MATH MODEL RESEARCH GROUP

DEPARTMENT OF MATHEMATICS

FEDERAL UNIVERSITY OF TECHNOLOGY (FUT), MINNA, NIGERIA

BOOK OF PROCEEDINGS

for the

International Conference on MATHEMATICAL MODELLING, OPTIMIZATION AND ANALYSIS OF DISEASE DYNAMICS (ICMMOADD 2024)

HYBRID (VIRTUAL & PHYSICAL)

Theme:

CONTEMPORARY ISSUES ON THE CONTROLS OF DISEASES EPIDEMICS AND PANDEMIC

DATE: Thursday 22nd February, 2024 **TIME:** 10:00am Prompt

VENUE: Department of Mathematics, Federal University of Technology Minna, Nigeria

PROFESSOR N. I. AKINWANDE FNMS

Convener

ISBN: 978-978-789-930-4

MATH MODEL RESEARCH GROUP
DEPARTMENT OF MATHEMATICS
FEDERAL UNIVERSITY OF TECHNOLOGY, MINNA, NIGERIA

BOOK OF PROCEEDINGS

for the

International Conference

on

MATHEMATICAL MODELLING, OPTIMIZATION AND ANALYSIS OF DISEASE DYNAMICS (ICMMOADD) 2024

HYBRID (VIRTUAL & PHYSICAL)

Theme:

CONTEMPORARY ISSUES ON THE CONTROLS OF DISEASES EPIDEMICS AND PANDEMIC

DATE: Thursday 22nd February, 2024 **TIME:** 10.00am Prompt
VENUE: Department of Mathematics, Federal University of Technology, Minna, Nigeria

PROFESSOR N. I. AKINWANDE FNMS
Convener

ISBN: 978-978-789-930-4

EDITORIAL BOARD

CENTRAL ORGANIZING COMMITTEE

NAME	STATUS	INSTITUTION
Prof. N. I. Akinwande	Convener	Dept. of Mathematics, F. U. T., Minna
Dr. S. A. Somma	Secretary	Dept. of Mathematics, F. U. T., Minna
Mrs. N. O. Abdurrahman	Ass. Secretary	Dept. of Mathematics, F. U. T., Minna
Prof. R. O. Olayiwola	Member	Dept. of Mathematics, F. U. T., Minna
Prof. F. A. Kuta	Member	Dept. of Microbiology, F. U. T., Minna
Prof. A. I. Enagi	Member	Dept. of Mathematics, F. U. T., Minna
Prof. S. Abdulrahman	Member	Dept. of Mathematics, F. U. Birnin Kebbi
Prof. M. D. Shehu	Member	Dept. of Mathematics, F. U. T., Minna
Prof. G. A. Bolarin	Member	Dept. of Mathematics, F. U. T., Minna
Dr. A. Usman	Member	Dept. of Statistics, F. U. T., Minna
Dr. T. T. Ashezua	Member	Dept. of Mathematics, JSTU, Makurdi
Dr. O. M. Adetutu	Member	Dept. of Statistics, F. U. T., Minna
Dr. F. A. Oguntolu	Member	Dept. of Mathematics, F. U. T., Minna
Dr. R. I. Gweryina	Member	Dept. of Mathematics, JSTU, Makurdi
Dr. P. T. Adajime	Member	Dept. of Epidemiology, BSU, Makurdi

LOCAL ORGANIZING COMMITTEE

Prof. N. I. Akinwande	Chaiman	Dr. R. Muhammad	Member
Dr. S. A. Somma	Secretary	Dr. N. Nyor	Member
Mrs. N. O. Abdurrahman	Ass. Secretary	Dr. S. I. Yusuf	Member
Prof. Y. M. Aiyesimi	Member	Dr. O. R. Jimoh	Member
Prof. Y. A. Yahaya	Member	Dr. F. A. Oguntolu	Member
Prof. U. Y. Abubakar	Member	Dr. A. Lawal	Member
Prof. M. Jiya	Member	Dr. A. Yusuf	Member
Prof. D. Hakimi	Member	Dr. K. J. Audu	Member
Prof. A. A. Muhammed	Member	Dr. (Mrs) Deborah Bako	Member
Prof. R. O. Olayiwola	Member	Dr. N. O. Salihu	Member
Prof. A. Ndanusa	Member	Mr. A. B. Zhiri	Member
Prof. A. I. Enagi	Member	Mr. C. U. Ugwu	Member
Prof. M.D. Shehu	Member	Mr. J. A. Jiddah	Member
Prof. G. A. Bolarin	Member	Mr. A. Gana	Member
Prof. (Mrs) A. T. Cole	Member	Mr. B. D. Bako	Member
Dr. U. Mohammed	Member		

TABLE OF CONTENT

PLENARY PAPERS

MATHEMATICAL MODELLING

FLUID DYNAMICS AND NUMERICAL ANALYSIS

STATISTICS AND OPTIMIZATION

ADDENDUM

PLENARY SPEAKERS

Professor Oluwole Daniel Makinde
Faculty of Military Science, Stellenbosch University, Saldanha 7395, South Africa

Dr. Adajime Terlumun Paul
Department of Epidemiology and Community Health, College of Health Sciences, Benue State University, Makurdi

PLENARY PAPERS

Disease Dynamics and Its Impact on Economy with Optimal Control: A Mathematical Model

Oluwole Daniel Makinde
Faculty of Military Science, Stellenbosch University, Private Bag X2, Saldanha 7395, South Africa

Abstract

Outbreak of infectious diseases are more destructive on the economic growth of nations around the world. This economic impact severity was observed during the recent global Covid-19 pandemic, leading to the rise in public health expenditure, diminished productivity, loss of life, business closures, trade disruption, obliteration of the tourism industry, revenue decline due to the government's inability to raise revenue because of quarantine and curfews. Since infectious diseases are not likely to disappear in the near future, proactive measures are required in order to save lives and safeguard economic prosperity. In this talk, a deterministic mathematical model for Covid-19 transmission dynamics with its global economic impact is qualitatively analysed via stability theory of differential equations. Positivity and invariant region of solutions together with disease-free and endemic equilibria were determined. The model basic reproduction number R_0 was obtained and the sensitivity indices of its embedded parameters were determined. It is observed that the model exhibits a forward bifurcation; this validates the stability of the Covid-19 disease-free equilibrium whenever $R_0 < 1$. Using Pontraygin's maximum principle with two variable control strategies (i.e. protective strategy and environmental fumigation), the optimal control analysis is implemented and their cost effectiveness determined. Numerical results displayed graphical suggest that the use of protective control is the most cost-effective strategy to combat the Covid-19 pandemic and boost the economy.

Keywords: Disease dynamics, Economic impact, Basic reproduction number, Sensitivity analysis, Bifurcation analysis, Optimal control analysis, Cost-effectiveness analysis

COVID-19 PANDEMIC IN NIGERIA: PUBLIC HEALTH RESPONSE TOWARDS EPIDEMIC CONTROL

Adajime T. Paul
Department of Epidemiology and Community Health, College of Health Sciences, Benue State University, Makurdi.

Abstract

The Coronavirus pandemic of 2019 brought intense fear throughout the world by its devastating health consequences on humans while overwhelming the health systems of many counties in the world. The first instance of the virus in Nigeria was an imported case from Italy on 27 February 2020. The incidence of COVID-19 grew steadily in Nigeria, moving from an imported case and elitist pattern to community transmission. The United States had the highest number of infections and deaths in the world. This was followed by Brazil, India, Mexico, and Peru. As of 24 February 2023, there were 10.8 million COVID-19 cases on the world, with 228,738 deaths, and 9.8 million recoveries (93.8%). In Nigeria, 180,661 have been confirmed and 2163 deaths have been recorded in 36 states and the Federal Capital Territory. The Federal Government of Nigeria established the Presidential Task Force (PTF) for the Control of Coronavirus (COVID-19) disease on 7th March 2020. The PTF is the focal point of government's efforts to tackle the COVID-19 pandemic. Nigerian households faced increased economic precarity: unemployed workers migrated back to the low productivity agricultural sector, and reports of food insecurity increased substantially. Before COVID-19, about 40 percent of Nigerians were living below the national poverty line, and millions more were vulnerable to falling into poverty. Simulations suggest that the crisis pushed more than 10 million Nigerians below the poverty line. Food assistance, conditional cash transfers and school feeding programme were additional interventions implemented to cushion the effects. The Federal Government also responded by setting up treatment sites across the country for the diagnosis and treatment of this ailment as well as supported many prevention interventions including vaccination programme. These interventions impacted the lives of the people positively, however came with challenges that are yet to be completely addressed.

Key Words: COVID-19 virus, pandemic, control, intervention, vaccination.

COVID-19 PANDEMIC IN NIGERIA: PUBLIC HEALTH RESPONSE TOWARDS EPIDEMIC CONTROL

INTRODUCTION

The coronavirus pandemic of 2019 brought intense fear throughout the world by its devastating health consequences on humans while overwhelming the health systems of must counties in the world.[1] The WHO defines an epidemic as "the occurrence in a community or region of cases of an illness, specific health-related behavior, or other health-related events clearly in excess of normal expectancy. A pandemic is defined by the WHO as "an epidemic occurring

worldwide, or over a very wide area, crossing international boundaries and usually affecting a large number of people.[1]

History of Epidemics in Nigeria

Over the years, epidemics and later pandemics have really shaped the history of health in Nigeria, creating superfluous burden of morbidity and mortality in the country and disrupting the existing socio-economic, religious and political activities in the country.[2] On 31 December 2019, the World Health Organization (WHO) was notified of a novel coronavirus disease in China that was later named COVID-19. This outbreak was declared a pandemic on 11th, March 2020. The first instance of the virus in Nigeria was an imported case from Italy on 27 February 2020. The incidence of COVID-19 grew steadily in Nigeria, moving from an imported case and elitist pattern to community transmission. By April 11, 2020, 318 confirmed cases and 10 deaths from COVID-19 have occurred in Nigeria. [2]

Epidemiology

The "2019 Novel Coronavirus" was first identified in January 2020. Early cases were associated with a seafood and live animal market in Wuhan City, China. The first cases were reported in December 2019. From December 18, 2019, through December 29, 2019, five patients were hospitalized with acute respiratory distress syndrome and one of these patients died.[3] By January 2, 2020, 41 admitted hospital patients had been identified as having laboratory-confirmed COVID-19 infection, less than half of these patients had underlying diseases, including diabetes, hypertension, and cardiovascular disease. More than 200 countries have been affected with over 700 million cases, and approximately 7 million deaths, and 180 million recoveries worldwide.[4] The World Health Organization reported that at the end of 2021, the United States had the highest number of infections and deaths in the world. This was followed by Brazil, India, Mexico, and Peru. As of 24 February 2023, there were 10.8 million COVID-19 cases on the continent, with 228,738 deaths (CFR: 2.1%), and 9.8 million recoveries (93.8%). Africa accounted for 1.3% of cases reported globally (757.2 million) and 1.2% of deaths (6.8 million). Of this total, the WHO African Region (WHO AFR) accounted for 82.7% of cases (8.9 million) and 76.2% of deaths (174,191 deaths).[5] In Nigeria, 180,661 have been confirmed, 165,122 cases have been discharged and 2163 deaths have been recorded in 36 states and the Federal Capital Territory.[4]

NATIONAL STARTEGIC RESPONSE FOR THE CONTROL OF COVID-19 IN NIGERIA

On the 23rd of January 2020, the World Health Organization International Health Regulations (IHR) Emergency Committee advised that all countries should be prepared for containment, including active surveillance, early detection, isolation and case management, contact tracing and prevention of onward spread of 2019-nCoV infection, and to share full data with the WHO.

After the pronouncement of this declaration, a nation COVID-19 control team was set by the president of Nigeria.

The Presidential Task force

The Federal Government of Nigeria established the Presidential Task Force (PTF) for the Control of Coronavirus (COVID-19) disease on 7th March 2020. The PTF is the focal point of government's efforts to tackle the COVID-19 pandemic and has an initial mandate of six months. The overall goal of the PTF is to stop further transmission of COVID-19 within Nigeria, ensure provision of basic treatment to those infected, and reduce the overall social and economic impact of the pandemic on the country.[6]

The PTF was chaired by Boss Mustapha with minister of health and the chairman of NCDC as members. The core mandate was:

- Provide overall policy
- Enable delivery of control priorities through; provision of treatment centers, set up of emergency operations center, provision of commodities for IPC, sensitization and awareness creation, and set up of diagnostic laboratories for COVID-19.

Other mandates include:

- Approve recommendations for funding and budget, provide recommendation for interventions such as; school closure, social distancing suspension and flight limitations
- Define targets and monitor the progress for meeting up targets
- Partnership engagement with states, bilateral and multilateral bodies and other countries and agencies.
- Keep the public informed of emergency development regarding preparedness and response. [6]

Functional Areas

- PTF National Pandemic Response Center
- Epidemiology and Surveillance
- Risk communication and Community Engagement
- Laboratory
- Resource mobilization
- Security, Logistics and Mass Care
- Infection, Prevention and Control
- Research
- Case Management
- Finance Monitoring and Compliance
- Point of Entry

The PTF established the National Pandemic Response Centre (NPRC), the technical coordinating structure responsible for providing strategic guidance on the national response, estimating MDA resource needs and allocations, and coordinating all response stakeholder efforts. Stakeholders included MDAs, donors, development partners, nongovernment

organizations, and civil society. The organized private sector established the Coalition Against COVID-19 (CACOVID) to coordinate their engagement. The NPRC, led by the PTF national coordinator, included Secretariat, led by a chief of secretariat (CoS) and an incident manager, who coordinated 9 functional pillars. Each pillar was led by different government MDAs with mandate and oversight for their pillar; for example, NCDC oversaw surveillance and laboratory and FMOH led case management. Staff from the US Centers for Disease Control and Prevention (CDC), US Agency for International Development (USAID), WHO, UNICEF, e-Health Africa, CREDO, and the Bill and Melinda Gates Foundation supported the NPRC. The PTF convened a multidisciplinary advisory group to provide evidence-based briefing papers, informing real-time decision making. The group comprised health policy and service experts, including epidemiologists, modelers, public health experts, social scientists, foreign and domestic academicians, and NPRC staff. [7]

The National Pandemic Response Centre (NPRC)

To provide effective technical guidance and direction, the NPRC developed a comprehensive pandemic response plan (PRP), the blueprint for the coordinated national COVID-19 strategy, in addition to the NCDC-developed public health incident action plan. The PRP included activities beyond health, such as disaster management, humanitarian affairs, information, security, finance, trade, and investment. The PRP described complementary response roles of national and state governments (Table 2), private sector, and development partners. The PRP divided the response into 6 phases based on the national and WHO epidemic response plans, with specific tasks for each phase following specific trigger events.[8]

Phase 1: Preparedness and No Cases

This phase, focus on monitoring global trends and preparation for surveillance; as well as early detection of high-risk passengers for follow-up, isolation of symptomatic passengers, and transfer of passengers to designated isolation centers for testing.[6]

Phase 2: Mitigation & Response to Sporadic Cases

This phase focused on the activation of health and non-health multi-sectoral structures to identify and contain the viral spread through public sensitization on preventive and protective measures by providing timely information and provision of consumables for the response.[8]

Phase 3: Intensified Response to Cluster(s) of Connected Cases

Activities in this phase were focused on intensified and heightened surveillance towards containment; expedited sample collection, testing, and reporting; mass care to alleviate containment measures; and prompt isolation and management of suspected/ confirmed cases with improved outcomes.[6]

Phase 4: Peak of the Pandemic due to Community transmission
This phase is activated as a result of increased cases of community transmission in one or more states. It calls for a recommendation for the declaration of a national emergency and heightened response in both health and non-health sectors.[8]

Phase 5: Post Peak
In this phase, there is a decline in new/confirmed cases by at least 10% per week for at least two consecutive weeks. The activities involve continuous health activities such as surveillance, laboratory testing, case management and infection, prevention, and control measures. [8]

Phase 6: Post-Pandemic Recovery
This involves phasing out pandemic activities, building the preparedness and resilience capacity of existing health and non-health institutions/infrastructure. It also focuses on rebuilding social welfare and promoting economic growth in the country.[8]

EFFECTS OF COVID-19 PANDEMIC AND RESPONSES

Work and COVID-19 in Nigeria.
Findings from a sample of household heads interviewed in successive rounds of the Nigeria COVID-19 National Longitudinal Phone Survey (NLPS) indicate that employment contracted sharply and job turnover increased. Even though many Nigerians returned to work after the easing of strict lockdown measures in the early phase of the COVID-19 crisis, most households remain in an economically precarious situation.[9] Many households reported lower income. Nigerian households faced increased economic precarity: unemployed workers migrated back to the low productivity agricultural sector, and reports of food insecurity increased substantially. To curb this, some institutions stated offering online and home delivery services to reduce contact with people[10]. Also, NIRSAL microfinance bank covid-19 loan in Nigeria, a federal government intervention program through the CBN to curb the consequences of Corona virus on households, small and medium scale enterprises and impact positively on the life's of its citizenry. [11]

The Effect of COVID-19 on Education and Social life
In response to the pandemic, the government implemented multiple measures, both at the federal and state levels, including the adoption of a Contingency Plan to ensure that the school community was protected. The plan aimed to ensure the continuation of education, provide safe water and hygiene facilities in schools, and train and sensitize the school community on preventive measures.[12] During the school closures, Nigeria strived for learning continuity despite the abrupt closure, with distance learning reaching approximately 60 percent of school children, a strong performance compared to other countries in the region. The use of online teaching methods were employed to solve this challenge[13]. Lockdowns on religious and public events where put in place nationwide to curtail the spread as well as other regulatory measures.

The Nigerian government implemented bans on international travels from all countries, especially high-risk countries.[14]
The Tertiary Education Trust Fund (TETFund), NCDC and other stakeholders constituted the National COVID-19 Research Consortium, with members drawn from the academia and research institutes. The consortium is mandated to undertake research on all aspects of COVID-19 to ensure effective prevention and control. [15]

Effect of COVID-19 Pandemic on health

Nigeria ranks among the top ten countries heavily affected by COVID-19 in Africa. Nigeria's COVID-19 response focuses on strengthening laboratory systems and enhancing risk communication and surveillance. The available indicators—such as the total number of deaths, the case fatality rate, and the total number of confirmed cases—show that Nigeria has fared reasonably well in responding to the COVID-19 pandemic despite a significant decline in the delivery of essential health services. Yet, COVID-19 has had a substantial negative impact on service delivery for both disease control programs and essential health care services. The federal government funded the construction of molecular laboratories in all the states to ensure quick diagnosis of epidemic prone diseases [13]. In addition, the Central Bank of Nigeria (CBN), Nigeria's apex regulatory bank, announced a 1.15 trillion naira (approximately 3 billion dollars) COVID-19 Pandemic Intervention Fund intended for Healthcare Sector Research and Development Intervention Scheme (HSRDIS) aimed at strengthening the public healthcare system with strategic funding of research and development of improved or new drugs, diagnostics and vaccines for infectious diseases in Nigeria, especially COVID-19.[15]

Nigeria's Social Protection System during COVID-19 and beyond.

Before COVID-19, about 40 percent of Nigerians were living below the national poverty line, and millions more were vulnerable to falling into poverty. Simulations suggest that the crisis pushed more than 10 million Nigerians below the poverty line. Recognizing the extraordinary scope of this challenge, the government has launched important new initiatives through the National Social Investment Programs, but critical financing gaps and institutional challenges continue to undermine the effectiveness of the social protection system.[16] Most safety nets are limited in scope, and social-protection programs cover only a small fraction of their target populations. While technological innovations can improve the effectiveness of social protection programs and enhance their ability to reach poor and vulnerable households, the government must establish a fiscally sustainable social protection system that integrates the disparate programs implemented at the federal, state, and local levels.[13]
Other programs and policies include:

- Economic Stimulus Bill. The bill was proposed on March 24, 2020, to provide socioeconomic relief to Nigerian citizens and businesses due to the negative impact of COVID-19 on businesses and livelihoods. The bill was aimed at reducing taxes by 50% for businesses registered under the Companies and Allied Matters Act to enable them to sustain their businesses and prevent staff layoffs.[11]

- National Conditional Cash Transfer. The federal government announced the plan to transfer 20,000 Naira to poor and vulnerable households on the National Social Register (NSR). The NSR has about 2.6 million households, which the federal government promised to increase to 3.6 million during COVID-19 lockdown (Dixit et al., 2020).[11]
- Food Assistance. The Federal Ministry of Humanitarian Affairs, Disaster Management and Social Development announced the decision to provide food to vulnerable households due to the lockdown that hindered socioeconomic activities and incapacitated finances of families.[11]
- School Feeding Program. The school feeding program has been in existence before the onset of COVID-19 in Nigeria. Students in Nigerian public schools were given free daily meals provided by federal school-funded school feeding programs. This program targeted 24 million school children.[11]

MANAGEMENT OF COVID-19 PANDEMIC

One of the cardinal steps in the response to an epidemic is case identification. Cases are identified through screening of individuals who have symptoms and signs that are related to the disease been investigated.

Symptoms associated with COVID-19

Presenting signs and symptoms of COVID-19 vary. Most persons experience fever (83–99%), cough (59–82%), fatigue (44–70%), anorexia (40–84%), shortness of breath (31–40%), myalgias (11–35%). Other non-specific symptoms, such as sore throat, nasal congestion, headache, diarrhoea, nausea and vomiting, have also been reported. Loss of smell (anosmia) or loss of taste (ageusia) preceding the onset of respiratory symptoms has also been reported. Additional neurological manifestations reported include dizziness, agitation, weakness, seizures, or findings suggestive of stroke including trouble with speech or vision, sensory loss, or problems with balance in standing or walking. Older people and immunosuppressed patients in particular may present with atypical symptoms such as fatigue, reduced alertness, reduced mobility, diarrhoea, loss of appetite, confusion, and absence of fever.[17]

Screening: The primary objective of the COVID-19 global response was to slow and stop transmission. This was to be achieved through finding, isolation and testing of every suspected case, and provision of timely appropriate care of patients with COVID-19. A simple set of questions based on the WHO case definition are used to identify a suspected case.[18] This is best done by establishing screening protocols at all health access points and during contact tracing activities. The case definition of COVID-19 is “any patient with acute respiratory illness (acute respiratory illness in an area of moderate or high COVID-19 prevalence with no other explanation) within the last 10 days (fever and either cough, difficulty breathing or shortness of breath); and in absence of an alternative diagnosis that explains the clinical presentation and residing or working in the last 14 days in an area identified by NCDC as a moderate or high prevalence region”. Persons with symptoms that meet the case definition for suspected COVID-19 enter into the COVID-19 care pathway and should immediately be given a medical mask. [18]

Laboratory diagnosis

Diagnostic technical guidance for the diagnosis of COVID-19 pandemic include:

1. Antigen-detection in the diagnosis of SARS-CoV-2 infection.
2. Use of SARS-CoV-2 antigen-detection rapid diagnostic tests for COVID-19 self-testing

It is recommended that, for all suspected COVID-19 cases, at minimum, respiratory specimens for nucleic acid amplification testing (NAAT) should be collected.[18] It is important to note that, in the first week of symptom onset relatively high viral loads are generally observed in the upper respiratory tract (URT) specimens. For the collection of URT samples, the collection of nasopharyngeal and oropharyngeal specimens. For the lower respiratory tract (LRT), samples are more likely to be positive after the first week of illness. [19]

COVID-19 Self-testing

Strong recommendation for COVID-19 self-testing, using SARS-CoV-2 Ag-RDTs, was offered in addition to professionally administered testing services (low to moderate certainty evidence). COVID-19 self-testing, as with any testing, should always be voluntary and never mandatory or coercive.[18]

Management of mild COVID-19: symptomatic treatment

Patients with mild symptoms may present to an emergency unit, primary care/outpatient department, or be encountered during community outreach activities, such as home visits. It is recommend that patients with suspected or confirmed mild COVID-19 be isolated to contain virus transmission according to the established COVID-19 care pathway. This can be done at a designated COVID-19 health facility, community facility or at home (self-isolation). [17] Because of co-infections with COVID-19, in areas with other endemic infections that cause fever (such as malaria, dengue, etc.), febrile patients are tested and treated for endemic infections per routine protocols irrespective of the presence of respiratory signs and symptoms. Patients with mild COVID-19 are given symptomatic treatment such as antipyretics for fever and pain, adequate nutrition and appropriate rehydration.[18]

Management of moderate COVID-19

Patients with moderate disease usually present to an emergency unit or primary care/outpatient department. Some were encountered during community outreach activities, such as home visits. [20] Patients with suspected or confirmed moderate COVID-19 were usually isolated to contain viral transmission. These patients usually do not require emergency interventions or hospitalization; however, isolation was necessary for all suspect or confirmed cases.

Management of severe COVID-19

For severe cases, immediate administration of supplemental oxygen therapy is key during resuscitation to target SpO2 ≥ 94% and to any patient without emergency signs and hypoxaemia (i.e. stable hypoxaemic patient) to target SpO2 > 90% or ≥ 92–95% in pregnant women.[20]

Key recommendations:

- Adults with emergency signs (obstructed or absent breathing, severe respiratory distress, central cyanosis, shock, coma and/or convulsions) are placed on emergency airway management and oxygen therapy during resuscitation to target SpO2 ≥ 94%.
- After stabilizing the patients, target > 90% SpO2 in non-pregnant adults and ≥ 92–95% in pregnant women.
- Appropriate oxygen delivery devices are used to administer oxygen (e.g. use nasal cannula for rates up to 5 L/min; Venturi mask for flow rates 6–10 L/min; and face mask with reservoir bag for flow rates 10–15 L/min). In adults, techniques such as positioning, e.g. high supported sitting, are used to optimize oxygenation, ease breathlessness and reduce energy expenditure.
- In adult patients with evidence of increased secretion production, secretion retention, and/or weak cough, airway clearance management are placed on secretion clearance techniques such as gravity-assisted drainage and active cycle of breathing technique.

PREVENTION AND CONTROL

Key IPC strategies to limit or prevent transmission of COVID-19

The response to the COVID-19 outbreak must be optimal using certain strategies and practices. At the facility level, IPC programme with a dedicated and trained team or at least an IPC focal point should be in place. The five IPC strategies required to prevent or limit transmission of COVID-19 in health care facilities include the following:

- **Early recognition and source control of COVID19.**

All patients who present to a health facility during this COVID-19 outbreak were screened for the disease using the case definition. Such patients were isolated and arranged for the commencement of further care if need be and for transportation to a designated COVID-19 treatment center. [21]

- **Application of standard precautions for all patients at all times**

Response regarding standard precautions is to reduce the risk of transmission of microorganisms from both recognized and unrecognized sources of infection. Elements of of the response include:

Hand hygiene

Hand hygiene is includes either cleansing hands with an alcohol-based hand rub (ABHR) containing at least 70% alcohol, or with soap, under running water and drying with disposable towels [22]

Respiratory hygiene

Response emphasized respiratory hygiene measures such as use of medical mask and display graphic information on the need to cover nose and mouth.

Environmental cleaning

This involves, consistent and correct environmental cleaning and disinfection. All surfaces in health-care facilities especially high-touch surfaces, should be routinely cleaned and disinfected.[21]

Waste management
Health-care waste produced during the care of patients with suspected or confirmed COVID-19 is considered to be infectious and should be collected safely in clearly marked lined containers and sharp safe boxes.[21]

- **Implement administrative controls.**

Most health facilities ensured that they have an IPC programme, with their healthcare workers adequately trained on basic IPC procedures and able to implement standard precautions as well as droplet and contact precaution. Adequate provision of appropriate commodity supplies for prevention of disease transmission e.g. Medical masks, certified N95masks, gloves, hand hygiene equipment, respiratory hygiene and waste disposal materials.

- **Use of environmental and engineering controls including ventilation**

Control strategies such as adequate spatial separation of patients, adequate ventilation and appropriate cleaning of the environment should be implemented.[21] The following engineering controls should be put in place:

Provide isolation rooms that are well ventilated (wide open windows that open to the outside, away from other wards with doors closed and preferably with an anteroom. Rooms should provide air flow of at least 160 L/s per patient with at least 12 air exchanges per hour and controlled direction of air flow (air flow should be away from the healthcare worker towards the patient to the outside through the open window. Air should not flow from the patient's room into the hallway or other rooms/wards.[22]

Provide physical barriers or partitions to guide patients through triage areas.

Provide closed suctioning systems for airway suctioning for intubated patients.

- **COVID-19 Vaccinations**

The largest vaccination response program in Nigeria was that of COVID-19.[23] On March 2, 2021, about 4 million doses of the AstraZeneca/Oxford vaccine arrived in the country, through the COVID-19 Vaccine Global Access (COVAX) facility, a partnership between Coalition between Epidemic Preparedness Innovations (CEPI), Global Alliance for Vaccines and Immunizations (GAVI), United Nations Children's Fund (UNICEF), and WHO.[3] This is an attempt to ensure equitable distribution of the COVID-19 vaccines globally.[4] Frontline health workers were prioritized groups to receive the vaccines due to their exposures in the course of investigation and treatment. Since the arrival of the first wave of vaccines, the country has

received more than 67 million doses of COVID-19 vaccines, out of which 31.1 million people have been fully vaccinated. Currently, apart from Oxford vaccine, six (6) more vaccines have been approved for use of in Nigeria. These include: Moderna vaccine, Pfizer/BioNTech, Gamaleya, Janssen (Johnson & Johnson),[3]

CHALLENGES OF COVID 19 RESPONSE

Corruption and lack of government willingness to invest adequately in social protection programs has resulted in poor coverage and low impact of social protection programs in Nigeria.[11] The National Conditional Cash Transfer Program during the lockdown did not achieve the set objective due to the lack of transparency in the system from non-digitalization of the process.[11] Testing and contact tracing were faced with some challenges such as inadequate equipment, shortage of funds, and inadequate expertise.[14] The COVID-19 vaccination programme had so many challenges including; entry of substandard and falsified vaccines into markets, theft of vaccines within the distribution systems, leakages in emergency funding designated for the development and distribution of vaccines, nepotism, favouritism, and corrupted procurement systems.[24] In Nigeria, COVID-19 vaccine uptake was generally low. In December 2021, due to this challenge, over one million doses of AstraZeneca vaccines became expired. The acceptance rate was poor (20%-58.2%). Identified reasons for this for the poor uptake include: conspiracy theories, side effects and misinformation spread on social media.[25] Other reasons for poor uptake include: education, religion, and prior COVID-19 diagnoses. [26]

CONCLUSION

It is evident that Nigeria was not as well prepared for the COVID-19 outbreak response due to poor health care system and key determinants of health.[27] This pandemic presents an opportunity for policy makers to look inward and strengthen Nigeria health system that will stand emerging pandemic of any magnitude.

REFERENCES

1. Amzat J, Aminu K, Kolo VI, Akinyele AA. Since January 2020 Elsevier has created a COVID-19 resource centre with free information in English and Mandarin on the novel coronavirus COVID- 19 . The COVID-19 resource centre is hosted on Elsevier Connect , the company ' s public news and information . 2020;(January).
2. Odusanya OO. Nigeria in the COVID era: Health system strengthening for national security and prosperity. Nigerian Postgraduate Medical Journal. 2022 Jul 1;29(3):192-7.
3. Sokunbi TO, Oluyedun AT, Adegboye EA, Oluwatomisin GP, Ibrahim AD. COVID-19 vaccination in Nigeria: Challenges and recommendations for future vaccination initiatives. Public Health Challenges. 2023 Mar;2(1):e57.
4. Simon-Oke IA, Nasiru R, Afolabi OJ. Corona Virus (COVID-19) Vaccine: Challenges and Prospects in Nigeria: A Review. J Infect Dis Epidemiol. 2022;8:279.
5. World Health Organization. COVID-19 response in Africa bulletin: situation and response in the WHO AFRO Region.

6. Ehanire EO. Nigeria ' s COVID-19 Response. 2020;
7. Spina S, Marrazzo F, Migliari M, Stucchi R, Sforza A, Fumagalli R. The response of Milan's Emergency Medical System to the COVID-19 outbreak in Italy. The Lancet. 2020 Mar 14;395(10227):e49-50.
8. Okunade K. January-March 2018 An Official Publication of The National Postgraduate Medical College of Nigeria. 2018;(January):19–26.
9. Engelhardt G V., Clancy D, Cussen M, Lydon R, Lydon CC, Fisher LA, et al. Measuring Living Standards: Household Consumption and Wealth Indices. Reg Sci Urban Econ [Internet]. 2009;37(1):1–11.
10. Okeke C, Uzochukwu B, Onyedinma C, Onwujekwe O. An assessment of Nigeria ' s health systems response to COVID -19. 2022;56(3):74–84.
11. Adeoye AO, Okunola JL. Poverty Implications of COVID-19 and Government Social Protection Programs in Nigeria. 2022;16(1):242–51.
12. Jacob ON, Ndubuisi AG, Terfa AC. Impact of Covid-19 on Nigerian Educational Institutions. Central Asian Journal of Medical and Natural Science. 2021 Feb 6;2(1):153-61.
13. Bolu O, Mustapha B, Ihekweazu C, Muhammad M, Hassan A, Abdulwahab A, et al. Effect of Nigeria Presidential Task Force on COVID-19. 2022;28(13).
14. Ilesanmi OS, Afolabi AA. Six months of COVID-19 response in Nigeria: lessons, challenges, and way forward. Journal of Ideas in Health. 2020 Sep 27;3(Special1):198-200. Ilesanmi OS, Afolabi AA. Six months of COVID-19 response in Nigeria: lessons, challenges, and way forward. Journal of Ideas in Health. 2020 Sep 27;3(Special1):198-200.
15. Etteh CC, Adoga MP, Ogbaga CC. COVID-19 response in Nigeria: health system preparedness and lessons for future epidemics in Africa. Ethics, Medicine and Public Health. 2020 Oct 1;15:100580.
16. Analysis AN, Food OF, Trends S, Major IN, Hotspots M. Populations at risk : Implications of COVID-19 for hunger , migration and displacement. 2020;(November).
17. NCDC. National interim guidelines for clinical management of COVID-19. Nigeria Centre for Disease Control. 2020.
18. World Health Organization. Clinical management of COVID-19: living guideline, August, 2023. World Health Organization; 2023.
19. Ministry F, Health OF. Interim Guidelines for Clinical Management of COVID-19. Niger Cent Dis Control. 2020;(3).
20. World Health Organization. Living guidance for clinical management of COVID-19: living guidance, 23 November 2021. World Health Organization; 2021.
21. World Health Organization. Infection prevention and control during health care when coronavirus disease (COVID-19) is suspected or confirmed: interim guidance, 12 July 2021. World Health Organization; 2021.
22. World Health Organization. Infection Prevention and Control (IPC) for Novel Coronavirus (COVID-19). Training module. WHO. 2020.

23. Olutuase VO, Jaja CJI, Akuoko CP, Adewuyi EO, Khanal V. Medicines and vaccines supply chains challenges in Nigeria : a scoping review. BMC Public Health [Internet]. 2022;1–15.
24. Cui X, Wang P, Wei Z. Emergency use of COVID-19 vaccines recommended by the World Health Organization (WHO) as of June 2021. Drug discoveries & therapeutics. 2021 Aug 31;15(4):222-4.
25. Olu-Abiodun O, Abiodun O, Okafor N. COVID-19 vaccination in Nigeria: A rapid review of vaccine acceptance rate and the associated factors. PloS one. 2022 May 11;17(5):e0267691.
26. Akande OW, Igumbor EU, Elimian KO, Ohonsi CE, Nwozor L, Oden O, et al. COVID-19 vaccine effectiveness studies in Nigeria : Quo vadis ? 2022;12.
27. Anyanwu MU, Festus IJ, Nwobi OC, Jaja CJ, Oguttu JW. A perspective on Nigeria's preparedness, response and challenges to mitigating the spread of COVID-19. Challenges. 2020 Sep 21;11(2):22.

MATHEMATICAL MODELLING

The Stability and Bifurcation Analysis of COVID-19 and Tuberculosis Co-infection Dynamics

[1]Abegye S. Y, [2]Akinwande N.I, [3]Akpan C.E
[1]Department of Mathematics/Statistics, Isa Mustapha Agawi I Polytechnic, Lafia, Nigeria
[2]Department of Mathematics, Federal University of Technology Minna, Nigeria
[3]Department of Mathematics, Federal University of Lafia, Nigeria.
Email: yakubupurity@gmail.com

Abstract

The World Health Organization declared COVID-19 as a public health menace in early 2020, due to the havoc the disease had caused resulting to the death of million of people across the globe. Due to its chaotic spread, and its co -infection with other diseases increased much more mortality rate. In particular, COVID-19 and tuberculosis diseases has similar symptoms, although they have different incubation periods. This paper was formulated to study the co-infection of COVID-19 and TB to investigate their synergic dynamism described by Mathematical model. An extensive study was conducted on both the analytical and numerical analysis of the model. The sub-models of the individual diseases were first analyzed and their both sensitivity and simulation analysis were carried out. The basic properties of the co-infection model was studied, its basic reproduction number was also computed using next generation method. It was proved that the co-infection with it's individual dieases can be eliminated when the basic reproduction number is less than one and greater than one at disease free equilibrium and at endemic equilibrium point respectively.We show that tuberculosis has postive impact on the transmission of COVID-19. It was observed also that the co-infection exbit forward bifurcation. From the sensitivity and simulation analysis it was demonstrated that the contact rate has positive influence on the transmision of the individual and the co-infection diseases.

Keywords: Bifurcation, co-infection, COVID-19, sensitivity, stability, Tuberculosis.

INTRODUCTION

Several pathogens may be responsible for diseases outbreak in human [2] and animals [5].Tuberculosis and COVID-19 can infect human simultaneously. Tuberculosis (TB) had infected over 10 million people and responsible for 1.2 million death cases worldwide [1]. Similarly, a population of over 100 million people infected with COVID – 19 with over 2 million death cases has been reported globally. During the COVID-19 pandemic in 2019, caused by novel beta coronavirus known as, severe acute respiratory syndrome corona-virus 2 (SARS-CoV-2), which took place first in Wuhan (Hubei), China. Since December 2019, there was increase in the number of individuals infected with the disease that became a threat to global public health and the world economy [21]. During the pandemic, the most suitable and safety measure is the lockdown measure that has a positive impact in curtailing the spread of COVID-19.

It is well known that Tuberculosis (TB) is caused by *Mycobacterium tuberculosis* that is transmitted from an individual to another via the released of microscopic droplets into the atmosphere through an infected person. This occurs when the infected patient coughs or sneezes then the tuberculosis bacterium disseminate [16]. Most people infected with these bacteria do not show any signs or

symptom this is described as latent tuberculosis stage. In a situation where the sign appears, this is known as the active tuberculosis stage. This is a condition where the cough is bloody; there is a weight loss, nocturnal sweats and fever are displaced [2]. The possibility of an individual exhibiting symptom or not is the function of the person's immune system. There are people whose immune system prevent the replication of the bacteria and consequently hinders the occurrence of the disease (latent TB stage) and in some other people their immunity is weak, so the bacteria develops and multiplies, causes the person to become infected [16]. TB is preventable and curable, yet it has defiled many efforts made for its total eradication because of the presence of latent TB patients and active TB infectious individuals. Treatment is usually administered to those with active tuberculosis through the use of antibiotic. Prevention of TB includes vaccination, isolation and chemoprophylaxis e.t.c.

COVID- 19 diseases has a similar transmission mode and symptoms like that of tuberculosis. For COVID- 19, the disease is transmitted also from one person to another when a healthy individual is in close contact with an infected person (either dead or alive patients). Instances have shown that human corpses are transmissible source of the virus also. The spread of COVID- 19 is possibly occurs through human faces shed to the environment. In upholding African traditions and customs of burial practices such as washing of dead bodies before dressing, has in deep sense fuelled the transmission of the virus in Africa. An individual infected with COVID – 19 diseases can be asymptomatic or symptomatic. In asymptomatic, the victim is infected with the virus, but does not exhibit any symptoms like fever, cough and shortness of breath but can transmit the virus to others making it difficult for isolation. In symptomatic, the infected person shows symptoms like fever, cough and shortness of breath and liable to spread the disease to others. Prevention measures for these diseases include vaccination, good hygiene, and use of face masks, physical distancing. Furthermore, treatment measures consist of prescription of antiviral medication, isolation and quarantine measures [4].The two diseases are very contagious and they can spread primarily through close contact with the infected person. It has been shown from researches and clinical evidences that TB co-exists with COVID-19, promoting twice or more increase in fatality and a 25% decrease in the recovery of the individual diseases. The harm is more devastating than the mortality rate of COVID-19 and TB globally. This association of these two diseases became one of the popular co - dynamic during the COVID- 19 pandemic. Although, several co - infections existed before COVID-19 emergency. Yet, COVID-19 co-infection with other diseases had exceeded the previous record of co-infection that ever existed [22].

Several studies had been conducted on COVID-19 co-infections and other infectious disease in various literatures. For instance, the co-dynamics Cholera-COVID-19 model control was formulated and analyzed by [10]. Similarly, Dengue-COVID-19 was designed and analyzed by [19], TB- HIV model in [3] and TB-COVID-19 in [9]. Marimuthu *et al*. [12], formulated a TB-COVID-19 co-infected by estimating people with and without intervention control measures. It was shown from their study that with no intervention the co-infection occurred at a relative small time while with intervention it takes a longer time. In particular, it was estimated from the model that at the peak of the epidemic about 27,968 TB-COVID-19 cases were reported with intervention mechanisms and 20,880 cases in absence of proper interventions.

Goudiady *et al*. [9], proposed a mathematical model on COVID-19 and Tuberculosis by incorporating public campaign awareness, COVID - 19 prevention and treatment of tuberculosis and COVID - 19 using optimal control. The basic properties of the model were discussed and the stability analyses were shown. Five strategies were employed as control measures during the

investigation. It was found that the strategy which focuses on the prevention of COVID - 19, its treatment and co - infection prevention offers a better preventive measure with a lower cost.

Bandekar and Ghosh [6], designed a co - infection model on TB and COVID - 19 considering waning immunity and face mask in the dynamics. Detailed stability analysis and bifurcation were carried out on the sub-models and discussions were also made on the impact of the most sensitive parameters like infection rate, waning immunity and face mask efficacy. The optimal control incorporate relative time control, improved TB treatment, and enhance COVID - 19 test and isolation facilities to combat the disease transmission were discussed. The result of their simulation shows that different control measures used are potentially instrumental in lowering the spread of the disease. They suggested that during pandemic, attention should be given to treatment of individual diseases in order to curtail co - infection of COVID - 19 with other diseases.

Inayaturnmat *et al*. [11], designed a seven (7) compartmental flow chart of tuberculosis and COVID–19 co – infection model with isolation and treatment. Two equilibria points were obtained at the disease – free equilibrium and endemic equilibrium points. In first instances, they show that at this equilibrium both tuberculosis and COVID– 19 infection are absent while the second connotes a situation where not only tuberculosis and COVID – 19 infections are found but the co – infections also existed. Analytical and numerical analyses of the co – infection were carried out. They used Latin hypercube sampling (LHS) to study the effect of the parameters of the model and they assumed that the parameters follow uniform distributions where 1000 samples were sorted by ranking. Partial rank correlation coefficient (PRCC) was used to obtain the correlation between the parameter with the compartments. Three compartments were selected for analysis namely: those infected with tuberculosis, COVID – 19 and the co – infection. They observed that the recovery rate and the infection rate of each COVID-19 and tuberculosis are the most sensitive. Optimal control was also carried out on the co – infection model as a control measure on tuberculosis and corona-virus. Simulation conducted revealled that isolation reduces the numbers of individuals infected with corona-virus and treatment has a long time impact on the population.

Rwezaura *et al*. [20], discussed a nine (9) compartmental populations with vaccination on corona-virus infected population and treatment for TB infected patients. The two equilibria points of the two diseases were analyzed in which it was shown that the local asymptotic stability at the disease – free and endemic equilibria exist when the reproduction numbers are below unity. They further, show that the TB sub – model undergoes forward bifurcation. Their model was tested using fmincon optimization toolbox in MATLAB in other to fit the daily confirmed cumulative cases of corona-virus of Indonesia from February 11, 2021 to August 26, 2021 and many parameters were estimated from. Through the application of Pontryagin's Principle, they established the possibility for co – infection of the model by stating conditions necessary for the existence of optimal control and the optimality. Several control measures were employed like: face-mask, vaccination on corona-virus population, treatment on both TB and corona-virus were incorporated in the model. The numerical simulation results show that the control measure against incident corona-virus prevented the occurrence of new cases of over 27, 878, 840 while preventive measure on TB and treatment averted 5,379,795 individuals from contacting corona-virus as new cases.

Ram *et al*. [18], assessed the impact of COVID - 19 on tuberculosis diseases using a proposed mathematical model. The stability analysis theory was used to analyzed the model qualitatively and

quantitatively. They show that at endemic equilibrium point the model is stable and unstable when $R_0 < 1$ and $R_0 > 1$ respectively. Also, they used Lyapunov function to described global stability at endemic point of the system. The bifurcation analysis was carried out and discussion was made on the behavior of the model's stability. The result from the simulation analysis evidently shows that both COVID - 19 and tuberculosis diseases mollified by controlling the transmission rate.

From the forgoing literatures, it is evidently clear that none of the authors commented on the impact of latent - symptomatic co-infection. In this research, we modified [13] by introducing an additional co-infection: latent TB - symptomatic COVID - 19 populations. This study is significant in that it captures the population of those latent-symptomatic COVID-19 which is a condition that is most severe than latent-asymptomatic condition. More importantly, [2] has shown that individuals with weak immune system in latent TB stage are liable to be infected with other diseases than those with strong immune system in latent TB stage, in that TB bacteria to progress to active stage within a short period. In this work we conducted to basically focus on the stability and bifurcation analysis. Furthermore the impact of TB on COVID - 19 is also shown with numerical simulation using some data from Nigeria during the outbreak and recent TB data

2. Materials and method

We consider a mixed population where an individual in the populations has equal chances of interacting with each other. The transmission of the modified model is described by adopting a deterministic compartmental modeling technique, at any time t. An extension of [13] consist of nine human populations was considered: susceptible individuals (S), those who are infected with COVID - 19 that does not show symptoms but are infectious with COVID - 19, known as asymptomatic I_A, COVID - 19 symptomatic I_S that shows both symptoms and are infectious, TB infected individuals who does not show signs of symptoms and does not transmit TB is known as latent TB (L_T), active TB (I_T), latent - asymptomatic co - infection (L_{TA}), latent - symptomatic co - infection (L_{TS}), active TB - symptomatic COVID-19 co - infection (I_{TS}) and recovered individuals (R). Bearing these in mind, the entire population in time t is denoted by

$$N(t) = S(t) + L_T(t) + I_T(t) + I_A(t) + I_S(t) + L_{TA}(t) + L_{TS}(t) + I_{TS}(t) + R(t) \qquad (1)$$

The contact between the susceptible individuals and active TB patients enhances the susceptible individuals to be infected with TB by a force of infection λ_T described in equation (2). The effective contact rate for TB transmission is denoted by β_T. The latent TB becomes infectious when they are not treated and become infected with symptomatic COVID-19 resulting to latent TB - symptomatic population $L_{TS}(t)$ [8] at the force of infection of $b_2\lambda_C$ where β_C is the effective contact rate for COVID-19. Due to effective contact with those infected with COVID -19, the susceptible individuals acquire COVID-19 infection with a force of infection λ_C represented in equation (3) with effective contact rate is β_C. Also, the rate at which those in latent TB population $L_T(t)$ moves to active TB is at the rate of τ and recovers at the rate of γ. The latent TB population becomes co-infected with asymptomatic COVID-19 and symptomatic COVID-19 with a force of infection $b_1\lambda_C$ and $b_2\lambda_C$ respectively. The active TB individual recovers at the rate of ω while the rest transfers to active TB - symptomatic COVID-19 co-infection population $I_{TS}(t)$ at the rate of ν and δ_T as the rate due to die by active TB.

The susceptible acquire asymptomatic COVID - 19 through contact with asymptomatic infected individuals at the force of infection λ_C. $I_A(t)$ progress to symptomatic COVID - 19 and the latent TB - asymptomatic corona-virus co-infection $L_{TS}(t)$ at the rate of ϵ and force of infection $a_1\lambda_T$ respectively or recovers at the rate of φ. The symptomatic corona - virus becomes infected with latent TB and active TB with the force of infection at $a_2\lambda_T$ and the rate of η respectively. These co-infection diseases; latent TB - symptomatic COVID – 19 and active TB - symptomatic COVID–19 denoted by $L_{TS}(t)$ and $I_{TS}(t)$ where it is assumed here that $I_{TS}(t)$ is more infectious and severe than $L_{TS}(t)$. Death induced by symptomatic corona-virus occurs at the rate of δ_C. The latent TB - asymptomatic corona-virus progresses to latent TB - symptomatic corona-virus at the rate of θ and migrate to $I_S(t)$ and $I_T(t)$ at the rate of $c\phi$ and $d\phi$ respectively. The co-infection experienced induced death rate at δ_1 or recovers at the rate $[1-(c+d)]\phi$. The compartment $L_{TS}(t)$ moves to $I_{TS}(t)$ at the rate of σ and death induced rate δ_2 or recovers at the rate of κ. The population $I_{TS}(t)$ migrate away from the class at the rate of $e\psi, f\psi$ and death induced rate δ_3 or recovers at the rate $[1-(e+f)]\psi$.

The new model schematic diagram is demonstrated in Figure 1, we assumed that interaction between individuals is considered to be homogeneous and all populations die naturally at the rate of μ. The conditions of individuals with latent TB are aggravated to active TB and susceptible individuals becomes infected with TB through contact with active TB individuals by a force of infection λ_T, given as:

$$\lambda_T(t) = \frac{\beta_T}{N(t)}(L_T(t) + I_T(t) + I_{TS}(t)) \qquad (2)$$

where β_T is the effectual contact rate for TB bacteria. Similarly, susceptible populations becomes infected with COVID-19 through contact with asymptomatic or symptomatic individuals by a force of infection λ_C, given by

$$\lambda_C(t) = \frac{\beta_C}{N(t)}(I_A(t) + I_S(t) + L_{TA}(t) + L_{TS}(t) + I_{TS}(t)) \qquad (3)$$

where β_C is the effectual contact rate for COVID-19 transmission. The co – infected individuals with tuberculosis in the asymptomatic and symptomatic COVID–19 infections ($L_{TA}(t), L_{TS}(t)$ and $I_{TS}(t)$ classes) are assumed to transmitted COVID–19 at the same rate λ_C as those with only COVID–19 infection ($I_A(t)$ and $I_S(t)$). The co - infection class $I_{TS}(t)$ can transmit tuberculosis at the same rate λ_T as individuals with active TB alone ($I_T(t)$ class). From the description and the assumptions of the model it follows that the governing mathematical non-linear differential equations is given by:

$$\begin{aligned}
\frac{dS}{dt} &= \Lambda - (\lambda_T + \lambda_c)S - \mu S \\
\frac{dL_T}{dt} &= \lambda_T S - (b_1 + b_2)\lambda_c L_T - AL_T \\
\frac{dI_T}{dt} &= \tau L_T + f\psi I_{TS} + d\phi L_{TA} - BI_T \\
\frac{dI_A}{dt} &= \lambda_C S - a_1\lambda_T I_A - CI_A \\
\frac{dI_S}{dt} &= \epsilon I_A + c\phi L_{TA} + c_{13}I_A + e\psi I_{TS} - a_2\lambda_T I_S - DI_S \qquad (4)
\end{aligned}$$

$$\frac{dL_{TA}}{dt} = a_1\lambda_T I_A + b_1\lambda_c L_T - EL_{TA}$$

$$\frac{dL_{TS}}{dt} = a_2\lambda_T I_S + b_2\lambda_c L_T + \theta L_{TA} - FL_{TS}$$

$$\frac{dI_{TS}}{dt} = \sigma L_{TS} + \eta L_S + \upsilon I_T - GI_{TS}$$

$$\frac{dR}{dt} = \varphi I_A + \gamma L_T + \omega I_T + \xi I_S + \kappa L_{TS} + [1-(c+d)]\phi L_{TA} + [1-(e+f)]\psi I_{TS} - \mu R$$

where, λ_T, λ_C as described in (2) and (3) and $A = \mu + \gamma + \tau, B = \mu + \delta_T + \nu, C = \mu + \epsilon + \varphi, D = \mu + \delta_C + \eta + \xi, E = \mu + \delta_1 + \theta + \phi, F = \mu + \delta_2 + \sigma + \kappa,$ and $G = \mu + \delta_3 + \psi$. Also the initial conditions $S(0) \geq 0, L_T(0) \geq 0, I_T(0) \geq 0, I_A(0) \geq 0, I_S(0) \geq 0, L_{TA}(0) \geq 0, L_{TS}(0) \geq 0, I_{TS}(0) \geq 0$ and $R(0) \geq 0$.

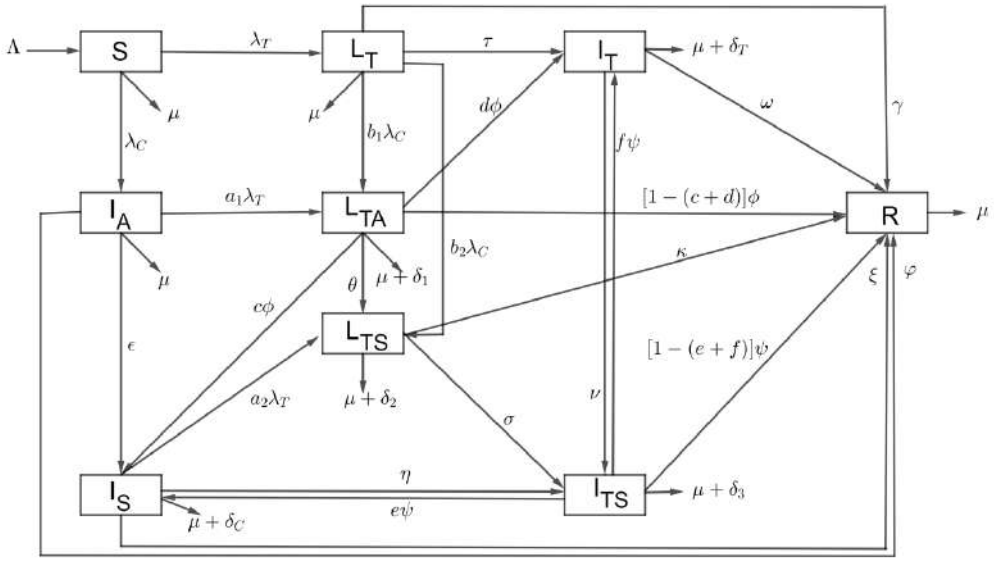

Figure 1: The schematic diagram describing the TB-COVID-19 model

Table 1:Description of parameters and values of TB-COVID-19 model

Parameters	Description	Values	Sources
Λ	Recruitment rate of susceptible population	500	[1]
μ	Natural death rate of individuals	0.17937	[1]
β_C	COVID-19 rate of transmission	0.38974	[4]
δ_C	Death rate due to COVID-19	0.043	[10]
δ_T	Death rate due active TB	0. 570776	Estimated
β_T	TB rate of transmission	0.39818	[1]
δ_1	Death rate due L_{TA}	0.023	[13]

δ_2	Death rate due to L_{TS}	0.035	Estimated
δ_3	Death rate due to I_{TS}	0.251	[13]
ϵ	Transfer rates from I_A to I_S	0.46	[17]
φ	Recovery rate of I_A	0.13978	[13]
ξ	Recovered rate of I_S	0.2016	[17]
ϕ	Rate at which L_{TA} leaves to I_T	0.01	Estimated
$]\eta$	Infectious rate of TB from COVID-19	0.001	[18]
ψ	Rate at which I_{TS} leaves the class	0.5	[18]
θ	Rate at which L_{TA} migrate to L_{TS} class	0.02	[18]
ν	Infectious rate of COVID-19 from TB	0.001	[19]
κ	Recovered rate of L_{TS}	0.35	Estimated
γ	Recovered rate of L_T	0.256	[23]
τ	Fraction of L_T that progress to I_T	0.11538	[1]
a_1	The rate at which I_A becomes infected with L_T	0.379	Estimated
a_2	The rate at which I_S becomes infected with L_T	0.13	Estimated
b_1	Transfer rate of L_T to L_{TA}	0.49	Estimated
b_2	Transfer rate of L_T to L_{TS}	0.35	Estimated
ω	The rate at which I_T recovers	0.09	[12]
σ	The rate at which L_{TS} progress to I_{TS}	0.002	[12]
c	Recovery rate of L_{TA} from latent TB	0.14	[18]
d	Recovery rate of L_{TA} from asympt. COVID-19	0.032	[12]
e	Recovery rate of I_{TS} from active TB	0.021	[13]
f	Recovery rate of I_{TS} from sympt. COVID-19	0.032	[13]

The basic properties of Tuberculosis-COVID-19 co-infection model

2.1 Positivity and boundedness of the co-infection model

Lemma 1. If $S(t)$, $L_T(0), I_T(0), I_A(0), I_S(0), L_{TA}(0), L_{TS}(0), I_{TS}(0)$ and $R(t)$ are not negative with the stated initial conditions above then the solutions $(S(t), L_T(0), I_T(0), I_A(0), I_S(0), L_{TA}(0), L_{TS}(0), I_{TS}(0), R(t))$ of the co-infection are all positive for all $t > 0$.

Proof. We illustrate this with the first ode in equations (4) as follows;

$$\frac{dS}{dt} = \Lambda - (\lambda_T + \lambda_c)S - \mu S,$$

The above equation can be further written as;

$$\frac{dS}{dt} \geq -\mu S$$

Solving this equation using separating the variable method of integration and applying the initial condition with respect to t, we have

$$S(t) \geq S_0 e^{-\mu t} > 0 \qquad (5)$$

Using the same approach for equation (4), the remaining solutions of the odes are;

$$L_T(t) \geq L_{0T} e^{-At} > 0$$
$$I_T(t) \geq I_{0T} e^{-Bt} > 0$$

$$\begin{aligned} I_A(t) &\geq I_{0A}e^{-Ct} > 0 \\ I_S(t) &\geq I_{0S}e^{-Dt} > 0 \\ L_{TA}(t) &\geq L_{0TA}e^{-Et} > 0 \\ L_{TS}(t) &\geq L_{0TS}e^{-Ft} > 0 \\ I_{TS}(t) &\geq I_{0TS}e^{-Gt} > 0 \\ R(t) &\geq R_0e^{-\mu t} > 0 \end{aligned} \qquad (6)$$

Therefore, it is very clear that the solution set $\Phi = \{(S, L_T, I_T, I_A, I_S, L_{TA}, L_{TS}, I_{TS}, R)$ of the model (4) is positive for all $t > 0$.

Invariant region

The system (4) is considered epidemiologically and mathematically well-posed, when all parameters and variables of the model are not negative for all time t. The co-infection model will be analyzed in a suitable feasible region as follows:

Lemma 2: The region $\Phi = \{(S, L_T, I_T, I_A, I_S, L_{TA}, L_{TS}, I_{TS}, R) \epsilon \mathbb{R}_+^9 : N(t) \leq \frac{\Lambda}{\mu}\}$ is a positive invariant for the system (4) with non-negative initial condition in $\mathbb{R}_+^9$.

Proof: Consider, $(S, L_T, I_T, I_A, I_S, L_{TA}, L_{TS}, I_{TS}, R) \epsilon \mathbb{R}_+^9$ as any solution for our model (4). Then the sum of the differential equation of system (4) is given by

$$\frac{dN}{dt} = \Lambda - \mu N - (\delta_T I_T + \delta_C I_S + \delta_1 L_{TA} + \delta_2 L_{TS} + \delta_3 I_{TS}) \leq \Lambda - \mu N \qquad (7)$$

From the initial condition of the variables, it follows that $N(t) \geq 0$ and since it was established that the region Φ is positive invariant and attracting, $N(t) \geq 0$ is obviously bounded for every $t > 0$. Furthermore, adopting Birkhoff and Rota's comparison theorem as found in [20], the solution of equation (7) is,

$$N(t) \leq N(0)e^{-\mu t} + \frac{\Lambda}{\mu}(1 - e^{-\mu t}) \qquad (8)$$

Indeed, $N(t) \leq \frac{\Lambda}{\mu}$ it then follows that $N(0) \leq \frac{\Lambda}{\mu}$. Hence we can conclude that the region Φ is positively invariant. It follows that the region Φ, has a solutions in the model system (4) with initial conditions in Φ will remain in the region for all time $t > 0$.

3. Model Analysis

To properly understand the behavior of the model, we shall investigate the sub-models by analyzing their equilibrium points before proceeding further to discuss the analysis of the co-infection

3.1. COVID-19 sub-model

In absence of those infected with TB from equations (4), the COVID-19 model equation reduces to:

$$\begin{cases} \frac{dS}{dt} = \Lambda - \lambda_c S - \mu S \\ \frac{dI_A}{dt} = \lambda_c S - (\mu + \epsilon + \varphi) I_A \\ \frac{dI_S}{dt} = \epsilon I_A - (\mu + \delta_C + \xi) I_S \\ \frac{dR}{dt} = \varphi I_A + \xi I_S - \mu R \end{cases} \quad (9)$$

with $N(t) = S(t) + I_A(t) + I_S(t) + R(t)$. The feasible region of COVID-19 sub-model is given as $\Phi_C = \{(S, I_A, I_S, R) \epsilon \mathbb{R}_+^4 : N(t) \leq \frac{\Lambda}{\mu}\}$

3.*1.1 The Local stability of COVID-19 sub-model*

The disease-free equilibrium (DFE) represents the model steady state solutions in the absence of the disease. By setting the odes to zeros, the disease-free equilibrium denoted by E_0 is given as

$$E_0 = \left(\frac{\Lambda}{\mu}, 0,0,0\right).$$

The basic reproduction number denoted by R_0^C is the threshold parameter of the expected number of secondary COVID-19 infections produced in a completely susceptible community by a typical infected person. This threshold parameter plays a crucial role in the mathematics of epidemiology [22]. If $R_0^C < 1$, this illustrate a condition when an average of COVID-19 infected individuals produces less than one new infection during the infectious period and the disease goes to extinction. If $R_0^C > 1$, then each infectious COVID-19 patient produces an average of more than one new infection and the disease spreads and persist in the population [22]. Considering $\mathcal{F}_i$ and $\mathcal{V}_i$ as the matrices of new infection in the infected compartments and the remaining transfer terms represented by:

$$\mathcal{F}_i = \begin{pmatrix} \frac{\beta_C}{N}(I_A + I_S) \\ 0 \end{pmatrix} \text{ and } \mathcal{V}_i = \begin{pmatrix} (\mu + \epsilon + \varphi) I_A \\ (\mu + \delta_C + \eta + \xi) I_S - \epsilon I_A \end{pmatrix}$$

Then evaluating the matrices denoted by F and V using Jacobian matrix of $\mathcal{F}_i$ and $\mathcal{V}_i$ at DFE and further determined the eigenvalues of the matrices. It is found that the largest spectrum radius for the COVID-19 sub-model is given as

$$R_0^C = \frac{\beta_C(\mu+\delta_C+\eta+\xi+\epsilon)}{(\mu+\epsilon+\varphi)(\mu+\delta_C+\eta+\xi)} \quad (10)$$

By interpretation, R_0^C represent the average number of secondary asymptomatic and symptomatic COVID-19 cases produced by asymptomatic or symptomatic person at his or her effective infectious period at the time the person entered an entirely COVID-19 susceptible population which is governed by eight parameters.

Theorem 3.1. The disease free equilibrium E_0 of the model 9, is given by equation 10, is locally asymptotically stable (LAS) if $R_0^C \leq 1$ and unstable if $R_0^C > 1$

Proof: From the above theorem we shall use Jacobian matrix to establish this fact. Consider a point $D = (S, I_A, I_S, R)$ and a Jacobian matrix denoted by $J_{E_0}(D)$ of equation 9, we have

$$J_{E_0}(D) = \begin{pmatrix} -\mu & -\beta_C & -\beta_C & 0 \\ 0 & \beta_C - A & \beta_C & 0 \\ 0 & \epsilon & -B & 0 \\ 0 & \varphi & 0 & -\mu \end{pmatrix} \quad (11)$$

where $A = \mu + \epsilon + \varphi$ and $B = \mu + \delta_C + \xi + \eta$. Since the first and the last elements of the diagonal matrix in 11 are both negative it implies, $\lambda_{1,2} = -\mu$, hence we can deduced the other two eigenvalues by matrix reduction shown in the matrix below;

$$J_{E_{01}}(D) = \begin{pmatrix} \beta_C - A & \beta_C \\ \epsilon & -B \end{pmatrix} \quad (12)$$

It follows that the,
Trace of $J_{E_{01}}(D) = tr(D)$ that $\beta_C < (2\mu + \epsilon + \varphi + \xi)$ and the $det\left(J_{E_{01}}(D)\right) = 1 - R_0^C$
By implication, if $R_0^C < 1$ then $det\left(J_{E_{01}}(D)\right) > 0$ if $R_0^C < 1$ and $det\left(J_{E_{01}}(D)\right) < 0$ if $R_0^C > 1$ is unstable.

3.1.2. Endemic Equilibrium Point (EEP)

The infection of corona-virus is considered to persist in a given population is usually described by the endemic equilibrium point. Consider $E_1 = (S, I_A, I_S, R) > 0$ as the EEP of the system (9). Thus, we rewrite equation 9 in endemic form as:

$$\begin{cases} S^* = \frac{\Lambda}{\mu + \lambda_C^*} \\ I_A^* = \frac{\lambda_C^* S^*}{A} \\ I_S^* = \frac{\lambda_C^* S^* \epsilon}{AB} \\ R^* = \frac{\lambda_C^* S^* \varphi}{A\mu} \end{cases} \quad (13)$$

Therefore, simplifying these endemic states in equation 13 in terms of λ_C^* we have,

$$\lambda_C^* = \frac{R_0^C - 1}{(\mu+\xi)(\mu+\varphi+\epsilon)+(\mu+\varphi)(\delta_C+\eta)} \quad (14)$$

The result obtained from equation (14) shows that force of infection is positive at the endemic equilibrium point if and only if $R_0^C > 1$. The above analogy proves the endemic equilibrium point of the corona-virus sub-model.

3.2. Tuberculosis sub-model

Similarly, in absence of those infected with COVID-19 from equations (4), the model reduces to a TB sub-model given by:

$$\begin{cases} \frac{dS}{dt} = \Lambda - \lambda_T S - \mu S \\ \frac{dL_T}{dt} = \lambda_T S - C L_T \\ \frac{dI_T}{dt} = \tau L_T - D I_T \\ \frac{dR}{dt} = \gamma L_T + \omega I_T - \mu R \end{cases} \quad (15)$$

where $\lambda_T = \frac{\beta_T I_T}{N}, N = S + L_T + I_T + R, C = \mu + \gamma + \tau$ and $D = \mu + \delta_T + \nu + \omega$.

3.2.1. The Local stability of Tuberculosis sub-model

At the state where there is no infection it gives the disease=free equilibrium point of TB sub-model given as $E_0 = (S_0, 0,0,0)$ where $S_0 = \frac{\Lambda}{\mu}$. The local stability of a system depends on the basic reproduction number that is usually to predict the eradication or persistence of a given disease in a population. Adopting, the next generation approach, using $\mathbb{F}$ and $\mathbb{V}$ to represent matrices for infection and transmission is expressed as;

$$\mathbb{F} = \begin{pmatrix} \frac{\beta_T I_T S}{N} \\ 0 \end{pmatrix} \text{ and } \mathbb{V} = \begin{pmatrix} C L_T \\ D I_T - \tau L_T \end{pmatrix}$$

Following the same argument shown about corona-virus sub-model in section 3.1, then the basic reproduction number for TB sub-model is given by:

$$R_0^T = \frac{\beta_T \tau}{(\mu+\gamma+\tau)(\mu+\delta_T+\nu+\omega)} \quad (16)$$

Equation (16) described the TB disease transmission potential of tuberculosis is governs by seven parameters. The equation portrays the new infection that occurs at the presence of a single infectious person in a completely susceptible population. The elimination of any epidemic in a given population is only possible when $R_0^T < 1$ and increases exponentially if $R_0^T > 1$ [22].

Theorem 3.2. The disease-free equilibrium of the Tuberculosis sub-model is locally asymptotically stable (LAS) if the threshold quantity is less than unity.

In biological terms, for $R_0^T < 1$ implies that the tuberculosis disease can easily be eradicated from the community. This is possible if the initial size of the sub-population of the model is found on the basin of the attraction of the DFE. We use linearization approach to examine the local stability of tuberculosis by considering the Jacobian matrix $J_{E_0} = (S, L_T, I_T, R)$ and then determining this Jacobian matrix E_0^T is given by;

$$J_{E_{01}} = \begin{pmatrix} -\mu & 0 & \beta_T & 0 \\ 0 & -C & \beta_T & 0 \\ 0 & \tau & -D & 0 \\ 0 & \gamma & \omega & -\mu \end{pmatrix} \quad (17)$$

Since the first and the last elements of the diagonal matrix in 17 are both negative that is, $\lambda_{1,2} = -\mu$, hence we can deduced the other two eigenvalues by matrix reduction shown in the matrix below;

$$J_{E_{02}} = \begin{pmatrix} -C & \beta_T \\ \tau & -D \end{pmatrix} \quad (18)$$

It is obtained that the trace of $J_{E_{02}} = -(2\mu + \gamma + \tau + \omega) < 0$ and the $\det(J_{E_{02}}) = 1 - R_0^T$, therefore, $\det(J_{E_{02}}) > 0$ if $R_0^T < 1$. This shows that the DFE point is asymptotically stable if, $R_0^T < 1$, which complete the proof.

3.2.2. Endemic Equilibrium Point of Tuberculosis sub-model

In order to obtain the endemic equilibrium point of the TB sub-model, we solve the odes in equation (15) by replacing S, L_T, I_T, R and λ_T by S^*, L_T^*, I_T^*, R^* and λ_T^*, these equations becomes,

$$\begin{cases} S^* = \frac{\Lambda}{\mu + \lambda_T^*} \\ L_T^* = \frac{\lambda_T^* S^*}{C} \\ I_T^* = \frac{\lambda_T^* S^* \tau}{CD} \\ R^* = \frac{\lambda_T^* S^* (D\gamma + \omega\tau)}{CD\mu} \end{cases} \quad (19)$$

Therefore, simplifying equation (19) in terms of λ_T^*, we have

$$\lambda_T^* = \frac{\mu(1 - R_0^{-T})}{D(\mu+\gamma) + \tau(\mu+\omega)} \quad (20)$$

Following equation (20), it shows that the endemic exist if and only if $R_0^T > 1$ and $D(\mu + \gamma) + \tau(\mu + \omega) > 0$.

3.3 The Tuberculosis and COVID-19 Co-infection Model

In this section we proceed to solve the equilibrium points of the full model (4) by setting the right hand side of the model equations to zero:

$$\begin{aligned}
&\Lambda - (\lambda_T + \lambda_c)S - \mu S = 0 \\
&\lambda_T S - (b_1 + b_2)\lambda_c L_T - c_{11} L_T = 0 \\
&\tau L_T + f\psi I_{TS} + d\phi L_{TA} - c_{12} I_T = 0 \\
&\lambda_C S - a_1 \lambda_T I_A - c_{13} I_A = 0 \\
&\epsilon I_A + c\phi L_{TA} + c_{13} I_A + e\psi I_{TS} - a_2 \lambda_T I_S - c_{14} I_S = 0 \\
&a_1 \lambda_T I_A + b_1 \lambda_c L_T - c_{15} L_{TA} = 0 \\
&a_2 \lambda_T I_S + b_2 \lambda_c L_T + \theta L_{TA} - c_{16} L_{TS} = 0 \\
&\sigma L_{TS} + \eta L_S + \upsilon I_T - c_{17} I_{TS} = 0 \\
&\varphi I_A + \gamma L_T + \omega I_T + \xi I_S + \kappa L_{TS} + [1 - (c + d)]\phi L_{TA} + [1 - (e + f)]\psi I_{TS} - \mu R = 0
\end{aligned} \quad (21)$$

where λ_T and λ_c are defined as shown in equation 2 and 3 above. The disease-free equilibrium point of the full model is defined as $E_0^{TC} = \left(\frac{\Lambda}{\mu}, 0,0,0,0,0,0,0,0\right)$. We apply the next generation method to

determine the stability of the co-infection. Using equation (21), we defined two matrices $\mathcal{F}_i$ and $\mathcal{V}_i$ for newly infected terms and the remaining transfer terms, given as

$$\mathcal{F}_i = \begin{pmatrix} \lambda_T S \\ 0 \\ \lambda_C S \\ 0 \\ 0 \\ 0 \\ 0 \end{pmatrix} \text{ and } \mathcal{V}_i = \begin{pmatrix} (b_1 + b_1)\lambda_C L_T + AL_T \\ -\tau L_T - f\psi I_{TS} - d\phi L_{TA} + BI_T \\ a_1\lambda_T I_A + CI_A \\ -\epsilon I_A - c\phi L_{TA} - e\psi I_{TS} - a_2\lambda_T I_S + DI_S \\ -a_1\lambda_T I_A - b_1\lambda_C L_T + EL_{TA} \\ -a_2\lambda_T I_S - b_2\lambda_C L_T - \theta L_{TA} + FL_{TS} \\ -\nu I_T - \sigma L_{TS} - \eta I_S + GI_{TS} \end{pmatrix}$$

The Jacobian matrix of the two matrices at disease-free equilibrium is:

$$F = \begin{pmatrix} \beta_T & \beta_T & 0 & 0 & 0 & 0 & 0 \\ 0 & 0 & 0 & 0 & 0 & 0 & 0 \\ 0 & 0 & \beta_C & \beta_C & \beta_C & \beta_C & \beta_C \\ 0 & 0 & 0 & 0 & 0 & 0 & 0 \\ 0 & 0 & 0 & 0 & 0 & 0 & 0 \\ 0 & 0 & 0 & 0 & 0 & 0 & 0 \\ 0 & 0 & 0 & 0 & 0 & 0 & 0 \end{pmatrix} \text{ and } V = \begin{pmatrix} A & 0 & 0 & 0 & 0 & 0 & 0 \\ -\tau & B & 0 & 0 & -d\phi & 0 & -f\psi \\ 0 & 0 & C & 0 & 0 & 0 & 0 \\ 0 & 0 & -\varepsilon & D & -c\phi & 0 & -e\psi \\ 0 & 0 & 0 & 0 & E & 0 & 0 \\ 0 & 0 & 0 & 0 & -\theta & F & 0 \\ 0 & -\upsilon & 0 & -\eta & 0 & -\sigma & G \end{pmatrix}$$

Hence,

$$V^{-1} = \begin{pmatrix} \frac{1}{A} & K_{12} & 0 & K_{14} & 0 & 0 & K_{17} \\ 0 & K_{22} & 0 & K_{24} & 0 & 0 & K_{27} \\ 0 & K_{32} & \frac{1}{C} & K_{34} & 0 & 0 & K_{37} \\ 0 & K_{42} & 0 & K_{44} & 0 & 0 & K_{47} \\ 0 & K_{52} & 0 & K_{54} & \frac{1}{E} & \frac{\theta}{EF} & K_{57} \\ 0 & K_{62} & 0 & K_{64} & 0 & \frac{1}{F} & K_{67} \\ 0 & K_{72} & 0 & K_{74} & 0 & 0 & K_{77} \end{pmatrix}$$

where

$$K_{12} = \frac{\tau(DG - e\psi\eta)}{A(BDG - Be\psi\eta - Df\psi\upsilon)}, K_{14} = \frac{e\psi\upsilon\tau}{A(BDG - Be\psi\eta - Df\psi\upsilon)}, K_{17} = \frac{\upsilon\tau D}{A(BDG - Be\psi\eta - Df\psi\upsilon)},$$

$$K_{22} = \frac{DG - e\psi\eta}{BDG - Be\psi\eta - Df\psi\upsilon}, K_{24} = \frac{e\psi\upsilon}{BDG - Be\psi\eta - Df\psi\upsilon}, \quad K_{27} = \frac{\upsilon D}{BDG - Be\psi\eta - Df\psi\upsilon}$$

$$K_{32}=\frac{f\psi\eta\varepsilon}{C(BDG-Be\psi\eta-Df\psi\upsilon)},K_{34}=\frac{\varepsilon(BG-f\psi\upsilon)}{C(BDG-Be\psi\eta-Df\psi\upsilon)},\quad K_{37}=\frac{\eta\varepsilon B}{C(BDG-Be\psi\eta-Df\psi\upsilon)},$$

$$K_{42}=\frac{f\psi\eta}{BDG-Be\psi\eta-Df\psi\upsilon},$$

$$K_{44}=\frac{BG-f\psi\upsilon}{BDG-Be\psi\eta-Df\psi\upsilon},K_{47}=\frac{\eta B}{BDG-Be\psi\eta-Df\psi\upsilon},$$

$$K_{52}=\frac{DFGd\phi+Df\psi\sigma\theta+Fc\phi\eta f\psi-Fd\phi e\psi\eta}{EF(BDG-Be\psi\eta-Df\psi\upsilon)},\quad K_{54}=\frac{BFd\phi+Be\psi\sigma\theta-Fc\phi f\psi\upsilon+Fd\phi e\psi\upsilon}{EF(BDG-Be\psi\eta-Df\psi\upsilon)},$$

$$K_{57}=\frac{BD\sigma\theta+BFc\phi\eta+DFd\phi\upsilon}{EF(BDG-Be\psi\eta-Df\psi\upsilon)},\quad K_{62}=\frac{f\psi\sigma D}{F(BDG-Be\psi\eta-Df\psi\upsilon)},$$

$$K_{64}=\frac{e\psi\sigma B}{F(BDG-Be\psi\eta-Df\psi\upsilon)},\quad K_{67}=\frac{\sigma BD}{F(BDG-Be\psi\eta-Df\psi\upsilon)},$$

$$K_{72}=\frac{f\psi D}{BDG-Be\psi\eta-Df\psi\upsilon},\quad K_{74}=\frac{e\psi B}{BDG-Be\psi\eta-Df\psi\upsilon},\quad K_{77}=\frac{BD}{BDG-Be\psi\eta-Df\psi\upsilon}$$

Five of the eigenvalues for the matrix FV^{-1} are zeroes. The other two eigenvalues are:

$$\lambda_1=\ R_1=\frac{1}{2AC(BDG-Be\psi\eta-Df\psi\nu)}\left[\alpha_1+(\alpha_2+\alpha_3+\alpha_4+\alpha_5+\alpha_6+\alpha_7+\alpha_8+\alpha_9)^{\frac{1}{2}}\right] \quad (22)$$

$$\lambda_2=R_2=\frac{1}{2AC(BDG-Be\psi\eta-Df\psi\nu)}\left[\alpha_1-(\alpha_2+\alpha_3+\alpha_4+\alpha_5+\alpha_6+\alpha_7+\alpha_8+\alpha_9)^{\frac{1}{2}}\right] \quad (23)$$

Where

$\alpha_1=AB\beta_C(DG+GE+\eta\epsilon)+CD\beta_T(BG+G\tau+\nu\tau)-A\psi\beta_C(Be\eta+Df\upsilon+f\upsilon\epsilon)-C\psi\beta_T(Be\eta+Df\upsilon+e\eta\epsilon)$

$\alpha_2=A^2B^2\beta_C^2(D^2G^2+G^2\epsilon^2+e\psi^2\eta^2+\epsilon^2)+2A^2B^2\beta_C^2(DG^2\epsilon+DG\eta\epsilon+G\eta\epsilon^2)-2A^2B^2\beta_C^2\eta\psi\epsilon(DG+Ge+e\eta)$

$\alpha_3=A^2f\psi^2\nu^2\beta_C^2(D^2+2DE+e^2)-2A^2BDf\psi\nu\beta_C^2(DG+2GE+\eta\epsilon)+2A^2e\psi f\psi\nu\eta\beta_C^2(D+\epsilon)-2A^2Bf\psi\nu\epsilon^2(D\eta+G)$

$\alpha_4=2AB^2C\beta_C\beta_T(e\psi\eta^2\epsilon-D^2G^2-DG^2\epsilon-DG\eta\epsilon+Ge\psi\eta\epsilon-e\psi^2\eta^2)+2BCDG\beta_C\beta_T(2e\psi\eta-ADG\tau)$

$\alpha_5=ABCD\beta_C\beta_T(DGf\psi\nu+Ge\psi\eta\tau+Gf\psi\nu\epsilon-e\psi\eta f\psi\upsilon)-2ABCDG\tau\beta_C\beta_T(D\nu+G\epsilon+\eta\epsilon+\nu\epsilon)$

$\alpha_6=2ABC\tau\beta_C\beta_T(e\psi\eta\upsilon+Df\psi\epsilon\nu+D\eta\epsilon\nu+Ge\psi)2ABCe\psi\beta_C\beta_T(\eta^2\tau\epsilon-\eta^2\psi\tau-\eta f\psi\nu\epsilon+2\eta\nu\tau\epsilon)$

$$\alpha_7 = 2ACD^2f\psi\beta_C\beta_T(G\psi\nu\tau - \psi\nu^2 + \nu^2\tau) + 2ACDf\psi\nu\beta_C\beta_T(G\epsilon - e\psi\eta\tau + 2\eta\epsilon - \nu\psi\epsilon + \nu\tau\epsilon)$$

$$\alpha_8 = 2ACe\psi\eta f\psi\nu\tau\epsilon\beta_C\beta_T + B^2C^2\beta_T^2(D^2G^2 - 2DGe\psi\eta + e\psi^2\eta^2) + 2BGC^2D^2(\tau - 2f\psi\nu + 2\nu\tau) + 2BC^2D\eta e\psi\beta_C^2(\nu - 2G\tau)$$

$$\alpha_9 = C^2\beta_C^2(D^2G^2\tau^2 + f\psi^2\nu^2D^2 + D^2\nu^2\tau^2 + e\psi^2\eta^2\tau^2) - 2C^2\tau C^2\beta_T^2[De\psi\eta(\nu + \tau\nu + G\tau - f\psi\nu) + D^2\nu(Gf\psi - G\tau + f\psi\nu) - Be\psi^2\eta^2]$$

Therefore, the basic reproduction number R_0^{TC} of the co-infection model (4) is given by;

$$R_0^{TC} = max\{R_1, R_2\} \quad (24)$$

3.3.1. The Local stability of the TB-COVID-19 co-infection model at DFE

Using linearization method, the local stability of the disease-free equilibrium point for the co-infection can be analyzed as follows. The Jacobian matrix of the co-infection from equation (4) is shown below;

$$J_{E_0^{TC}} = \begin{pmatrix} -\mu & -\beta_T & -\beta_T & -\beta_C & -\beta_C & -\beta_C & -\beta_C & -\beta_C - \beta_T & 0 \\ 0 & -A & -\beta_T & 0 & 0 & 0 & 0 & 0 & 0 \\ 0 & \tau & -B & 0 & 0 & d\phi & 0 & f\psi & 0 \\ 0 & 0 & 0 & -C & \beta_C & \beta_C & \beta_C & \beta_C & 0 \\ 0 & 0 & 0 & \varepsilon & -D & -c\phi & \beta_C & e\psi & 0 \\ 0 & 0 & 0 & 0 & 0 & -E & 0 & 0 & 0 \\ 0 & 0 & 0 & 0 & 0 & \theta & -F & 0 & 0 \\ 0 & 0 & \nu & 0 & \eta & 0 & \sigma & -G & 0 \\ 0 & \gamma & \omega & \varphi & 0 & [1-(c+d)]\phi & \kappa & [1-(e+f)]\psi & -\mu \end{pmatrix} \quad (25)$$

The characteristics equation of $\left|\lambda I - J_{E_0^{TC}}\right| = 0$ gives the first three eigenvalues from the first, last entries and sixth row column six of (25) as $\lambda_{1,2} = -\mu$ and $\lambda_3 = -E$. Hence the matrix (25) reduces to:

$$J_{1E_0^{TC}} = \begin{pmatrix} -A & \beta_T & 0 & 0 & 0 & 0 \\ \tau & -B & 0 & 0 & 0 & f\psi \\ 0 & 0 & -C & \beta_C & \beta_C & \beta_C \\ 0 & 0 & \varepsilon & -D & \beta_C & e\psi \\ 0 & 0 & 0 & 0 & -F & 0 \\ 0 & \nu & 0 & \eta & \sigma & -G \end{pmatrix}$$

As performed by [13], we further reduced the above matrix into two block matrices shown below:

$$J_{2E_0^{TC}} = \begin{pmatrix} -A & \beta_T & 0 & 0 \\ \tau & -B & 0 & 0 \\ 0 & 0 & -C & \beta_C \\ 0 & 0 & \varepsilon & -D \end{pmatrix} \text{ and } \quad J_{3E_0^{TC}} = \begin{pmatrix} -F & 0 \\ \sigma & -G \end{pmatrix}$$

The characteristics polynomials of $J_{2E_0^{TC}}$ and $J_{3E_0^{TC}}$ matrices are;

$J_{2E_0^{TC}} = \lambda^4 + (A+B+C+D)\lambda^3 + [AB + (A+B)(C+D) - \beta_C\epsilon - \beta_T\tau]\lambda^2 + [AB(C+D)$
$+CD(A+B) - \beta_C\epsilon(A+B) - \beta_T\tau(C+D)]\lambda + [ABCD - \beta_C\epsilon AB - \beta_T\tau CD - \beta_T\beta_C\epsilon\tau]$

$J_{3E_0^{TC}} = (F+\lambda)(G+\lambda)$ Therefore,

$J_{1E_0^{TC}} = (F+\lambda)(G+\lambda)\{\lambda^4 + (A+B+C+D)\lambda^3 + [AB + (A+B)(C+D) - \beta_C\epsilon - \beta_T\tau]\lambda^2$
$+[AB(C+D) \quad +CD(A+B) - \beta_C\epsilon(A+B) - \beta_T\tau(C+D)]\lambda + +[ABCD - \beta_C\epsilon AB - \beta_T\tau CD -$
$\beta_T\beta_C\epsilon\tau\} = 0$

It follows that $\lambda_1 = -F$ and $\lambda_2 = -G$ with a polynomial

$$P_4(\lambda) = \lambda^4 + a_1\lambda^3 + a_2\lambda^2 + a_3\lambda + a_4 = 0 \qquad (26)$$

where

$$a_1 = A + B + C + D$$
$$a_2 = AB + CD + (A+B)(C+D) - \beta_C\epsilon - \beta_T\tau$$
$$a_3 = AB(C+D) + CD(A+B) - \beta_C\epsilon(A+B) - \beta_T\tau(C+D)$$
$$a_4 = ABCD - \beta_C\epsilon AB - \beta_T\tau CD - \beta_T\beta_C\epsilon\tau$$
$$= AB\{(1 - R_0^C) - \beta_C D\} - CD[(1 - R_0^T) - AB] - \beta_T\beta_C\epsilon\tau$$

Therefore, following the Routh-Hurwitz stability criteria, roots of (26) of the reduced matrix posses' negative real parts if the following condition holds;

$$a_1 > 0, a_3 > 0, a_4 > 0 \qquad (27)$$

and

$$a_1a_2a_3 > a_3^2 + a_1^2a_4 \qquad (28)$$

It follows that the conditions 27 and 28 holds if $R_0^C < 1$ and $R_0^T < 1$ consequently, we have proved the expected result.

3.3.2. Global stability of the co-infection at DFE

In considering the global stability of the co-infection, we sub-divided the model (4) into two ode's as used by [13] as follows:

$$\begin{cases} \frac{dX}{dt} = F(X,Z) \\ \frac{dZ}{dt} = G(X,Z), G(x,0) \end{cases} \qquad (29)$$

where $X = (S,R)$ with $X\epsilon\mathbb{R}_+^2$ and $Z = (L_T, I_T, I_A, I_S, L_{TA}, L_{TS}, I_{TS})$ with $Z\epsilon\mathbb{R}_+^7$ these represent the non-infectious and infectious compartments respectively. It follows that $V_0 = (X,0)$ where $X_0 = (\frac{\Lambda}{\mu}, 0)$ as the disease-free equilibrium. For global asymptotic stability to exist, then,

H_1: $\frac{dX}{dt} = F(X,0)$, the equilibrium point V_0 is globally stable

H_2: $G(X,Z) = AZ - \hat{G}(X,Z), \hat{G} \geq 0$ for $(X,Z)\epsilon\Omega$ where $A = D_ZG(V_0,0)$ is Metzler matrix, and the feasible region is denoted by Ω .

From equation (4) we defined the matrix as:

$$\frac{dX}{dt} = F(X,Z)$$

$$= \begin{bmatrix} \Lambda - \mu S \\ \varphi I_A + \gamma L_T + \omega I_T + \xi I_S + \kappa L_{TS} + [1-(c+d)]\phi L_{TA} + +[1-(c+d)]\psi I_{Ts} - \mu R \end{bmatrix}$$

So,

$$F(X,0) = \begin{bmatrix} \Lambda - \mu S \\ 0 \end{bmatrix} \text{ and}$$

$$\frac{dZ}{dt} = G(X,Z)$$

$$= \begin{bmatrix} \lambda_T S - (b_1 + b_1)\lambda_C L_T - AL_T \\ \tau L_T + f\psi I_{TS} + d\phi L_{TA} - BI_T \\ \lambda_C S - a_1\lambda_T I_A - CI_A \\ \epsilon I_A + C\phi L_{TA} + e\psi I_{TS} - a_2\lambda_T I_S - DI_S \\ a_1\lambda_T I_A + b_1\lambda_C L_T - EL_{TA} \\ a_2\lambda_T I_S + b_2\lambda_C L_T + \theta L_{TA} - FL_{TS} \\ \nu I_T + \sigma L_{TS} + \eta I_S - GI_{TS} \end{bmatrix}$$

Therefore, the Metzler matrix, is given by

$\hat{G}(X,Z) = AZ - G(X,Z)$ is obtained as follows;

$$\hat{G} = \begin{bmatrix} G_1(\hat{X},Z) \\ G_2(\hat{X},Z) \\ G_3(\hat{X},Z) \\ G_4(\hat{X},Z) \\ G_5(\hat{X},Z) \\ G_6(\hat{X},Z) \\ G_7(\hat{X},Z) \end{bmatrix} = \begin{bmatrix} \lambda_T(1-S) + (b_1 + b_1)\lambda_C L_T \\ d\phi L_{TA} \\ \lambda_C(1-S) + a_1\lambda_T I_A \\ \beta_C L_{TS} + a_2\lambda_T I_S \\ b_1\lambda_C L_T - a_1\lambda_T I_A \\ -a_2\lambda_T I_S - b_2\lambda_C L_T \\ 0 \end{bmatrix} \quad (30)$$

From equation (30), since, $(-a_2\lambda_T I_S - b_2\lambda_C L_T) < 0$, it implies that the second criteria is not satisfied. The implication is that V_0 and the disease-free equilibrium point E_0^{TC} can't be globally asymptotically stable.

3.3.4. The bifurcation of the co-infection

We represent the populations in our model (4) with the following

$$S = x_1, L_T = x_2, I_T = x_3, I_A = x_4, I_S = x_5, L_{TA} = x_6, L_{TS} = x_7, I_{TS} = x_8, R = x_9$$

The modified model becomes:

$$\frac{dx_1}{dt} \equiv f_1 = \Lambda - (\lambda_T + \lambda_c)x_1 - \mu x_1$$
$$\frac{dx_2}{dt} \equiv f_2 = \lambda_T x_1 - (b_1 + b_2)\lambda_c x_2 - (\mu + \gamma + \tau)x_2$$
$$\frac{dx_3}{dt} \equiv f_3 = \tau x_2 + f\psi x_8 + d\phi x_6 - (\mu + \delta_T + \nu)x_3$$
$$\frac{dx_4}{dt} \equiv f_4 = \lambda_C x_1 - a_1\lambda_T x_4 - (\mu + \epsilon + \varphi)x_4$$
$$\frac{dx_5}{dt} \equiv f_5 = \epsilon x_4 + c\phi x_6 + e\psi x_8 - a_2\lambda_T x_5 - (\mu + \delta_C + \eta + \xi)x_5 \quad (31)$$
$$\frac{dx_6}{dt} \equiv f_6 = a_1\lambda_T x_4 + b_1\lambda_c x_2 - (\mu + \delta_1 + \theta + \phi)x_6$$
$$\frac{dx_7}{dt} \equiv f_7 = a_2\lambda_T x_5 + b_2\lambda_c x_2 + \theta x_6 - (\mu + \delta_3 + \sigma + \kappa)x_7$$
$$\frac{dx_8}{dt} \equiv f_8 = \sigma x_7 + \eta x_5 + \upsilon x_3 - (\mu + \delta_3 + \psi)x_8$$
$$\frac{dx_9}{dt} \equiv f_9 = \varphi x_4 + \gamma x_2 + \omega x_3 + \xi x_5 + \kappa x_7 + [1 - (c + d)]\phi x_6 + [1 - (e + f)]\psi x_8 - \mu x_9$$

where

$\lambda_T = \frac{\beta_T}{N}(x_2 + x_3 + x_8)$ and $\lambda_C = \frac{\beta_C}{N}(x_4 + x_5 + x_6 + x_7 + x_8)$

The Jacobian matrix of the above system (31) at the disease-free equilibrium E_0^* at a chosen bifurcation parameter $\beta_C = \beta_C^*$ was obtained by equating $R_0^C = 1$ and $\beta_C^* = \frac{(\mu+\epsilon+\varphi)(\mu+\delta_C+\eta)}{\mu+\delta_C+\eta+\epsilon}$ hence,

$$J_{E_0^*} = \begin{pmatrix} -\mu & -\beta_T & -\beta_T & -a_{14}^* & -a_{14}^* & -a_{14}^* & -a_{14}^* & -a_{15} & 0 \\ 0 & a_{22} & \beta_T & 0 & 0 & 0 & 0 & \beta_T & 0 \\ 0 & \tau & -a_{33} & 0 & 0 & d\phi & 0 & f\psi & 0 \\ 0 & 0 & 0 & -a_{44} & -a_{14}^* & -a_{14}^* & -a_{14}^* & -a_{14}^* & 0 \\ 0 & 0 & 0 & \varepsilon & -a_{55} & c\phi & 0 & e\psi & 0 \\ 0 & 0 & 0 & 0 & 0 & -a_{66} & 0 & 0 & 0 \\ 0 & 0 & 0 & 0 & 0 & \theta & -a_{77} & 0 & 0 \\ 0 & 0 & \upsilon & 0 & \eta & 0 & \sigma & -a_{88} & 0 \\ 0 & \gamma & \omega & \varphi & \xi & [1-(c+d)]\phi & \kappa & [1-(e+f)]\psi & -\mu \end{pmatrix} \quad (32)$$

where

$a_{14}^* = \frac{(\mu+\epsilon+\varphi)(\mu+\delta_C+\eta)}{\mu+\delta_C+\eta+\epsilon}, a_{15}^* = \beta_T + a_{14}^*, a_{22} = \beta_T - (\mu + \gamma + \tau), , a_{33} = \mu + \delta_T + \nu + \omega,$
$a_{44} = a_{14}^* - (\mu + \epsilon + \varphi),\ \ a_{55} = \mu + \delta_C + \eta + \epsilon,\ \ a_{66} = \mu + \delta_1 + \theta + \phi,\ \ a_{77} = \mu + \delta_2 + \kappa + \sigma,$
$a_{88} = \mu + \delta_3 + \psi.$

We now denote the right hand eigenvalue $w = (w_1, w_2, w_3, w_4, w_5, w_6, w_7, w_8)$ where,

$w_1 = -\frac{1}{\mu}\{\frac{\beta_T[f\psi(a_{22}-\beta_T)-\beta_T(a_{33}+\tau)]}{a_{22}a_{33}+\beta_T\tau} + \frac{a_{14}^*[e\psi a_{44}+\epsilon a_{15}-a_{14}^*(\epsilon+e\psi+a_{55})]+a_{15}a_{44}a_{55}}{a_{44}a_{55}+a_{14}^*\epsilon}\}w_8,\ w_2 = -\frac{\beta_T(f\psi+a_{33})}{a_{22}a_{33}+\beta_T\tau}w_8,$

$w_3 = \frac{f\psi a_{22}-\beta_T}{a_{22}a_{33}+\beta_T\tau}w_8,\ w_4 = -\frac{a_{14}^*e\psi+a_{14}^*a_{55}}{a_{22}a_{33}+\beta_T\tau}w_8,\ w_5 = -\frac{a_{44}e\psi-a_{14}^*\epsilon}{a_{22}a_{33}+\beta_T\tau}w_8,\ w_7 = 0, w_8 = w_8 > 0,$

$$w_9 = \frac{1}{\mu}\{\frac{f\psi\omega a_{22}-\beta_T(\tau\omega+\gamma f\psi+a_{33}\gamma)}{\mu(a_{22}a_{33}+\beta_T\tau)} + \frac{[1-(e+f)](a_{44}a_{55}+a_{14}^*\epsilon)\psi-a_{14}^*\varphi(e\psi+a_{55})}{\mu(a_{22}a_{33}+\beta_T\tau)}\}w_8$$

Similarly, the left hand eigenvalue $v = (v_1, v_2, v_3, v_4, v_5, v_6, v_7, v_8)^T$ is given by $v_1 = 0$, $v_2 = -\frac{\tau v}{a_{22}a_{33}+\beta_T\tau}v_8$, $v_3 = \frac{a_{22}v}{a_{22}a_{33}+\beta_T\tau}v_8$, $v_4 = -\frac{\epsilon\eta}{a_{14}^*\epsilon + a_{44}a_{55}}v_8$, $v_5 = \frac{a_{55}\eta}{a_{14}^*\epsilon + a_{44}a_{55}}v_8$,
$v_6 = \left\{\frac{a_{22}vd\phi}{a_{66}(a_{22}a_{33}+\beta_T\tau)} + \frac{a_{77}\eta(c\phi a_{44} - a_{14}^*\epsilon)+\theta[\sigma(a_{14}^*\epsilon + a_{44}a_{55})-a_{14}^*\epsilon\eta]}{a_{77}(a_{14}^*\epsilon + a_{44}a_{55})}\right\}v_8$, $v_7 = \frac{\sigma(a_{14}^*\epsilon + a_{44}a_{55})-a_{14}^*\epsilon\eta}{a_{77}(a_{14}^*\epsilon + a_{44}a_{55})}v_8$,
$v_8 = v_8 > 0, v_9 = 0$. We now proceed to determine the direction of the bifurcation as we obtained the values of a and b. Since $v_1 = v_9 = 0$ then we considered $k = 2,3,4,5,6,8$.
$a = \sum_{k,i,j=1}^{9} v_k w_i w_j \frac{\partial f_k}{\partial w_i \partial w_j}(0,0)$
The expansion of $a = v_2\left[w_1w_1\frac{\partial^2 f_2}{\partial w_1\partial w_1} + \cdots + w_1w_9\frac{\partial^2 f_2}{\partial w_1\partial w_9}\right] + \cdots$
$+ v_8\left[w_1w_1\frac{\partial^2 f_8}{\partial w_1\partial w_1} + \cdots + w_1w_9\frac{\partial^2 f_8}{\partial w_1\partial w_9}\right]$ (33)

Let us represent these components of a as $a = \ell_1 + \ell_2 + \ell_3 + \ell_4 + \ell_5 + \ell_6 + \ell_7$ from equation (33). The computed value of a from the values of ℓ_i for $i = 1, \ldots, 7$, is given as follows;
$\ell_1 = -\frac{2\mu\tau\nu\beta_T}{a_{22}a_{33}+\beta_T\tau}A_0\left\{\frac{\beta_T - a_{22}}{a_{22}a_{33}+\beta_T\tau} + \frac{(b_1+b_2)(e\psi + a_{55})(a_{44}-a_{14}^*)(\mu+\epsilon+\varphi)(\mu+\delta_C+\eta)}{(\mu+\delta_C+\eta+\epsilon)(a_{14}^*\epsilon + a_{44}a_{55})(a_{22}a_{33}+\beta_T\tau)}\right\}$ where
$A_0 =$
$= \left[\frac{\beta_T(a_{14}^*\epsilon + a_{44}a_{55})(f\psi+(a_{22}-\beta_T)-\beta_T(a_{33}+\tau))+(a_{22}a_{33}+\beta_T\tau)(a_{14}^*(e\psi a_{44}+a_{15}\epsilon-a_{14}^*(\epsilon+e\psi+a_{55}))+a_{15}a_{44}a_{55}}{(a_{14}^*\epsilon + a_{44}a_{55})(a_{22}a_{33}+\beta_T\tau)}\right]$
Therefore, $\ell_1 < 0, \ell_2 = 0$.
$\ell_3 = -\frac{2\mu\epsilon\eta v_2 w_8^2}{\Lambda a_{14}^*\epsilon + a_{44}a_{55}}\left[\frac{(\mu+\epsilon+\varphi)(\mu+\delta_C+\xi)(e\psi+a_{55})(a_{14}^*-a_{44})}{\mu(\mu+\delta_C+\xi+\epsilon)(a_{14}^*\epsilon + a_{44}a_{55})}A_1 + A_2\right] < 0$ where
$A_1 = \frac{\beta_T(f\psi a_{22}-\beta_T(f\psi+a_{33}+\tau))}{a_{22}a_{33}+\beta_T\tau} + \frac{a_{14}^*(e\psi a_{44}+a_{15}\epsilon-a_{14}^*(\epsilon+e\psi+a_{55}))+a_{15}a_{44}a_{55}}{a_{14}^*\epsilon + a_{44}a_{55}}$ and $A_2 = \frac{a_1 a_{14}^*(f\psi+a_{33})(a_{33}+\beta_T)(e\psi+a_{55})}{(a_{22}a_{33}+\beta_T\tau)(a_{14}^*\epsilon + a_{44}a_{55})}$
$\ell_4 = -\frac{2a_2\beta_T a_{44}\mu\eta v_8 w_8^2(a_{44}e\psi - a_{14}^*\epsilon)(f\psi+a_{33})(\beta_T+a_{22})}{(a_{22}a_{33}+\beta_T\tau)(a_{14}^*\epsilon + a_{44}a_{55})^2} < 0$ if $a_{44}e\psi > 0$ $a_{14}^*\epsilon$
$\ell_5 = -\frac{2\mu v_8 w_8^2(e\psi+a_{55})(f\psi+a_{33})}{\Lambda}A_3A_4 < 0$ where $A_3 = \frac{a_1\beta_T a_{14}^*(\beta_T+a_{22})}{(a_{22}a_{33}+\beta_T\tau)(a_{14}^*\epsilon + a_{44}a_{55})} + \frac{b_1(\mu+\epsilon+\varphi)(\mu+\delta_C+\xi)(a_{14}^*-a_{44})}{(\mu+\delta_C+\xi+\epsilon)(a_{22}a_{33}+\beta_T\tau)(a_{14}^*\epsilon + a_{44}a_{55})}$ and

$A_4 = \frac{a_{22}vd\phi}{a_{66}(a_{22}a_{33}+\beta_T\tau)} + \frac{a_{77}\eta(c\phi a_{44} - a_{14}^*\epsilon)+\theta[\sigma(a_{14}^*\epsilon + a_{44}a_{55})-a_{14}^*\epsilon]}{a_{77}(a_{22}a_{33}+\beta_T\tau)}$
$\ell_6 = -\frac{2\mu\beta_T v_8 w_8^2}{a_{77}\Lambda(a_{22}a_{33}+\beta_T\tau)}[A_5 + A_6] < 0$ where
$A_5 = \frac{b_2(\mu+\epsilon+\varphi)(\mu+\delta_C+\eta)(f\psi+a_{33})[a_{14}^*\epsilon + a_{44}a_{55}-(e\psi+a_{55})]}{(\mu+\delta_C+\xi+\epsilon)(a_{22}a_{33}+\beta_T\tau)(a_{14}^*\epsilon + a_{44}a_{55})}$ and $A_6 = \frac{(a_{44}e\psi + a_{14}^*\epsilon)[\beta_T(f\psi + a_{33}+\tau)-f\psi a_{22}]}{(a_{22}a_{33}+\beta_T\tau)(a_{14}^*\epsilon + a_{44}a_{55})}$

Since f_8 for $k = 8$ does not have the product of $x_i x_j$ hence $\ell_7 = 0$. Therefore, from the computation of $\ell_i's$ for $i = 1, 2, \ldots, 7$ above are all negative, this implies that $a < 0$.

We now determine the value of b, using the formula and evaluating at k =4;

$b = \sum_{i,j=1}^{9} v_k w_j \frac{\partial f_k}{\partial w_j \partial \beta_C}$
$b = \sum_{i,j=1}^{9} v_4 w_j \frac{\partial f_4}{\partial w_j \partial \beta_C}$
$b = -\frac{\epsilon\eta v_8 w_8(e\psi+a_{55})(a_{44}-a_{14}^*)}{(a_{14}^*\epsilon + a_{44}a_{55})^2} < 0$ if $a_{44} > a_{14}^*$

The bifurcation analysis of model (4) is summarized below using the theorem.

Theorem 3.3 Since the parameter $a < 0$ and $b < 0$, the bifurcation direction of model (4) at $R_0^C = 1$ is forward. It can be observed that $a < 0$ and $b < 0$ as shown in the above section, implies the direction of TB and COVID-19 co-infection diseases is a forward bifurcation at $R_0^C = 1$ for the fact that the co-infection has no re-infection. The implication is that, a stable equilibrium point loses stability as a parameter is varied, and two new equilibrium points, one stable and the other unstable are created. The stable equilibrium point moves forward in parameter space as the parameter is increased [11].

3.3.5 The impact of Tuberculosis on COVID-19

In order to ascertain the impact of tuberculosis on COVID-19, we adopt the approach used in [13]. This is obtained by expressing the basic reproduction number of R_0^C in terms of R_0^T which is easily enhanced since the parameter μ appeared in both R_0^C and R_0^T.We can re-write equation (16) as

$$R_0^T = \frac{\beta_T \tau}{(\mu + d_1)(\mu + d_2)} \tag{34}$$

where $d_1 = \gamma + \tau, d_2 = \delta_T + \nu + \omega$. Solving for μ in equation (34) and substituting it in equation (10), we have,

$$R_0^C = \frac{R_0^T\left(S_1 + \frac{\sqrt{S_2}}{2}\right)}{\left[\frac{\sqrt{S_2}}{2} + (\epsilon + \phi)R_0^T - \frac{d_1 + d_2}{2}R_0^T\right]\left[\frac{\sqrt{S_2}}{2} + (\delta_C + \eta)R_0^T - \frac{d_1 + d_2}{2}R_0^T\right]} \tag{35}$$

where $S_1 = R_0^T(\delta_C + \eta + \epsilon) - \frac{d_1 + d_2}{2}$ and $S_2 = R_0^T(R_0^T(d_1 + d_2)^2 + 4\beta_T\tau)$. In order to determine the impact of TB and COVID-19, we evaluate $\frac{\partial R_0^C}{\partial R_0^T}$ using equation (35) and simplifying sufficiently to have;

$$\frac{\partial R_0^C}{\partial R_0^T} = \frac{\beta_T\left(S_1 + \frac{\sqrt{S_2}}{2}\right)\left\{1 + R_0^T\left[\frac{d_1 + d_2}{2} - (\delta_C + \eta)\right] + R_0^T\left[\frac{d_1 + d_2}{2} - (\epsilon + \phi)\right]\right\}}{H_1^2 H_2^2} \tag{36}$$

where $H_1 = \left[\frac{\sqrt{S_2}}{2} + (\epsilon + \phi)\,R_0^T - \left(\frac{d_1 + d_2}{2}\right)R_0^T\right]$ and $H_2 = \left[\frac{\sqrt{S_2}}{2} + (\delta_C + \eta)\,R_0^T - \left(\frac{d_1 + d_2}{2}\right)R_0^T\right]$

It had been shown here that the partial derivative of R_0^C with respect to R_0^T is positive. This analysis portray that any increase in the population of the infected population will positively influence the transmission of corona-virus.

4. Numerical simulation

In the previous sections, we focused on the analytical behaviors of the sub-models and modeled dynamics (4). In this section, we shall perform some numerical solutions of sub-models and the co-infection model. The solutions of the dynamics equations are solved with the help of ode45 solver in MATLAB. The parameters values are also shown in table 1 above. The data used in this numerical simulation of tuberculosis sub-model were obtained from the record given during the 2023 Tuberculosis Day celebration in March 24 in Abuja, Nigeria as cited in [1] and [15]. Similarly, COVID-19 sub-model data were obtained from [4]. The initial data for the variable $S =$

$1.6 \times 10^7, L_T = 3.5 \times 10^6, I_T = 4.83 \times 10^5$ were collected from [1], $I_A = 266, I_S = 217$, [16], $L_{TA} = 45, I_{TS} = 25, [18]$ and $R = 1.45 \times 10^5$ and $L_{TS} = 25$ were estimated.

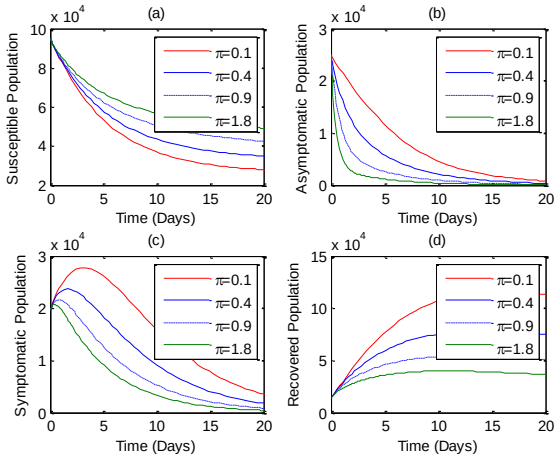

Figure 2: Simulation results showing the effect of emhanced recovery rate on asymptomatic COVID-19 population with respect to time when $\varphi = \pi$ from 0.1 to 1.8 where (a) Susceptible (b) asymptomatic (c) symptomatic and (d) Recovered populations.

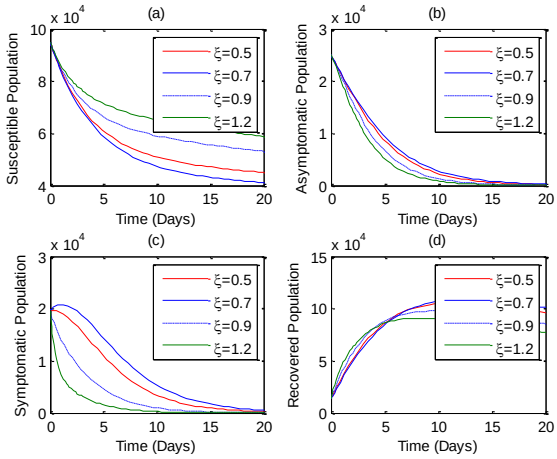

Figure 3: Plots showing the effect of treatment on the symptomatic population when the value of ξ was varied from 0.5 to 1.2 with time for (a) Susceptible (b) asymptomatic (c) symptomatic and (d) Recovered populations.

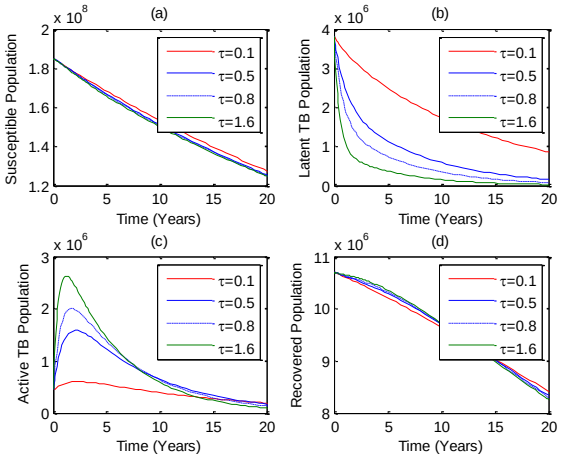

Figure 4: The diagram present the changes in each TB sub-model population with respect to time by varying τ from 0.1 to 1.6 as it progresses from Latent TB to active TB where (a) susceptible population (b) Latent TB (c) Active TB (d) Recovered Population.

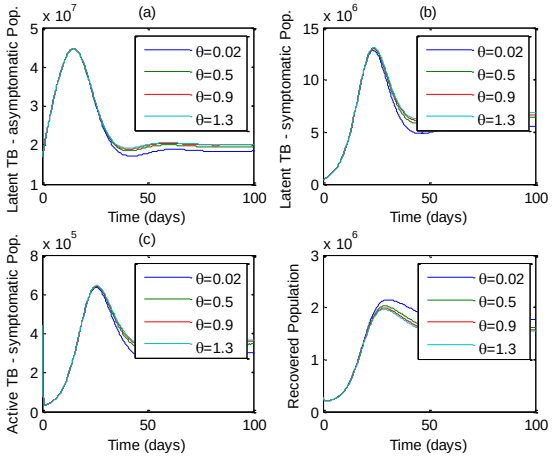

Figure 5: The simulation of model (4) showing the behavior of (a) Latent TB- asymptomatic (b) Latent TB-symptomatic (c) Active TB-symptomatic and (d) Recovered population as θ was varied from 0.02 to 1.3.

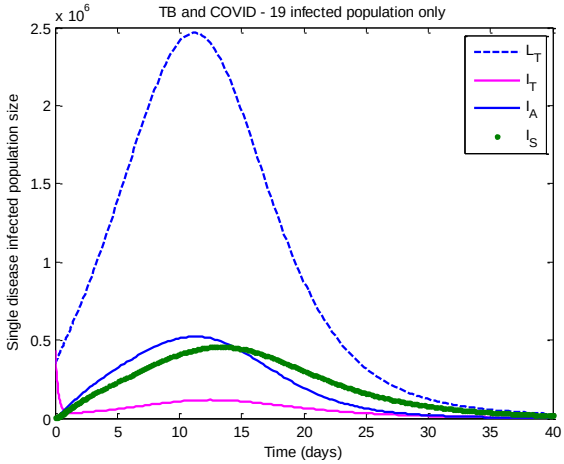

Figure 6: The simulation diagram displacing the plots of TB and COVID-19 single infected populations.

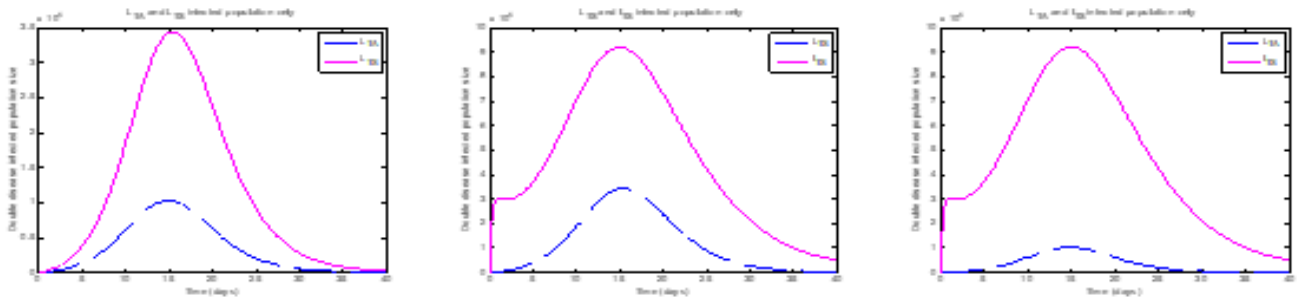

(a) (b) (c)

Figure 7: (a) A plot comparing the behavior of Latent TB-asymptomatic and Latent TB-symptomatic COVOD-19 (b) a plot comparing the behavior of Latent TB-symptomatic and active TB-symptomatic COVOD-19 and (c) a diagram comparing the behavior of Latent TB-asymptomatic and active TB-symptomatic COVOD-19.

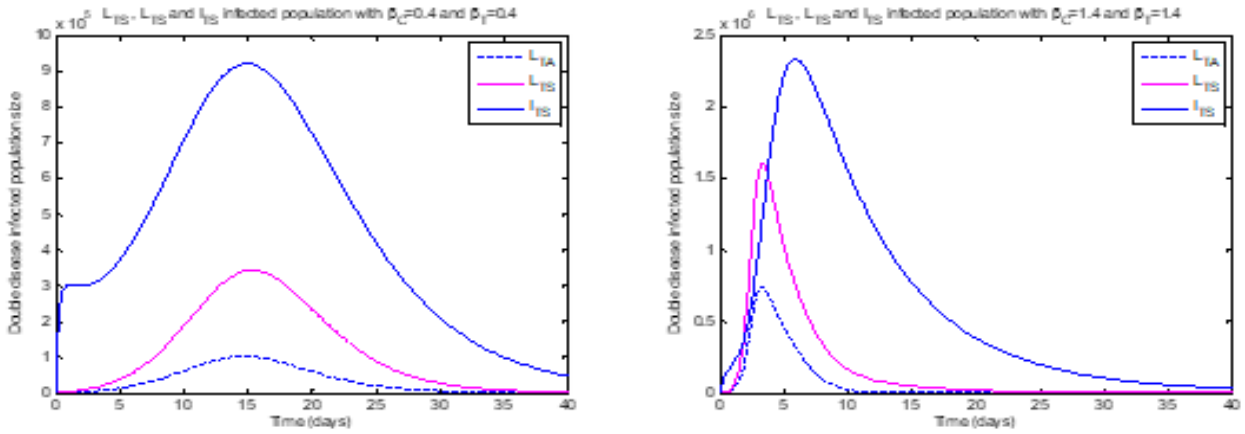

Figure 8: (a) A plot comparing the behavior of three co-infection diseases with $\beta_C = \beta_T = 0.4, \nu = 0.001$ and $\eta = 0.002$ (b) a plot comparing the behavior of three co-infection diseases with $\beta_C = \beta_T = 1.4, \nu = 1.001$ and $\eta = 1.002$

5. Discussion

Figure 2; illustrate the behavior of COVID 19 sub- model populations when asymptomatic corona-virus individuals were treated as the rate of recovery $\varphi = \pi$ was varied from 0.1 to 1.8. The susceptible population (a) was positively affected but for asymptomatic (b) and symptomatic (c) COVID - 19 declined in population since effective treatment reduces disease growth. In Figure 2d, gives a situation where treatment enhances growth as all treated populations recovers.

Figure 3; demonstrated a situation where symptomatic corona-virus was treated as the rate of recovery ξ was varied from 0.5 to 1.2. It was observed that the susceptible population (a) was favored but for asymptomatic (b) and symptomatic (c) COVID - 19 declined in population to extinction. The diseases ceased to exist as from days 10 as effective treatment was conducted. In figure 3d, illustrate a situation where treatment enhances growth for all treated population.

Figure 4; demonstrated the behavior of the susceptible, Latent TB, active TB and recovery population of people who gets infected with active TB. It can be seen that the susceptible population declines (a) as they progress to latent population. The latent population (b) collapsed as more people moved to the active population and became infected with active TB. In figure 4c, the population increases as many individuals get infected with active TB at the rate of 0.8 within time 0 to 3 days before it declined. In the recovered population (d) there is a decline in its population since more persons are getting infected instead of recovering. This scenario had been demonstrated in section 4 owning to the fact that when the reproduction number of the sub-model is greater than one.

Figure 5 shows the effect of the rate of progression of latent TB - asymptomatic COVID- 19 to latent TB - symptomatic COVID 19 when the parameters θ was varied from 0.02 to 1.3 that is, the populations denoted by L_{TA}, L_{TS}, I_{TS} and R. It is shown that the latent- asymptomatic population increases due to the inflow from other populations and decreases at θ = 0.02. The inflow from the L_{TA} population to L_{TS}increases its population to a peak before it begins to decrease when θ was varied to 0.5 (5b). Similarly, at $\theta = 0.9$ and $\theta = 1.3$ for (c) and (d) the same scenario occurs. Since all the populations were all infected, the recovery population decreases.

The time series plots of TB and COVID -19 single infected populations are shown in figure 6 the varying populations of each disease that eventually goes to extinction with time according to this order I_T, I_A, L_T and I_S. Figures 6a, 6b, and 6c shows the graphs drawn for each respective pair of diseases: L_{TA} and L_{TS}, L_{TS} and I_{TS}, and then L_{TA} and I_{TS} from model (4). The simulation in each of these pairs shows a gradual growth of each population to the 15th day before then began to decrease till extinction. In figure 7a, L_{TA} goes to extinction at the 33rd day and L_{TS} at the 40th day while in figure 7b, L_{TA} goes to extinction at the 35th day and while I_{TS} at above 40th day and in 7c, L_{TA} goes to extinction at the 30th day and L_{TS} at above 40th day. The phenomenon of these pairs of co-infection finds its importance in diseases control strategies.

The simulations of figures 8a and 8b illustrate the behaviors of the three co-infected diseases when the contact rate for tuberculosis and COVID-19 was fixed at 0.4, $\eta = 0.001, \nu = 0.001$ and when these parameters were varied to $\beta_C = \beta_T = 1$, $\eta = 1.001$ and $\nu = 1.001$ respectively. The two figures show a similar arrangement in which the population goes to extinction with time. In figure 8a, it takes 30, 35, above 40 days for L_{TA}, L_{TS} and $I_{TA}$to go to extinction but for figure 8b, their extinction period were reduced to 10, 20 and below 40 days. This shows that the three diseases can co-exist and demonstrate the population nature of severity arranged accordingly in a given order L_{TA}, L_{TS} and I_{TA} [18].

6. Conclusion

The first part of this work examined the behavior of the spread of COVID - 19 and tuberculosis as sub-models. The individual basic reproduction numbers (R_0^C and R_0^T) using the next generation method was obtained. The important threeshold quantity R_0^C and R_0^T, that determined the nature of diseases transmission were computed. It was shown that the systems are locally asymptotically stable if $R_0^C < 1$ and $R_0^T < 1$ and unstable otherwise, which implies that the diseases can be eradicated at DFE. It was also established that the dynamics exist at endemic equilibrium point if $R_0^C > 1$ and $R_0^T > 1$. From the simulation analysis conducted, it reveals that the result obtained agrees with the analytical analysis. Similarly, the properties of the the co-infection model was studied and its threshold quantity R_0^{CT} was obtained by adopting the next generation technique. Both local and global stabilities were conducted which were proved to be stable and unstable at $R_0^{CT} < 1$ and $R_0^{CT} > 1$ respectively. It was proved that tuberculosis has a positive impact on the transmission of COVID - 19. Several simulation cases were conducted to support the analytical result, and it is observed that diseases co-relate appropriately. The result of simulation reveals that an increase in the rate of those infected with active tuberculosis and those infected with symptomatic COVID-19 enhances the increase of the co-infection diseases and verse versa [13] and [22]. Also, the three co-infection co-exist and portray severity in an ascending order L_{TA}, L_{TS} and I_{TA}.

References

[1] Abegye S. Y and Kpanja S.S. (2023). Sensitivity analysis of mathematical modeling of tuberculosis dynamics with a control measure. *Abj- Statistics , 6* (3), 17 - 34.

[2] Abegye S. Y., Akpan C. E.. and Kpanji S. S. (2024). Dymanical Behavior of Tuberculosis Transmission of a weak and string letently immune population. *IOSR Journal of Mathematics , 20* (2), 22 - 33.

[3] Ahmad A., Farman M., Akgul A., Bukhari N. and Imtiaz S. (2020). Mathematical analysis and numerical simulation of co-infection of TB-HIV. *Arab Journal of Basic and Applied Sciences , 27* (1), 431 - 441.

[4] Akinwande et al. (2022). Mathematical model of COVID-19 transmission dynamics incorporating booster vaccine program and environmental contamination. *Heliyon , 23* (2), 1 - 14.

[5] Akpan C. E and Ibrahim M. O. (2020). Sensitivity Analysis for Avian Influenza (Bird flu) epidemic Model with Exposed class. *Adian Journal of Mathematics and Application , 30* (5), 1 - 32.

[6] Banddekar S. R. and Ghosh M. (2022). A co-infection model on TB-COVID-19 with optinal control and sensitivity analysis. *Journal of Mathematics and computers in simulation , 23* (5), 1 - 31.

[7] Diabat´e A. B., Sangar´e, B., and Koutou, O. (2023). Optimal control analysis of a COVID-19 and tuberculosis co-infection model with in imperfect vaccine for COVID-19. *SeMA Journal , 18* (2), 1 - 28.

[8] Ding C., Hu M., Guo W., Li X., Wang S., Shangguan Y., Zhang Y., Yang S., and Xu K. (2022). Prevalence trends of latent tuberculosis infection at the global, regional and country level from 1990 - 2019. *Intertional Journal of Infectious Diseases , 21* (5), 46 - 52.

[9] Goudiaby M., Gning L., Diagne M., Rwezaura H. and Tchuenche J. (2022). Optimal control analysis of a COVID -19 and Tuberculosis co-dynamics model. *Informatics in Medicine Unlocked , 2* (8), 849 - 861.

[10] Hazam, I.M, Foul A and Alrasheedi A. (2021). A dynamic optimal control model for covid-19 and cholera co-infection in Yemen. *Diferential Equation , 2021* (1), 1 - 30.

[11] Inayaturohmat F., Anggriani N. and Supriatma A. K. (2022). A mathematical model of Tuberculosis and COVID-19 coinfection with the effect of Isolation and treatment. *Frontiers in Applied Mathematics and Statistics , 8* (3), 39 - 58.

[12] Marimuthu et al. (2020). COVID-19 and TB: A Mathematical model based forecasting in Delhi, India. *Journal of Tuberculosis , 15* (2), 177 - 181.

[13] Mekonen K. G., Feyissa B.s., Obus L.L. and Hassan A. (2022). Mathematical modeling and Analysis of TB and COVID-19 co-infection. *Journal of Applied Mathematics , 7* (1), 1 - 20.

[14] Odume et al. (2020). Impact of COVID-19 on TB active casefinding in Nigeria. *Public health action , 10* (4), 157 - 162.

[15] Ogbudebe et al. (2023). Identifying hot spots of tuberculosis in Nigeria using an early warning outbreak recognition system: Retrospective analysis of implications for active case finding interventions. *JMIR Public Health and Surveillance , 9* (1), 403 - 418.

[16] Ojo M. M., Peter O. J., Goufo E. F. D. and Nisar K. S. (2023). A mathematical model for the co- dynamics of COVID-19 and Tuberculosis. *Mathematics and Computters in Simulations , 20* (7), 499 -520.

[17] Okuonghae D. and Omame A. (2022). Analysis of a mathematical model for COVID-19 population dynamics in Lagos, Nigeria. *Chaos, Solitons and Fractals , 13* (9), 110 - 132.

[18] Ram et al. (2023). Mathematical modeling and analysis of COVID-19 and tuberculosis transmission dynamics. *ELSEVIER , 23* (4), 1 - 13.

[19] Rehman U. A, Singh R and Agarwai P. (2021). Modeling, analysis and prediction of new variants of covid-19 and dengue co-infection on complex network. *Chaos Solitons Fractals , 12* (5), 234 - 263.

[20] Rwezaura H., Diagne M., Omame A., de Espindola A. and Tchuenche J. (2022). Mathematical Modeling and Optimal control of SARS-CoV-2 and Tuberculosis co=inecftion a case study of Indonesia. *Modeling Earth Systems and Environment , 8* (4), 5493 - 5520.

[21] Singhet et al. (2023). Mathematical Modeling and anlysisof COVID-19 and Tuberculosis transmission dynamics. *Informics in Medicine unlocked , 38* (5), 101 -115.

[22] Verma V. S., Kaushik H. and Bhadauria A.S. (2023). Mathematical modeling of tuberculosis and COVID-19 co-infection in India. A real data analysis on concomitant diseases. *Application & Applied Mathematics,18* (1), 65 - 89.

[23] WHO and others. (2023). COVID-19 weekly epidemiological update, edition edition. *World Health Organization , 12* (2), 1 - 10.

Modeling the Dynamics of Illicit Drug Abuse and Its Related Infection and Violence

[1*]Kalabu Salisu Ahmad, [2]Yusuf Bala, [3]Usamatu Usman and [4]Aminu Haruna
[1*,2,3,4] Department of Mathematics and Statistics, Federal Polytechnic Bauchi, Nigeria
[1*]skalabuahmad@fptb.edu.ng
[2]byusuf@fptb.edu.ng
[3]haminu@fptb.edu.ng
[4]uusamatu@fptb.edu.ng

Abstract

The prevalence of drug abuse and its related diseases and violence continue to escalate worldwide despite existing control measures. In order to promote good health and well-being, eliminate poverty or promote decent work and economic growth, and promote peace and justice among the United Nations' Sustainable Development Goals (SDGs), there is an urgent need to understand the dynamics of those identified problems for more strategic and prompt control actions. Therefore this research considers existing theoretical literature concerning the dynamics of the problems and adopts a mathematical modeling framework and comes up with a system of differential equations that presents the problems for more understanding of the dynamics of the problems in the human population. Moreover, the equilibrium points and basic reproduction number of the model have been obtained. The research effort concludes the problems of drug abuse, related infection and violence can be eliminated in human population by taking care of the parameters in the basic reproduction number of the model. However, the research effort can be extended where a particular disease can be considered in place of I_D and any relevant measures for controlling the problems.

Keywords: Illicit Drug-Abuse, Diseases, Violence, SDGs, Socio-Economic Development

1. Introduction

Controlling diseases to promote Good Health and Well-Being, controlling violence to promote Peace and Justice, and eliminating Poverty to promote Economic Growth are among the 17 goals which the world is moving towards sustaining by the United Nations (UN, 2023) but unfortunately, the consequences of drug abuse in the human population world over including the related illnesses and violence hinder development in many countries of the world based on revelation from the United Nations Office on Drug and Crime (UNODC, 2013) as according to the World Drug Report (WDR, 2022), the epidemic of non-medical use of tramadol in North Africa, West Africa, the Near and Middle East and South West Asia, continued to alarm great health risks in recent years. It has been revealed that weed remains the most commonly abused drug where 200 million individuals consumed it with more than 11 million people who inject drugs and 62 million individuals who use opioids in 2019. It has been projected that the number of people who use or abuse drugs in Africa will increase by about 75% by the year 2030 (UNODC, 2021) with the most unfortunate situation that drug abuse occurs more frequently in young people than in other age groups (UNODC 2, 2023), and in order to achieve those UNs' objectives, this terrible situation of drug abuse needs to be addressed urgently.

2. Literature Review

Drug abuse is the illicit consumption of any naturally occurring or pharmaceutically prepared substance for changing the consumer's feeling, thinking, or behavior with no consideration given to the resulting dangerous physical and mental side-effects it produces on the consumers (Salisu, *et al*., 2021). Addiction is defined as a chronic, relapsing brain disease that is characterized by compulsive drug acquisition and use, despite the numerous harmful consequences it results. It is considered a brain disease because drugs change the brain's shape and functions National Institute on Drugs and Addiction (NIDA, 2014). This is considered as the next progression stage of drug abuse. Drug dependence is regarded as a stage of drug abuse when the abuser can no longer perform without consuming the addicted drug. This is considered as next progression stage of drug addiction. Drug tolerance is the administration of a higher quantity of drugs to obtain the effect it has on the organism which a lower dose or administration cannot produce as a result of tolerance by the body system of the organism (Abraham, 2012). This is considered as next progression stage of drug dependence. Mental illness is developed in abusers as a result of long time consumption of drugs of abuse. Drug abuse and mental illness often co-exist as drug impairs the brain (NIDA, 2014). This is considered as next progression stage of drug tolerance. Once a person is declared mentally ill, such a person is considered insignificant or irrelevant in terms of productivity. Drugs or substances abuse especially alcoholism do not only induce significant defects in the body's immune cells (i.e., pathogens) by interfering with multiple aspects of the immune response but also results increased risk and severity of infections. Alcohol abuse severity of infection has been demonstrated particularly well for infections or drug related illnesses of respiratory tract, especially bacterial pneumonia and tuberculosis, prevalence of hepatitis C and HIV (Patricia, 2010). Violence is considered as any form of unwanted behavior or action that causes physical or psychological discomfort, threat, harm, deprivations, or even death to one-self as personal violence, or other individual(s) as interpersonal violence. Violence could be domestic or otherwise (Salisu, *et al*. 2021). Different kinds of violence have been claiming the lives of people all over the world where it has been projected that by the year 2030, The number of annual direct conflict deaths is anticipated to exceed 100,000 (Claire, 2017). There is relationship between drug abuse and violence in the sense that involvement in drug abuse can increase the risks of being perpetrator of violence, while experiencing violence can in turn, increase the risks of initiating illicit drug abuse (Amanda, *et al*., 2009).

Understanding of the economic costs of- production of drugs of abuse, economic deprivation on the abusers, drugs-related illnesses treatments, and drugs-related crimes control is necessary to develop policies that reduce such costs and investing into the economy. Even though it is difficult to ascertain due to the conservative interest in some of the estimates for individual substances, an estimated turnover of around $400 billion per annum is considered realistic in drug production where the figure can be compared to estimates of over $500 billion that are based solely on the average of minimum and maximum prices in the United States (UNODC, 2023). It has been identified that drug addiction amongst youths is one of the global menace that has negatively affected their development and productivity (Eguda *et al*. 2022). Addictive substances such as alcohol and tobacco account for nearly 5 million deaths annually worldwide and psychological researchers predicted that the ideation of suicide in People Living with HIV (PLHIV) include- development of concurrent substance-use, past history of personal depression, and hopelessness in life (Jamerlia 2021). Moreover, in Nigeria

for instance, groups mostly affected by HIV/AIDS infection are injecting drug abusers, commercial sex workers, and homosexuals where the three groups constitute only 3.4% of the population but contributing about 32% new HIV/AIDS infections (Adewolfe, 2021).

Based on the literatures considered by the research, there is need to more comprehensively understand the dynamics of drug abuse, drug-related diseases and violence for taking more sophisticated and urgent control measure for strengthening of the economy instead of using huge sums of money in production of drugs and control of drug-related diseases and violence world over.

3. Methodology of the Model Formulation

In order to formulate the model we based the research on the existing theoretical literature concerning the dynamics of drugs-abuse and its related infections and violence; and we also use the following assumptions to realize the model:

i. Total population is sub-divided into eight (8) classes of individuals where Susceptible persons are designated by S, Light drug abusers designated by L, drug Addicted persons designated by A, drug Dependent persons designated by D, drug Tolerant persons designated by T, drug Mentally ill persons designated by M, those who acquired various kind of drug-related Illnesses designated by I_D and drug-related Violent persons designated by V_D;

ii. Due to disgusting state of higher class abusers (in D, T and M), there is no effective contacts between susceptible persons and those in the higher classes of abusers;

iii. New recruitment into the system is in the susceptible class; and

iv. The population is not affected by migration.

3.1 The model variables and parameters

Variables/Parameters	Description
$S(t)$	Number of susceptible individuals at time t
$L(t)$	Number of light drug abusing individuals at time t
$A(t)$	Number of addicted drug abuse individuals at time t
$D(t)$	Number of dependent drug abusing individuals at time t
$T(t)$	Number of tolerant drug abusers at time t
$M(t)$	Number of mentally ill drug abusers at time t
$I_D(t)$	Number of drug-related Infected individuals at time t

$V_D(t)$	Number of drug-related Violent persons at time t
Λ	New recruitment rate into the population
γ	Is drug abuse transmission rate
ρ	Is transmission modification parameter for addicted persons
α	Is natural death rate in all the subclasses
σ_1	Is acquired infection rate from L to I_D
σ_2	Is acquired infection rate from A to I_D
σ_3	Is acquired infection rate from D to I_D
σ_4	Is acquired infection rate from T to I_D
σ_5	Is acquired infection rate from M to I_D
δ_1	Is progression rate from L to A
δ_2	Is progression rate from A to D
δ_3	Is progression rate from D to T
δ_4	Is progression rate from T to M
π_1	Is acquired violence rate from L to V_D
π_2	Is acquired violence rate from A to V_D
π_3	Is acquired violence rate from D to V_D
π_4	Is acquired violence rate from T to V_D
π_5	Is acquired violence rate from M to V_D
μ_1	Is drug abuse induced death rate in L
μ_2	Is drug abuse induced death rate in A
μ_3	Is drug abuse induced death rate in D
μ_4	Is drug abuse induced death rate in T
μ_5	Is drug abuse induced death rate in M
μ_6	Is death rate due to infection in I_D
μ_7	Is death rate due to violence in V_D

3.2 The model flow diagram

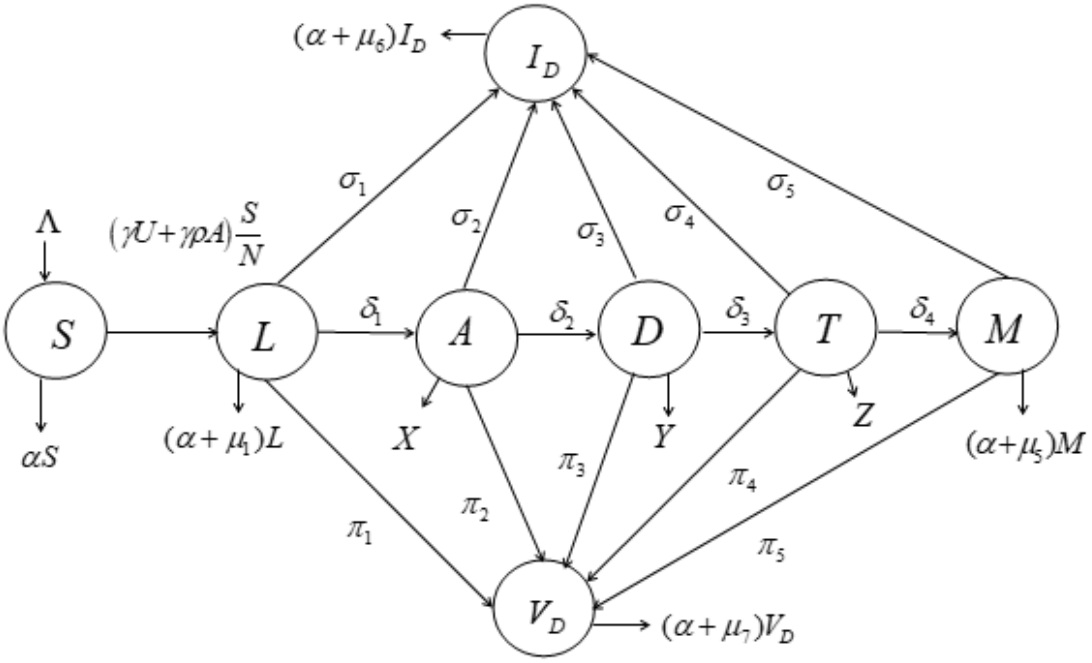

Figure 1: Flow diagram of the model.

with $X=(\alpha+\mu_2)$, $Y=(\alpha+\mu_3)$ and $Z=(\alpha+\mu_4)$.

3.3 The Model Equations

$$\frac{dS}{dt}=\Lambda-(\gamma L+\gamma\rho A)\frac{S}{N}-\mu S \tag{1}$$

$$\frac{dL}{dt}=(\gamma L+\gamma\rho A)\frac{S}{N}-(\sigma_1+\pi_1+\alpha+\mu_1)L \tag{2}$$

$$\frac{dA}{dt} = \delta_1 L - \left(\sigma_2 + \pi_2 + \alpha + \mu_2\right) A \tag{3}$$

$$\frac{dD}{dt} = \delta_2 A - \left(\sigma_3 + \pi_3 + \alpha + \mu_3\right) D \tag{4}$$

$$\frac{dT}{dt} = \delta_3 D - \left(\sigma_4 + \pi_4 + \alpha + \mu_4\right) T \tag{5}$$

$$\frac{dM}{dt} = \delta_4 T - \left(\sigma_5 + \pi_5 + \alpha + \mu_5\right) M \tag{6}$$

$$\frac{dI_D}{dt} = \sigma_1 L + \sigma_2 A + \sigma_3 D + \sigma_4 T + \sigma_5 M - \left(\alpha + \mu_6\right) I_D \tag{7}$$

$$\frac{dV_D}{dt} = \pi_1 L + \pi_2 A + \pi_3 D + \pi_4 T + \pi_5 M - \left(\alpha + \mu_7\right) V_D \tag{8}$$

where,

$$N = S + L + A + D + T + M + I_D + V_D \tag{9}$$

Subject to the initial condition,

$$S(0) = S_0, L(0) = L_0, A(0) = A_0, D(0) = D_0, T(0) = T_0, M(0) = M_0, I_D(0) = I_{D0}, V_D(0) = V_{D0} \tag{11}$$

4. Model Analysis

To analyze the model, we obtained drug abuse, infection and violence free as well as endemic equilibrium points of the model, and basic reproduction number of the model at the problems-free equilibrium point.

4.1 The Equilibrium Points

At infection and violence free, we equate the rate of changes, drug abuse, infection and violence variables to zero in equations (1) to (8) and obtained the drug abuse infection and violence free equilibrium point thus:

$$E_0 = (S, L, A, D, T, M, I_D, V_D) = \left(\frac{\Lambda}{\mu}, 0, 0, 0, 0, 0, 0, 0\right) \tag{12}$$

Whereas at the that point, every individual in the entire population stands the chance to be susceptible therefore,

$$S \le N \tag{13}$$

In the presence of drug abuse, infection and violence, we equate the rate of changes to zero and obtained the simplified form of the endemic equilibrium point thus:

$$E_1 = \begin{pmatrix} S, \\ L, \\ A, \\ D, \\ T, \\ M, \\ I_D, \\ V_D \end{pmatrix} = \begin{pmatrix} \frac{\pi - g_1 L}{\mu}, \\ \frac{g_2 A}{\delta_1}, \\ \frac{L\left(\mu g_1 N - \gamma\left(\pi - g_1 L\right)\right)}{\pi\rho\left(\pi - g_1 L\right)}, \\ \frac{\delta_2 A}{g_3}, \\ \frac{\delta_3 D}{g_4}, \\ \frac{\delta_4 T}{g_5}, \\ \frac{g_6\left(B_1 + B_2 + B_3 + B_4 + B_5\right)}{\delta_1 g_3 g_4 g_5 \pi\rho\left(\pi - g_1 L\right)}, \\ \frac{g_7\left(B_6 + B_7 + B_8 + B_9 + B_{10}\right)}{\delta_1 g_3 g_4 g_5 \pi\rho\left(\pi - g_1 L\right)} \end{pmatrix} \tag{14}$$

with,

$$B_1 = \sigma_1 g_2 g_3 g_4 g_5 \pi\rho\left(\pi - g_1 L\right) A,\ B_2 = \sigma_2 \delta_1 g_3 g_4 g_5 L\left(\mu g_1 N - \gamma\left(\pi - g_1 L\right)\right),$$
$$B_3 = \sigma_3 \delta_2 A \delta_1 g_4 g_5 \pi\rho\left(\pi - g_1 L\right),\ B_4 = \sigma_4 \delta_3 D \delta_1 g_3 g_5 \pi\rho\left(\pi - g_1 L\right),\ B_5 = \sigma_5 \delta_4 T \delta_1 g_3 g_4 \pi\rho\left(\pi - g_1 L\right),$$
$$B_6 = \pi_1 g_2 g_3 g_4 g_5 \pi\rho\left(\pi - g_1 L\right) A,\ B_7 = \pi_2 \delta_1 g_3 g_4 g_5 L\left(\mu g_1 N - \gamma\left(\pi - g_1 L\right)\right),$$
$$B_8 = \pi_3 \delta_2 A \delta_1 g_4 g_5 \pi\rho\left(\pi - g_1 L\right),\ B_9 = \pi_4 \delta_3 D \delta_1 g_3 g_5 \pi\rho\left(\pi - g_1 L\right),\ B_{10} = \pi_5 \delta_4 T \delta_1 g_3 g_4 \pi\rho\left(\pi - g_1 L\right); \tag{15}$$

and,

$$g_1 = \left(\sigma_1 + \pi_1 + \alpha + \mu_1\right),\ g_2 = \left(\sigma_2 + \pi_2 + \alpha + \mu_2\right),\ g_3 = \left(\sigma_3 + \pi_3 + \alpha + \mu_3\right),\ g_4 = \left(\sigma_4 + \pi_4 + \alpha + \mu\ \right),$$
$$g_5 = \left(\sigma_5 + \pi_5 + \alpha + \mu_5\right),\ g_6 = \left(\alpha + \mu_6\right),\ g_7 = \left(\alpha + \mu_7\right) \tag{16}$$

4.2 Basic Reproduction Number

We used the next generation matrix approach according to (Driessche and Watmough, 2002) and obtained the basic reproduction number based on which we analyzed the local stability of the model. The Jacobian matrix of the transmission matrix of the model (1) to (8) evaluated at (12) and (13) while considering $S = N$ is,

$$F = \begin{pmatrix} \gamma & \gamma\rho & 0 & 0 & 0 & 0 & 0 \\ \delta_1 & 0 & 0 & 0 & 0 & 0 & 0 \\ 0 & \delta_2 & 0 & 0 & 0 & 0 & 0 \\ 0 & 0 & \delta_3 & 0 & 0 & 0 & 0 \\ 0 & 0 & 0 & \delta_4 & 0 & 0 & 0 \\ \sigma_1 & \sigma_2 & \sigma_3 & \sigma_4 & \sigma_5 & 0 & 0 \\ \pi_1 & \pi_2 & \pi_3 & \pi_4 & \pi_5 & 0 & 0 \end{pmatrix}$$

And the inverse of the transition matrix is,

$$V^{-1} = \begin{pmatrix} \frac{1}{g_1} & 0 & 0 & 0 & 0 & 0 & 0 \\ 0 & \frac{1}{g_2} & 0 & 0 & 0 & 0 & 0 \\ 0 & 0 & \frac{1}{g_3} & 0 & 0 & 0 & 0 \\ 0 & 0 & 0 & \frac{1}{g_4} & 0 & 0 & 0 \\ 0 & 0 & 0 & 0 & \frac{1}{g_5} & 0 & 0 \\ 0 & 0 & 0 & 0 & 0 & \frac{1}{g_6} & 0 \\ 0 & 0 & 0 & 0 & 0 & 0 & \frac{1}{g_7} \end{pmatrix}$$

Now the basic reproduction number $(\Re_0)$ which is the threshold eigenvalues of the $\left(FV^{-1}\right)$ matrix is,

$$\Re_0 = \frac{1}{g_1}\left(\gamma + \sqrt{\frac{\gamma}{g_2}\left(\gamma g_2 + 4\rho\delta_1 g_1\right)}\right) \tag{16}$$

In order to ensure stability of the problems-free steady state of the model, the basic reproduction number has to be kept less than zero by watching the parameters involved especially the most sensitive amongst.

5. Results and Discussion

Mathematical model depicting the dynamics of drug abuse, related infection and violence has been posed and problems-free and endemic equilibrium points of the model have been obtained. The basic reproduction number of the model has been obtained and used in order to guide on achieving the problems-free society.

6. Conclusion

We obtained a mathematical model that describes the dynamics of drug abuse, related infection and violence, and realized the steady states as well as the basic reproduction number of the model which translates to possibility of eradication of the problems in human population. Moreover, controlling drug abuse will go a long way in controlling its related diseases and violence which can speeds up achieving some of the SDGs in the world. However, this research effort has been done without specifically considering any disease that is acquired through drug abuse in place of I_D, and specific control measure(s) for the problems. Therefore, the model gives room for further studies and possible extensions.

References

Abraham, P. (2012). Intermittent Adaptation: A Mathematical Model of Drug Tolerance, Dependence and Addiction (Chapter 2). Computational Neuroscience of Drug Addiction, Springer Series in Computational Neuroscience 10, DOI 10.1007/978-1-4614-0751-5_2.

Adewolfe, I. (2021). HIV and AIDs in Nigeria. https://www.avert.org.

Amanda, A., Zara, A., Karen, H., Mark. A. B., Harry, S. & Qutub, S. (2009). Interpersonal Violence and Illicit Drug Use. WHO, https://www.who.org.

Claire, Mc-E. & G, H. (2017). Global Violent Deaths (Time to Decide). A publication of the Small Arms Survey with support from the Swiss Agency for Development and Cooperation. ISBN 978-2-940548-46-0.

Driessche, P. V. D. & Watmough, J. (2002). Reproduction numbers and sub-threshold endemic equilibria for compartmental models of disease transmission. *Mathematical Biosciences,* 180, 29 – 48.

Eguda, F. Y., Ocheme, C. A., Sule, M. M., Abah, Samuel, E. & Hamza, G. A. (2022). Analysis of a Mathematical Model of the Population Dynamics of Drug Addiction Among Youths. *Dutse Journal of Pure and Applied Sciences* (DUJOPAS), Vol. 8 No. 1a, https://dx.doi.org/10.4314/dujopas.v8i1a.6 ISSN (Print): 2476-8316 ISSN (Online): 2635-3490.

Jamerlia E. W. (2021). HIV/AIDS and Substance Use Among Older Adults. Walden University, https://scholarworks.waldenu.edu/dissertations.

NIDA (2014). Drugs, Brain and Behavior The Science of Addiction. USA: NIH. NIH Pub. No 14-5605. www.humanconnectomeproject.org.

Patricia, E. M., Kyle, I. H., Ping, Z., Jay, K. K. & Steve, N. (2010). Alcohol and Health, Focus on: Alcohol and the Immune System. Alcohol Research and Health, 33(1,2).

Salisu, K. A., Bala, Y., Audu, A. & Ayinde, M. A. (2021). Mathematical Modelling for the Dynamics of Drug-Abuse and Violence Co-menace. *The Pacific Journal of Science and Technology*, Volume 22, Number 1, pp. 47-60, http://www.akamaiuniversity.us/PJST.htm.

WDR (2022). Executive Summary Policy Implications Booklet 1. United Nations Office on Drug and Crime, https://www.unodc.org.

UN (April, 2023). THE 17 GOALS | Sustainable Development. https://sdgs.un.org.

UNODC (2021). World Drug Report Booklet 2. UN publication, ISBN: 9789211483611, https://www.unodc.org.

UNODC (2013). Economic Consequences of Drug Abuse. International standards on drug use prevention, https://www.unodc.org.

UNODC (April, 2023). Economic And Social Consequences Of Drug Abuse And Illicit Trafficking, (Number 6). United Nations Office on Drug and Crime, https://www.unodc.org.

Homotopy Perturbation Analysis of the Spread and Control of Lassa Fever

Tsado Daniel[1*], Oguntolu Festus Abiodun[2] and Somma Samuel Abu[3]
[1-3] Department of Mathematics, Federal University of Technology, Minna, Nigeria
[1*]damielrhodatsado@gmail.com

Abstract

Lassa fever, a viral infection transmitted by rodents, has emerged as a significant global health concern in recent times. It continues to garner significant attention daily basis owing to its rapid transmission and deadly nature. In this study, the Homotopy Perturbation Analysis was conducted to examine the spread and control of Lassa fever. The human population was categorized into susceptible, exposed, infected, and recovered compartments, while the rodent population was divided into susceptible and infected recovered compartments. By applying the Homotopy Perturbation Analysis to the nonlinear differential equations associated with these compartments, we were able to obtain the analytical solution for the spread and control of Lassa fever. The nonlinear differential equations were integrated into the Homotopy Perturbation framework and solved to form a power series solution. Finally, the final approximate solutions were obtained and simulation results were generated from the general solution graphically.

Keywords — Homotopy Perturbation Method, Lassa fever**,** Nonlinear Differential Equations

1. INTRODUCTION

In light of their rapid transmission and the severity of diseases such as HIV/AIDS, measles, tuberculosis, cholera, diarrhea, COVID-19, and Lassa fever Lassa fever infection continues to receive a lot of attention daily (Olumuyiwa *et al*., 2020; Agbata *et al.*, 2021). Lassa Fever is a zoonotic illness characterized by acute hemorrhagic symptoms, which is caused by the Lassa virus. This virus is primarily transmitted from animals to humans, with the Mastomys natalensis serving as its reservoir host. (Rodent) (Akinpelu and Akinwande, 2019; Anorue and Okeke, 2020). According to reports, one in every five infections leads to a severe case of the disease, wherein the virus impacts crucial organs like the liver, spleen, and kidneys (WHO, 2017). The virus can be transmitted to individuals by coming into contact with household items, food, water, or air that has been contaminated by the droppings or urine of infected multimammate rats (*Mastomyces natalensis*). Additionally, direct contact with infected rats or exposure to the virus blood, tissue, secretions, or excretions of a person with Lassa virus can lead to person–person transmission. Contaminated medical equipment, like reused needles, also poses a risk of transmission (CDC, 2019; Collins and Okeke, 2021; Anorue and Okeke, 2020; Bakare *et al.*, 2020).

The period of incubation for Lassa fever can vary between 6 to 21 days. The initial symptoms typically include fever, weakness, and malaise, followed by headache, sore throat, muscle pain, chest pain, nausea, vomiting, diarrhoea, cough, and abdominal pain. In severe cases, patients may experience facial swelling, fluid accumulation in the lungs, bleeding from various parts of the body, low blood pressure, presence of protein in the urine, shock, seizures, tremors, disorientation, and even coma in advanced stages (Sulaiman and Ibrahim, 2018; WHO, 2017). Fatal cases typically result in death within 14 days of onset. The disease becomes particularly severe in the late stages of pregnancy, with over 80% of cases experiencing maternal death and/or fetal loss during the third trimester (Sulaiman and Ibrahim, 2018; WHO, 2017).

Ribavirin appears to be an effective antiviral drug for treating for Lassa fever virus during the initial stages of the illness (WHO, 2017). In the event of a Lassa fever outbreak within a community, swift isolation of infected individuals, proper infection prevention and control measures, and thorough contact tracing are essential to halt the spread of the disease. It is crucial to promote "community hygiene" practices that deter rodents, such as securing food in rodents-proof containers, disposing of garbage away from homes, and maintaining clean living spaces. Additionally, family members should take precautions to avoid contact with blood and bodily fluids when caring take precautions to avoid contact and bodily fluids when caring for sick individuals, while healthcare and laboratory workers must adhere to strict infection control protocols to minimize the risk of exposure to contaminated materials (WHO, 2017; CDC, 2019; Adebayo *et al.*, 2015).

Dr. Ji Huan He, a Chinese researcher, introduced Homotopy Perturbation Method (HPM) in 1998 to solve both linear and nonlinear differential and integral equations. This method, which involves a series expansion, is particularly useful in tacking non-linear partial differential equations Jiya (2010). The HPM method utilizes a power series to convert the original non-linear differential equation into a series of linear differential equations Padma *et al.* (2021). This method combines the traditional perturbation and the homotopy method Anorue and Okeke (2020), providing a direct approach to obtaining analytical or approximatively solutions for a wide range of problems in various domains, by integrating topological homotopy with traditional perturbation techniques Otoo *et al,* this approach has proven successful in solving linear and nonlinear functional equations, yielding exact solutions and ensuring accurate quantitative predictions using the Homotopy Perturbation technique (HPM) Mechee and Al-Juaifri (2018). The accuracy of the Homotopy Perturbation Method (HPM) has led to its application in epidemic modeling.

2. Literature Review

In the study conducted by Mechee and Al-Juaifri (2018), they suggested utilizing the Homotopy Perturbation method approach for the SIR model with vital dynamics and constant population. The application of this approach yielded an effective and highly precise approximate solution. Padma *et al.* (2021) also employed the Homotopy Perturbation Method to solve the SIR infectious disease model by integrating vaccination. The (HPM) was utilized to derive an approximate solution for each compartment of the model. The resulting approximate solution was then utilized to visually represent the model, providing a better comprehension of the dynamics of the infectious disease. Furthermore, Ayoade *et al.* (2020) introduced Homotopy Perturbation Method to a SIR mumps model and the theoretical outcomes validated the effectiveness and suitability of HPM in solving epidemic models. Ojo *et al.* (2021) developed a deterministic model using systems of ordinary differential equations to investigate the transmission dynamic of Lassa fever in the population. The population was divided into human and rodent compartments. Their findings suggest that implementing control strategies and methods aimed at reducing rodent populations and minimizing transmission from rodents to humans would contribute to the effective management of Lassa fever in the population. In a separate study, Padma *et al*. (2021) utilized the modified Homotopy perturbation method to solve and analyze the transmission of the SIR model of this disease. The derived analytical expression of the population of the susceptible group S(t), the infected group I(t), and the recovered group R(t) at all-time values. The Homotopy Perturbation Method was then applied to the nonlinear differential equations representing the different compartments. By incorporating the nonlinear differential equations into Homotopy Perturbation constructor, they obtained the analytical solution for the transmission dynamics of Lassa fever in the form of a power series. Peter and Awoniran (2018) utilized the modified Homotopy perturbation method to solve and examine the transmission of the SIR model of

the particular disease. The analytical expression for the population of the susceptible group S(t), the infected group I(t), and the recovered group R(t) is derived for all time. Hence, this study aims to employ the Homotopy Perturbation Method to deduce the analytical solution of the spread and control of Lassa fever. The study also addresses the impact of different parameters, we conducted numerical simulation using MAPLE 17 and compared the results with our analytical findings. In this, article, we employ the homotopy perturbation analysis to investigate the spread and control of Lassa fever.

2.1. Basic Ideas of Homotopy Perturbation Method

The fundamental concept of HPM is demonstrated in this section.

Consider (1) that provides the differential equation

,

$$A(U)-f(r)=0,\ r\in\Omega \tag{1}$$

subject to the boundary condition (2).

$$B\left(U,\frac{\partial U}{\partial n}\right)=0,\quad r\in\Gamma \tag{2}$$

A is a general differential operator, B is a boundary operator, $f(r)$ is a known analytical function and Γ represents the boundary of the domain Ω. The operator A can be split into linear (L) and nonlinear (N) components. Hence, equation (1) can be expressed as (3).

$$L(U)+N(U)-f(r)=0 \tag{3}$$

An artificial parameter p can be embedded in (3) as (4).

$$L(U)+p(U)-f(r)=0 \tag{4}$$

Where $P\in[0,1]$ is an embedding parameter (also called as an artificial parameter)

Using the homotopy technique, proposed by He (1999), we construct a homotopy;

$H:v(r,p):\Omega\times[0,1]\to R$ which satisfies (5)

$$H(V,\mathrm{P})=(1-P)\left[L(V)-L(U_0)\right]+P\left[A(V)-f(r)\right]=0 \tag{5}$$

And (6)

$$H(V,\mathrm{P})=L(V)-L(U_0)+PL(U_0)+p\left[N(V)-f(r)\right]=0 \tag{6}$$

At $p=0$

$$H(\mathrm{v},0)=L(\mathrm{v})-L(\mathrm{u}_0)=0 \tag{7}$$

And at $p=1$

$$H(\mathrm{v},1)=L(\mathrm{u})+N(\mathrm{u})-f(\mathrm{r})=0 \tag{8}$$

The transition process of p from zero to unity is just that of $v(r,\ p)$ from $u_0(r)$ to $u(r)$. In topology, this is referred to as deformation $L(\mathrm{v})-L(\mathrm{u}_0)$ and $L(\mathrm{u})+N(\mathrm{u})-f(\mathrm{r})$ is called homotopic. Following the HPM, we can introduce the embedding parameter p as a small parameter and express that the solutions of equations (7) and (8)can be written as a power series p as indicated in (9)

$$V=V_0+pV_1+p^2V_2+... \tag{9}$$

The results in the approximate solution of equation (1) may then also be obtained as (10)

$$U=\lim_{p\to 1} v=v_0+pv_1+p^2v_2+... \tag{10}$$

Which is the convergence series solution

3. Methodology

3.1 Disease Model

The nonlinear differential equations system is derived from the compartments model and incorporated in the Homotopy Perturbation Method. Subsequently, the equations were resolved to obtain analytical solutions for individual compartments. The spread of Lassa fever involves the interplay between human populations and rodent populations Usman and Adamu, (2018).

In this study, a six-compartmental model for the spread and control of Lassa fever is constructed using ordinary differential equations. The total human population at time t denoted by N is divided into four compartments namely; susceptible $S_h(t)$, exposed $E_h(t)$, infectious $I_h(t)$, and recovered $R_h(t)$. Thus, the total human population $N_h(t)$ is given as:

$$N_h(t)=S_h(t)+E_h(t)+I_h(t)+R_h(t) \tag{11}$$

Again, the total rodent population at a time t denoted by $N_r(t)$ which is divided into two compartments, namely: susceptible rodents $S_r(t)$ and infectious rodents $I_r(t)$. Thus, the total rodent population $N_r(t)$ is given as:

$$N_r(t)=S_r(t)+R_r(t) \tag{12}$$

3.2 Formulation of the Model

1)Susceptible Human (S_h)

This indicates the individuals within the entire human population that are susceptible to the disease. The population of susceptible humans S_h is populated by immigration or birth at a rate ϕ_h, and from recovered individuals due to their loss of immunity at the rate $\chi_h R_h$. The

susceptible human population is depopulated by infection following effective contact with infected individuals at the rates. The parameter ℓ_h represents the effective transmission probability of humans, which could be through direct contact with contaminated food by the urine or excretes of an infectious infected rodent, or laboratory transmissions that is sharing of medical equipment with infectious individuals without adequate sterilization Mayowa and Emile, (2022).We assume that all susceptible humans are further reduced by natural death at rate μ_h.

2) Exposed Human (E_h)

The Exposed humans are those that carry the bacteria but are not capable of infecting susceptible humans. The exposed human population is proven from an infection occurring from the susceptible population. This populace is reduced by natural death μ_h and the disease progression to the infectious population at the rate δ_h. It is imperative to note that, exposed humans are infected with the Lassa fever virus but are not showing symptoms yet. Following the disease incubation period which is between $6-21$ days (Sulaiman and Ibrahim, 2018; WHO, 2017). Such individuals progress to infectious population. This is the stage whereby they start showing symptoms of the disease.

3) Infected Human (I_h)

An infected human is any individual who has the pathogen and shows symptoms of the disease. The infectious human compartment is generated as a result of the rate from the exposed human population. The population is reduced by the recovery rate due to treatment at rate γ_h and disease-induced death (death caused by Lassa fever) at the rate ρ_h and natural death at the rate μ_h.

4) Recovered Human (R_h)

Following early treatment of individuals and diagnosed of Lassa fever disease, such individuals recover and progress to increase the recovered human population. However, since recovered individuals can be re-infected of the disease Mayowa and Emile, (2022) the recovered human populace is reduced by loss of immunity at rate γ_h and natural death at the rate μ_h.

5)Susceptible Rodent (S_r)

Susceptible rodents' population is established by the birth of rodents at a certain rate ϕ_r.This group is reduced by natural death at a specific rate μ_r, and is additionally decreased after being infected with Lassa virus from coming into contact with an infectious human or rodent at the rate. The parameters ℓ_r represents the effective transmission probability from human-to rodent and the effective transmission probability from rodent-to-rodent.

5) Infected Rodent (I_r)

The infectious rodent population is derived from infection occurring from the susceptible rodent population, while depopulated by natural death of rodents at rate μ_r.

3.3 *Nonlinear Equations of the Model*

The nonlinear system of differential equations is obtained by merging the equations for the various compartments.

$$\left.\begin{aligned}
\frac{dS_h}{dt} &= \phi_h + \chi_h R_h - \ell_h S_h - \mu_h S_h = 0 \\
\frac{dE_h}{dt} &= \ell_h S_h - (\delta_h + \mu_h) E_h = 0 \\
\frac{dI_h}{dt} &= \delta_h E_h - (\gamma_h + \rho_h + \mu_h) I_h = 0 \\
\frac{dR_h}{dt} &= \gamma_h I_h - (\mu_h + \chi_h) R_h = 0 \\
\frac{dS_r}{dt} &= \phi_r - \ell_r S_r - \mu_r S_r = 0 \\
\frac{dI_r}{dt} &= \ell_r S_r - \mu_r S_r = 0
\end{aligned}\right\} \tag{13}$$

Where,

ϕ_h	Recruitment rate of humans through birth or immigration
χ_h	Immunity waning rate of humans
δ_h	Disease progression rate from exposed to infectious human
γ_h	Recovery rate of infectious humans
μ_h	Natural death rate of humans
ρ_h	Disease induced death rate for humans
ℓ_h	Transmission probability from human-to-human and human-to-rodents
ℓ_r	Transmission probability from human-to-rodent and rodent-to-rodent
ϕ_r	Recruitment rate of rodents through birth
μ_r	Natural death rate of rodents

Let the initial conditions or approximate are as follows;

$$S_h(0) = s_o, \mathrm{E}_h(0) = e_o, \mathrm{I}_h(0) = i_o, \mathrm{R}_h(0) = \mathrm{r}_o, S_r(0) = k_o, \mathrm{I}_r(0) = r_o \tag{14}$$

3.4 Assumptions of Homotopy Perturbation Method

To ascertain the analytical solution of the model, the embedding parameter " p " from (5) is utilized as a small parameter based on the Homotopy perturbation approach. It assumed that the solution of the equations can be represented as a power series in the form of (15)

$$V = V_0 + pV_1 + p^2V_2 + \ldots \tag{15}$$

Setting $p = 1$ results in the approximate solution of equation (15)

$$U = \lim_{p \to 1} v = v_0 + pv_1 + p^2v_2 + \ldots \tag{16}$$

This method retains all the advantages of the traditional perturbation method while removing its limitations.

3.5 Application of the Homotopy Perturbation Method to the Compartmental Disease Model Equations

The Homotopy Perturbation Method is utilized to equations (13) by employing Homotopy constructor equation in order to obtain an approximate solution,

$$H(v, p) = (1 - p)\left[L(v) - L(v_0)\right] + p\left[L(v) + N(v) - f(r)\right] = 0 \tag{17}$$

In order to initiate the process of deriving the analytical or approximate solution of the model, we employ Homotopy Perturbation assumption stated in (9) as per the assumption;

$$S_h(t) = S_0 + pS_1 + p^2S_2 + \ldots \tag{18}$$

$$E_h(t) = E_0 + pE_1 + p^2E_2 + \ldots \tag{19}$$

$$I_h(t) = I_0 + pI_1 + p^2I_2 + \ldots \tag{20}$$

$$R_h(t) = R_0 + pR_1 + p^2R_2 + \ldots \tag{21}$$

$$S_r(t) = K_0 + pK_1 + K^2S_2 + \ldots \tag{22}$$

$$I_r(t) = F_0 + FI_1 + F^2I_2 + \ldots \tag{23}$$

With the initial conditions given by
$S_{hi}(0) = 0, \mathrm{E}_{hi}(0) = 0, \mathrm{I}_{hi}(0) = 0, \mathrm{R}_{hi}(0), S_{ri}(0) = 0, \mathrm{I}_{ri}(0) = 0 \forall_i = 1, 2, 3, \ldots\ldots$

Next, nonlinear differential (13) are substituted one after the other into the homotopy constructor in (17);

Firstly, substituting the first equation (13) into (17) gives

$$(1-p)\frac{dS}{dt} + p\left[\frac{dS}{dt} + \phi_h + \chi_h R_h - \ell_h S_h - \mu_h S_h\right] = 0 \tag{24}$$

$$\frac{dS}{dt} - p\frac{dS}{dt} + p\frac{dS}{dt} + p\phi_h + p\chi_h R_h - p\ell_h S_h - p\mu_h S_h = 0 \tag{25}$$

$$\frac{dS}{dt} + p\phi_h + p\chi_h R_h - p\ell_h S_h - p\mu_h S_h = 0 \tag{26}$$

Again, substituting (18) and (21) into (26)

$$\frac{d}{dt}\left(S_0 + pS_1 + p^2 S_2 + \ldots\right) + p\phi_h + \chi_h\left(R_0 + pR_1 + p^2 R_2 + \ldots\right) - p\ell_h\left(S_0 + pS_1 + p^2 S_2 + \ldots\right)$$
$$-p\mu_h\left(S_0 + pS_1 + p^2 S_2 + \ldots\right)$$

(27)

Then again, grouping the coefficient powers of p in (27)

$$p^0 : \frac{ds}{dt} = 0 \tag{28}$$

$$p^1 : \frac{ds_1}{dt} + \phi_h + \chi_h R_0 - \ell_h S_0 - \mu_h S_0 = 0 \tag{29}$$

$$p^2 : \frac{ds_2}{dt} + \chi_h R_1 - \ell_h S_1 - \mu_h S_1 = 0 \tag{30}$$

Also, by substituting second equation (13) into (17)

$$(1-p)\frac{dE}{dt} + p\left[\ell_h S_h - (\delta_h + \mu_h)E_h\right] = 0 \tag{31}$$

$$\frac{dE}{dt} - p\frac{dE}{dt} + p\frac{dE}{dt} + p\ell_h S_h - p(\delta_h + \mu_h)E_h = 0 \tag{32}$$

$$\frac{dE}{dt} + p\ell_h S_h - p(\delta_h + \mu_h)E_h = 0 \tag{33}$$

Again, substituting (18) and (19) into (33)

$$\frac{d}{dt}\left(E_0 + pE_1 + p^2 E_2 + \ldots\right) + p\ell_h\left(S_0 + pS_1 + p^2 S_2 + \ldots\right)$$
$$-p(\delta_h + \mu_h)\left(E_0 + pE_1 + p^2 E_2 + \ldots\right) = 0 \tag{34}$$

Then again, grouping the coefficient powers of p in (34)

$$p^0 : \frac{dE_0}{dt} = 0 \tag{35}$$

$$p^1 : \frac{dE_1}{dt} + \ell_h S_0 - (\delta_h + \mu_h) E_0 \tag{36}$$

$$p^2 : \frac{dE_2}{dt} + \ell_h S_1 - (\delta_h + \mu_h) E_1 \tag{37}$$

Also, by substituting third equation (13) into (17)

$$\frac{dI_h}{dt} = \delta_h E_h - (\gamma_h + \rho_h + \mu_h) I_h = 0 \tag{38}$$

$$(1-p)\frac{dI}{dt} + p\left(\delta_h E_h - (\gamma_h + \rho_h + \mu_h) I_h = 0\right) \tag{39}$$

$$\frac{dI}{dt} - p\frac{dI}{dt} + p\frac{dI}{dt} + P(\delta_h E_h) - p(\gamma_h + \rho_h + \mu_h) I_h = 0 \tag{40}$$

$$\frac{dI}{dt} + P(\delta_h E_h) - p(\gamma_h + \rho_h + \mu_h) I_h = 0 \tag{41}$$

Again, substituting (19) and (20) into (41)

$$\frac{d}{dt}\left(I_0 + pI_1 + p^2 I_2 + ...\right) + p\delta_h\left(E_0 + pE_1 + p^2 E_2 + ...\right) - p(\gamma_h + \rho_h + \mu_h)\left(I_0 + pI_1 + p^2 I_2 + ...\right) \tag{42}$$

Then again, grouping the coefficient powers of pin (42)

$$p^0 : \frac{dI_0}{dt} = 0 \tag{43}$$

$$p^1 : \frac{dI_1}{dt} + \delta_h E_0 - (\gamma_h + \rho_h + \mu_h) I_0 \tag{44}$$

$$p^2 : \frac{dI_2}{dt} + \delta_h E_1 - (\gamma_h + \rho_h + \mu_h) I_1 \tag{45}$$

Also, by substituting the fourth equation (13) into (17)

$$(1-p)\frac{dR}{dt} + p\left[\gamma_h I_h - (\mu_h + \chi_h) R_h\right] = 0 \tag{46}$$

$$\frac{dR}{dt} - p\frac{dR}{dt} + p\frac{dR}{dt} + p\gamma_h I_h - p(\mu_h + \chi_h) R_h \tag{47}$$

$$\frac{dR}{dt} + p\gamma_h I_h - p(\mu_h + \chi_h) R_h \tag{48}$$

Again, substituting (20) and (21) into (48)

$$\frac{d}{dt}\left(R_0 + pR_1 + p^2R_2 + ...\right) + p\gamma_h\left(I_0 + pI_1 + p^2I_2 + ...\right) - p\left(\mu_h + \chi_h\right)\left(R_0 + pR_1 + p^2R_2 + ...\right) \tag{49}$$

Then again, grouping the coefficient powers of p in equation (49)

$$p^0 : \frac{dR_0}{dt} = 0 \tag{50}$$

$$p^1 : \frac{dR_1}{dt} + \gamma_h I_0 - \left(\mu_h + \chi_h\right)R_0 = 0 \tag{51}$$

$$p^2 : \frac{dR_2}{dt} + \gamma_h I_1 - \left(\mu_h + \chi_h\right)R_1 = 0 \tag{52}$$

Also, by substituting fifth equation (13) into (17)

$$\left(1-p\right)\frac{dS}{dt} + p\left[\frac{dS}{dt} + \phi_r - \ell_r S_r - \mu_r S_r\right] = 0 \tag{53}$$

$$\frac{dS}{dt} - p\frac{dS}{dt} + p\frac{dS}{dt} + p\phi_r - p\ell_r S_r - p\mu_r S_r = 0 \tag{54}$$

$$\frac{dS}{dt} + p\phi_r - p\ell_r S_r - p\mu_r S_r = 0 \tag{55}$$

Again, substituting (22) into (55)

$$\begin{aligned}&\frac{d}{dt}\left(K_0 + pK_1 + p^2K_2 + ...\right) + p\phi_r - p\ell_r\left(K_0 + pK_1 + p^2K_2 + ...\right)\\ &-p\mu_h\left(K_0 + pK_1 + p^2K_2 + ...\right)\end{aligned} \tag{56}$$

Then again, grouping the coefficient powers of p in equation (3.292)

$$p^0 : \frac{dK}{dt} = 0 \tag{57}$$

$$p^1 : \frac{dK_1}{dt} + \phi_r - (\ell_r - \mu_r)K_0 = 0 \tag{58}$$

$$p^2 : \frac{dK_2}{dt} + \phi_r - (\ell_r - \mu_r)K_1 = 0 \tag{59}$$

Also, by substituting sixth equation (13) into (17)

$$(1-p)\frac{dI}{dt} + p\left[\ell_r S_r - \mu_r I_r\right] = 0 \tag{60}$$

$$\frac{dI}{dt} - p\frac{dI}{dt} + p\frac{dI}{dt} + p\ell_r S_r - p\mu_r I_r = 0 \tag{61}$$

$$\frac{dI}{dt} + p\ell_r S_r - p\mu_r I_r = 0 \tag{62}$$

Again, substituting (22) and (23) into (62)

$$\frac{d}{dt}\left(F_0 + pF_1 + p^2F_2 + ...\right) + p\ell_r\left(K_0 + pK_1 + p^2K_2 + ...\right)$$
$$-p\mu_r\left(K_0 + pK_1 + p^2K_2 + ...\right) = 0 \tag{63}$$

Then again, grouping the coefficient powers of p in equation (63)

$$p^0 : \frac{dF_0}{dt} = 0 \tag{64}$$

$$p^1 : \frac{dF_1}{dt} + \ell_r K_0 - \mu_r F_0 \tag{65}$$

$$p^2 : \frac{dF_2}{dt} + \ell_r K_1 - \mu_r F_1 \tag{66}$$

Firstly, the equations obtained by combining the coefficient powers of p are integrated with respect to time t. The equation related with powers p^o " are integrated first and from the initial conditions of homotopy perturbation;

Thus, integrating equation (28) that is $\int \frac{dS}{dt} = 0$

(67)

$$S_{ho}(t) = s_0 \tag{68}$$

Integrating equation (35) that is $\int \frac{dE}{dt} = 0$ (69)

$$E_{ho}(t) = e_0 \quad (70)$$

Integrating equation (43) that is $\int \frac{dI}{dt} = 0$

(71)

$$I_{ho}(t) = l_0 \quad (72)$$

Integrating equation (50) that is $\int \frac{dR}{dt} = 0$ (73)

$$R_{ho}(t) = r_0 \quad (74)$$

Integrating equation (57) that is $\int \frac{ds}{dt} = 0$

(75)

$$S_{ro}(t) = k_0 \quad (76)$$

Integrating equation (64) that is $\int \frac{dI}{dt} = 0$ (77)

$$I_{ro}(t) = f_0 \quad (78)$$

The procedure is continued by integrating the equations associated with powers s^1 with respect to time t; Thus, integrating (29) that is

$$\int \frac{ds_1}{dt} = \phi_h + \chi_h R_0 - \ell_h S_0 - \mu_h S_0 \quad (79)$$

$$\int ds_1 = \left[\phi_h + \chi_h R_0 - \ell_h S_0 - \mu_h S_0\right] dt \quad (80)$$

Substituting (68) and (74) into (80)

$$\int ds_1 = \left[\phi_h + \chi_h r_0 - \ell_h s_0 - \mu_h s_0\right] dt \quad (81)$$

$$s_1 = \int \left[\phi_h + \chi_h r_0 - \ell_h s_0 - \mu_h s_0\right] dt \quad (82)$$

$$s_1(t) = \left[\phi_h + \chi_h r_0 - \ell_h s_0 - \mu_h s_0\right] t + c \quad (83)$$

At $(t) = 0; S(0) = 0;$ $\quad c = 0$

$$s_1(t) = \left(\phi_h + \chi_h r_0 - \ell_h s_0 - \mu_h s_0\right) t \quad (84)$$

Integrating (36)

$$\int \frac{dE_1}{dt} = \ell_h S_0 - (\delta_h + \mu_h) E_0 \tag{85}$$

$$\int dE_1 = \left(\ell_h S_0 - (\delta_h + \mu_h) E_0\right) dt \tag{86}$$

Substituting (68) and (70) into (86)

$$E_1 = \int \left(\ell_h s_0 - (\delta_h + \mu_h) e_0\right) dt \tag{87}$$

$$E_1(t) = \left(\ell_h s_0 - (\delta_h + \mu_h) e_0\right) t + c \tag{88}$$

At $t = 0; E_1(0) = 0; c = 0$

$$E_1(t) = \left(\ell_h s_0 - (\delta_h + \mu_h) e_0\right) t \tag{89}$$

Integrating (43)

$$\int \frac{dI_1}{dt} = \delta_h E_0 - (\gamma_h + \rho_h + \mu_h) I_0 \tag{90}$$

$$\int dI_1 = \left(\delta_h E_0 - (\gamma_h + \rho_h + \mu_h) I_0\right) dt \tag{91}$$

Substituting (70) and (72) into (91)

$$I_1 = \int \left(\delta_h e_0 - (\gamma_h + \rho_h + \mu_h) l_0\right) dt \tag{92}$$

$$I_1(t) = \left(\delta_h e_0 - (\gamma_h + \rho_h + \mu_h) l_0\right) t + c \tag{93}$$

$t = 0; \mathrm{I}_1(0) = 0; c = 0$

$$I_1(t) = \left(\delta_h e_0 - (\gamma_h + \rho_h + \mu_h) l_0\right) t \tag{94}$$

Integrating (51)

$$\int \frac{dR_1}{dt} = \gamma_h I_0 - (\mu_h + \chi_h) R_0 \tag{95}$$

$$\int dR_1 = \left(\gamma_h I_0 - (\mu_h + \chi_h) R_0\right) dt \tag{96}$$

Substituting (72) and (74) into (96)

$$R_1 = \int \left(\gamma_h l_0 - (\mu_h + \chi_h) r_0\right) dt \tag{97}$$

$$R_1(t) = \left(\gamma_h l_0 - (\mu_h + \chi_h) r_0\right) t + c \tag{98}$$

$t = 0; \mathrm{R}_1(0) = 0; c = 0$

$$R_1(t) = \left(\gamma_h l_0 - \left(\mu_h + \chi_h\right) r_0\right) t \tag{99}$$

Integrating (58) that is

$$\int \frac{dk_1}{dt} = \phi_r - \ell_r K_0 - \mu_r K_0 \tag{100}$$

$$\int dk_1 = \left[\phi_r - \ell_r K_0 - \mu_r K_0\right] dt \tag{101}$$

Substituting (76) into (101)

$$k_1 = \int \left[\phi_r - \ell_r k_0 - \mu_r k_0\right] dt \tag{102}$$

$$k_1(t) = \left[\phi_r - \ell_r k_0 - \mu_r k_0\right] t + c \tag{103}$$

At $(t) = 0; \mathrm{K}_1(0) = 0; \quad \mathrm{c} = 0$

$$k_1(t) = \left(\phi_r - \ell_r k_0 - \mu_r k_0\right) t \tag{104}$$

Integrating (78)

$$\int \frac{df_1}{dt} = \ell_r K_0 - \mu_r f_0 \tag{105}$$

$$\int df_1 = \left(\ell_r K_0 - \mu_r F_0\right) dt \tag{106}$$

Substituting (76) and (78) into (106)

$$F_1 = \int \left(\ell_r k_0 - \mu_r f_0\right) dt \tag{107}$$

$$F_1(t) = \left(\ell_r k_0 - \mu_r f_0\right) t + c \tag{108}$$

At $t = 0; \mathrm{F}_1(0) = 0; c = 0$

$$F_1(t) = \left(\ell_r k_0 - \mu_r f_0\right) t \tag{109}$$

Lastly, the coefficients with power p^2 are also integrated with respect to t.

Integrating (30)

$$\int \frac{ds_2}{dt} + \chi_h R_1 - \ell_1 S_1 - \mu_h S_1 = 0 \tag{110}$$

$$\int \frac{ds_2}{dt} = -\chi_h R_1 + \ell_1 S_1 + \mu_h S_1 \tag{111}$$

Substituting $R_1(t); \mathrm{S}_1(\mathrm{t})$ into (111)

$$ds_2 = \int -\chi_h\left(\gamma_h l_0 - \left(\mu_h + \chi_h\right) r_0\right)t + \ell_h\left(\phi_h + \chi_h r_0 - \ell_h s_0 - \mu_h s_0\right)t + \mu_h\left(\phi_h + \chi_h r_0 - \ell_h s_0 - \mu_h s_0\right)t \tag{112}$$

$$ds_2 = \int\left(-\chi_h\left(\gamma_h l_0 - \left(\mu_h + \chi_h\right) r_0\right) + \ell_h\left(\phi_h + \chi_h r_0 - \ell_h s_0 - \mu_h s_0\right) + \mu_h\left(\phi_h + \chi_h r_0 - \ell_h s_0 - \mu_h s_0\right)\right)tdt \tag{113}$$

$$ds_2 = \frac{1}{2}t^2\left(-\chi_h\left(\gamma_h l_0 - \left(\mu_h + \chi_h\right) r_0\right) + \ell_h\left(\phi_h + \chi_h r_0 - \ell_h s_0 - \mu_h s_0\right) + \mu_h\left(\phi_h + \chi_h r_0 - \ell_h s_0 - \mu_h s_0\right)\right) + c \tag{114}$$

At; $t = 0,\ S_2(0) = 0;\ c = 0$

$$ds_2 = \frac{1}{2}t^2\left(-\chi_h\left(\gamma_h l_0 - \left(\mu_h + \chi_h\right) r_0\right) + \ell_h\left(\phi_h + \chi_h r_0 - \ell_h s_0 - \mu_h s_0\right) + \mu_h\left(\phi_h + \chi_h r_0 - \ell_h s_0 - \mu_h s_0\right)\right) \tag{115}$$

From (37);

$$\frac{dE_2}{dt} = -\ell_h S_1 + \left(\delta_h + \mu_h\right) E_1 \tag{116}$$

Substituting $E_1(t)$ and $S_1(t)$ into (116)

$$\frac{dE_2}{dt} = -\ell_h\left(\phi_h + \chi_h r_0 - \ell_h s_0 - \mu_h s_0\right)t - \left(\delta_h + \mu_h\right)\left(\ell_h s_0 - \left(\delta_h + \mu_h\right)e_0\right)t \tag{117}$$

$$\int \frac{dE_2}{dt} = \int\left[-\ell_h\left(\phi_h + \chi_h r_0 - \ell_h s_0 - \mu_h s_0\right)t - \left(\delta_h + \mu_h\right)\left(\ell_h s_0 - \left(\delta_h + \mu_h\right)e_0\right)\right]tdt \tag{118}$$

$$\frac{dE_2}{dt} = -\frac{1}{2}t^2\left[-\ell_h\left(\phi_h + \chi_h r_0 - \ell_h s_0 - \mu_h s_0\right)t - \left(\delta_h + \mu_h\right)\left(\ell_h s_0 - \left(\delta_h + \mu_h\right)e_0\right)\right] + c \tag{119}$$

At; $t = 0; E_2(0) = 0; \mathrm{C} = 0$

$$\frac{dE_2}{dt} = -\frac{1}{2}t^2\left[-\ell_h\left(\phi_h + \chi_h r_0 - \ell_h s_0 - \mu_h s_0\right)t - \left(\delta_h + \mu_h\right)\left(\ell_h s_0 - \left(\delta_h + \mu_h\right)e_0\right)\right] \tag{120}$$

From (45)

$$\frac{dI_2}{dt} = -\delta_h E_1 + \left(\gamma_h + \rho_h + \mu_h\right) I_1 \tag{121}$$

Substituting $I_1(t)$ and $E_1(t)$ into (121)

$$\frac{dI_2}{dt} = -\delta_h\left(\ell_h s_0 - \left(\delta_h + \mu_h\right)s_0\right)t + \left(\gamma_h + \rho_h + \mu_h\right)\left(\delta_h e_0 - \left(\gamma_h + \rho_h + \mu_h\right)l_0\right)t \tag{122}$$

$$\int dI_2 = \int\left[-\delta_h\left(\ell_h s_0 - \left(\delta_h + \mu_h\right)s_0\right) + \left(\gamma_h + \rho_h + \mu_h\right)\left(\delta_h e_0 - \left(\gamma_h + \rho_h + \mu_h\right)l_0\right)t\right]tdt \tag{123}$$

$$I_2(t) = -\frac{1}{2}t^2\left[\delta_h\left(\ell_h s_0 - (\delta_h + \mu_h)s_0\right) + (\gamma_h + \rho_h + \mu_h)\left(\delta_h e_0 - (\gamma_h + \rho_h + \mu_h)l_0\right)\right] + C \quad (124)$$

At; $t = 0; \mathrm{I}_2(0) = 0; C = 0$

$$I_2(t) = -\frac{1}{2}t^2\left[\delta_h\left(\ell_h s_0 - (\delta_h + \mu_h)s_0\right) + (\gamma_h + \rho_h + \mu_h)\left(\delta_h e_0 - (\gamma_h + \rho_h + \mu_h)l_0\right)\right] \quad (125)$$

From equation (52);

$$\frac{dR_2}{dt} = -\gamma_h I_1 + (\mu_h + \chi_h)R_1 \quad (126)$$

Substituting $I_1(t)$ and $R_1(t)$ into (126)

$$\frac{dR_2}{dt} = -\gamma_h\left(\delta_h e_0 - (\gamma_h + \rho_h + \mu_h)l_0\right)t + (\mu_h + \chi_h)\left(\gamma_h l_0 - (\mu_h + \chi_h)r_0\right)t \quad (127)$$

$$\int dR_2 = \int\left[\left(-\gamma_h\left(\delta_h e_0 - (\gamma_h + \rho_h + \mu_h)l_0\right)\right) + (\mu_h + \chi_h)\left(\gamma_h l_0 - (\mu_h + \chi_h)r_0\right)\right]tdt \quad (128)$$

$$R_2 = \frac{1}{2}\left(-\gamma_h\left(\delta_h e_0 - (\gamma_h + \rho_h + \mu_h)l_0\right)\right) + (\mu_h + \chi_h)\left(\gamma_h l_0 - (\mu_h + \chi_h)r_0\right) + C \quad (129)$$

At; $t = 0; \mathrm{R}_2(0) = 0; C = 0$

$$R_2 = \frac{1}{2}\left(-\gamma_h\left(\delta_h e_0 - (\gamma_h + \rho_h + \mu_h)l_0\right)\right) + (\mu_h + \chi_h)\left(\gamma_h l_0 - (\mu_h + \chi_h)r_0\right) \quad (130)$$

From equation (59);

$$\frac{dk_2}{dt} + \phi_r - \ell_r K_1 - \mu_r K_1 = 0 \quad (131)$$

Substituting $K_1(t)$ into equation (131)

$$dk_2 = -\phi_r + \ell_r\left(\phi_r - \ell_r k_0 - \mu_r k_0\right)t + \mu_h\left(\phi_r - \ell_r k_0 - \mu_r k_0\right)t \quad (132)$$

$$\int dk_2 = \int\left[-\phi_r + \ell_r\left(\phi_r - \ell_r k_0 - \mu_r k_0\right) + \mu_h\left(\phi_r - \ell_r k_0 - \mu_r k_0\right)\right]tdt \quad (133)$$

$$dk_2 = -\frac{1}{2}t^2\left[\phi_r + \ell_r\left(\phi_r - \ell_r k_0 - \mu_r k_0\right) + \mu_h\left(\phi_r - \ell_r k_0 - \mu_r k_0\right)\right] + c \quad (134)$$

At; $t = 0,\ \mathrm{k}_2(0) = 0;\ c = 0$

$$dk_2 = -\frac{1}{2}t^2\left[\phi_r + \ell_r\left(\phi_r - \ell_r k_0 - \mu_r k_0\right) + \mu_h\left(\phi_r - \ell_r k_0 - \mu_r k_0\right)\right] \quad (135)$$

From equation (66);

$$\frac{dF_2}{dt} + \ell K_1 - \mu_r F_1 \tag{136}$$

Substituting $F_1(t)$ and $K_1(t)$ into equation (136)

$$\frac{dF_2}{dt} = -\ell_r\left(\phi_r - \ell_r k_0 - \mu_r k_0\right)t + \mu_r\left(\ell_r k_0 - \mu_r f_0\right)t \tag{137}$$

$$\int dF_2 = \int\left(-\ell_r\left(\phi_r - \ell_r k_0 - \mu_r k_0\right) + \mu_r\left(\ell_r k_0 - \mu_r f_0\right)\right)t\,dt \tag{138}$$

$$dF_2 = -\frac{1}{2}t^2\left(\ell_r\left(\phi_r - \ell_r k_0 - \mu_r k_0\right) + \mu_r\left(\ell_r k_0 - \mu_r f_0\right)\right) + c \tag{139}$$

At; $t = 0; \mathrm{F}_2(0) = 0; \mathrm{C} = 0$

$$dF_2 = -\frac{1}{2}t^2\left(\ell_r\left(\phi_r - \ell_r k_0 - \mu_r k_0\right) + \mu_r\left(\ell_r k_0 - \mu_r f_0\right)\right) \tag{140}$$

From (18) to (23), the approximate solution at $P = 1$ is written as;

$$S_h(t) = S_0 + S_1(t) + S_2(t) + \ldots \tag{141}$$

$$E_h(t) = E_0(t) + E_1(t) + E_2(t) + \ldots \tag{142}$$

$$I_h(t) = I_0(t) + I_1(t) + I_2(t) + \ldots \tag{143}$$

$$R_h(t) = R_0(t) + R_1(t) + R_2(t) + \ldots \tag{144}$$

$$S_r(t) = K_0(t) + K_1(t) + K_2(\mathrm{t}) + \ldots \tag{145}$$

$$I_r(t) = F_0(t) + F_1(t) + F_2(t) + \ldots \tag{146}$$

Hence, the final approximate solutions of (141) to (146) are obtained as follows;

$$S_h(t) = s_0 + \left(\phi_h + \chi_h r_0 - \ell_h s_0 - \mu_h s_0\right)t - \frac{1}{2}\left(\chi_h\left(\gamma_h l_0 - \left(\mu_h + \chi_h\right)r_0\right) + \ell_h\left(\phi_h + \chi_h r_0 - \ell_h s_0 - \mu_h s_0\right) + \mu_h\left(\phi_h + \chi_h r_0 - \ell_h s_0 - \mu_h s_0\right)\right)t^2 \tag{147}$$

$$E_h(t) = e_0 + \left(\ell_h s_0 - \left(\delta_h + \mu_h\right)s_0\right)t - \frac{1}{2}\left[\ell_h\left(\phi_h + \chi_h r_0 - \ell_h s_0 - \mu_h s_0\right)t - \left(\delta_h + \mu_h\right)\left(\ell_h s_0 - \left(\delta_h + \mu_h\right)e_0\right)\right]t^2 \tag{148}$$

$$I_h(t) = l_0 + \left(\delta_h e_0 - \left(\gamma_h + \rho_h + \mu_h\right)l_0\right)t - \frac{1}{2}\left[\delta_h\left(\ell_h s_0 - \left(\delta_h + \mu_h\right)s_0\right) + \left(\gamma_h + \rho_h + \mu_h\right)\left(\delta_h e_0 - \left(\gamma_h + \rho_h + \mu_h\right)l_0\right)\right]t^2 \tag{149}$$

$$R_h(t) = r_0 + \left(\gamma_h l_0 - (\mu_h + \chi_h) r_0\right) t - \frac{1}{2}\left(\gamma_h \left(\delta_h e_0 - (\gamma_h + \rho_h + \mu_h) l_0\right)\right) + (\mu_h + \chi_h)\left(\gamma_h l_0 - (\mu_h + \chi_h) r_0\right) t^2 \quad (150)$$

$$S_r(t) = k_0 + \left(\phi_r - \ell_r k_0 - \mu_r k_0\right) t - \frac{1}{2}\left[\phi_r + \ell_r\left(\phi_r - \ell_r k_0 - \mu_r k_0\right) + \mu_h\left(\phi_r - \ell_r k_0 - \mu_r k_0\right)\right] t^2 \quad (151)$$

$$I_r(t) = f_0 + \left(\ell_r k_0 - \mu_r f_0\right) t - \frac{1}{2}\left(\ell_r\left(\phi_r - \ell_r k_0 - \mu_r k_0\right) + \mu_r\left(\ell_r k_0 - \mu_r f_0\right)\right) t^2 \quad (152)$$

Therefore, equations (147) through (152) represent the analytical solution for the different compartments. These equations are structured as a series of solutions, each representing specific compartments considered analyzed in the study. By simulating various parameters values based on these equations, one can ascertain their impact on the population being studied.

4. Results and Discussion

This section shows, the parameter values, graphs generated from the general solution (147) to (152) and discussion of the results.

Table 1. Parameter values for the series solutions Variables/ Parameters

Parameters	Value	Reference
ϕ_h	1.20	(Peter et al., 2020a)
χ_h	Assumed	
δ_h	0.00385	(Peter et al., 2020a)
γ_h	Assumed	
μ_h	0.003465	(Lakshmikantham et al., 1989
ρ_h	0.00019231	(White et al., 1996)
ℓ_h	0.025	(Abdulraheem, 2002)
ℓ_r	0.0182	(Peter et al., 2020a)
ϕ_r	0.00001	(Abdulraheem, 2002)
μ_r	0.0038	(Lakshmikantham et al., 1989)
$\mathbf{S}_h(0)$	100	(Peter et al., 2020b)
$E_h(0)$	20	(Peter et al., 2020b)
$I_h(0)$	10	(Peter et al., 2020b)
$R_h(0)$	5	(Peter et al., 2020b)
$\mathbf{S}_r(0)$	1000	(Peter et al., 2020b)
$I_r(0)$	20	(Peter et al., 2020b)

4.1 Results

This section shows graphs generated from the general solution of our equation (147) to (152) using MAPLE.

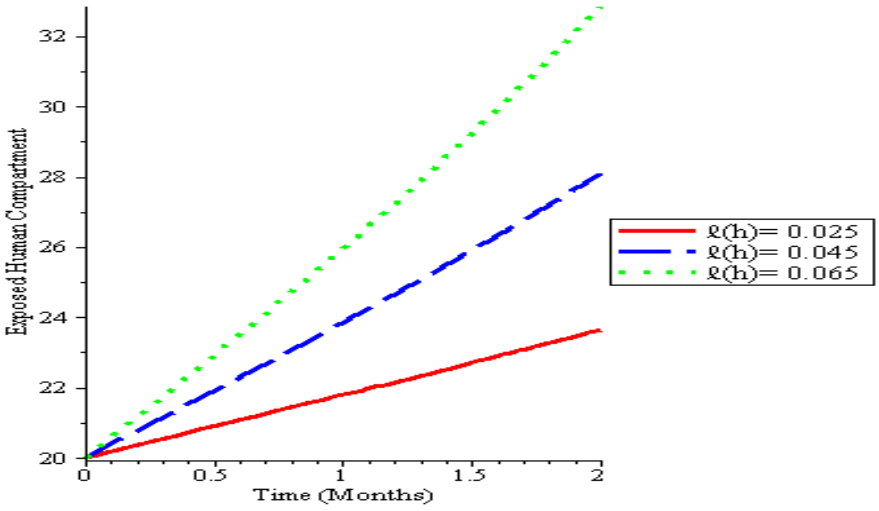

Fig. 1: Simulations of result show the relationship between the Exposed Human Compartment and time (t) for various values of $\ell_h = 0.025, \ell_h = 0.045$ and $\ell_h = 0.065$.

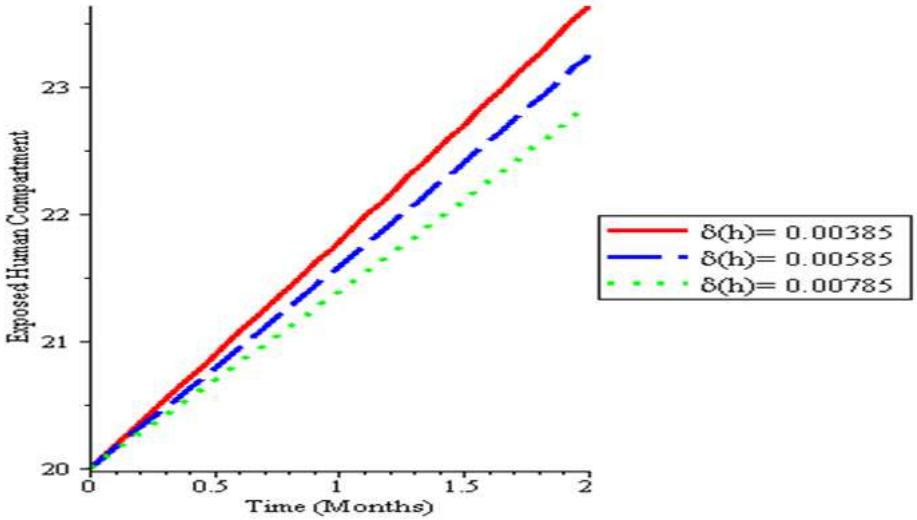

Fig. 2: Presents a graphical representation of the Exposed Human Compartment over time (t) for various values of $\delta_h = 0.00385$, $\delta_h = 0.00585$ and $\delta_h = 0.00785$.

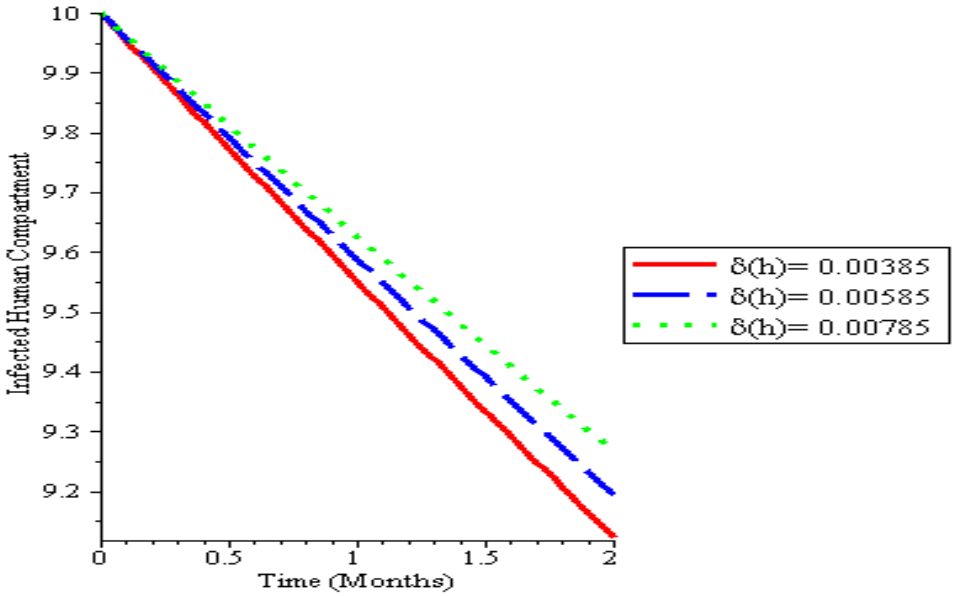

Fig. 3: Represents the graph of the Infected Human Compartment over time (t) for various values of $\delta_h = 0.00385$, $\delta_h = 0.00585$ and $\delta_h = 0.00785$.

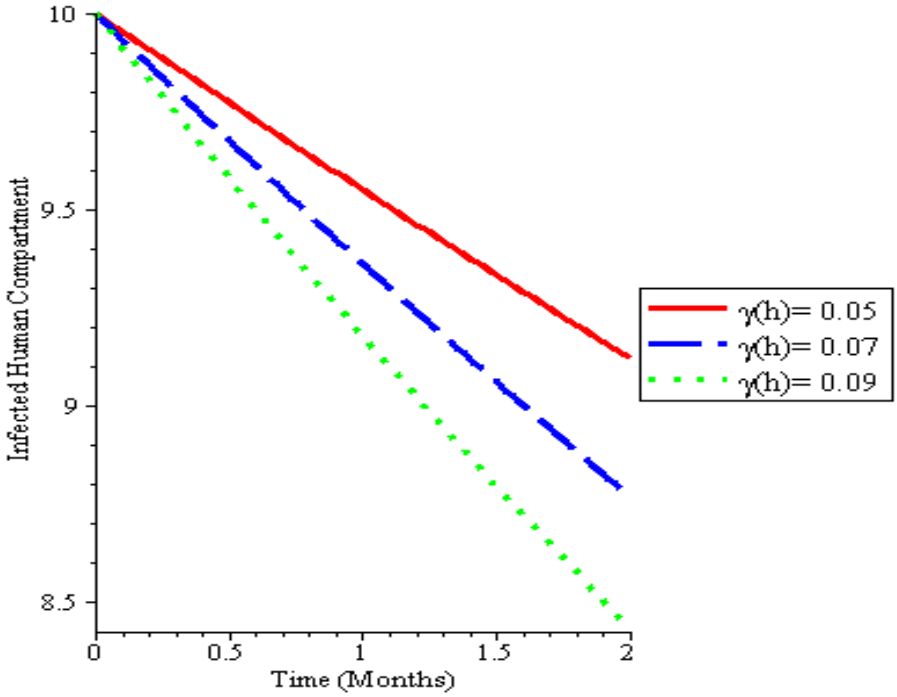

Fig. 4 Displays the graph of the Infected Human Compartment over time (t) for various values of $\gamma_h = 0.05$, $\gamma_h = 0.07$ and $\gamma_h = 0.09$.

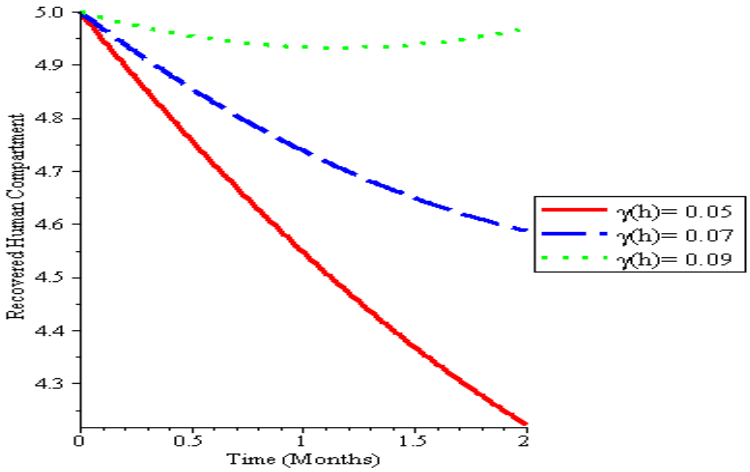

Fig. 5: Present the graph illustrating the Infected Human Compartment against time (t) for varying values of $\gamma_h = 0.05$, $\gamma_h = 0.07$ and $\gamma_h = 0.09$.

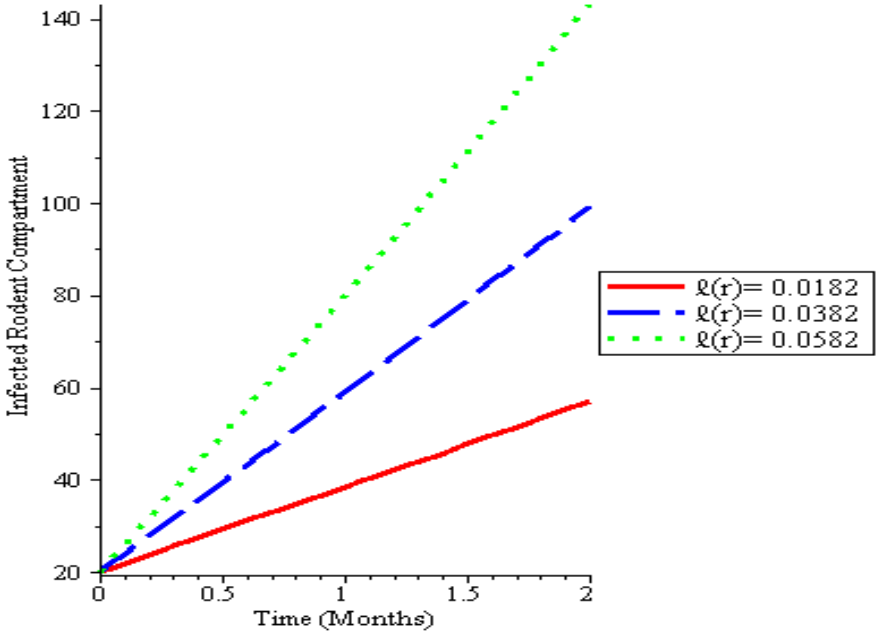

Fig. 6: Illustrates the graph of the Infected Rodent Compartment over time (t) for various values of $\ell_r = 0.0182$, $\ell_r = 0.0382$ and $\ell_r = 0.0582$.

4.2 Discussion of the Results

Figure 1. The graph distinctly demonstrates that an increase in ℓ_h leads to a higher population in the exposed human compartment, subsequently reducing the susceptible human class. This reduction is attributed to contact, which may occur through direct exposure to contaminated food via urine or excretes of an infectious rodent, as well as through laboratory transmissions involving the sharing of medical equipment with infected individuals without proper sterilization.

Figure 2. The graph conspicuously indicates that with an increase in δ_h, the population of the exposed human compartment decreases, subsequently resulting in an increase in the infected human compartment due to the progression of the disease within the population.

Figure 3: The graph clearly indicates a decrease in the infected human compartment with time (t), but experiences an increment when increases δ_h. This is a consequence of the disease progressing from the human exposed class

Figure 4. The graph illustrates a reduction in the infected human compartment over time, and it further diminishes as the recovery rate increases. This highlights the effectiveness and efficiency of the recovery rate.

Figure 5. The graph illustrates that the number of individuals in the recovered human compartment decreases over time. However, it increases as the recovery rate rises, showcasing the effectiveness and efficiency of the recovery rate.

Figure 6.The graph distinctly shows that as ℓ_r increases, the infected rodent compartment becomes populated, leading to a reduction in the susceptible rodent class. This occurs due to the effective transmission probability from human to rodent and the effective transmission probability from rodent to rodent.

5. Conclusion

In this paper, the equations representing the different compartments are transformed into first-order non-linear differential equations. The system of non-linear equations is then solved using the homotopy perturbation method, the final approximate solutions are derived and the simulation results are compared, revealing a satisfactory agreement,

References

Abdulraheem, I. S. (2002). Public's Health Importance of Lassa fever epidemiology, clinical features and current management review of literature, *Africa Journal of Clinical and Experimental* Microbiology, Vol 3(1), 33–37.

Adebayo, D., Nwobi, E.A., Vincent T., and Gonzalez, J.P. (2015), Response Preparedness to Viral Hemorrhagic Fever in Nigeria, Risk Perception, Attitude towards Lassa fever. Epidemiology(sunnyvale), Vol. 5(3), 1- 5 doi:10.4172/2161-1165.1000199.

Agbata, B., Shior, M., Olorunnishola, O., Ezugorie, I., and Obeng-Denteh, W. (2021). Analysis of Homotopy Perturbation Method (HPM) and its application for solving infectious disease models, *International Journal of Mathematics and Statistics Studies*, Vol. 9(4), 27–38.

Akinpelu, F.O. and Akinwande R., (2018), Mathematical Model for Lassa Fever and Sensitivity Analysis,

Journal of Scientific and Engineering Research, Vol. 5(6), 1-9.

Anorue, O. F. and Okeke, A. A. (2020). Mathematical Model for Lassa Fever Transmission and Control.

Mathematics and Computer Science, Vol 5(6),110-118. doi: 10.11648/j.mcs.20200506.13

Amanat, A. K. and Musammet, T. A. (2020). Solving Highly Nonlinear Partial Differential Equations Using Homotopy Perturbation Method, *American Journal of Applied Mathematics*. Vol. 8(6), 334-343. doi: 10.11648/j.ajam.20200806.16.

Ayoade, A. A., Peter, O. J., Abioye, A.I., Aminu, T.F., and Uwaheren, O. A. (2020). Application of Homotopy perturbation method to a sir mumps model, Advances in Mathematics: *Scientific Journal*, Vol. 9(3): 329–1340.

Bakare, E., Are, E., Abolarin, O., Osanyinlusi, S., Ngwu, B., and Ubaka, O.N. (2020). Mathematical modelling and analysis of transmission dynamics of lassa fever. *Journal of Applied Mathematics, Medicine and Environmental Science*, 1 -21.

Centers for Disease Control and Prevention of Lassa Fever (2014), Atlanta, Georgia. Available from: https://www.cdc.gov/vhf/lassa/ index.html. Retrieved on 04-06-2020.

Centers for Disease Control and Prevention of Lassa Fever (2019), Atlanta, Georgia. Available from: https://www.cdc.gov/vhf/lassa/ index.html. Retrieved on 04-06-2020.

Collins. O. C. and Okeke J. E. (2021). Analysis and control measures for Lassa fever model under socio

economic conditions, International Conference on Recent Trends in Applied Research, *Journal of*

Physics, Vol.1734,1-9, doi:10.1088/1742-6596/1734/1/012049.

He, J. H. (1998). "Approximate analytical solution for seepage flow with fractional derivatives in porous

media," Computational Methods Applied Mechanical Engineering, Vol. 167, 57–68.

Jiya, M. (2010). "Application of Homotopy Perturbation Method (HPM) for the Solution of some Non-Linear Differential Equations", *Pacific Journal of Science and Technology*. Vol. 11(2), 268- 272.

Mayowa, M. O., and Emile, F.D. G. (2022). Modeling, analyzing and simulating the dynamics of Lassa fever in Nigeria, *Journal of the Egyptian Mathematical Society*, Vol. 30(1), 1 – 31, doi.org/10.1186/s42787- 022-00138-x

Mechee, M. S., and Al-Juaifri, G. A. (2018). Application of homotopy perturbation method for sir model with vital dynamics and constant population", *American Journal of Applied Sciences*, Vol. 15(1), 10–21.

Otoo, H., Takyi-Appiah, S., and Nsiah, A. (2022). Analytical Solution of the Transmission Dynamics of

Diarrhea using Homotopy Perturbation Method, *European Journal of Engineering and Technology*

Research, Vol. 7 (6), 161 – 168. DOI: http://dx.doi.org/10.24018/ejeng.2022.7.6.2943

Olumuyiwa, J. P., Adesoye, I. A., Festus, A. O., Titilayo, A. O., Michael, O. A., Abdullaziz, G. Z., and

Timilehin, G.S., (2020). Modelling and optimal control analysis of Lassa fever disease Informatics in
Medicine Unlocked, Vol. 20, 1- 11, https://doi.org/10.1016/j.imu.2020.100419

Padma, S., Vanaja, R., and Rajendran, L. (2021), Theoretical Model for the Control of Lassa Fever and
Transmission Using Homotopy Perturbation Method. *Turkish Online Journal of Qualitative Inquiry*,
Vol. 12 (3), 4172-4184.

Peter, O.J. and Awoniran, A.F. (2018). "Homotopy Perturbation Method for Solving SIR Infectious Disease
Model by Incorporating Vaccination", *Pacific Journal of Science and Technology*, Vol. 19(1): 133-140.

Peter, O. J., Adebisi, A. F., Ajisope, M. O., Ajibade, F. O., Abioye, A. I. & Oguntolu, F. A.. (2020a). Global
Stability analysis of Typhoid fever model. *Advance System Science Applied*, Vol.20, 20–31. https://doi.org/10.25728/assa.2020.20.2.792.

Rekha, S., Balaganesan, P., and Renuka, J. (2021). Homotopy Perturbation Method for Mathematical Modelling
of Dengue Fever, *Journal of Physics*, Vol. 1724, 1-12, doi:10.1088/1742-6596/1724/1/012056.

Sambo, D., and Chinwendu, E. M. (2020). Mathematical Model of the Transmission Dynamics of Lassa Fever
Infection with Controls, Mathematical Modelling and Applications, Vol. 5(2), 65-86, doi: 10.11648/j.mma.20200502.13.

Sulaiman, U., and Ibrahim, I. A., (2018). Modelling the Transmission Dynamics of the Lassa Fever Infection
Mathematical Theory and Modeling, Vol. 8(5), 42 – 63.

Tahmina, A. M. and Mansur, C. M. A. (2019). Homotopy Perturbation Method for Solving Highly Nonlinear
Reaction-Diffusion-Convection Problem, *American Journal of Mathematics and Statistics*, Vol. 9(3):
136-141, DOI: 10.5923/j.ajms.20190903.04

Usman, S. & Adamu, I. I. (2018), Modelling the Transmission Dynamics of Lassa Fever Infection,
Mathematical Theory and Modelling, Vol. 8(15), 42-63.

White, A., Begon, M. & Bowers, R. G. (1996). Host-pathogen cycles in self-regulated forest insect systems:
resolving conflicting predictions. *Am Nat*, Vol.148, 220–245.

World Health Organization. (2017) Lassa Fever. World Health Organization, Geneva. Available from:
http://www. who.int/mediacentre/factsheets/fs179/en. Retrieved on 04-06-2020.

World Health Organization. (2019) Lassa Fever. World Health Organization, Geneva. Available from:
http://www. who.int/mediacentre/factsheets/fs179/en. Retrieved on 04-06-2020.

Impact of Educational Strategies on the Control of Marital Conflict: A Mathematical Modelling Approach

Bako D.

Department of Mathematics Federal University of Technology Minna
e-mail and Phone Number: deborah.bako@futminna.edu.ng; 08034077299

Abstract

The study examines the impact of different education strategies on controlling marital conflict, focusing on the effective contagion rate as an indicator of conflict spread. The analysis compares the outcomes of educating 80% of married men and 20% of married women versus educating 20% of married men and 80% of married women about the dangers of divorce. The findings reveal that the former strategy fails to reduce the effective contagion rate to zero, indicating ongoing conflict propagation within the population. In contrast, the latter approach shows a significant reduction in the effective contagion rate initially, although it starts to rise again along the trend. To achieve optimal control of marital conflicts, a balanced approach is recommended, with a 50% coverage rate of education for both genders. This balanced strategy aims to strike a gender equilibrium, ensuring a substantial portion of the population receives education on the dangers of divorce. Implementing this comprehensive education approach holds promise for minimizing conflict spread, promoting healthier marital relationships, and fostering stable family units. However, further research is needed to consider additional factors and long-term effects in understanding and addressing marriage conflict dynamics.

Keywords: Marital conflict, Education strategies, Mathematical model

Introduction

Marriage is a complex and dynamic institution that involves the union of two individuals, often with the intention of creating a lasting and fulfilling partnership. However, conflicts within marriages are inevitable and can have significant ramifications on the well-being of both spouses and their overall relationship. Marriage conflicts encompass a wide range of issues, including disagreements over finances, parenting styles, communication breakdowns, infidelity, and differences in values and expectations. Numerous authors have contributed to our understanding of the causes of marriage conflict. According to Gottman and Silver (2015), conflicts often arise from deep-rooted differences in core values and incompatible personality traits. Additionally, Fincham and Beach (2010) highlight the role of situational factors, such as financial stress or work-related demands, in triggering conflicts within marriages. In their seminal work, Johnson and Greenberg (2013) emphasize the significance of attachment styles and the impact of past experiences on present relationship dynamics. These authors collectively underscore the multifaceted nature of marriage conflict, emphasizing the importance of examining both individual and contextual factors.

Marriage conflicts can have far-reaching consequences for the well-being of individuals and the stability of the relationship. Extensive research by Amato and Previti (2003) demonstrates that unresolved conflicts often contribute to marital dissatisfaction, increased likelihood of separation or divorce, and negative effects on physical and mental health. Conflictual marriages can also adversely affect children's development, as highlighted by Cummings and Davies (2010). Their studies reveal that ongoing marital conflict can lead to increased behavioral problems and emotional distress among children. These findings underscore the urgency of understanding the consequences of marriage conflict and developing effective interventions.

Marital conflict is a universal phenomenon that transcends cultural, socioeconomic, and geographic boundaries. It is an essential area of study, as understanding the nature and dynamics of marital conflicts can shed light on the challenges faced by couples globally. Marital conflict manifests in diverse ways across different cultures. Research conducted by Hofstede (2001) on cultural dimensions revealed that societies vary in their approaches to conflict resolution, ranging from more collectivist cultures that prioritize harmony and avoiding conflict to individualistic cultures that emphasize open confrontation. For example, in collectivist cultures, such as Japan and Korea, maintaining harmony within the family unit takes precedence over expressing individual needs, potentially leading to suppressed conflicts.

On the other hand, in individualistic cultures like the United States, direct and assertive communication may be more common during marital conflicts. These cultural variations highlight the importance of considering context and cultural norms when studying marital conflict. The increasing interconnectedness brought about by globalization has had a profound impact on marital relationships worldwide. As societies become more globalized, traditional gender roles and expectations within marriages undergo transformation. For instance, the entry of women into the workforce and the erosion of traditional gender norms have contributed to shifts in power dynamics and decision-making processes within relationships. These changes can lead to conflicts as couples negotiate new roles and responsibilities.

Marital conflict, like a social infection, can spread through social interaction, affecting individuals and their relationships. Drawing upon the metaphor of infection, this perspective suggests that marital conflict can be contagious, with negative emotions and behaviors transmitted between partners and even to others within their social networks. Understanding marital conflict as a social contagion offers valuable insights into the dynamics of conflict spread, its consequences, and potential strategies for prevention and intervention. Similar to the transmission of infectious diseases, marital conflict can be transmitted through various channels of social interaction. Research by Feinberg and colleagues (2007) has shown that conflicts between spouses can spill over into interactions with children, affecting parent-child relationships and potentially spreading conflict to the next generation. Additionally, conflicts within a marriage can influence the behavior and emotional well-being of family members, friends, and acquaintances who witness or are indirectly exposed to the conflict (Lavner, Karney, & Bradbury, 2016).

Through verbal and nonverbal communication, emotional contagion, and observational learning, marital conflict can be transmitted and replicated in social networks, perpetuating a cycle of discord.

The spread of marital conflict has significant consequences for individuals and their social environments. Individuals who are repeatedly exposed to conflict within their social networks may experience heightened stress, emotional distress, and negative affect (Lavner et al., 2016). Witnessing or being involved in ongoing marital conflicts can lead to increased conflict sensitivity and negative relationship expectations, affecting the quality of their own relationships (Rhoades, 2008). Moreover, the social contagion of marital conflict can contribute to the erosion of social support networks, as conflict spreads and affects relationships beyond the marital dyad.

Understanding marital conflict as a social infection provides insights into potential strategies for prevention and intervention. Just as public health efforts focus on preventing the spread of infectious diseases, interventions aimed at reducing marital conflict should target both individuals and their social networks. Couples therapy and relationship education programs, such as those developed by Markman and colleagues (Markman, Rhoades, Stanley, Ragan, & Whitton, 2010), can equip couples with conflict resolution skills and enhance relationship satisfaction, thereby reducing the transmission of conflict to others.

Authors have proposed various strategies for resolving marriage conflicts and promoting healthier relationships. Notably, Gottman and Gottman (2017) advocate for a constructive approach, emphasizing the importance of open communication, active listening, and mutual respect in resolving conflicts. Similarly, Markman, Stanley, and Blumberg (2010) propose the use of structured interventions, such as couples therapy and relationship education programs, to facilitate effective conflict resolution and enhance relationship satisfaction. Furthermore, Christensen and Jacobson (2000) advocate for the implementation of preventive measures, such as premarital counseling, to address potential sources of conflict before they escalate. These authors highlight the significance of proactive strategies in reducing the prevalence and intensity of marriage conflicts.

2. Model Formulation

The total population is compartmentalized into six sub-populations, which consist of susceptible male (S_m), married male (M_m), divorced male (D_m), susceptible female (S_f), married female (M_f), divorced female (D_f) as shown in the diagram below:

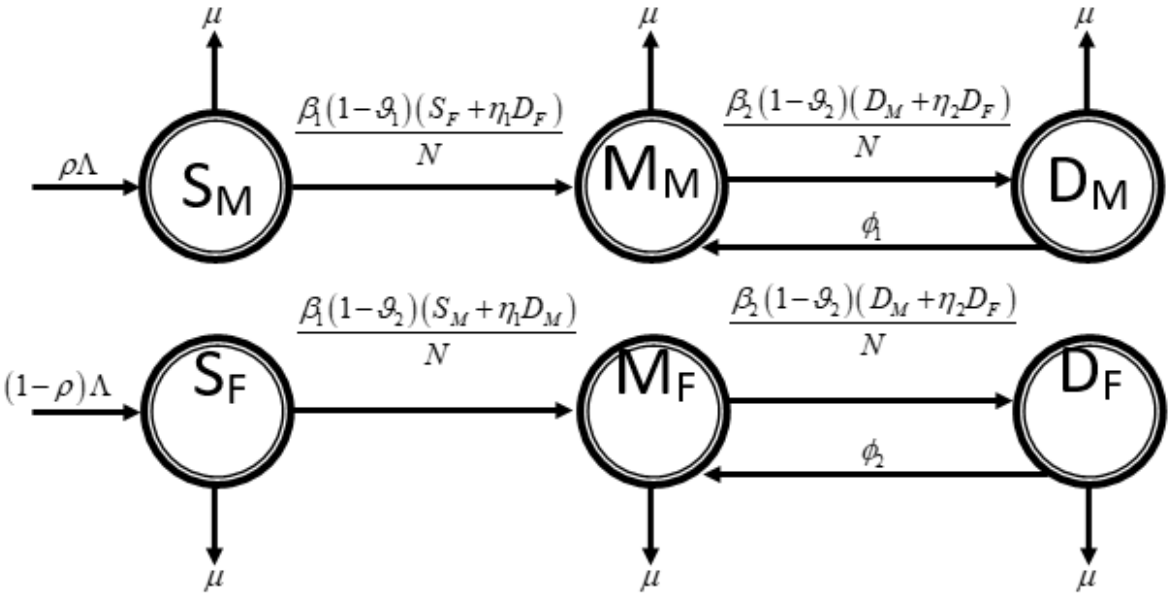

Figure 1: Schematic diagram of the Marital Conflict Model

A full description of the parameters used in the model are given below

Parameter	Description
Λ	Recruitment number of human
ρ	Birth rate of male
β_1	Contact rate of susceptible and divorced individuals
β_2	Contact rate of divorced individuals
μ	Per capita natural mortality rate
ϑ_1	Control rate for reducing conflict by men
ϑ_2	Control rate for reducing conflict by women
η_1	Modification parameter for the reduction of conflict by men

η_2	Modification parameter for the reduction of conflict by women
ϕ_1	Rate at which divorced men remarry
ϕ_2	Rate at which divorced women remarry
N	Total human population

The corresponding mathematical equations of the schematic diagram can be described by a system of Ordinary Differential Equations (ODEs) given below:

$$\frac{dS_M}{dt} = \rho\Lambda - \frac{\beta_1(1-\vartheta_1)(S_F + \eta_1 D_F)S_M}{N} - \mu S_M \tag{1}$$

$$\frac{dM_M}{dt} = \frac{\beta_1(1-\vartheta_1)(S_F + \eta_1 D_F)S_M}{N} - \frac{\beta_2(1-\vartheta_2)(D_M + \eta_2 D_F)M_M}{N} + \phi_1 D_M - \mu M_M \tag{2}$$

$$\frac{dD_M}{dt} = \frac{\beta_2(1-\vartheta_2)(D_M + \eta_2 D_F)M_M}{N} - (\phi_1 + \mu)D_M \tag{3}$$

$$\frac{dS_F}{dt} = (1-\rho)\Lambda - \frac{\beta_1(1-\vartheta_1)(S_M + \eta_1 D_M)S_F}{N} - \mu S_F \tag{4}$$

$$\frac{dM_F}{dt} = \frac{\beta_1(1-\vartheta_1)(S_M + \eta_1 D_M)S_F}{N} - \frac{\beta_2(1-\vartheta_2)(D_M + \eta_2 D_F)M_M}{N} + \phi_2 D_F - \mu M_F \tag{5}$$

$$\frac{dD_F}{dt} = \frac{\beta_2(1-\vartheta_2)(D_M + \eta_2 D_F)M_F}{N} - (\phi_2 + \mu)D_F \tag{6}$$

3. Effective Contagion Rate (R_{eff})

The threshold quantity (R_{eff}) is the effective contagion rate of the model (1) – (6) for the stability analysis for controlling marital conflict. It measures the average number of new conflict generated by a typical marital conflict in a population comprising of completely susceptible married couples.

Using the next generation operator technique described by (Diekmann & Heesterbeek, 2000), the effective contagion rate $\left(R_{eff}\right)$ of model (1) to (6), which is the spectral radius $\left(\rho\right)$ of the next generation matrix. This is given by:

$$F = \begin{pmatrix} \frac{\beta_2\left(1-\vartheta_1\right)M_M{}^0}{N^0} & \frac{\beta_2\left(1-\vartheta_2\right)\eta_2 M_M{}^0}{N^0} \\ \frac{\beta_2\left(1-\vartheta_1\right)M_F{}^0}{N^0} & \frac{\beta_2\left(1-\vartheta_2\right)\eta_2 M_F{}^0}{N^0} \end{pmatrix}$$

$$V^{-1} = \begin{pmatrix} \frac{1}{k_1} & 0 \\ 0 & \frac{1}{k_2} \end{pmatrix}$$

$$R_{eff} = \frac{\beta_2\left(1-\vartheta_2\right)\left(k_1\eta_2 M_F{}^0 + k_2 M_M{}^0\right)}{k_1 k_2 N^0}$$

3.0 Results and Discussions

3.1 Estimation of Variables and Population-dependent Parameters Values

S/N	Parameter	Value	Source
1	Λ	3000	Estimated
2	ρ	300	Estimated
3	β_1	0.005	Estimated
4	β_2	0.0027	Estimated
5	μ	0.9	Estimated
6	ϑ_1	0.3	Estimated
7	ϑ_2	0.00005	Estimated
8	η_1	0.01	Estimated

9	η_2	0.6	Estimated
10	ϕ_1	(0,1)	Varied for computational reasons
11	ϕ_2	0.5	Assumed
12	N	5000	Assumed

3.2 Effect of the rate of control strategies on susceptible married couples on the dynamics and control of marital conflicts

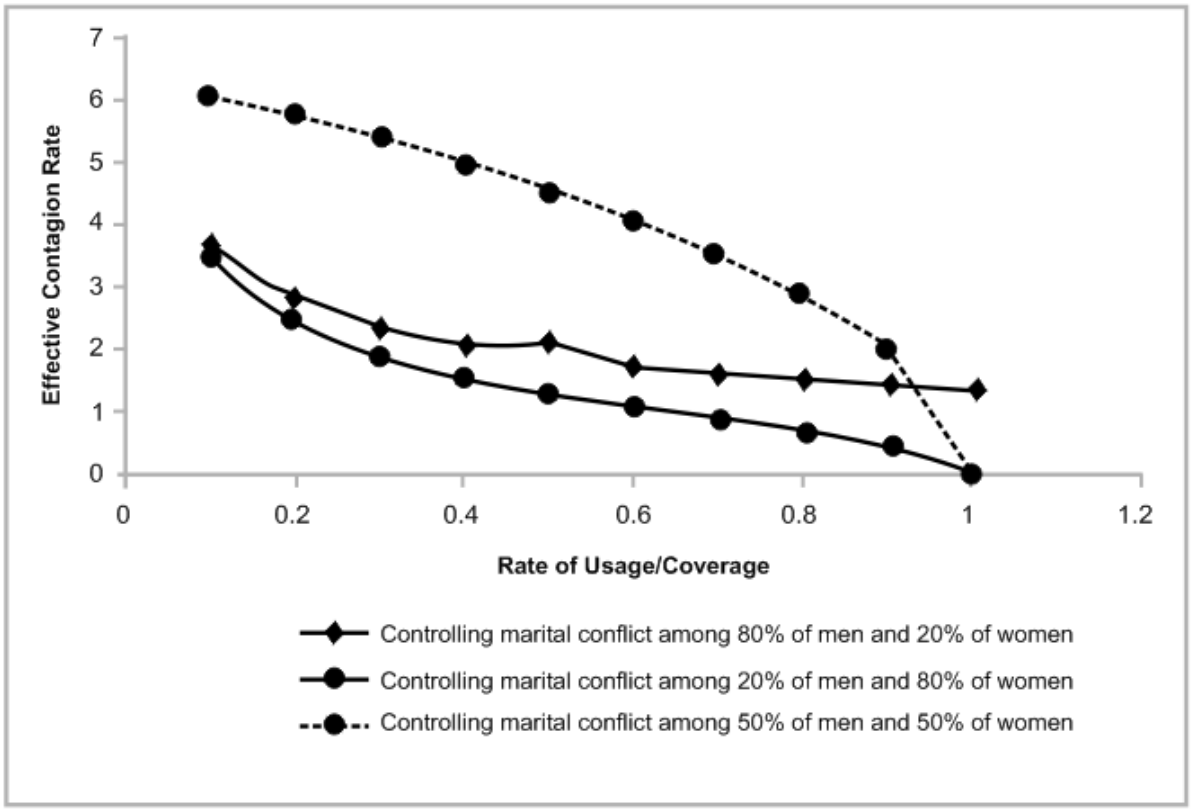

Figure 2: Effect of three different control strategies on the dynamics and control of marital conflict

The analysis of Figure 2 highlights the impact of different education strategies on controlling marriage conflict. Focusing on educating 80% of married men and 20% of married women about the dangers of divorce proves to be ineffective, as the effective contagion rate never reaches zero. This indicates that conflict continues to persist and spread within the population. In contrast, when 20% of married men and

80% of married women receive education on the dangers of divorce, there is a notable reduction in the effective contagion rate. However, it is important to note that even though the effective contagion rate drops to zero initially, it starts to rise again along the trend.

To achieve optimal control of marital conflicts in a society, a balanced approach is recommended. Implementing a 50% coverage rate of education for both married men and women demonstrates promising results in minimizing the spread of marital conflict. This strategy aims to strike a balance between the genders, ensuring that a significant portion of the population receives education on the dangers of divorce. By adopting this approach, it is expected that the effective contagion rate can be effectively managed and kept at a lower level. Overall, the findings suggest that a comprehensive education strategy involving both married men and women is crucial for effective control of marriage conflict. The specific balance of educational coverage can play a vital role in minimizing the spread of conflict within a society and promoting healthier and more stable marital relationships.

4. Conclusion

This research provides valuable insights into the impact of education strategies on controlling marriage conflict. The findings clearly demonstrate that focusing solely on educating a specific gender group is ineffective in reducing the spread of conflict within a population. While educating 80% of married men and 20% of married women shows limited effectiveness, a more balanced approach of educating 20% of married men and 80% of married women yields better results in reducing the effective contagion rate initially. However, it is crucial to note that the effective contagion rate starts to rise again along the trend, indicating that sustained efforts are necessary to maintain control over marriage conflict. To achieve optimal control, it is recommended to implement a balanced approach, with a 50% coverage rate of education for both married men and women. This approach acknowledges the importance of addressing both genders and ensuring that a substantial proportion of the population receives education on the dangers of divorce. By adopting this comprehensive education strategy, societies can strive towards minimizing the spread of marital conflict and promoting healthier and more stable marital relationships. It is crucial for policymakers, educators, and professionals in the field of relationship counseling to recognize the significance of providing education to both genders and tailor intervention programs accordingly.

However, it is important to acknowledge the limitations of this study. The analysis focused on the impact of education strategies on the effective contagion rate, neglecting other potential factors that contribute to marriage conflict. Future research should explore additional variables, such as cultural and socioeconomic factors, as well as consider long-term follow-ups to assess the sustainability of the effects observed.

References

Amato, P. R., & Previti, D. (2003). People's reasons for divorcing: Gender, social class, the life course, and adjustment. Journal of Family Issues, 24(5), 602-626.

Christensen, A., & Jacobson, N. S. (2000). Reconcilable differences: Rebuild your relationship by rediscovering the partner you love without losing yourself. The Guilford Press.

Cummings, E. M., & Davies, P. T. (2010). Marital conflict and children: An emotional security perspective. Guilford Press.

Diekmann, O., & Heesterbeek, J. A. P. (2000). *Mathematical epidemiology of infectious diseases: Model building, analysis and integration*. New York: Wiley.

Fincham, F. D., & Beach, S. R. (2010). Conflict in marriage: Implications for working with couples. Annual Review of Psychology, 61, 429-453.

Gottman, J. M., & Gottman, J. S. (2017). The science of couples and family therapy: Behind the scenes at the Love Lab. Routledge.

Gottman, J. M., & Silver, N. (2015). The seven principles for making marriage work. Harmony.

Johnson, S. M., & Greenberg, L. S. (2013). Emotionally focused couples therapy: Creating secure connections. Routledge.

Markman, H. J., Stanley, S. M., & Blumberg, S. L. (2010). Fighting for your marriage: Positive steps for preventing divorce and preserving a lasting love. Jossey-Bass.

Feinberg, M. E., Kan, M. L., & Hetherington, E. M. (2007). The longitudinal influence of coparenting conflict on parental negativity and adolescent maladjustment. Journal of Marriage and Family, 69(3), 687-702.

Lavner, J. A., Karney, B. R., & Bradbury, T. N. (2016). Does couples' communication predict marital satisfaction, or does marital satisfaction predict communication? Journal of Marriage and Family, 78(3), 680-694.

Hofstede, G. (2001). Culture's consequences: Comparing values, behaviors, institutions, and organizations across nations (2nd ed.). Sage Publications.

Mathematical Model of Hepatitis B in a Susceptible Population with Control Strategies

Adagba Ibrahim Abdullahi [1], Akpan Collins Emmanuel [2], Mbah Moses Anayo [3].
Department of Mathematics, Federal University of Lafia, Nigeria.
Email: adagbaibrahimabdullahi@gmail.com

Abstract

A mathematical model based on the Susceptible-Latent-Infected-Chronic-Treatment-Exclusion-Recovered (SLICTER) compartments for hepatitis B was formulated. The population is assumed to be recruited by birth. Existing hepatitis B data was used in validating the model to fathom the transmission dynamics of HBV as it will aid in preventing, controlling, eradicating the disease, help in policy formulation and improve lives. It was proved that the global dynamics were completely determined by the basic reproductive number R_0. If $R_0 < 1$, the disease free-equilibrium is locally and globally stable and the disease always die out. And if $R_0 > 1$, an endemic equilibrium exist and is locally bistable in the interior of the feasible region, and the disease remain at an endemic equilibrium state if it at the onset exist. Sensitivity analysis were performed on the model parameters in the basic reproductive number R_0 to determine the effect of different parameter values on the spread of HBV. Four control strategies was considered and the analysis shows that the implementation of maximum vaccination at birth, combined treatment and exclusion along with regular sensitization (awareness) will help greatly in eradicating the virus. The system was solved using the classical Runge-Kutta scheme of order four, forward in time of 50 years and the algorithm were implemented using MATLAB.

Key words: Basic reproductive number, Bi-stability, Control Strategies, Dynamics, Hepatitis B, Model, Sensitivity Analysis,

1.0 INTRODUCTION

Hepatitis is an inflammation of the liver caused by viruses, bacterial infections, or constant vulnerability to alcohol intake, drugs, or toxic chemicals, such as those obtained in aerosol sprays and paint thinners. Inflammation is the painful, red growth that results when tissues of the body become wounded or infected.

Hepatitis B, is one of the major and common infectious disease of the liver worldwide. It constitutes a serious public health problem and more dangerous on account of its tendency to become chronic, sometimes giving rise to cirrohsis of the liver or worse still, liver cancer. Hepatitis B is a potential life-threatening infection caused by Hepatitis B virus (HBV), Adagba and Joseph (2022). The World Health Organization, WHO (2022) reported that as many as 296 million people were living with Hepatitis B infection in 2019, With 1.5 million new infections each year and resulted in an estimated 820,000 deaths mostly from cirrhosis and hepatocellular carcinoma (primary liver cancer). HBV infection exhibits an acute infection stage and a chronic liver infection, which is determined by the degree of virus replication and the intensity of host immune response. Infection in newborns, who are incapable

of constructing a defective immune response, is more likely to result in chronic infection (90%) than that in adults (5%), in whom most primary infections are self-limited. Safe and effective vaccine is available for all age groups to prevent HBV infection and development of chronic disease. More than 150 countries have vaccine immunization programs, with routine infant vaccination designated as a high priority in all countries. When viral replication is observed in a patient, efficient therapy is needed to control the risk of disease progression. It is estimated that, if left untreated, approximately (15-25)% of chronically infected individuals would develop liver cirrhosis and HCC after decades of infection. And there is abundant evidence that antiviral therapy, in patients with long-term virological response, can improve liver histology by providing indirect support and possibly even reversing liver damage, Zhang and Suxia (2018). HBV is transmitted by parenteral or mucosal exposure to HBsAg positive body fluids from persons who have acute or chronic HBV infection. It replicates in hepatocytes through a unique reverse transcription process. The clinical course of acute hepatitis B is indistinguishable from that of other types of acute viral hepatitis. The incubation period typically ranges from 60 to 90 days. Clinical signs and symptoms occur more often in adults than in infants or children; infants and young children usually are asymptomatic. Approximately 50% of adults who have acute infections are asymptomatic.

The pre-icteric, prodromal, phase from initial symptoms to onset of jaundice usually lasts 3 to 10 days. It is nonspecific and is characterized by abrupt onset of fever, malaise, anorexia, nausea, abdominal discomfort, and dark urine beginning 1 to 2 days before the onset of jaundice. The icteric phase is variable but usually lasts from 1 to 3 weeks and is characterized by jaundice, light or gray stools, hepatic tenderness, and hepatomegaly (splenomegaly is less common). During convalescence, malaise and fatigue may persist for weeks or months, while jaundice, anorexia, and other symptoms disappear.

Most acute HBV infections in children and young adults result in complete recovery with elimination of HBsAg from the blood and the production of anti-HBs, creating immunity to future infection. In contrast, as many as 90% of HBV infections in infants progress to chronic infection. Perinatal transmission from mother to infant at birth (vertical transmission) is highly efficient. Prior to the widespread availability of postexposure prophylaxis, the proportion of infants born to HBsAg-positive women that acquired HBV infection was approximately 30% for those born to HBeAg negative mothers and 85% for those born to HBeAg positive mothers. With post exposure prophylaxis, comprised of HepB vaccine and Hepatitis B Immune Globulin (HBIG) at birth, followed by completion of the HepB vaccine series, 0.7% through 1.1% of infants develop infection; infants born to mothers with high viral loads are at greatest risk for infection despite receipt of HepB vaccine and HBIG, Penina and Sarah (2021). The epidemiology of hepatitis B is said to be geographically diverse, essentially regarding population prevalence, age and mode of contraction and the likelihood of progression to the chronic infection. The disease has caused epidemics in Asia and Africa and it is endemic in China.

2. Literature Review

Many researchers have made utmost attempts and contributions to fathom the epidemiology of hepatitis B. In this chapter we present some theories and models related to our study work.

One of interest is the work published by Oyelami (2014). A book detailing some techniques needed in analyzing the stability of a dynamical system. In his work, he considered several of these techniques viz; stability through (ϵ–δ) argument, stability via Routh Hurwitz criterion, stability via fundamental matrices and finally by the use of scalar functional called lyapunov stability technique. For clarity purpose consider the initial value problem (IVP) below.

$$X(t) = f\big(t, x(t)\big), x(t_0) = x_0$$

Where $f \in C(IX\Omega, E^n)$, Ω is open and connected subset of E^n. Assuming f has the

property that the solution $x(t,t_0,x_0)$ exists and is unique, that is if $x(t,t_0,x_0)$ is a solution and f satisfies the hypotheses of the Picard-Linderloft existence and uniqueness theorem.
The core or central question of stability is there a special solution $\phi(t,t_0,x_0)$ existing on the interval $[t_0,+\infty)$ such that a small perturbations would result in small deviations from system behaviour ? If such a solution exists, then we say such a system is stable, otherwise it is unstable.

Wiah et al. (2011) contributed their quota to the understanding of the dynamics of HBV by presenting a simplified mathematical model of immune responds to Hepatitis B Virus (HBV) infection. Their work focused on the control of the infection by the interferons, the innate and adaptive immunity. The model was compartmentalized as appropriate and the resulting model equations were solved numerically. The mathematical analysis of their model showed that both disease-free and endemic equilibrium point exist and they derive conditions for their stability. They went ahead to perform sensitivity analysis on the model parameters, to account for the variability and speed of adaptation.

The model is based on human immune response against HBV infection, they considered a simplified model of population-dynamics type which consists of the following interactions; The liver cells are assumed to be in one of four possible states: healthy (H), infected (I), dead (D), or resistant (R) to infection. The total number of liver cells (i.e., H + I + D + R) is assumed constant. The virus particles (V) interact with healthy cells and infect them. Infected cells release new virus particles upon their death. Proliferation of healthy cells causes regeneration and decrease in the proportion of dead cells. Dead cells stimulate the activation of APC (M). APC stimulate the production of interferon α and β (F) that interact with healthy cells and convert them to a resistant state. APC also stimulate the proliferation of effector cells (E) that destroy infected cells. Finally, they stimulate the production of plasma cells (P) which, in turn, produce antibodies (A) that neutralize (kills) virus. This neutralization is modulated by the antigenic compatibility (S) between virus and antibodies currently produced by

the organism. S quantifies the affinity between antibodies and virus. These interactions are used in the construction of a system of 10-dimensional ordinary differential equations describing the dynamics of the main variables, which correspond to the components of the immune response.

Stability, sensitivity analysis and numerical simulation was carried and they found that although each component of innate and adaptive immune response contributes to the recovery of HBV infection, the simulations suggest that, in the absence of one component of innate immunity, the remaining two defense mechanisms are sufficient for viral clearance.

Another model of interest to this study was published by Inam et al. (2021). They presented a work on the mathematical analysis of hepatitis B epidemic model with optimal control. The paper described a mathematical model developed to control global HBV problem by education campaign (awareness), vaccination, and treatment. They employed a compartmental model expressed by a set of ordinary differential equations (ODEs) based on the characteristics of of the HBV infection. With regards to the transmission dynamics of HBV.

A lot has been done by several researchers to fathom the spread of HBV in to order to contribute to knowledge, bring its spreads under control, aid decision making and improve livelihood. Come what may, a lot more need be done as we still have many homes that still share household items like cups, spoons, plates, towel, etc. Hence, we have a long way to go in preventing, controlling and eradicating the virus. In order to fathom HBV epidemiology, attempt need be made to incorporate virtually all the key factors that have effect on its transmission but some of the models presented did not capture one or more salient features of the epidemiology of hepatitis B or did not incorporate both the vertical and horizontal mode of transmission and either no vaccination or treatment compartments. Furthermore, some of the researchers that included vaccination either as a compartment or as a strategy forgot that the HBV vaccine does not confer lifelong immunity. As it wane overtime, a proportion of the recovered compartment moves back into the susceptible compartment and become susceptible. In an outbreak of an endemic disease, its difficult for the Government to provide treatment for everyone because of the high cost of treatment, shortage of hospitals to admit all the patients as observed in 2020 during the outbreak of Covid-19 and lack of access to rural areas are few among several reasons. The proportion of people especially children and young adults who are not receiving treatment or does not have access to treatment with higher tendency of having contacts with other members of the population greatly affects the spread of the virus by increasing transmission rate, thereby making it difficult to forestall transmission and eradicate the disease. For this age structure, It is known that they can undergo spontaneous clearance as a result of strong immune response and move to the recovered compartment after some time. This help to reduce the amount of exposure to the virus, lower the cost needed to treat the entire population, and may also help to prevent the transmission of the virus to others. For these reasons, the need to include the two compartments (The adults receiving treatment and the isolated children and young adults) in the epidemiological model of HBV become imperative.

3.0 Methods

We present a mathematical model that involves the integral characteristics of the virus. The model will help to study the epidemiology of the disease, in turn, the results will help in understanding its patterns and there after aid in seeking for the control strategies that will prevent its spread and eradicate the disease.

In our study, we extend the model presented by Inam *et al.* (2021). In extending their work, we included two compartments (Treatment and Exclusion) leading to SLICTER model. Also, we considered the waning effect of HBV vaccine as well as four interventions (Awareness, Vaccination, Reduction in contact rates, Anti-viral treatment and Isolation) for the control strategies. These will help to have a better understanding of the epidemiology of HBV. In using the SLICTER model we divide the host population into seven compartments of individuals: the susceptible compartment (S), the latent compartment (L), the infectious individuals with acute cases compartment (I), the chronic compartment (C), the compartment of individuals that are receiving treatment (T), the compartment of individuals that are not receiving treatment but being isolated, but for the sake of confusion with the (I) compartment, we use (E) to represent this compartment and finally the recovered compartment (R).

The (S) compartment includes individuals that are liable to catch the disease but for time being are disease free. The (L) compartment consists of individuals that have caught the disease due to successful contact with an acute or/and chronic carriers but at present not contagious. The (I) compartment comprises of individuals who have the disease and are contagious. The (T) compartment consists of individuals that are receiving anti-viral treatment. The (E) compartment includes children of above age 5 and young adults that are not receiving anti-viral treatment but being excluded (isolated). The (R) compartment comprises of individuals that have recovered from the disease as a result of anti-viral treatment, spontaneous clearance and vaccinated individuals. So that the total population N(t) at any given time is:

$$N(t) = S(t) + L(t) + I(t) + C(t) + T(t) + E(t) + R(t)$$

The population will be recruited by birth at the rate μ, proportion of birth without vaccination at the rate ω. The parameter v shows the proportion of children who are un-immunized born to infected mothers. As a result of effective awareness campaign we assumed that the newborns are to be successfully immunized at rate $\mu\omega$ or unsuccessfully at rate $\mu(1-\omega)$, the population $\mu\omega vC$ is assumed to enter into the chronic carrier compartment and the rest $\mu\omega(1-vC)$ stays in the susceptible compartment. where β and ε are the disease transmission rates relative to infected individuals in I(t) and C(t) compartments respectively. σ is the transfer rate to the acute (infection) compartment while Ω_1 and Ω_2 are rate of infectious individuals moving to treatment and isolated compartment respectively and θ is the transfer rate to the chronic (infection) compartment. The rate of chronic individuals moving to the treatment and isolated compartment are α_1 and α_2. τ_1 and τ_2 are the recovery rate due to antiviral

treatment and spontaneous clearance respectively. γ is the vaccination rate and λ is the rate of waning of HBV vaccine. μ_0 and μ_1 are the natural mortality rate and the HBV induced death rate. The assumptions made in using the model are:

1. There is no inherited immunity and immunity via vaccine is not lifelong

2. The members of the population mix homogeneously

3. The rate of birth and death are equal.

4. We assume that the people progressing from the infectious class to the chronic class is lower than the sum of the individuals moving to treatment and isolated compartments respectively. Also, the rate of individuals moving out of the chronic compartment is greater than the rate at which individuals moves in. It is equally worthy to note that we assume those receiving treatment and being isolated can die as a result of natural death but not HBV induced death. The figure below represents the flow diagram of the SLICTER model of hepatitis with vital dynamics.

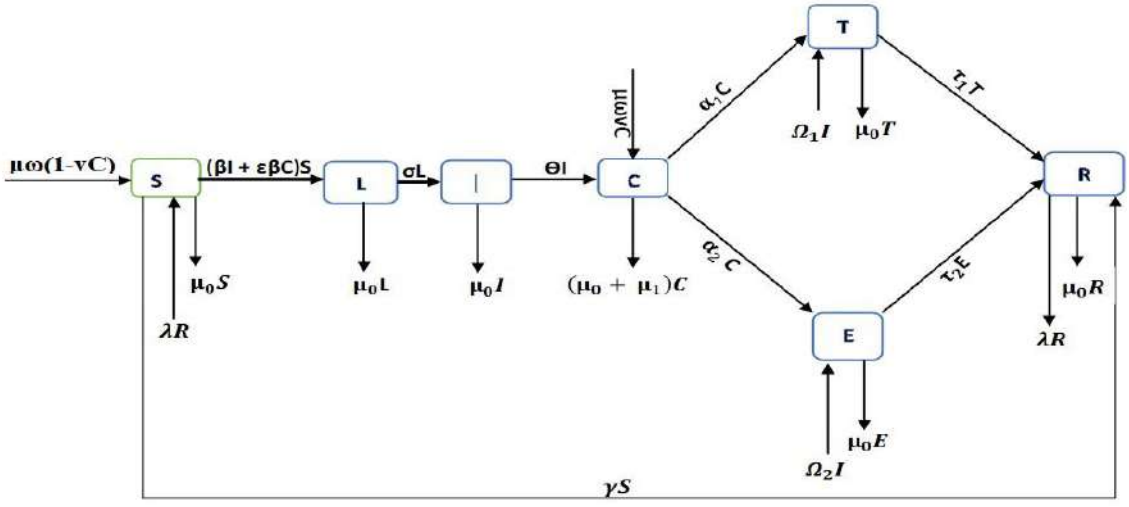

Figure 1: Flow diagram of SLICTER model of HBV with vital dynamics

Based on the descriptions, assumptions and the model flow diagram the following model equations are obtained.

$$\frac{dS}{dt} = \mu\omega(1 - \nu C(t)) + \lambda R(t) - (\mu_0 + \beta I(t) + \varepsilon\beta C(t) + \gamma)S(t) \quad (1)$$

$$\frac{dL}{dt} = (\beta I(t) + \varepsilon\beta C(t))S(t) - (\mu_0 + \sigma)L(t) \quad (2)$$

$$\frac{dI}{dt} = \sigma L(t) - (\mu_0 + \theta + \Omega_1 + \Omega_2)I(t) \quad (3)$$

$$\frac{dC}{dt} = \mu\omega\nu C(t) + \theta I(t) - (\mu_0 + \mu_1 + \alpha_1 + \alpha_2)C(t) \quad (4)$$

$$\frac{dT}{dt} = \Omega_1 I(t) + \alpha_1 C(t) - (\mu_0 + \tau_1)T(t) \quad (5)$$

$$\frac{dE}{dt} = \Omega_2 I(t) + \alpha_2 C(t) - (\mu_0 + \tau_2)E(t) \quad (6)$$

$$\frac{dR}{dt} = \tau_1 T(t) + \tau_2 E(t) + \gamma S(t) - (\mu_0 + \lambda)R(t) \quad (7)$$

Combining the equations above give the system of HBV dynamics equations below.

$$\begin{cases} \frac{dS}{dt} = \mu\omega(1 - \nu C(t)) + \lambda R(t) - (\mu_0 + \beta I(t) + \varepsilon\beta C(t) + \gamma)S(t) \\ \frac{dL}{dt} = (\beta I(t) + \varepsilon\beta C(t))S(t) - (\mu_0 + \sigma)L(t) \\ \frac{dI}{dt} = \sigma L(t) - (\mu_0 + \theta + \Omega_1 + \Omega_2)I(t) \\ \frac{dC}{dt} = \mu\omega\nu C(t) + \theta I(t) - (\mu_0 + \mu_1 + \alpha_1 + \alpha_2)C(t) \\ \frac{dT}{dt} = \Omega_1 I(t) + \alpha_1 C(t) - (\mu_0 + \tau_1)T(t) \\ \frac{dE}{dt} = \Omega_2 I(t) + \alpha_2 C(t) - (\mu_0 + \tau_2)E(t) \\ \frac{dR}{dt} = \tau_1 T(t) + \tau_2 E(t) + \gamma S(t) - (\mu_0 + \lambda)R(t) \end{cases} \quad (8)$$

With the initial conditions S(0) = $S_0 > 0$, L(0) = $L_0 \geq 0$, I(0) = $I_0 \geq 0$, C(0) = $C_0 \geq 0$, T(0) = $T_0 \geq 0$, E(0) = $E_0 \geq 0$, R(0) = $R_0 \geq 0$.

3.1 Model Analysis

3.1.1 *Positivity and Boundedness of solutions*

Theorem 1. Let $\pi(0)$ = (S(0), L(0), I(0), C(0), T(0), E(0), R(0))$\in R_+^7$ be the initial condition for model (8). Hence, the set of solutions { S(t), L(t), I(t), C(t), T(t), E(t), R(t)} is non negative for all t > 0 and N $\leqslant \frac{\mu\omega}{\mu_0}$.

Proof: Let $t_1 = \sup \{t > 0 : S(t_0) > 0, L(t_0) > 0, I(t_0) > 0, C(t_0) > 0, T(t_0) > 0, E(t_0) > 0, R(t_0) > 0, \forall t_0 \in [0,t] \}$. Since S(0), L(0), I(0), C(0), T(0), E(0) and R(0) are all non negative then $t_1 > 0$. If $t_1 < \infty$, using the variation of the constant formula of the first equation of model (1) at t_1 we have;

$$\frac{dS}{dt} = \mu\omega(1 - \nu C(t)) + \lambda R(t) - (\mu_0 + \beta I(t) + \varepsilon\beta C(t) + \gamma)S(t).$$

This is linear and can be written as;

$$\frac{dS}{dt} = (\mu_0 + \beta I(t) + \varepsilon\beta C(t) + \gamma)S(t) = \mu\omega(1 - \nu C(t)) + \lambda R(t) \tag{9}$$

with IF = eR $(\mu 0+\beta I(t)+\varepsilon\beta C(t)+\gamma)dt$ multiplying both sides of (9) by IF

and rearranging we have;

$$\frac{d}{dt}\left[S(t)e^{(\mu_0+\gamma)t+\int_0^t \chi(y)dy}\right] = \left[\mu\omega(1 - \nu C(t)) + \lambda R(t)\right] e^{(\mu_0+\gamma)+\int_0^t \chi(y)dy}, \tag{10}$$

Therefore,

$$S(t_1)e^{(\mu_0+\gamma)t_1+\int_0^{t_1} \chi(y)dy} - S(0) = \int_0^{t_1} [\mu\omega(1 - \nu C(r)) + \lambda R(r)] \cdot \left[e^{(\mu_0+\gamma)r+\int_0^r \chi(y)dy}\right] dr \tag{11}$$

Hence,

$$S(t_1) = S(0)e^{(-\mu_0-\gamma)t_1-\int_0^{t_1} \chi(y)dy} + \left[e^{(-\mu_0-\gamma)t_1-\int_0^{t_1} \chi(y)dy}\right] \int_0^{t_1} \mu\omega(1 - \nu C(r)) + \lambda R(r) \left[e^{(\mu_0+\gamma)r+\int_0^r \chi(y)dy}\right] dr \geqslant 0 \tag{12}$$

We can go on to prove for other state variables using the same approach for any time t_1, that each state variable satisfy the initial condition as in the case of S above. Furthermore, we show that the region denoted by the set $\pi(t)$ is positively invariant for the formulated HBV transmission model (8) with $\pi(t) \geqslant 0 \in R_+^7$

From (8) we obtain,

$$\frac{dN}{dt} = \mu\omega - \mu_0 N - \mu_1 C(t) \tag{13}$$

But μ_1 and the state variable C are positive in (8), thus, we have;

$$\frac{dN}{dt} = \mu\omega - \mu_0 N \tag{14}$$

Since (14) is linear, solving by the use of integrating factor and using the initial condition N(0) = N_0 we have;

$$N \leqslant \frac{\mu\omega}{\mu_0} - \frac{1}{\mu_0}(\mu\omega - \mu_0 N_0)e^{-\mu t} \tag{15}$$

Conclusively, we have $N(t) \to \frac{\mu\omega}{\mu_0}$ as $t \to \infty$, This means that $0 < N \leqslant \frac{\mu\omega}{\mu_0}$. Furthermore, if $N > \frac{\mu\omega}{\mu_0}$, then the solution either enter $\pi(t)$ in a finite time or N(t) approaches. So, it can be concluded that $\pi(t)$ attracts all the solutions in R_+^7 and hence all the properties are being hold for the system become positive invariant (This means that the state of the system is in the positive state at any time t, and will remain in that state for all future times), unique and bounded in the region by $\pi(t)$. Thus, given certain constraints, the feasible region or state space of the system is;

$$\pi = \{(S, L, I, C, T, E, R) \in R_+^7 : 0 < N \leqslant \frac{\mu\omega}{\mu_0}\} \tag{16}$$

3.2 Disease-Free Equilibrium

We will have a disease free equilibrium when there is no case of HBV infection and to solve for the equilibrium points, we equate RHS of (8) to 0 as we have in (17).

$$\begin{cases} \mu\omega(1-\nu C(t)) + \lambda R(t) - (\mu_0 + \beta I(t) + \varepsilon\beta C(t) + \gamma)S(t) = 0 \\ (\beta I(t) + \varepsilon\beta C(t))S(t) - (\mu_0 + \sigma)L(t) = 0 \\ \sigma L(t) - (\mu_0 + \theta + \Omega_1 + \Omega_2)I(t) = 0 \\ \mu\omega\nu C(t) + \theta I(t) - (\mu_0 + \mu_1 + \alpha_1 + \alpha_2)C(t) = 0 \\ \Omega_1 I(t) + \alpha_1 C(t) - (\mu_0 + \tau_1)T(t) = 0 \\ \Omega_2 I(t) + \alpha_2 C(t) - (\mu_0 + \tau_2)E(t) = 0 \\ \tau_1 T(t) + \tau_2 E(t) + \gamma S(t) - (\mu_0 + \lambda)R(t) = 0 \end{cases} \quad (17)$$

Solving equation (17) for DFE points and noting that in the absence of HBV disease, L=I=C=T=E=0. We have the disease free equilibrium points denoted by; $D_0 = (S^0, L^0, I^0, C^0, T^0, E^0, R^0)$ as:

$$D_0 = \left\{ \frac{\mu\omega(\mu_0 + \lambda)}{(\mu_0 + \gamma)(\mu_0 + \lambda) - \gamma\lambda}, 0, 0, 0, 0, 0, \frac{\gamma\mu\omega}{(\mu_0 + \gamma)(\mu_0 + \lambda) - \gamma\lambda} \right\} \quad (18)$$

The Basic Reproductive Number R_0^{HBV}

The basic reproductive number of hepatitis B virus epidemiological threshold is represented by the symbol $R_0^{HBV} = \rho F V^{-1}$, and ρ denotes the dominant eigenvalue, F and V are the new infection and transmission term respectively. To derive the expression in terms of parameters for the of the system (8), we have;

$$R_0^{HBV}$$

$$F = \begin{bmatrix} (\beta I + \varepsilon\beta C)S \\ 0 \\ 0 \\ 0 \end{bmatrix}, V = \begin{bmatrix} (\beta I(t) + \varepsilon\beta C(t))S(t) - (\mu_0 + \sigma)L(t) \\ \sigma L(t) - (\mu_0 + \theta + \Omega_1 + \Omega_2)I(t) \\ \mu\omega\nu C(t) + \theta I(t) - (\mu_0 + \mu_1 + \alpha_1 + \alpha_2)C(t) \end{bmatrix}$$

$$F^* = S^0 \begin{bmatrix} 0 & \beta & \varepsilon\beta \\ 0 & 0 & 0 \\ 0 & 0 & 0 \end{bmatrix},$$

$$V^* = \begin{bmatrix} -(\mu_0 + \sigma) & 0 & 0 \\ \sigma & -(\mu_0 + \theta + \Omega_1 + \Omega_2) & 0 \\ 0 & \theta & \mu\omega\nu - (\mu_0 + \mu_1 + \alpha_1 + \alpha_2) \end{bmatrix}$$

At hepatitis B DFE, the Jacobian matrices for F and V are evaluated giving the following,

re $\Lambda = \mu_0 + \theta + \Omega_1 + \Omega_2, \Xi = \mu_0 + \mu_1 + \alpha_1 + \alpha_2$. Then we have;

$$FV^{-1} = \begin{bmatrix} \frac{\beta\sigma(\varepsilon\theta+\Xi-\mu\omega\nu)S^0}{\Lambda(\mu_0+\sigma)(\mu\omega\nu-\Xi)} & \frac{\beta(\mu\omega\nu-\Xi-\varepsilon\theta)S^0}{\Lambda(\mu\omega\nu-\Xi)} & \frac{\beta\varepsilon S^0}{\mu\omega\nu-\Xi} \\ 0 & 0 & 0 \\ 0 & 0 & 0 \end{bmatrix}$$

(20)

The largest absolute value (spectral radius) of the eigenvalues of the matrix (20) gives the basic reproductive number ;

$$R_0^{HBV} = \frac{\beta\sigma\mu\omega(\mu_0+\lambda)(\varepsilon\theta+\Xi-\mu\omega\nu)}{\Lambda(\mu_0+\sigma)(\Xi-\mu\omega\nu)(\mu_0+\gamma)(\mu_0+\lambda)-\gamma\lambda)} \tag{21}$$

Where $\Lambda(\mu_0+\sigma)(\Xi-\mu\omega\nu)(\gamma\lambda+(\mu_0+\gamma)(\mu_0+\lambda)) > 0$, (21) embodies the average number of secondary infections caused by an acute and/or chronic patient when introduced into the susceptible population.

Theorem 2. If $R_0^{HBV} < 1$ then the equilibrium point D_0 is locally asymptotically stable otherwise unstable if $R_0^{HBV} > 1$.

$$J_{D_0} = \begin{bmatrix} -\mu_0-\gamma & 0 & -\beta S^0 & -\mu\omega\nu-\varepsilon\beta S^0 & 0 & 0 & 0 \\ 0 & -\mu_0-\sigma & \beta S^0 & \varepsilon\beta S^0 & 0 & 0 & 0 \\ 0 & \sigma & -\Lambda & 0 & 0 & 0 & 0 \\ 0 & 0 & \theta & \mu\omega\nu-\Xi & 0 & 0 & 0 \\ 0 & 0 & \Omega_1 & \alpha_1 & -\mu_0-\tau_1 & 0 & 0 \\ 0 & 0 & \alpha_2 & \Omega_2 & 0 & -\mu_0-\tau_2 & 0 \\ \gamma & 0 & 0 & 0 & \tau_1 & \tau_2 & -\mu_0-\lambda \end{bmatrix} \tag{22}$$

Proof:

The desired Jacobian matrix J_{D0} of the model (8) at DFE is;

By expanding the determinant of the characteristic equation $|J(D_0)-\lambda| = 0$, we obtained $\lambda_1 = -\mu_0-\gamma < 0, \lambda_2 = -\mu_0-\tau_1 < 0, \lambda_3 = -\mu_0-\tau_2 < 0, \lambda_4 = -\mu_0-\tau_2 < 0$, The remaining three eigenvalues are eigenvalues of

$$J_{D_1} = \begin{bmatrix} -\mu_0 - \sigma & \beta S^0 & \varepsilon\beta S^0 \\ \sigma & -\Lambda & 0 \\ 0 & \theta & \mu\omega\nu - \Xi \end{bmatrix} \tag{23}$$

Again, by expanding the determinant of the characteristic equation $|JD_1|$ we have the characteristic polynomial;

Where;

$K_1 = \Lambda + \sigma + \mu_0 + \xi - \mu\omega\nu,$

$K_2 = \Xi\Lambda + \Xi\sigma + \Xi\mu_0 + \Lambda\sigma + \Lambda\mu_0 - \beta\sigma S^0 - \Lambda\mu\omega\nu - \mu\omega\nu\sigma - \mu\omega\nu\mu_0$ and

$K_3 = \Xi\Lambda\sigma + \Xi\Lambda\mu_0 + \beta\mu\nu\omega\sigma S^0 - \varepsilon\sigma\theta S^0 - \Xi\beta\sigma S^0 - \Lambda\mu\omega\nu\sigma - \Lambda\omega\nu\mu\mu_0$

$$\lambda^3 + K_1\lambda^2 + K_2\lambda + K_3 = 0 \tag{24}$$

The characteristic polynomial in (24) follows the Routh-Hurwitz criteria where the associated Hurwiz matrito (24) is;

$$\begin{bmatrix} K_1 & K_3 & 0 \\ 1 & K_2 & 0 \\ 0 & K_1 & K_3 \end{bmatrix} \tag{25}$$

Comparing (24) with the polynomial $P(\lambda) = P_n\lambda^n + P_{n-1}\lambda^{n-1} + +P_{n-2}\lambda^{n-2} + P_0$ for n = 3, $P_3 = 1$, $P_2 = K_1, P_1 = K_2, P_0 = K_3$. The necessary and sufficient condition for the polynomial to have roots with negative real part are;

(i). $(P_3)^1 D_1 > 0, \Rightarrow K_1 > 0$

(ii). $(P_3)^2 D_2 > 0, \Rightarrow K_1K_2 > K_3,$

(iii). $(P_3)^3 D_3 > 0, \Longrightarrow K_1K_2K_3 - K_3^2 > 0, \Longrightarrow K_3 > 0$

Hence, it suffices to conclude that the DFE is locally asymptotically stable if $R_0^{HBV} > 1$ and the necessary Routh-Hurwitz conditions are met otherwise its unstable.

Theorem 3. If $R_0^{HBV} < 1$ then the equilibrium point D_0 is globally asymptotically stable otherwise unstable if $R_0^{HBV} > 1$.

Proof: The Lyapunov function defined below will be used to prove the theorem.

$$V(t) = (S - S^0 - R^0) + L + I + C + T + E + R \tag{26}$$

Differentiating equation (26) and using model (8) we obtain; $\frac{dV}{dt} = \frac{dS}{dt} + \frac{dL}{dt} + \frac{dI}{dt} + \frac{dC}{dt} + \frac{dT}{dt} + \frac{dE}{dt} + \frac{dR}{dt}$

$$\frac{dV}{dt} = \mu\omega - \mu_0 N - \mu_1 C$$

$$\frac{dV}{dt} = \frac{-[\gamma\lambda+(\mu_0+\gamma)(\mu_0+\lambda)](S-S^0-R^0)}{\gamma-\mu_0-\lambda} - \mu_0 N - \mu_1 C$$

$$\frac{dV}{dt} = -[\frac{(\gamma\lambda+(\mu_0+\gamma))(\mu_0+\lambda)(S-S^0-R^0)}{\gamma-\mu_0-\lambda} + \mu_0 N + \mu_1 C] < 0$$

Therefore, $\frac{dV}{dt} < 0$ if $R_0^{HBV} < 1$. Hence, by the well known LaSalle's invariant principle, we conclude that the point D_0 is globally asymptotically stable.

3.4. Endemic Equilibrium

The endemic equilibrium point is the point where the system (8) settle down into a steadystate where the virus exists in the population. This is denoted by $D_0^* =$

$(S^*, L^*, I^*, C^*, T^*, E^*, R^*)$.

Expressing the other state variables in terms of I^* From (8) we obtain;

$$\begin{cases} S^* = \frac{a_2a_3a_4\mu\omega a_1\gamma\nu\theta I^*+\gamma\lambda\tau_1\Omega_1[(a_1+\alpha_1\theta)I^*]+a_2\tau_2\Omega_2(a_1+\alpha_2\theta)I^*}{a_1a_2a_3a_4[(a_1a_5+\varepsilon\beta\theta I^*)-a_1a_2a_3]} \\ L^* = \frac{\beta a_2a_3a_4\mu\omega(a_1I^*+\varepsilon)(a_1-\gamma\nu\theta I^*)+\gamma\lambda\{\tau_1\Omega_1(a_1+\alpha_1\theta)+a_2\tau_2\Omega_2(a_1+\alpha_2\theta)\}I^*}{a_1^2a_2a_3a_4a_6[(a_1a_5+\varepsilon\beta\theta I^*)-a_1a_2a_3]} \\ C^* = \frac{\theta I^*}{a_1} \\ T^* = \frac{\Omega_1(a_1+\alpha_1\theta)I^*}{a_1a_2} \\ E^* = \frac{\Omega_2(a_1+\alpha_2\theta)I^*}{a_1a_3} \\ R^* = \frac{a_3\tau_1\Omega_1[(a_1+\alpha\theta)I^*]+a_2\tau_2\Omega_2[(a_1+\alpha_2\theta)I^*]+a_1a_2a_3\gamma S^*}{a_1a_2a_3a_4} \end{cases} \quad (27)$$

$a_1 = \Xi - \mu\omega\nu, a_2 = \mu_0 + \tau_1, a_3 = \mu_0 + \tau_2, a_4 = \mu_0 + \lambda, a_5 = \mu_0 + \beta I, a_6 = \mu_0 + \sigma.$

Substituting the expression of L^* above into the third equation of system (8), we obtain;

$I^* = \frac{-B\pm\sqrt{B^2-4AC}}{2A}$

Where;

$$A = (\varepsilon\theta + a_1)(a_1a_2a_3a_4\beta\theta)(\Lambda\epsilon a_1a_5a_6 + \gamma\sigma\mu\omega\nu),$$

$$B = (\varepsilon\theta + a_1)\{\Lambda a_1^3a_2a_3a_4a_6(a_5 - a_2a_3) + \sigma\beta a_2a_3a_4\mu\omega(\varepsilon\gamma\nu\theta - a_1^2) - \gamma\lambda[a_1\tau_1\Omega_1(1+\theta) + a_2\tau_2\Omega_2(a_1 + \alpha_2\theta)]\},$$

$$C = \Lambda\varepsilon a_1^2a_2a_3a_6[\gamma\lambda + a_4(\mu_0 + \gamma)]R_0^{HBV}$$

Theorem 4. If $R_0^{HBV} > 1$ then the endemic equilibrium point D_0^* is locally asymptotically stable otherwise unstable.

Proof: To check for the possibility whether system (8) exhibits a backward or forward bifurcation or possibly a bi-stable endemic equilibrium states, we adopt the following method:

$$\begin{cases} S = x_1, L = x_2, I = x_3, C = x_4, T = x_5, E = x_6, R = x_7 \end{cases} \quad (28)$$

Therefore, system (8) is transformed as;

$$\begin{cases} \frac{dx_1}{dt} &= \mu\omega(1-\nu x_4) + \lambda x_7 - (\mu_0 + \beta x_3 + \varepsilon\beta x_4 + \gamma)x_1 \\ \frac{dx_2}{dt} &= (\beta x_3 + \varepsilon\beta x_4)x_1 - (\mu_0 + \sigma)x_2 \\ \frac{dx_3}{dt} &= \sigma x_2 - (\mu_0 + \theta + \Omega_1 + \Omega_2)x_3 \\ \frac{dx_4}{dt} &= \mu\omega\nu x_4 + \theta x_3 - (\mu_0 + \mu_1 + \alpha_1 + \alpha_2)x_4 \\ \frac{dx_5}{dt} &= \Omega_1 x_3 + \alpha_1 x_4 - (\mu_0 + \tau_1)x_5 \\ \frac{dx_6}{dt} &= \Omega_2 x_3 + \alpha_2 x_4 - (\mu_0 + \tau_2)x_6 \\ \frac{dx_7}{dt} &= \tau_1 x_5 + \tau_2 x_6 + \gamma x_1 - (\mu_0 + \lambda)x_7 \end{cases} \tag{29}$$

We choose β as the bifurcation parameter and solving for $\beta^* = \beta$ in (21) when $R_0^{HBV} = 1$we obtain;

$$\beta^* = \frac{\Lambda(\mu_0 + \sigma)a_1}{\sigma(\varepsilon\theta + a_1)S^0} \tag{30}$$

$$J_{D_0,\beta^*} = \begin{bmatrix} -p_1 & 0 & -\beta S^0 & -p_2 & 0 & 0 & 0 \\ 0 & -p_3 & \beta S^0 & p_8 & 0 & 0 & 0 \\ 0 & \sigma & -\Lambda & 0 & 0 & 0 & 0 \\ 0 & 0 & \theta & p_4 & 0 & 0 & 0 \\ 0 & 0 & \Omega_1 & \alpha_1 & -p_5 & 0 & 0 \\ 0 & 0 & \alpha_2 & \Omega_2 & 0 & -p_6 & 0 \\ \gamma & 0 & 0 & 0 & \tau_1 & \tau_2 & -p_7 \end{bmatrix} \tag{31}$$

$p_1 = \mu_0 + \gamma, p_2 = \mu\omega\nu + \varepsilon\beta S^0, p_3 = \mu_0 + \sigma, p_4 = \mu\omega\nu - \Xi, p_5 = \mu_0 + \tau_1, p_6 = \mu_0 + \tau_2, p_7 = \mu_0 + \lambda, p_8 = \varepsilon\beta S^0.$

We linearize the system (29) around the disease-free equilibrium when $\beta^* = \beta$ and obtained;

The center manifold theory will be used to analyze the dynamic of the system (29) near $\beta = \beta^*$ because of its simple zero eigenvalues. In addition, we obtain the left and the right eigenvectors of J_{D0,β^*} associated with the zero eigenvalue. The right eigenvector is given by;

$W = (w_1, w_2, w_3, w_4, w_5, w_6, w_7)$. From (31) we have;

$$\begin{bmatrix} -p_1 & 0 & -\beta^* S^0 & -p_2 & 0 & 0 & 0 \end{bmatrix} \begin{bmatrix} w_1 \end{bmatrix} \quad \begin{bmatrix} 0 \end{bmatrix}$$

From (32) we have the

$$\begin{cases} -p_1 w_1 - \beta^* S^0 w_3 - p_2 w_4 = 0, \\ -p_3 w_2 + \beta^* S^0 w_3 + p_8 w_4 = 0 \\ \sigma w_2 - \Lambda w_3 = 0 \\ \theta w_3 + p_4 w_4 = 0 \\ \Omega_1 w_3 + \alpha_1 w_4 - p_5 w_5 = 0 \\ \alpha_2 w_3 + \Omega_2 w_4 - p_6 w_6 = 0 \\ \gamma w_1 + \tau_1 w_5 + \tau_2 w_6 - p_7 w_7 = 0 \end{cases} \tag{33}$$

following equations;

From (33),

$$w_1 = \frac{((\mu\omega\nu - \Xi)\beta^* S^0 + (\mu\omega\nu + \varepsilon\beta^* S^0))w_3}{(\mu_0 + \gamma)(\mu\omega\nu - \Xi)}$$

$$w_2 = \frac{\{\varepsilon\theta - \mu\omega\nu + \Xi\}\beta^* S^0 w_3}{(\mu\omega\nu - \Xi)(\mu_0 + \sigma)},$$

$$w_3 = w_3 > 0,$$

$$w_4 = -\frac{\theta w_3}{\mu\omega\nu - \Xi},$$

$$w_5 = \frac{\{\theta\alpha_1 - \Omega_1(\mu\omega\nu - \Xi)\}w_3}{(\mu\omega\nu - \Xi)(\mu_o + \tau_1)},$$

$$w_6 = \frac{\alpha_2\{\mu\omega\nu - \Xi - \theta\Omega_2\}w_3}{(\mu\omega\nu - \Xi)(\mu_2 + \tau_2)},$$

$$w_7 = \frac{\{-(\mu\omega\nu + \Xi)p_5p_6p_7(\mu\omega\nu + \Xi)\beta^* S^0 + p_6p_7p_1(\theta\alpha_1 - \Omega_1 p_4) + p_1p_5p_7\alpha_2(p_4 - \theta\Omega_2\}w_3}{p_1p_4p_5p_6p_7}$$

,

Let $G = (g_1, g_2, g_3, g_4, g_5, g_6, g_7)^T$ be the left eigenvector associated with the zero eigenvalue

$$J_{D_0,\beta^*} = \begin{bmatrix} -p_1 & 0 & 0 & 0 & 0 & 0 & \gamma \\ 0 & -p_3 & \sigma & 0 & 0 & 0 & 0 \\ -\beta^* S^0 & \beta^* S^0 & -\Lambda & \theta & \Omega_1 & \alpha_2 & 0 \\ -p_2 & p_8 & 0 & p_4 & \alpha_1 & \Omega_2 & 0 \\ 0 & 0 & 0 & 0 & -p_5 & 0 & \tau_2 \\ 0 & 0 & 0 & 0 & 0 & -p_6 & \tau_2 \\ 0 & 0 & 0 & 0 & 0 & 0 & -p_7 \end{bmatrix} \begin{bmatrix} g_1 \\ g_2 \\ g_3 \\ g_4 \\ g_5 \\ g_6 \\ g_7 \end{bmatrix} = \begin{bmatrix} 0 \\ 0 \\ 0 \\ 0 \\ 0 \\ 0 \\ 0 \end{bmatrix} \tag{34}$$

of $J_{D0,\beta*}$, and we have;

$$\begin{cases} -p_1 g_1 + \gamma g_7 = 0, \\ -p_3 g_2 + \sigma g_3 = 0 \\ -\beta^* S^0 g_1 + \beta^* S^0 g_2 - \Lambda g_3 + \theta g_4 + \Omega_1 g_5 + \alpha_2 g_6 = 0 \\ -p_2 g_1 + p_8 g_2 + p_4 g_4 + \alpha_1 g_5 + \Omega_1 g_6 = 0 \\ -p_5 g_5 + \tau_2 g_7 = 0 \\ -p_6 g_6 + \tau_2 g_7 = 0 \\ -p_7 g_7 = 0 \end{cases} \tag{35}$$

From (34) we have the following equations;

Solving system (35) above yields;

$$G = \left(0, \frac{\sigma g_3}{\mu_0+\sigma}, g_3, \frac{\Lambda g_3}{\varepsilon\theta+\Xi-\mu\omega\nu}, 0, 0, 0\right), \; g_3 > 0.$$

By the property W · V = 1, we can find the expressions for w_3 and g_3 that satisfies the equality if we choose;

$w_3 = 1$ and

$$g_3 = \frac{(\varepsilon\theta+\Xi-\mu\omega\nu)(\mu_0+\sigma)^2(\mu\omega\nu-\Xi)}{(\varepsilon\theta+\Xi-\mu\omega\nu)(\Xi-\mu\omega\nu)\Lambda+(\mu_0+\sigma)(\mu\omega\nu-\Xi)(\varepsilon\theta+a_1)-\theta\Lambda(\mu_0+\sigma)}$$

Now, we proceed to obtain the associated bifurcation parameters, a and b,which are defined

as;

$$\begin{aligned} a &= \sum_{k,j,i=1}^{7} w_k g_i g_j \frac{\partial^2 f_k(D_0)}{\partial x_i \partial x_j} \quad , \\ b &= \sum_{k,i=1}^{7} w_k g_i \frac{\partial^2 f_k(D_0)}{\partial x_i \partial \beta^*} \end{aligned} \tag{36}$$

Where,

e associated bifurcation coefficients a and b, we obtain the non-vanishing partial derivatives of model system (37) evaluated at disease free equilibrium (D_0). Hence, it follows that;

$$\begin{aligned} a =& w_1 g_1 g_3 \frac{\partial^2 f_1}{\partial x_1 \partial x_3}(D_0) + w_1 g_1 g_4 \frac{\partial^2 f_1}{\partial x_1 \partial x_4}(D_0) + w_2 g_1 g_3 \frac{\partial^2 f_2}{\partial x_1 \partial x_3}(D_0) \\ &+ w_2 g_1 g_4 \frac{\partial^2 f_2}{\partial x_1 \partial x_4}(D_0) \\ b =& w_1 g_1 \frac{\partial^2 f_1}{\partial x_1 \partial \beta^*}(D_0) + w_2 g_1 \frac{\partial^2 f_1}{\partial x_1 \partial \beta^*}(D_0) \end{aligned} \tag{38}$$

Therefore, $a = 0$, $b = 0$ and since the bifurcation coefficients are both zero, it indicates that system (8) exhibits a bi-stability endemic equilibrium states. This means that the system can exist in a stable state with a low prevalence if the number of individuals with HBV immunity is large, therefore can keep the virus in a low state, or stable state with a high prevalence if the number of individuals with immunity is very low. Hence, we conclude that the endemic equilibrium point D_0^* is locally asymptotically stable when R_0^{HBV} crosses the

threshold$R_0^{HBV} = 1$.

3.5 *Permanence of the System*

A system is said to be permanent if it can maintain itself or does not die out over time. For if system (8) is a weak permanence system, the endemic equilibrium may be unstable or non-existent when perturbed from the equilibrium. At the other hand, if system (8) is a strong permanence system, the endemic equilibrium will be stable over time due to any

perturbation.

We assumed that system (8) is a strong permanence system if there are constants $M_1, m_1 > 0$ such that for each positive solution of (S(t), L(t), I(t), C(t), T(t), E(t), R(t)) of system (8) with initial conditions $S(0) = S_0 > 0$, $L(0) = L_0 > 0$, $I(0) = I_0 > 0$, $C(0) = C_0 > 0$, $T(0) = T_0 >$

0, $E(0) = E_0 > 0$, $R(0) = R_0 > 0$ satisfies;

$$M_1 \geqslant \lim_{t\to+\infty} SupS(t) \geqslant \lim_{t\to+\infty} InfS(t) \geqslant m_1$$

$$M_1 \geqslant \lim_{t\to+\infty} SupL(t) \geqslant \lim_{t\to+\infty} InfL(t) \geqslant m_1$$

$$M_1 \geqslant \lim_{t\to+\infty} SupI(t) \geqslant \lim_{t\to+\infty} InfI(t) \geqslant m_1$$

$$M_1 \geqslant \lim_{t\to+\infty} SupC(t) \geqslant \lim_{t\to+\infty} InfC(t) \geqslant m_1$$

$$M_1 \geqslant \lim_{t\to+\infty} SupT(t) \geqslant \lim_{t\to+\infty} InfT(t) \geqslant m_1$$

$$M_1 \geqslant \lim_{t\to+\infty} SupE(t) \geqslant \lim_{t\to+\infty} InfE(t) \geqslant m_1$$

$$M_1 \geqslant \lim_{t\to+\infty} SupR(t) \geqslant \lim_{t\to+\infty} InfR(t) \geqslant m_1$$

3.6 The Herd Immunity Threshold (V_c)

In a large population of individuals where there is an outbreak of HBV, if a large enough number of individuals have immunity, then the incidence of HBV will reduce. Hence, the possibilities that a chain of HBV transmission will be interrupted is very high, resulting in a self-contained, small outbreaks that will die out quickly. Thus, individuals that are not immune will be protected by the wall that is set up by the vaccinated ones. The herd immunity threshold (V_c) is the percentage of the population that needs to be immune to control transmission of HBV. Paul et al. (2011), used an equation for estimating the herd immunity threshold. The equation, in terms of HBV basic reproductive number is given as;

$$V_c = 1 - \frac{1}{R_0^{HBV}}$$

Where V_c is the critical vaccination level. Therefore, we have;

$$V_c = \frac{\beta\sigma\mu\omega(\mu_0+\lambda)(\varepsilon\theta+\Xi-\mu\omega\nu)-\Lambda(\mu_0+\sigma)(\Xi-\mu\omega\nu)(\gamma\lambda+(\mu_0+\gamma)(\mu_0+\lambda))}{\beta\sigma(\varepsilon\theta+\Xi-\mu\omega\nu)}$$

(39)

As the amount of HBV vaccination increases, the herd immunity threshold increases. This means that the level of HBV vaccination is directly proportional to the herd immunity thresh-

old.

4.0 Results and Discussion

4.1 *Sensitivity Analysis*

Here, we present the sensitivity of the parameters involved in theR_0^{HBV} of model (8). It will help to know which of the parameters have significant impact on the spread of HBV. To calculate the sensitivity index of any given parameter say ρ, we use;

$$\Psi_{\rho}^{R_0^{HBV}} = \left(\frac{\partial R_0^{HBV}}{\partial \rho}\right)\left(\frac{\rho}{R_0^{HBV}}\right) \tag{40}$$

Hence, the sensitivity index peculiar to each parameter in$R_0^{HBV}$is calculated as follows:

$$
\begin{aligned}
\Psi_{\beta}^{R_0^{HBV}} &= 1, \\
\Psi_{\sigma}^{R_0^{HBV}} &= \frac{\mu_0}{\mu_0+\sigma}, \\
\Psi_{\mu}^{R_0^{HBV}} &= \frac{(\Xi-\mu\omega\nu)(\epsilon\theta+\Xi-\mu\omega\nu)+\mu\omega\nu(\varepsilon\theta+2\Xi-2\mu\omega\nu)}{(\Xi-\mu\omega\nu)(\varepsilon\theta+\Xi-\mu\omega\nu)}, \\
\Psi_{\omega}^{R_0^{HBV}} &= \frac{(\Xi-\mu\omega\nu)(\varepsilon\theta+\Xi-\mu\omega\nu)+\mu\omega\nu(\varepsilon\theta+2\Xi-2\mu\omega\nu)}{(\Xi-\mu\omega\nu)(\varepsilon\theta+\Xi-\mu\omega\nu)} \\
\Psi_{\varepsilon}^{R_0^{HBV}} &= \frac{\varepsilon\theta}{\Xi-\mu\omega\nu}, \\
\Psi_{\theta}^{R_0^{HBV}} &= \frac{\Lambda\varepsilon\theta-\theta(\varepsilon\theta+\Xi-\mu\omega\nu)}{\Lambda(\varepsilon\theta\Xi-\mu\omega\nu)}, \\
\Psi_{\nu}^{R_0^{HBV}} &= \frac{\mu\omega\nu}{(\Xi-\mu\omega\nu)(\varepsilon\theta+\Xi-\mu\omega\nu)}, \\
\Psi_{\mu_1}^{R_0^{HBV}} &= \frac{-\mu_1\varepsilon\theta}{(\Xi-\mu\omega\nu)(\varepsilon\theta+\Xi-\mu\omega\nu)}, \\
\Psi_{\gamma}^{R_0^{HBV}} &= \frac{-\gamma\mu_0}{(\mu_0+\gamma)(\mu_0+\lambda)-\gamma\lambda}, \\
\Psi_{\Omega_1}^{R_0^{HBV}} &= \frac{-\Omega_1}{\Lambda}, \\
\Psi_{\Omega_2}^{R_0^{HBV}} &= \frac{-\Omega_2}{\Lambda}, \\
\Psi_{\alpha_1}^{R_0^{HBV}} &= \frac{-\alpha_1\varepsilon\theta}{(\Xi-\mu\omega\nu)(\varepsilon\theta+\Xi-\mu\omega\nu)}, \\
\Psi_{\alpha_2}^{R_0^{HBV}} &= \frac{-\alpha_2\varepsilon\theta}{(\Xi-\mu\omega\nu)(\varepsilon\theta\Xi-\mu\omega\nu)}, \\
\Psi_{\lambda}^{R_0^{HBV}} &= \frac{\lambda(((\mu_0+\gamma)(\mu_0+\lambda)-\gamma\lambda)-\mu_0(\mu_0+\lambda)}{(\mu_0+\lambda)((\mu_0+\gamma)(\mu_0+\lambda)-\gamma\lambda)} \\
\Psi_{\mu_0}^{R_0^{HBV}} &= \Delta_1-\Delta_2-\Delta_3
\end{aligned}
$$

Where

$$
\begin{aligned}
\Delta_1 &= \frac{\mu_0(\varepsilon\theta+\Xi+\mu_0+\lambda-\mu\omega\nu)}{(\mu_0+\lambda)(\varepsilon\theta+\Xi-\mu\omega\nu)} \\
\Delta_2 &= \frac{\mu_0(\Lambda+\sigma+\mu_0)}{\Lambda(\mu_0+\sigma)} \\
\Delta_3 &= \frac{\mu_0(\Xi-\mu\omega\nu)(2\mu_0+\gamma+\lambda)+((\mu_0+\gamma)(\mu_0+\lambda)-\gamma\lambda)}{((\mu_0+\gamma)(\mu_0+\lambda)-\gamma\lambda)(\Xi-\mu\omega\nu)}
\end{aligned}
$$

For the purpose of simulation, the parametric values and sensitivity index of the parameters involved in R_0^{HBV} are given in Table 4.1.

Table 1: Sensitivity indices of the parameters in R_0^{HBV}

Parameter	Value	Source	Sensitivity index
μ	0.0121	Inam et al. (2021)	+ 1.05
B	0.091	Inam et al. (2021)	+ 1
E	0.00003	Inam et al. (2021)	$+ 4.3\times10^{-7}$
Σ	0.2	Inam et al. (2021)	+ 0.26
N	0.46	Inam et al. (2021)	+ 0.11
Ω	0.85	Inam et al. (2021)	+ 10.96
Λ	0.06-0.03	Hussam et al. (2020)	+ 0.08
μ_0	0.0693	Inam et al. (2021)	- 6.14
μ_1	0.01	Inam et al. (2021)	$- 2.1\times10^{-8}$
Θ	0.003	Inam et al. (2021)	- 0.01
Γ	0.01	Hussam et al. (2020)	- 0.08
α_1	0.0936	Hussam et al. (2020)	$- 8.4\times10^{-9}$
α_2	0.0411	Assumed	$- 8.5\times10^{-8}$
Ω_1	0.0736	Hussam et al. (2020)	- 0.36
Ω_2	0.0321	Assumed	- 0.16

The sensitivity index of each of the parameters involved in R_0^{HBV} aids in the analysis of HBV extinction or persistence in the population. From Table 4.1, it is worthy to note that the parameters $\mu, \beta, \varepsilon, \sigma, \nu, \omega, \lambda$ with positive sensitivity indices are directly proportional to the R_0^{HBV}. This means that an increase or decrease in the values of these parameters will result in an increase or decrease in the R_0^{HBV}, thereby increasing or decreasing the burden of HBV in the population. On the other hand, the parameters μ_0, μ_1, θ, γ, α_1, α_2, Ω_1, Ω_2 with negative sensitivity indices are inversely proportional to the R_0^{HBV}. This shows that an increase in the values of these parameters will decrease R_0^{HBV}. Hence, decreasing the burden of HBV in the population. While decreasing the values of these parameter leads to an increase in the R_0^{HBV}. Therefore, leading to increase of HBV burden in the population.

4.2 Numerical Simulations

Here, we investigate qualitatively the effect of control strategies on model (41) in order to demonstrate the importance of the control measures or strategies. To solve the system, we will use the Runge-Kutta scheme of order four with forward in time [0,50].

The initial condition for the state variables of model (8) are S(0) = 100, L(0) = 30, I(0) = 20, C(0) = 5, T(0) =15, E(0) = 5, R(0) =15, along with the parametric values of $\tau_1 = 0.9738$, $\tau_2 = 0.500$ and with those in Table 4.1. And for the weight constants $\beta_1 = 0.091, \beta_2 = 100000, \beta_3 = 1, \beta_4 = 0.005, \beta_5 = 0.100, \beta_6 = 0.05, \beta_7 = 91, \beta_8 = 2000, \beta_9 = 0.100, \beta_{10} = 70, \beta_{11} = 5$.

First, we present the plot of the state variables of hepatitis B without control then follow it up with plots of each state variables in the system without and with controls.

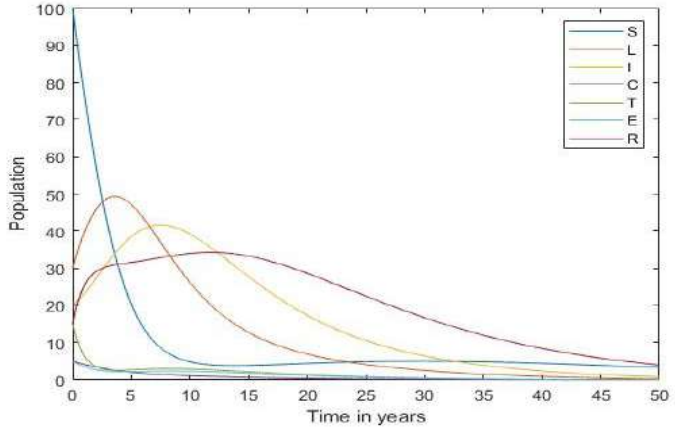

Figure 2: The plot of the state variables without controls

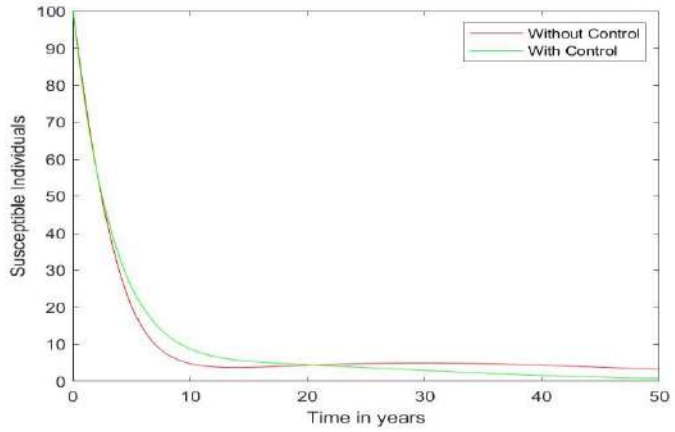

Figure 3: The plot of Susceptible class without and with controls

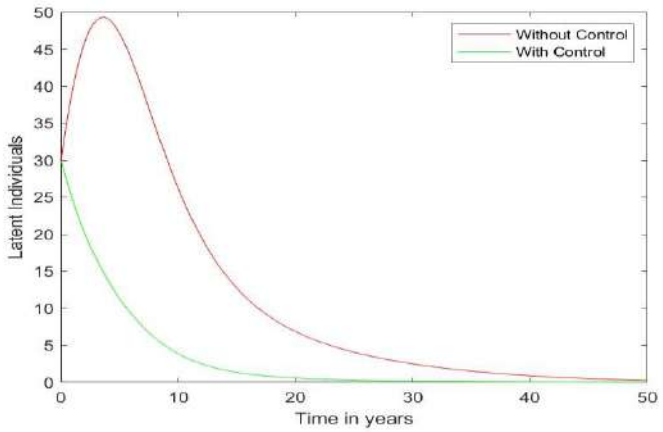

Figure 4: The plot of Latent class without and with controls

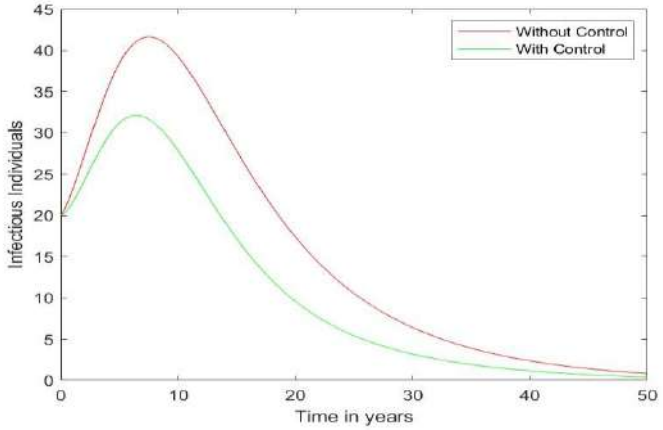

Figure 5: The plot of Infectious class without and with controls

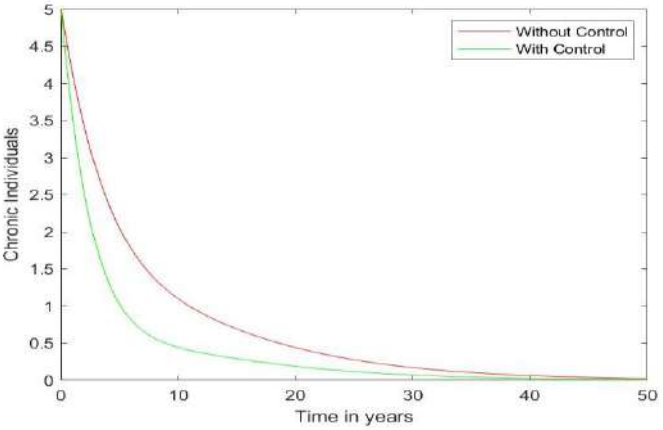

Figure 6: The plot of Chronic class without and with controls

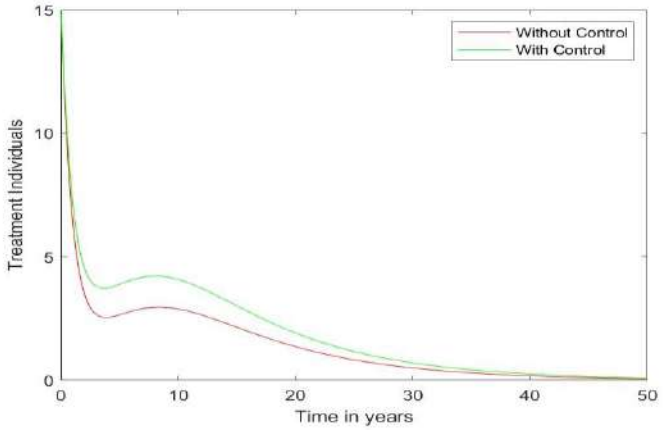

Figure 7: The plot of Treatment class without and with controls

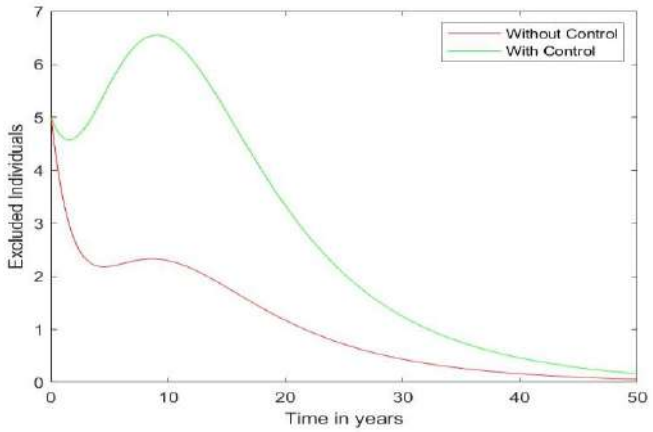

Figure 8: The plot of Exclusion class without and with controls

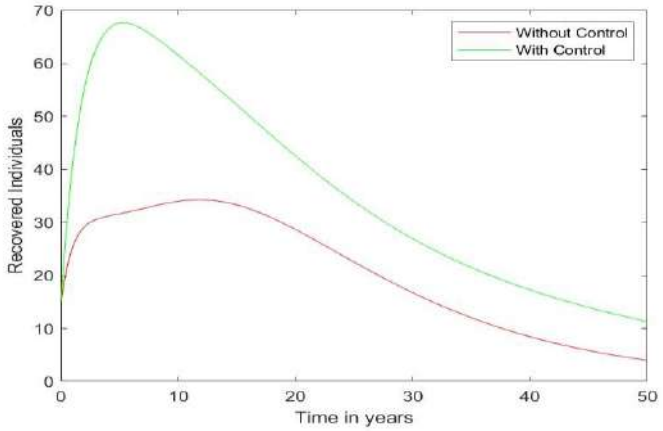

Figure 9: The plot of Recovered class without and with controls

4.3 Discussion

In this work we have been able to extend a mathematical model of HBV by incorporating HBV waning parameter and two more compartments (Treatment and Exclusion). In addition we considered four (4) control measures for the model with the prime target of reducing the susceptible population and increasing the recovered population as seen in Fig 3 and Fig 9. The result shows that after some time those in the recovered class loss immunity as the HBV vaccine wane and become susceptible again. This is one of factor that accounts for the decline in the recovered class as seen in Fig 9. In addition, it was noticeable that before the introduction of our proposed control strategies there is a reduction in latent Fig 3, infectious Fig 4 and chronic individuals Fig 5 which we traced to the incorporated treatment and exclusion compartments in our model.

Furthermore, the analysis of our model shows that there is local and global stability for the disease free equilibrium and the endemic equilibrium by bifurcation analysis is bi-stable. This means that the disease can exist in low or high state in the population. The sensitivity analysis reveals the parameters that has significant role in the epidemiology of HBV. From Table 1, the parameters with positive index are directly proportional to the R_0^{HBV} while the parameters with negative index are inversely proportional to the basic reproductive number.

Also, we observed from the numerical simulation that the proposed four (4) control strategies (Awareness, reduction in rate of contacts, vaccination and treatment and isolation) played a vital role in bringing the spread of HBV under control. These control strategies if implemented will arrest the spread of HBV in the population even before the forward 50th year under consideration.

Finally, it is the responsibility of the government to provide her citizens medical policies and care when there is an outbreak of an epidemic. Providing all these control strategies might be expensive and unrealistic. Hence, we suggest the implementation of maximum vaccination at birth, combined treatment and exclusion along with regular sensitization (awareness) of her citizens about the epidemic.

5.0 Conclusion

We have seen from the analysis how different parameter values increase or decrease the HBV burden in the population. Increasing the parameter values with positive sensitivity index will increase the HBV burden in the population vice versa while increasing the parameter values with negative sensitivity index will play a greater role in reducing drastically, the challenges post by HBV. The most significant among these parameters with positive sensitivity index we attempt to minimize is the birth without vaccination at $\mu\omega$ and among the parameters with negative sensitivity index, the vaccination rate γ is

the most significant we attempt to maximize; As the rate of birth without vaccination increases, the burden of HBV increases vice versa while at the other hand, as the vaccination rate increases, the burden of HBV in the population decreases and vice versa. The dynamics of HBV is completely determined by the basic reproductive number R_0^{HBV} as an increase in R_0^{HBV} will lead to an increase of HBV burden vice versa. Furthermore, as a result of the vaccination, anti-viral treatment and isolation of HBV incorporated in the model, even before implementing the proposed control strategies; it was observed that the Susceptible and Recovered population decline over time and tends to be equal while the other compartments tends to zero over the forward in time of 50 years as seen in Fig. 4.1. With the implementation of the control strategies, it was noticed that there is a rapid decline in the number of individuals within each compartment as expected. Hence, the need to adopt and implement the proposed strategies in order to bring the spread of HBV under control within a short time.

The SLICTER model with its sensitivity and control analysis gave us a better understanding of HBV dynamics and serves as a tool needed in bringing its threat under control with the aid of the proposed control strategies. Primarily, adequate attention should be given to HBV sensitization and maximum vaccination at birth in order to meet up with the critical vaccination level v_c and this should be done alongside social distancing in order to minimize the rate of contact. And in a case of a failed vaccination and one become infected, it is advisable to go for anti-viral treatment and isolation. Putting these measures together will help in bringing the virus under control, improving lives and eventually eradicating the disease from the population.

References

Abegye S.Y., Akpan C.E., Shammah S.K (2024). Dynamical Behavior of Tuberculosis of a Weak and Strong Latently Immune Population. IOSR Journal mathematics (IOSR-JM),20: 22-33.

Abdulfatai, A. M., Abubakar, A., Dethi´ e, D., and Inalegwu, M. A. (2023). On the optimal´ control of intervention strategies for hepatitis b model. *Abstract and Applied Analysis*, 2023:19 pages.

Adagba, A. I. and Joseph, C. S. (2022). A mathematical modeling of hepatitis b in a susceptible population. *International Journal of Multidisciplinary Research and Growth Evaluation*, 3(6):382–393.

Akanni, J. O., Abidemi, A., Jenyo, O. O., and Akinpelu, F. O. (2018). Mathematical modelling of transmission dynamics and optimal control of isolation, vaccination and treatment for hepatitis b virus. *General Letters in Mathematics*, 5(3):132–147.

Akpan, C.E. and Ibrahim, M.O. (2020) Sensitivity analysis for Avian Influenza (Bird Flu) Epidemic model with exposed class. Asian Journal of Mathematics and Applications, : 24 pages.

Awuah-Mensah, K. A. (2018). Epidemiological model of the transmission and spread of hepatitis b pandemic in ghana doctoral and masters thesis, edith cowan university. *This Thesis is posted at Research Online. https://ro.ecu.edu.au/theses/2123*.

Bassey, B. E. (2020). Optimal control dynamics: Multi-therapies with dual immune response for treatment of dual delayed hiv-hbv infections. *I.J. Mathematical Sciences and Computing*, 2(2):18–60.

Blessing, O. E. and Simeon, C. I. (2018). Mathematical model and analysis of hepatitis b virustransmission dynamics. *Method Article*, 7(1312).

Calvin, T. and Severin, F. (2019). Modeling and mathematical analysis of an initial boundary value problem for the hepatitis b virus infection. *Mathematical Analysis and Applications*, page 36.

Dotia, A., Ibrahim, M., Ejieji, C., Kareem, B., Ahmed, B., and Ajanaku, B. (2019). Optimal control on hepatitis b virus model with non-monotonic incidence function. *Journal of*

Science and Technology Research, 1(1):149–157.

Firaol, A. W., Dawit, M. G., and Alemneh, H. T. (2023). Mathematical model analysis of efective intervention strategies on transmission dynamics of hepatitis b virus. *Scientific reports*, 13(8737).

Hussam, A., Mohammad, A. S., Mahmoud, H. D., Bashir, A., Saif, U., Muhammad, A. K., and Syed, A. A. S. (2020). Optimal control analysis of hepatitis b virus with treatment and vaccination. *Results in Physics*, 19:2211–3797.

Inam, Z., Muhammad, N. J., Nigar, A., Dalal, A., Kottakkaran, S. N., and Gul, Z. (2021).

Mathematical analysis of hepatitis b epidemic model with optimal control. *Advances in Difference Equations*, 2021(451).

Kumama, R. C. (2023). Optimal control and bifurcation analysis of hiv model. *Computational and Mathematical Methods in Medicine*, 2023:21 pages.

Malede, A. B., Okelo, J. A., and David, M. T. (2023). mathematical model of hepatitis b disease with optimal control and cost-effectiveness analysis. *Computational and Mathematical Methods in Medicine*, 2023:29 pages.

Oyelami, B. O. (2014). Ordinary differential equations and applications. *Tomssy Press*, pages 330–353.

Paul, F., ken, E., and David L., H. (2011). ”herd immunity”: A rough guide. *Clinical Infectious Disease*, 52(7):911–916.

Penina, H. and Sarah, S. (2021). Epidemiology and prevention of vaccine preventable diseases. *Centers for Disease Control and Prevention*.

Shanta, K. and Haider, A. B. (2020). Optimal control strategies for preventing hepatitis b infection and reducing chronic liver cirrhosis incidence. *Infectious Disease Modelling*, 5:91–110.

Sirajo, A., Akinwande, N. I., Awojoyogbe, O. B., and Usman, Y. A. (2013). Mathematical analysis of the control of hepatitis b virus in a population with vital dynamics. *The Pacific*

Journal of Science and Technology, 14(188-204):11.

Titus, I. C., Edmund, O. E., and Godwin, C. E. M. (2018). A mathematical model of the dynamics of hepatitis b virus (hbv) infection with controls. *International Journal of Trend in Scientific Research and Development*, 2(5):2456 – 6470.

WHO (2022). Key facts on hepatitis b. *World Health Organization*, 2022.

Wiah, E., Dontwi, I., and Adetunde, I. (2011). Using mathematical model to depict the immune response to hepatitis b virus infection. *Journal of Mathematics research*, 3(2):11.

Zhang, J. and Suxia, Z. (2018). Application and optimal control for an hbv model with vaccination and treatment. *Discrete Dynamics in Nature and Society*, 2018:13 pages.

Mathematical Analysis of an Epidemic Model of Diphtheria Disease Dynamics with Vaccination and Isolation of Infectious individuals

Salisu Usaini

Department of Mathematics, Aliko Dangote university of Science and Technology, Wudil-Kano, Nigeria

salisu.usaini@kustwudil.edu.ng

Abstract

We reviewed an epidemic diphtheria model to carry out more rigorous mathematical analysis. We obtained a control parameter $\mathcal{R}_v$ which determines the persistence or extinction of diphtheria disease. The presented model has diphtheria infection-free and diphtheria infection presence equilibria. The latter equilibrium state is stable locally asymptotically if $\mathcal{R}_v > 1$ and the former one is locally asymptotically stable whenever $\mathcal{R}_v < 1$. Sensitivity analysis results indicate that of more interest, the rate of isolating individuals infected with diphtheria and the fraction of vaccinated susceptible persons are the most sensitive parameters other than the effective contact rate. Moreover, we showed that there is an inverse relationship between each of these parameters and the vaccinated reproductive number, $\mathcal{R}_v$. Indeed, an increase of one or both of them results in reducing the value of $\mathcal{R}_v$ and leads to containing the spread of the bacteria in a community.

Keywords: diphtheria, stability analysis, sensitivity index

1. Introduction

Diphtheria is a contagious disease produced by bacteria known as *Corynebacterium diphtheriae*. Such bacteria make toxin which causes sickness to people. Diphtheria infection can spread in a population from person to person, through respiratory droplets, such as coughing or sneezing. People also contract the bacteria by touching open wounds of infected individuals. Therefore, people with high risk of infection include those in the same household or come into contact with the infectious and persons having direct exposure to excretions from the suspected infection site like mouth and skin of the infected person (CDC, 2024). Diphtheria disease incubate for a period of 2-5 days.

Diphtheria is classified based on the nature of appearance for clinical purposes depending on the site of the infection. These are respiratory diphtheria which is further divided into three including: Nasal diphtheria, Pharyngeal and tonsillar diphtheria as well as Laryngeal diphtheria and cutaneous diphtheria. Onset of respiratory one is slow with characteristics of mild fever, sore throat, difficulty swallowing, malaise, loss of appetite and hoarseness (if the larynx is involved). For respiratory diphtheria a pseudo membrane (a thick, gray coating forms by dead tissues) will appear within two to three days of illness in the throat or nose causing difficulty in breath and swallow. Moreover, a toxin produces by bacteria slays

healthy tissues in the respiratory system and damage heart, nerve, and kidney if gets into blood stream (CDC, 2024).

Immunization of all ages is a preventive measure for diphtheria disease. Diphtheria is treated with antibiotics to kill and get rid of the bacteria irrespective of infection site. Diphtheria antitoxin is used to treat respiratory diphtheria infections as it stops the bacteria toxin from damaging the body (CDC, 2024).

Diphtheria infection was among the leading causes of childhood death worldwide before the advent diphtheria toxoid vaccine in 1923. A diphtheria disease dynamics model with quarantine was presented in (Adewale *et al.*, 2017). The model analysis reveals that high quarantine rate of exposed individuals lowers the reproductive number thereby reducing the size of infectious persons. Therefore, intensifying quarantine rate of exposed individuals prevent the endemic persistence of diphtheria disease in a community. In 2018, Ilahi and Widiana (2018) proposed an epidemic model of diphtheria disease for assessing vaccination effect on bacterial infection. The model analysis and simulation results indicate that vaccine has positive impact in containing the spread of diphtheria. In the following year a simple SIR model of diphtheria transmission dynamics with natural immunity of infectious individuals was proposed by Husain (2019). He concludes that the rate of recovery and effective contact parameter play important role for controlling disease persistence.

Recently, an optimal control mathematical model of diphtheria was also presented in (Izzati, Andriani and Robi'aqolbi, 2020), with quarantine and vaccination strategies as control measures. The analysis indicates that an optimal control strategy could minimize diphtheria disease persistence. A mathematical model of diphtheria disease dynamics was also proposed to get insights on the dynamics of the bacteria (Izzati and Andriani, 2021). Stability results of the model equilibria were presented. Numerical simulations showed that disease persistence could be affected by basic vaccination coverage and natural immunity of the population. In a similar note, Kanchanarat *et al*., (2022) proposed a transmission dynamics model of diphtheria aimed at assessing the effect of imperfect vaccine on disease spread. The analysis reveals that diphtheria could be eradicated if the immunization coverage exceeds the required level of optimal immunization coverage. Two influential factors for containing diphtheria infections are determined via sensitivity analysis. Moreover, numerical simulations indicate that the time period spent by infected individuals before the appearance of clinical signs has an effect on the required maximum level of immunization coverage for diphtheria elimination.

In this paper, we extended the model of Izzati and Andriani (2021) by incorporating diphtheria transmission of exposed individuals. Moreover, we addressed some drawbacks of their model in terms of formulation and analysis as follows:

i. We changed quarantine of infected individuals to isolation as exposed individuals supposed to be quarantined,
ii. We obtained the endemic equilibrium point and proved its stability result which were not presented in their paper,
iii. We proved the existence of transcritical bifurcation phenomenon as they mentioned without proof,
iv. Sensitivity analysis of the model parameters were carried out

Remaining part of this paper is organized in this way: Section 2 describes the model of diphtheria disease. We carried out the model analysis in section 3. Then we provide the concluding remarks in the last section.

2. The model of diphtheria

The human diphtheria infection model as presented by Izzati and Andriani in 2021 classified the human population, N into five distinct classes of susceptible (S), exposed (susceptible humans who come into contact with infected individuals, E), infected (I), isolated (J), and recovered (R) individuals. Thus, the total human population at time t is

$$N(t) = S(t) + E(t) + I(t) + J(t) + R(t).$$

It is assumed that

i. who do not get vaccinated are included in the susceptible groups (S)
ii. vaccinated are immune and move to recovered class (R)
iii. the transmission of diphtheria disease is via effective contact between the susceptible and infected individuals.
iv. exposed humans with strong natural immunity do not become infectious and are moved to the susceptible class. While those who have weak natural immunity could be infectious for a time period.
v. the infectious individuals (I) receive treatment and progress to isolated class.
vi. the isolated individuals reduce by either recovery or diphtheria infection.
vii. recovery confers permanent immunity. That is, there is no reinfection after recovery.
viii. individuals of each class can die naturally at the rate, τ. Moreover, infected individuals can die due to the diphtheria disease infection at the rate θ.

Based on the above assumptions, the model is presented in equation (1) and the rates of transfer between the five classes is shown in Figure 1. The parameters of model (1) are presented in Table 1.

$$\left.\begin{aligned}
\frac{dS}{dt} &= (1-p)\mu N - \lambda S - \tau S + \phi E \\
\frac{dE}{dt} &= \lambda S - \alpha E - \phi E - \tau E \\
\frac{dE}{dt} &= \alpha E - \gamma I - \tau I - \theta I \\
\frac{dJ}{dt} &= \gamma I - \tau J - \eta J \\
\frac{dR}{dt} &= p\mu N + \eta J - \tau R
\end{aligned}\right\} \quad (1)$$

with $\lambda = \frac{\beta(\varepsilon E + I)}{N}$, nonnegative state variables and model parameters.

Table 1. Values of model parameters as in (Izzati and Andriani, 2021)

Parameter	Description	Nominal value
P	Fraction of vaccinated human	0.3
μ	Rate of birth	0.019
τ	Natural death rate	0.006
α	Progression rate from E to I	0.57
β	Effective contact rate	0.23
ϕ	Rate at which exposed become susceptible	0.3
γ	Isolation rate	0.3
ε	Modification parameter	0.5

θ	Mortality rate due to Diphtheria	0.05

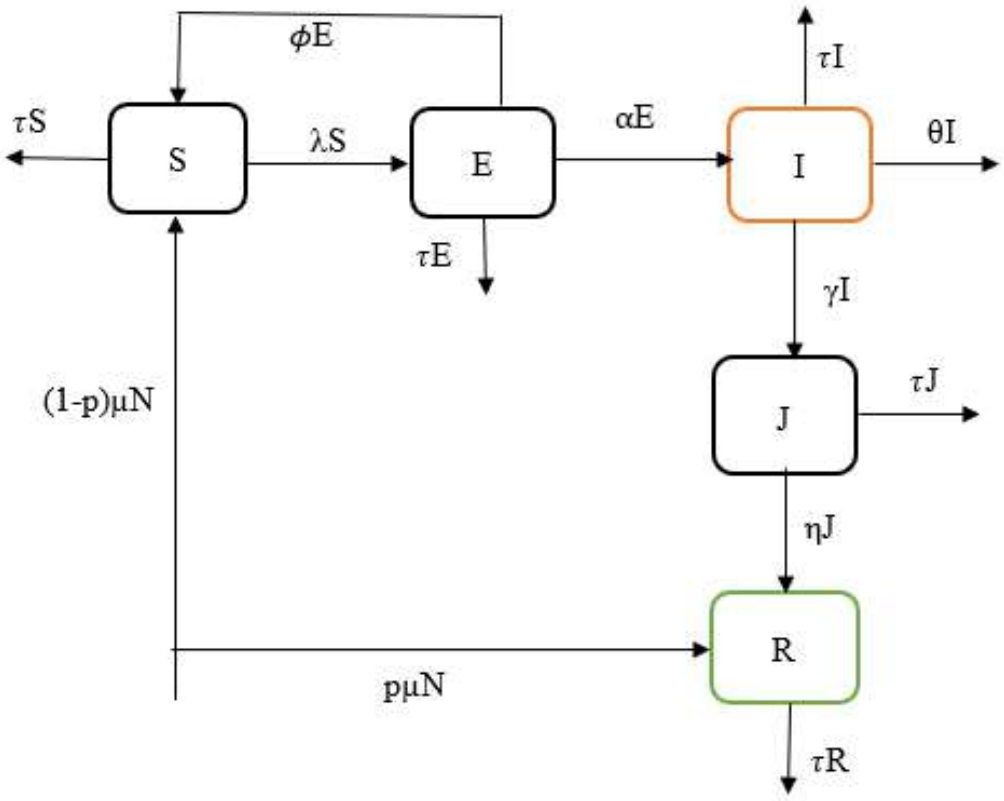

Figure 1: Flow diagram of model (1)

3. Analysis of the model

3.1 Equilibrium points of model (1)

When there is no diphtheria infection ($E = I = 0$) so that an infection-free equilibrium denoted by $\mathcal{H} = (S_0, E_0, I_0, J_0, R_0)$ is given by

$$\mathcal{H} = \left(\frac{(1-p)\mu}{\tau}, 0, 0, 0, \frac{p\mu}{\tau}\right).$$

If the disease is present, we denote by $\mathcal{H}^* = (S^*,\ E^*, I^*, J^*, R^*)$ an endemic equilibrium of model (1). Then using Maple 18 software, we obtain

$$S^* = \frac{k_1\mu(1-p)[\tau(\alpha + k_2k_3) + \alpha\gamma(\eta+\tau)] + k_2k_3p(\alpha+\tau)}{\tau\{k_3(\tau k_1(\alpha k_2 + 1) + (\alpha+\tau)[k_2\alpha\beta + (\mathcal{R}_1 - 1)]) + k_1\alpha\gamma(\eta+\tau)\}}$$

$$E^* = \frac{k_1k_2k_3\mu(\mathcal{R}_v - 1)}{k_3(\tau k_1(\alpha k_2 + 1) + (\alpha + \tau)[k_2\alpha\beta + (\mathcal{R}_1 - 1)]) + k_1\alpha\gamma(\eta + \tau)}$$

$$I^* = \frac{\alpha k_1k_2k_3\mu(\mathcal{R}_v - 1)}{k_2\{k_3(\tau k_1(\alpha k_2 + 1) + (\alpha + \tau)[k_2\alpha\beta + (\mathcal{R}_1 - 1)]) + k_1\alpha\gamma(\eta + \tau)\}}$$

$$J^* = \frac{\alpha\gamma k_1k_2k_3\mu(\mathcal{R}_v - 1)}{k_2\{k_3(\tau k_1(\alpha k_2 + 1) + (\alpha + \tau)[k_2\alpha\beta + (\mathcal{R}_1 - 1)]) + k_1\alpha\gamma(\eta + \tau)\}}$$

$$R^* = \frac{\mu\{pk_1^2k_2^2k_3(\mathcal{R}_v - 1) + \Psi + k_1k_2(\mathcal{R}_0 - 1)(\alpha\eta\gamma - k_2k_3p\phi)\}}{k_2\{k_3(\tau k_1(\alpha k_2 + 1) + (\alpha + \tau)[k_2\alpha\beta + (\mathcal{R}_1 - 1)]) + k_1\alpha\gamma(\eta + \tau)\}}$$

with $\mathcal{R}_1 = \frac{\beta\varepsilon}{k_1}, \mathcal{R}_0 = \frac{\beta(\varepsilon k_2 + \alpha)}{k_1k_2}, k_1 = \alpha + \phi + \tau, k_2 = \tau + \gamma + \theta, k_3 = \tau + \eta.$ For this endemic equilibrium to exist, $\mathcal{R}_v > 1$ such that $\mathcal{R}_1 > 1$ and $\alpha\eta\gamma - k_2k_3p\phi > 0$.

For linear stability of these equilibrium points, a threshold parameter called basic reproduction number (here vaccinated reproductive number) is required which can be obtained using the method proposed in (Van den Driessche and Watmough, 2002). Let F be a matrix for the infection term and V a matrix for transition terms. Then

$$F = \begin{pmatrix} \frac{\beta\varepsilon S}{N} & \frac{\beta S}{N} & 0 \\ 0 & 0 & 0 \\ 0 & 0 & 0 \end{pmatrix} \text{ and } V = \begin{pmatrix} k_1 & 0 & 0 \\ -\alpha & k_2 & 0 \\ 0 & -\gamma & k_3 \end{pmatrix},$$

So that

$$\mathcal{R}_v = \rho(FV^{-1}) = \frac{\beta(1-p)(\varepsilon k_2 + \alpha)}{k_1k_2}.$$

This threshold parameter $\mathcal{R}_v$ is an average size of secondary infections an index infective is produced in a population of people at risk for which a fraction is vaccinated.

3.2 Local stability of equilibrium points

Here, we present the local stability results of the infection-free equilibrium and diphtheria infection presence equilibrium. In the absence of diphtheria disease, the linearized system (1) gives the following Jacobian matrix, denoted by $J(\mathcal{H})$

$$J(\mathcal{H}) = \begin{pmatrix} -\tau & q_1 & -q_3 & 0 & 0 \\ 0 & q_2 & q_3 & 0 & 0 \\ 0 & \alpha & -k_2 & 0 & 0 \\ 0 & 0 & \gamma & -k_3 & 0 \\ 0 & 0 & 0 & \eta & -\tau \end{pmatrix} \tag{2}$$

with $q_1 = -\beta\varepsilon(1-p) + \phi, q_2 = \beta\varepsilon(1-p) - k_1, q_3 = \beta(1-p)$.

It can be seen by inspection that the first three eigenvalues of the matrix $J(\mathcal{H})$ are the following: $-\tau$, $-\tau$, $-k_3$ and the remaining two eigenvalues are of the sub-matrix of $J(\mathcal{H})$ denoted by $J_0(\mathcal{H})$. This matrix is obtained by deleting the first row and first column, the last row and last column and the fourth row and fourth column of the matrix $J(\mathcal{H})$. Thus

$$J_0 = (\mathcal{H}) = \begin{pmatrix} q_2 & q_3 \\ \alpha & -k_2 \end{pmatrix}.$$

The trace and determinant of this matrix are

$$\mathrm{tr}(J_0) = q_2 - k_2 = -k_1\left(1 - \frac{\beta\varepsilon(1-p)}{k_1}\right) - k_2 < 0$$

and

$$\det(J_0) = -k_2 q_2 - \alpha q_3 = k_1 k_2 (1 - \mathcal{R}_v) > 0,$$

if $\mathcal{R}_v < 1$. Thus, J_0 has eigenvalues with negative real parts and so as those of $J(\mathcal{H})$. It follows that, the infection-free equilibrium $\mathcal{H}$ is asymptotically stable locally if $\mathcal{R}_v$ is less than unity.

Also, evaluating Jacobian matrix of system (1) around infection presence equilibrium, $\mathcal{H}^*$gives

$$J(\mathcal{H}^*) = \begin{pmatrix} -\omega_1 - \tau & \omega_2 + \phi & -\omega_3 & \omega_2 & \omega_2 \\ \omega_1 & -\omega_2 - k_1 & \omega_3 & -\omega_2 & -\omega_2 \\ 0 & \beta & -k_2 & 0 & 0 \\ 0 & 0 & \gamma & -k_3 & 0 \\ 0 & 0 & 0 & \varepsilon & -\tau \end{pmatrix}$$

with $\omega_1 = \frac{\alpha I^*(N^* - S^*)}{N^{*2}}, \omega_2 = \frac{\alpha I^* S^*}{N^{*2}}, \omega_3 = \frac{\alpha I^*(N^* - I^*)}{N^{*2}}$. Then using elementary row operations with Maple 18 software on $J(\mathcal{H}^*)$, we obtained an upper triangular matrix J^*. Thus, the diagonal entries of this matrix which are the eigenvalues of $J(\mathcal{H}^*)$ are the following.

$$-(\delta + \omega_1), \qquad -\frac{N^{*2}\tau(k_1 + \omega_1) + \alpha\tau I^* S^* + \alpha^2 I^*(N^* - S^*)}{N^{*2}((\tau + \omega_1)},$$

$$-\frac{N^{*2}\tau k_2(k_1k_3+\omega_1)\mp\alpha\tau k_2S^*I^*+\alpha^2k_2I^*(N^*-S^*)}{N^{*2}\tau(k_1+\omega_1)+\alpha\tau\alpha S^*I^*+\alpha^2I^*(N^*-S^*)},$$

$$-\frac{N^{*2}\tau k_2(k_1+k_3\omega_1)+\Phi+\alpha\tau S^*I^*(\beta\gamma+k_2k_3)}{N^{*2}\tau(k_1+\omega_1)+\alpha\tau\alpha S^*I^*+\alpha^2I^*(N^*-S^*)},$$

$$-\left(1+\frac{\alpha\beta S^*I^*(\gamma\varepsilon+\tau k_3)}{\Upsilon}\right),$$

Where $\Phi=\alpha k_3(\alpha k_2I^*(N^*-S^*)-\beta\tau S^*(N^*-I^*),$

$\Upsilon=N^{*2}\tau k_2k_3(k_1+\omega_1)+\alpha\tau S^*I^*(\beta\gamma+k_2k_3)+\Phi$

These five eigenvalues are negative if Φ is greater than zero and so, $\mathcal{H}^*$ is asymptotically stable locally.

3.3 Bifurcation analysis

As mentioned without proof in (Izzati and Andriani, 2021) a bifurcation occurs due to the existence of unique endemic equilibrium point which is called transcritical (forward) bifurcation. It is also known as a change of stability as the infection-free equilibrium exchange stability with the infection presence equilibrium at bifurcation point. This point is biologically called inversion boundary as a point after which the disease invades the population.

Theorem 1

Model (1) exhibits a transcritical bifurcation at the disease-free equilibrium $\mathcal{H}$ if the bifurcation parameter $\beta^*=\frac{k_1k_2}{(1-p)(\varepsilon k_2+\alpha)}$.

Proof

Let f be a vector defined from model (1) as

$$f(S,E,I,J,R;\ \beta)=\begin{pmatrix}(1-p)\mu N-\lambda S-\tau S+\phi E\\ \lambda S-\alpha E-\phi E-\tau E\\ \alpha E-\gamma I-\tau I-\theta I\\ \gamma I-\tau J-\eta J\\ p\mu N+\eta J-\tau R\end{pmatrix} \quad (3)$$

The Jacobian matrix $J(\mathcal{H})$ evaluated at $\mathcal{H}$, as presented in (2) has the determinant

$$\det(\mathcal{H})=\delta^2\prod_{i=1}^{3}k_i\,(\mathcal{R}_v-1),$$

which is zero if $\mathcal{R}_v = 1$ or $\beta = \frac{k_1 k_2}{(1-p)(\varepsilon k_2 + \alpha)}$. The trace of $J(\mathcal{H})$ is given by

$$tr\big(J(\mathcal{H})\big) = -\left[2\tau + \sum_{i=1}^{3} k_i - \beta\varepsilon(1-p)\right] \neq 0.$$

Thus, one of the eigenvalues of the Jacobian matrix $J(\mathcal{H})$ is a simple zero. This allow us to establish the existence of a transcritical bifurcation at the equilibrium $\mathcal{H}$ using Sotomayor theorem (Perko, 2001). To verify the conditions for transcritical bifurcation given in this theorem, let $V = (v_1, v_2, v_3, v_4, v_5)^T$ be an eigenvector of the matrix $J(\mathcal{H})$ corresponding to the zero eigenvalue. Then using the standard computation of an eigenvector, we obtain

$$V = \begin{pmatrix} 0 & 1 & \frac{\beta(1-p)}{k_2} & 0 & 0 \end{pmatrix}^T. \tag{4}$$

Then, let $W = (w_1, w_2, w_3, w_4, w_5)^T$ be an eigenvector of the transpose of the Jacobian matrix $J(\mathcal{H})$. Such an eigenvector associated to the zero eigenvalue is the following

$$W = \begin{pmatrix} \frac{\beta(1-p)(\alpha+k_2) - k_2\phi}{k_2} & 1 & \frac{\alpha}{k_2} & \frac{\alpha\gamma}{k_2 k_3} & \frac{\alpha\eta\gamma}{\tau k_2 k_3} \end{pmatrix}^T. \tag{5}$$

The derivative of the vector field $f(S, E, I, J, R;\ \beta)$ in (3) in relation to the bifurcation parameter β at the infection-free equilibrium, $\mathcal{H}$ is

$$f_\beta(\mathcal{H};\ \beta) = (0 \quad 0 \quad 0 \quad 0 \quad 0)^T$$

And so,

$$W^T f_\beta(\mathcal{H};\ \beta) = \begin{pmatrix} Q_1 & 1 & \frac{\alpha}{k_2} & \frac{\alpha\gamma}{k_2 k_3} & \frac{\alpha\eta\gamma}{\delta k_2 k_3} \end{pmatrix}^T \begin{pmatrix} 0 \\ 0 \\ 0 \\ 0 \\ 0 \end{pmatrix} = 0 \tag{6}$$

where $Q_1 = \frac{\beta(1-p)(\alpha+k_2) - k_2\phi}{k_2}$.

Now, $Df_\beta(S, E, I, J, R;\ \beta)V = \frac{\partial f_\beta}{\partial S}v_1 + \frac{\partial f_\beta}{\partial E}v_2 + \frac{\partial f_\beta}{\partial I}v_3 + \frac{\partial f_\beta}{\partial J}v_4 + \frac{\partial f_\beta}{\partial R}v_5$. Evaluating this expression at $\mathcal{H}$ and using equation (4), we get

$$Df_\beta(\mathcal{H};\ \beta) = \begin{pmatrix} -\frac{\mu(1-p)(k_2\varepsilon+1)}{\tau k_2} & \frac{\mu(1-p)(k_2\varepsilon+1)}{\tau k_2} & 0 & 0 & 0 \end{pmatrix}^T.$$

Thus,

$$W^T[Df_\beta(\mathcal{H};\ \beta)] = \begin{pmatrix} Q_1 & 1 & \frac{\alpha}{k_2} & \frac{\alpha\gamma}{k_2k_3} & \frac{\alpha\eta\gamma}{\delta k_2k_3} \end{pmatrix}^T \begin{pmatrix} -\frac{\mu(1-p)(k_2\varepsilon+1)}{\tau k_2} \\ \frac{\mu(1-p)(k_2\varepsilon+1)}{\tau k_2} \\ 0 \\ 0 \\ 0 \end{pmatrix}$$

$$= -\frac{\mu(1-p)([(\alpha+k_2)-\phi k_2](k_2\varepsilon+1)+\beta+k_2)}{\tau k_2} \neq 0. \qquad (7)$$

Also $D^2f(x;\beta)(V,V)$ is defined in [4] as follows: $D^2f(x;\beta)(V,V) = \sum_{k,i,j}^{5} \frac{\partial^2 f_k}{\partial x_i \partial x_j} v_i v_j$.

Expanding and evaluating this using (4) at the point $\mathcal{H}$, we obtain

$$D^2f(\mathcal{H};\beta)(V,V) = \begin{pmatrix} Q_2 \\ -Q_2 \\ 0 \\ 0 \\ 0 \end{pmatrix},$$

$$Q_2 = \frac{2\beta(1-p)[k_2\varepsilon\tau + \beta(1-p)(1+\varepsilon+\tau)]}{\mu k_2}$$

Hence,

$$W^T[D^2f(\mathcal{H};\beta)(V,V)] = \begin{pmatrix} Q_1 & 1 & \frac{\alpha}{k_2} & \frac{\alpha\gamma}{k_2k_3} & \frac{\alpha\eta\gamma}{\tau k_2k_3} \end{pmatrix}^T \begin{pmatrix} Q_2 \\ -Q_2 \\ 0 \\ 0 \\ 0 \end{pmatrix}$$

$$= Q_2(Q_1 - 1)\ \neq 0. \qquad (8)$$

Equations (6), (7) and (8) are the conditions for transcritical bifurcation which are satisfied (see, Theorem 1, Perko, 2001). Hence, the result.

3.4 Sensitivity analysis

The occurrence of transcritical bifurcation indicates that the diphtheria disease extinction or persistence depends on the vaccinated reproductive number, $\mathcal{R}_v$. However, a model parameter with greatest effect on this number would have the same effect on the diphtheria disease persistence. To investigate such a parameter, we can apply sensitivity indices as presented in (Chitnis, 2008).

Following Chitnis (2008), the associated sensitivity indices of the parameters of $\mathcal{R}_v$ are as follows:

$$\Phi_{\beta}^{\mathcal{R}_v} = \frac{\partial \mathcal{R}_v}{\partial \beta} \times \frac{\beta}{\mathcal{R}_v} = +1$$

$$\Phi_{p}^{\mathcal{R}_v} = \frac{\partial \mathcal{R}_v}{\partial \beta} \times \frac{p}{\mathcal{R}_v} = -\frac{p}{1-p}$$

$$\Phi_{\varepsilon}^{\mathcal{R}_v} = \frac{\partial \mathcal{R}_v}{\partial \varepsilon} \times \frac{\varepsilon}{\mathcal{R}_v} = \frac{\varepsilon k_2}{\varepsilon k_2 + \alpha}$$

$$\Phi_{\delta}^{\mathcal{R}_v} = \frac{\partial \mathcal{R}_v}{\partial \delta} \times \frac{\tau}{\mathcal{R}_v} = -\frac{\tau\left[\varepsilon {k_2}^2 + \alpha(k_1 + k_2)\right]}{k_1 k_2(\varepsilon k_2 + \alpha)}$$

$$\Phi_{\gamma}^{\mathcal{R}_v} = \frac{\partial \mathcal{R}_v}{\partial \gamma} \times \frac{\gamma}{\mathcal{R}_v} = -\frac{\alpha\gamma}{k_2(\varepsilon k_2 + \alpha)}$$

$$\Phi_{\theta}^{\mathcal{R}_v} = \frac{\partial \mathcal{R}_v}{\partial \theta} \times \frac{\theta}{\mathcal{R}_v} = -\frac{\alpha\theta}{k_2(\varepsilon k_2 + \alpha)}$$

$$\Phi_{\alpha}^{\mathcal{R}_v} = \frac{\partial \mathcal{R}_v}{\partial \alpha} \times \frac{\alpha}{\mathcal{R}_v} = -\frac{\alpha(\varepsilon k_2 - \phi - \tau)}{k_2(\varepsilon k_2 + \alpha)}$$

$$\Phi_{\phi}^{\mathcal{R}_v} = \frac{\partial \mathcal{R}_v}{\partial \phi} \times \frac{\phi}{\mathcal{R}_v} = -\frac{\phi}{k_1}$$

We evaluated the above sensitivity indices using values of the model parameters in Table 1. Then, resulting values of these indices are shown in Table 2 on increasing sensitiveness.

Table 2 Values of sensitivity indices of $\mathcal{R}_v$ on increasing sensitiveness

Parameter	Sensitivity index
β	+1

γ	-0.642162
P	-0.428571
ϕ	-0.342466
ε	0.237968
α	-0.111347
θ	-0.107027
τ	-0.019693

As depicted in Figure 2, there is direct relationship between the reproductive number $\mathcal{R}_v$ and each parameter β, ε and α. That is, an increase of any of these parameters results in the rise of the value of $\mathcal{R}_v$ leading to the disease persistence and vice-versa.

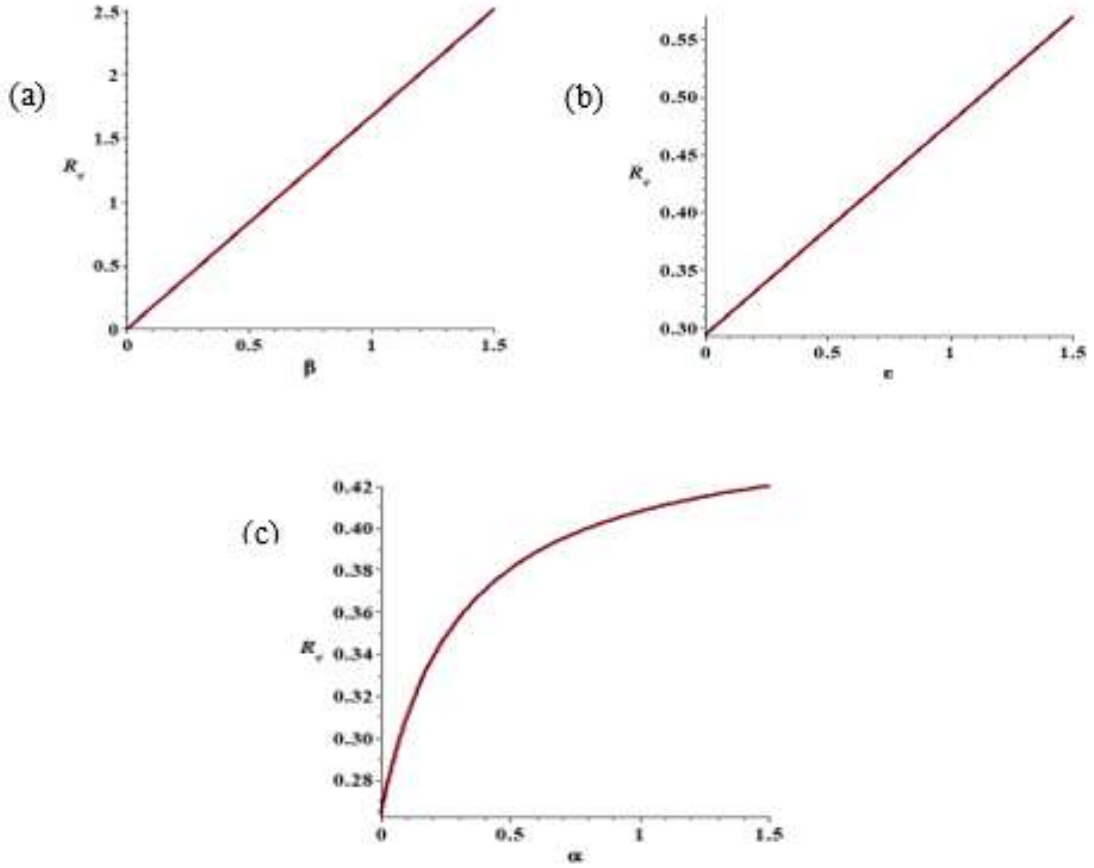

Figure 2. Sensitivity analysis of $\mathcal{R}_v$, showing direct relationship with β, ε and α

Figure 3 indicates inverse relationship between the reproductive number $\mathcal{R}_v$ and each parameter $p, \delta, \gamma, \theta$ and ϕ. It follows that increasing the value of each of these parameters will decrease the value of $\mathcal{R}_v$. Thus, contain disease persistence a population. We are interested in the control parameters γ and p for easy disease eradication. The diphtheria disease could be eliminated from a community by either high isolation rate of infectious individuals or vaccinating high proportion of susceptible individuals. Moreover, combining the two strategies will be the best way of diphtherial disease eradication in a community.

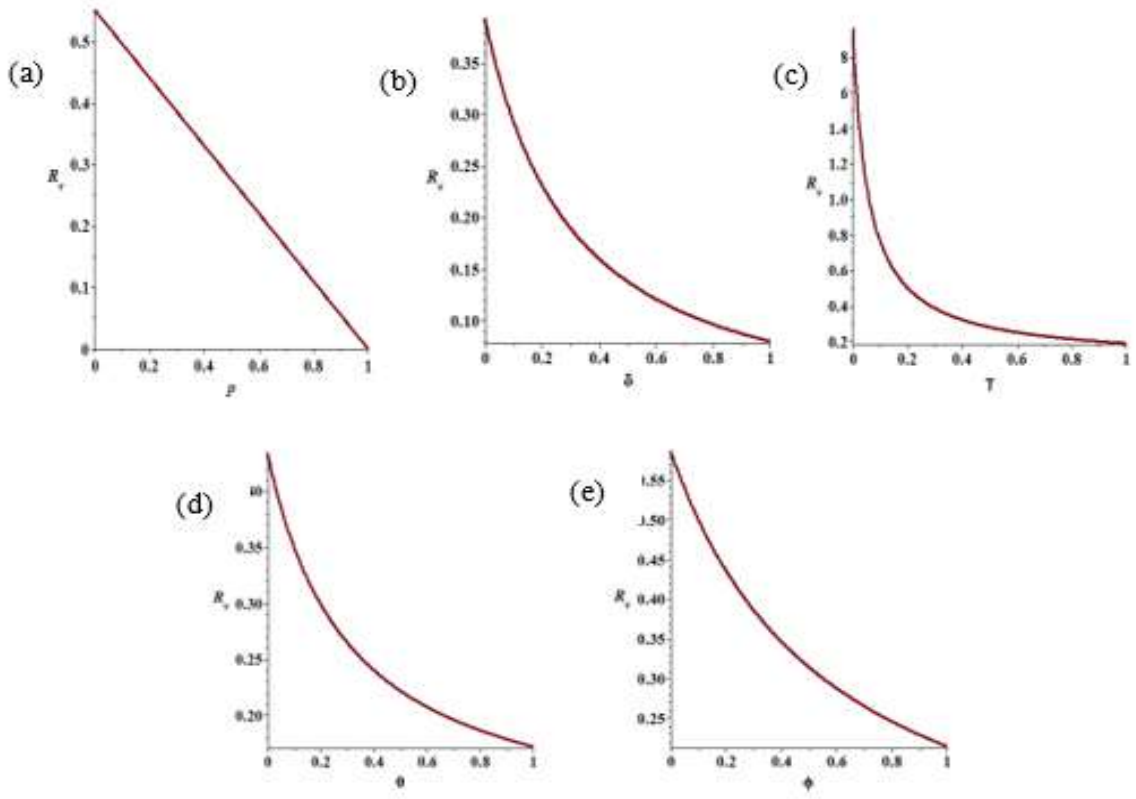

Figure 3. Sensitivity analysis of $\mathcal{R}_v$ showing inverse relationship with p, τ, γ, θ and ϕ

4. Conclusion

We presented an extended version of the model of diphtheria transmission dynamics proposed by Izzati and Andriani (2021). For the extension, we incorporate the transmission of bacteria by exposed individuals and changed quarantine of infected individuals to isolation. In addition to the infection-free equilibrium presented in (Izzati and Andriani, 2021), a unique infection presence equilibrium also exists. We proved the occurrence of transcritical bifurcation phenomenon as mentioned without proof in (Izzati and Andriani, 2021). Moreover, the most important parameters for diphtheria disease eradication were explored via sensitivity analysis. Such parameters are isolation rate of infectious individuals γ and proportion of vaccinated individuals p. In fact, the high isolation rate of infectious individuals or vaccinating high proportion of susceptible individuals would contain the spread of the bacteria. For further research, a booster vaccination can be incorporated in the model.

References

Adewale, S. O., Olopade, I. A., Adeniran, G. A., Ajao, S. O., Mohammed, I. T. (2017), Mathematical Analysis of Quarantine on the Dynamical Transmission of Diphtheria Disease, *International Journal of Science and Engineering Investigations*, vol. 6(64), 7-17.

Archary, M. *et al.* (2018). Diphtheria: NICD Recommendations for Diagnosis, Management and Public Health Response, Guidelines-Diphtheria-2018/05/28-v3

CDC, Diphtheria, https://www.cdc.gov/diphtheria/about/causes-transmission.html\#print accessed 11th January 2024.

Chitnis, N., Hyman, J. M. and Cushing, J. M. (2021), Determining important parameters in the spread of malaria through the sensitivity analysis of a mathematical model, *Bulletin of Mathematical Biology*, Vol. 70, 1272, doi:10.1007/s11538-008-9299-0.

Ilahi, F. and Widiana, A. (2018), The effectiveness of vaccine in the outbreak of diphtheria: mathematical model and simulation, *IOP Conf. Series: Materials Science and Engineering*, Vol. 434, 012006 doi:10.1088/1757-899X/434/1/012006

Izzati, N., Andriani, A. and Robi'aqolbi, R. (2020), Optimal control of diphtheria epidemic model with prevention and treatment, *Journal of Physics: Conference Series*, 1663, 012042 IOP Publishing doi:10.1088/1742-6596/1663/1/012042

Izzati, N., and Andriani, A. (2021), Dynamical analysis of diphtheria epidemic model with natural immunity rate on exposed individuals, *Journal of Physics: Conference Series,* 1869, 012117, doi:10.1088/1742-6596/1869/1/012117

Kanchanarat, S., Chinviriyasit, S., Chinviriyasit, W. (2022), Mathematical Assessment of the Impact of the Imperfect Vaccination on Diphtheria Transmission Dynamics, *Symmetry*, 14, 2000. https://doi.org/10.3390/ sym14102000

Perko, L. (2001), *Differential Equations and Dynamical Systems*, Third Edition, New York, 2001.

Van den Driessche, P., and Watmough, J. (2002), Reproduction Numbers and Sub-Threshold Endemic Equalibria for Compartmental Models of Disease Transmission, *Mathematical Biosciences*, Vol. 180, 29-48.

Analyzing Pneumonia Dynamics: A Mathematical and Optimal Control Approach with Emphasis on Immunization Campaigns

[1]Mohammed IdayatTemilade, [2]Olopade Isaac Adesola, [3]Adeniran deyemiGbenga and [2]Philemon Musa Emmanuel

[1]Department of Mathematics and social sciences, Osun state polytechnic Iree. Nigeria.

[2]Department of Mathematics and Statistics, Federal University Wukari, PMB 1020, Taraba State, Nigeria.

[3]Department of Physical Sciences, Chrisland University, P.M.B. 2131, Abeokuta, OgunState,Nigeria

[1]iskiludayat@gmail.com

[2]isaac.olopade@fuwukari.edu.ng

[3]gbadeniran@chrislanduniversity.edu.ng

[2]emmanuelmusa540@gmail.com

Abstract

Pneumonia poses a significant threat to children aged zero (0) to five (5) in the developing world, leading to high morbidity and mortality rates. Despite this, there has been limited focus on optimal control measures for childhood pneumonia. To address this gap, a new five-compartmental mathematical model to explore the impact of contact and transmission rates on the dynamic spread of pneumonia is developed. The disease-free-equilibrium model was analyzed, and the basic reproduction number (R_{0P}) was computed using the Next Generation Matrix (NGM) method. Sensitivity analysis highlighted the substantial influence of contact and transmission rates on the basic reproduction number (R_{0P}) . Numerical simulations conducted using Maple and the introduction of optimal control strategies demonstrated that increasing immunization campaigns can effectively reduce the dynamic spread of pneumonia infection.

Keywords: Optimal control, Pneumonia, Simulation, Transmission rate

1. Introduction

Pneumonia is an infection of the lungs that is caused by bacteria, viruses, fungi or parasites. It is most dangerous for older adults, babies and people with other diseases or impaired immune systems (rudan *et al.*, 2011). Pneumococcal is spread through contact with people who are ill or who carry the bacteria in their throat. One can get pneumococcal pneumonia from respiratory droplets from the nose or mouth of an infected person. It is common for people, especially children, to carry the bacteria in their throats

without being sick. After a person is infected and diagnosed with pneumonia, he should be on medication for a particular period of time; the infection is contagious for 10 to 14 days after the infected person stops getting treatment (WHO, 2006, UNICEF, 2011).When a person breathes pneumonia-causing germs into his lungs and his body's immune system cannot prevent its entry, the organisms settle in small air sacs called alveoli and continue multiplying. As the body sends white blood cells to attack the infection, the sacs become filed with fluid and pus causing pneumonia. Pneumonia has Bacterial, Viral, Fungal, and other primary causes. Other substances that caused pneumonia are smoke, abuse alcohol, those that have other medical conditions, such as chronic obstructive pulmonary disease (COPD), emphysema, asthma or HIV/AIDS (Singh and Aneja, 2011). This pneumonia is not common but may occur among those with weak immunity due to AIDS, immunosuppressive drugs and other medical problems (Ebby, 2005).

Pneumonia is of two type viz: typical and atypical. Typical pneumonia produces cough, fever, dyspnea, sudden onset of chills, pleura tic chest pain and usually no constitutional symptoms but historically atypical pneumonia is nonproductive of cough, lesser fever, less dyspnea, less chill, less pleurisy, chest pain but its constitutional symptoms are myalgia, arthralgia and rhinitis which are very common. Physically, typical pneumonia comes with more respiratory distress, higher fever and consolidation findings while all these are not present in atypical pneumonia. People who are older than 65 years of age and those that have recently recovered from a cold or flu have an increased risk of developing pneumonia and children younger than one year of age have a weakened or impaired immune system.

2. Literature Review

In order to know the dynamical spread of pneumonia disease, many researchers have worked on the mathematical model of this infectious disease. Tilahun (2019), worked on seven compartmental mathematical model. He stated in his research that in other to make endemic equilibrium unstable so that it merges to disease free equilibrium, high efficacy treatment vaccination programme are necessary as optimal control. He showed that reduction in contact rate of either pneumonia or meningitis has a great effect on controlling pneumonia and meningitis co-infection at population level. Mohammed (2019) worked on 14 compartmental model basically malaria-pneumonia co-infection and their optimal control at population level. It was established in her research that all the control strategies mentioned should be applied simultaneously for quick eradication of both diseases in the society. Marcus and Newton (2021) also examined the dynamics of the pneumonia disease from a mathematical perspective via a deterministic SEIR model. They observed that pneumonia free equilibrium is locally asymptotically stable for R_0 is less than one and pneumonia endemic equilibrium is globally asymptotically stable in the invariant region whenever $R_0 > 1$. In their research, sensitivity analysis revealed that transmission rates and the rates at which exposed individuals become infectious as the most sensitive parameters via center manifold theory. Getachew *et al., (2017*) also worked on modeling and optimal control of pneumonia disease with cost-effective strategies. A nonlinear mathematical model for the transmission dynamics of pneumonia disease

in a population of varying sizes was proposed and analyzed. Their research based on five deterministic mathematical compartmental models used control mechanisms to control disease prevention through education, treatment, and screening. They concluded that a combination of prevention and treatment are the most cost-effective intervention strategies to combat the pneumonia pandemic.

3. Methodology

In this paper, we consider the childhood stage, and vaccinated individuals which cannot gain permanent immunity for life because there is a certain age that vaccine can wane, denoted by omega "ω". The vaccine for pneumonia is perfect for a certain period and not be considered as hundred percent perfect. Meanwhile, we are considering childhood stage pneumonia, and we neglected the vaccination of adult individuals.

The formulation of our model is based on the following assumption that the human population is not assumed to be constant since migration, emigration, morbidity and mortality rates occurred. The susceptible human is increased by the recruitment of people (either by birth or immigration) into the population at the rate π_H, recovered people from pneumonia disease at the rate of $\boldsymbol{\alpha}$ and the vaccinated individuals who gained immunity for life at the rate of ω as well. This class of susceptible humans decreased by natural death $\boldsymbol{\mu}_H$ and transmission rate of the infected individual at λ_P. The fraction ρ of the newly recruited individuals are assumed to show no symptoms joined the vaccinated class of pneumonia. This class of individuals reduced by the natural death of vaccinated individuals with pneumonia and decreased at the rate ω of which the vaccine wanes. The population of exposed pneumonia individuals increased by the infection of fast progressor at the rate of $(1 - \varepsilon_2)$. This class is decreased by humans' natural death rate μ_H and the rate ϕ_1 at which disease progressed or spread into the population. The population of infected individuals with pneumonia is increased by the fraction ε_2 of the newly infected individuals and the progression rate of the disease into the population at the rate of ϕ_1. This infected class was reduced by the natural death rate of infected individuals at the rate of μ_H, pneumonia induced mortality at the rate of δ_1 and some individuals in this class received treatment at the rate of τ_1, which moved to recovered class. The group of individuals that received treatment at the rate of τ_1 which left infected pneumonia class joined the class of recovered individual. So this recovered class also decreased by the natural death of people in this class and by total recovered individuals from pneumonia at the rate $\boldsymbol{\alpha}$ which moves to susceptible class. Then:

$$\frac{dS_p}{dt} = (1-\rho)\pi_H - \lambda_p S_H - \mu_H S_H + \alpha R_p + \omega V_p, \qquad (3.1)$$

$$\frac{dV_p}{dt} = \rho\pi_H - \mu_H V_p - \omega V_p, \qquad (3.2)$$

$$\frac{dE_p}{dt} = (1- \varepsilon_2)\lambda_p S_H - \mu_H E_P - \phi_1 E_P, \quad (3.3)$$

$$\frac{dI_p}{dt} = \varepsilon_2\lambda_p S_H + \phi_1 E_P - \mu_H I_P - \delta_1 I_P - I_P\tau_1, \quad (3.4)$$

$$\frac{dR_p}{dt} = \tau_1 I_P - \mu_H R_P - \boldsymbol{\alpha} R_P. \quad (3.5)$$

where S, V, E, I and R stand for susceptible, vaccinated, exposed, infected and recovered class respectively.

3.1 Transmission Rates

Transmission by single infected individual acquire infections with pneumonia is represented by λ_p and given as

$$\lambda_p = \frac{\omega_p C(E_p+\eta_3 I_P)}{N_H} \quad (3.6)$$

Where C is the probability that one individual is being infected with pneumonia by a single infectious human and $\omega_p$is the effective contact rate for pneumonia while $\eta_3$is the modification parameter which led to the risk of infectiousness of individuals in the infected class.

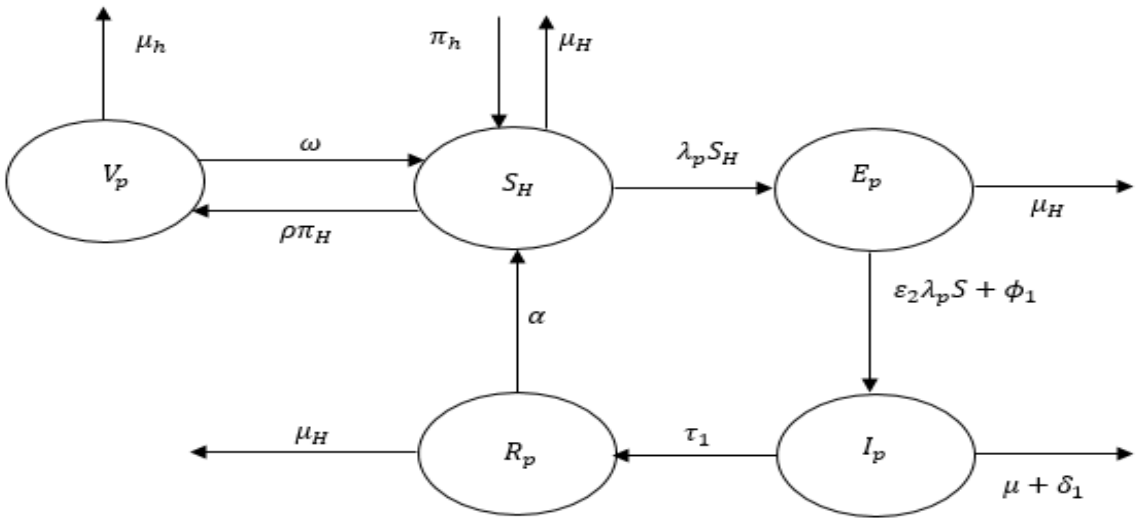

Figure 3.1.The flow chart of the model.

3.2 Existence and uniqueness of the model

We adopted the idea of Derrick and Grossman to analyze the solution of the existence and uniqueness of pneumonia model as follows

$$D = \{(S_H, V_p, E_p, I_p, R_p) : |S_H - S_{H_0}| \leq a,\ |V_p - V_{p_0}| \leq b,\ |E_p - E_{p_0}| \leq c,\ |I_p - I_{p_0}| \leq d,\ |R_p - R_{p_0}| \leq e, |t - t_0| \leq f \quad (3.7)$$

Proof

$$\frac{dS_H}{dt} = f_1(S_H, V_p, E_p, I_p, R_p) = (1-\rho)\pi_H - \lambda_H - \lambda_p S_H - \mu_H S_H + \alpha R_p + \omega V_p,$$

$$\frac{dV_p}{dt} = f_2(S_H, V_p, E_p, I_p, R_p) = \rho\pi_H - \mu_H V_p - \omega V_p,$$

$$\frac{dE_p}{dt} = f_3(S_H, V_p, E_p, I_p, R_p) = (1- \varepsilon_2)\lambda_p S_H - \mu_H E_P - \phi_1 E_P,$$

$$\frac{dI_p}{dt} = f_4(S_H, V_p, E_p, I_p, R_p) = \varepsilon_2\lambda_p S_H + \phi_1 E_P - \mu_H I_P - \delta_1 I_P - I_P\tau_1,$$

$$\frac{dR_p}{dt} = f_5(S_H, V_p, E_p, I_p, R_p) = \tau_1 I_P - \mu_H R_P - \boldsymbol{\alpha} R_P.$$

Then

$$\begin{Bmatrix} \frac{\partial f_1}{\partial S_H}|_{(0,0,0,0,0)} = -\mu_H \\ \frac{\partial f_1}{\partial V_p}|_{(0,0,0,0,0)} = \omega \\ \frac{\partial f_1}{\partial E_p}|_{(0,0,0,0,0)} = 0 \\ \frac{\partial f_1}{\partial I_p}|_{(0,0,0,0,0)} = 0 \\ \frac{\partial f_1}{\partial R_p}|_{(0,0,0,0,0)} = \alpha \end{Bmatrix} \begin{Bmatrix} \frac{\partial f_2}{\partial S_H}|_{(0,0,0,0,0)} = 0 \\ \frac{\partial f_2}{\partial V_p}|_{(0,0,0,0,0)} = -(\mu_H + \omega) \\ \frac{\partial f_2}{\partial E_p}|_{(0,0,0,0,0)} = 0 \\ \frac{\partial f_2}{\partial I_p}|_{(0,0,0,0,0)} = 0 \\ \frac{\partial f_2}{\partial R_p}|_{(0,0,0,0,0)} = 0 \end{Bmatrix} \begin{Bmatrix} \frac{\partial f_3}{\partial S_H}|_{(0,0,0,0,0)} = 0 \\ \frac{\partial f_3}{\partial V_p}|_{(0,0,0,0,0)} = 0 \\ \frac{\partial f_3}{\partial E_p}|_{(0,0,0,0,0)} = -(\mu_H + \emptyset_1) \\ \frac{\partial f_3}{\partial I_p}|_{(0,0,0,0,0)} = 0 \\ \frac{\partial f_3}{\partial R_p}|_{(0,0,0,0,0)} = 0 \end{Bmatrix}$$

$$\left\{\begin{array}{c} \frac{\partial f_4}{\partial S_H}|_{(0,0,0,0,0)} = 0 \\ \frac{\partial f_\$}{\partial V_p}|_{(0,0,0,0,0)} = 0 \\ \frac{\partial f_4}{\partial E_p}|_{(0,0,0,0,0)} = \emptyset_1 \\ \frac{\partial f_4}{\partial I_p}|_{(0,0,0,0,0)} = -(\mu_H + \delta + \tau_1) \\ \frac{\partial f_4}{\partial R_p}|_{(0,0,0,0,0)} = 0 \end{array}\right\}\left\{\begin{array}{c} \frac{\partial f_5}{\partial S_H}|_{(0,0,0,0,0)} = 0 \\ \frac{\partial f_5}{\partial V_p}|_{(0,0,0,0,0)} = 0 \\ \frac{\partial f_5}{\partial E_p}|_{(0,0,0,0,0)} = 0 \\ \frac{\partial f_5}{\partial I_p}|_{(0,0,0,0,0)} = -\tau_1 \\ \frac{\partial f_5}{\partial R_p}|_{(0,0,0,0,0)} = -(\mu_H + \alpha) \end{array}\right\} \quad (3.8)$$

Hence, the problem has a unique solution and the model is mathematically and epidemiologically well posed.

3.3 Disease Free Equilibrium

The disease free equilibrium (DFE) is the stage where there is neither disease nor infection in the society. This shall be denoted as $\varepsilon_0$then,

$$\frac{dS_H}{dt} = \frac{dV_p}{dt} = \frac{dE_p}{dt} = \frac{dI_p}{dt} = \frac{dR_p}{dt} = 0 \quad and \quad \lambda_p = 0 \quad (3.9)$$

$$V_p = \frac{\rho\pi_H}{\mu_H+\omega}, \quad S_H = \frac{(\mu_H-\rho+\omega)\pi_H}{\mu_H(\mu+\omega)} \quad and \quad E_p = 0$$

Also

$$\varepsilon_2\lambda_p S_H + \emptyset_1 E_p - (\mu_H + \delta + \tau_1)I_p = 0$$

Since $I_p = 0$, then

$$\tau_1 I_p - (\mu_1 + \alpha)R_p = 0, Then\ R_p = 0$$

$$\therefore \varepsilon_0 = (S_H, V_p, E_p, I_p, R_p) = \left(\frac{(\mu-\rho+\omega)\pi_H}{\mu(\mu+\omega)}, \frac{\rho\pi_H}{\mu_H+\omega}, 0, 0, 0\right) \quad (3.10)$$

3.4 Existence of endemic equilibrium

The endemic is the stage where pneumonia infection has become pandemic in the society which shall be denoted as ε_0^* and determined as follows:

$$\varepsilon_0^* = \left(S_H^*, V_p^*, E_p^*, I_p^*, R_p^*\right)$$

where

$$\frac{dS_H}{dt} = \frac{dV_p}{dt} = \frac{dE_p}{dt} = \frac{dI_p}{dt} = \frac{dR_p}{dt} = 0$$

At endemic steady stage the expression λ_p is denoted by λ^{**}

$$\varepsilon_0^* = \omega_p C \frac{(E_p^* + \eta_3 I_p)}{N^*} \tag{3.11}$$

Let $K_1 = (\mu_h + \phi_1),\ K_2 = (\mu_H + \delta_1 + \tau_1),\ K_3 = (\mu_h + \alpha)\ and\ K_4 = (\mu_H + \omega)$

then

$$(1 - \rho)\pi_H - \lambda_p S_H^* - \mu S_H^* + \alpha R_p^* = 0$$

$$(1- \varepsilon_2)\lambda_p^* S_H^* - \mu E_p^* - \phi_1 E_p^* = 0,$$

where

$S_H^* = \frac{(1-\rho)\pi_H + \alpha R_p^* + \omega V_p^*}{(\lambda_p^* + \mu_h)E_p^*}$, $I_p^* = \frac{(1-\varepsilon_2)\lambda_p^* S_H^*}{K_1}$, $V_p^* = \frac{\rho\pi_H}{K_4}$

$\varepsilon_2\lambda_p^* S_H^* + \phi_1 E_p^* - (\mu + \delta + \tau_1)I_p^* = 0$

where

$E_p^* = \frac{(1-\varepsilon_2)\lambda_P^* S_H^*}{K_1}$, $R_p^* = \frac{\tau_1 I_p^*}{K_3}$, and $\tau_1 I_p^* - (\mu + \alpha)R_p^* = 0$

Then,

$I_p^* = \frac{S_H^*(K_1\varepsilon_2\lambda_p + \phi_1\lambda_p - \phi_1\varepsilon_2\lambda_p)}{K_1K_2}$ where $P_1 = \frac{K_1\varepsilon_2 + (1-\varepsilon_2)\phi_1}{K_1K_2}$

also,

$R_p^* = \frac{\tau_1 I_p^*}{K_3} = \frac{\tau P_1 \lambda^* S_H}{K_3} = P_2\lambda^*{}_p S^*{}_H$ Where $P_2 = \frac{\tau}{K_3}\left(\frac{\varepsilon_2}{K_2} + \frac{(1-\varepsilon_2)\phi_1}{K_1K_2}\right)$

from equation (3.1), $N^* = S_P^* + V_P^* + E_P^* + I_P^* + R_P^*$

Then,

$$\lambda_p{}^* N^* = \omega_p C(E^*{}_p + \eta_3 I^*{}_p)\ \lambda^*{}_p\left(S^* + \frac{\ell\pi_H}{K_4} + \frac{(1-\varepsilon_2)\lambda_P^* S^*{}_H}{K_1} + P_1\lambda^* S^*{}_H + P_2\lambda^* S^*{}_H\right)$$

$$= \omega_p C\left(\frac{(1-\varepsilon_2)\lambda^* S^*{}_H}{K_1} + \eta_3 P_1\lambda^*{}_p S^*{}_H\right)$$

Divide through by $\lambda^*{}_p S^*{}_H$, we obtain

$$1 + P_3\lambda^* = \omega_p C\left(\frac{(1-\varepsilon_2)\lambda^* S^*{}_H}{K_1} + \eta_3 P_1\right)$$

Where $P_3 = \frac{\ell\pi\lambda^*}{S^*} + \frac{1-\varepsilon_2}{K_1} + P_1 + P_2$, then

$$\lambda^* = \frac{1}{P_3}\left(\frac{\omega_p C(_1-\varepsilon_2) + \eta_3 P_1 K_1}{K_1} - 1\right) = \frac{\omega_P C\frac{(1-\varepsilon_2)}{K_1} + \eta_3 P_1}{P_3} - 1. \qquad (3.12)$$

3.4 Derivation of basic reproduction number

We adopt the idea of the next generation matrix used by Driessche and Watmough to calculate the basic reproduction number (R_{0p}) of the pneumonia model. The Jacobian derivative of F and V are

$$F = \begin{bmatrix} 0 & 0 & 0 & 0 \\ 0(1-\varepsilon_2)\omega_p C & (1-\varepsilon_2)\eta_3\omega_p C & 0 \\ 0 & \varepsilon_2\omega_p C & \varepsilon_2\omega_p C\eta_3 & 0 \\ 0 & 0 & 0 & 0 \end{bmatrix} \qquad V = \begin{bmatrix} K_4 & 0 & 0 & 0 \\ 0 & K_1 & 0 & 0 \\ 0 & -\phi_1 & K_2 & 0 \\ 0 & 0 & -\tau_1 & K_3 \end{bmatrix} \qquad (3.13)$$

Then,

$$FV^{-1} = \begin{bmatrix} 0 & 0 & 0 & 0 \\ 0 & \frac{(1-\varepsilon_2)\omega_p C}{K_1} + \frac{(1-\varepsilon_2)\omega_p C\eta_3\phi_1}{K_1K_2} & \frac{(1-\varepsilon_2)\omega_p C\eta_3}{K_2} & 0 \\ 0 & \frac{\varepsilon_2\omega_p C}{K_1} + \frac{\varepsilon_2\omega_p C\eta_3\phi_1}{K_1K_2} & \frac{\varepsilon_2\omega_p C\eta_3}{K_2} & 0 \\ 0 & 0 & 0 & 0 \end{bmatrix}.$$

the basic reproduction number (R_{0p}) is

$$R_{0P} = \frac{\omega_p C\left(\varepsilon_2\eta_3 K_1 + K_2 + \eta_3\phi_1 - \varepsilon_2 K_2 - \varepsilon_2\eta_3\phi_1\right)}{K_1 K_2} \tag{3.14}$$

where $K_1 = (\mu_H + \phi_1)$, $K_2 = \left(\mu_H + \delta + \tau\right)$, and $K_3 = \left(\mu_H + \alpha\right)$. (3.15)

(3.14) is the basic reproduction number of pneumonia model in this paper which measures the average number of new infections generated by a typical infected individual in the society.

3.5 Local Stability of disease free equilibrium

This shall be established using the theorem below.

Theorem 1**.**The model (3.1-3.5) is locally asymptotically stable (LAS), if $R_{oP} < 1$ and unstable when $R_{oP} > 1$.

Proof**:** Now, to determine the local stability of ε_0 the following jacobian matrix J_P is computed corresponding to its equilibrium point.

$$J_p = \begin{bmatrix} -\mu_h & \omega & 0 & 0 & \alpha \\ 0 & -(\mu_h + \omega) & 0 & 0 & 0 \\ 0 & 0 & -(\mu_h + \phi) & 0 & 0 \\ 0 & 0 & \phi_1 & -(\mu + \delta + \tau) & 0 \\ 0 & 0 & 0 & \tau & -(\mu + \alpha) \end{bmatrix} \tag{3.16}$$

We obtain the characteristic equation using $\left|J_p - \lambda I\right| = 0$,for I is 5 by 5 identity matrix.

Now, $\lambda I = \begin{bmatrix} \lambda & 0 & 0 & 0 & 0 \\ 0 & \lambda & 0 & 0 & 0 \\ 0 & 0 & \lambda & 0 & 0 \\ 0 & 0 & 0 & \lambda & 0 \\ 0 & 0 & 0 & 0 & \lambda \end{bmatrix}$, (3.17)

Hence, $\left|J_p - \lambda I\right| = 0$ becomes:

$$\begin{vmatrix} -\mu_H-\lambda_1 & \omega & 0 & 0 & \alpha \\ 0 & -(\mu_H+\omega)-\lambda_2 & 0 & 0 & 0 \\ 0 & 0 & -(\mu_H+\phi_1)-\lambda_3 & 0 & 0 \\ 0 & 0 & \phi_1 & -(\mu_H+\delta_1+\tau_1)-\lambda_4 & 0 \\ 0 & 0 & 0 & \tau_1 & -(\mu_H+\alpha)-\lambda_5 \end{vmatrix} = 0 \quad (3.18)$$

From (3.18), $\lambda_1 = -\mu_H$, while λ_2, λ_3, λ_4 and λ_5 are obtained from

$$\begin{vmatrix} -(\mu_H+\omega)-\lambda_2 & 0 & 0 & 0 \\ 0 & -(\mu_H+\phi_1)-\lambda_3 & 0 & 0 \\ 0 & \phi_1 & -(\mu_H+\delta_1+\tau_1)-\lambda_4 & 0 \\ 0 & 0 & \tau_1 & -(\mu_H+\alpha)-\lambda_5 \end{vmatrix} = 0 \quad (3.19)$$

Hence, the corresponding eigen values of this equation are as follows

$$\lambda_1 = -\mu_H, \lambda_2 = -(\mu_H+\omega), \lambda_3 = -(\mu_H+\phi_1), \lambda_4 = -(\mu_H+\delta_1+\tau_1) \quad and \ \lambda_5 = -(\mu_H+\alpha) \quad (3.20)$$

Since all the roots are negatives, real and distinct,. Hence, the disease free equilibrium of the pneumonia model (3.1-3.5) is locally asymptotically stable (LAS).

3.6 Global Stability of disease free equilibrium for Pneumonia

Theorem 2: The disease free equilibrium of the system of equation (3.1-3.5) is globally asymptotically stable (GAS) whenever $R_{0p} < 1$ and unstable if $R_{0p} > 1$.

Proof.

It follows that $S = N_H - V_p - E_p - I_p - R_p$ at steady state. The proof is based on using the comparison theorem describe in (Lakshkanthan*et al*, 1989) to prove the global stability. The rate of change of the variables representing the infected components of the system can be written as follows:

$$\frac{dV_p}{dt} = \rho\pi_H - \mu_H V_p - \omega V_P$$

$$\frac{dE_p}{dt} = (1-\varepsilon_2)\lambda_p\left(N_H^* - V_p - E_p - I_p - R_p\right) - \mu_H E_p - \phi_1 E_p$$

$$\frac{dV_p}{dt} = \varepsilon_2\lambda_p\left(N_H^* - V_p - E_p - I_p - R_p\right) - \phi_1 E_p \text{-- } \mu_H I_p - \delta I_p - \tau_1 I_p$$

$$\frac{dR_p}{dt} = \tau_1 I_p - \mu_H R_p - \delta R_p$$

$$D^* = \left\{\left(V_p, E_p, I_p, R_p\right) \in \mathbb{R}_+^4 : V_p + E_p + I_p + R_p \leq N_H^*\right\} \qquad (3.21)$$

For the model the associated reproduction number R_{0p}, the DFE of the model is globally asymptotically stable, inD^* if $R_{0p} < 1$, using the comparison method gives

$$\begin{bmatrix} \frac{dV_p}{dt} \\ \frac{dE_p}{dt} \\ \frac{dI_p}{dt} \\ \frac{dR_p}{dt} \end{bmatrix} = (F - V)\begin{bmatrix} V_p \\ E_p \\ I_p \\ R_p \end{bmatrix} - F_i\begin{bmatrix} V_p \\ E_p \\ I_p \\ R_p \end{bmatrix} \qquad (3.22)$$

where

$$(F - V) = \begin{bmatrix} -K_4 & 0 & 0 & 0 \\ 0 & (1-\varepsilon_2)\omega_P C - K_1 & (1-\varepsilon_2)\eta_3\omega_P C & 0 \\ 0 & \varepsilon_2\omega_P C + \phi_1 & \varepsilon_2\eta_3\omega_P C - K_2 & 0 \\ 0 & 0 & \tau_1 & -K_3 \end{bmatrix}. \qquad (3.23)$$

According to CastiloCharez*etal*(2002) , all eigenvalues of the matrix (F - V) have negative real parts, then

$$\begin{bmatrix} -K_4 - \lambda & 0 & 0 & 0 \\ 0 & (1-\varepsilon_2)\omega_P C - K_1 - \lambda & (1-\varepsilon_2)\eta_3\omega_P C & 0 \\ 0 & \varepsilon_2\omega_P C + \phi_1 & \varepsilon_2\eta_3\omega_P C - K_2 - \lambda & 0 \\ 0 & 0 & \tau_1 & -K_3 - \lambda \end{bmatrix} = 0 \qquad (3.24)$$

From equation (3.24) we find the determinant and arrive at the following characteristic equation

$$\lambda^4 + \left(k_3 - \varepsilon_2\,\omega_p\,\eta_3\,c + k_2 - \omega_p\,c + \varepsilon_2\,\omega_p\,c + k_1 + k_4\right)\lambda^3 + \left(\right.$$
$$-k_3\,\varepsilon_2\,\omega_p\,\eta_3\,c + k_3\,k_2 - k_3\,\omega_p\,c + k_3\,\varepsilon_2\,\omega_p\,c + k_3\,k_1 + k_3\,k_4$$
$$- \eta_3\,\omega_p\,c\,\phi_1 + \eta_3\,\omega_p\,c\,\phi_1\,\varepsilon_2 - \varepsilon_2\,\omega_p\,\eta_3\,c\,k_1 - \varepsilon_2\,\omega_p\,\eta_3\,c\,k_4$$
$$- k_2\,\omega_p\,c + k_2\,\varepsilon_2\,\omega_p\,c + k_2\,k_1 + k_2\,k_4 - k_4\,\omega_p\,c + k_4\,\varepsilon_2\,\omega_p\,c$$
$$\left. + k_4\,k_1\right)\lambda^2 + \left(-k_3\,\eta_3\,\omega_p\,c\,\phi_1 + k_3\,\eta_3\,\omega_p\,c\,\phi_1\,\varepsilon_2 - k_3\,\varepsilon_2\,\omega_p\,\eta_3\,c\,k_1\right.$$
$$- k_3\,\varepsilon_2\,\omega_p\,\eta_3\,c\,k_4 - k_3\,k_2\,\omega_p\,c + k_3\,k_2\,\varepsilon_2\,\omega_p\,c + k_3\,k_2\,k_1 + k_3\,k_2\,k_4$$
$$- k_3\,k_4\,\omega_p\,c + k_3\,k_4\,\varepsilon_2\,\omega_p\,c + k_3\,k_4\,k_1 + \eta_3\,\omega_p\,c\,\phi_1\,\varepsilon_2\,k_4$$
$$- k_4\,\varepsilon_2\,\omega_p\,\eta_3\,c\,k_1 - \eta_3\,\omega_p\,c\,\phi_1\,k_4 + k_4\,k_2\,\varepsilon_2\,\omega_p\,c - k_4\,k_2\,\omega_p\,c$$
$$\left. + k_4\,k_2\,k_1\right)\lambda - k_3\,k_4\left(-\eta_3\,\omega_p\,c\,\phi_1\,\varepsilon_2 + \varepsilon_2\,\omega_p\,\eta_3\,c\,k_1 + \eta_3\,\omega_p\,c\,\phi_1\right.$$
$$\left. - k_2\,\varepsilon_2\,\omega_p\,c + k_2\,\omega_p\,c - k_2\,k_1\right) \tag{3.25}$$

Let the coefficient of $\lambda^3 = a_4$, $\lambda^2 = a_3, \lambda^1 = a_2$ and a_1 = constant and applying Routh-Hurwitz criteria of order four, we obtained

$$a_4 = K_3 + K_4 - \varepsilon_2\omega_p C\eta_3 + K_1 - (1-\varepsilon_2)\omega_p C + K_2$$

$$a_3 = -\omega_p C((1-\varepsilon_2)(-\eta_3 K_3 + K_3 - \eta_3 K_1 + K_2 + K_4 - \varepsilon_2\omega_p C\eta_3 K_3 + K_2 K_3 - \eta_3\phi_1) + K_3 K_2 + K_3 K_1 + K_2 K_4 + K_4 K_1$$

$$a_2 = K_1 K_2 K_3 + K_1 K_3 K_4 + K_2 K_3 K_4 + K_1 K_2 K_4 - (1-\varepsilon_2)\omega_p C(\eta_3\phi_1 K_3 + K_2 K_3 + K_3 K_4 + \eta_3\phi_1 K_4 + K_2 K_4 - \eta_3 K_1 K_4 - \eta_3 K_3 K_4$$

$$a_1 = K_3 K_4(-\omega_P C((1-\varepsilon_2)(-\eta_3\phi_1) + \varepsilon_2\eta_3 K_1 - \varepsilon_2 K_2 + K_2) - K_1 K_2)$$

Where n = 4: $a_4 > 0,\ a_3 > 0\ and\ a_1 > 0,\ a_3 a_2 > a_1^2 + a_4^2$, then for $a_1 > 0, we\ have$

$$K_3 K_4(-\omega_P C((1-\varepsilon_2)(-\eta_3\phi_1) + \varepsilon_2\eta_3 K_1 - \varepsilon_2 K_2 + K_2) - K_1 K_2) > 0 \tag{3.26}$$

we arrived at

$$\frac{\omega_p C\{K_2 - \varepsilon_2 K_2 + \varepsilon_2\eta_3 K_1 + \eta_3\phi_1 - \varepsilon_2\eta_3\phi_1\}}{K_1 K_2} < 1 \tag{3.27}$$

we infer from (3.27) that $R_{0p} < 1$. We conclude that the linearized differential inequality above is stable for $R_{0p} < 1$which is in agreement with the claim of Castilo Chavez *et al* 2002 and (3.20), since eigenvalues of the matrix (F - V) have negative real parts.

3.7 Sensitivity analysis of the model

The sensitivity index is defined as the ratio of the relative change in R_{0p} to the relative change in the parameter say *w*, the sensitivity values of each parameter in this work were shown in the table (2) below and each one is calculated using.

$$X_w^{R_{0p}} = \frac{\partial R_{op}}{\partial w} \times \frac{w}{R_{0p}} \quad (3.28)$$

Table 1: Description of parameters used and their respective values

Parameters	Definitions	Values	Sources
π_H	Human recruitment rate	2000	Assumed
μ_H	Natural death rate of the human	0.0002	[2]
ρ	Fraction of vaccinated recruited individual	0.05	[20]
ω	The rate at which vaccine wanes for pneumonia	0.01	[20]
$\propto$	Rate of recovered moves to the susceptible class	0.2	[20]
ε_2	Fast progression for pneumonia	0.338	[5]
ϕ_1	Progression rate for pneumonia	0.01096	[7]
τ_1	Treatment rate for infected pneumonia	0.0238	[15]
δ_1	Induced mortality rate for pneumonia	0.33	[7]
ω_p	Capital contact rate for pneumonia	0.049	[20]
C	Probability of one individual transmit infection	0.1205	[20]
η_3	Modification parameter for pneumonia	0.008883	[1]

TABLE 2: Pneumonia model parameters with their respective sensitivity values

PARAMETERS	**SENSITIVITY VALUES**
μ_H	-0.02367185947
τ_1	-0.2325904914
δ_1	$-0.0060733253$32
η_3	0.259907081$\dot{3}$
ε_2	-0.4931129892
ϕ_1	$-0.737664323$9
ω_P	1.0000000$\dot{0}$
C	1.0000000$\dot{0}$

3.8 Optimality of the model

To obtain an optimal control for the system, the controls u_i where i = 1, 2, 3 were introduced to curtail the spread of the diseases. Then, u_1 stands for the prevention effort in order to protect susceptible individual from contacting the pneumonia disease. Also u_2 represents the control on the awareness of pneumonia vaccine (immunization) through education/campaign by organizing seminars and conferences while u_3 is the control on treatment made to minimize pneumonia infection. After incorporating u_i into the equation (3.1), then optimal control model goes thus:

$$\frac{dS_p}{dt} = (1-\rho)\pi_H + (1-u_1)\lambda_p S_H - \mu_H S_H + \alpha R_p + \omega V_p, \quad (3.29a)$$

$$\frac{dV_p}{dt} = \rho\pi_H - \mu_H V_p - u_2\omega V_p, \quad (3.29b)$$

$$\frac{dE_p}{dt} = (1-u_1)(1-\varepsilon_2)\lambda_p S_H - \mu_H E_P - \phi_1 E_P, \quad (3.29c)$$

$$\frac{dI_p}{dt} = (1-u_1)\varepsilon_2\lambda_p S_H + \phi_1 E_P - \mu_H I_P - \delta_1 I_P - (1-u_3) I_P \tau_1, \quad (3.29d)$$

$$\frac{dR_p}{dt} = (1-u_3)\tau_1 I_P - \mu_H R_P - \boldsymbol{\alpha} R_P. \quad (3.29e)$$

3.9 Analysis of Optimal Control

To study the optimal levels of the controls, the control set U is lebesque measurable and it is defined as $U = u_1(t), u_2(t), u_3(t)$ for u_I, I = 1, 2, 3 and $0 \le t \le J$. The aim is to obtain a controlu_I on S_H, V_p, E_P, R_P and I_P that minimize the proposed objective functional J. The objective function J is given as;

$$J(u_1, u_2, u_3) = \int_1^{t_f} \{f_1 V_p + f_2 E_p + f_3 I_p + \sum_{1=1}^{3} A_i u_i^2\} dt \quad (3.30)$$

Here the constants f_1, f_2, f_3 are positive weights on individual that received vaccine for pneumonia, exposed pneumonia and infected human by pneumonia. Weight co-efficient $A_i, i = 1, 2, 3$ are measure of relative cost of the interventions associated to control u_I is quadratic because it was assumed that costs are non-linear in its nature. The aim here is to minimize the number of $f_1 V_p, f_2 E_p$ *and* $f_3 I_p$ costs of control $u_1(t), u_2(t), u_3(t)$. Thus optimal controls (u_1, u_2, u_3) shall be seeking to such that,

$$J(u_1, u_2, u_3) = Min\{J(u_I : i = 1, 2, 3) \; such \; that \; u \in U\}$$

$$where \; U = \{(u_1, u_2, u_3) \; such \; that \; each \; u_I : i = 1, 2, 3 \quad (3.31)$$

$$is \; measurable \; with \; 0 \le u_I \le 1 \;\; t \in [0, t_f] \to [0,1] \}$$

The terms$A_1u_1^2$, $A_2u_2^2$, and $A_3u_3^2$ are the costs on campaign for pneumonia immunization, exposed pneumonia.

3.10 Hamiltonian and Optimality System

In order to establish the optimality of the system and to show that the system is also Hamiltonian, we implore the idea of the maximum principle where the necessary conditions are satisfied by optimal pair would be arrived. Also, this principle shall converts equations (3.29b) and (3.29c) into the problem of minimizing point wise to a Hamiltonian *H* with respect to u_I. Therefore, to find an optimal solution, firstly, we shall seek for the Lagrangian and Hamiltonian of the system for the optimal control problem. Then the Lagrangian (L) of the optimal problem is given by

$$L = f_1V_p + f_2E_p + f_3I_p + \sum_{1=1}^{3} A_iu_i^2 \qquad (3.32)$$

In order to have minimal value of Lagrangian the Hamiltonian *H* for the control problem is obtained as follows

$$H = L\left(f_1V_p + f_2E_p + f_3I_p + \sum_{1=1}^{3} A_iu_i^2\right) + y_1\frac{dS_H}{dt} + y_2\frac{dV_p}{dt} + y_3\frac{dE_p}{dt} + y_4\frac{dI_p}{dt} + y_5\frac{dR_p}{dt} \quad (3.33)$$

where the value of $\frac{dS_H}{dt}, \frac{dV_p}{dt}, \frac{dE_p}{dt}, \frac{dI_p}{dt}, \frac{dR_p}{dt}$ has been given in equation (3.33)

Theorem 3

Given the control model (3.1), there exists an optimal control pair $u^* = u_i^* \in U$ for $I = [1, 3]$ such that $J(u_i^*) = Min\{J\left((u_1, u_2, u_3\right)\}$ subject to control system (3.33)

Proof

To prove the existence of an optimal control pair, we verify the following highlighted properties of the model:

(i) The set of the entire controls variable and corresponding state variables are non-empty

(ii) The set of controls is convex and closed

(iii) The optimal system (right hand side of the state problem) is bounded by linear function in the state and control variables. Whereas this determines the compactness needed for the existence of the optimal control.

(iv) The integrand in the objective functional (3.33) is concave on the control set.

(v) There exist positive numbers and a constant *w* such that the integrand of $L = \left(V_p, E_p, I_p, u_1, u_2, u_3\right)$ of the objective functional are satisfied such that

$$J(u_i) \geq P_1(|u_i|^2)^{\frac{w}{2}} - P_2 \quad for \quad i = 1,2,3. \qquad (3.34)$$

because the state variables are biunded, this completes the existence of an optimal control.

Theorem 4

For an optimal control set u_1, u_2, u_3 and optimal state solution $S_H^*,\ V_P^*, E_p^*, I_p^*\ and\ R_p^*$ of the corresponding state system (3.1-3.5) that minimizes the objectives functional $J(u_1, u_2, u_3)$ over ∪.

Proof

By Pontryagin's maximum principle, the form of the adjoint equations and transversality conditions are standard results. Then, differentiating the Hamiltonian function H with respect to each states variables $y_1, y_2, y_3, y_4\ and\ y_5$ respectively which are evaluated at the optimal control function $u_1, u_2\ and\ u_3$.So, re-written the adjoint system and with the following transversality conditions

$$y_1(t_f) = y_2(t_f) = y_3(t_f) = y_4(t_f) = y_5(t_f) = 0 \qquad (3.35)$$

Solving $\frac{\partial H}{\partial u_i}$, for i= 1, 2, 3 and evaluating at the optimal control on the interior of control set, where $0 < u_i \leq 1$ gives

$$\frac{\partial H}{\partial u_1} = 2A_1u_1 - S_H^*(-y_1 + y_3(1 - \varepsilon_2) + y_4\varepsilon_2)\lambda_p \qquad (3.36a)$$

$$\frac{\partial H}{\partial u_2} = 2A_2u_2 - V_p^*\omega(y_1 - y_2) \qquad (3.36b)$$

$$\frac{\partial H}{\partial u_3} = 2A_3u_3 - I_p^*\tau_1(y_4 - y_5) \qquad (3.36c)$$

Then,

$$u_1^* = \max\{0, \min(1, \frac{S_H^*(-y_1 + y_3(1-\varepsilon_2) + y_4\varepsilon_2)\lambda_p}{2A_1})\} \qquad (3.37a)$$

$$u_2^* = \max\left\{1, min\left(1, \frac{V_p^*\omega(y_1 - y_2)}{2A_2}\right)\right\} \qquad (3.37b)$$

$$u_3^* = \max\left\{1, min\left(1, \frac{I_p^*\tau_1(y_4 - y_5)}{2A_3}\right)\right\} \qquad (3.37c)$$

In compact notation

$$u_1^* = \max\{0, \min(1, \gamma_1)\}$$

$$u_2^* = \max\{0, \min(1, \gamma_2)\}$$

$$u_3^* = \max\{0, \min(1, \gamma_3)\}$$

where $y_1, y,\ and\ y_3$ can be deduce from equation (3.36).

4. Results and Discussion

4.1 Numerical Analysis and discussion of results

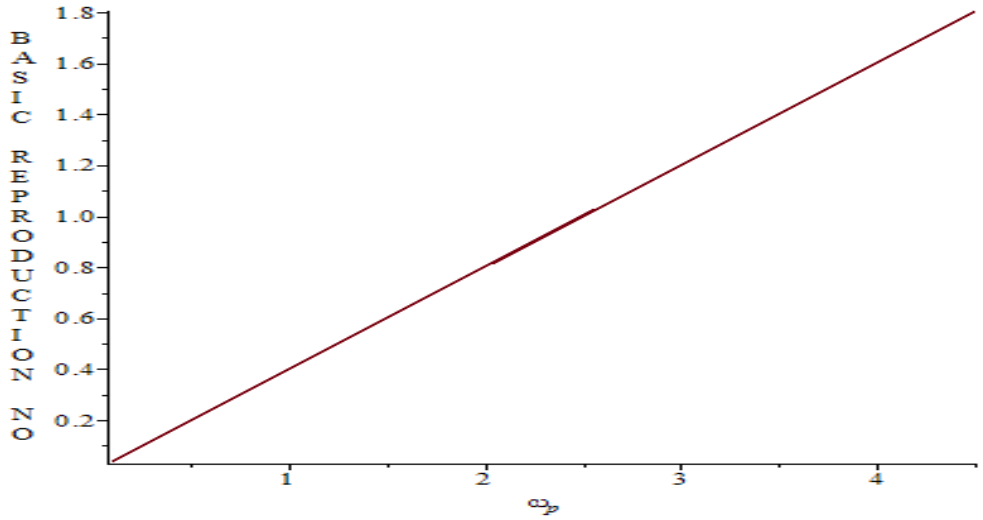

Figure 2: The graph of R_{0p} against ω_p

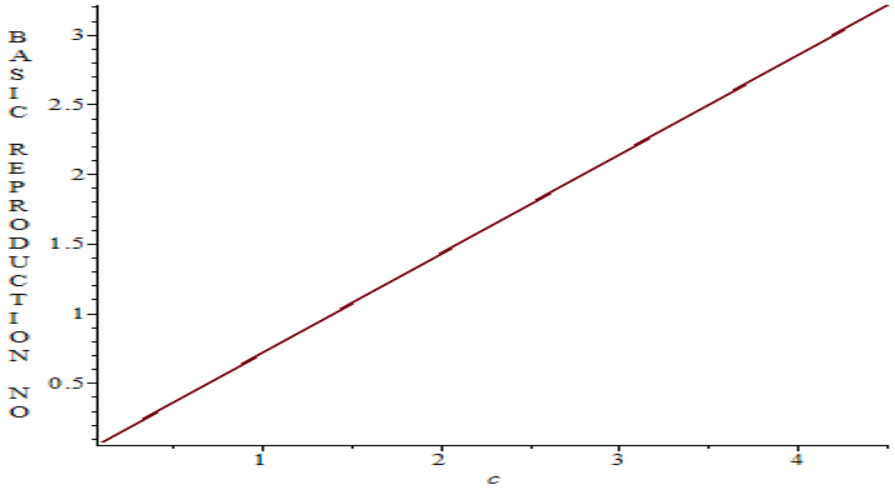

Figure 3: The graph of R_{0p} against c.

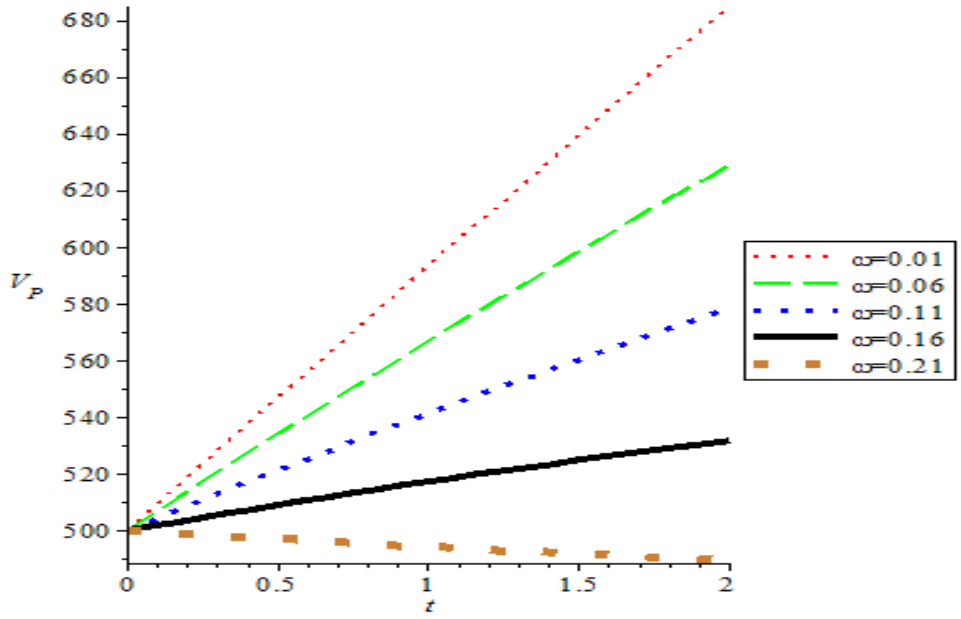

Figure 4: Graph of V_P against t with different values of ω

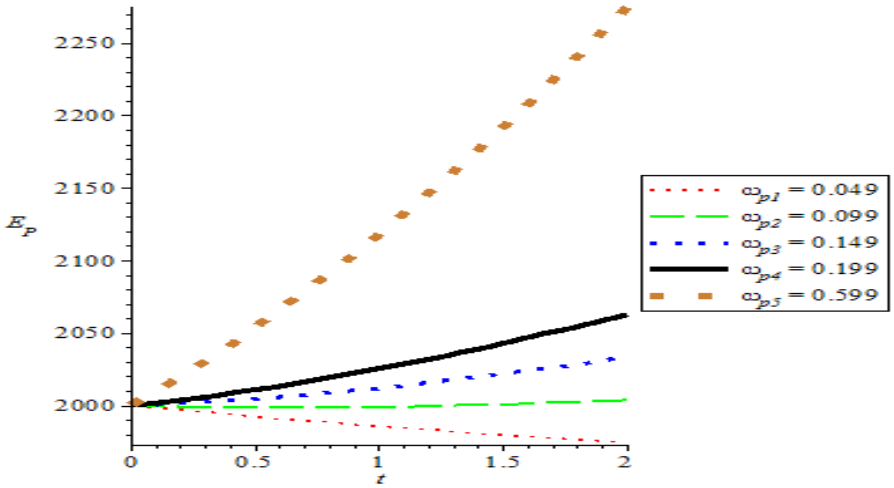

Figure 5: The graph of E_p against time(t) with different values of ω_p.

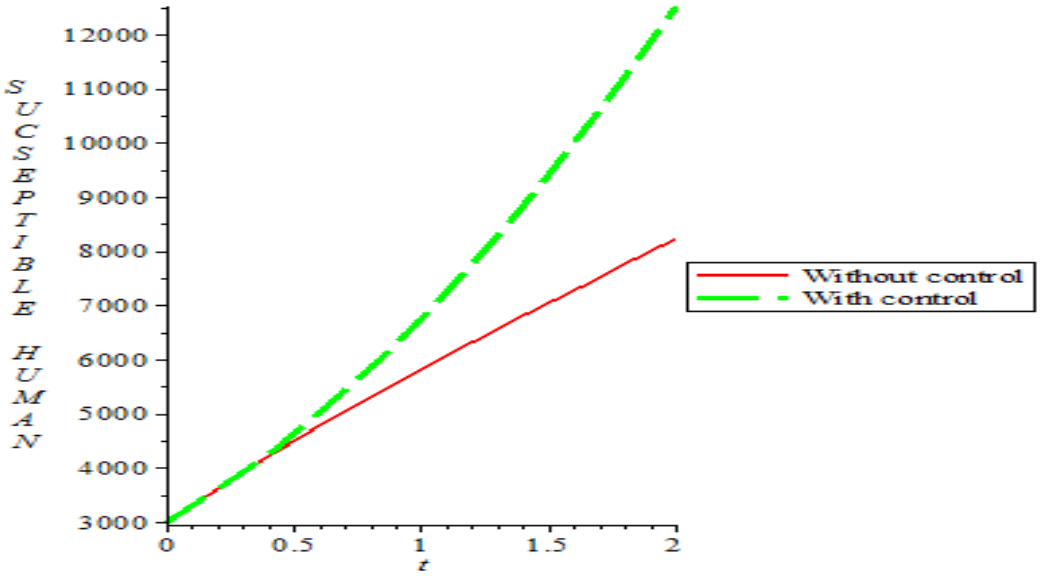

Figure 6: Graph of optimal control on susceptible individuals against time t in years.

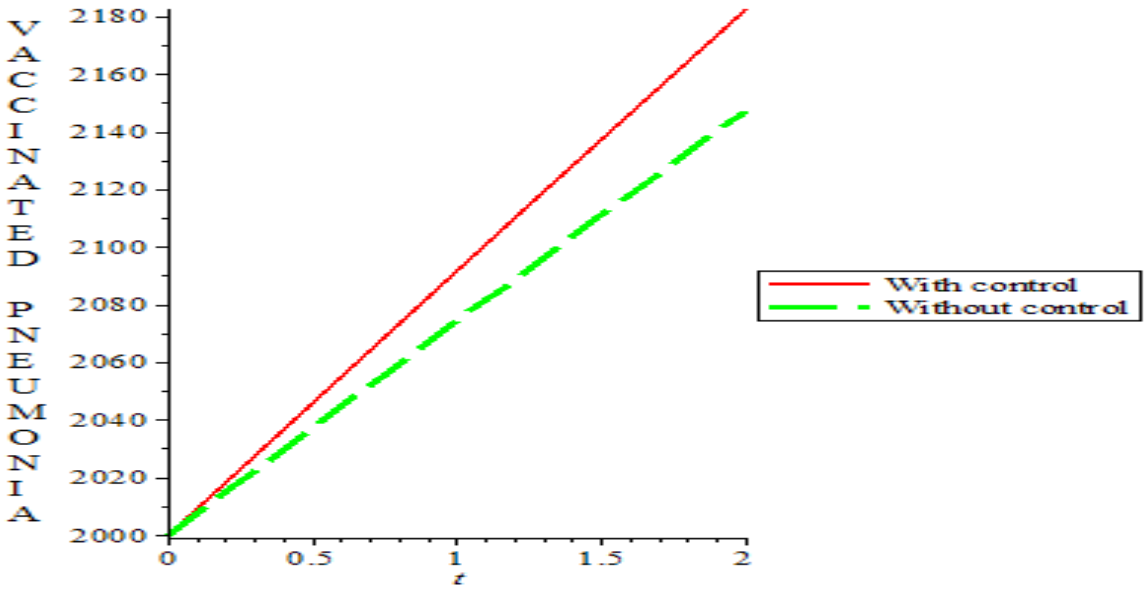

Figure 7: Graph of optimal control on individuals that received pneumonia vaccine against time t in years.

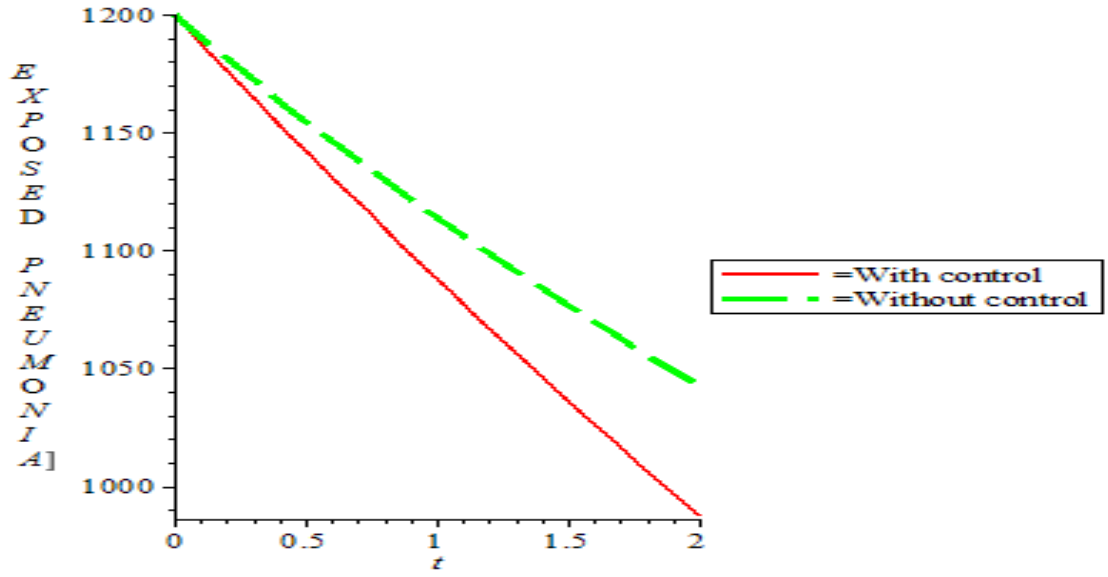

Figure 8: Graph of optimal control on individuals that were exposed to pneumonia against time t in years.

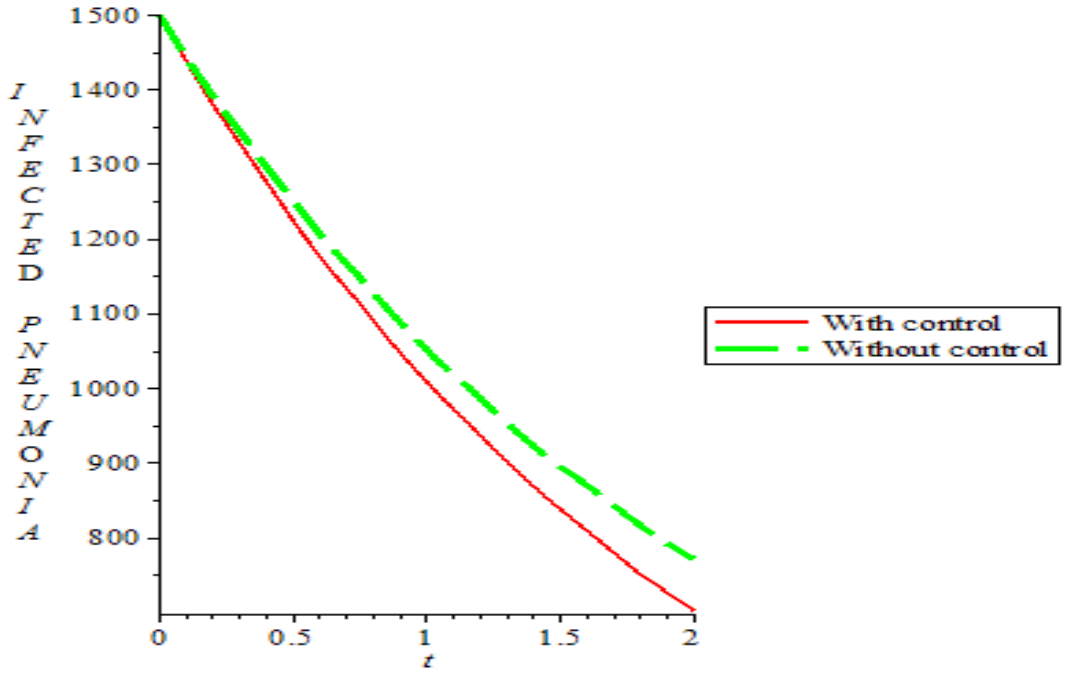

Figure 9: Graph of optimal control on infected individuals with pneumonia against time t in years.

According to the sensitivities analysis (table 1) of the model, it could be seen that transmission rate (ω_p) and effective contact rate (C) have greater influence on the basic reproduction number of pneumonia (R_{0p}) because their sensitivities values are 1.000 and 1.000. Hence these two parameter (i.e. $\omega_p \; and \; C$) are the most sensitive parameters on the analysis of R_{0p} while the higher these parameters, the higher the basic reproduction number (R_{0p}) which measures the average number of secondary infectious individual generated by a single infected person. This shows that the more the transmission and contact rates, the more the pneumonia epidemic in the society, awareness should be made to the public by the government or communities leaders so that anywhere there is pneumonia infection or disease, the rate of contact by innocent people should be avoided or reduced. Also, the infected individual with pneumonia should be separated in order to reduce the transmission rate of pneumonia because this disease is an airborne type.

Figure 2 shows the effect of pneumonia contact rate on basic reproduction number of pneumonia. It reveals that the increment in contact rate yields increment in reproduction number of pneumonia. Since basic reproduction number measures the average number of secondary infectious individual caused by single-infected individual, then the more individual contact pneumonia disease if the higher the basic reproduction number. Hence, there would be an epidemic of the disease if the rate at which individual contact pneumonia increased. The figure 2 also shows that the more the infected individual transmits the pneumonia infection, the more the spread of this disease in the society. Hence, the basic reproduction number (R_{0p}) will be greater than one and endemicity of pneumonia would occur in such community. So, the transmission rate must be reduced in order to avoid or reduce the quick spread of pneumonia. The figure 3 shows the effect at which vaccine for pneumonia wanes on the individual that receives pneumonia vaccine. Vaccine for pneumonia is well posed but can wane at anytime. Hence, the person that received vaccine for pneumonia can contact this disease whenever the vaccine wanes. So, whenever the vaccines wanes shows there would be no immunity for such vaccinated people and the tendency of contacting the pneumonia would be high. Therefore, the population of this vaccinated class gets reduced. The high value of the rate at which vaccine wanes tends to reduce the population of vaccinated class. According to the graph, the population of vaccinated class at ω= 0:01 were greater than the number of vaccinated population when the ω= 0:21 .This implies that the higher the rate at which vaccine wanes the lesser the population in the vaccinated class. Also, figure 5 reveals that increase in contact rate of pneumonia disease leads to increase in the population of exposed class of pneumonia with respect to time especially when the contact rate was highly increased to 0:599.

The graph 6 shows the effect of applying all controls on susceptible population in this research work and without any control as well. It could be seen that when controls were applied, the population of susceptible class grows faster than when no control was applied. The dotted green line represent when all

controls were applied while the red one is for without control at all. So ,one can conclude that there should be effective control application on pneumonia in the society in order to avoid the epidemic of pneumonia. In figure 7, the effect of applying pneumonia vaccine (immunization) and education or campaign on its awareness by organizing seminars and conferences on the vaccinated class of pneumonia in this work were tested. It was seen that the red line that represent with control and dotted green line that represent without control move at the same rate at initial stage which is due to the fact that the control is yet to take effect since it is immunization. But immediately that the control took effect it leads to increase in population of the vaccinated class. Meanwhile, graph 8 shows the effect of preventing effort from contacting pneumonia (u_1) and treatment to minimize pneumonia infection u_2 on exposed individual to pneumonia. It was observed that the red line which represents with control falls in a proportional rate, that is to say the control is inversely proportional to population of exposed class. So the more the control rates lesser will be number of exposed individual and vice versal. Whereas, the dotted green line that stands for without control fall in a steady rate. Figure 9 reveals the effect of both prevention effort from contacting pneumonia (u_1) and provision of treatment for pneumonia u_3 on infected individuals with pneumonia. Since the population of this infected class can spread the pneumonia infection, then appling contols and without controls fall at thesame rate before those that receives control move faster than those without control.

5. Conclusion

Conclusively, the effect of applying pneumonia vaccine (immunization) and education or campaign on vaccine awareness by organizing seminars and conferences on the society especially for children and adult people in the society were shown in this work. The reason is that without campaign or education on awareness of vaccine the children of within age five(5) and adult of sixty-five (65) years above may not be aware till this pneumonia deadly disease kill them at home. Also, for the fact that pneumonia is a contagious disease, if both infected and exposed individuals with pneumonia were not properly kept or treated, thereby, epidemic of pneumonia will occur because there would be high contact rate.

References

Adewale, S.O., Mohammed, I. T. &Olopade, I. A. (2014). Mathematical analysis of effect of habitat area on the dynamical spread of measles. *International Organization of Scientific Research Journal of Engineering (IOSRJEN)4(3): 43 - 57.*

Adewale, S. O., Podder, C. N. and Gumel, A. B. (2009). *Mathematical analysis of a TB transmission model with DOT. Canadian Applied Mathematics Quarterly.* 1(17):1-36.

AdewaleS. O.,OlopadeI. A., AdeniranG.A., Mohammed I.T. &AjaoS. O. (2015). Mathematical analysis ofeffectsofısolationonebola transmission dynamics.*Research JournalofMathematics.2015;2(2):1-20.*

Adewale, S.O., Adeniran, G. A.,Olopade, I.A., Ajao, S. O. & Mohammed, I. T. (2017). Mathematical and sensitivity spread of cholera. *International Journal of Innovations and Applied Studies. 19(1): 46-54.*

Adult Pneumonia Clinical Guideline (Community and Hospital Acquired) Hunter New England Local Health District. Version 1, April 2012.

Aluko, O.B. Babatunde, O.H., Isikilu, I.T.&Ojo, B. (2012). Modelling and simulation of spread of malaria epidemic. *International Journal of Scientific and Statistical Computing (IJSSC).3(10): 20– 27.*

Amber M. S, Jonathan A. M, and Frederick R. A, (2011). Mathematical model of a three

stage innate immune response to a pneumococcal lung infection. *Journal of Theoretical Biology,* 2(76):106-116.

Anderson R.M and May R.M, (1991). Infectious disease of human dynamics and control.

Oxford University Press, London New York.

Birkhoff and G.C. Rota, (1989).Ordinary Differential Equations, 4th Edition, John Wiley and Sons, Inc; New York.

Derricks W.R. and Grossman S.I. (1976). Elementary Differential Equations with application. Addison Wesley Publications Company, Philippine.

Dickamann and Hesterbeek J.A.P (2002). Mathematical Epideminology of infectious Disease: Model building, Analysis and Interpretation, New York Willey.

Driessche P.V and Watmough J. (2002). Reproduction numbers and Sub-threshold endemic equilibra for compartmental models of disease transmission. *Mathematical Bioscience*, 180; 29-48

Ebby, O., (2005). Community-Acquired Pneumonia: From Common Pathogens to Emerging Resistance. *Emergency Medicine Practice:* 7(12)

Castillo-chavev, C. Blower, S. Vander Derichee, P. Krischne, D. and Yakubu A.A.(Eds) (2002). Mathematical Approaches for Emerging and Reemerging infectious diseases. An introduction IMA Volumes in Mathematics and its application. Springer Verlag, New York, 125, 229-250.

GetachewTeshomeTilahun, Oluwole Daniel Makinde and David Malonza, (2017).Modelling and Optimal Control of Pneumonia disease with Cost-effective Strategies.*Journal of Biological Dynamics*. 11(2): 400 –426.

Kateete, D., Kajumbula, H., Deogratias K., and Ssevviri, A. (2012).Narsophageal Carriage Rate of Streptococcus Pneumoniae in Ugandan Children with Sickle Cell Disease. BMC Research Notes, 5(28): 321-416

Kermack W.O and Mackendrick A. G. (1932). A Contribution to the Mathematics Theory of Epidemic Proc. Roy. Soc. (A138): 58-83.

Lakshmikantham, V. Leela, S. and Martynyuk A.A (1989). Stability Analysis of Nonlinear Systems. Marcel Dekker, Inc., New York and Basel.

Marcus, I.O. and Newton, I.O.(2021). Mathematical modeling and Analysis of [neumonia infection dynamics. *Science world journal, vol. 16 No(2) page 73-80.*

Marrie, T.J, (2011). Epidemiology, Pathogenesis and Microbiology of Community-Acquired Pneumonia in Adults.

Mohammed, I. T. (2019). Mathematical Modeling and Optimal control of Malaria–Pneumonia Co-infection, *Unpublished PhD Thesis,* LadokeAkintola University of Technology, Ogbomoso, Nigeria.

OlopadeI. A.,MohammedI. T., PhilemonM. E., AjaoS. O., AdeniranG. A.,SagoniyiS. &AdewaleS. O. (2024). Mathematical analysis of optimal control of human immunodeficiency virus (HIV) co-infection with tuberculosis. Asian Research Journal of Current Sciences.2024; 6(1): 23-53.

OlopadeI. A., SagoniyiS.O., PhilemonM. E., MohammedI. T., AdeniranG. A., AjaoS. O., Aisha U. M. &Adamu A. K. (2024). Mathematical modelling and analyzing the dynamics of condom efficacy and compliance in the spread of HIV. Asian Research Journal of Current Sciences.2024; 6(1): 54-65.

Olopade I.A,AdesanyaA.O.&MohammedI.T. (2017).Mathematical analysisofthe global dynamics of an SVEIR epidemic model withherdimmunity.InternationalJournalof ScienceandEngineering Investigations. (IJSEI).2017;6(69):141-148.

OlopadeI.A.,AdewaleS.O,MohammedI.T., Adeniran G.A.,AjaoS.O.&OgunsolaA.W. (2021). Effectofeffective contacttracingin curtainingthe spread ofCovid-19. *Asian Journal of Research in Biosciences*.2021;3(2):118-134.

OlopadeI.A,AdewaleS.O,MohammedI.T, AjaoS.O.&OyedemiO.T. (2016). Mathematical analysisof theroleof detection in the dynamical spreadofHIV-TBCo-infection.*JournalofAdvancesin Mathematics*.2016;11(10):5715-5740.

Pontryagin, L.S., Boltyanskii, V.G.,Gamkrelize,R.V. and Mishchenko, E.F.(1986). The Mathematical Theory of Optimal Processes, John Wiley & Sons, New York.

Rudan, C. Boschi-Pinto, Z. Biloglar, K. Muholland, and H. Campbell (2011).Epidemiology and Eutomology of Childhood Pneumonia.*Bulletin of the World Health Organization.*

Singh, V. and Aneja, S. (2011).Pneumonia Management in the Developing World. Pediatric Respiratory Reviews, 12(1): 52-59.

Tilahun, G.T. (2019). Mathematical Model for Co-infection of Pneumonia and Meningitis with Optimal Control.*Ph.D. Thesis, the Pan African University.P1-71.*

Word Health Organization (2005).Technical Basis for the WHO Recommendations on the Management of Pneumonia in Children at First-Level Health Facilities. WHO/ARI/91.20

World Health Organization (WHO) The United Nations Children's Fund (UNICEF), Global Aeron plan for prevention and control of Pneumonia (GAPP) [Internet]. WHO (General) 2009 Nov [cited: 2011] Oct. Available from: http/www.unicef.org/media/files/GAPP3 – web. Pdf)

Population dynamics of a mathematical model for Campylobacteriosis

T. T. Ashezua[1], M. T. Salemkaan[2] and S. A. Somma[3]
[1,2]Department of Mathematics, Joseph Sarwuan Tarka University Makurdi, Nigeria
[3]Department of Mathematics, Federal University of Technology, Minna, Nigeria

Corresponding author's email/Phone number: timothy.ashezua@uam.edu.ng, 07032230542

Abstract

The bacterium campylobacter is the cause of campylobacteriosis, a major cause of foodborne illness that goes by the most common name for diarrheal illnesses. This paper develops and analyzes a new mathematical model for campylobacteriosis. It is demonstrated that in cases where the corresponding reproduction number is smaller than unity, the model's disease-free equilibrium is both locally and globally stable. The numerical simulation results indicate that increasing the treatment rate for both symptomatic and asymptomatic disease-infected individuals resulted in a decrease in the number of asymptomatic and symptomatic individuals, respectively, and a rise in the population's number of recovered individuals.

Keywords: Reproduction number, stability, mathematical simulation, campylobacteriosis.

1.0 Introduction

The bacterium campylobacter is the source of campylobacteriosis, a major cause of foodborne illness that is thought to be the most prevalent indicator of diarrheal illnesses (WHO, 2020). The World Health Organization estimates that the burden of food-borne illnesses claims the lives of approximately 33 million healthy people and causes 1 in 10 people to become ill. The majority of illnesses resulting from eating unsafe food are diarrheal diseases, accounting for 550 million illnesses per year, of which 220 million are in children under the age of five (WHO, 2020). The majority of the time, campylobacter infections are mild (asymptomatic); however, in very young children, the elderly, and people with compromised immune systems, they can be fatal (symptomatic) (WHO, 2020, Health direct, 2024).

Common symptoms of campylobacter infection are; fever, cramping in the stomach, and diarrhea, which is frequently bloody. After diarrhea, nausea and vomiting are possible. Following infection, symptoms typically appear two to five days later and persist for approximately one week. Some people experience complications like arthritis, irritable bowel syndrome, and temporary paralysis (CDC, 2023). The majority

of people with campylobacter infections recover without the need for antibiotics, Centers for Disease Control and Prevention reported that (patients are advised to stay hydrated for the duration of their diarrhea), however severe cases may require antibiotic treatment. The groups most likely to experience severe cases of the disease are the elderly (65 years of age and older), pregnant women, and individuals with weakened immune systems (CDC, 2019).

Throughout the years, mathematical models of infectious diseases have offered helpful insights into the dynamics of infectious disease transmission, prevention, and control (Gulmel *et al*., 2018 are one example of this). However, only a small number of mathematical models have been created and applied to campylobateriosis in order to comprehend the disease's dynamics of transmission, management, and prevention; for instance, refer to (Rawson *et al.* 2019, Nyasagare et al. 2019, Osman *et al.* 2020, Chuma and Mussa, 2021). In 2019, Rawson and colleagues created and studied a mathematical model of the campylobacter in broiler flocks dynamics. In their investigations, the pathways of infection among co-housed birds were modeled using a system of stochastic differential equations. Nyasagare *et al.* (2019) developed and examined a mathematical model of campybacteriosis in animal and human populations using the S-I-R approach. Using an S-I-R model for both human and animal populations, Osman *et al.* (2020) developed and examined a mathematical model for campylobacteriosis using a modified finite difference method with optimal control. Chuma and Mussa (2021) created and examined an epidemic model that included sanitation control, treatment, and public health education to explain the dynamics of the campylobacteriosis disease. They did not divide the exposed class into asymptomatic and symptomatic classes in their work. A novel deterministic mathematical model for analyzing the dynamics of campylobacteriosis transmission in a population is presented in this work. The following presumptions form the basis of the model:

(i) The exposed class is split into asymptomatic and symptomatic classes, respectively. This is in line with the information obtained from (Osman *et al.* 2020, Health direct, 2024).

(ii) Asymptomatic individuals can recover without treatment and equally develop symptoms to progress to the symptomatic class while symptomatic patients might need antibiotics treatment (CDC, 2019).

In all the aforementioned mathematical models of Campylobacteriosis, none of them considered the assumptions (i) and (ii). Hence, in the present study, the exposed class have been split into the asymptomatic and symptomatic classes. Also, treatment of the asymptomatic and symptomatic patients are included as intervention strategies in our model to curtail the spread of the disease in the population.

2.0 Model Formulation

The total population at time t, denoted by $N(t)$, is divided into the human $(N_h(t))$ and animal $(N_v(t))$ populations. The total population of humans is further sub-divided into the five mutually-exclusive compartments of the susceptible $(S_h(t))$, exposed $(E_h(t))$, asymptomatic $(I_a(t))$, symptomatic $(I_s(t))$, and recovered $(I_a(t))$ humans. Also, the total animal population is sub-divided into the susceptible $(S_v(t))$, infected $(I_v(t))$ and recovered $(R_v(t))$ sub-population. Thus,

$$\begin{aligned} N(t) &= N_h(t) + N_v(t) \\ N_h(t) &= S_h(t) + E_h(t) + I_a(t) + I_s(t) + R_h(t), \\ N_v(t) &= S_v(t) + I_v(t) + R_v(t). \end{aligned} \tag{2.1}$$

The susceptible population (for both human and animals) are recruited through immigration at rates $\Lambda_h(\Lambda_v)$, respectively. Humans in E_h class progresses to class I_a and I_s at rate θ while ρ is the proportion of humans that progressed to class I_a. The humans in classes I_a and I_s recover from campylobacteriosis at rates γ_1 and γ_2, respectively. Furthermore, natural death rate $\mu_h(\mu_v)$ occurs in all the epidemiological classes of human (animal) population while humans (animals) in classes I_s and I_v suffer an additional Campylobacteriosis induced death at a rate $\delta_h(\delta_v)$, respectively. Humans and other animals that are susceptible to the disease can contract campylobacteriosis by eating contaminated food or water or by coming into close contact with infected humans or animals (i.e. those in the I_a, I_s and I_v classes), at a rate $\beta_1\lambda$ and $\beta_2\lambda$, respectively, given by

$$\beta_1(I_a + I_s + I_v), \tag{2.2}$$

and

$$\beta_2(I_a + I_s + I_v). \tag{2.3}$$

Animals recover from campylobacteriosis at a rate γ_3.

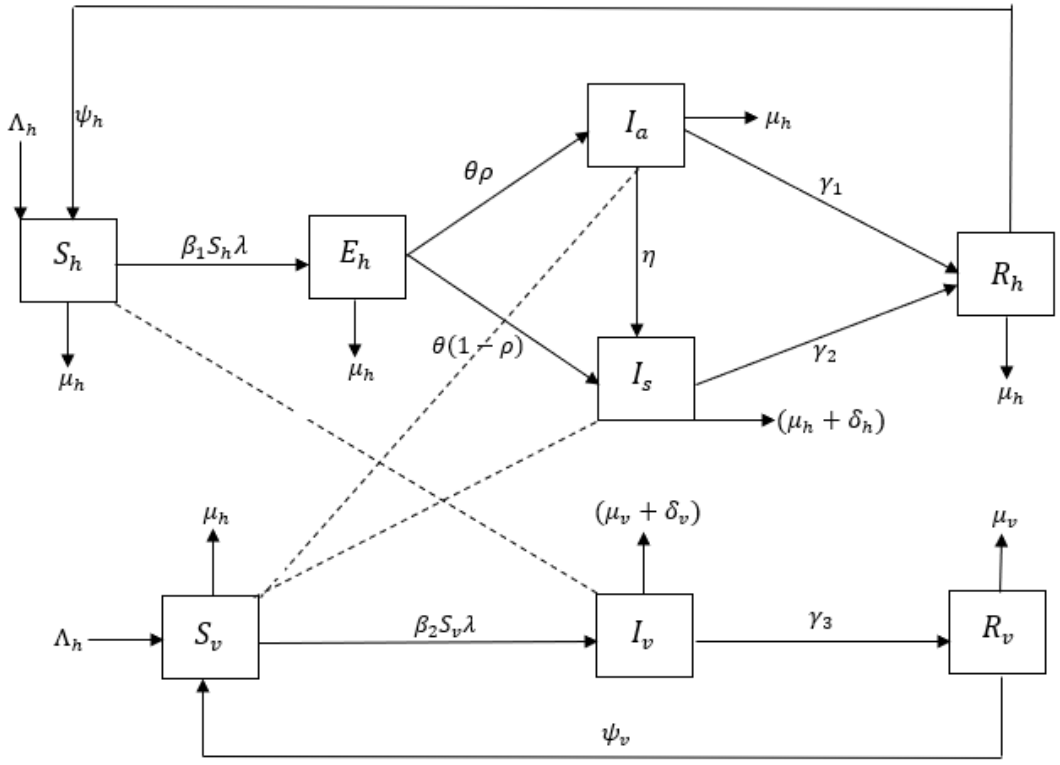

Figure 1. Schematic diagram for model (2.4).

Table 1: Description of variables and parameters in the Campylobacteriosis model (2.4).

Variables/parameters	Interpretation
S_h	Susceptible human population
E_h	Exposed human population
I_a	Asymptomatic human population
I_s	Symptomatic human population
R_h	Recovered human population
S_v	Susceptible animal population
I_v	Infected animal population
R_v	Recovered animal population
$\Lambda_h(\Lambda_v)$	Recruitment rate into the susceptible human (animal) compartments
$\beta_1(\beta_2)$	Infection rates
θ	Progression rate
ρ	Proportion of exposed humans moving to class I_a

η	Progression rate from I_a to I_s
$\gamma_1(\gamma_2)$	Treatment rates for the human
γ_3	Treatment rate for the animals
$\mu_h(\mu_v)$	Human (animal) natural death rate
$\psi_h(\psi_v)$	Loss of immunity
$\delta_h(\delta_v)$	Human (animal) disease-induced death rate
λ	Force of infection

When all of these definitions and presumptions are combined, the system of differential equations in (2.4) yields the new Campylobacteriosis model. Figure 1 displays the model's flow diagram, and Table 1 lists the variables in the model.

$$\begin{aligned}
\frac{dS_h(t)}{dt} &= \Lambda_h - \beta_1\lambda S_h - \mu_h S_h + \psi_h R_h,\\
\frac{dE_h(t)}{dt} &= \beta_1\lambda S_h - [\theta\rho + \theta(1-\rho) + \mu_h]E_h,\\
\frac{dI_a(t)}{dt} &= \theta\rho E_h - (\eta + \gamma_1 + \mu_h)I_a,\\
\frac{dI_s(t)}{dt} &= \theta(1-\rho)E_h + \eta I_a - (\gamma_2 + \mu_h + \delta_h)I_s, \qquad (2.4)\\
\frac{dR_h(t)}{dt} &= \gamma_1 I_a + \gamma_2 I_s - (\mu_h + \psi_h)R_h,\\
\frac{dS_v(t)}{dt} &= \Lambda_v - \beta_2\lambda S_v - \mu_v S_v + \psi_v R_v,\\
\frac{dI_v(t)}{dt} &= \beta_2\lambda S_v - (\gamma_3 + \mu_v + \delta_v)I_v,\\
\frac{dR_v(t)}{dt} &= \gamma_3 I_v - (\mu_v + \psi_v)R_v.
\end{aligned}$$

where the forces of infection for human and animals are as given in equations (2.2) and (2.3), respectively.

Theorem 2.1.: When starting with positive data, every solution in the model (2.4) stays positive over time. Additionally, the model is a dynamic system on the area that has, $\Omega = \Omega_1 \cup \Omega_2 \subset \Re_+^5 \times \Re_+^3$ with,

$$\Omega_1 = \left\{ \left(S_h, E_h, I_a, I_s, R_h\right) : S_h + E_h + I_a + I_s + R_h = N_h \le \frac{\Lambda_h}{\mu_h} \right\},$$
$$\Omega_2 = \left\{ \left(S_v, I_v, R_v\right) : S_v + I_v + R_v = N_v \le \frac{\Lambda_v}{\mu_v} \right\}, \tag{2.5}$$

Proof. Following similar approach as in Gumel *et al.,* (2018), it is easy to see that the following first-order inequality equations follow from the equations for humans (susceptible individuals) and animals (susceptible animals) in model (2.4):

$$\frac{dS_h}{dt} + \left(\beta_1 \lambda + \mu_h\right) S_h > 0, \text{ and } \frac{dS_v}{dt} + \left(\beta_2 \lambda + \mu_v\right) S_v > 0$$

Applying integrating factor to the inequalities

$$\alpha_{S_h}(t) = \exp^{\int [\beta_1 \lambda(\tau) + \mu_h] d\tau}, \alpha_{S_v}(t) = \exp^{\int [\beta_2 \lambda(\tau) + \mu_v] d\tau},$$

and observing that

$$\alpha S_h(t) \left[\frac{dS_h(t)}{dt} + (\beta_1 \lambda + \mu_h) S_h \right] = \frac{dS_h \alpha S_h}{dt},$$
$$\alpha S_v(t) \left[\frac{dS_v(t)}{dt} + (\beta_1 \lambda + \mu_v) S_A \right] = \frac{dS_v \alpha S_v}{dt},$$

then integrating from 0 to gives $S_h(t) \ge 0$ and $S_v(t) \ge 0$ at all times, respectively, with respect to time. Nevertheless, the remaining equations are not amenable to this direct method. However, the conservation law is obtained by summing the model's first five and final three equations (2.4).

$$\left.\begin{aligned} \frac{dN_h}{dt} &= \Lambda_h - \mu_h N_h - \delta_h I_s \\ \frac{dN_v}{dt} &= \Lambda_v - \mu_v N_v - \delta_a I_v \end{aligned}\right\} \tag{2.6}$$

Thus, the general a priori estimates below can be demonstrated to hold using a standard comparison theorem.

$$\left.\begin{aligned} 0 \le N_h(t) &\le N_h(0) \exp^{-\mu_h t} + \frac{\Lambda_h}{\mu_h}\left(1 - \exp^{-\mu_h t}\right) \\ 0 \le N_v(t) &\le N_v(0) \exp^{-\mu_v t} + \frac{\Lambda_v}{\mu_v}\left(1 - \exp^{-\mu_v t}\right) \end{aligned}\right\} \tag{2.7}$$

We determine that there is only one global solution in the domain Ω. The right-hand side of the model (2.4) is locally Lipschitz (Stuart and Humphties 1998). Consequently, the dynamical system on Ω in model (2.4). Conversely, if a solution is found outside of the area Ω, that is, $N_h \le \frac{\Lambda_h}{\mu_h}$ and $N_v \le \frac{\Lambda_v}{\mu_v}$, then the conservation law mentioned above implies that $\frac{dN_h}{dt} \le 0$ and $\frac{dN_v}{dt} \le 0$. Thus, it can be seen from the estimates above that $N_h(t)$ tends to $\frac{\Lambda_h}{\mu_h}$ and $N_v(t)$ tends to $\frac{\Lambda_v}{\mu_v}$ as $t \to \infty$.. As a result, the region Ω is interesting.

3 Mathematical Analysis

3.1 Asymptotic Stability of Disease-free Equilibrium (DFE)

The DFE of the model (2.4) is given by

$$E_1 = (S_h^0, E_h^0, I_a^0, I_s^0, R_h^0, S_v^0, I_v^0, R_v^0) = (\frac{\Lambda_h}{\mu_h}, 0,0,0,0, \frac{\Lambda_v}{\mu_v}, 0,0).$$

Using model (2.4) and an operator method for the next generation (van den Driessche and Watmough, 2002), the local stability of E_1 will be established. It follows that matrices F and V, the notation found in van den Driessche and Watmough (2002) is used for the new infection terms and the remaining transition terms, respectively.

$$F = \begin{pmatrix} 0 & \frac{\beta_1 \Lambda_h}{\mu_h} & \frac{\beta_1 \Lambda_h}{\mu_h} & \frac{\beta_1 \Lambda_h}{\mu_h} \\ 0 & 0 & 0 & 0 \\ 0 & 0 & 0 & 0 \\ 0 & \frac{\beta_2 \Lambda_v}{\mu_v} & \frac{\beta_2 \Lambda_v}{\mu_v} & \frac{\beta_2 \Lambda_v}{\mu_v} \end{pmatrix} \text{ and } V = \begin{pmatrix} k_1 & 0 & 0 & 0 \\ 0 & k_2 & 0 & 0 \\ -k_3 & -\eta & k_4 & 0 \\ 0 & 0 & 0 & k_6 \end{pmatrix},$$

where,

$$k_1 = [\theta\rho + \theta(1-\rho) + \mu_h], k_2 = (\eta + \gamma_2 + \mu_h), k_3 = \theta(1-\rho), k_4 = (\gamma_4 + \mu_h + \delta_h), \\ k_5 = (\mu_h + \psi_h), k_6 = (\gamma_3 + \mu_v + \delta_v), k_7 = (\mu_v + \psi_v). \quad (3.1).$$

Hence, the effective reproduction number of the model (2.4), denoted by R_c, is given by

$$R_c = \frac{\Lambda_h k_3 k_6 \mu_v \beta_1 + \Lambda_v k_1 k_4 \mu_h \beta_2}{\mu_h \mu_v k_1 k_4 k_6} \tag{3.2}$$

The following findings are derived from the Theorem 2 Van den Driessche and Watmough's (2002)

Lemma 3.1: The DFE (E_1) of the model (2.4) is locally asymptotically stable whenever $R_c < 1$ and unstable if otherwise.

The threshold quantity R_c measures the average number of new Campylobacteriosis infections generated by an index case in a completely susceptible population (van den Driessche and Watmough, 2002). Specifically, R_c denotes the mean quantity of newly acquired Campylobacteriosis infections within the human (animal) population, resulting from the introduction of a single infected individual into a fully susceptible human (animal) population. Lemma 3.1's epidemiological implication is that, if the initial sizes of the model's subpopulation are within the DFE's (E_1) basin of attraction, campylobacteriosis can be eradicated from the population when R_c is less than unity. As a result, a small number of humans or animals carrying the infection may enter the community; this will not cause significant outbreaks of the disease, and it will eventually go extinct. It is vital to demonstrate that the DFE is globally-asymptotically stable (GAS) if $R_c < 1$ and the initial subpopulation sizes do not affect the eradication of campylobacteriosis.

Theorem 3.2. The DFE (E_1) of the model (2.4) is globally asymptotically stable in Ω whenever $R_c \leq 1$.

Proof. The proof of Theorem 3.2 will be established using the Theorem of comparison (Lakshmikantham *et al.,* 1989). The following is the matrix-vector form for the equations on the model's (2.4) infected components:

$$\frac{dL(t)}{dt} = \left[(F - V) - \left(1 - \frac{S_h}{N_h}\right) H_1 - \left(1 - \frac{S_v}{N_v}\right) H_2 \right] L(t), \tag{3.3}$$

where $L(t) = (E_h(t), I_a(t), I_s(t), R_h(t), I_v(t), R_v(t))^T$ and the matrices F and V are given in section 3. Furthermore,

$$H_1 = \begin{pmatrix} \frac{\beta_1 \Lambda_h}{\mu_h} & \frac{\beta_1 \Lambda_h}{\mu_h} & \frac{\beta_1 \Lambda_h}{\mu_h} & \frac{\beta_1 \Lambda_h}{\mu_h} \\ 0 & 0 & 0 & 0 \\ 0 & 0 & 0 & 0 \\ 0 & 0 & 0 & 0 \end{pmatrix},$$

and

$$H_2 = \begin{pmatrix} 0 & 0 & 0 & 0 \\ 0 & 0 & 0 & 0 \\ 0 & 0 & 0 & 0 \\ 0 & \frac{\beta_2 \Lambda_v}{\mu_v} & \frac{\beta_2 \Lambda_v}{\mu_v} & \frac{\beta_2 \Lambda_v}{\mu_v} \end{pmatrix}.$$

Since H_1 and H_2 are nonnegative matrices and $S_h(t) \le N_h(t)$ and $S_v(t) \le N_v(t)$ in Ω, it follows that

$$\frac{dL(t)}{dt} \le [(F - V)]L(t) \tag{3.4}$$

The differential inequality system (3.4) is stable whenever $R_c < 1$, based on the fact that all of the matrix eigenvalues have negative real parts. Thus, according to comparison theorem of (Lakshmikantham *et al* 1989).

$$\lim_{t\to\infty}(E_h(t), I_a(t), I_s(t), R_h(t), I_v(t), R_v(t)) = (0,0,0,0,0,0). \tag{3.5}$$

It can be shown by substituting (3.5) into (2.1) that $S_h \to \frac{\Lambda_h}{\mu_h}$ and $S_v \to \frac{\Lambda_v}{\mu_v}$ as $t \to \infty$. thus,

$$\lim_{t\to\infty}(S_h(t), E_h(t), I_a(t), I_s(t), R_h(t), S_v(t), I_v(t), R_v(t) = (\tfrac{\Lambda_h}{\mu_h}, 0,0,0,0, \tfrac{\Lambda_h}{\mu_h}, 0,0) = E_1^*. \tag{3.6}$$

Hence, every solution to the equation of the model (2.4) and initial conditions in Ω, approaches the DFE (E_1) as $t \to \infty$ whenever $R_c < 1$ .The epidemiological implication of Theorem 3.2 is that irrespective of the number of infectives in the population, if the threshold quantity R_c can be kept below unity, campylobacteriosis will be effectively controlled in the community

4 Numerical Simulation

In this section, numerical simulations for the transmission dynamics of campylobacteriosis are performed on model (2.4) with the parameter values from Table 2 and the assumed initial data. The model (2.4) is solved numerically using MATLAB ODE45 solver. In Figure 2, an increase in the progression rate of the asymptomatic individuals to the symptomatic class experienced an increase in the population of the symptomatic individuals. In Figures 3 and 4 (as expected), an increase in the treatment rate of the asymptomatic and symptomatic individuals led to a decrease in the number of infected (both asymptomatic and symptomatic) individuals in the population. This suggests that if treatment of infected (both asymptomatic and symptomatic) individuals is deployed early enough, it will lead to the timely eradication of the disease in the population.

Table 2. The parameter values of the model (2.4) per year.

Parameter	Nominal value	Reference
β_1	0.03	Osman *et al.* (2020)
β_2	0.004	Parshotama (2011)
Λ_h	0.002	Osman *et al.* (2020)
Λ_v	0.005	Osman *et al.* (2020)
μ_h	0.0001	Osman *et al.* (2020)
μ_v	0.0002	Parshotama (2011)
θ	0.20	Assumed
ρ	0.6	Assumed
ϕ	0.3	Assumed
γ_1	0.4	Assumed
γ_2	0.7	Assumed
δ_h	0.001	Osman *et al.* (2020)
δ_v	0.003	Osman *et al.* (2020)
γ_3	0.05	Parshotama (2011)
ψ_h	0.004	Osman *et al.* (2020)
ψ_v	0.007	Parshotama (2011)
η	0.5	Assumed

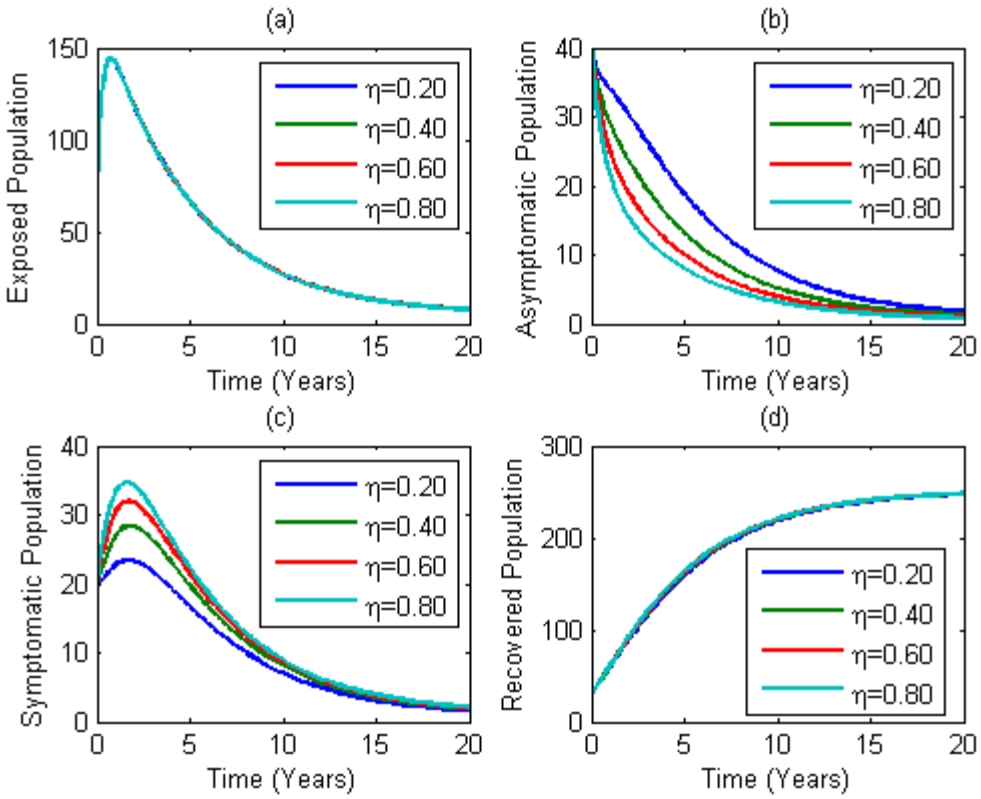

Figure 2. Simulation of model (2.4) showing the population of exposed, asymptomatic, symptomatic and recovered individuals. Here, the progression rate from the asymptomatic to symptomatic class η is varied from 0.20 to 0.80.

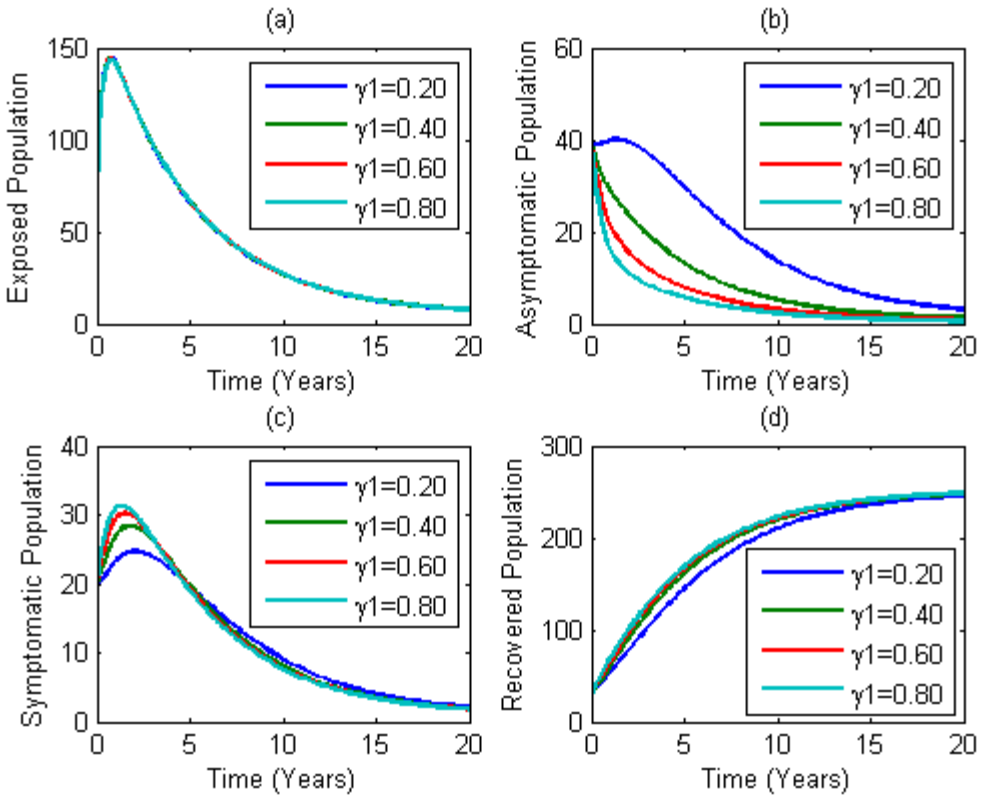

Figure 3. Simulation of model (2.4) showing the population of exposed, asymptomatic, symptomatic and recovered individuals. Here, the treatment rate of the asymptomatic individuals, γ_1 is varied from 0.20 to 0.80.

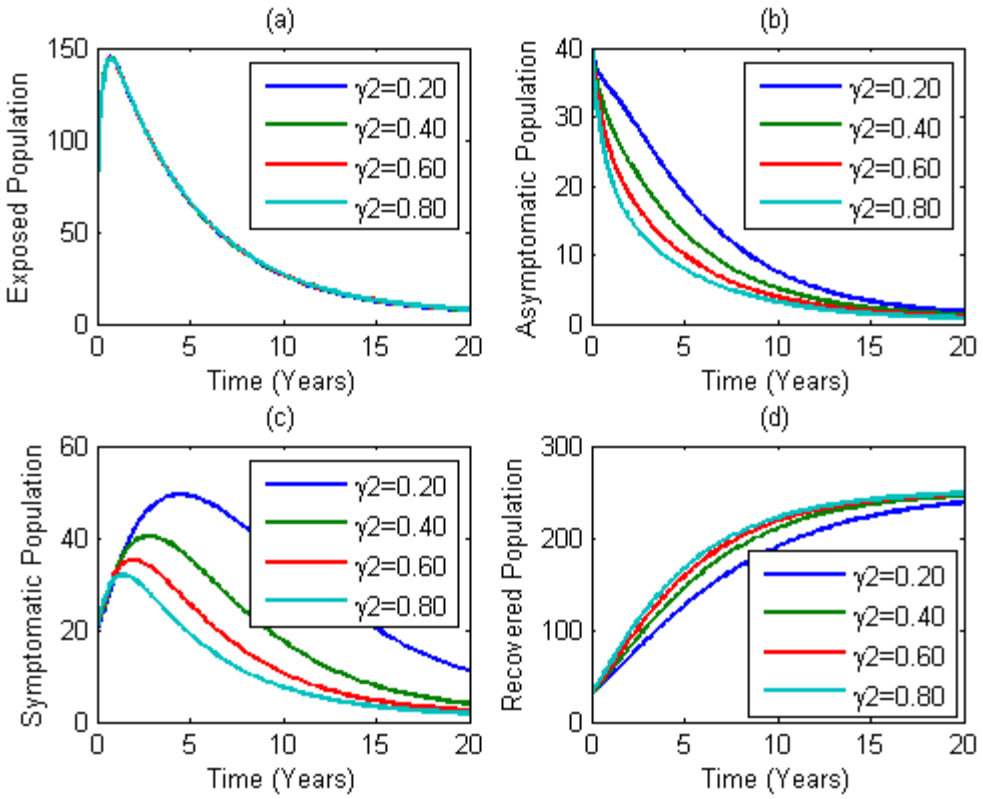

Figure 4. Simulation of model (2.4) showing the population of exposed, asymptomatic, symptomatic and recovered individuals. Here, the treatment rate of the symptomatic individuals, γ_2 is varied from 0.20 to 0.80.

5 Conclusion

In order to better understand the dynamics of Campylobacteriosis infection transmission in a population, this study offers a novel deterministic mathematical model with treatment as a control strategy. It is shown that for model (2.4), if the corresponding reproduction number is less than unity, the disease-free equilibrium (DFE) is locally asymptotically stable. The disease-free equilibrium was discovered to be globally asymptotically stable whenever the corresponding reproduction number is less than unity using the comparison theorem. The numerical simulation results show that a decrease in the population of asymptomatic individuals and an increase in the population of recovered individuals occurred when the treatment rate for both symptomatic and asymptomatic disease-infected individuals was increased.

Few mathematical models have been developed to date to investigate the dynamics of campylobacteriosis transmission as well as its prevention and control. Therefore, additional investigation of the

Campylobacteriosis model in this work is required to determine model parameters related to the reproduction number that are essential to containing the disease's spread. In light of this, we suggest further analysis our model as follows:

(i) Sensitivity analysis of the model parameters associated with the reproduction number be carried out.
(ii) Further theoretical results, such as the type of bifurcation the model (2.4) can exhibit should be explored.

References

Centers for Disease Prevention and Control (2019). Diagnosis and treatment. Retrieved on the 27th January, 2024 from https://www.cdc.gov/campylobacter/diagnosis.html#:~:text=The%20test%20could%20be%20a,genetic%20material%20of%20the%20bacteria.&text=Most%20people%20recover%20from%20Campylobacter,as%20long%20as%20diarrhea%20lasts

Centers for Disease Prevention and Control (2023). Campylobacter (campylobacteriosis). Retrieved on 27th January, 2024 from https://www.cdc.gov/campylobacter/fag.html.

Chuma, F. M. and Mussa, Z. S. (2021). Campylobacteriosis transmission dynamics in Human: Modelling the effects of public health education, treatment, and sanitation. *Tanzania Journal of Science*, 47(1): 315-331.

Gumel, A. B., Lubuma, J. M. S., Sharomi, O. and Terefe (2018). Mathematics of a sex-structured model for syphilis transmission dynamics. *Mathematical Methods in Applied Sciences*, 41(18): 8488-8513.

Gweryina, R. I., Madubueze, C. E. and Kaduna, F. S. (2021). Mathematical assessment of the role of denial on COVID-19 transmission with non-linear incidence and treatment functions. *Scientific African*, 12: e00811.

Havelar, A. H., van Pelt, W., Ang, C. W. et. al. (2009). "Immunity to campylobacteriosis: its role in risk assessment and epidemiology". Critical Reviews in Microbiology, 35(1): 1-22.

Healthdirect (2024). Campylobacter infection. Retrieved on the 27th January, 2024 from https://www.healthdirect.gov.au/campylobacterinfection#:~:text=Most%20people%20recover%20in%20about,your%20baby%20throughout%20their%20illness

Iboi, E. and Okuonghae, D. (2016). Population dynamics of a mathematical model for syphilis. Applied Mathematical Modeling, 40: 3573-3590.

Lakshimikantham, S., Leela, S. and Martynyuk, A. A. (1989). Stability analysis of nonlinear systems, Marcel Dekker, New York.

Nyasagare, B. N., Osman, S. and Wainaina, M. (2019). Modelling and analysis of campylobacter of campylobacteriosis in human and animal population. *Global Journal of pure and Applied Mathematics,* 15(5): 551-567.

Osman, S., Togbenon, H. A. and Otoo, D. (2020). Modelling the dynamics of campylobacteriosis using nonstandard finite difference approach with optimal control. Computational and Mathematical Methods in Medicine. Volume 2020, Article ID 8843299, 12 pages. https://dot.org/10.1155/2020/8843299.

Parshotama, A. (2011). "Modelling of a zoonotic pathogen (campylobacter) in a dairy head" in 19th International Congress on Modelling and Simulation, Perth, Australia.

Rawson, T., Dawkins, M. S. and Bonsall, M. B. (2019). A mathematical model of campylobacter dynamics within a broiler flock. Frontiers in Microbiology, 10: 1940. doi: 3389/fmicb.2019.01940.

Stuart, A. M. and Humphties (1998). Dynamical systems and numerical analysis.

van den Driessche, P. and Watmough, J. (2002). Reproduction numbers and sub-threshold endemic equilibria for compartmental models of disease transmission. *Mathematical Biosciences*, 180: 29-48.

World Health Organization (2020). Campylobacter. Retrieved from https://www.who.int/news-room/fact-sheets/detail/campylobacter on 27th January, 2024.

Numerical Simulation of Adaptive Immunity Effects in an Intrahost Chikungunya Virus Model Using the Homotopy Perturbation Method

Morufu Oyedunsi Olayiwola[1] Adedapo Ismaila Alaje [2], Isaac Ademola Adewale[3] John Femi Odeleye [4]

[1, 2, 3, 4] Department of Mathematical Sciences, Osun State University, Osogbo, Nigeria

[1]olayiwola.oyedunsi@uniosun.edu.ng

[2]adedapo.alaje@uniosun.edu.ng

[4]isaac.adewale@uniosun.edu.ng

[5]john.odeleye @uniosun.edu.ng

Abstract

This study utilizes the homotopy perturbation method (HPM) to numerically solve a nonlinear system of differential equations representing the adaptive immune response in an intrahost chikungunya virus model. Results highlight HPM's efficiency in solving the model, with graphical representations showing that cytotoxic T lymphocytes (CTLs) and antibodies significantly strengthen the immune system, contributing to a robust defence mechanism. Visual representations of the findings are provided.

Keywords: Adaptive Immunity Response, Chikungunya Virus Model, HPM.

1. Introduction

The Chikungunya virus, named for the contorted posture it induces, is transmitted by Aedes mosquitoes (WHO, 2023). This mosquito-borne illness has led to global outbreaks in Africa, Asia, Europe, the Americas, and the Pacific. While no specific antiviral treatment exists, efforts focus on preventing the virus through strategies aimed at avoiding mosquito bites. As of January 2022, ongoing research is dedicated to developing a vaccine (CDC, 2023). Chikungunya fever, attributed to the Chikungunya virus (CHIKV), exhibits clinical symptoms like fever, rash, headache, pain, myalgia, arthritis, conjunctivitis, and vomiting, manifesting 5–7 days after mosquito contact (Hajji *et al.,* 2022). Initially identified in Tanzania in 1952, the virus re-emerged globally in 2004, posing a significant public health challenge. Control measures, including mathematical modelling, are employed to curb its spread (Alade *et al.,* 2023). This article explores the various aspects of Chikungunya viral transmission preventive strategies, and the latest developments in vaccine research.

2. Literature Review

Understanding the spread and control of fatal diseases involves mathematical modeling, often utilizing ordinary or partial differential equations (Alaje *et al.,* 2023; Olayiwola *et al.,* 2023; Olayiwola *et al.,* 2024). Notable among these models are the Yunus *et al*., (2023) and Adebisi *et al.*, (2024) studies on the transmission dynamics of COVID-19.

Solving mathematical models before simulation is crucial for investigating parameter influence. Obtaining analytical solutions is challenging, prompting the use of numerical techniques like the homotopy perturbation method (He 1999, 2003; Alaje *et al.* 2021, 2022, 2023; Olayiwola *et al.* 2023a, 2023b). For instance, Kolawole *et al.* (2023) analyzed the impact of vaccination, treatment, and human compliance on COVID-19 transmission using the homotopy perturbation method. And this same method was applied to study EIAV infection (Balamuralitharan *et al.*, 2018) and hepatitis B virus (Aniji *et al.*, 2020). Across these studies, the method consistently demonstrated significant proficiency in handling both linear and nonlinear models, establishing itself as a potent tool.

While researchers have explored within-host chikungunya virus dynamics (Alade *et al.*, 2023; Olaniyi *et al.*, 2023), no study has applied a computational technique to provide an analytical solution to the model. This study addresses this gap, utilizing the homotopy perturbation method to solve and analyze adaptive immunity's role in the within-host Chikungunya virus model presented by (Alade *et al.,* 2023).

3. Methodology

The mathematical model that described the intrahost Chikunguya disease dynamics previously studied in (Alade et al., 2023; Olaniyi et al., 2023) is

$$\begin{aligned}
\frac{dS(t)}{dt} &= \lambda - dS(t) - bS(t)V(t) \\
\frac{dI(t)}{dt} &= bS(t)V(t) - aI(t) - \varepsilon I(t)Z(t) \\
\frac{dV(t)}{dt} &= mI(t) - rV(t)B(t) - qB(t) \\
\frac{dB(t)}{dt} &= \eta + cV(t)B(t) - \delta B(t) \\
\frac{dZ(t)}{dt} &= \gamma + \omega I(t)Z(t) - \mu Z(t)
\end{aligned} \tag{1}$$

Subject to initial conditions

$$S(0) = s_0, I(0) = i_0, V(0) = v_0, B(0) = b_0, Z(0) = z_0 \tag{2}$$

In the model, $S(t)$, $I(t)$, $V(t)$, $B(t)$, and $Z(t)$ represent the levels of uninfected cells, infected cells, CHIKV particles, antibodies, and CTLs. Production rates for uninfected cells, antibodies, and CTLs are denoted by constant rates λ, η, and γ, while CHIKV particles are produced at a rate mI. The per capita mortality rates for $S(t)$, $I(t)$, $V(t)$, $B(t)$, and $Z(t)$ are d, a, r, δ, and μ, respectively. Uninfected cells become infected at a rate bSV. Infected cells and CHIKV particles are eliminated by CTLs at rates ϵIZ and antibodies at a rate qVB, respectively. Antibodies and CTLs proliferate at rates cVB and ωIZ.

3.1. Homotopy Perturbation Method

For the computation of the model result using homotopy perturbation, we outline the methodology which begins by considering the following differential equation:

$$D(\varpi) = g(\upsilon), \qquad \upsilon \in \Phi. \tag{3}$$

Subject to the boundary condition

$$\psi(\varpi, \varpi_n) = 0 \quad \upsilon \in \Pi. \tag{4}$$

The differential operator, denoted as D, operates on an analytic function $g(\upsilon)$. The boundary operator is represented by ψ, and the external normal vector derivative, denoted as ϖ_n, is drawn from Φ. The boundary of the domain, referred to as Φ, is denoted by Π.

Operator $D(\varpi)$ contains the linear and nonlinear parts such that

$$D(\varpi) = \ell_T(\varpi) + \eta_T(\varpi), \tag{5}$$

This yields

$$\ell_T(\varpi) + \eta_T(\varpi) = g(\upsilon), \qquad r \in \Phi. \tag{6}$$

We can construct a Homotopy for (6) so that

$$H(f, p) = (1-p)\left[\ell_T(f) - \ell_T(\varpi_0)\right] + p\left[D(f) - g(\upsilon)\right] = 0. \tag{7}$$

Where $\rho \in [0,1]$ is an embedding parameter. And (7) yields

$$H(f, p) = \ell_T(f) - \ell_T(\varpi_0) + p[\ell_T(\varpi_0)] + p\left[\eta_T(\varpi_0) - g(\upsilon)\right] = 0, \tag{8}$$

As $p \to 0$, equation (8) gives:

$$H(f,0) = \ell_T(f) - \ell_T(\varpi_0) = 0 \tag{9}$$

And when $p \to 1$,

$$H(f,1) = D(f) - g(\upsilon) = 0. \tag{10}$$

The solution to (10) can be obtained iteratively by assuming a power series of ρ such that

$$f(t) = f_0(t) + pf_1(t) + p^2 f_2(t) + \cdots p^n f_n(t) \tag{11}$$

Evaluating (10) using (11), and comparing coefficients of equal powers of p and subsequently solving yields the values of $f_0(t)$, $f_1(t)$, $f_2(t)$. And the approximate solution of (10) is:

$$f(t) = \lim_{p \to 1} f_n(t) = f_0(t) + f_1(t) + f_2(t) + \cdots \tag{12}$$

3.2. Model Solution via HPM

In this section, we apply the homotopy perturbation method to obtain an approximate solution for the Chikungunya virus model (1) using Procedure (3-12).

$$\begin{aligned}
&(1-p)\frac{dS(t)}{dt}+p\left(\frac{dS(t)}{dt}-(\lambda-dS(t)-bS(t)V(t))\right)=0\\
&(1-p)\frac{dI(t)}{dt}+p\left(\frac{dI(t)}{dt}-(bS(t)V(t)-aI(t)-\varepsilon I(t)Z(t))\right)=0\\
&(1-p)\frac{dV(t)}{dt}+p\left(\frac{dV(t)}{dt}-(mI(t)-rV(t)B(t)-qB(t))\right)=0\\
&(1-p)\frac{dB(t)}{dt}+p\left(\frac{dB(t)}{dt}-(\eta+cV(t)B(t)-\delta B(t))\right)=0\\
&(1-p)\frac{dZ(t)}{dt}+p\left(\frac{dZ(t)}{dt}-(\gamma+\omega I(t)Z(t)-\mu Z(t))\right)=0
\end{aligned} \tag{13}$$

We can assume the following power series of p as solution for the model variables in (13) such that

$$S(t)=\sum_{n=0}^{\infty}p^n s_n(t),\ I(t)=\sum_{n=0}^{\infty}p^n i_n(t),V(t)=\sum_{n=0}^{\infty}p^n v_n(t)\ \ B(t)=\sum_{n=0}^{\infty}p^n b_n(t),\ R(t)=\sum_{n=0}^{\infty}p^n r_n(t) \tag{14}$$

Evaluating (13) using (14) and subsequently collecting coefficients of powers of p, for $n\geq 1$ yields the following system

At $n=1$, coefficients of p^1 are:

$$\begin{aligned}
&\frac{ds_1(t)}{dt}=\lambda-ds_0(t)-bs_0(t)v_0(t)\\
&\frac{di_1(t)}{dt}=bs_0(t)v_0(t)-ai_0(t)-\varepsilon i_0(t)z_0(t)\\
&\frac{dv_1(t)}{dt}=mi_0(t)-rv_0(t)b_0(t)-qb_0(t)\\
&\frac{db_1(t)}{dt}=\eta+cv_0(t)b_0(t)-\delta b_0(t)\\
&\frac{dz_1(t)}{dt}=\gamma+\omega i_0(t)z_0(t)-\mu z_0(t)
\end{aligned} \tag{15}$$

Solving system (14), using the initial conditions $S(0)=s_0, I(0)=i_0, V(0)=v_0, B(0)=b_0, Z(0)=z_0$, the first approximate solution of the model is obtained as

$$
\begin{aligned}
s_1(t) &= (\lambda - ds_0 - bs_0v_0)t \\
i_1(t) &= (bs_0v_0 - ai_0 - \varepsilon i_0z_0)t \\
v_1(t) &= (mi_0 - rv_0b_0 - qb_0)t \\
b_1(t) &= (\eta + cv_0b_0 - \delta b_0)t \\
z_1(t) &= (\gamma + \omega i_0z_0 - \mu z_0)t
\end{aligned} \tag{16}
$$

At $n=2$, coefficients of p^2 are

$$
\begin{aligned}
\frac{ds_2(t)}{dt} &= (-ds_1(t) - b(s_0(t)v_1(t) + s_1(t)v_0(t))) \\
\frac{di_2(t)}{dt} &= b(s_0(t)v_1(t) + s_1(t)v_2(t)) - ai_1(t) - \varepsilon(i_0(t)z_1(t) + i_1(t)z_0(t)) \\
\frac{dv_2(t)}{dt} &= mi_1(t) - r(v_0(t)b_1(t) + v_1(t)b_0(t)) - qb_1(t) \\
\frac{db_2(t)}{dt} &= \eta + c(v_1(t)b_0(t) + v_0(t)b_1(t)) - \delta b_1(t) \\
\frac{dz_2(t)}{dt} &= \gamma + \omega(i_0(t)z_1(t) + i_1(t)z_0(t)) - \mu z_1(t)
\end{aligned} \tag{17}
$$

Solving (17) yields the second approximate results given by

$$
\begin{aligned}
s_2(t) &= (-d(\lambda - ds_0 - bs_0v_0) - b(s_0(mi_0 - rv_0b_0 - qb_0) + v_0(\lambda - ds_0 - bs_0v_0)))\frac{t^2}{2} \\
i_2(t) &= \left(b\begin{pmatrix} s_0(mi_0 - rv_0b_0 - qb_0) \\ + v_0(\lambda - ds_0 - bs_0v_0) \end{pmatrix} - a(bs_0v_0 - ai_0 - \varepsilon i_0z_0) - \varepsilon\begin{pmatrix} i_0(\gamma + \omega i_0z_0 - \mu z_0) \\ + (bs_0v_0 - ai_0 - \varepsilon i_0z_0)z_0 \end{pmatrix}\right)\frac{t^2}{2} \\
v_2(t) &= \left(m(bs_0v_0 - ai_0 - \varepsilon i_0z_0) - r\begin{pmatrix} v_0(\eta + cv_0b_0 - \delta b_0) \\ + (mi_0 - rv_0b_0 - qb_0)b_0 \end{pmatrix} - q(\eta + cv_0b_0 - \delta b_0)\right)\frac{t^2}{2} \\
b_2(t) &= (c((mi_0 - rv_0b_0 - qb_0)b_0 + v_0b_1(t)) - \delta(\eta + cv_0b_0 - \delta b_0))\frac{t^2}{2} \\
z_2(t) &= (\omega(i_0(\gamma + \omega i_0z_0 - \mu z_0) + (bs_0v_0 - ai_0 - \varepsilon i_0z_0)z_0) - \mu(\gamma + \omega i_0z_0 - \mu z_0))\frac{t^2}{2}
\end{aligned}
$$

This procedure can be continued till the desired number of iteration is achieved. And the solution for the model variables is obtained as

$$
S(t) = \sum_{n=0}^{2} s_n(t),\ I(t) = \sum_{n=0}^{2} p^n i_n(t),\ V(t) = \sum_{n=0}^{2} p^n v_n(t)\ \ B(t) = \sum_{n=0}^{2} p^n b_n(t),\ R(t) = \sum_{n=0}^{2} p^n r_n(t) \tag{18}
$$

3.3. Convergence of Solution

In this section, we assess the model results obtained in equation (14) through numerical evaluation. The parameter values employed are based on those provided by Alade *et al.* (2023): λ = 1.826, μ = 1.2, c =

1.2129, $d = 0.7979$, $\gamma = 0.5$, $\omega = 0.5$, $\epsilon = 0.04441$, $m = 2.02$, $q = 0.5964$, $r = 0.4418$, $\eta = 1.402$, $\delta = 1.251$, $a = 0.5$, and $b = 0.9$. The initial conditions for cell state variables are set as follows: $S0 = 1.4$, $I0 = 0.8$, $V0 = 0.6$, $B0 = 1.0$, and $Z0 = 0.5$. And the following results are obtained

$$S(t) = 1.4\text{-}0.29906t + 0.13804787000t^2\text{-}0.10452491166t^3$$

$$I(t) = 0.8 + 0.338360t + 0.30451698100t^2 - 0.20416867300t^3$$

$$V(t) = 0.6 + .754520t\text{-}0.20343833557t^2 + 0.07198051767t^3$$

$$A(t) = 1.0 + 0.878740t + 0.22767390788t^2 + 0.14610077555t^3 \qquad (19)$$

$$Z(t) = 0.5 + 0.100t + 0.022950000000t^2 + 0.00304037483t^3$$

Theorem 5: Let N be an operator from Hilbert space H in to H and let $Q(t) = (S(t), I(t), V(t), A(t), Z(t))^T \in R^5$ contains the exact solution of model (1) then the solution $\sum_{n=0}^{\infty} Q_n(t)$ obtained by via the homotopy perturbation method converges to $Q(t)$ whenever $\|Q_{n+1}\| \le \varepsilon \|Q_n\|$ $0 \le \lambda_n < 1$.

Proof: As demonstrated by He (2003) and applied in Ayati et al, (2015), for every $n \in N$, it has been shown that the solution Q_n converges provided that $0 \le \varepsilon_n < 1$ whenever

$$\varepsilon_n = \begin{cases} \dfrac{\|Q_{n+1}\|}{\|Q_n\|} & \|Q_n\| \neq 0 \\ 0 & \|Q_{n+1}\| = 0 \end{cases} \qquad (20)$$

Applying (20) to (19) the following results on Table 3.1 are obtained.

Table 3.1: Numerical results of third order convergence test

Variables	Formula	Results
$S(t)$	$\varepsilon_1 = \|s_3\|/\|s_2\|$	$0.75716424774 < 1$
$I(t)$	$\varepsilon_2 = \|i_3\|/\|i_2\|$	$0.67046728384 < 1$
$V(t)$	$\varepsilon_3 = \|v_3\|/\|v_2\|$	$0.35381983119 < 1$
$B(t)$	$\varepsilon_4 = \|b_3\|/\|b_2\|$	$0.64171066779 < 1$

$Z(t)$	$\varepsilon_5 = \|z_3\| / \|z_2\|$	$0.1324782061 < 1$

The results presented in Table 3.1 not only validate the theorem but also confirm the convergence of the model solution through the Homotopy Perturbation Method (HPM). This validation assures the accurate predictions of cell interaction and development during numerical simulations.

4. Results and Discussion

4.1 Numerical Simulation

In this segment, we apply the numerical results using Python 3.11.5 software, running on an Hp-15 laptop with Windows 11, equipped with a 12GB RAM, 1TB ROM and a 2.76 hertz processor. The graphical representation of the simulation results is presented below.

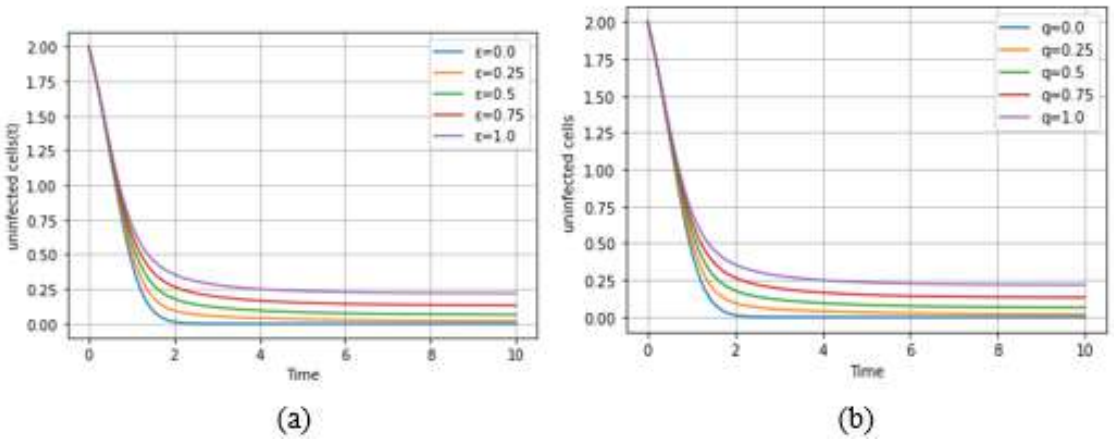

Figure 1: dynamics of uninfected cells to consumption rates of CTLs and Antibodies

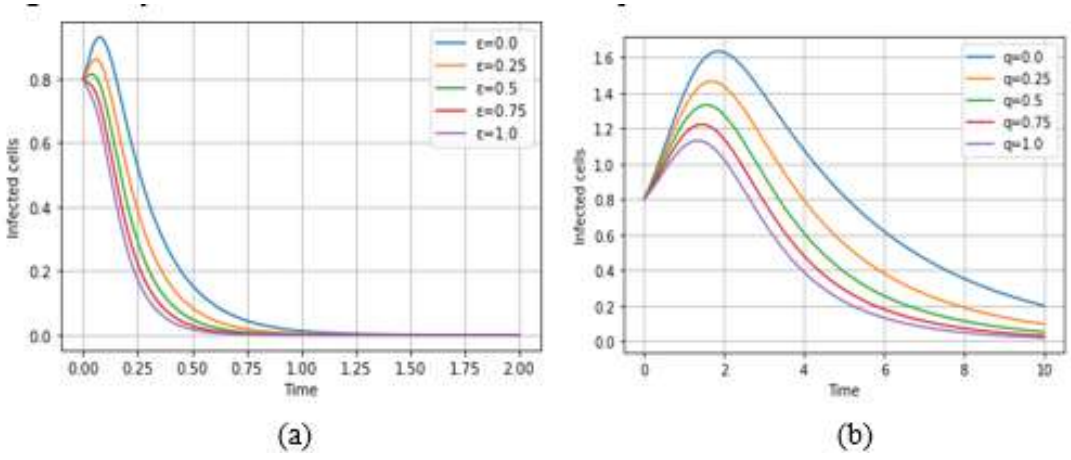

Figure 2: dynamics of infected cells to consumption rates of CTLs and Antibodies

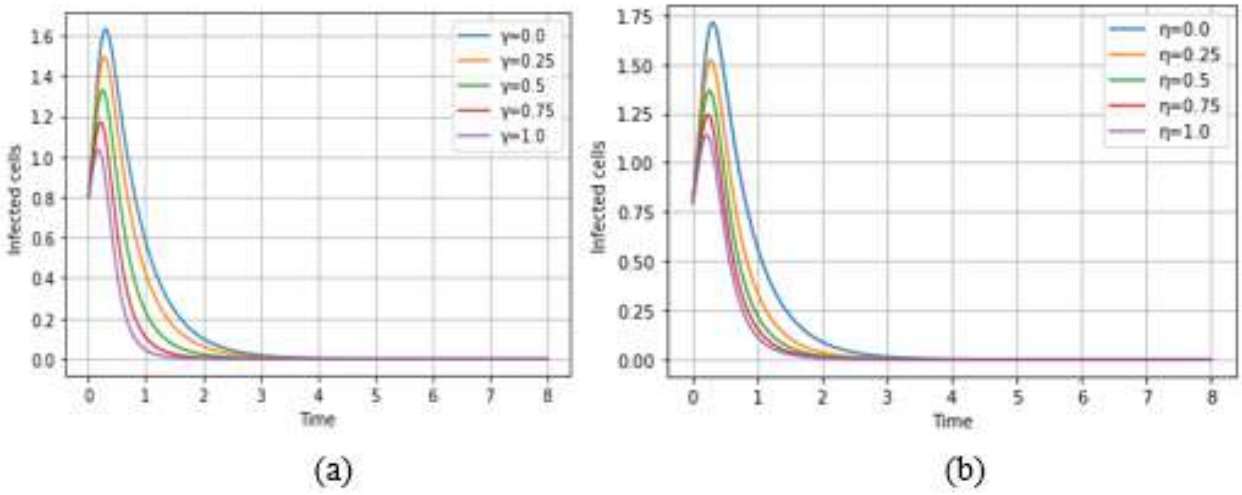

Figure 3: dynamics of infected cells to variation inhost supply of CTLs and Antibodies.

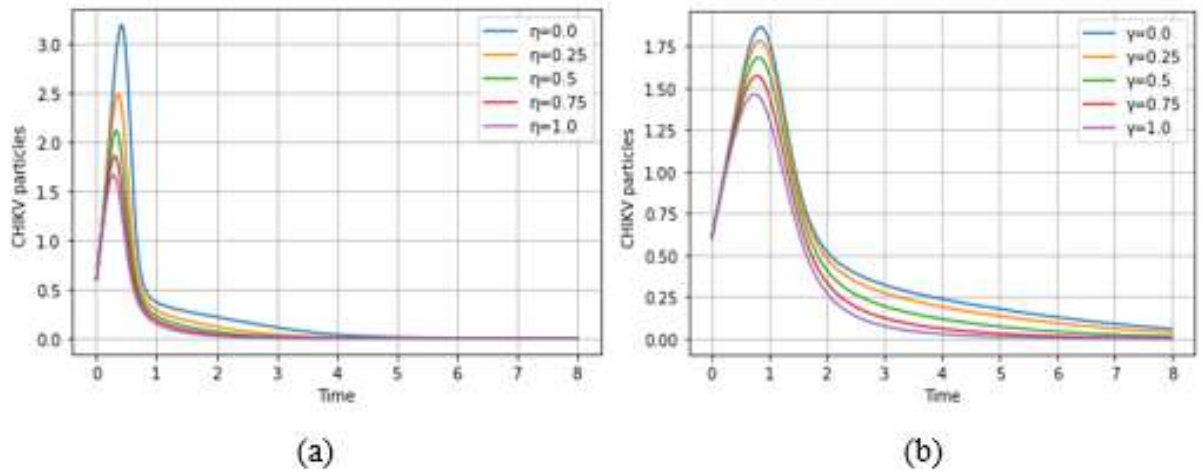

Figure 4: Concentration of CHIKV particle to inhost variational supply of CTLs and Antibodies.

We have successfully applied the homotopy perturbation method to conduct numerical simulations on our model. The results from these simulations illustrate the dynamics of uninfected cells (Figure 1) and infected cells (Figure 2) in response to varying consumption rates of CTLs and antibodies. Additionally, Figures 3 and 4 demonstrate the response of infected cells and CHIKV particle concentration to changes

in the host's supply of CTLs and antibodies. Specifically, Figures 1(a) and (b) show that an increase in antibodies and CTLs results in a more effective defense against infected cells and CHIKV particles, leading to a reduced rate of uninfected cell infection. In Figures 2(A) and 2(B), it is evident that the elimination of infected cells occurs more rapidly when confronting CTLs and antibodies, respectively. Higher concentrations of CTLs and antibodies are associated with a more significant decline in the population of infected cells.

Figures 3(A) and (B) strongly support the findings of Figure 2, indicating that a higher supply of antibodies and CTLs to the host effectively limits the proliferation of infected cells. A similar response is observed for CHIKV particle concentration in Figures 4(A) and (B). These results align well with the earlier findings presented by Alade *et al.* (2023), suggesting that adaptive immune responses lead to a faster reduction in the concentrations of infected cells and viral particles. This strengthens the claim that the homotopy perturbation method is a valuable analytical and simulation tool.

4.2 Abbreviations

CHIKV: Chikunguyan Virus

CTLs: Cytotoxic T-cells

EIAV: Equine Infectious Anemia Virus

5. Conclusion

In conclusion, this study has investigated the influence of adaptive immunity on the SIVBZ model, employing the homotopy perturbation method. The demonstrated effectiveness of this method, supported by a theorem proven through the Ratio test, highlights its efficiency in achieving convergence with less computational effort. Utilizing the Python Software for simulation, our results underscore the crucial role played by adaptive immunity in the effective eradication of the Chikungunya virus. This research contributes valuable insights into the potential applications of the homotopy perturbation method for understanding and optimizing adaptive immune responses in combating viral infections.

References

Adebisi, A. F., Olayiwola, M. O., Adediran, I. A., & Alaje, A.I. (2024). A Novel Mathematical Model and Homotopy Perturbation Method Analyzing the Effects of Saturated Incidence and Treatment Rate on COVID-19 Eradication. *Iranian Journal of Science*, 48, https://doi.org/10.1007/s40995-024-01608-w

Alade, T.O., Abidemi, A., Tunç, C., & Ghaleb, S.A. (2021). Global stability of generalized within-host chikungunya virus dynamics models. *International Journal of Applied Mathematics*, Vol. 16(1), 8.

Alade, T.O., Alnegga, M., Olaniyi, S. A., & Abidemi, A. (2023). Mathematical modelling of within-host chikungunya virus dynamics with adaptive immunity. *Modeling Earth Systems and Environment*. http://dx.doi.org/10.1007/s40808-023-01737.

Alaje, A. I., & Olayiwola, M. O. (2023). A fractional-order mathematical model for examining the spatiotemporal spread of COVID-19 in the presence of vaccine distribution. *Healthcare Analytics*, 4. https://doi.org/10.1016/j.health.2023.100230

Alaje, A. I., Olayiwola, M. O., Adedokun, K. A., *et al.* (2023). Modified homotopy perturbation method and its application to analytical solitons of fractional-order Korteweg–de Vries equation. *Beni-Suef University Journal of Basic and Applied Sciences*, Vol.11, 1-17. https://doi.org/10.1186/s43088-022-00317-w

Alaje, A. I., Olayiwola, M. O., Adedokun, K. A., *et al.* (2023). The modified homotopy perturbation method and its application to the dynamics of price evolution in Caputo-fractional order Black Scholes model. *Beni-Suef University Journal of Basic and Applied Sciences,* Vol. 12, 93. https://doi.org/10.1186/s43088-023-00433-1

Alaje, A. I., Olayiwola, M. O., Ogunniran, M. O., Adedeji, J. A., & Adedokun, K. A. (2021). Approximate analytical methods for the solution of fractional order integro-differential equations. *Nigerian Journal of Mathematics and Applications*, Vol. 31, 175-190.

Aniji, M. Kavitha N., Balamuralitharan, S. (2020). Mathematical modelling of hepatitis B virus infection for antiviral therapy using LHAM. *Advances in Differential Equations*. doi:10.1186/s13662-020-02770-2.

Ayati, Z., & Biazar, J. (2015). On the convergence of Homotopy perturbation method. *Journal of the Egyptian Mathematical Society*, Vol. 23(2), 424-428. https://doi.org/10.1016/j.joems.2014.06.015

Balamuralitharan, S., Geethamalini, S. (2018). *Solutions of epidemic of EIAV infection by HPM. Journal of Physics:* Conference Series, 1000, 012023.

Centers for Disease Control and Prevention. (2023). Chikungunya. Retrieved from http://www.cdc.gov/chikungunya/index.html Accessed: 10th March, 2023.

Elaiw, A.M., Alade, T.O., & Alsulami, S.M. (2019). Global dynamics of delayed chikv infection model with multitarget cells. *Journal of Applied Mathematics and Computation*, Vol, 60, 303–325. http://dx.doi.org/10.1007/s12190-018-1215-7.

Hajji, M.E., Zaghdani, A., & Sayari, S. (2022). Mathematical analysis and optimal control for Chikungunya virus with two routes of infection with nonlinear incidence rate. *International Journal of Biomathematics*, 15 (1). http://dx.doi.org/10.1142/S1793524521500881

He, J. H. (2003). Homotopy perturbation method: A new nonlinear analytical technique. *Applied Mathematics and Computation*, Vol. 135(1), 73-79.

He, J.H. (1999). Homotopy perturbation technique. *Computational Methods in Applied Mechanics and Engineering*, Vol. 178(3-4), 257.

Kolawole, M. K., Olayiwola, M. O., Alaje, A. I., *et al.* (2023). Conceptual analysis of the combined effects of vaccination, therapeutic actions, and human subjection to physical constraint in reducing the prevalence of COVID-19 using the homotopy perturbation method. *Beni-Suef University Journal of Basic and Applied Sciences*, Vol. 12. https://doi.org/10.1186/s43088-023-00343-2

Olaniyi, S., Alade, T. O., Chuma, F. M., Ogunsola, A. W., Aderele, O. R., & Abimbade, S. F. (2023). A fractional-order nonlinear model for within-host Chikungunya virus dynamics with adaptive immunity using Caputo derivative operator. *Healthcare Analytics*, 4, 100205. https://doi.org/10.1016/j.health.2023.100205

Olayiwola, M. O., & Adedokun, K. A. (2023). A novel tuberculosis model incorporating a Caputo fractional derivative and treatment effect via the homotopy perturbation method. *Bulletin of the National Research Centre*, Vol. 47(1), 121.

Olayiwola, M. O., Alaje, A. I., Olarewaju, A. Y., & Adedokun, K. A. (2023). A Caputo fractional order epidemic model for evaluating the effectiveness of high-risk quarantine and vaccination strategies on the spread of COVID-19. *Healthcare Analytics*, 3. https://doi.org/10.1016/j.health.2023.100179

Olayiwola, M. O. & Alaje, A. I. (2024). Mathematical modelling of diphtheria transmission and vaccine efficacy using Nigeria. *Modelling earth systems and environment*, 10. https://doi.org/10.1007/s40808-024-01976-7

WHO, Chikunvirus Fact Sheets, World Health Organization Press, Geneva, 2023, Accessed 10th March.

Yunus, A. O., Olayiwola, M. O., Adedokun, K. A., *et al.* (2022). Mathematical analysis of fractional-order Caputo's derivative of coronavirus disease model via Laplace Adomian decomposition method. *Beni-Suef University Journal of Basic and Applied Sciences*, Vol.11, 144. https://doi.org/10.1186/s43088-022-00326-9

Yunus, A. O., Olayiwola, M. O., Omoloye, M. A., & Oladapo, A. O. (2023). A fractional-order model of Lassa disease using the Laplace-Adomian Decomposition Method. *Healthcare Analytics*, Vol. 3, 100167. doi:10.1016/j.health.2023.100167.

An Appraisal on the Application of Reproduction Number for the Stability Analysis of Disease - Free Equilibrium State for S-I-R Type Models

N. I. Akinwande[1], S. A. Somma[2]*, T. T. Ashezua[3], R. I. Gweryina[4], O. N. Abdurahman[5],

[1,2,5]Department of Mathematics, Federal University of Technology Minna, Nigeria
[3,4]Department of Mathematics, Joseph Sarwuan Tarka University, Makurdi, Nigeria
[2*]Corresponding author: sam.abu@futminna.edu.ng
+2348068037304
[1]ninuola.wande@futminna.edu.ng
[3]ttashezua@gmail.com
[4]gweryina.reuben@uam.edu.ng
[5]nurat.a@futminna.edu.ng

Abstract

One of the key ideas in mathematical biology is the basic reproduction number, which can be utilized to comprehend how a disease epidemic profile might evolve in the future. The basic reproduction number, represented by R_0, is the anticipated number of secondary cases that a typical infectious individual would cause in a population that is fully susceptible. This threshold parameter is highly valuable in characterizing mathematical problems related to infectious diseases. If $R_0 < 1$, this suggests that, on average, during the infectious period, an infected individual produces less than one new infected individual, suggesting that the infection may eventually be eradicated from the population. On the other hand, if $R_0 > 1$, every infected person develops an average of multiple new infections, it suggests that the disease may continue to spread throughout the population. We discuss the Reproduction number in this work and provide some examples, both for straightforward and complicated situations.

1.0 The Basic Reproduction Number

One of the key ideas in mathematical biology that is used to predict the future of an epidemic is the basic reproduction number. Diekmann O. & Heesterbeck, 2000), (Murray, 2002) state that the basic reproduction number, represented by, is the anticipated number of secondary cases that a typical infectious individual would cause in a fully susceptible population. This threshold parameter is highly valuable as it describes mathematical issues related to the dynamics of infectious diseases.

If $R_0 < 1$, this implies that, on average, an infected individual produces less than one new infected individual during the infectious period and the infection can be brought under control or totally eliminated from the population. Conversely, if $R_0 > 1$, then each infected individual produces, on average, more than one new infection, and the disease persists in the population. For a single infected compartment, R_0 is simply the product of the infection rate and the mean duration of the infection. But for complicated models, this simple computation of R_0 is not applicable and the need for a more robust computation is required and will be demonstrated in the second example after giving the analytical framework. We therefore compute the basic reproduction number R_0, using the next generation operator approach by (Van de Driessche, 2002). The method is described as illustrated next.

1.1 Computation of Basic Reproduction Number

Suppose that there are a total number of n compartments in the S-I-R model under consideration with m compartments corresponding to the infected classes.

Let

$F_i(x)$ = the rate of appearance of new infections in compartment i.

$V_i^+(x)$ = the rate of transfer of individuals into compartment i by all other means; (inflow).

$V_i^-(x)$ = the transfer of individuals out of the compartment i. (outflow)

The disease transmission model is given by the system of equations

$$x_i' = f_i(x) = F_i(x) - V_i(x) \tag{1.1}$$

where,

$$V_i = V_i^-(x) - V_i^+ \tag{1.2}$$

One other important step is to obtain the disease-free equilibrium point x_0. We then compute matrices F and V which are $m \times m$ matrices, where m represents number of the infected classes, defined by

$$F = \left[\frac{\partial F_i}{\partial x_j}(x_0) \right] \tag{1.3}$$

and

$$V = \left[\frac{\partial V_i}{\partial x_j}(x_0)\right] \text{ with } 1 \le i, \quad j \le m, \tag{1.4}$$

and F is non-negative and V is a non-singular M-matrix (a matrix with inverse, belonging to the class of positive matrices). Since F is non-negative and V is non-singular, then V^{-1} is non-negative and also FV^{-1} is non-negative. We then compute matrix FV^{-1}, defined as the next generation matrix (Diekmann O. & Heesterbeck, 2000).

The basic reproduction number (reproduction ratio) R_0 is then defined as

$$R_0 = \rho\left(FV^{-1}\right) \tag{1.5}$$

where

$\rho(A)$ = the spectral radius of matrix A, (or the maximum modulus of the eigenvalues of A).

The following steps are followed in computing the basic reproduction number using the next generation operator approach:

1. Identify classes for which:
   (i) An infection event increases this class (gain/inflow terms).
   (ii) Loss from this class means of current or future infection (loss/outflow terms)
2. Compute the disease-free equilibrium
3. List the gain and loss terms for each class.
4. Create a matrix (F) of gain terms of each class partially differentiated with respect to each and evaluated at the disease-free equilibrium
5. Create a matrix (V) of loss terms of each class partially differentiated with respect to each and evaluated at the disease-free equilibrium
6. Invert matrix V to get V^{-1}
7. Evaluate matrix $G = FV^{-1}$
8. R_0 is the dominant Eigen-value of G.

2.0 Example 1

Consider the following SIR model

$$\frac{dS}{dt} = \pi - \beta SI - \mu S \tag{1}$$

$$\frac{dI}{dt} = \beta SI - (\mu + \gamma)I \tag{2}$$

$$\frac{dR}{dt} = \gamma I - \mu R \tag{3}$$

We compute the basic reproduction number for the above model.

The disease-free equilibrium state for the model is given by $(S, I, R) = \left(\frac{\pi}{\mu}, 0, 0\right) = E_0$.

Gains to class $I =$ βSI (4)

Loss from class $I =$ $(\mu + \gamma)I$ (5)

$$F_i = (\beta SI) \tag{6}$$

And so

$$V_i = (\mu + \gamma)I \tag{7}$$

Differentiating (6) and (7) partially with respect to I at E_0

$$F = \left(\frac{\beta\pi}{\mu}\right) \tag{8}$$

$$V = (\mu + \gamma) \tag{9}$$

$$V^{-1} = \left(\frac{1}{(\mu + \gamma)}\right) \tag{10}$$

The product of (8) and (10) yields

$$FV^{-1} = \left(\frac{\beta\pi}{\mu}\right)\left(\frac{1}{(\mu+\gamma)}\right) = \frac{\beta\pi}{\mu(\mu+\gamma)} \tag{11}$$

The basic reproduction number R_0, is therefore given by

$$R_0 = \frac{\beta\pi}{\mu(\mu+\gamma)} \tag{12}$$

Analysis and interpretation

The Disease-Free equilibrium DFE is stable if

$$R_0 = \frac{\beta\pi}{\mu(\mu+\gamma)} < 1 \tag{13}$$

i.e if

$$\beta < \frac{\mu(\mu+\gamma)}{\pi} = \beta_{max} \tag{14}$$

Which gives the threshold for the infection rate β.

For the effective control of the disease from the population we must have

$$\beta < \beta_{max} \tag{15}$$

Otherwise, the disease will persist in the population.

3.0 Example 2 - Scabby Mouth Disease Model

3.1 Preamble

Abdurrahman *et al.* (2021) in their work titled A Mathematical Model of Scabby Mouth Disease Incorporating the Quarantine Class obtained the Reproduction Number and analyzed the DFE stability. The aspect of the work relating to this application is presented in this section.
The authors proposed a mathematical model to study the transmission and control of scabby mouth disease in sheep, incorporating the vaccinated and quarantine classes. The Disease-free equilibrium (DFE) was obtained and the reproduction number was also computed. The DFE was analyzed for local stability using the condition that the DFE is locally stable if $R_0 < 1$.

3.2 Model Equation Formulation

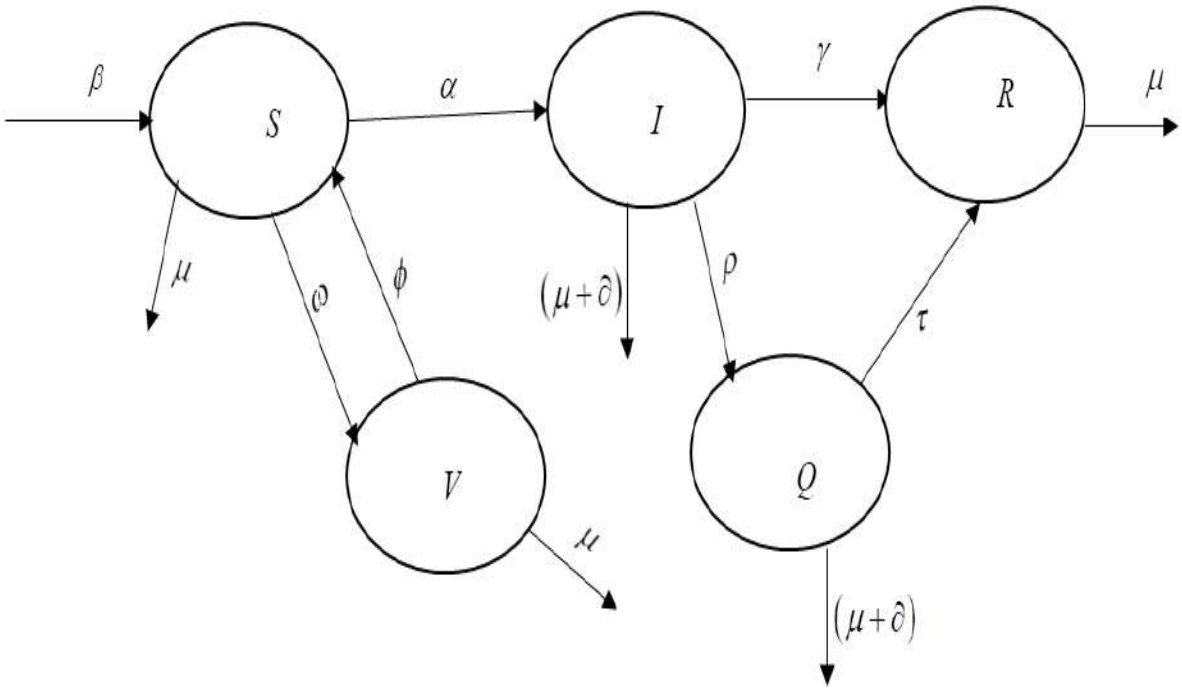

Figure 1: Schematic Diagram

The governing equations are given as:

$$\frac{dS}{dt} = \beta + \phi V - \frac{\alpha SI}{N} - (\omega + \mu)S \tag{16}$$

$$\frac{dI}{dt} = \frac{\alpha SI}{N} - (\gamma + \rho + \mu + \partial)I \tag{17}$$

$$\frac{dQ}{dt} = \rho I - (\tau + \mu + \partial)Q \tag{18}$$

$$\frac{dV}{dt} = \omega S - (\phi + \mu)V \tag{19}$$

$$\frac{dR}{dt} = \gamma I + \tau Q - \mu R \tag{20}$$

Table 3.1: Definition of Variables and Parameters.

Variables and Parameters	Description
S	Susceptible class
I	Infected Class

V	Vaccinated Class
Q	Quarantine Class
R	Recovered Class
β	Recruitment/Birth Rate
α	infection rate
ρ	Rate at which the infected class is quarantined
∂	death due to complication from infection
ω	Vaccination rate
ϕ	loss of immunity
μ	natural death rate
γ	recovery rate
τ	treatment rate

Let

$$k_1 = (\omega + \mu), k_2 = (\gamma + \rho + \mu + \partial), k_3 = (\tau + \mu + \partial), k_4 = (\phi + \mu)\,; \tag{21}$$

3.4 Equilibrium state of the model

At equilibrium state,

$$\frac{dS}{dt} = \frac{dI}{dt} = \frac{dQ}{dt} = \frac{dV}{dt} = \frac{dR}{dt} = 0 \tag{22}$$

Let $\begin{pmatrix} S \\ I \\ Q \\ V \\ R \end{pmatrix} = \begin{pmatrix} S_0^* \\ I_0^* \\ Q_0^* \\ V_0^* \\ R_0^* \end{pmatrix}$ (23)

We have the following equations

$$\beta + \varphi V_0^* - \frac{\alpha S_0^* I_0^*}{N_0^*} - k_1 S_0^* = 0 \tag{24}$$

$$\frac{\alpha S_0^* I_0^*}{N_0^*} - k_2 I_0^* = 0 \tag{25}$$

$$\rho I_0^* - k_3\, Q_0^* = 0 \tag{26}$$

$$\omega S_0^* - k_4 V_0^* = 0 \tag{27}$$

$$\gamma I_0^* + \tau Q_0^* - \mu R_0^* = 0 \tag{28}$$

From equation (25)

$$(\alpha S_0^* - k_2)\, I_0^* = 0 \tag{29}$$

$$\Rightarrow I_0^* = 0 \tag{30}$$

From (24)

$$\beta + \phi V_0^* - k_1 S_0^* = 0 \tag{31}$$

$$\Rightarrow V_0^* = \frac{k_1 S_0^* - \beta}{\phi} \tag{32}$$

From equation (27),

$$V_0^* = \frac{\omega S_0^*}{k_4} \tag{33}$$

comparing equation (32) and (33), we have

$$\frac{\omega S_0^*}{k_4} = \frac{(k_1 S_0^* - \beta)}{\phi} \tag{34}$$

$$S_0^* = \frac{\beta k_4}{k_1 k_4 - \omega\phi} \tag{35}$$

Substituting equation (35) into (33), we have

$$V_0^* = \frac{\omega\beta}{k_1 k_4 - \omega\phi} \tag{36}$$

Substituting equation (30) into (26), we have

$$k_3\, Q_0^* = 0 \tag{37}$$

$$\Rightarrow Q_0^* = 0 \tag{38}$$

substituting equations (30) and (36) into equation (28),

$$\mu R_0^* = 0 \tag{39}$$

$$\Rightarrow R_0^* = 0 \tag{40}$$

$$\begin{pmatrix} S_0^* \\ I_0^* \\ Q_0^* \\ V_0^* \\ R_0^* \end{pmatrix} = \begin{pmatrix} \frac{\beta k_4}{k_1 k_4 - \omega\phi} \\ 0 \\ 0 \\ \frac{\omega\beta}{k_1 k_4 - \omega\phi} \\ 0 \end{pmatrix} \tag{41}$$

$$N_0^* = \frac{\beta k_5}{k_1 k_4 - \omega\phi} \tag{42}$$

Where $k_5 = k_4 + \omega$ (43)

3.5 Computation of the Reproduction Number R_0

he basic reproduction number is the average number of secondary infections produced when one infective is introduced into the host population where everyone is susceptible (Benyah, 2009)

When$R_0 < 1$ The infection will die out over time while if $R_0 > 1$ the infection will persist in the population. In this model the reproduction number is given as the largest eigen-value or spectral radius of FV^{-1} . WhereF_i is the rate of appearance of new infection in compartment i, $V_i$is the transfer of infection from one compartment i to another.

$$FV^{-1} = \left(\frac{dF_i}{dx_i}\right)\left(\frac{dV_i}{dx_i}\right)^{-1} \tag{44}$$

$$F_i = \begin{pmatrix} \frac{\alpha SI}{N} \\ \rho I \end{pmatrix} \tag{45}$$

At DFE,

$$F = \begin{pmatrix} \frac{\alpha S_0^*}{N_0^*} & 0 \\ \rho & 0 \end{pmatrix} = \begin{pmatrix} \frac{\alpha k_4}{k_5} & 0 \\ \rho & 0 \end{pmatrix} \tag{46}$$

$$\frac{S_0}{N_0} = \frac{k_4}{k_5} \tag{47}$$

$$V_i = \begin{pmatrix} k_2 I \\ k_3 Q \end{pmatrix} \tag{48}$$

$$V_i = \begin{pmatrix} \frac{dV_i}{dI} \\ \frac{dV_i}{dQ} \end{pmatrix} = \begin{pmatrix} k_2 & 0 \\ 0 & k_3 \end{pmatrix} \tag{49}$$

$$|V| = \left|\begin{pmatrix} k_2 & 0 \\ 0 & k_3 \end{pmatrix}\right| = (k_2 k_3) \tag{50}$$

$$AdjV = \begin{pmatrix} k_3 & 0 \\ 0 & k_2 \end{pmatrix} \tag{51}$$

$$V^{-1} = \begin{pmatrix} \frac{1}{k_2} & 0 \\ 0 & \frac{1}{k_3} \end{pmatrix} \tag{52}$$

$$FV^{-1} = \begin{pmatrix} \frac{\alpha k_4}{k_2 k_5} & 0 \\ 0 & 0 \end{pmatrix} \tag{53}$$

$$|FV^{-1} - I\lambda| = 0 \tag{54}$$

$$\begin{vmatrix} \frac{\alpha k_4}{k_2 k_5} - \lambda & 0 \\ 0 & -\lambda \end{vmatrix} = 0 \tag{55}$$

$$-\lambda\left(\frac{\alpha k_4}{k_2 k_5} - \lambda\right) = 0 \tag{56}$$

$$\lambda_1 = 0, \lambda_2 = \frac{\alpha k_4}{k_2 k_5} \tag{57}$$

Therefore, the reproduction number

$$R_0 = \frac{\alpha k_4}{k_2 k_5} \tag{58}$$

3.6 Local Stability Analysis of the DFE

$$J(E^0) = (S_0^* I_0^* Q_0^* V_0^* R_0^*) \tag{59}$$

$$J(E^0) = \begin{pmatrix} -\alpha I - k_1 & -\alpha S & 0 & \phi & 0 \\ \alpha I & \alpha S - k_2 & 0 & 0 & 0 \\ 0 & \rho & -k_3 & 0 & 0 \\ \omega & 0 & 0 & -k_4 & 0 \\ 0 & \gamma & \tau & 0 & -\mu \end{pmatrix} \tag{60}$$

Substituting (39) into (54) we have that

$$\begin{pmatrix} -k_1 & -\frac{\alpha\beta k_4}{k_1 k_4 - \omega\phi} & 0 & \phi & 0 \\ 0 & \frac{\alpha\beta k_4}{k_1 k_4 - \omega\phi} - k_2 & 0 & 0 & 0 \\ 0 & \rho & -k_3 & 0 & 0 \\ \omega & 0 & 0 & -k_4 & 0 \\ 0 & \gamma & \tau & 0 & -\mu \end{pmatrix} \tag{61}$$

$$\begin{pmatrix} -k_1 & -\frac{\alpha\beta k_4}{k_1 k_4 - \omega\phi} & 0 & \phi & 0 \\ 0 & \frac{\alpha\beta k_4}{k_1 k_4 - \omega\phi} - k_2 & 0 & 0 & 0 \\ 0 & \rho & -k_3 & 0 & 0 \\ \omega & 0 & 0 & -k_4 & 0 \\ 0 & \gamma & \tau & 0 & -\mu \end{pmatrix} \tag{62}$$

$$\begin{vmatrix} -k_1 & -\frac{\alpha k_4(k_1-\beta)}{\omega\phi} & 0 & \phi & 0 \\ 0 & \frac{k_2\phi\omega+\alpha k_4(k_1-\beta)}{\omega\phi} & 0 & 0 & 0 \\ 0 & 0 & -k_3 & 0 & 0 \\ 0 & 0 & 0 & \frac{\phi\omega-k_1k_4}{k_1} & 0 \\ 0 & 0 & 0 & 0 & -\mu \end{vmatrix} \tag{63}$$

$$\begin{pmatrix} -k_1-\lambda_1 & -\frac{\alpha k_4(k_1-\beta)}{\omega\phi} & 0 & \phi & 0 \\ 0 & \frac{k_2\phi\omega+\alpha k_4(k_1-\beta)}{\omega\phi} - \lambda_2 & 0 & 0 & 0 \\ 0 & 0 & -k_3-\lambda_3 & 0 & 0 \\ 0 & 0 & 0 & \frac{\phi\omega-k_1k_4}{k_1} - \lambda_4 & 0 \\ 0 & 0 & 0 & 0 & -\mu-\lambda_5 \end{pmatrix} \tag{64}$$

$$\begin{pmatrix} \lambda_1 = -k_1 \\ \lambda_2 = \frac{-k_2\phi\omega+\alpha k_4(k_1-\beta)}{\omega\phi} \\ \lambda_3 = -k_3 \\ \lambda_4 = \frac{\phi\omega-k_1k_4}{k_1} \\ \lambda_5 = -\mu \end{pmatrix} \tag{65}$$

For the Disease-Free state to be achieved λ_2 and $\lambda_4$have to be negative. For $\lambda_2$to be negative we have that

$$-k_2\phi\omega + \alpha k_4(k_1-\beta) < 0 \tag{66}$$

$$\Rightarrow \alpha k_4(k_1-\beta) < k_2\phi\omega \tag{67}$$

$$\frac{\alpha k_4(k_1-\beta)}{k_2\phi\omega} < 1 \tag{68}$$

Comparing (58) to (68)

$\Rightarrow R_0 < 1$which implies that the disease will die out if this inequality holds.

On the other hand, $\lambda_4 < 0$ implies that

$$\Rightarrow \phi\omega < k_1 k_4 \tag{69}$$

$$\Rightarrow \phi\omega < (\omega+\mu)(\phi+\mu) \tag{70}$$

$$\Rightarrow \phi\omega < \phi\omega + \omega\mu + \mu\phi + \mu^2 \tag{71}$$

$$\Rightarrow -\omega\mu < \mu\phi + \mu^2 \tag{72}$$

$$\omega > -(\phi+\mu) \tag{73}$$

3.7 Conclusion

The DFE is locally stable if $R_0 = \frac{\alpha k_4}{k_2 k_5} < 1$ which implies that

$$\alpha < \frac{k_2 k_5}{k_4} < \frac{(\gamma+\rho+\mu+\partial)(\phi+\mu+\omega)}{(\phi+\mu)} = \alpha_{max} \tag{74}$$

Hence, the infection rate should not exceed α_{max} in order to effectively control the disease.

4.0 Example 3 - A TB model

Ashezual *et al*. (2017), in their work titled A Mathematical Model of Scabby Mouth Disease Incorporating the Quarantine Class obtained the Reproduction Number and analyzed of the DFE stability.

$$\left.\begin{aligned}
\frac{dS}{dt} &= \pi - (1-k)\alpha_1\lambda S - k\alpha_2\lambda S - \mu S \\
\frac{dL}{dt} &= (1-k)\alpha_1\lambda S - (\phi\alpha_3\lambda + \gamma)L - \mu L \\
\frac{dI}{dt} &= k\alpha_2\lambda S + (\phi\alpha_3\lambda + \gamma)L - (\upsilon + \mu + d)I + \alpha_4\lambda\omega R \\
\frac{dR}{dt} &= \upsilon I - \alpha_4\lambda\omega R - \mu R
\end{aligned}\right\} \tag{75}$$

With, $$\lambda = \beta c \frac{I}{N} \tag{76}$$

$S(t)$ Number of susceptible individuals at time t

$L(t)$ Number of exposed individuals at time t

$I(t)$ Number of infected individuals at time t

$R(t)$ Number of recovered individuals at time t

The disease-free equilibrium state for the model is given by

$$(S, L, I, R) = \left(\frac{\pi}{\mu}, 0, 0, 0\right) = E_0. \tag{77}$$

This represents the state in which there is no TB infection and is known as the disease-free equilibrium point.

$$F_i = \begin{pmatrix} (1-k)\alpha_1 \beta c \dfrac{I}{N} S \\ k\alpha_2 \beta c \dfrac{I}{N} S \\ 0 \\ 0 \end{pmatrix} \tag{78}$$

and

$$V_i = \begin{pmatrix} (\phi\alpha_3\lambda + \gamma)L + \mu L \\ -(\phi\alpha_3\lambda + \gamma)L - \alpha_4\lambda\omega R + (\upsilon + \mu + d)I \\ -\pi + (1-k)\alpha_1\lambda S + k\alpha_2\lambda S + \mu S \\ -\upsilon I + \alpha_4\lambda\omega R + \mu R \end{pmatrix} \tag{79}$$

We then obtain the partial derivatives of (78) and (79) with respect to (L, I) and by substituting the disease-free equilibrium point E_0 we get a 2×2 matrix since there are two infectious classes.

$$F = \begin{pmatrix} 0 & (1-k)\alpha_1 \beta c \dfrac{S}{N} \\ 0 & k\alpha_2 \beta c \dfrac{S}{N} \end{pmatrix} \tag{80}$$

and

$$V = \begin{pmatrix} (\gamma+\mu) & 0 \\ -\gamma & (\upsilon+\mu+d) \end{pmatrix} \tag{81}$$

Taking the inverse of (81) gives:

$$V^{-1} = \begin{pmatrix} \frac{1}{(\gamma+\mu)} & 0 \\ \frac{\gamma}{(\gamma+\mu)(\upsilon+\mu+d)} & \frac{1}{(\upsilon+\mu+d)} \end{pmatrix} \tag{82}$$

By computing the product of (80) and (82), we obtain

$$FV^{-1} = \begin{pmatrix} \frac{(1-k)\alpha_1 c\beta\gamma}{(\gamma+\mu)(\upsilon+\mu+d)} & \frac{(1-k)\alpha_1 c\beta}{(\upsilon+\mu+d)} \\ \frac{k\alpha_2 c\beta\gamma}{(\gamma+\mu)(\upsilon+\mu+d)} & \frac{k\alpha_2 c\beta}{(\upsilon+\mu+d)} \end{pmatrix} \tag{83}$$

From (83), we calculate the eigenvalues to determine the basic reproduction number, R_0 by taking the spectral radius (dominant eigenvalue) of the matrix FV^{-1}. This is computed by $|J-\lambda I| = 0$, hence the matrix becomes

$$\begin{vmatrix} \frac{(1-k)\alpha_1 c\beta\gamma}{(\gamma+\mu)(\upsilon+\mu+d)} - \lambda & \frac{(1-k)\alpha_1 c\beta}{(\upsilon+\mu+d)} \\ \frac{k\alpha_2 c\beta\gamma}{(\gamma+\mu)(\upsilon+\mu+d)} & \frac{k\alpha_2 c\beta}{(\upsilon+\mu+d)} - \lambda \end{vmatrix} = 0 \tag{84}$$

From (84), we obtain two eigenvalues, λ_1 and λ_2 which are given by

$$\lambda_1 = \frac{c\beta[\alpha_2 k(\gamma+\mu)+\alpha_1\gamma(1-k)]}{(\gamma+\mu)(\upsilon+\mu+d)} \tag{85}$$

and

$$\lambda_2 = 0 \tag{86}$$

Clearly, λ_1 is the dominant eigenvalue and therefore becomes the effective reproduction number R_{es} for the model. This is called the effective reproduction number because of the control parameters contained in the dominant eigenvalue.

5.0 Example 4 Vector-Host Model

In their research, Akinwande (2017) described the relationship between a population of humans and mosquitoes, with the human population represented as $S_h \to I_h \to S_h$ and the mosquito dynamics represented in $S_m \to I_m$ a model where S_h denotes susceptible humans, I_h is the human population that is infected, and S_M stands for both susceptible mosquitoes and I_M infected mosquitoes.

According to such a model, the mode of transmission occurs in each population in two stages:
Humans become infected (I_h) when they come into contact (i.e. λ_h, biting rate) with mosquitoes carrying the infection, which then spreads to other susceptible humans (S_h). When a susceptible mosquito (S_m) bites a human who is infected, it can spread the virus to other mosquitoes. Infected humans move into the removed compartment at a rate α and the removed compartment move to the susceptible compartment at a rate r. Additionally, we take into account that while infected humans die at a rate υ, mosquitoes and humans also have constant natural death rates w_h and w_m. Human and mosquito birth rates are b_h and b_m, respectively.

$$\dot{S}_h = b_h + rR_h - \lambda_h S_h I_m - w_h S_h \tag{87}$$

$$\dot{I}_h = \lambda_h S_h I_m - (w_h + \alpha + \upsilon) I_h \tag{88}$$

$$\dot{R}_h = \alpha I_h - (w_h + r) R_h \tag{89}$$

while that for mosquitoes is

$$\dot{S}_m = b_m - \lambda_m S_m I_h - w_m S_m \tag{90}$$

$$\dot{I}_m = \lambda_m S_m I_h - w_m I_m \tag{91}$$

with

$$T_h = S_h + I_h + R_h \tag{92}$$

$$T_m = S_m + I_m \tag{93}$$

The disease-free equilibrium state of the system (87) - (91) is:

$$x_0 = \left(\frac{b_h}{w_h}, 0, 0, \frac{b_m}{w_m}, 0 \right) \tag{94}$$

The Jacobian for system (87) - (91) for new infections and transfer from one compartment to another is provided by the next generation method as follows:

$$F_i = \begin{pmatrix} 0 \\ \lambda_h S_h I_m \\ 0 \\ 0 \\ \lambda_m S_m I_h \end{pmatrix} \tag{95}$$

and

$$V_i = \begin{pmatrix} w_h S_h - b_h - r R_h \\ (w_h + \alpha + \upsilon) I_h \\ (w_h + r) R_h - \alpha I_h \\ w_m S_m - b_m \\ w_m I_m \end{pmatrix} \tag{96}$$

Taking the partial derivatives with respect to I_h and I_m, and solving at the disease-free equilibrium produces

$$F = \begin{pmatrix} 0 & \lambda_h \\ \lambda_m & 0 \end{pmatrix} \tag{97}$$

and

$$V = \begin{pmatrix} (w_h + \alpha + \upsilon) & 0 \\ 0 & w_m \end{pmatrix} \tag{98}$$

The inverse of (98) yields

$$V^{-1} = \begin{pmatrix} \frac{1}{(w_h + \alpha + \upsilon)} & 0 \\ 0 & \frac{1}{w_m} \end{pmatrix} \tag{99}$$

The product of (97) and (99) gives

$$FV^{-1} = \begin{pmatrix} 0 & \frac{\lambda_h}{w_m} \\ \frac{\lambda_m}{(w_h + \alpha + \upsilon)} & 0 \end{pmatrix} \tag{100}$$

Next, we compute

$\left|FV^{-1} - \lambda I\right| = 0$ as

$$\begin{vmatrix} -\lambda & \frac{\lambda_h}{w_m} \\ \frac{\lambda_m}{(w_h + \alpha + \upsilon)} & -\lambda \end{vmatrix} = 0 \tag{101}$$

The evaluation of (101) gives

$$\lambda^2 - \frac{\lambda_m \lambda_h}{w_m (w_h + \alpha + \upsilon)} = 0 \tag{102}$$

From (102), we obtain the eigenvalues

$$\lambda = \pm \sqrt{\frac{\lambda_m \lambda_h}{w_m (w_h + \alpha + \upsilon)}} \tag{103}$$

From (103) we define our basic reproduction number, R_0 as the spectral radius (dominant eigenvalue) of the next generation matrix FV^{-1} since the basic reproduction number cannot be negative. Therefore

$$R_0 = + \sqrt{\frac{\lambda_m \lambda_h}{w_m (w_h + \alpha + \upsilon)}} \tag{104}$$

Interpretation and Analysis

$\frac{\lambda_h}{(w_h+\alpha+\upsilon)}$ represents the average number of newly infected humans that an infected mosquito spreads throughout the course of its infectivity from a population of humans that are only susceptible to the virus, and $\frac{1}{(w_h+\alpha+\upsilon)}$ is the average amount of time that each infected person spends prior to any kind of transfer. Also, $\frac{\lambda_m}{w_m}$ represents the quantity of infected mosquitoes that an infected human generates during its infectious period from a population of purely susceptible mosquitoes close to the DFE and $\frac{1}{w_m}$ is the average number of hours an infectious mosquito stays within the infectious chamber. The following scenarios will be taken into consideration for the system's stability:

(i) If $\lambda_m\lambda_h > w_m(w_h+\alpha+\upsilon) \Rightarrow R_0 > 1$, hence, the equilibrium is unstable, which implies that if a disease is introduced into the human and mosquito populations, it will persist.

(ii) If $\lambda_m\lambda_h < w_m(w_h+\alpha+\upsilon) \Rightarrow R_0 < 1$, thus there is stability in the equilibrium. In that case, the illness might not persist.

As a result, this provides guidance to the vector control and public health agencies regarding the efforts to be made to stop the disease's spread.

6.0 Example 5 - A COVID-19 Pandemic Mathematical Model

Akinwande *et al.* (2023) proposed a model on Covid-19 pandemic, the disease Free Equilibrium was computed, the effective reproduction number was calculated and the stability analysis of the DFE was performed. Below is the model formulation:

6.1 Model Formulation

By dividing the entire human population $N(t)$ at time t nine sub-populations of susceptible $S(t)$, first dose vaccinated $V_1(t)$, second dose vaccinated $V_2(t)$, latently infected $L(t)$, quarantined $Q(t)$, asymptomatic infectious $I_a(t)$, symptomatic infectious $I_s(t)$, hospitalized (isolated) $P(t)$ and removed $R(t)$. a model for the dynamics of COVID-19 transmission within a population in the presence of first and second doses of vaccination is fomulated.

Susceptible individuals are recruited at a constant rate Λ. The individuals in susceptible class are infected through contact with an infected person at the probability τ_1 and effective contact rate $\tau_1 c$ and moved to latent class. The individuals in first dose vaccinated class are infected through contact with an infected

person at the probability τ_2 and effective contact rate $\tau_2 c$ and moved to latent class. Also, the susceptible vaccinated individuals moved to first dose vaccinated class at vaccination rate ρ_1. First dose vaccinated individuals moved to second dose vaccinated class at vaccination rate ρ_2 after getting second dose of vaccine. First dose vaccinated individuals moved to susceptible class at waning rate ω. Second dose vaccinated individuals moved to removed class at progression rate ρ_3. People in latent class move to quarantine class and infected class at the quarantine rate θ and progression rate σ respectively. Some individuals in latent class recovered from the disease through natural immune and move to removed class at the recovery rate γ_1. The individual in quarantine class move to isolation class and removed class at the isolation rate ϕ_1 and recovery rate γ_2 respectively. The individuals in infected classes move to isolation class at the isolation rates ϕ_2 and ϕ_3. Those in isolation class are moved to the removed class at the recovery rate γ_3. Those in symptomatic infectious class and hospitalized (isolated) class can die due to COVID - 19 at disease-induced death rate δ_1 and δ_2 respectively. Those in symptomatic infectious class have reduced infectiousness compared to asymptomatic infectious class at the rates η.

The formulation of our model is guided by the following assumptions:

1. Individual in first dose vaccinated class can reverse back to susceptible class as a result of the waning of the vaccine.

2. There is permanent immunity after recovery.

3. While all infected classes are contagious, both hospitalized (isolated) and quarantined individuals have negligible contact rates and are therefore thought to be non-infectious under ideal (normal) conditions.

4. The risk of infection is further decreased with the second dosage.

5. Every individual has equal chance of contracting the disease.

The above description leads to the flow diagram in Figure 6.1.

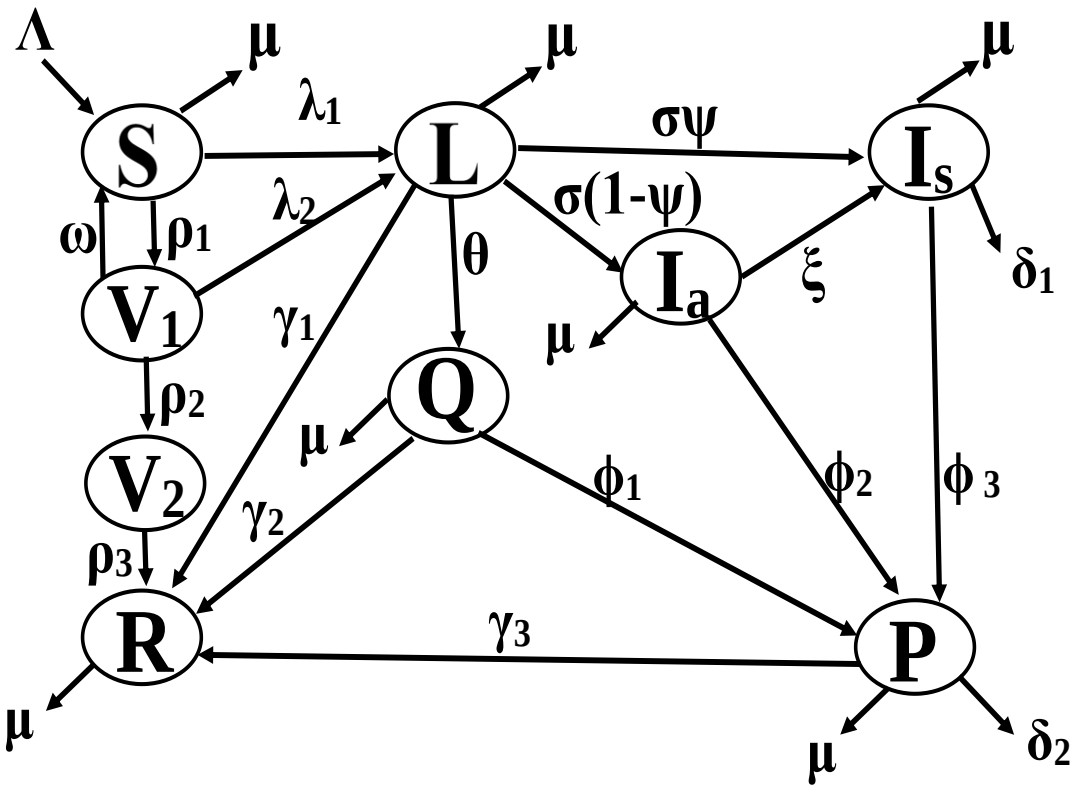

Figure 6.1: Flow diagram of COVID-19 dynamics

Using these definitions, assumptions and Figure 6.1 we arrive at the following non-linear system of equations that model the transmission dynamics and control of COVID-19 pandemic in a homogeneously mixing population:

$$\frac{dS}{dt} = \Lambda + \omega V_1 - \lambda_1 S - (\rho_1 + \mu)S \tag{105}$$

$$\frac{dV_1}{dt} = \rho_1 S - \lambda_2 V_1 - (\omega + \rho_2 + \mu)V_1 \tag{106}$$

$$\frac{dV_2}{dt} = \rho_2 V_1 - (\rho_3 + \mu)V_2 \tag{107}$$

$$\frac{dL}{dt} = \lambda_1 S + \lambda_2 V_1 - (\sigma + \theta + \gamma_1 + \mu)L \tag{108}$$

$$\frac{dQ}{dt} = \theta L - (\phi_1 + \gamma_2 + \mu)Q \tag{109}$$

$$\frac{dI_a}{dt} = \sigma(1-\psi)L - (\phi_2 + \xi + \mu)I_a \tag{110}$$

$$\frac{dI_s}{dt} = \sigma\psi L + \xi I_a - (\phi_3 + \delta_1 + \mu)I_s \tag{111}$$

$$\frac{dP}{dt} = \phi_1 Q + \phi_2 I_a + \phi_3 I_s - (\gamma_3 + \delta_2 + \mu)P \tag{112}$$

$$\frac{dR}{dt} = \rho_3 V_2 + \gamma_1 L + \gamma_2 Q + \gamma_3 P - \mu R \tag{113}$$

With initial conditions:

$$S(0) = S_0,\ V_1(0) = V_{10},\ V_2(0) = V_{20},\ L(0) = L_0,\ Q(0) = Q_0,\ I_a(0) = I_{a0},\ I_s(0) = I_{s0},\ P(0) = P_0,\ R(0) = R_0 \tag{114}$$

Movement out of the susceptible class, S into latently infected class, L occurs at a rate

$$\lambda_1 = \frac{\tau_1 c(1-\varepsilon\varphi)(I_a + \eta I_s)}{N} \tag{115}$$

Movement out of the first dose vaccinated class, V_1 into latently infected class, L occurs at a rate

$$\lambda_2 = \frac{\tau_2 c(1-\varepsilon\varphi)(I_a + \eta I_s)}{N} \tag{116}$$

where,

$$N(t) = S(t) + V_1(t) + V_2(t) + L(t) + Q(t) + I_a(t) + I_s(t) + P(t) + R(t) \tag{117}$$

The parameters and variables of the model indicated in Figure 6.1 are defined in Tables 6.1 and 6.2.

Table 6.1: Description of Variables

S/N	Variable	Description
1	S	Susceptible class.
2	V_1	First Dose Vaccinated class
3	V_2	Second Dose Vaccinated class
4	L	Latent class
5	Q	Quarantined class
6	I_a	Asymptomatic Infectious class
7	I_s	Symptomatic Infectious class.
8	P	Hospitalized (Isolated) class
9	R	Removed class
10	N	Total Population

Table 6.2: Description of Parameters

S/N	Parameters	Description
1	Λ	Constant recruitment into the population via birth or immigration
2	ρ_1	First Dose Vaccination rate
3	ρ_2	Second Dose Vaccination rate
4	ρ_3	Progression rate from V_2 to R
5	ω	Waning rate of first dose
6	μ	Natural death rate
7	δ_1	The disease-induced death rate of I_a.
8	δ_2	The disease-induced death rate of P.
9	τ_1	Covid-19 transmission probability per contact from S.
10	τ_2	Covid-19 transmission probability per contact from V_1.
11	c	Average contact rate, and thus $\beta = \pi c$ is the effective contact rate in the absence of any control measure.
12	ε	Efficacy of public enlightenment
13	φ	Rate of compliance to public enlightenment.
14	ϕ_1	Rate of hospitalization of L.

15	ϕ_2	Rate of hospitalization of I_a.
16	ϕ_3	Rate of hospitalization of I_s.
17	θ	Rate of quarantine L to Q
18	η	Modification parameter associated with reduced infectiousness of I_s compared to I_a.
19	σ	Progression rate of disease from L to I_a and I_s
20	ψ	Proportion of L that goes to I_s.
21	γ_1	Self- immune recovery of the L individuals
22	γ_2	Self- immune recovery of the Q individuals
23	γ_3	Recovery of P individuals due to treatment
24	ξ	Progression Rate from I_a to I_s

6.2 Disease Free Equilibrium (DFE)

The disease-free equilibrium of model system (105) – (116) is obtained by setting

$$\frac{dS}{dt}=\frac{dV_1}{dt}=\frac{dV_2}{dt}=\frac{dL}{dt}=\frac{dQ}{dt}=\frac{dI_a}{dt}=\frac{dI_s}{dt}=\frac{dP}{dt}=\frac{dR}{dt}=0, \tag{118}$$

and in the absence of disease, $L=Q=I_a=I_s=P=0$ and further simplification gives: $DFE(E_0)=(S^0,V_1^0,V_2^0,L^0,Q^0,I_a^0,I_s^0,P^0,R^0)=$

$$\left(\frac{\Lambda k_2}{k_1k_2-\rho_1\omega},\frac{\Lambda\rho_1}{k_1k_2-\rho_1\omega},\frac{\Lambda\rho_1\rho_2}{k_3(k_1k_2-\rho_1\omega)},0,0,0,0,\frac{\Lambda\rho_1\rho_2\rho_3}{\mu k_3(k_1k_2-\rho_1\omega)}\right) \tag{119}$$

where,

$$k_1=\rho_1+\mu,\quad k_2=\omega+\rho_2+\mu,\quad k_3=\rho_3+\mu$$

6.3 Computation of the Basic Reproduction Number, $\Re_0$

Since the infection components in this model are L, Q, I_a, I_s and P, then from (105) –(116)

$$F_i=\begin{pmatrix}\frac{c(1-\varepsilon\varphi)(I_a+\eta I_s)(\tau_1S+\tau_2V_1)}{N}\\0\\0\\0\\0\end{pmatrix} \tag{120}$$

Partial differentiation of F_i with respect to L, Q, I_a, I_s and P gives the new infection matrix

$$F = \begin{pmatrix} 0 & 0 & \frac{c(1-\varepsilon\varphi)(\tau_1 S^0 + \tau_2 V_1^0)}{N^0} & \frac{c(1-\varepsilon\varphi)\eta(\tau_1 S^0 + \tau_2 V_1^0)}{N^0} & 0 \\ 0 & 0 & 0 & 0 & 0 \\ 0 & 0 & 0 & 0 & 0 \\ 0 & 0 & 0 & 0 & 0 \\ 0 & 0 & 0 & 0 & 0 \end{pmatrix} \tag{121}$$

On the other hand,

$$V_i = \begin{pmatrix} (\sigma + \theta + \gamma_1 + \mu)L \\ -\theta L + (\phi_1 + \gamma_2 + \mu)Q \\ -\sigma(1-\psi)L + (\phi_2 + \xi + \mu)I_a \\ -\sigma\psi L - \xi I_a + (\phi_3 + \delta_1 + \mu)I_s \\ -\phi_1 Q - \phi_2 I_a - \phi_3 I_s + (\gamma_3 + \delta_2 + \mu)P \end{pmatrix} \tag{122}$$

Partial differentiation of V_i with respect to L, Q, I_a, I_s and P gives the transition matrix

$$V = \begin{pmatrix} k_4 & 0 & 0 & 0 & 0 \\ -\theta & k_5 & 0 & 0 & 0 \\ -\sigma(1-\psi) & 0 & k_6 & 0 & 0 \\ -\sigma\psi & 0 & -\xi & k_7 & 0 \\ 0 & -\phi_1 & -\phi_2 & -\phi_3 & k_8 \end{pmatrix} \tag{123}$$

It follows that

$$V^{-1} = \begin{pmatrix} \frac{1}{k_4} & 0 & 0 & 0 & 0 \\ A_3 & \frac{1}{k_5} & 0 & 0 & 0 \\ -A_4 & 0 & \frac{1}{k_6} & 0 & 0 \\ -A_5 & 0 & A_7 & \frac{1}{k_7} & 0 \\ -A_6 & A_8 & A_9 & A_{10} & \frac{1}{k_8} \end{pmatrix} \tag{124}$$

It follows that the next generation matrix is given by

$$FV^{-1} = \begin{pmatrix} -A_1A_4 - A_2A_5 & 0 & \frac{A_1}{k_6} + A_2A_7 & \frac{A_2}{k_7} & 0 \\ 0 & 0 & 0 & 0 & 0 \\ 0 & 0 & 0 & 0 & 0 \\ 0 & 0 & 0 & 0 & 0 \\ 0 & 0 & 0 & 0 & 0 \end{pmatrix} \tag{125}$$

Where,

$$k_4 = \sigma + \theta + \gamma_1 + \mu, \quad k_5 = \phi_1 + \gamma_2 + \mu, \quad k_6 = \phi_2 + \xi + \mu, \quad k_7 = \phi_3 + \delta_1 + \mu, \quad k_8 = \gamma_3 + \delta_2 + \mu$$

$$A_1 = \frac{c(1-\varepsilon\varphi)(\tau_1 S^0 + \tau_2 V_1^0)}{N^0}, \quad A_2 = \frac{c(1-\varepsilon\varphi)\eta(\tau_1 S^0 + \tau_2 V_1^0)}{N^0}, \quad A_3 = \frac{\theta}{k_4 k_5}, \quad A_4 = \frac{\sigma(\psi - 1)}{k_4 k_6},$$

$$A_5 = \frac{\sigma(\xi\psi - \psi k_6 - \xi)}{k_4 k_6 k_7}, \; A_6 = \frac{(\sigma\psi\xi k_5\phi_3 - \sigma\psi k_5 k_6\phi_3 + \sigma\psi k_5 k_7\phi_2 - \sigma\xi k_5\phi_3 - \sigma k_5 k_7\phi_2 - \theta k_6 k_7\phi_1)}{k_4 k_5 k_6 k_7 k_8},$$

$$A_7 = \frac{\xi}{k_6 k_7}, \qquad A_8 = \frac{\phi_1}{k_5 k_8}, \qquad A_9 = \frac{\phi_3\xi + \phi_2 k_7}{k_6 k_7 k_8}, \qquad A_{10} = \frac{\phi_3}{k_7 k_8}$$

The spectral radius for FV^{-1} gives the effective reproduction number (basic reproduction number with controls) denoted by $\Re_0^c$ which is given by

$$\Re_0^c = -A_1A_4 - A_2A_5 = \frac{c(1-\varepsilon\varphi)(\sigma k_7(1-\psi) + \sigma\eta(\xi(1-\psi) + k_6\psi))(\tau_1 S^0 + \tau_2 V_1^0)}{k_4 k_6 k_7 N^0} = \frac{c(1-\varepsilon\varphi)\sigma\mu(k_7(1-\psi) + \eta(\xi(1-\psi) + k_6\psi))(\tau_1 k_2 + \tau_2\rho_1)}{k_4 k_6 k_7(\mu(k_2 + \rho_1) + \rho_1\rho_2)} \tag{126}$$

which provides a measurement for the disease risk during COVID-19 transmission.

6.4 Local Asymptotic Stability of DFE

Theorem 4: The DFE, E_0 of the model equations (105) – (116) is locally asymptotically stable if R_0.

Proof: The stability of E_0 is established from the roots of the characteristic polynomial, which says that the equilibrium is stable if the roots of the characteristic polynomial are all negative. The Jacobian Matrix of equations (105) to (116) is given as:

$$J=\begin{bmatrix} -\lambda_1-k_1 & \omega & 0 & 0 & 0 & \frac{B_1S}{N} & \frac{B_2S}{N} & 0 & 0 \\ \rho_1 & -\lambda_2-k_2 & 0 & 0 & 0 & \frac{B_3V_1}{N} & \frac{B_4V_1}{N} & 0 & 0 \\ 0 & \rho_2 & -k_3 & 0 & 0 & 0 & 0 & 0 & 0 \\ \lambda_1 & \lambda_2 & 0 & -k_4 & 0 & \frac{B_1S}{N}+\frac{B_3V_1}{N} & \frac{B_2S}{N}+\frac{B_4V_1}{N} & 0 & 0 \\ 0 & 0 & 0 & \theta & -k_5 & 0 & 0 & 0 & 0 \\ 0 & 0 & 0 & \sigma(1-\psi) & 0 & -k_6 & 0 & 0 & 0 \\ 0 & 0 & 0 & \sigma\psi & 0 & \xi & -k_7 & 0 & 0 \\ 0 & 0 & 0 & 0 & \phi_1 & \phi_2 & \phi_3 & -k_8 & 0 \\ 0 & 0 & \rho_2 & \gamma_1 & \gamma_2 & 0 & 0 & \gamma_3 & -\mu \end{bmatrix} \quad (127)$$

At DFE (127) becomes,

$$J(E_0)=\begin{bmatrix} -k_1 & \omega & 0 & 0 & 0 & B_1B_5 & B_2B_5 & 0 & 0 \\ \rho_1 & -k_2 & 0 & 0 & 0 & B_3B_6 & B_4B_6 & 0 & 0 \\ 0 & \rho_2 & -k_3 & 0 & 0 & 0 & 0 & 0 & 0 \\ 0 & 0 & 0 & -k_4 & 0 & B_7 & B_8 & 0 & 0 \\ 0 & 0 & 0 & \theta & -k_5 & 0 & 0 & 0 & 0 \\ 0 & 0 & 0 & \sigma(1-\psi) & 0 & -k_6 & 0 & 0 & 0 \\ 0 & 0 & 0 & \sigma\psi & 0 & \xi & -k_7 & 0 & 0 \\ 0 & 0 & 0 & 0 & \phi_1 & \phi_2 & \phi_3 & -k_8 & 0 \\ 0 & 0 & \rho_2 & \gamma_1 & \gamma_2 & 0 & 0 & \gamma_3 & -\mu \end{bmatrix} \quad (128)$$

Applying elementary row operation on (128) gives

$$\begin{bmatrix} -k_1 & \omega & 0 & 0 & 0 & B_1B_5 & B_2B_5 & 0 & 0 \\ 0 & B_9 & 0 & 0 & 0 & B_{10} & B_{11} & 0 & 0 \\ 0 & 0 & -k_3 & 0 & 0 & -B_{12} & -B_{13} & 0 & 0 \\ 0 & 0 & 0 & -k_4 & 0 & B_7 & B_8 & 0 & 0 \\ 0 & 0 & 0 & 0 & -k_5 & \dfrac{\theta B_7}{k_4} & \dfrac{\theta B_8}{k_4} & 0 & 0 \\ 0 & 0 & 0 & 0 & 0 & -B_{14} & \dfrac{\sigma(1-\psi)B_8}{k_4} & 0 & 0 \\ 0 & 0 & 0 & 0 & 0 & 0 & B_{15} & 0 & 0 \\ 0 & 0 & 0 & 0 & 0 & 0 & 0 & -k_8 & 0 \\ 0 & 0 & 0 & 0 & 0 & 0 & 0 & 0 & -\mu \end{bmatrix} \tag{129}$$

where,

$$\left.\begin{aligned} &B_1 = \tau_1 c(1-\varepsilon\varphi), \quad B_2 = \tau_1 c\eta(1-\varepsilon\varphi), \quad B_3 = \tau_2 c(1-\varepsilon\varphi), \quad B_4 = \tau_2 c\eta(1-\varepsilon\varphi), \\ &N^0 = \frac{\Lambda k_2}{k_1k_2-\rho_1\omega} + \frac{\Lambda\rho_1}{k_1k_2-\rho_1\omega} + \frac{\Lambda\rho_1\rho_2}{k_3(k_1k_2-\rho_1\omega)} + \frac{\Lambda\rho_1\rho_2\rho_3}{\mu k_3(k_1k_2-\rho_1\omega)} = \frac{\Lambda(\mu A_{10}+\rho_1\rho_2)}{\mu(k_1k_2-\rho_1\omega)}, \\ &A_{10} = k_2+\rho_1, \quad B_5 = \frac{S^0}{N^0} = \frac{\mu k_2}{\mu A_{10}+\rho_1\rho_2}, \quad B_6 = \frac{V_1^0}{N^0} = \frac{\mu\rho_1}{\mu A_{10}+\rho_1\rho_2} \\ &B_7 = B_1B_5+B_3B_6, \quad B_8 = B_2B_5+B_4B_6, \quad B_9 = \frac{\rho_1\omega-k_1k_2}{k_1}, \quad B_{10} = \frac{k_1B_3B_6+\rho_1B_1B_5}{k_1}, \\ &B_{11} = \frac{k_1B_4B_6-\rho_1B_2B_5}{k_1}, \quad B_{12} = \frac{\rho_2(k_1B_3B_6+\rho_1B_1B_5)}{\rho_1\omega-k_1k_2}, \quad B_{13} = \frac{\rho_2(k_1B_4B_6-\rho_1B_2B_5)}{\rho_1\omega-k_1k_2}, \\ &B_{14} = \frac{k_4k_6-\sigma(1-\psi)B_7}{k_4}, \quad B_{15} = \frac{\xi\sigma(1-\psi)B_8+\sigma\psi k_6B_8-k_4k_6k_7+\sigma(1-\psi)k_7B_7}{k_4k_6-\sigma(1-\psi)B_7} \end{aligned}\right\} \tag{130}$$

The characteristic equation of (130) is given as

$$\begin{vmatrix} -k_1-\lambda & \omega & 0 & 0 & 0 & B_1B_5 & B_2B_5 & 0 & 0 \\ 0 & B_9-\lambda & 0 & 0 & 0 & B_{10} & B_{11} & 0 & 0 \\ 0 & 0 & -k_3-\lambda & 0 & 0 & -B_{12} & -B_{13} & 0 & 0 \\ 0 & 0 & 0 & -k_4-\lambda & 0 & B_7 & B_8 & 0 & 0 \\ 0 & 0 & 0 & 0 & -k_5-\lambda & \frac{\theta B_7}{k_4} & \frac{\theta B_8}{k_4} & 0 & 0 \\ 0 & 0 & 0 & 0 & 0 & -B_{14}-\lambda & \frac{\sigma(1-\psi)B_8}{k_4} & 0 & 0 \\ 0 & 0 & 0 & 0 & 0 & 0 & B_{15}-\lambda & 0 & 0 \\ 0 & 0 & 0 & 0 & 0 & 0 & 0 & -k_8-\lambda & 0 \\ 0 & 0 & 0 & 0 & 0 & 0 & 0 & 0 & -\mu-\lambda \end{vmatrix} = 0 \quad (131)$$

$$(-k_1-\lambda)(B_9-\lambda)(-k_3-\lambda)(-k_4-\lambda)(-k_5-\lambda)(-B_{14}-\lambda)(B_{15}-\lambda)(-k_8-\lambda)(-\mu-\lambda)=0 \quad (132)$$

$$\lambda_1=-k_1,\ \lambda_2=B_9,\lambda_3=-k_3,\ \lambda_4=-k_4,\ \lambda_5=-k_5,\ \lambda_6=-B_{14},\ \lambda_7=B_{15},\ \lambda_8=-k_8,\ \lambda_9=-\mu \quad (133)$$

It is observed from equation (133) that for the DFE to be stable λ_2 and λ_7 must be less than zero ($\lambda_2<0$ and $\lambda_7<0$) ;

This implies that,

$$\left.\begin{array}{l} \lambda_2<0 \\ B_9<0 \\ \dfrac{\rho_1\omega-k_1k_2}{k_1}<0 \\ \rho_1\omega-k_1k_2<0 \\ \rho_1\omega<k_1k_2 \\ \rho_1<\dfrac{k_1k_2}{\omega} \end{array}\right\} \quad (134)$$

From equation (134) the DFE will be stable if $\rho_1<\dfrac{\mu k_2}{\omega-k_2}$

$$\left.\begin{array}{l} \lambda_7<0 \\ B_{15}<0 \\ \dfrac{\xi\sigma(1-\psi)B_8+\sigma\psi k_6B_8-k_4k_6k_7+\sigma(1-\psi)k_7B_7}{k_4k_6-\sigma(1-\psi)B_7}<0 \\ \xi\sigma(1-\psi)B_8+\sigma\psi k_6B_8-k_4k_6k_7+\sigma(1-\psi)k_7B_7<0 \\ \xi\sigma(1-\psi)B_8+\sigma\psi k_6B_8+\sigma(1-\psi)k_7B_7<k_4k_6k_7 \end{array}\right\} \quad (135)$$

Divide (135.5.28) $k_4k_6k_7$ gives

$$\frac{\xi\sigma(1-\psi)B_8+\sigma\psi k_6B_8+\sigma(1-\psi)k_7B_7}{k_4k_6k_7}<1 \tag{136}$$

The Left Hand Side of (134) is equivalent to the Right Hand Side of (127). Hence,

$$R_0<1 \tag{137}$$

Therefore, the DFE is locally asymptotically stable if $\rho_1<\frac{\mu k_2}{\omega-k_2}$ and $R_0<1$.

7.0 Concluding Remarks

We have presented a discourse on the methods of computation of basic reproduction number which is one of the fundamental concepts in mathematical biology that is used to analyze the stability of Disease Free Equilibrium state. The note will be of great assistance to researchers in epidemiological modelling.

References

Abdurrahman, N. O. Somma, S.A., Akinwande, N.I. & Aboyeji, F.(2021). Mathematical Model of Scabby Mouth Disease Incorporating the Quarantine Class. *Nigerian Mathematical Society Conference Proceeding.* Sokoto.

Benyah, F. (2009). Introduction to Mathematical Modeling;. In *7th Regional College on Modeling, Simulation and Optimization, .* Ghana: University of Cape Coast.

N.I. Akinwande, S.A. Somma, R.O. Olayiwola, T.T. Ashezua, R.I. Gweryina, F.A. Oguntolu, O.N. Abdurahman, F.S. Kaduna, T.P. Adajime, F.A. Kuta, S. Abdulrahman, A.I. Enagi, G.A. Bolarin, M.D. Shehu, A. Usman, (2023). "Modelling the impacts of media campaign and double dose vaccination in controlling COVID-19 in Nigeria". *Alexandria Engineering Journal*.

Diekmann O. & Heesterbeck, J. A. (2000). *Mathematical Epidemiology of Infectious Diseases Model Building, Analysis and Inter.* New York: Wiley.

Murray, J. D. (2002). Mathematical Biology, An Introduction. (T. Edition., Ed.) *Springer,, Volume 17, .*

T. T. Ashezua, R. O. Olayiwola and N. I. Akinwande (2017) "Global Stability Analysis and solution of an infection-age structured Mathematical Model for Tuberculosis Disease Dynamics" Journal of the Nigerian Association of Mathematical Physics Volume 42, July, 2017, pages 93-102

Van de Driessche, P. &. (2002). Reproduction Number and sub-threshold Endemic Equilibrium for Compartmental Models of Diseases Transmission; 180,. *Mathematical Bioscience*, 29-48.

The Roles of Mathematical Modelling in Green Energy, Governance, and Democracy. (Analysis of Chickenpox Epidemics in Kogi State, Nigeria as a Case Study)

M. M., Shior [1] B.C..Agbata, ,[2] Odeh, J.O.,,[1] A.U.,Ezeafulukwe, [3] J, Amos[4]
[11]Department of Mathematics/ Computer Science, Benue State University, Makurdi, Nigeria.
[2]Department of Mathematics and Statistics, Faculty of Science, Confluence University of Science and Technology, Osara, Nigeria
[3]Department of Mathematics, Faculty of Physical Sciences, University of Nigeria Nsukka, Nigeria.
[4]Department of Mathematical Science, Faculty of Natural Sciences, Prince Abubakar Audu, University, Nigeria

Corresponding Author: *mshior@bsum.edu.ng*

Abstract

This paper explores the multifaceted role of mathematical modeling in understanding and managing infectious diseases, examining its implications for green energy, governance, and democracy. The mathematical modeling of infectious diseases has proven instrumental in shaping effective public health policies, guiding governance strategies, and influencing democratic decision-making. The interplay between these domains showcases the interconnectedness of mathematical modeling with societal resilience and sustainable development. A deterministic model was formulated using system of differential equation with aim to investigate roles of mathematical modelling in governance, democracy and green energy. The key features, including the disease-free equilibrium, endemic equilibrium, and stability properties, were analyzed. It was discovered that the disease-free equilibrium is locally and asymptotically stable when the basic reproduction number (R_0) is less than 1, indicating disease control, and unstable otherwise, suggesting potential outbreaks. Sensitivity analysis and numerical simulations were conducted considering the total population of Kogi State as at December 2023 estimated to be 4,466, 800 (data obtained from National Population Commission of Nigeria) in order to validate the model against real-world observations. The analysis revealed the crucial role of mathematical epidemiology in governance, democracy and green energy, especially in the context of the Nigeria region. By introducing a hospitalized compartment, the model captured the dynamics of severe cases and the impact on disease transmission. The sensitivity analysis highlighted parameters influencing the model's behavior, providing insights into factors that significantly affect chickenpox dynamics. Various applications of mathematical epidemiology in governance, democracy and green were discussed intensively.

Keywords: Africa, Basic reproduction Number, Chickenpox, Democracy, Governance, Green energy, Hospitalization, Infectious Disease, Mathematical modelling, Numerical Simulation. Sensitivity Analysis,

1. Introduction

Mathematical modeling of infectious diseases is closely tied to governance, democracy, and green energy. In governance, models help authorities plan and implement effective public health policies, allocate resources, and make informed decisions during outbreaks. Democracy is impacted as governments communicate and enforce measures, requiring public cooperation. Green energy can be affected indirectly as disruptions in societal functions during pandemics may influence energy consumption patterns [6].

Furthermore, the modeling of infectious diseases can highlight vulnerabilities in healthcare systems, prompting governments to invest in resilient and sustainable healthcare infrastructure, indirectly linking to green energy efforts. Overall, mathematical modeling in this context is crucial for understanding, responding to, and mitigating the impact of infectious diseases on society [15]. Chickenpox, caused by the Varicella-Zoster virus (VZV), has a long history in Africa, affecting populations across the continent [14]. The epidemiological landscape of chickenpox in Africa is influenced by factors such as population density, healthcare infrastructure, and socio-economic conditions. While historical records may not extensively document chickenpox in Africa, the disease has been a part of the infectious diseases landscape for centuries [11]. The introduction of vaccination against chickenpox has played a crucial role in altering the disease's dynamics. However, the accessibility and implementation of vaccination programs in various African countries have varied, impacting the overall prevalence and severity of chickenpox in the region. The treatment of chickenpox in Africa aligns with global practices, focusing on symptom management and, in severe cases, antiviral therapy [11,14]. Access to healthcare resources and medications, however, can pose challenges in some regions. Community awareness and education regarding the importance of seeking medical attention for chickenpox complications are vital. Antiviral medications such as acyclovir can be prescribed to reduce the severity and duration of symptoms, especially in high-risk populations. Public health efforts in Africa are increasingly emphasizing the importance of vaccination as a preventive measure. Varicella vaccines are being integrated into routine immunization schedules, contributing to the reduction of chickenpox incidence and its associated complications [8]. The virus spreads through respiratory droplets and direct contact with the fluid from the chickenpox blisters. It is particularly contagious during the early stages of the infection, making person-to-person transmission common [4]. It is a global phenomenon, affecting individuals of all ages. While most cases occur in childhood, the virus can also manifest in adults. The prevalence varies across regions, influenced by vaccination rates and healthcare infrastructure. Chickenpox is typically a self-limiting disease, but complications can arise, particularly in vulnerable populations. Severe cases may lead to pneumonia, encephalitis, or secondary bacterial infections. Pregnant women and immune compromised individuals are at higher risk for complications [3]. Diagnosis is often based on clinical presentation and a history of exposure. Laboratory tests, such as polymerase chain reaction (PCR) or serological assays, can confirm the diagnosis by detecting VZV antibodies or the virus itself. The varicella vaccine is a highly effective preventive measure against chickenpox. It has significantly reduced the incidence and severity of the disease [3,4]. Vaccination is recommended in childhood, and a booster shot may be administered in adolescence. Early symptoms include fever, headache, and malaise, followed by

the characteristic itchy rash. The rash progresses from macules to papules, vesicles, and finally, crusts. The presence of lesions in various stages is a hallmark of chickenpox [14].

The basic Susceptible-Infectious-Recovered (SIR) model forms the foundation, characterizing the transitions between susceptible, infectious, and recovered individuals. However, a comprehensive understanding of the disease dynamics requires the inclusion of a hospitalized compartment to account for severe cases requiring medical attention. Hospitalization rates, treatment durations, and the impact on overall transmission dynamics are essential factors considered in this extended model. [1] formulated mathematical for the control of chickenpox with vaccination and treatment strategies. They used a deterministic mathematical model to formulate five dimensional ordinary differential equations modelling chickenpox with treatment and vaccination strategies. [12] also developed and analyzed a model for a varicella zoster virus model with vaccination.

This article aims to contribute to the existing body of knowledge by presenting a refined mathematical model that better reflects the nuanced dynamics of chickenpox, especially in the context of hospitalization. Insights gained from this model can inform public health strategies, vaccination campaigns, and resource allocation in healthcare systems.

2.0 Effects of Hospitalization in the Management of Chickenpox in Africa

Chickenpox, caused by the Varicella-Zoster virus (VZV), generally presents as a self-limiting disease. However, in some cases, especially in vulnerable populations, severe complications may arise, necessitating hospitalization. The effects of hospitalization in the management of chickenpox in Africa are crucial considerations for public health strategies and healthcare systems [14].

Complication Management: Hospitalization allows for the proper management of complications such as pneumonia, encephalitis, and bacterial infections, which can be more prevalent in certain regions of Africa due to varying healthcare access and socio-economic conditions.

Supportive Care: Severe cases of chickenpox may require supportive care, including intravenous fluids, pain management, and respiratory support. Hospitalization ensures the availability of necessary resources and expertise to provide comprehensive care [12].

Prevention of Secondary Infections: Hospital settings facilitate infection control measures, reducing the risk of secondary bacterial infections, a concern particularly in areas with limited access to healthcare and hygiene facilities.

Monitoring High-Risk Groups: Vulnerable populations, such as pregnant women and immune compromised individuals, benefit from close monitoring during hospitalization to prevent and manage potential complications [6].

Public Health Surveillance: Hospitalization data contribute to public health surveillance, aiding in the understanding of the disease burden and informing vaccination strategies and healthcare resource allocation.

Impact on Healthcare Infrastructure: The strain on healthcare infrastructure due to severe chickenpox cases underscores the importance of vaccination programs to reduce hospitalization rates and alleviate pressure on medical facilities [9, 12].

Mathematical epidemiology plays a crucial role in informing governance, democracy, and green energy policies by providing quantitative insights into disease spread, population dynamics, and sustainable practices.

1. **Governance: Disease Modeling:** Mathematical models help policymakers predict and manage disease outbreaks. For instance, the SEIR model (Susceptible-Exposed-Infectious-Removed) aids in understanding the progression of infectious diseases, enabling timely interventions.

Resource Allocation: Models assist in optimizing resource allocation, guiding decisions on healthcare infrastructure, vaccine distribution, and public health measures, enhancing the efficiency of governance [6,12].

2. **Democracy: Informed Decision-Making:** Transparent communication of mathematical models fosters an informed public, allowing citizens to understand the rationale behind policy decisions. This contributes to a democratic process by involving the populace in decision-making.

Public Health Policies: Democratic societies benefit from mathematical epidemiology as it guides the development and implementation of evidence-based public health policies, ensuring the well-being of the population [15].

3. **Green Energy: Population Dynamics:** Mathematical models are used to project population growth and energy consumption patterns, aiding in the development of sustainable green energy policies.

Environmental Impact Assessment: Epidemiological modeling extends to assessing the environmental impact of policies, helping governments make informed decisions regarding green energy initiatives and their implications on public health [6].

3.0 Model Formulation

The total population $N(t)$ is divided into five epidemiological compartments, the susceptible individuals (S), the exposed individuals (E), the infected individuals (I), hospitalized individuals (H), and recovered individuals (R). Supposed Λ denotes the constant recruitment where every individuals is recruited into the population by birth or immigration and every susceptible human becomes exposed at the rate β, where α, denotes rate of infection and $f\omega$ is the rate at which infected humans become hospitalized. $(1-f)\omega$ is the remaining fraction of infected individuals that recovered from chicken pox whereas σ is the recovering rate of hospitalized individuals and μ denotes natural death rate. ε_1 and ε_2 are disease induced death rates associated with infection and hospitalization respectively.

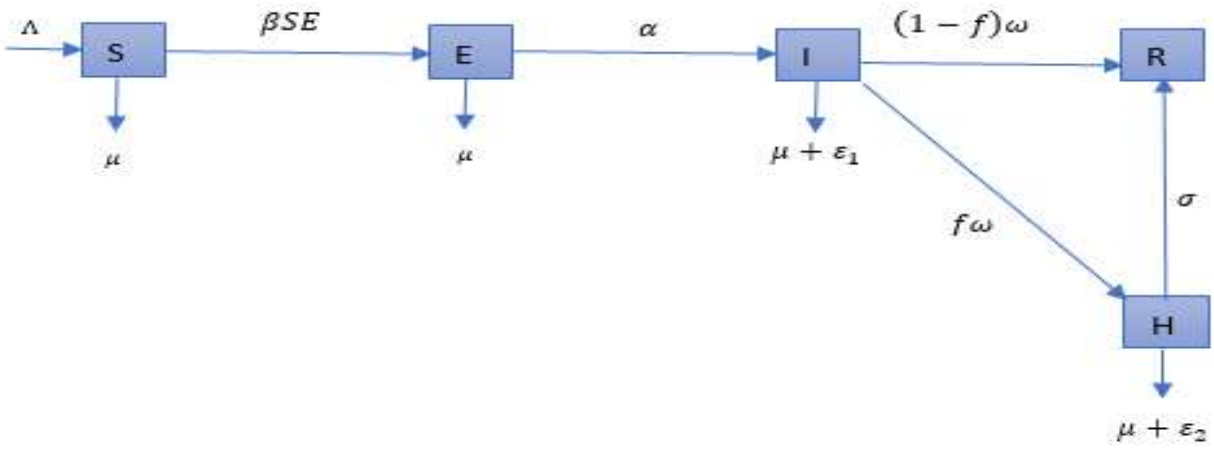

Fig: 1 Schematic diagram for the Model

Model Equation

$$\frac{ds}{dt} = \Lambda - (\beta E + \mu)\mathrm{S}$$
$$\frac{dE}{dt} = \beta SE - (\alpha + \mu)\mathrm{E}$$
$$\frac{dI}{dt} = \alpha E - (\omega + \mu + \varepsilon_1)\mathrm{I} \qquad (1)$$
$$\frac{dH}{dt} = f\omega I - (\mu + \varepsilon_2 + \sigma)\mathrm{H}$$
$$\frac{dR}{dt} = (1-\mathrm{f})\omega I + \sigma H - \mu R$$

3.1 Variables and Parameters Interpretation

Variables	**Interpretation**
$\mathrm{S}(t)$	Susceptible humans at time t
$E(t)$	Exposed humans at time t
$\mathrm{H}(t)$	Hospitalized humans at time t
$\mathrm{I}(t)$	Infected humans at time t
$\mathrm{R}(t)$	Recovered humans at time t
Parameter	**Description**
Λ	Constant recruitment rate

β	Rate of exposure to chicken pox
α	Constant recruitment rate
μ	Natural death rate
$f\omega$	Rate of hospitalization
σ	Rate at which hospitalized individuals recovered
$(1-\mathrm{f})\omega$	Remaining fractions of infected individuals that recovered
ε_1	Disease induced death rate
ε_2	Disease induced death rate associate with hospitalization

3.1 Invariant Region of the Model

The solutions of the proposed model are feasible for all t > 0, if they enter the invariant region D, which is given by:

$$D=\left\{\left(S,E,I,H,R\right):S>0,E>0,I>0,H>0,R>0,N<\frac{\Lambda}{\mu}\right\}$$

Proof

The total population of the model is given as

$$N\left(t\right)=S+E+I+H+R$$

The sum of the differential equations is

$$N^{'}\left(t\right)=S^{'}+E^{'}+I^{'}+H^{'}+R^{'}$$

On evaluating the algebraic terms, we obtain

$$N^{'}(t)=\Lambda-\left(S+E+I+H+R\right)\mu-\left(\varepsilon_1 I+\varepsilon_2 H\right)$$

$$N^{'}(t)=\Lambda-\mu N-\left(\varepsilon_1 I+\varepsilon_2 H\right)$$

$$\frac{dN}{dt}\leq\Lambda-\mu N$$

Solving the differential equation using the integrating factor method, we obtained

$$N(t)\leq\frac{\Lambda}{\mu}+\left(N(0)-\frac{\Lambda}{\mu}\right)e^{-\mu t}$$

Applying Birkhoff and Rota's theorem on the inequality, we obtain

$$0 \le N \le \frac{\Lambda}{\mu} \text{ as } t \to \infty$$

Thus, D is a positively invariant set under the flow described by the model (1) so that no solution path leaves through the boundary of region D.Thus, in this region, the model can be considered as being epidemiologically and mathematically well posed [7,13].

3.2 Positivity of Solution of the Model

It is necessary to prove that all state variable of the model in are non-negative for all time (t), for the model to be epidemiologically and mathematically well posed in a feasible region D given by:

$$D = \left\{ (S, E, I, H, \mathrm{R}) \in R_+^5 : (S + E + I + H + R) \le N \right\}$$

This is done by considering,

$$\left\{ (S, E, I, H, R) \ge 0 \in R_+^5 \right\}$$

Lemma 1:

Let the initial data for the model (1) be $(S, E, I, H, R) > 0$. Then the solutions (S, E, I, H, R) of the model (2) are positive for all time $t > 0$

Proof

Let $t_1 = \sup\{t > 0 : S > 0, E > 0, I > 0, H > 0, R > 0 \in [0, t]\}$. Thus $t > 0.$

We have from the first equation that

$$\frac{dS}{dt} = \Lambda - (\beta E + \mu)S$$

$$\frac{dS}{dt} \ge -(\beta E + \mu)S$$

This can also be written as

$$\int \frac{dS}{S} \ge -\int (\beta E + \mu)dt$$

We obtained:

$$\ln S \ge -(\beta E + \mu)t + C$$

$$S(t) \geq Ce^{-(\beta E+\mu)t}$$

Applying the initial condition; when $t=0,\ S(0)=C$

Therefore, $S(t) \geq S(0)e^{-(\beta E+\mu)t} \geq 0$ since $(\beta E+\mu)>0$

Similarly, it can be shown that $S, E, I, H, R > 0$

3.3 Asymptotic Stability of the Disease Free Equilibrium of the Model

The steady state where there is no infection (or absence of the disease), a point where $E=I=H=R=0$ is called the disease-free equilibrium point (DFE) which is given

$$\eta_0 = \left\{S^*, E^*, I^*, H^*, R^* > 0\right\} = \left\{\frac{\Lambda}{\mu}, 0, 0, 0, 0\right\}$$

3.4 Basic Reproduction Number of the Model

The basic reproduction number of infected individuals denoted by R_0 is defined as the average number of secondary infections produced by a single infectious individual introduced in a wholly susceptible population during his or her entire infectious period. We calculate the basic reproduction number by using the next generation operator method on the dynamical system (1) [5].

Hence, it follows that

$R_0 = \rho\left(FV^{-1}\right)$ where ρ is the dominant eigenvalue of FV^{-1}

$$F = \begin{bmatrix} \frac{\beta\Lambda}{\mu} & 0 & 0 \\ 0 & 0 & 0 \\ 0 & 0 & 0 \end{bmatrix} \quad V = \begin{bmatrix} (\alpha+\mu) & 0 & 0 \\ -\alpha & (\omega+\varepsilon_1+\mu) & 0 \\ 0 & -f\omega & (\omega_2+\sigma+\mu) \end{bmatrix} \quad F.V^{-1} = \begin{bmatrix} \frac{\beta\Lambda}{\mu(\alpha+\mu)} & 0 & 0 \\ 0 & 0 & 0 \\ 0 & 0 & 0 \end{bmatrix}$$

Therefore the basic reproduction number of the model is

$$R_0 = \frac{\beta\Lambda}{\mu(\alpha+\mu)}$$

3.5 Local Asymptotic Stability of the DFE of the Model

Theorem 1

The disease-free equilibrium point of the is locally asymptotically stable (LAS) if $R_0 < 1$, *and unstable if* $R_0 > 1$.

Proof

Using Jacobian matrix to prove the local stability of the disease free equilibrium point

$$J(\varepsilon_0) = \begin{bmatrix} -\mu & \frac{-\beta\Lambda}{\mu} & 0 & 0 & 0 \\ 0 & \frac{\beta\Lambda}{\mu} - (\alpha+\mu) & 0 & 0 & 0 \\ 0 & \alpha & -(\omega+\varepsilon+\mu) & 0 & 0 \\ 0 & 0 & f\omega & -(\omega_2+\sigma+\mu) & 0 \\ 0 & 0 & \sigma & (1-f)\omega & -\mu \end{bmatrix}$$

Since the diagonal of the first and last column consist of only the diagonal element, we can reduce $J(\varepsilon_0)$ to

$$J_1(\varepsilon_0) = \begin{bmatrix} \frac{\beta\Lambda}{\mu} - (\alpha+\mu) & 0 & 0 \\ \alpha & -(\omega+\varepsilon+\mu) & 0 \\ 0 & f\omega & -(\omega_2+\sigma+\mu) \end{bmatrix}$$

The characteristics polynomial of $J_1(\varepsilon_0)$ is

The characteristics polynomial of $J_1(\varepsilon_0)$ is

$$\lambda^3 - \frac{\left(\beta\Lambda - \alpha\mu + \mu^2 + \omega\mu + \sigma\mu + \omega_2\mu + \varepsilon_1\mu\right)\lambda^2}{\mu} + \frac{\left(2\Lambda\beta\mu + \Lambda\beta\omega + \Lambda\beta\sigma + \Lambda\beta\omega_2 + \Lambda\beta\varepsilon_1 - 2\alpha\mu^2 - \alpha\mu\omega - \alpha\mu\sigma - \alpha\mu\omega_2 - \alpha\mu\varepsilon_1 - \mu^3 + \mu\omega\sigma + \mu\omega\omega_2 + \mu\sigma\varepsilon_1 + \mu\omega_2\varepsilon_1\right)\lambda}{\mu} - \frac{(\omega_2+\sigma+\mu)(\omega+\mu+\varepsilon_1)(\alpha(\mu(\mu+\theta))(1-R_0))}{\mu}$$

Applying Routh-Hurwitz criterion to the Characteristics polynomial, we have that

$$\left(1 - R_0^H\right) > 0$$

$$\Rightarrow R_0^H < 1$$

Thus the DFE point of the model is locally asymptotically stable.

3.7 Global Asymptotic Stability of the Disease free equilibrium Point of the Model.

To investigate the global stability of the disease free equilibrium, we use the technique implemented by Castillo-Chavez and Song.

To do this, we write the equation in the uninfected class as

$$\frac{dX}{dt} = F\left(X, Z\right)$$

And we re-write the equation in the infected class as

$$\frac{dz}{dt} = G(X, Z)$$

Where $X = S \in \mathbb{R}^1_+$ denotes the uninfected population and

$Z = \left(E, I, H, R\right) \in \mathbb{R}^4_+$ denotes the infected population

$\varepsilon_0 = (X^*, 0)$ represents the disease free equilibrium of the system, and it globally asymptotically stable if it satisfies the following conditions:

$H_1 : \frac{dX}{dt} = F\left(X^*, 0\right), X^*$ is globally asymptotically stable

$H_2 : \frac{dZ}{dt} = D_Z G\left(X^*, 0\right) Z - \hat{G}\left(X, Z\right)$

$\hat{G}\left(X, Z\right) \geq 0$ for all $\left(X, Z\right) \in D$ and where $D_Z G\left(X^*, 0\right)$ is an M- matrix (i.e the diagonal elements are no-negative and it is also the Jacobian of $\hat{G}\left(X, Z\right) \geq 0$ evaluated at $(X^*, 0)$.

If the system satisfies the above condition, then the theorem below holds [,7, 9, 13].

Theorem 2

The equilibrium point $\varepsilon_0 = (X^*, 0)$. *is globally asymptotically stable if* $R_0 \leq 1$

$$F(X, Z) = \begin{bmatrix} \Lambda - (\beta \mathrm{E} + \mu)\mathrm{S} \\ (1 - \mathrm{f})\omega I + \sigma H - \mu R \end{bmatrix}$$

$$G(X, Z) = \begin{bmatrix} \beta SE - (\alpha + \mu)\mathrm{E} \\ \alpha E - (\omega + \mu + \varepsilon_1)\mathrm{I} \\ f\,\omega I - (\mu + \varepsilon_2 + \sigma)\mathrm{H} \end{bmatrix}$$

At disease free equilibrium,

H_1 :

$$\frac{dS}{dt} = \Lambda - \mu S$$

$$\frac{dR}{dt} = 0$$

H_2 :

$$D_Z G\left(X^*,0\right)Z = \begin{bmatrix} \left(\frac{\beta\Lambda}{\mu} - (\alpha+\mu)\right)E \\ \alpha E - (\omega+\mu+\varepsilon_1)\mathrm{I} \\ f\,\omega I - (\mu+\varepsilon_2+\sigma)\mathrm{H} \end{bmatrix}$$

$$\hat{G}\left(X,Z\right) = D_Z G\left(X^*,0\right)Z - G\left(X,Z\right)$$

$$\hat{G}\left(X,Z\right) = \begin{bmatrix} \beta E\left(\frac{\Lambda}{\mu} - S\right) \\ 0 \\ 0 \end{bmatrix}$$

Clearly, $\frac{\Lambda}{\mu} \geq S$ this implies that $\hat{G}\left(X,Z\right) \geq 0$.

Therefore the disease free equilibrium of the model is globally asymptotically stable.

Therefore, the disease free equilibrium of the model is globally asymptotically stable.

3.8 Endemic Equilibrium Point of the Model

The endemic equilibrium point is the steady state where there is persistence or prevalence of a disease in the population.

To obtain the endemic equilibrium we set the RHS of the differential equations in (1) to zero and solve for the state variables.

Thus, at the endemic equilibrium point,

$$\frac{dS}{dt} = \frac{dE}{dt} = \frac{dI}{dt} = \frac{dH}{dt} = \frac{dR}{dt} = 0.$$

Let $\varepsilon^{**} = \left(S^{**}, E,^{**} I^{**}, H^{**}, R^{**}\right)$ be the endemic equilibrium point.

We have that,

$$S^{**} = \frac{\alpha+\mu}{\beta}$$

$$E^{**} = \frac{\beta\Lambda - \mu(\alpha+\mu)}{\beta(\alpha+\mu)}$$

$$I^{**} = \frac{\alpha\beta\Lambda - \alpha\mu(\alpha+\mu)}{\beta(\alpha+\mu)(\omega+\mu+\varepsilon_1)}$$

$$H^{**} = \frac{\alpha\beta f\omega\Lambda - \alpha\mu f\omega(\alpha+\mu)}{\beta(\alpha+\mu)(\omega+\mu+\varepsilon_1)(\mu+\varepsilon_2+\sigma)}$$

$$R^{**} = \frac{(\omega+\mu+\varepsilon_1)(1-f)\omega(\alpha\beta\Lambda - \alpha\mu(\alpha+\mu)) + \alpha\beta f\omega\sigma\Lambda - \alpha\mu f\omega\sigma(\alpha+\mu)}{\beta(\alpha+\mu)(\omega+\mu+\varepsilon_1)(\mu+\varepsilon_2+\sigma)}$$

3.9 Sensitivity Analysis of the Model

Sensitivity analysis is carried out to determine the parameters that enhance the spread of chickenpox as well as control of the infection in a population.

The sensitivity index of the reproduction number of the model with respect to any parameter say x is given by:

$$\Im_x^{R_0} = \frac{\partial R_0}{\partial x} \times \frac{x}{R_0}$$

Given that

$$R_0 = \frac{\beta\Lambda}{\omega(\alpha+\mu)}$$

$$\Im_\beta^{R_0} = 1.0000$$

$$\Im_\Lambda^{R_0} = 1.0000$$

$$\Im_\mu^{R_0} = -\frac{\mu}{\alpha+\mu} = -0.9868$$

$$\Im_\alpha^{R_0} = -\frac{\theta}{\mu+\theta} = -0.0131$$

$$\Im_\omega^{R_0} = -\frac{\theta}{\mu+\theta} = -1$$

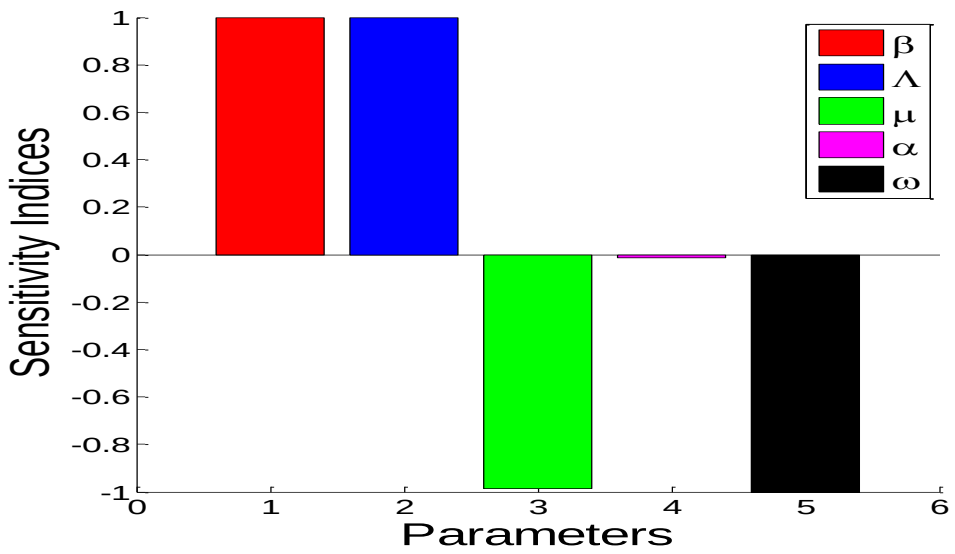

Figure 2 Sensitivity bar chat

3.10 Numerical Simulations of the Model

Numerical simulation plays a crucial role in the mathematical modeling of chickenpox by allowing researchers to simulate and analyze the dynamic interactions within a population. Through computational methods, mathematical models can incorporate various factors influencing the spread of chickenpox, such as transmission rates, population density, vaccination strategies, and immunity dynamics [9]. Simulation enables researchers to explore different scenarios and assess the impact of interventions, like vaccination campaigns or social distancing measures, on the spread of chickenpox. It aids in understanding the disease dynamics over time, identifying critical parameters, and optimizing control strategies. By running simulations, scientists can observe the progression of the disease under different conditions, helping to predict outbreaks, assess the effectiveness of public health measures, and inform policy decisions. Overall, numerical simulation enhances the precision and practical applicability of mathematical models in understanding and managing the spread of chickenpox within populations [1,9]

Table 2. Parameter values of the model (1) with the total population of Kogi State, Nigeria as at December 2023 estimated to 4,466,800 (Data obtained from National population Commission of Nigeria)

Parameter	Value	Source
Λ	0.01	[1]
μ	0.03	[1]
ε_1	0.06	Assumed
ε_2	0.01	Assumed
ω	0.001	[2]

f	0.000584	[1]
α	0.00004	Assumed
σ	0.08	Assumed
β	0.02	[1]
θ	0.2	Assumed

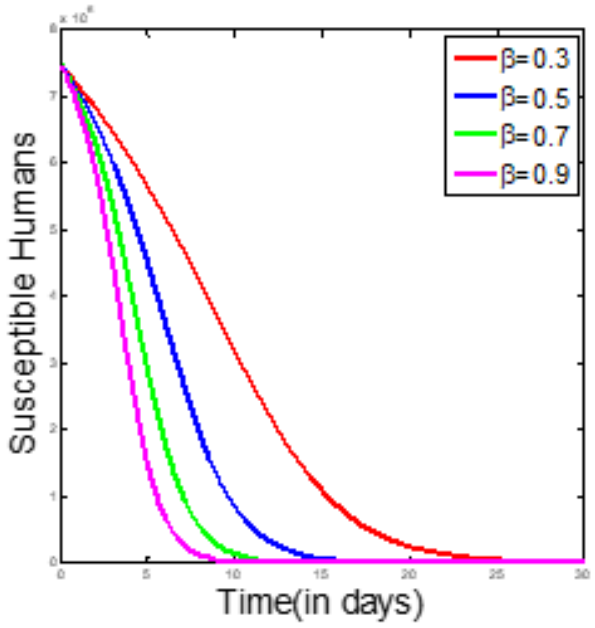

Figure 3a

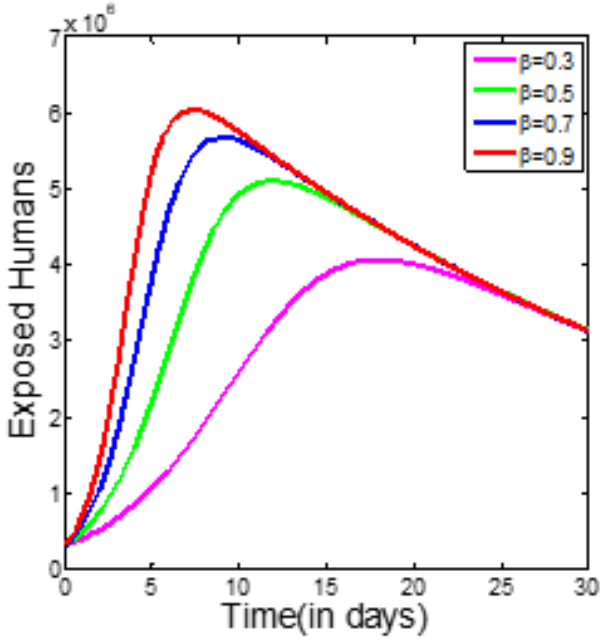

Figure 3b

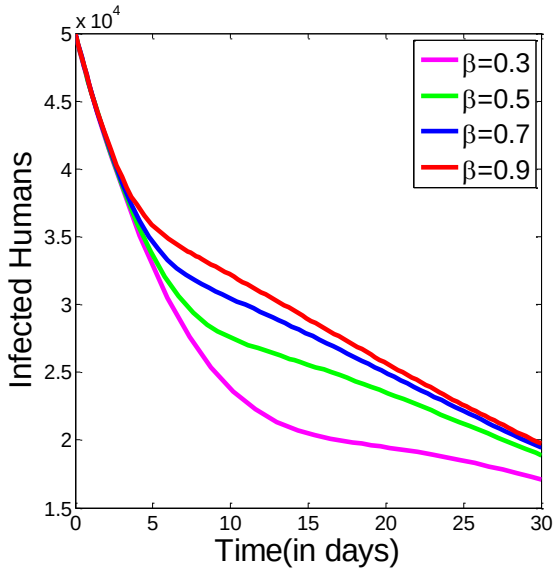

Figure 3c

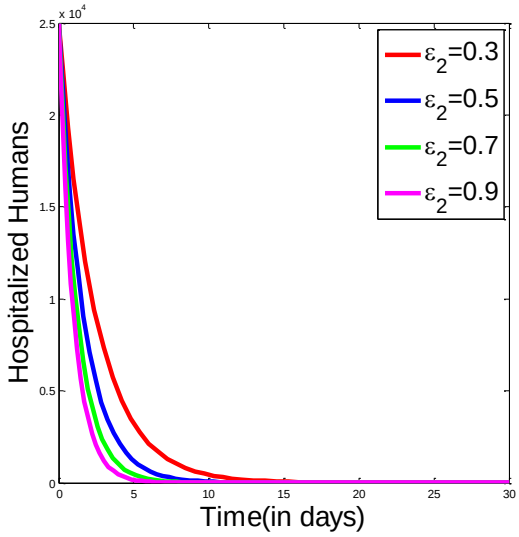

Figure 3d

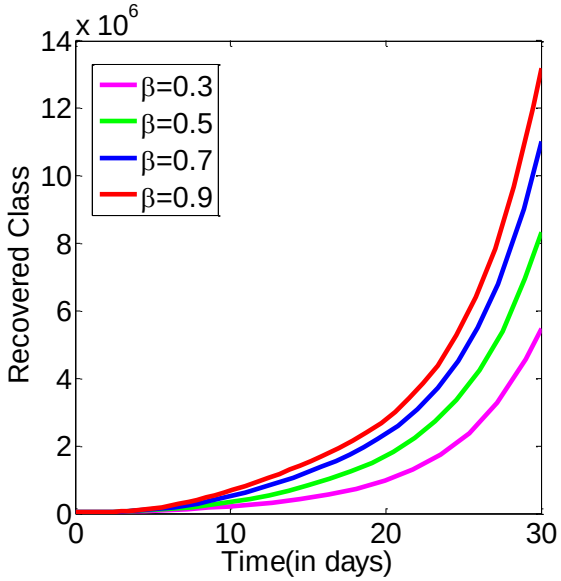

Figure 3e

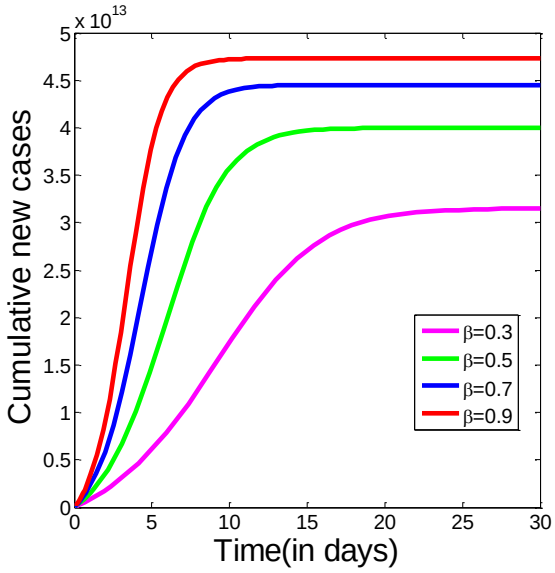

Figure 3f

4. **Conclusion**

From the sensitivity analysis and the resultant bar chat in figure 2, it is observed that the parameters with positive sensitivity indices enhance the transmission of the disease within the human population. Thus, parameters like β and Λ enhance the endemicity of the disease within the population. Also, parameters

such as μ, ω with negative sensitivity indices will ultimately curb the prevalence of the disease within the human population. In figure 3a, the number of susceptible individuals decreases to zero with time, though in figure 3b, the number of exposed individuals increases initially and later decreases quickly as it approaches zero which indicates disease control. In figure 3c, the number of infected individuals decreases rapidly with time which leads to decrease in the number of hospitalized individuals in figure 3d, this shows that effective hospitalization and awareness can tame the spread of chickenpox. The effective treatment observed in 3d produced to high recovery rate in figure 3e while figure 3f gives the cumulative new case of each compartment of the model. our mathematical model offers valuable insights into the transmission dynamics of chickenpox, considering the impact of hospitalization on disease management. The local and global stability analyses provided a thorough understanding of the equilibrium states, crucial for predicting potential outbreaks. Sensitivity analysis emphasized the importance of certain parameters in influencing disease dynamics. Notably, the results indicated that effective hospitalization significantly contributes to disease control, especially in regions like Africa with diverse healthcare challenges. Numerical simulations further validated the model, aligning our findings with real-world observations. The enumeration of the effects of hospitalization in the management of chickenpox in Africa underscores the importance of targeted public health interventions and healthcare infrastructure improvements to mitigate the impact of severe cases and reduce overall disease burden.

In conclusion, the role of mathematical modeling in infectious diseases extends far beyond the realms of epidemiology. Its impact on green energy, governance, and democracy underscores the need for interdisciplinary collaboration in addressing complex global challenges. As we navigate the complexities of the modern world, leveraging mathematical models becomes crucial for informed decision-making, resilient governance, and sustainable development. This paper underscores the importance of integrating mathematical modeling into the fabric of our societal responses to infectious diseases, paving the way for a more resilient and interconnected future.

Conflict of interest

The authors declare that they have no competing interest

Funding

We didn't receive funding for the publication of this article

Availability of data.

The data used in this study are referenced and presented in table 2 above.

References

1. Agbata B.C, Omale, D, Ojih, P.B, Omatola, I.U (2019). Mathematical analysis of chickenpox transmission dynamics with control measures. *Continental J. Applied Sciences* 14(2), 6-23
2. Agbata B.C, Ode O.J, Ani B.N, Odo C.E, Olorunnishola O.A. (2019).Mathematical assessment of the transmission dynamics of HIV/AID with treatment effects. *IJMSS*, 7(4), 40-52

3. American Academy of Pediatrics. (2018). Varicella-Zoster Infections. In Red Book: 2018 Report of the Committee on Infectious Diseases (31st ed., pp. 889-902). Elk Grove Village, IL: American Academy of Pediatrics.
4. Centers for Disease Control and Prevention. (2021). Chickenpox (Varicella). Retrieved from https://www.cdc.gov/chickenpox/index.html
5. Diekmann O, Heesterbeek JAP (2000) Mathematical epidemiology of infectious diseases: model building, analysis and interpretation. Wiley, New York
6. Ferguson, N. M. (2020). Impact of Non-Pharmaceutical Interventions (NPIs) to Reduce COVID-19 Mortality and Healthcare Demand. Imperial College COVID-19 Response Team.
7. Hethcote H W (2000) The mathematics of infectious diseases. *Soc Ind Appl Math Rev* 42:599–653
8. Njuguna, H. N, Yusuf U, Wamola B,. (2016). Burden and correlates of varicella zoster virus complications in Kenya. East African Medical Journal, 93(10), S35-S40.
9. Okon, I.M., Acheneje, G.O., Agbata, B.C., Onalo, P.O., Odeh, O.J., Shior, M.M (2023): A mathematical model for computation of alcoholism epidemics in Nigeria: A case of Lokoja metropolis (05, 12, 2023). ICIET 2023,
10. O'Neill, B. C. (2017). The Road to Sustainable Development: A New Vision for the Environmental, Social, and Economic Pillars. Annual Review of Environment and Resources.
11. Ogunbanjo, G .A, Dlakwa H .D. (2006). Chickenpox: presentation and management in adults in family practice. South African Family Practice, 48(6), 16-16d.,
12. Stephen Edward, Dmitry kuznetsor, Silas Mirau. (2014) Modelling and stability analysis for a varicella zoster virus modelwith vaccination. Applied and computational mathematics vol, 3 no 4, 2014 pp 150-162, doil 10:11648ij.acm. 20140304.16
13. van den Driessche P, Watmough J (2002) Reproduction number and sub-threshold endemic equilibria forcomputational models of disease transmission. *Math Biosci* 180:29–48
14. World Health Organization Regional Office for Africa. (2019). Immunization in the African Region 2018 Update. Retrieved from https://www.afro.who.int/sites/default/files/2019-05/Immunization%20in%20the%20African%20Region%202018%20Update.pdf
15. World Health Organization. (2018). Varicella vaccines: WHO position paper, June 2018. Weekly Epidemiological Record, 93(25), 313–326.

Mathematical Analysis of the Efficacy of Isolation in Mitigating the Spread of Rift Valley Fever Among Livestock

Olopade Isaac Adesola[1*], Mohammed Idayat Temilade[2], Philemon Musa Emmanuel[1], Sangoniyi Sunday Oloruntoyin[3], Adeniran Gbenga Adeyemi[4]. Ajao Saheed Oladele[5], and Adamu Abdul Kareem[1]

[1]Department of Mathematics and Statistics, Federal University Wukari, PMB 1020, Taraba State, Nigeria.

[2]Department of Mathematics and Social Sciences, Osun State Polytechnic Iree. Nigeria.

[3]Department of Mathematics and Computing Science Education, Emmanuel Alayande University of Education, Oyo, Oyo State, Nigeria.

[4]Department of Physical Sciences, Chrisland University, P.M.B. 2131, Abeokuta, Ogun State, Nigeria

[5]Department of Mathematics and Computer Science, Elizade University, Ondo State, Nigeria

[1*]isaac.olopade@fuwukari.edu.ng

[2]iskiludayat@gmail.com

[1]philemonmusa540@gmail.com

[3]sangoniyisunday@gmail.com

[4]gbadeniran@chrislanduniversity.edu.ng

[5]saheed.ajao@elizadeuniversity.edu.ng

[1]kareem@fuwukari.edu.ng

Abstract

This study delves into the intricate transmission dynamics of Rift Valley fever (RVF), involving interactions between mosquitoes and livestock, utilizing a compartmental model. The investigation incorporates the isolation of infected individuals as a control measure.

Calculation of the basic reproduction number R_0 using the next-generation matrix sheds light on the disease-free equilibrium state. It is found that the equilibrium state is locally asymptotically stable when R_0 less than 1, i.e. is. ($R_0 < 1$).Indicating potential control of RVF within a livestock population where R_0 remains below this threshold. However, when R0 exceeds 1, i.e. ($R_0 > 1$), the disease may become endemic, highlighting the critical importance of monitoring R_0 levels.

Furthermore, sensitivity analysis is conducted to pinpoint essential parameters vital for livestock policymakers and veterinary workers to consider. Through numerical simulations, the study assesses the effectiveness of early detection and isolation of infected livestock, alongside other integrated control measures. These simulations offer valuable insights into the dynamic behaviour of RVF, aiding in the development of effective strategies for disease management and prevention.

Keywords: Detection, Equilibrium Points, Isolation, Rift-Valley Fever, Sensitivity, Stability

1. Introduction

Rift Valley fever (RVF) is a viral zoonotic disease with significant implications for public health, livestock production, and economic stability, primarily affecting regions of Africa and the Arabian Peninsula. The disease is caused by the Rift Valley fever virus (RVFV), belonging to the Phlebovirus genus within the Bunyaviridae family (Adeyeye *et al.,* 2011), (Bird *et al.,* 2009), (Mpeshe *et al.* 2011; 2014). RVFV is transmitted primarily through the bites of infected mosquitoes, with both animal and human populations susceptible to infection. Rift Valley fever (RVF) particularly impacts domesticated animals like farm animals, sheep, goats, and camels, although it can also pose a chance to humans. Transmission of the virus usually takes place through bites from inflamed mosquitoes, drastically species belonging to the Aedes and Culex genera. moreover, touch with inflamed animal tissues or fluids can make contributions to the unfolding of the virus. (Bird *et al.*, 2016). RVF was initially documented in Kenya in 1931. Since its discovery, Cases of the disease have been documented in various regions of Africa and beyond, with notable occurrences reported in Madagascar in 1979, the Arabian Peninsula in 2000, and the Comoros archipelago in 2007 (Nanyingi *et al.,* 2014), (Sissoko *et al.,* 2009). In subsequent events, such as the virus's introduction to Egypt in 1977 through the trade of infected animals and a significant outbreak in Kenya, Somalia, and Tanzania in 1997-1998 exacerbated by El Niño and extensive flooding, the global significance of RVF has been underscored (Kanouté *et al.,* 2017). A concerning development emerged when RVF spread beyond the African continent in 2000, reaching Saudi Arabia and Yemen following the trade of infected animals from the Horn of Africa. This marked the first documented instance of the virus extending beyond Africa, raising concerns about potential dissemination to other regions, including Asia and Europe. Given the multifaceted impact of RVF on both animal and human health, comprehensive strategies for surveillance, control, and prevention are imperative to mitigate its adverse effects on public health and the economy (WHO, 2023). In animals, RVF can cause a wide range of clinical signs including fever, abortion storms in pregnant animals, high mortality rates in newborns, and hepatitis (Oguntolu *et al.,* 2022). In humans, RVF manifests as a febrile illness with symptoms such as fever, headache, muscle pain, joint pain, photophobia, and gastrointestinal symptoms. In severe cases, RVF can lead to complications such as hemorrhagic fever, encephalitis, retinitis, and death. Certain populations, such as farmers, herders, slaughterhouse workers, and veterinarians, are at increased risk of infection due to their close contact with livestock (Marion *et al.,* 2018), (Salih *et al.,* 2022).

Many researchers have utilized mathematical models as valuable instruments for studying disease epidemiology in various populations (Musibau *et al.,* 2022), (Bird *et al.,* 2009), (Fischer et *al.,* 2014), (Gachohi *et al.,* 2016), (Fawzy and Helmy 2022), (Métras *et al.,* 2017), (Pedro *et al.,* 2014; 2016), (Ajao *et al.,* 2023), (Akinwumi *et al.,* 2021), (Adewale *et al.,* 2015a; 2015b, 2015c; 2016). Previous studies have extensively explored the transmission dynamics and contagious properties of Rift Valley fever in both livestock and human communities.

In a study conducted by (et al., 2018), an eco-epidemiological compartmental mathematical model was formulated. This model integrated ambient temperature and water availability, utilizing empirical environmental data sourced from Kenya to accurately reflect real-world conditions. This model effectively accounts for the intermittent nature of Rift Valley fever (RVF) occurrences, elucidating low-level circulation that often evades detection, intermittently emerging, and occasionally reappearing after prolonged periods. The research offers insights into the intricate dynamics of RVF concerning environmental influences, highlighting the sporadic patterns of its occurrence. In a study conducted by (Nielsen et al., 2021), an evaluation was performed to gauge the effectiveness of surveillance and control strategies for Rift Valley fever (RVF) in both Mayotte and the continental European Union (EU).

Mathematical models were employed as part of this assessment. The research aimed to evaluate the efficiency of different approaches in preventing and controlling RVF outbreaks in these areas.

This study aims to develop a comprehensive model that integrates the effectiveness of isolating infected and infectious livestock, with the goal of better understanding how this isolation strategy influences the dynamics of disease within the animal population. Our objective is to explore and quantify the efficacy of isolating infected and infectious animals in reducing the spread of the disease among livestock.
In Section 2 of this paper, we elaborate on the formulation of the model, outlining the variables and parameters involved—section 3 delves into the mathematical analysis of the model, examining its stability and dynamics. The findings of our study are presented in Section 4, where we discuss the implications of the model's outcomes. In Section 5, we engage in further discussions and draw conclusions based on our findings, emphasizing the significance of isolating infected and infectious livestock as a control measure in disease management strategies. Through this research, Our objective is to contribute to the advancement of more effective measures for mitigating disease transmission within animal populations.

2. Model Formulation

In constructing our model, we assume that livestock contract the infection primarily through contact with infectious mosquitoes. Additionally, a consistent natural death rate denoted by δ is applied uniformly across all compartments. For further details on parameters, please refer to Table 2.2.
Our model comprises two main populations: livestock and mosquitoes. Within the livestock population, there are six compartments, namely S_L Susceptible, V_L Vaccinated, E_L Exposed, Sy_L Symptomatic, Ay_L Asymptomatic, I_L Isolated, and R_L Recovered. Each of these compartments represents a distinct stage of infection or immunity within the livestock population. Meanwhile, the vector population is subdivided into two compartments: S_V Susceptible and I_V Infected. These compartments capture the different states that mosquitoes can occupy concerning their susceptibility to and infection with the virus. This detailed compartmentalization allows us to capture the nuanced dynamics of disease transmission between livestock and mosquitoes, enabling a more comprehensive understanding of Rift Valley fever's spread and control strategies.

Livestock

$$
\begin{aligned}
S_L' &= \pi_L - \lambda_L S_L - \mu_L S_L + \omega_L R_L \\
E_L' &= (1-\theta_L)\lambda_L S_L - (\kappa_L + \mu_L)E_L \\
A'y_L &= (1-\alpha_L)\kappa_L E_L - (\mu_L + \delta_L + \overline{\sigma_L})Ay_L \\
S'y_L &= \theta_L \lambda_L S_L + \alpha_L \kappa_L E_L - (\mu_L + \delta_L + \sigma_L + \gamma_L)Sy_L \\
I_L &= \gamma_L Sy_L - (\mu_L + \delta_L + \Lambda_L)I_L \\
R_L' &= \sigma_L Sy_L + \overline{\sigma_L} Ay_L + \Lambda_L I_L - (\mu_L + \omega_L)R_L
\end{aligned} \tag{1.1}
$$

Vector

$$
\begin{aligned}
S_V' &= \pi_V - \lambda_V S_V - \mu_V S_V \\
I_V' &= \lambda_V S_V - \mu_V I_V \\
\lambda_L &= \frac{\beta_{VL}\phi I_V}{N_L} \text{ and } \lambda_V = \frac{\beta_{LV}\phi(E_L + Ay_L + Sy_L)}{N_V}
\end{aligned} \tag{1.2}
$$

Table 2.1. Description of Variables

Variables	Description
S_L	Susceptible Livestock Individual
E_L	Exposed Livestock Individuals
Sy_L	Symptomatic Livestock Individual
Ay_L	Asymptomatic Livestock Individual
I_L	Isolated Livestock Individual
R_L	Recovered Livestock Individual
S_V	Susceptible Vector Individual
I_V	Infected Vector Individuals

Table 2.2 Description of Parameters

Parameters	Description
β_{VL}	Probability of transmission from an infectious vector to susceptible livestock.
β_{LV}	Probability of transmission from an infectious livestock to susceptible vector.
ϕ	Biting rate of vector
π_L	Recruitment rate of Livestock
π_V	Recruitment of vector
λ_L	Force of infections of livestock

λ_V	Force of infections of vector
μ	Natural death
ω_L	Loss of Immunity
θ_L	Active infection
κ_L	Progression rate
α_L	Detection rate of asymptomatic
δ_L	Induced death from disease
γ_L	Isolation of Symptomatic individual
σ_L	Recovery of Symptomatic individual
$\overline{\sigma_L}$	Recovery of Asymptomatic individual
Λ	Recovery of Isolated individual

For better analysis, the following representation holds

$$
\begin{aligned}
S_L' &= \pi_L - \lambda_L S_L - \mu_L S_L + \omega_L R_L \\
E_L' &= (1-\theta_L)\lambda_L S_L - K_1 E_L \\
A'y_L &= (1-\alpha_L)\kappa_L E_L - K_2 A y_L \\
S'y_L &= \theta_L \lambda_L S_L + \alpha_L \kappa_L E_L - K_3 S y_L \\
I_L &= \gamma_L S y_L - K_4 I_L \\
R_L' &= \sigma_L S y_L + \overline{\sigma_L} A y_L + \Lambda_L I_L - K_5 R_L \\
S_V' &= \pi_V - \lambda_V S_V - \mu_V S_V \\
I_V' &= \lambda_V S_V - \mu_V I_V
\end{aligned}
\tag{1.3}
$$

Where

$$
\begin{aligned}
K_1 &= (\kappa_L + \mu_L) \\
K_2 &= (\mu_L + \delta_L + \overline{\sigma_L}) \\
K_3 &= (\mu_L + \delta_L + \sigma_L + \gamma_L) \\
K_4 &= (\mu_L + \delta_L + \Lambda_L) \\
K_5 &= (\mu_L + \omega_L)
\end{aligned}
$$

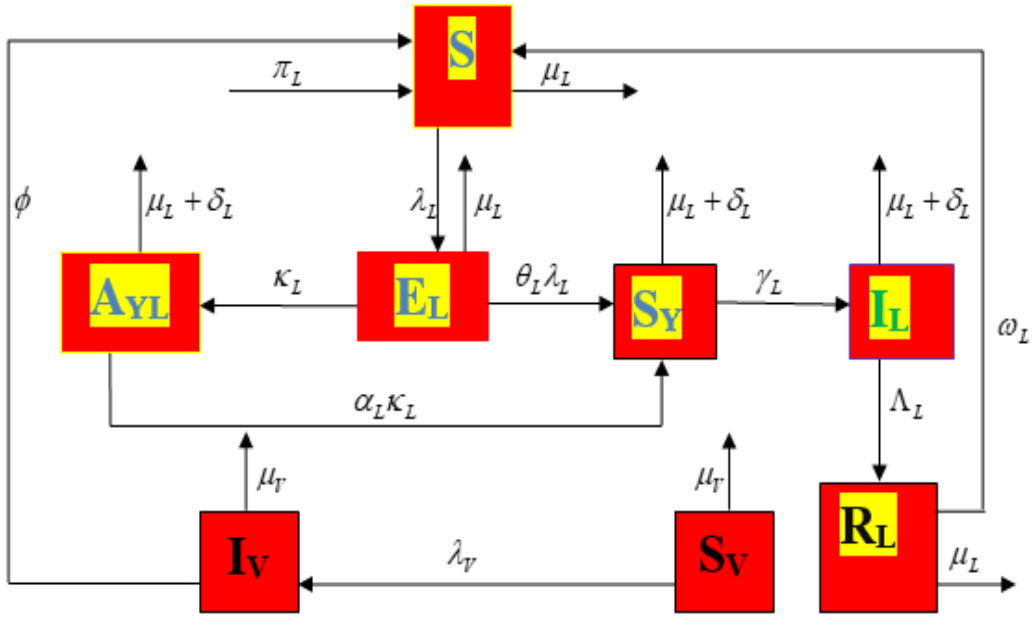

Figure 1. Schematic Diagram of the RVF Model.

2.1Analysis of the model

Lemma 1: The close set $D = D_L \times D_V \subset R_+^8$ is positive invariant for the model equation (1.3) with non-negative initial condition in R_+^8.

Proof: Consider the biologically-feasible region $D = D_L \times D_V \subset R_+^8$ with

$$D_L = \left\{ (S_L, E_L, Ay_L, Sy_L, I_L, R_L) \in R_+^6 : N_L \le \frac{\pi_L}{\mu} \right\} \tag{1.4}$$

And

$$D_V = \left\{ (S_V, I_V) \in R_+^2 : N_V \le \frac{\pi_V}{\mu} \right\}. \tag{1.5}$$

We will demonstrate that D is positive invariant (i.e all solutions within D remain within D for all time $t > 0$). Therefore:

$\frac{dN_L}{dt} = \pi_L - \mu N_L - \delta_L (Ay_L + Sy_L + I_L)$ and $\frac{dN_V}{dt} = \pi_V - \mu_V N_V$

Where $N_L = S_L + E_L + Ay_L + Sy_L + I_L + R_L$ and $N_V = S_V + I_V$

It follows that

$$\frac{dN_L}{dt} \le \pi_L - \mu N_L \tag{1.6}$$

And

$$\frac{dN_V}{dt} \le \pi_V - \mu_V N_V \tag{1.7}$$

A standard comparison theorem can be utilized to demonstrate that

$$N_L(t) \le N_L(0)e^{-N_L t} + \frac{\pi_L}{\mu_L}(1-e^{-N_L t})$$

And

$$N_V(t) \le N_V(0)e^{-N_V t} + \frac{\pi_V}{\mu_V}(1-e^{-N_V t})$$

In particular $N_L(t) \le \frac{\pi_L}{\mu_L}$ and $N_V(t) \le \frac{\pi_V}{\mu_V}$

If $N_L(0) \le \frac{\pi_L}{\mu_L}$ and $N_V(0) \le \frac{\pi_V}{\mu_V}$. Hence, all solutions of the model with the initial condition persist within this region for $t > 0$. This suggests that the region D is positive-invariant, and thus, the model can be deemed epidemiologically and mathematically well-posed.

2.2 Disease Free Equilibrium

The model equation (1.3) has a disease free equilibrium which is derived by setting all the right hand sides of the equations in (1.3) to zero which is given by;

$$\varepsilon_0 = (S_L, E_L, Ay_L, Sy_L, R_L, I_L, S_V, I_V) = \left(\frac{(1-\rho)\pi_L}{\mu_L}, 0,0,0,0,0, \frac{\pi_V}{\mu_V}, 0\right)$$

2.2 *Existence of Endemic Equilibrium Point of* $R-V$ *Fever*

The endemic equilibrium is given point is given below;

$$S_L^{**} = \frac{(1-\rho)\pi_L + \omega_L R_L^{**}}{\lambda_L^{**} + \mu_L},\ E_L^{**} = \frac{(1-\theta_L)\lambda_L^{**} S_L^{**}}{K_1},\ A_L^{**} y_L = \frac{(1-\alpha_L)\kappa_L E_L^{**}}{K_2}$$

$$S^{**} y_L = \frac{\theta_L \lambda_L^{**} S_L^{**} + \alpha_L \kappa_L E_L^{**}}{K_3},\ I_L^{**} = \frac{\gamma_L Sy_L^{**}}{K_4},\ R_L^{**} = \frac{\sigma_L S^{**} y_L + \overline{\sigma_L} A^{**} y_L + \Lambda_L I_L^{**}}{K_5}$$

$$S_V^{**} = \frac{\pi_V}{\lambda_V^{**} + \mu_V^{**}},\ I_V^{**} = \frac{\lambda_V^{**} S_V^{**}}{\mu_V}$$

Thus, the endemic equilibrium arises whenever the basic reproduction number $R_0 > 1$.

2.3Basic Reproduction Number

Using next generation matrix method (Olopade *et al.,* 2016; 2017; 2021a; 2021b; 2022). The non-negative matrix F (representing new infection terms) and the non-singular matrix V (depicting other remaining transfer terms) of the model (1.3) are given respectively;

$$V(F = \begin{pmatrix} 0 & 0 & 0 & 0 & (1-\theta_L)\beta_{VL}\phi\mu_V \\ 0 & 0 & 0 & 0 & 0 \\ 0 & 0 & 0 & 0 & \theta_L\beta_{VL}\phi\mu_V \\ 0 & 0 & 0 & 0 & 0 \\ \beta_{LV}\phi\mu_L & \beta_{LV}\phi\mu_L & \beta_{LV}\phi\mu_L & 0 & 0 \end{pmatrix} \quad (1.8)$$

And

$$V=\begin{pmatrix} K_1 & 0 & 0 & 0 & 0 \\ -(1-\alpha_L)\kappa_L & K_2 & 0 & 0 & 0 \\ -\alpha_L\kappa_L & 0 & K_3 & 0 & 0 \\ 0 & 0 & -\gamma_L & K_4 & 0 \\ 0 & 0 & 0 & 0 & \mu_V \end{pmatrix} \tag{1.9}$$

$$R_{1,2}=\frac{\pm\sqrt{\begin{matrix}K_1K_2K_3\mu_L\beta_{LV}\beta_{VL}(-K_2\alpha_L\kappa_L\theta_L+K_3\alpha_L\kappa_L\theta_L+K_1K_2\theta_L-K_2K_3\theta_L \\ +K_2\alpha_L\kappa_L-K_3\alpha_L\kappa_L-K_3\theta_L\kappa_L+K_2K_3+K_3\kappa_L)\phi\end{matrix}}}{K_1K_2K_3}$$

R_0 Is the maximum value of the two Eigen-values determines R_0, the associated reproduction number for the rift valley fever model. This reproduction number, denoted by $R_0=\rho(FV^{-1})$, R_0 Is the maximum value of the two Eigen values $R_{1,2}$ hence, the associated reproduction number R_0 for $R-V$ malaria model is given by $R_0=\rho(FV^{-1})$, where ρ represents the spectral radius of the dominant Eigen-value of the next generation matrix FV^{-1}. Thus

$$R_0=\frac{\sqrt{\begin{matrix}K_1K_2K_3\mu_L\beta_{LV}\beta_{VL}(-K_2\alpha_L\kappa_L\theta_L+K_3\alpha_L\kappa_L\theta_L+K_1K_2\theta_L-K_2K_3\theta_L \\ +K_2\alpha_L\kappa_L-K_3\alpha_L\kappa_L-K_3\theta_L\kappa_L+K_2K_3+K_3\kappa_L)\phi\end{matrix}}}{K_1K_2K_3} \tag{2.0}$$

Is the average number of infections caused by one infected vector introduced into the completely susceptible populations of both livestock and vectors.

2.4Local Stability of Disease Free Equilibrium

Theorem 1:The disease free equilibrium of the model equation (1.3) is locally asymptotically stable if $R_0<1$ and unstable if $R_0>1$.

Proof: To ascertain the local stability of ε_0, we compute the Jacobian matrix corresponding to the Disease-Free Equilibrium. Evaluating the stability of the disease-free equilibrium at $\varepsilon_0=\left(\frac{(1-\rho)\pi_L}{\mu_L},0,0,0,0,0,\frac{\pi_V}{\mu_V},0\right)$.

$$J(\varepsilon_0)=\begin{pmatrix} -\mu_L & 0 & 0 & 0 & 0 & \omega_L & 0 & 0 \\ 0 & -K_1 & 0 & 0 & 0 & 0 & 0 & 0 \\ 0 & (1-\alpha_L)\kappa_L & -K_2 & 0 & 0 & 0 & 0 & 0 \\ 0 & \alpha_L\kappa_L & 0 & -K_3 & 0 & 0 & 0 & 0 \\ 0 & 0 & 0 & \gamma_L & -K_4 & 0 & 0 & 0 \\ 0 & 0 & \overline{\sigma_L} & \sigma_L & \Lambda_L & -K_5 & 0 & 0 \\ 0 & 0 & 0 & 0 & 0 & 0 & -\mu_V & 0 \\ 0 & 0 & 0 & 0 & 0 & 0 & 0 & -\mu_V \end{pmatrix} \tag{2.1}$$

The characteristic equation of (2.1) above are obtained as $|J\varepsilon_0 - \lambda I|$=0, where I is the (8*8) identity matrix. Then, $|J\varepsilon_0 - \lambda I| =$

$$J(\varepsilon_0 - \lambda I) = \begin{pmatrix} -\mu_L - \lambda & 0 & 0 & 0 & 0 & 0 & 0 & 0 \\ 0 & -K_1 - \lambda & 0 & 0 & 0 & 0 & 0 & 0 \\ 0 & (1-\alpha_L)\kappa_L & -K_2 - \lambda & 0 & 0 & 0 & 0 & 0 \\ 0 & \alpha_L\kappa_L & 0 & -K_3 - \lambda & 0 & 0 & 0 & 0 \\ 0 & 0 & 0 & \gamma_L & -K_4 - \lambda & 0 & 0 & 0 \\ 0 & 0 & \overline{\sigma_L} & \sigma_L & \Lambda_L & -K_5 - \lambda & 0 & 0 \\ 0 & 0 & 0 & 0 & 0 & 0 & -\mu_V - \lambda & 0 \\ 0 & 0 & 0 & 0 & 0 & 0 & 0 & -\mu_V - \lambda \end{pmatrix} \quad (2.2)$$

The Eigen-values are $-K_1, -K_2, -K_3, -K_4, -K_5, -\mu_L$ and $-\mu_V$ twice.

Hence, the disease equilibrium point is locally asymptotically stable since all the Eigen values are real and negative. This theorem implies that if the initial sizes of the sub-populations of the model lie within the basin of attraction of the disease-free equilibrium, the disease is controllable provided $R_o < 1$

2.5 Global Stability of Disease Free Equilibrium

We study the global stability of equilibrium without disease and we implement the approach of (Philemon *et al.,* 2023), then the equations of the model may be rewritten in the form;

$$\frac{dM}{dt} = F(M, I)$$

$$\frac{dI}{dt} = G(M, I)$$

With $G(P,0) = 0$, where $P \in \Re^3$ represents the uninfected classes (S_L, R_L, S_V) and $I \in \Re^5$ represents the infected classes $(E_L, Ay_L, Sy_L, I_L, I_V)$. Also, $\varepsilon_o = (M^*, 0)$ denotes the disease-free equilibrium of the model.

The two conditions (H1) and (H2) stated below must be satisfied for the model to be globally stable;

(H1): For $\frac{dM}{dt} = F(M,0)$, M^* is globally asymptotically stable

(H2): $G(M, I) = AI - \hat{G}(M, I)$, $\quad \hat{G}(M, I) \geq 0$ for $(M, I) \in D$

Where $A = D_I G(M^*, 0)$ is an M-matrix (the off-diagonal elements of A are non-negative) and D is the region is the feasible region where the model is biologically meaningful. If (H1) and (H2) are satisfied, then the following theorem holds;

Theorem 2: The disease-free equilibrium $\varepsilon_o = (M^*, 0)$ is a globally asymptotically stable equilibrium of the model if $R_0 < 1$ and that the conditions (H1) and (H2) are satisfied

Proof:

Now $M = (S_L, R_L, S_V)$ and $I = (E_L, Ay_L, Sy_L, I_L, I_V)$

$$F(M,0)=\begin{pmatrix}(1-\rho)\pi_L-\mu_L S_L\\0\\0\end{pmatrix} \tag{2.3}$$

And

$$AI=\begin{pmatrix}-K_1 & 0 & 0 & 0 & (1-\theta_L)\beta_{VL}\phi\\(1-\alpha_L)\kappa_L & -K_2 & 0 & 0 & 0\\\alpha_L\kappa_L & 0 & -K_3 & 0 & \theta_L\beta_{VL}\phi\\0 & 0 & \gamma_L & -K_4 & 0\\\beta_{LV}\phi & \beta_{LV}\phi & \beta_{LV}\phi & 0 & -\mu_V\end{pmatrix}\begin{pmatrix}E_L\\Ay_L\\Sy_L\\I_L\\I_V\end{pmatrix} \tag{2.4}$$

$$\text{Then } \hat{G}(M,I)=\begin{pmatrix}(1-\theta_L)\beta_{VL}\phi\left(1-\frac{S_L}{N_L}\right)\\0\\\theta_L\beta_{VL}\phi\left(1-\frac{S_L}{N_L}\right)\\0\\\beta_{LV}\phi\left(1-\frac{S_V}{N_V}\right)\end{pmatrix} \tag{2.5}$$

Since $0\le\varepsilon\le 1$, clearly $\hat{G}(M,I)\ge 0$, $\varepsilon_o=\left(\frac{(1-\rho)\pi_L}{\mu_L},0,0\right)$ is a globally asymptotic stable equilibrium of the model equations. Thus, both conditions outlined above are met, indicating that the disease-free equilibrium is globally asymptotically stable. This biological implication suggests that the elimination of Rift Valley fever is independent of the initial sizes of the sub-populations when the basic reproduction number is less than one.

2.6 Sensitivity Analysis

Sensitivity analysis plays a pivotal role in understanding the significance of each parameter in disease transmission dynamics. By calculating the sensitivity index of parameters with respect to the basic reproduction number, we gain insight into the degree of influence each parameter holds over disease transmission. This analysis allows us to identify the most critical parameters that impact the basic reproduction number, shedding light on their importance in driving disease transmission. By conducting sensitivity analysis, we can prioritize interventions and target control measures towards parameters that exert the most significant influence on the spread of the disease. This comprehensive evaluation improves our comprehension of the fundamental mechanisms influencing transmission dynamics and guides the development of more effective strategies for disease control and prevention.

Definition: The normalized forward sensitivity index of a variable ω that depends differentiability on a parameter P is defined as

$$X_P^{R_0} = \frac{d\omega}{dP} \times \frac{P}{R_0} \tag{2.6}$$

The calculation of the sensitivity index is performed for each parameter using the data in Table 3.1. The results are presented in Table 3.2.

3. Numerical Analysis

The numerical approximation and validation of the model's theoretical calculations are conducted through the implementation of a fourth-order Runge-Kutta numerical scheme. This numerical scheme is implemented using the MAPLE 18 program software. The model's calculations are validated using a predefined set of estimated parameter values, as detailed in Table 3.1.

Table 3.1 Parameters and Values

Parameter	Value	Source
β_{VL}	0.7	(Pépin *etal.,* 2010), (Jupp *et al.,* 2002)
β_{LV}	0.21	(Pépin *etal.,* 2010), (Turell *et al.,* 1985)
ϕ	0.25	(Diallo *et al.,* 2008), (Chitnis *et al.,* 2013)
μ_L	0.05	(Gaff*et al.,* 2011), (Mehmood *et al.,* 2021)
μ_V	0.07	(Mehmood *et al.,* 2021), (Kasari*et al.,*2008)
ω_L	0.2	Assumed
Λ	0.2	Assumed
γ_L	0.3	Assumed
θ_L	0.3	(Adeyeye *et al.,*2011), (Jupp *et al.,* 2002)
κ_L	0.4	(Adeyeye *et al.,*2011), (Jupp *et al.,* 2002)
κ_V	0.07	(Chamchod *et al.,*2016), (Turell *et al.,* 1985)
α_L	0.3	Assumed
δ_L	0.10	(Adeyeye *et al.,*2011), (Kasari *et al.,*2008)
$\overline{\sigma_L}$	0.25	(Adeyeye *et al.,*2011), (Kasari *et al.,*2008)
σ_L	0.3	(Adeyeye *et al.,*2011), (Kasari *et al.,*2008)

Table 3.2 Numerical Sensitivity Index for RV-Malaria

Parameter	Sensitivity Value	Sensitivity Sign
β_{VL}	1.00000	+
β_{LV}	1.00000	+
ϕ	1.00000	+
θ_L	0.05371	+
κ_L	0.12227	+
α_L	0.00755	+

ρ	-0.12115
μ_L	-0.51223
δ_L	-0.30122
ω_L	-0.00027
γ_L	-0.25999
σ_L	-0.22598
$\overline{\sigma_L}$	-0.04354

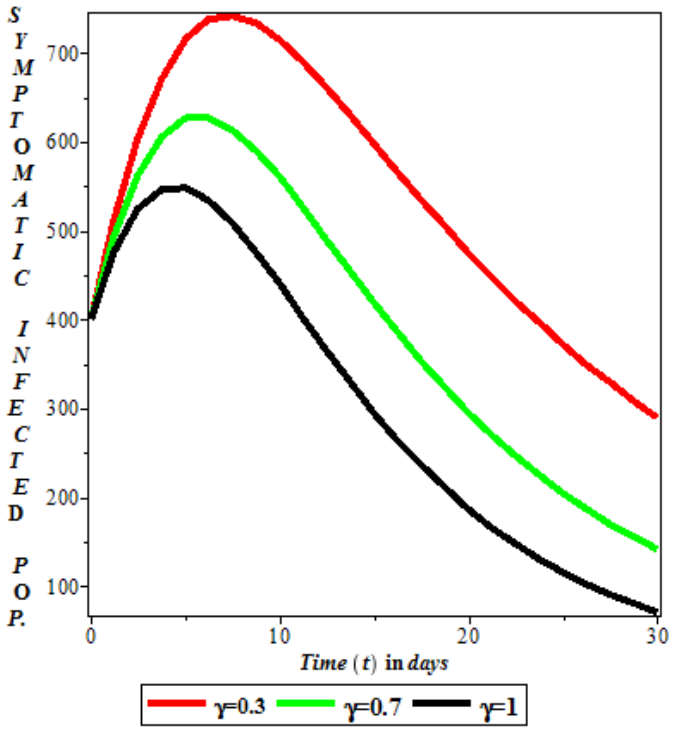

Figure 2.Symptomatic Population with Isolation Rate $\gamma_L = 0.3,\ 0.7 \& 1.0$

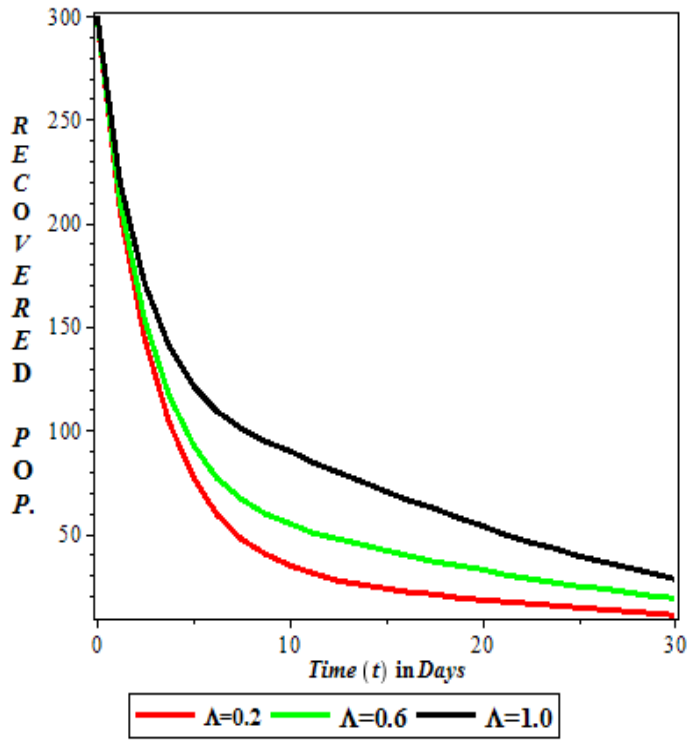

Figure 3.Recovered Population with Recovery of Isolated Individual Rate $\Lambda_L = 0.2,\ 0.6 \& 1.0$

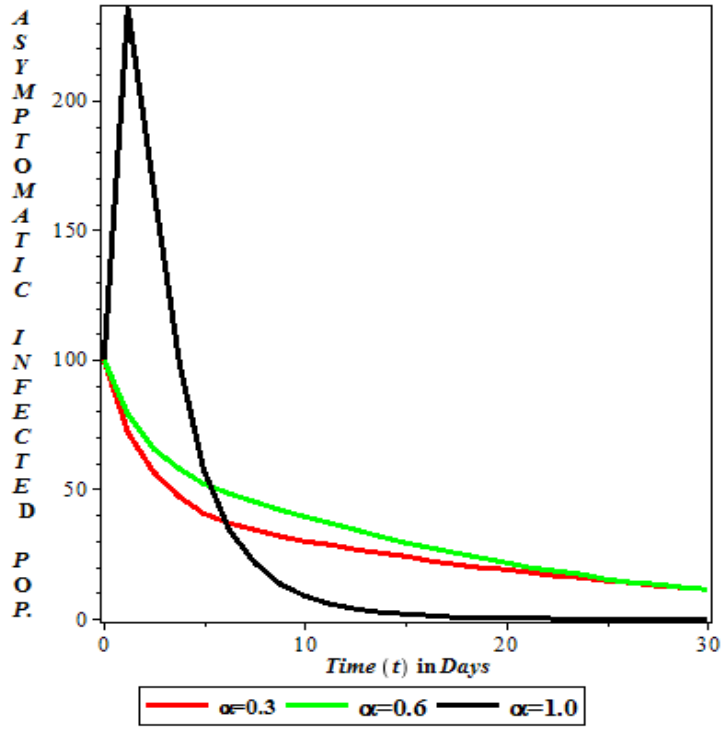

Figure 4.Asymptomatic Population with Detection Rate $\alpha_L = 0.3,\ 0.6 \& 1.0$

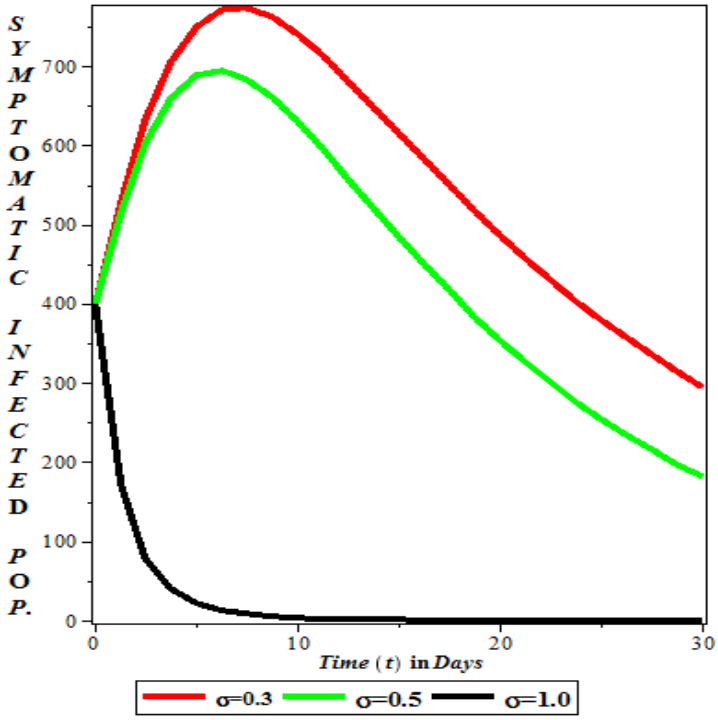

Figure 5.Symptomatic Population with Recovery Rate $\sigma_L = 0.3,\ 0.5 \& 1.0$

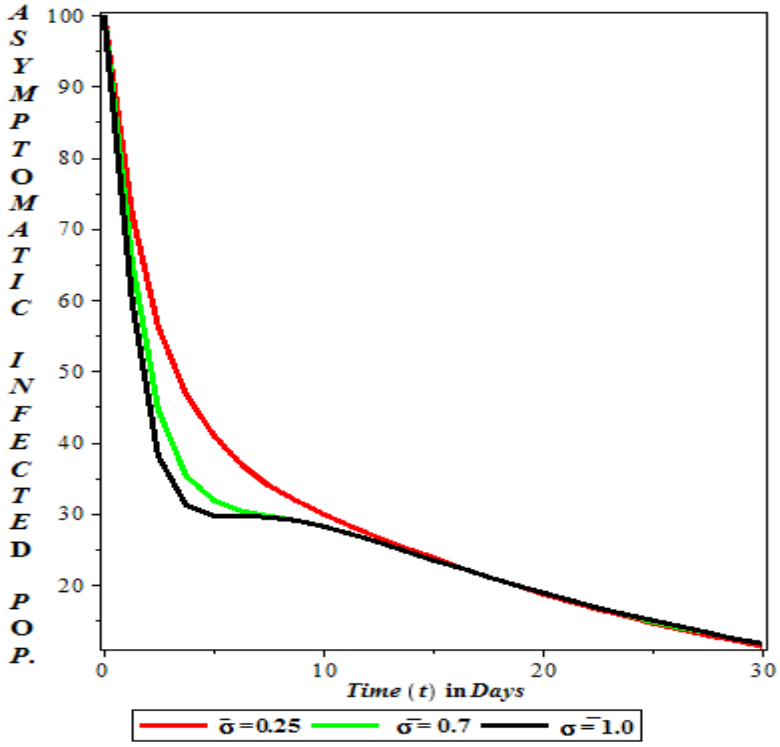

Figure 6.Asymptomatic Population with Recovery Rate $\bar{\sigma}_L = 0.25\ 0.7 \& 1.0$

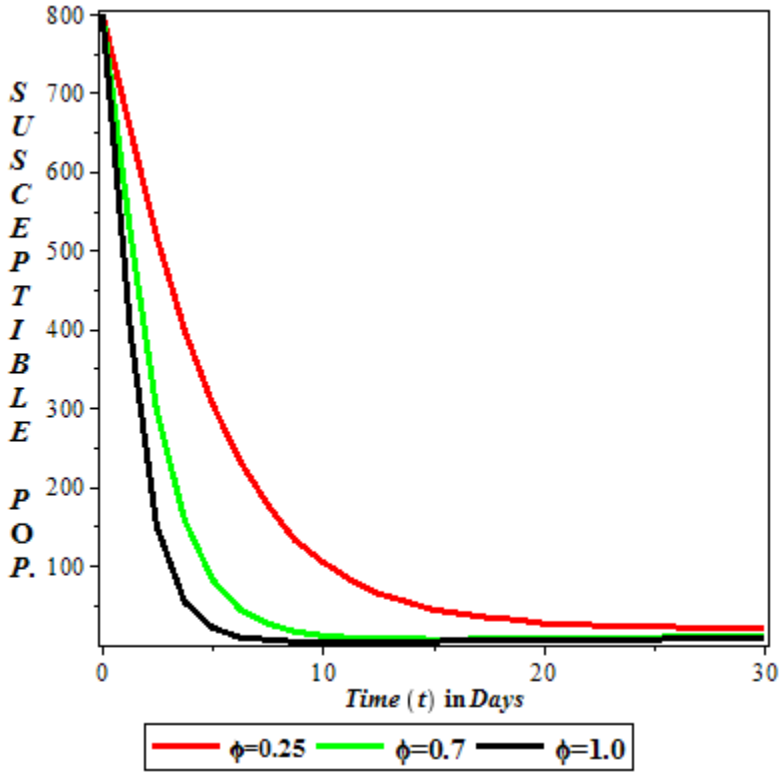

Figure 7. Susceptible Livestock with biting rate $\phi = 0.25\ 0.7\ \&\ 1.0$

4. Results and Discussion

A non-linear deterministic model for Rift Valley fever, considering the detection and isolation of infected livestock from susceptible individuals, is presented and thoroughly analyzed. This study aims to provide insights into the importance of early detection and isolation measures in minimizing and mitigating the spread of Rift Valley fever within livestock populations.

The model's mathematical and epidemiological viability is confirmed through the positivity of its solutions, suggesting that it is well-posed both mathematically and epidemiologically. The analysis considers the existence of both disease-free and endemic equilibrium points, with the basic reproduction number serving as a crucial indicator of disease dynamics. Specifically, the disease is predicted to either die out (i.e. when $R_0 < 1$) or spreads (i.e. when $R_0 > 1$), based on the value of the basic reproduction number.

The analysis of both local and global stability of the disease equilibrium is conducted, demonstrating its stability. Furthermore, numerical simulations of sensitivity analysis, performed using MAPLE 18 software, aim to identify parameters influencing the spread of Rift Valley fever among livestock. The results highlight parameters with negative indices, which reduce disease spread, and those with positive indices, which increase the basic reproduction number, thereby intensifying disease transmission.

An examination of Table 3.2 reveals that parameters with positive index values elevate the basic reproduction number, potentially leading to an endemic situation when it exceeds unity. Among the parameters, three stand out as the most sensitive contributors to the basic reproduction number: the transmission of infection from infective vectors to susceptible livestock, the transmission of infection from infective livestock to susceptible vectors, and the biting rate of

vectors. These findings underscore the critical role of these parameters in driving the spread of Rift Valley fever within livestock populations.

Figure 2 illustrates the significance of isolating the symptomatic infected population, a pivotal measure in epidemiology for curtailing the transmission of infectious diseases. This practice involves segregating individuals showing symptoms from the general population to halt further spread. Effective implementation hinges on prompt identification, access to isolation facilities, adherence to protocols, and the contagious nature of the disease. Ultimately, it serves as a crucial tool in containing outbreaks and preserving public health. **Figure 3** depicts the reintegration rate of individuals who were previously isolated due to infection and have now recovered into the general population. This aspect holds significant importance in epidemiology, aiding in the comprehension of disease transmission dynamics and the evaluation of control measures' effectiveness. Monitoring this rate allows for the assessment of isolation protocols, determination of post-recovery immunity duration, and evaluation of the overall impact on managing infectious disease outbreaks. **Figure 4** illustrates the detection of Asymptomatic livestock population, focusing on identifying and diagnosing livestock infected with a disease but not exhibiting symptoms. This metric holds significance in controlling Rift Valley Fever, where asymptomatic livestock can transmit the virus. Improving detection rates through widespread testing among livestock is crucial for effectively managing outbreaks and implementing public health strategies. **Figure 5** presents the Symptomatic livestock population with recovery rate, indicating the number of livestock showing symptoms of a disease who subsequently recover over time. This visualization is crucial for understanding the progression of the rift valley fever disease and assessing the effectiveness of recovery measures among livestock. Monitoring the recovery rate among symptomatic livestock provides valuable insights into disease dynamics and informs healthcare strategies aimed at managing and treating affected livestock populations. **Figure 6** illustrates the Asymptomatic Livestock Population with Recovery Rate, depicting the number of livestock that are asymptomatic for a disease and subsequently recover over time. This phenomenon may occur due to the consumption of certain grasses that unknowingly possess medicinal properties beneficial to livestock health. Monitoring the recovery rate among asymptomatic livestock provides insights into natural remedies and their potential impact on disease management within animal populations. **Figure 7** emphasizes the seriousness of the situation where infected vectors transmit diseases to vulnerable livestock, exacerbating endemic conditions within the system due to the lack of effective intervention measures. It highlights the susceptibility of livestock populations to vector-borne infections and the pressing need for proactive and holistic interventions to limit their spread and alleviate their negative impacts. It underscores the vital importance of implementing timely and focused measures, including vector control strategies, vaccination campaigns, early detection of infected livestock and enhanced livestock management practices, to protect the health and welfare of susceptible livestock populations and mitigate the economic losses stemming from disease outbreaks.

5. Conclusion

In conclusion, addressing Rift Valley fever's impact on livestock populations necessitates a multifaceted and proactive strategy. This includes robust measures such as detecting and isolating asymptomatic and symptomatic infected livestock, implementing strategic management practices, and establishing early detection mechanisms. Veterinary practitioners are pivotal in championing and executing these strategies to ensure the health and longevity of livestock farming operations. By prioritizing these proactive approaches, stakeholders can effectively

mitigate the adverse effects of Rift Valley fever on livestock populations while promoting overall agricultural sustainability.

References

Adewale, S.O., Olopade, I.A., Adeniran, G.A., Mohammed, I.T., and Ajao, S.O., (2015b), Mathematical Analysis of Effects of Isolation On Ebola Transmission Dynamics. *Researchjournali's Journal of Mathematics*. 2(2), 1-20,.

Adewale, S.O., Olopade, I.A., Adeniran, G.A., and Ajao, S.O.(2015a), Mathematical Modelling and Sensitivity Analysis of HIV-TB Co-infection". *Journal of Advances in Mathematics,* Vol. 11(8), 5494-5519.

Adewale, S.O., Olopade, I.A., Ajao, and Mohammed, I.T., (2016), Mathematical Analysis of Sensitive Parameters on the Dynamical Spread of HIV. *International Journal of Innovative Research in Science, Engineering and Technology.* Vol. 5(5), 2624-2635.

Adewale, S.O., Olopade, I.A., Ajao, S.O., Adeniran, G.A., (2015c), Mathematical Analysis of Diarrhea in the Presence of Vaccine". *International Journal of Scientific and Engineering Research.* Vol. 6(12). 396-404.

Adeyeye, P. S., Ekong, N. N., Pilau, (2011), Rift valley fever: the Nigerian story. *Veterinaria Italiana,* Vol. 47(1), 35–40.

Ajao, S.O., Olopade, I.A., Akinwumi, T.O., Adewale, S. O., and Adesanya, A. O.,(2023), Understanding the Transmission Dynamics and Control of HIV Infection: A Mathematical Model Approach. *Journal of the Nigerian Society of Physical Sciences*, *5*(2), 1389.

Akinwumi, T.O., Olopade, I.A., Adesanya, A. O., and Alabi, M. O. Alabi, (2021), Mathematical Model for the Transmission of HIV/AIDS with Early Treatment". *Journal of Advances in Mathematics and Computer Science*, *36*(5), 35-51.

Bird, B. H. and McElroy, A. K. (2016), Rift Valley fever virus: unanswered questions. *Antiviral Res.* Vol. 132, 274–280.

Bird, B. H., Ksiazek, T. G., Nichol, S. T., and Maclachlan, N. J. (2009), Rift Valley fever virus. *J Am Vet Med Assoc.* Vol. 234(7), 883-893.

Chamchod, F., Cosner, C., Cantrell, R. S., Beier, J. C., and Ruan, S., (2016), Transmission Dynamics of Rift Valley Fever Virus: Effects of Live and Killed Vaccines on Epizootic Outbreaks and Enzootic Maintenance, *Frontiers in Microbiology*, Vol. 6, 15-68. DOI: 10.3389/fmicb.2015.01568

Chitnis, N., Hyman, J. M., and Manore, C. A., (2013), Modelling vertical transmission in vector-borne diseases with applications to Rift Valley fever, *Journal of Biological Dynamics,* Vol. 7(1), 11–40. DOI: 10.1080/17513758.2012.733427

Diallo, Y.B., Kebe, C.M.F., Dia, I., and Diallo, M. (2005), Aspects of bioecology of two Rift Valley fever virus vectors in Senegal (West Africa): Aedes vexans and Culex poicilipes (Diptera: Culicidae), *J. Med. Entomol.* 42(5), 739–750.

Fawzy, M., and Helmy, Y. A., (2019), The One Health Approach is Necessary for the Control of Rift Valley Fever Infections in Egypt: *A Comprehensive Review Viruses*, Vol. 11(2), DOI: 10.3390/v11020139

Fischer, E. A., Boender, G.-J., Nodelijk, G., de Koeijer, A. A., and Van Roermund H. J., (2013), The transmission potential of Rift Valley fever virus among livestock in the Netherlands: a modelling study. *Veterinary Research,* Vol. 44(1), 44-58, DOI: 10.1186/1297-9716.

Gachohi, J. M., Njenga, M. K., Kitala, P., and Bett, B., (2016), Modelling Vaccination Strategies against Rift Valley Fever in Livestock in Kenya. *PLOS Neglected Tropical Diseases*, Vol. 10(12), 05-49. DOI: 10.1371/journal.pntd.0005049

Gaff, H., Burgess, C., Jackson, J., Niu, T., Papelis, Y., and Hartley, D., (2011) Mathematical model to assess the relative effectiveness of Rift Valley fever counter-measures, *Int. J. Artif. Life Res,* 2(2) , 1–18.

Iacono, G. Lo, Cunningham, A. A., Bett, B., Grace, D., Redding, D. W., and Wood, J. L. N., (2018), Environmental limits of Rift Valley fever revealed using ecoepidemiological mechanistic models," *Proceedings of the National Academy of Sciences*, vol. 115(31), 7448–7456. DOI: 10.1073/pnas.1803264115

Jupp, P.G., Kemp, A., Grobbelaar, A., Leman, P., Burt, F.J., Alahmed, A.M., Mujalli, D., Khamees, M., and Swanepoel, R., (2002), The 2000 epidemic of Rift Valley fever in Saudi Arabia: Mosquito vector studies, *Med. Vet. Entomol.* 16(3), 245–252.

Kanouté, Y. B., Gragnon, B. G., Schindler, C., Bonfoh, B. and Schelling, E., (2017) Epidemiology of brucellosis, Q Fever and Rift Valley Fever at the human and livestock interface in northern Côte d'Ivoire. *Acta Tropica*, Vol. 165, 66–75. DOI: 10.1016/j.actatropica.2016.02.012

Kasari, T.R., Carr, D.A., Lynn, T.V., and Weaver, J.T., (2008), Evaluation of pathways for release of Rift Valley fever virus into domestic ruminant livestock, ruminant wildlife, and human populations in the continental United States, *J. Am. Vet. Med. Assoc.* 232(4), 514–529.

Marion, E, Hayden, M. H., Sun, J. (2018), Predictive environmental risk factors for Rift Valley fever epidemics in Nigeria. *BMC Infect Dis.* 18(1), 305.

Mehmood, Q., Irfan, M., Ogunkola, I. O., Jaguga, F., and Ullah, I., (2021), Rift valley fever and Covid-19 outbreak in kenya: a double whammy, Ethics, *Medicine, and Public Health*, Vol. 19, 06-85. DOI: 10.1016/j.jemep.2021.100685

Métras, R., Fournié, G., Dommergues, L., Camacho, A., Cavalerie, L., Mérot, P., Keeling, M. J., Cêtre-Sossah, C., Cardinale, E., and Edmunds, W. J.,(2017), Drivers for Rift Valley fever emergence in Mayotte: A Bayesian modelling approach. *PLOS Neglected Tropical Diseases*, Vol. 11(7) 57-67. DOI: 10.1371/journal.pntd.0005767

Mpeshe, H., Haario, and Tchuenche, J. M. (2011), A Mathematical Model of Rift Valley Fever with Human Host. *Acta Biotheoretica,* Vol. 59(3-4), 231–250. DOI: 10.1007/s10441-011-9132-2.

Musibau, O. O, Muritala, A. A., Isaac, A O., Adelani, O A., and. Akeem, O. Y. (2022), Mathematical analysis of sensitive parameters due to dynamic transmission of Ebola virus disease. *Comprehensive Research and Reviews in Multidisciplinary Studies*. 01(01), 001–016.

Nanyingi, M. O., Munyua, P., Kiama, and S. G. (2015), A systematic review of Rift Valley fever epidemiology. *Infect Ecol Epidemiol*, Vol. 51931-2014.

Nielsen, S. S., (2021), Scientific Opinion on the assessment of the control measures of the category A diseases of Animal Health Law: Highly Pathogenic Avian Influenza. *EFSA Journal*, Vol. 19(1), DOI: 10.2903/j.efsa.2021.6372.

Oguntolu, F. A., Yavalah, D. W., Udom, C. F., Peter, O. J., Oshinubi, K., (2022), Mathematical modelling for the transmission dynamics of Rift Valley fever virus with human host. *Jambura Journal of Mathematics.*Vol. 3(1), 17-22. https://doi.org/10.34312/jjbm.v3i1.14160.

Olopade, I.A., Adesanya, A. O. and Akinwumi, T. O. (20121a). Mathematical Transmission of SEIR Epidemic Model with Natural Immunity. *Asian Journal of Pure and Applied Mathematics;* 3(1):19-29.

Olopade, I.A., Adesanya, A. O. and Mohammed, I. T.(2017). Mathematical Analysis of the Global Dynamics of an SVEIR Epidemic Model with Herd Immunity. *International Journal of Science and Engineering Investigations.* (IJSEI) 6(69):141-148.

Olopade, I.A., Ajao, S. O., Adeniran, G. A., Adamu, A. K., Adewale, S. O. and Aderele, O. R. (2022). Mathematical Transmission of Tuberculosis (TB) with Detection of Infected Undetectected. *Asian Journal of Research in Medicine and Medical Sciences*, *4*(1), 100-119.

Olopade, I.A., Adewale, S.O., Mohammed, I.T., Adeniran, G. A., Ajao, S. O. and Ogunsola, A. W. (2021b). Effect of Effective Contact Tracing in Curtaining the Spread of Covid-19. *Asian* Journal of Research in Biosciences, *3*(2), 118-134.

Olopade, I.A., Adewale, S.O., Mohammed, I.T., Ajao, S.O. and Oyedemi, O. T. (2016).Mathematical Analysis of the Role of Detection in the Dynamical Spread of HIV-TB Co-infection". *Journal of Advances in Mathematics.* Vol. 11, No. 10. Pp. 5715-5740.

Pedro, S. A., Abelman, S. and Tonnang, H. E. Z., (2016), Predicting Rift Valley Fever Inter-epidemic Activities and Outbreak Patterns: Insights from a Stochastic Host-Vector Model. *PLOS Neglected Tropical Diseases,* Vol. 10(12), 51-67. DOI: 10.1371/journal.pntd.0005167

Pedro, S. A., Abelman, S., Ndjomatchoua, F. T., Sang, R. and Tonnang, H. E. Z. (2014), Stability, Bifurcation and Chaos Analysis of Vector-Borne Disease Model with Application to Rift Valley Fever. *PLoS ONE*, Vol. 9(10), 108-172, DOI: 10.1371/journal.pone.010817

Pépin, M., Bouloy, M., Bird, B.H., Kemp, A., and Paweska, J., (2010), Rift Valley fever virus (Bunyaviridae: Phlebovirus): An update on pathogenesis, molecular epidemiology, vectors, diagnostics and prevention, *Vet. Res.* Vol. 41, 61-72.

Philemon, M. E., Olopade, I. A., and Ogbaji, E. O., (2023). Mathematical Analysis of the Effect of Quarantine on the Dynamical Transmission of Monkey-Pox, *Asian Journal of Pure and Applied Mathematics*, *5*(1), 473–492. Retrieved from https://globalpresshub.com/index.php/AJPAM/article/view/1894

Salih, D. A., Ahmed, J. S., Askar, M. I. (2020), Rift Valley fever outbreak in Sudan, 2019, Epidemiological, clinical, and laboratory findings. *J. Med Virol.* 92(11), 3503-3507.

Sissoko, D., Giry, C., and Gabrie, P. (2009), Rift Valley fever, Mayotte, 2007-2008. *Emerg Infect Dis,* 15(4), 568-709.

Turell, J., Rossi, C.A., and Bailey, C.L., (1985), Effect of extrinsic incubation temperature on the ability of Aedestaeniorhynchus and Culex pipiens to transmit Rift Valley fever virus, *Am. J. Trop. Med. Hyg.* 34(6), 1211–1218.

Uwishema, O., Chalhoub, E., Torbati, T., David, S. C., Khoury, C., Ribeiro, Y. Nasrallah, L. L. P. A., Bekele, B. K., and Onyeaka, H., (2022), Rift Valley fever during the COVID–19 pandemic in Africa: A double burden for Africa's healthcare system, *Health Science Reports*, Vol. 5(1). DOI: 10.1002/hsr2.468

World Health Organization. Rift Valley fever. https://www.who.int/news-room/fact-sheets/detail/rift-valley-fever. Accessed December 1, (2023)

Basic Reproduction Number and the Existence of a COVID-19-Diabetes Complication-Free Equilibrium State

Yusuf, A.[1,3], Akinwande N. I.[1] ,Olayiwola R. O.[1],Kuta, F.A.[2] Somma, S. A.[1]

[1,] Department of Mathematics, Federal University of Technology, Minna, Nigeria.
[2,] Department of Microbiology, Federal University of Technology, Minna, Nigeria.
[3]Department of Mathematics, Ibrahim Badamasi Babangida University Nigeria

abdullahyusuf90@gmail.com

Abstract

In this paper, a COVID-19-Diabetes Complication-free Equilibrium was obtained, and the positivity of the solution was verified. We also determined the basic reproduction number using the next-generation Matrix and Jacobian matrix methods. It follows that the positive eigenvalues represent the two reproduction numbers where R_i represent the expected number of COVID-19 infectiousness produced by one COVID-19 infectious individual, where R_d represent the expected number of Diabetes without complication-induced COVID-19 infectiousness produced by one COVID-19 infectious individual.

Keywords: Basic Reproduction,COVID-19, Diabetes Complication and Equilibrium

1. Introduction

In 2019, diabetes resulted in approximately 4.2 million deaths. It is the 7th leading cause of death globally. The global Economic cost of diabetes-related health expenditure in 2017 was estimated at US$727 billion. In the United States, diabetes cost nearly US$327 billion in 2017. Average medical expenditures among people with diabetes are about 2 to 3 times higher (IDF, 2020; WHO, 2020).

The World as we know it has been ravaged by an ongoing coronavirus disease 2019 (COVID-19) Pandemic (WHO, 2021). Which emerged from the city of Wuhan in China, in December of 2019, caused by the novel coronavirus, SARS-COV2, a highly virulent

virus that has caused COVID-19 to be a lethal disease, a disease which targets the human respiratory system, started as an outbreak of pneumonia of unidentified cause. It swiftly became an overwhelming pandemic, thinning out to every country on earth, and wreaking a brutal public health and socio-economic burden globally and the patients were linked to a seafood and wet animal market in Wuhan, Hubei Province, China, an ongoing coronavirus disease 2019 (COVID-19) pandemic has decimated the world as we know it (WHO, 2021). SARS-COV2, a highly virulent virus that has caused COVID-19 to be a lethal disease, began as an outbreak of pneumonia of unknown origin in the Chinese city of Wuhan in December of 2019, caused by the novel coronavirus, SARS-COV2, a highly virulent virus that has caused COVID-19 to be a fatal disease, a disease that attacks the human respiratory system(Rothana and Byrareddy, 2020;

Gumel *et al.,* 2020; Branswell, 2020; Dong *et al.,* 2020; Roda *et al.,* 2020; Sun and Wang, 2020; Contreras *et al.,* 2020; Li *et al*., 2020; Zhu *et al.,*2020). It is reported that the virus might be bat origin (Zhou *et al.,* 2020). The virus's spread could be linked to a Hunan Seafood Wholesale Market (Huang *et al*., 2020; Zhu *et al.,* 2020b). By January 22, 2020, a total of 571 cases of COVID-19 were reported in 25 provinces in China (Rothana and Byrareddy, 2020; Lu, 2020). On January 30, 2020, about 7734 cases were confirmed in China, with 90 cases reported in about 13 countries (Rothana and Byrareddy, 2020) Including the United States, India, Canada, France, Germany and the United Arab Emirates.

People with certain underlying medical conditions may have a higher risk of severe illness from COVID-19. These conditions include diabetes, heart problems, obesity, and chronic kidney disease. Specifically, the available evidence suggests that people with type 2 diabetes have a higher risk of severe illness from COVID-19, according to the Centers for Disease Control and Prevention (CDC). People with type 1 or gestational diabetes may also have an increased risk, but the data is less conclusive (CDC,2021; IDF,2021).

In general, infections are more serious in people with diabetes. One reason is that diabetes affects the way the immune system works, making it harder for the body to fight viruses. Also, diabetes causes high blood sugar levels, and the International Diabetes Federation observes that the novel coronavirus may thrive in an environment of elevated blood glucose. Diabetes also keeps the body in a low-level state of inflammation, which makes its healing response to any infection slower. High blood sugar levels combined with a persistent state of inflammation make it much more difficult for people with diabetes to recover from illnesses such as COVID-19 (IDF, 2021).

Omame *et al.* (2022) They presented and analyzed the fractional optimal control model for COVID-19 and diabetes co-dynamics, using the Atangana-Baleanu derivative. They establish the positivity and boundedness of the solutions as was shown by the method of Laplace transform. The existence and uniqueness of the solutions of the model equation were established using the Banach fixed point Theorem and Leray–Schauder alternative Theorem.

Kouidere *et al*. (2021) Pont rya gin's maximum principle was used, to characterize the optimal controls and the optimality system as solved by an iterative method and some numerical simulations were performed to verify the theoretical analysis using MATLAB

In this paper, we verified the invariant region of the model and the positivity of the solution of the model. We also calculated the COVID-19 -Diabetes-Complication Free Equilibrium CDCFE, and the basic reproduction number using next-generation matrix and Jacobian matrix methods.

2. Model Formulation

The model equations are formulated using the first-order ordinary differential equation, with the total human population at time t, denoted by N. the total population is further divided into fourteen (14) compartment, which is susceptible to COVID-19(S_i), Diabetic without complication and also susceptible to COVID-19(S_d), Exposed to COVID-19(E_i), COVID-19 infectious (I_i), Quarantine for COVID-19(Q_i), Isolated for COVID-19(P_i), Recovered from

COVID-19(R_i), Diabetics without complication and also COVID-19Exposed (E_d), Diabetics without complication and also COVID-19Infectious(I_d), Quarantine for COVID-19 and also diabetes without complication(Q_d), Isolated for COVID-19and diabetes without complication(P_d), Recovered from COVID-19but having diabetes without complication (R_d), Diabetics with complication and also COVID-19Infectious (I_c), Isolated for COVID-19and diabetes with complication (P_c).

Recruitment to the susceptible to COVID-19 class is at a constant rate, The COVID-19 susceptible individuals may acquire the infection after effective contacts $\eta_{i1}, \eta_{i2}, \eta_{i3}, \eta_{i4}$ with Exposed to COVID-19, COVID-19infectious, Quarantine for COVID-19, and Isolated for COVID-19, the quarantined are recruited through contact with the exposed class at rate $\sigma_i$and return to the susceptible at a rateξ_i.

The quarantined class become COVID-19 infectious at a rate ρ_i τ_i, COVID-19infectious is recruited to isolated for COVID-19 and subsequently γ_i, is the rate at which isolated become recovered thus some of the recruited will become susceptible while some will be recruited to the class of Diabetic without complication and also susceptible to COVID-19, again recruitment to the diabetic without complication and also susceptible to COVID-19class at a constant rate.

The COVID-19 susceptible but diabetic without complication individuals may acquire infection after effective contact $\eta_{d1}, \eta_{d2}, \eta_{d3}, \eta_{d4}, \eta_{d5}, \eta_{d6}$ $\alpha_d$with Diabetics without complication and also COVID-19Exposed, Diabetics without complication and also COVID-19Infectious, Quarantine for COVID-19and diabetes without complication Isolated for COVID-19and diabetes without complication, Diabetics with complication and COVID-19 Infectious, Isolated COVID-19 and diabetes with complications, the quarantined are recruited through contact with the exposed class at rate $\sigma_d$and return to the susceptible at a rate. $\xi_d$the quarantine class become COVID-19 infectious at a rate ρ_d, and recruitment to COVID-19 infectious but diabetes with complication which move back to the susceptible class without complication and some to isolated with COVID-19but diabetes with complication, at a rate τ_dCOVID-19 infectious is recruited to isolated for COVID-19 and subsequently γ_d.

All individuals who are alive may die naturally at a rate similar to infectious and isolated individuals who experience an additional death burden occasioned by COVID-19, diabetes without complication and diabetes with complication at their respective rates $\delta_1, \delta_2, \delta_3$.

The force of infection is given by;

$$\alpha_i = m_i \left(\frac{\eta_{i1}E_i+\eta_{i2}Q_i+\eta_{i3}I_i+\eta_{i4}P_i}{N}\right) \quad (1)$$

$$\alpha_d = m_d \left(\frac{\eta_{d1}E_d+\eta_{d2}Q_d+\eta_{d3}I_d+\eta_{d4}P_d+\eta_{d5}I_c+\eta_{d6}P_c}{N}\right) \quad (2)$$

Where m_i, m_d the number of contacts made between the susceptible to COVID-19, Diabetic without complication and also susceptible to COVID-19, and the agents of virus transmission.

3 Assumptions of the Model

The models are formulated based on the following Assumptions:

- **i.** The diabetes disease infections can either be without complication (acute) or with complication (chronic).
- **ii.** There can be death due to complications from COVID-19.
- **iii.** There can be death due to complications from acute diabetes.
- **iv.** There can be death due to complications from chronic diabetes.
- **v.** There is no recovery from COVID-19 when there is diabetes with complications.
- vi. If the person who is co-infected with both COVID-19 and diabetes is effectively treated for diabetes, the person moves into the class of diabetes without complication but is still COVID-19-infected.
- **vii.** people with diabetes are more likely to have more severe symptoms and complications when infected with COVID-19.
- **viii.** We assume that persons who already have diabetes complications are likely to have worse outcomes if they contract COVID-19.
- **ix.** After effective treatment of COVID-19, persons from the recovered class may move back to diabetes without complications but are susceptible to COVID-19 class after a while.

Based on the assumptions, the equations governing the co-infection dynamics are given as,

$$\frac{dS_i}{dt} = \beta_i - \alpha_i S_i + \eta_i R_i + \xi_i Q_i - \mu S_i \quad (3)$$

$$\frac{dS_d}{dt} = \beta_d - \alpha_d S_d + \omega I_c + \theta R_i + \eta_d R_d + \xi_d Q_d - \mu S_d \quad (4)$$

$$\frac{dE_i}{dt} = \alpha_i S_i - A_{11} E_i \quad (5)$$

$$\frac{dQ_i}{dt} = \sigma_i E_i - A_2 Q_i \quad (6)$$

$$\frac{dI_i}{dt} = \rho_i Q_i - A_1 I_i \quad (7)$$

$$\frac{dP_i}{dt} = \tau_i I_i - A_3 P_i \quad (8)$$

$$\frac{dE_d}{dt} = \alpha_d S_d - A_{12} E_d \quad (9)$$

$$\frac{dQ_d}{dt} = \sigma_d E_d - A_5 Q_d \quad (10)$$

$$\frac{dI_d}{dt} = \rho_d Q_d - A_4 I_d \quad (11)$$

$$\frac{dP_d}{dt} = \tau_d I_d - A_6 P_d \quad (12)$$

$$\frac{dI_c}{dt} = (1-\alpha) I_d - A_7 I_c \quad (13)$$

$$\frac{dP_c}{dt} = \tau_c I_c - A_8 P_c \quad (14)$$

$$\frac{dR_i}{dt} = \gamma_i P_i - A_9 R_i \quad (15)$$

$$\frac{dR_d}{dt} = \gamma_d P_d - A_{10} R_d \quad (16)$$

Were

$\tau_i + \delta_1 + \mu = A_1,\ \rho_i + \xi_i + \mu = A_2, \gamma_i + \delta_1 + \mu = A_3, 1 - \alpha + \tau_d + \delta_2 + \mu = A_4$

$\rho_d + \xi_d + \mu = A_5, \gamma_d + \delta_2 + \mu = A_6, \omega + \tau_c + \delta_3 + \mu = A_7, \delta_3 + \mu = A_8, \eta_i + \theta + \mu = A_9, \eta_d + \mu = A_{10}, \sigma_i + \mu = A_{11}, \sigma_d + \mu = A_{12}$

4. Invariant Region of the model.

The entire population size can be determined by adding up equations (3) to (16) which will be examined in a biologically feasible region as follows. From the differential equation, we have

$$\frac{dN}{dt} = \beta_i + \beta_d - \mu N - \delta_1(I_i + P_i) - \delta_2(I_d + P_d) - \delta_3(I_c + P_c) \quad (17)$$

In the absence of the disease ($\delta_1 = \delta_2 = \delta_3 = 0$) then (17) becomes

$$\frac{dN}{dt} = \beta_i + \beta_d - \mu N - \delta_1(I_i + P_i) - \delta_2(I_d + P_d) - \delta_3(I_c + P_c) \leq \beta_i + \beta_d - \mu N \quad (18)$$

Theorem 1

The system (3) to (16) has solutions which are contained in the feasible region Ω for all t > 0

Proof:

Let $\Omega = S_i, S_d, E_i, E_d, I_i, I_d, I_c, Q_i, Q_d, P_i, P_d, P_c, R_i, R_d \in \Re^{14}$ be any solution of the system (3.1) to (3.14) with non-negative initial conditions.

Using the theorem on differential inequality, Birkoff and Rota (1982) on (18) gives $\frac{dN}{dt} \leq \beta_i + \beta_d - \mu N$

$$0 \leq N \leq \frac{\beta_i + \beta_d}{\mu} \quad (19)$$

Hence,

$$\beta_i + \beta_d - \mu N \geq k\ell^{-\mu t} \quad (20)$$

Where k is the constant, So therefore, the feasible solution of the model system is in the region

$$\Omega = \{(S_i, S_d, E_i, E_d, I_i, I_d, I_c, Q_i, Q_d, P_i, P_d, P_c, R_i, R_d) \in \Re^{14}$$
$$: S_i, S_d, E_i, E_d, I_i, I_d, I_c, Q_i, Q_d, P_i, P_d, P_c, R_i, R_d \geq 0, N \leq \frac{\beta_i+\beta_d}{\mu}\} \quad (21)$$

Which is positively invariant (i.e. solutions remain positive for all times, t) and the model is epidemiological meaningful and mathematically well-posed.

5. Positivity of Solution

Since the system is modelling the human population, all variables of the model must be non-negative.

let the initial data be
$\{(S_i(0), S_d(0), E_i(0), E_d(0), I_i(0), I_d(0), I_c(0), Q_i(0), Q_d(0), P_i(0), P_d(0), P_c(0), R_i$

$(0), R_d(0)) \geq 0\} \in \Omega \quad (22)$

For the system (3) to (16) is positive for all t > 0

Proof:

From (3)

$$\frac{dS_i}{dt} = \beta_i - \alpha_i S_i + \eta_i R_i + \xi_i Q_i - \mu S_i$$

$$\frac{dS_i}{dt} \geq_i - \{\alpha_i + \mu\} S_i$$

$$\frac{dS_i}{S_i} \geq -\{\alpha_i + \mu\} dt \quad (23)$$

Integrating (23) gives

$$\int \frac{dS_i}{S_i} \geq -\int (\alpha_i + \mu\} dt$$

$$S_i(t) \geq S_i(0) e^{-(\alpha_i+\mu\}t} \quad (24)$$

From (4)

$$\frac{dS_d}{dt} = \beta_d - \alpha_d S_d + \omega I_c + \theta R_i + \eta_d R_d + \xi_d Q_d - \mu S_d$$

$$\frac{dS_d}{dt} \geq -(\alpha_d + \mu) S_d$$

$$\frac{dS_d}{S_d} \geq -(\alpha_d + \mu) dt \quad (25)$$

Integrating (25) gives

$$\int \frac{dS_d}{S_d} \geq -\int (\alpha_d + \mu)dt$$

$$S_d(t) \geq S_d(0)e^{-(\alpha_d+\mu)t} \quad (26)$$

From (5)

$$\frac{dE_i}{dt} = \alpha_i S_i - (\sigma_i + \mu)E_i$$

$$\frac{dE_i}{dt} \geq -(\sigma_i + \mu)E_i$$

$$\frac{dE_i}{E_i} \geq -(\sigma_i + \mu)dt \quad (27)$$

Integrating (27) gives

$$\int \frac{dE_i}{E_i} \geq -\int (\sigma_i + \mu)dt$$

$$E_i(t) \geq E_i(0)e^{-(\sigma_i+\mu)t} \quad (28)$$

From (6)

$$\frac{dQ_i}{dt} = \sigma_i E_i - \rho_i Q_i - (\xi_i + \mu)Q_i$$

$$\frac{dQ_i}{dt} \geq -(\xi_i + \mu)Q_i$$

$$\frac{dQ_i}{Q_i} \geq -(\sigma_i + \xi_i + \mu)dt \quad (29)$$

Integrating (29)

$$\int \frac{dQ_i}{Q_i} \geq -\int (\xi_i + \mu)dt$$

$$Q_i(t) \geq Q_i(0)e^{-(\xi_i+\mu)t} \quad (30)$$

From (7)

$$\frac{dI_i}{dt} = \rho_i Q_i - (\tau_i + \delta_1 + \mu)I_i$$

$$\frac{dI_i}{dt} \geq -(\tau_i + \delta_1 + \mu)I_i$$

$$\frac{dI_i}{I_i} \geq -(\tau_i + \delta_1 + \mu)dt \tag{31}$$

Integrating (31)

$$\int \frac{dI_i}{I_i} \geq -\int (\tau_i + \delta_1 + \mu)dt$$

$$I_i(t) \geq I_i(0)e^{-(\tau_i+\delta_1+\mu)t} \tag{32}$$

From (8)

$$\frac{dP_i}{dt} = \tau_i I_i - (\delta_1 + \gamma_i + \mu)P_i$$

$$\frac{dP_i}{dt} \geq -(\gamma_i + \delta_1 + \mu)P_i$$

$$\frac{dP_i}{P_i} \geq -(\gamma_i + \delta_1 + \mu)dt \tag{33}$$

Integrating (33)

$$\int \frac{dP_i}{P_i} \geq -\int (\gamma_i + \delta_1 + \mu)dt$$

$$P_i(t) \geq P_i(0)e^{-(\gamma_i+\delta_1+\mu)t} \tag{34}$$

From (9)

$$\frac{dE_d}{dt} = \alpha_d S_d - (\sigma_d + \mu)E_d$$

$$\frac{dE_d}{dt} \geq -(\sigma_d + \mu)E_d$$

$$\frac{dE_d}{E_d} \geq -(\sigma_d + \mu)dt \tag{35}$$

Integrating (35) gives

$$\int \frac{dE_d}{E_d} \geq -\int (\sigma_d + \mu)dt$$

$$E_d(t) \geq E_d(0)e^{-(\sigma_d+\mu)t} \tag{36}$$

From (10)

$$\frac{dQ_d}{dt} = \sigma_d E_d - (\xi_d + \rho_d + \mu)Q_d$$

$$\frac{dQ_d}{dt} \geq -(\xi_d + \rho_d + \mu)Q_d$$

$$\frac{dQ_d}{Q_d} \geq -(\xi_d + \rho_d + \mu)dt \tag{37}$$

Integrating (37)

$$\int \frac{dQ_d}{Q_d} \geq -\int (\xi_d + \rho_d + \mu)dt$$

$$Q_d(t) \geq Q_d(0)e^{-(\xi_d+\rho_d+\mu)t} \tag{38}$$

From (11)

$$\frac{dI_d}{dt} = \rho_d Q_d - (1-\alpha)I_d - (\tau_d + \delta_2 + \mu)I_d$$

$$\frac{dI_d}{dt} \geq -(1 - \alpha + \tau_d + \delta_2 + \mu)I_d$$

$$\frac{dI_d}{I_d} \geq -(1 - \alpha + \tau_d + \delta_2 + \mu)dt \tag{39}$$

Integrating (39)

$$\int \frac{dI_d}{I_d} \geq -\int (1 - \alpha + \tau_d + \delta_2 + \mu)dt$$

$$I_d(t) \geq I_d(0)e^{-(\rho_d+\mu)dt} \tag{40}$$

From (12)

$$\frac{dP_d}{dt} = \tau_d I_d - (\gamma_d + \delta_2 + \mu)P_d$$

$$\frac{dP_d}{dt} \geq -(\gamma_d + \delta_2 + \mu)P_d$$

$$\frac{dP_d}{P_d} \geq -(\gamma_d + \delta_2 + \mu)dt \tag{41}$$

Integrating (41)

$$\int \frac{dP_d}{P_d} \geq -\int (\gamma_d + \delta_2 + \mu)dt$$

$$P_d(t) \geq P_d(0)e^{-(\gamma_d+\delta_2+\mu)t} \tag{42}$$

From (13)

$$\frac{dI_c}{dt} = (1-\alpha)I_d - \omega I_c - (\tau_c + \delta_3 + \mu)I_c$$

$$\frac{dI_c}{dt} = -(\omega + \tau_c + \delta_3 + \mu)I_c$$

$$\frac{dI_c}{dt} \geq -(\omega + \tau_c + \delta_3 + \mu)I_c \tag{43}$$

Integrating (43)

$$\int \frac{dI_c}{I_c} \geq -\int (\omega + \tau_c + \delta_3 + \mu)dt$$

$$I_c(t) \geq I_c(0)e^{-(\omega+\tau_c+\delta_3+\mu)t} \tag{44}$$

From (14)

$$\frac{dP_c}{dt} = \tau_c I_c - (\delta_3 + \mu)P_c$$

$$\frac{dP_c}{dt} \geq -(\delta_3 + \mu)P_c$$

$$\frac{dP_c}{P_c} \geq -(\delta_3 + \mu)dt \tag{45}$$

Integrating (45)

$$\int \frac{dP_c}{P_c} \geq -\int (\delta_3 + \mu)dt$$

$$P_c(t) \geq P_c(0)e^{-(\delta_3+\mu)t} \tag{46}$$

From (15)

$$\frac{dR_i}{dt} = \gamma_i P_i - (\theta + \eta_i + \mu)R_i$$

$$\frac{dR_i}{dt} \geq -(\theta + \eta_i + \mu)R_i$$

$$\frac{dR_i}{R_i} \geq -(\theta + \eta_i + \mu)dt \tag{47}$$

Integrating (47)

$$\int \frac{dR_i}{R_i} \geq -\int (\theta + \eta_i + \mu)dt$$

$$R_i(t) \geq R_i(0)e^{-(\theta+\eta_i+\mu)t} \tag{48}$$

From (16)

$$\frac{dR_d}{dt} = \gamma_d P_d - (\eta_d + \mu)R_d$$

$$\frac{dR_d}{dt} \geq -(\eta_d + \mu)R_d$$

$$\frac{dR_d}{R_d} \geq -(\eta_d + \mu)dt \tag{49}$$

Integrating (49)

$$\int \frac{dR_d}{R_d} \geq -\int (\eta_d + \mu)dt$$

$$R_d(t) \geq R_d(0)e^{-(\eta_d+\mu)t} \tag{50}$$

Therefore, we conclude that all solutions of system(3) to (16) are positive for all t > o

6. Equilibrium Points of the model

Existence of Steady States Solution In this section, model system (3) – (16) is qualitatively analyzed to investigate the condition of existence and stability of its associated equilibrium points. The equilibrium points are obtained by setting the right-hand side of the model system to zero, that is from the system of equations (3) to (16) at equilibrium states we have that at steady states the right-hand side of equation (3) to (16) is equal to zero, giving the following;

$$\frac{dS_i}{dt} = \frac{dS_d}{dt} = \frac{dE_i}{dt} = \frac{dE_d}{dt} = \frac{dI_i}{dt} = \frac{dQ_i}{dt} = \frac{dP_i}{dt} = \frac{dR_i}{dt} = \frac{dI_d}{dt} = \frac{dQ_d}{dt} = \frac{dP_d}{dt} = \frac{dR_d}{dt} = \frac{dI_c}{dt} = \frac{dP_c}{dt} = 0 \tag{51}$$

Let

$$(S_i, S_d, E_i, E_d, I_i, I_d, I_c, Q_i, Q_d, P_i, P_d, P_c, R_i, R_d) = (S_i^*, S_d^*, S_c^*, I_i^*, I_d^*, I_c^*, Q_i^*, Q_d^*, Q_c^*, P_i^*, P_d^*, P_c^*, R_i^*, R_d^*) \tag{52}$$

Therefore, the system (3) to (16) becomes

$$\beta_i + \eta_i R_i^* + \xi_i Q_i^* - (\alpha_i + \mu)S_i^* = 0 \tag{53}$$

$$\beta_d + \theta R_i^* + \omega I_c^* + \eta_d R_d^* + \xi_d Q_d^* - (\alpha_d + \mu)S_d^* = 0 \tag{54}$$

$$\rho_i Q_i^* - (\tau_i + \delta_1 + \mu)I_i^* = 0$$

$$\rho_i Q_i^* - A_1 I_i^* = 0 \tag{55}$$

$$\sigma_i E_i^* - (\rho_i + \xi_i + \mu)Q_i^* = 0$$

$$\sigma_i E_i^* - A_2 Q_i^* = 0 \tag{56}$$

$$\tau_i I_i^* - (\gamma_i + \delta_1 + \mu) P_i^* = 0$$

$$\tau_i I_i^* - A_3 P_i^* = 0 \tag{57}$$

$$\rho_d Q_d^* - (1 - \alpha + \tau_d + \delta_2 + \mu) I_d^* = 0$$

$$\rho_d Q_d^* - A_4 I_d^* = 0 \tag{58}$$

$$\sigma_d E_d^* - (\rho_d + \xi_d + \mu) Q_d^* = 0$$

$$\sigma_d E_d^* - A_5 Q_d^* = 0 \tag{59}$$

$$\tau_d I_d^* - (\gamma_d + \delta_2 + \mu) P_d^* = 0$$

$$\tau_d I_d^* - A_6 P_d^* = 0 \tag{60}$$

$$(1 - \alpha) I_d^* - (\omega + \tau_c + \delta_3 + \mu) I_c^* = 0$$

$$(1 - \alpha) I_d^* - A_7 I_c^* = 0 \tag{61}$$

$$\tau_c I_c^* - (\delta_3 + \mu) P_c^* = 0$$

$$\tau_c I_c^* - A_8 P_c^* = 0 \tag{62}$$

$$\gamma_i P_i^* - (\eta_i + \theta + \mu) R_i^* = 0$$

$$\gamma_i P_i^* - A_9 R_i^* = 0 \tag{63}$$

$$\gamma_d P_d^* - (\eta_d + \mu) R_d^* = 0$$

$$\gamma_d P_d^* - A_{10} R_d^* = 0 \tag{64}$$

$$\alpha_i S_i^* - (\sigma_i + \mu) E_i^* = 0$$

$$\alpha_i S_i^* - A_{11} E_i^* = 0 \tag{65}$$

$$\alpha_d S_d^* - (\sigma_d + \mu) E_d^* = 0$$

$$\alpha_d S_d^* - A_{12} E_d^* = 0 \tag{66}$$

7. COVID-19-Diabetes Complication Free Equilibrium (CDCFE)

At the COVID-19-Diabetes Complication-Free Equilibrium (CDCFE) point COVID-19 and Diabetes complications are absent. Thus all the affected classes will be zero.

Lemma 1: A COVID-19-Diabetes Complication-Free Equilibrium (CDCFE) state of the model (3)-(16) exists at a point

$$(S_i, S_d, E_i, E_d, I_i, I_d, I_c, Q_i, Q_d, P_i, P_d, P_c, R_i, R_d) = (\frac{\beta_i}{\mu}, \frac{\beta_d}{\mu}, 0,0,0,0,0,0,0,0,0,0,0,0) \quad (67)$$

Proof :

Let

$$E^0 = (S_i, S_d, E_i, E_d, I_i, I_d, I_c, Q_i, Q_d, P_i, P_d, P_c, R_i, R_d)$$
$$= ({S_i}^0, {S_d}^0, {E_i}^0 {E_d}^0, , {I_i}^0, {I_d}^0, {I_c}^0, {Q_i}^0, {Q_d}^0, {P_i}^0, {P_d}^0, {P_c}^0, {R_i}^0, {R_d}^0) \quad (68)$$

Be the CDCFE point by Setting the system equal to zero,

Where

$$E_i = 0, E_d = 0, I_i = 0, I_d = 0, I_c = 0, Q_i = 0, Q_d = 0, P_i = 0, P_d = 0, P_c = 0,$$

$$R_i = 0, R_d = 0$$

thus we have,

from (3)

$$\beta_i - \alpha_i {S_i}^* + \eta_i {R_i}^* + \xi_i {Q_i}^* - \mu {S_i}^* = 0$$

$$\beta_i - \alpha_i {S_i}^* + \eta_i(0) + \xi_i(0) - \mu {S_i}^* = 0$$

$$\beta_i - \alpha_i {S_i}^* - \mu {S_i}^* = 0$$

$$\beta_i - (\alpha_i + \mu) {S_i}^* = 0$$

$${S_i}^* = \frac{\beta_i}{(\alpha_i + \mu)} \quad (69)$$

Substitute (1) into (69) and evaluate to obtain

$$S_i = \frac{\beta_i}{\mu} \quad (70)$$

Again from (4)

$$\beta_d + \theta {R_i}^* + \omega {I_c}^* + \eta_d {R_d}^* + \xi_d {Q_d}^* - (\alpha_d + \mu) {S_d}^* = 0$$

$$\beta_d + \theta(0) + \omega(0) + \eta_d(0) + \xi_d(0) - (\alpha_d + \mu) {S_d}^* = 0$$

$$\beta_d - (\alpha_d + \mu) {S_d}^* = 0$$

$${S_d}^* = \frac{\beta_d}{(\alpha_d + \mu)} \quad (71)$$

Substitute (2) into (71) and evaluate to obtain

$$S_d = \frac{\beta_d}{\mu} \tag{72}$$

Thus, a CDCFE exists at the point

$$\left(S_i{}^0, S_d{}^0, E_i{}^0 E_d{}^0, , I_i{}^0, I_d{}^0, I_c{}^0, Q_i{}^0, Q_d{}^0, P_i{}^0, P_d{}^0, P_c{}^0, R_i{}^0, R_d{}^0\right) = (\frac{\beta_i}{\mu}, \frac{\beta_d}{\mu}, 0,0,0,0,0,0,0,0,0,0,0) \tag{73}$$

8. Computation of Reproduction Number (R_0)

In this section, we determine the threshold parameter that governs the spread of disease which is the effective reproduction number. The method for calculating is called the next-generation matrix (Diekmann and Heesterbeek, 2000). We apply the next-generation matrix operator to compute the basic reproduction number (Driessche and Watmough, 2002). The basic reproduction number is obtained by dividing the whole population into n compartments in which there are$m$infected compartments, $m < n$. Let $x_i, i = 1,2,3, \ldots m$be the number of infected individuals in the i^{th}compartment at time t. The largest eigenvalue or spectral radius of $FV^{-1}$is the basic reproduction number of the model.

$$FV^{-1} = \left[\frac{\partial F_i(E^0)}{\partial x_i}\right]\left[\frac{\partial V_i(E^0)}{\partial x_i}\right]^{-1} \tag{74}$$

Where F_i is the rate of appearance of new infection in the compartment, is the transfer of infection from one compartment $i$to another and $E^0$is the Disease-Free Equilibrium. Using this technique, we have the spectral radius of the next generation matrix, FV^{-1}that is, $R_0 = \rho(FV^{-1})$. Both $F$and$V$are obtained from the model equations (3)-(16). The COVID-19-comorbidity co-infection model has a COVID-19-Diabetes complication-free equilibrium (CDCFE), obtained by setting the disease classes and the right-hand sides of the equations in the model (3)-(16) to zero, given by

$$(S_i^*, S_d^*, E_i{}^*, E_d{}^*, I_i{}^*, I_d{}^*, I_c{}^*, Q_i{}^*, Q_d{}^*, P_i{}^*, P_d{}^*, P_c{}^*, R_i{}^*, R_d{}^*) = (A, B, 0,0,0,0,0,0,0,0,0,0,0)$$

Where,

$$A = S_i{}^* = \frac{\beta_i}{\mu}$$

$$B = S_d{}^* = \frac{\beta_d}{\mu}$$

$$f_i = \begin{pmatrix} f_1 \\ f_2 \\ f_3 \\ f_4 \\ f_5 \\ f_6 \\ f_7 \\ f_8 \\ f_9 \\ f_{10} \end{pmatrix} = \begin{pmatrix} \alpha_i S_i \\ \sigma_i E_i \\ \rho_i Q_i \\ \tau_i I_i \\ \alpha_d S_d \\ \sigma_d E_d \\ \rho_d Q_d \\ \tau_d I_d \\ (1-\alpha) I_d \\ \tau_c I_c \end{pmatrix} \tag{75}$$

$$f_i = \begin{pmatrix} f_1 \\ f_2 \\ f_3 \\ f_4 \\ f_5 \\ f_6 \\ f_7 \\ f_8 \\ f_9 \\ f_{10} \end{pmatrix} = \begin{pmatrix} S_i m_i \left(\frac{\eta_{i1} E_i + \eta_{i2} Q_i + \eta_{i3} I_i + \eta_{i4} P_i}{N} \right) \\ \sigma_i E_i \\ \rho_i Q_i \\ \tau_i I_i \\ S_d m_d \left(\frac{\eta_{d1} E_d + \eta_{d2} Q_d + \eta_{d3} I_d + \eta_{d4} P_d + \eta_{d5} I_c + \eta_{d6} P_c}{N} \right) \\ \sigma_d E_d \\ \rho_d Q_d \\ \tau_d I_d \\ (1-\alpha) I_d \\ \tau_c I_c \end{pmatrix} \tag{76}$$

$$f_i = \begin{pmatrix} f_1 \\ f_2 \\ f_3 \\ f_4 \\ f_5 \\ f_6 \\ f_7 \\ f_8 \\ f_9 \\ f_{10} \end{pmatrix} =$$

$$\begin{pmatrix} S_i m_i\left(\frac{\eta_{i1}}{N}\right) & S_i m_i\left(\frac{\eta_{i2}}{N}\right) & S_i m_i\left(\frac{\eta_{i3}}{N}\right) & S_i m_i\left(\frac{\eta_{i4}}{N}\right) & 0 & 0 & 0 & 0 & 0 & 0 \\ \sigma_i & 0 & 0 & 0 & 0 & 0 & 0 & 0 & 0 & 0 \\ 0 & \rho_{i_i} & 0 & 0 & 0 & 0 & 0 & 0 & 0 & 0 \\ 0 & 0 & \tau_i & 0 & 0 & 0 & 0 & 0 & 0 & 0 \\ 0 & 0 & 0 & 0 & S_d m_d\left(\frac{\eta_{d1}}{N}\right) & S_d m_d\left(\frac{\eta_{d2}}{N}\right) & S_d m_d\left(\frac{\eta_{d3}}{N}\right) & S_d m_d\left(\frac{\eta_{d4}}{N}\right) & S_d m_d\left(\frac{\eta_{d5}}{N}\right) & S_d m_d\left(\frac{\eta_{d6}}{N}\right) \\ 0 & 0 & 0 & 0 & \sigma_d & 0 & 0 & 0 & 0 & 0 \\ 0 & 0 & 0 & 0 & 0 & \rho_d & 0 & 0 & 0 & 0 \\ 0 & 0 & 0 & 0 & 0 & 0 & \tau_d & 0 & 0 & 0 \\ 0 & 0 & 0 & 0 & 0 & 0 & (1-\alpha) & 0 & 0 & 0 \\ 0 & 0 & 0 & 0 & 0 & 0 & 0 & 0 & \tau_c & 0 \end{pmatrix}$$

(77)

At COVID-19-diabetes complication- Free Equilibrium (CDCFE)

$$A = S_i^* = \frac{\beta_i}{\mu}$$

$$B = S_d^* = \frac{\beta_d}{\mu}$$

And also at COVID-19-diabetes complication- Free Equilibrium (CDCFE)

$$N = \hat{S_i} + \hat{S_d}$$

$$N = \frac{\beta_i}{\mu} + \frac{\beta_d}{\mu}$$

$$N = \frac{\beta_i + \beta_d}{\mu}$$

we have

$$F = \begin{pmatrix} f_1 \\ f_2 \\ f_3 \\ f_4 \\ f_5 \\ f_6 \\ f_7 \\ f_8 \\ f_9 \\ f_{10} \end{pmatrix} =$$

$$\begin{bmatrix} \frac{m_i\beta_i\eta_{i1}}{\beta_i+\beta_d} & \frac{m_i\beta_i\eta_{i2}}{\beta_i+\beta_d} & \frac{m_i\beta_i\eta_{i3}}{\beta_i+\beta_d} & \frac{m_i\beta_i\eta_{i4}}{\beta_i+\beta_d} & 0 & 0 & 0 & 0 & 0 & 0 \\ 0 & 0 & 0 & 0 & 0 & 0 & 0 & 0 & 0 & 0 \\ 0 & 0 & 0 & 0 & 0 & 0 & 0 & 0 & 0 & 0 \\ 0 & 0 & 0 & 0 & 0 & 0 & 0 & 0 & 0 & 0 \\ 0 & 0 & 0 & 0 & \frac{m_d\beta_d\eta_{d1}}{\beta_i+\beta_d} & \frac{m_d\beta_d\eta_{d2}}{\beta_i+\beta_d} & \frac{m_d\beta_d\eta_{d3}}{\beta_i+\beta_d} & \frac{m_d\beta_d\eta_{d4}}{\beta_i+\beta_d} & \frac{m_d\beta_d\eta_{d5}}{\beta_i+\beta_d} & \frac{m_d\beta_d\eta_{d6}}{\beta_i+\beta_d} \\ 0 & 0 & 0 & 0 & 0 & 0 & 0 & 0 & 0 & 0 \\ 0 & 0 & 0 & 0 & 0 & 0 & 0 & 0 & 0 & 0 \\ 0 & 0 & 0 & 0 & 0 & 0 & 0 & 0 & 0 & 0 \\ 0 & 0 & 0 & 0 & 0 & 0 & 0 & 0 & 0 & 0 \\ 0 & 0 & 0 & 0 & 0 & 0 & 0 & 0 & 0 & 0 \end{bmatrix} \quad (78)$$

$$v = \begin{pmatrix} v_1 \\ v_2 \\ v_3 \\ v_4 \\ v_5 \\ v_6 \\ v_7 \\ v_8 \\ v_9 \\ v_{10} \end{pmatrix} = \begin{bmatrix} -(\sigma_i + \mu)E_i \\ \sigma_i E_i - \rho_i Q_i - (\xi_i + \mu)Q_i \\ \rho_i Q_i - (\tau_i + \delta_1 + \mu)I_i \\ \tau_i I_i - (\gamma_i + \delta_1 + \mu)P_i \\ -(\sigma_d + \mu)E_d \\ \sigma_d E_d - (\xi_d + -\rho_d + \mu)Q_d \\ \rho_d Q_d - (1-\alpha)I_d - (\tau_d + \delta_2 + \mu)I_d \\ \tau_d I_d - (\gamma_d + \delta_2 + \mu)P_d \\ (1-\alpha)I_d - \omega I_c - (\tau_c + \delta_3 + \mu)I_c \\ \tau_c I \quad -(\delta_3 + \mu)P_c \end{bmatrix} \tag{79}$$

Differentiating (79)

$$V = \begin{bmatrix} b_1 & 0 & 0 & 0 & 0 & 0 & 0 & 0 & 0 & 0 \\ -\sigma_i & b_2 & \rho_i & 0 & 0 & 0 & 0 & 0 & 0 & 0 \\ 0 & -\rho_i & b_3 & 0 & 0 & 0 & 0 & 0 & 0 & 0 \\ 0 & 0 & -\tau_i & b_4 & 0 & 0 & 0 & 0 & 0 & 0 \\ 0 & 0 & 0 & 0 & b_5 & 0 & 0 & 0 & 0 & 0 \\ 0 & 0 & 0 & 0 & -\sigma_d & b_6 & 0 & 0 & 0 & 0 \\ 0 & 0 & 0 & 0 & 0 & -\rho_d & b_7 & 0 & 0 & 0 \\ 0 & 0 & 0 & 0 & 0 & 0 & -\tau_d & b_8 & 0 & 0 \\ 0 & 0 & 0 & 0 & 0 & 0 & -1+\alpha & 0 & b_9 & 0 \\ 0 & 0 & 0 & 0 & 0 & 0 & 0 & 0 & -\tau_c & b_{10} \end{bmatrix} \tag{80}$$

Were

$b_1 = \sigma_i + \mu, b_2 = \xi_i + \rho_i + \mu, b_3 = \tau_i + \delta_1 + \mu, b_4 = \gamma_i + \delta_1 + \mu, b_5 = \sigma_d + \mu,$
$b_6 = \xi_d + \rho_d + \mu, b_7 = 1 - \alpha + \tau_d + \delta_2 + \mu, b_8 = \gamma_d + \delta_2 + \mu, b_9 = \omega + \tau_c + \delta_3 + \mu, b_{10} = \tau_c + \delta_3 + \mu$

(81)

$$V^{-1} = \frac{adjV}{det\,V}$$

$$\begin{bmatrix}
\frac{1}{b_1} & 0 & 0 & 0 & 0 & 0 & 0 & 0 & 0 & 0 \\
\frac{\sigma_i b_3}{\left(b_2 b_3 + \rho_i^2\right) b_1} & \frac{b_3}{b_2 b_3 + \rho_i^2} & -\frac{\rho_i}{b_2 b_3 + \rho_i^2} & 0 & 0 & 0 & 0 & 0 & 0 & 0 \\
\frac{\rho_i \sigma_i}{b_1 \left(b_2 b_3 + \rho_i^2\right)} & \frac{\rho_i}{b_2 b_3 + \rho_i^2} & \frac{b_2}{b_2 b_3 + \rho_i^2} & 0 & 0 & 0 & 0 & 0 & 0 & 0 \\
\frac{\tau_i \rho_i \sigma_i}{\left(b_2 b_3 + \rho_i^2\right) b_1 b_4} & \frac{\tau_i \rho_i}{\left(b_2 b_3 + \rho_i^2\right) b_4} & \frac{\tau_i b_2}{\left(b_2 b_3 + \rho_i^2\right) b_4} & \frac{1}{b_4} & 0 & 0 & 0 & 0 & 0 & 0 \\
0 & 0 & 0 & 0 & \frac{1}{b_5} & 0 & 0 & 0 & 0 & 0 \\
0 & 0 & 0 & 0 & \frac{\sigma_d}{b_5 b_6} & \frac{1}{b_6} & 0 & 0 & 0 & 0 \\
0 & 0 & 0 & 0 & \frac{\rho_d \sigma_d}{b_6 b_5 b_7} & \frac{\rho_d}{b_6 b_7} & \frac{1}{b_7} & 0 & 0 & 0 \\
0 & 0 & 0 & 0 & \frac{\tau_d \rho_d \sigma_d}{b_7 b_6 b_5 b_8} & \frac{\tau_d \rho_d}{b_7 b_6 b_8} & \frac{\tau_d}{b_7 b_8} & \frac{1}{b_8} & 0 & 0 \\
0 & 0 & 0 & 0 & -\frac{(-1+\alpha)\,\rho_d \sigma_d}{b_7 b_6 b_5 b_9} & -\frac{(-1+\alpha)\,\rho_d}{b_7 b_6 b_9} & -\frac{-1+\alpha}{b_7 b_9} & 0 & \frac{1}{b_9} & 0 \\
0 & 0 & 0 & 0 & -\frac{\tau_c (-1+\alpha)\,\rho_d \sigma_d}{b_9 b_7 b_6 b_5 b_{10}} & -\frac{\tau_c (-1+\alpha)\,\rho_d}{b_9 b_7 b_6 b_{10}} & -\frac{\tau_c (-1+\alpha)}{b_9 b_7 b_{10}} & 0 & \frac{\tau_c}{b_9 b_{10}} & \frac{1}{b_{10}}
\end{bmatrix} \tag{82}$$

$$R_o = \rho(FV^{-1}) \tag{83}$$

$$\begin{bmatrix}
0 \\ 0 \\ 0 \\ 0 \\ 0 \\ 0 \\ 0 \\ 0 \\
\frac{m_i \beta_i \left(\eta_{i1} b_2 b_3 b_4 + \eta_{i1} b_4 \rho_i^2 + \eta_{i2} \sigma_i b_3 b_4 + \eta_{i3} \rho_i \sigma_i b_4 + \eta_{i4} \tau_i \rho_i \sigma_i\right)}{b_1 b_4 \left(\beta_d b_2 b_3 + \beta_d \rho_i^2 + \beta_i b_2 b_3 + \beta_i \rho_i^2\right)} \\
-\frac{m_d \beta_d \left(-\eta_{d1} b_6 b_7 b_8 b_9 b_{10} - \eta_{d2} \sigma_d b_7 b_8 b_9 b_{10} - \eta_{d3} \rho_d \sigma_d b_8 b_9 b_{10} - \eta_{d4} \tau_d \rho_d \sigma_d b_9 b_{10} + \eta_{d5} \rho_d \sigma_d b_8 b_{10} \alpha - \eta_{d5} \rho_d \sigma_d b_8 b_{10} + \eta_{d6} \tau_c \rho_d \sigma_d b_8 \alpha - \eta_{d6} \tau_c \rho_d \sigma_d b_8\right)}{b_5 b_6 b_7 b_8 b_9 b_{10} \left(\beta_i + \beta_d\right)}
\end{bmatrix} \tag{84}$$

Where $\lambda_1 = 0, \lambda_2 = 0, \lambda_3 = 0, \lambda_4 = 0, \lambda_5 = 0, \lambda_6 = 0, \lambda_7 = 0, \lambda_8 = 0$

$$\lambda_9 = \frac{m_i \beta_i \left(\eta_{i1} b_2 b_3 b_4 + \eta_{i1} b_4 \rho_i^2 + \eta_{i2} \sigma i b_3 b_4 + \eta_{i3} \rho_i \sigma_i b_4 + \eta_{i4} \tau_i \rho_i \sigma_i\right)}{b_1 b_4 \left(\beta_d b_2 b_3 + \beta_d \rho_i^2 + \beta_i b_2 b_3 + \beta_i \rho_i^2\right)}$$

$$\lambda_{10} = \frac{m_d \beta_d \begin{pmatrix} -\eta_{d1} b_6 b_7 b_8 b_9 b_{10} - \eta_{d2} \sigma_d b_7 b_8 b_9 b_{10} - \eta_{d3} \sigma_d \rho_d b_8 b_9 b_{10} - \eta_{d4} \sigma_d \rho_d \tau_d b_9 b_{10} \\ + \eta_{d5} \sigma_d \rho_d \alpha b_8 b_{10} - \eta_{d5} \sigma_d \rho_d b_8 b_{10} + \eta_{d6} \sigma_d \rho_d \alpha \tau_c b_8 - \eta_{d6} \sigma_d \rho_d \tau_c b_8 \end{pmatrix}}{b_5 b_6 b_7 b_8 b_9 b_{10} (\beta_i + \beta_d)}$$

$$R_i = \frac{m_i \beta_i \left(\eta_{i1} b_2 b_3 b_4 + \eta_{i1} b_4 \rho_i^2 + \eta_{i2} \sigma i b_3 b_4 + \eta_{i3} \rho_i \sigma_i b_4 + \eta_{i4} \tau_i \rho_i \sigma_i \right)}{b_1 b_4 \left(\beta_d b_2 b_3 + \beta_d \rho_i^2 + \beta_i b_2 b_3 + \beta_i \rho_i^2 \right)}$$

(85)

$$R_d = \frac{m_d \beta_d \begin{pmatrix} -\eta_{d1} b_6 b_7 b_8 b_9 b_{10} - \eta_{d2} \sigma_d b_7 b_8 b_9 b_{10} - \eta_{d3} \sigma_d \rho_d b_8 b_9 b_{10} - \eta_{d4} \sigma_d \rho_d \tau_d b_9 b_{10} \\ + \eta_{d5} \sigma_d \rho_d \alpha b_8 b_{10} - \eta_{d5} \sigma_d \rho_d b_8 b_{10} + \eta_{d6} \sigma_d \rho_d \alpha \tau_c b_8 - \eta_{d6} \sigma_d \rho_d \tau_c b_8 \end{pmatrix}}{b_5 b_6 b_7 b_8 b_9 b_{10} (\beta_i + \beta_d)}$$

(86)

Therefore, the reproduction number is given as

$$R_0 = max\{R_i, R_d\} \quad (87)$$

9. Results

It follows that the positive eigenvalues represent the two reproduction numbers where R_i represent the expected number of COVID-19 infectiousness produced by one COVID-19 infectious individual, where R_d represent the expected number of Diabetes without complication-induced COVID-19 infectiousness produced by one COVID-19 infectious individual.

10. Conclusion

The feasible solutions set of the model (3) to (16) enters the region which is positively invariant and the model is well-posed and biologically meaningful. The equilibrium points exist for the Disease Free that was calculated, We conclude that, the result above follows from Theorem 2 of (van den Driessche &Watmough, 2002).

REFERENCES

Andrew Omame, Ugochukwu K. Nwajeri, M. Abbas, Chibueze P. Onyenegecha, A fractional order control model for Diabetes and COVID-19 co-dynamics with Mittag-Leffler function, Peer review under responsibility of Faculty of Engineering, Alexandria University. Alexandria Engineering Journal (2022) 61, 7619–7635

Castillo-Chavez, C., Feng Z. & Huang, W. (2002). On the computation of Ro and its role in global stability. In C. Castillo-Chavez, S. Blower,P, Van den Driessche,D. Krirschner& A. A. Yakubu (Eds), *Mathematical approaches for emerging* and *re-emerging infectious diseases: An introduction. The IMA Volumes in Mathematics and its Applications,* 125, 229-250. New York: Springer-Verlag.

Centres for Disease Control and Prevention (CDC), Coronavirus Disease 2019 (COVID-19), Available on https:// www.cdc.gov/coronavirus/2019-ncov/index.html.

Gumel, Enahoro A. Iboib, Calistus N. Ngonghala, Elamin H. Elbashaf (2020).A primer on using mathematics to understand COVID-19 dynamics: Modeling, analysis and simulations, *KeAi Communications Co., Ltd. Infectious Disease Modelling*https://doi.org/10.1016/j.idm.2020.11.005

Huang C, Wang Y, Li X, Ren L, Zhao J, Hu Y.(2020). Clinical features of patients infected with 2019 novel coronavirus in Wuhan, China. Lancet.https://doi.org/10.1016/S0140-6736(20)30183-5.

International Diabetes Federation (2020).IDF Diabetes Atlas.13th Edition http://www.idf.org/diabetesatlas.

International Diabetes Federation (2021).About diabetes.www.idf.org/about-diabetes

Li Q, Guan X, Wu P. (2020).Early transmission dynamics in Wuhan, China, of novel coronavirus-infected pneumonia. N Engl J Med published online Jan 29.2020; DOI: 10.1056/NEJMoa2001316.

Lu H, Drug treatment options for the 2019-new coronavirus (2019-nCoV), Biosci. Trends 2020.doi.org/10.5582/bst.2020.01020.

Rosenwald, Michael S. (2020). History's deadliest pandemics, from ancient Rome to modern America.The Washington Post.Archived from the original on 7 April 2020 and retrieved 11 April 2020.

Rothana HA, Byrareddy SN, The epidemiology and pathogenesis of coronavirus disease (COVID-19) outbreak, J. Autoimmun. 2020; 109:102433.

The Nigeria Center for Disease Control,(2020). *https://covid19.ncdc.gov.ng*

Tingzhe Sun, Yan Wang (2020).Modelling COVID-19 epidemic in Heilongjiang province,Chinahttps://doi.org/10.1016/j.chaos.2020.109949 0960-0779, Elsevier Ltd. All rights reserved.

World Health Organization. Coronavirus.(2021). World Health Organization, cited January 10, 2021. Available: https://www.who.int/health-topics/coronavirus.

World Health Organization.Coronavirus. World Health Organization, cited June 10, 2020. Available: https://www.who.int/health-topics/coronavirus.

Yesenia Cruz Rosado (2009). Mathematical Model for detecting diabetes.Proceedings of the National Conference, University of Wisconsin La-Crosse, Wisconsin.

Zhou F., Yu T., Du R., Fan G., Liu Y., Liu Z., Xiang J., Wang Y., Song B., Gu X., et al. Clinical course and risk factors for mortality of adult inpatients with COVID-19 in Wuhan, China: A retrospective cohort study. *Lancet.* 2020;**395**:1054–1062. doi: 10.1016/S0140-6736(20)30566-3. [PMC free article] [PubMed] [CrossRef] [Google Scholar]

Zhou P, Yang XL, Wang XG, Hu B, Zhang L, Zhang W. (2020).A pneumonia outbreak associated with a new coronavirus of probable bat origin. Nature.2020. https://doi.org/10.1038/s41586-020-2012-7.

Zhu N, Zhang D, Wang W. (2020).A novel coronavirus from patients with pneumonia in China, 2019. N Engl J Med 2020; published Feb 20. DOI: 10.1056/NEJMoa2001017.

Mathematical Modelling of the Effects of Water Depth on Temperature of Lakes

[1]Evans, Patience. O., [2]Okoro, Samuel .I., [3]Faniyi, O.E., & [4]Umar, Aliyu M.
[1,2,3]Department of Mathematics, Anchor University, Lagos, Nigeria.
[4]Department of Mathematics, Federal Polytechnic Offa, Kwara State,
E-mail Corresponding Author: pevans@aul.edu.ng,
Phone Corresponding Author: +2347065530033

Abstract

This paper analysed the effect of water depth on the temperature of different lakes. The governing equations were formulated and solved using least square method embedded in mathematical software packages. The model equations showing the effect of water depth on the temperature of lake 1, 2 and 3 were linear. The thermocline depth and temperature for each lake were also determine. It was observed that as the depth increases the temperature decreases. The results shows that thermocline depth and temperature for each lake were (4.4m, 24.50^{0}C), (4.4m, 28.25^{0}C) and (4.4m, 26.99^{0}C) respectively. It can be concluded that linear models can be used to analyse the effect of water depths on lake's temperature and the thermocline of each lake can be determine. The linear models obtained competes favourably with other existing models.

Keywords: Depth, Lakes, Mathematical models, Thermocline, Temperature

1. INTRODUCTION

The least-squares regression approach stands as a prevalent technique within the domain of Regression Analysis. It serves as a mathematical framework employed to ascertain the optimal fitting line delineating the association between an independent and a dependent variable (Reddy & Henze, 2023).

The physical attribute of water temperature indicates how hot or cold the water is. Since the labels hot and cold are arbitrary, another way to define temperature is as the average thermal energy of a material. Temperature measures the average kinetic energy of atoms and molecules because thermal energy is the kinetic energy of atoms and molecules. Similar to heat flow, this energy can be exchanged across substances. Heat transfer from the air, sunshine, another water source, or thermal pollution can alter the temperature of water (FELC, 2024).

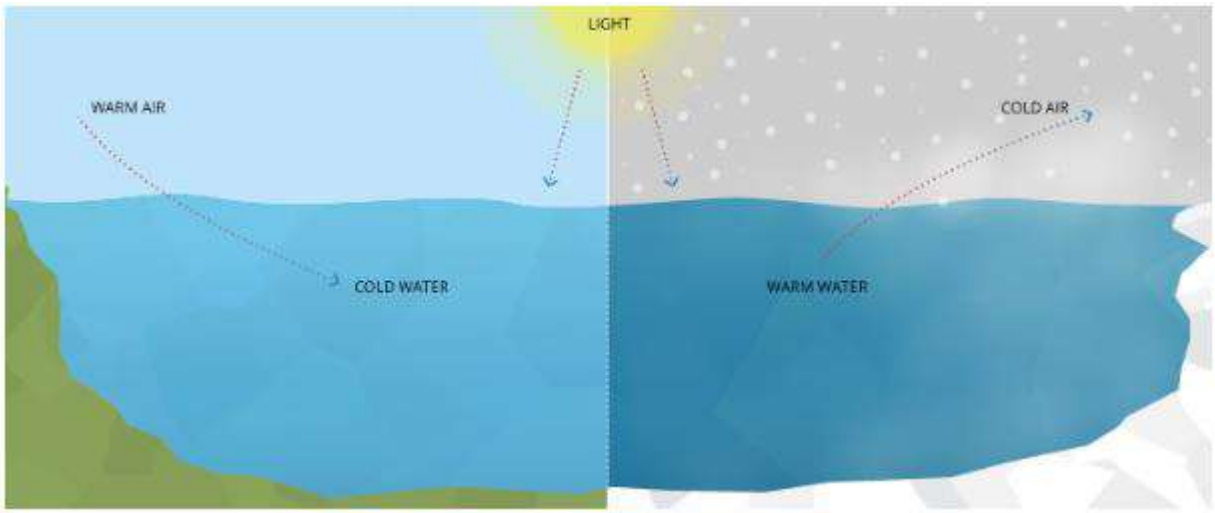

(FELC, 2024)

Plate 1: Water temperature plays a major role in the quality of aquatic life and habitats. Heat flow and the fluctuation of temperature determine what species will live and thrive in a body of water.

When evaluating the quality of water, temperature is an essential consideration. Temperature has its own impacts, but it also affects a number of other variables and changes the chemical and physical characteristics of water. In this context, the following parameters should be taken into consideration when calculating water temperature: pH, water density, dissolved oxygen and other dissolved gas concentrations, conductivity and salinity, compound toxicity, and metabolic rates and photosynthetic production. (FELC, 2024).

Recent research has shown that lakes all over the world are warming significantly. It is yet unknown, though, how coherent these tendencies are in space and time. Lakes are a good proxy for evaluating the effects of climate change because they are particularly sensitive to changes in environmental conditions. (Yu, *et al*. 2021). According to Piccolroaz,(2024) gives a summary of the various observational water temperature data sources used in lake water temperature modeling, such as satellite Earth observations and in situ monitoring. We first analyze and categorize the several models of lake water temperature that are currently available with model performance, including popular performance indicators and optimization techniques. Chikwendu *et., al*. (2015) worked on the application of spline and piecewise interpolation to heat transfer (cubic case) and did a comparative analysis with the result that the cubic spline interpolation method had less percentage error.

Considering the upper and the lower layer of the lake, we have the layer between them as the thermocline.

Thermocline is the boundary between warm surface and cold deep water in lakes and oceans. When the thermocline becomes higher or shallower than normal, it significantly affects the environment. A shallower or higher thermocline can lead to change in water circulation patterns, which in turn affect the oxygen and nutrient distribution of the water column. This can in turn impact the distribution of marine life, such as fish and other organisms that rely on specific water temperatures and nutrient levels. (Eville and Farrell, 1989)

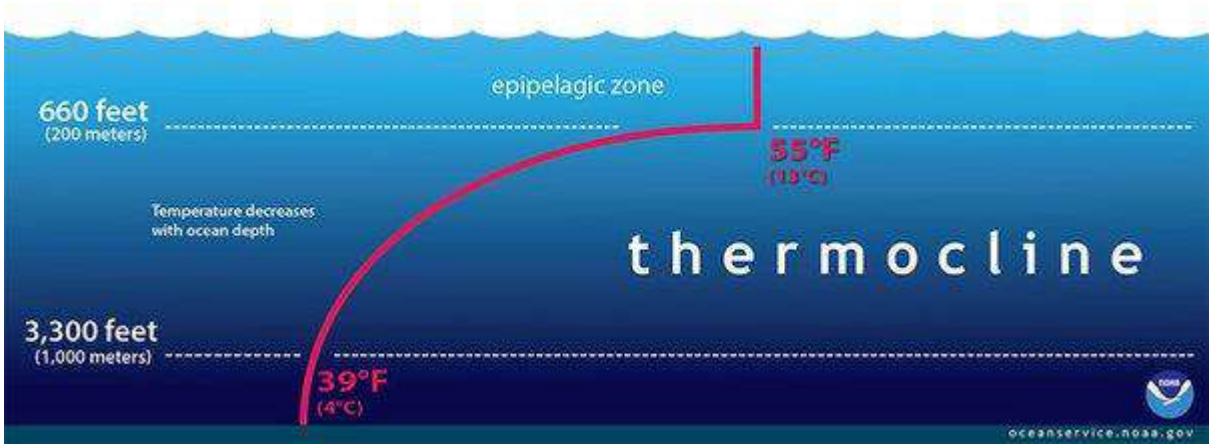

https://qph.cf2.quoracdn.net/main-qimg-fafa9a305272ae54cfbe48843bfc3e84-lq

Plate 2: Thermocline

Thermocline depth influences weather pattern and climate, as the ocean plays a vital role in regulating global temperature and atmospheric circulation. In general, thermocline depth can have significant consequences on climate change, weather pattern and marine ecosystem. (Eville and Farrell, 1989)

This research seeks to determine the effect of depth of the lake on temperature of the lake. Mathematical model that best describe the relationship will be formulated using the least square method. The temperature of the lake is the independent variable; depth of the lake is the dependent variables.

2. MODEL FORMULATION

Least Square method, which seeks to minimse the variance between the estimated values from the polynomial and the expected values from the dataset, will be used for the model formulation

The linear equation that govern the relationship between the depth of water and temperature is given by equation (1).

$$D = a\,T_{L1} + b \tag{1}$$

Which is a linear model

Where, D=Depth of water, m = Slope

T= Temperature, b = Y intercept

Normalizing equation (1), we obtain,

$$D - a\,T_{L1} - b = 0 \tag{2}$$

$$I = D - a\,T_{L1} - b = 0 \tag{3}$$

$$I = min \sum_{n=1}^{8} (D - a\,T_{L1} - b)^2 \tag{4}$$

Differentiating equation (4) with respect to a and b, we have,

$$\frac{dI}{da} = 2\sum (D_{L_1} - aT_{L_1} - b)(-T_{L_1}) = 0 \tag{5}$$

$$\frac{dI}{db} = 2\sum (D_{L_1} - aT_{L_1} - b)(-1) = 0$$

$$-\sum D_{L_1} T_{L_1} + a\sum T_{L_1}{}^2 + bT_{L_1} = 0 \tag{6}$$

$$-\sum D_{L_1} + aT_{L_1} + b = 0$$

$$a\sum T_{L_1}{}^2 + b\sum T_{L_1} = \sum D_{L_1} T_{L_1}$$

$$a\sum T_{L_1} + b\sum 1 = \sum D_{L_1} \tag{7}$$

Table 1: Formulation of effect of temperature on water depth of Lake 1

D	TL_1	D TL_1	TL_1^2
1	30	30	900
2	30	60	900
3	30	90	900
4	28	112	784
5	23	115	529
6	19	114	361
7	18	126	324
9	18	144	324
36	196	791	5022

By using the Matrix equation $ax = b$ equation (7) is transformed to become

$$\begin{pmatrix} \sum T_{L_1}{}^2 & \sum T_{L_1} \\ \sum T_{L_1} & \sum 1 \end{pmatrix} \begin{pmatrix} a \\ b \end{pmatrix} = \begin{pmatrix} \sum D_{L_1} T_{L_1} \\ \sum D_{L_1} \end{pmatrix} \tag{8}$$

$$\begin{pmatrix} 5022 & 196 \\ 196 & 8 \end{pmatrix} \begin{pmatrix} a \\ b \end{pmatrix} = \begin{pmatrix} 791 \\ 36 \end{pmatrix}$$

$$A = \begin{pmatrix} 5022 & 196 \\ 196 & 8 \end{pmatrix}$$

$$|A| = 5022(8) - 196(196) = 40176 - 38416$$

$$|A| = 1760$$

$$a = \begin{pmatrix} 791 & 196 \\ 36 & 8 \end{pmatrix}$$

$$|a| = 791(8) - 196(36) = 6328 - 7056$$

$$|a| = -728$$

$$a = \frac{|a|}{|A|} = \frac{-728}{1760} = -0.4136$$

$$b = \begin{pmatrix} 5022 & 791 \\ 196 & 36 \end{pmatrix}$$

$$|b| = 5022(36) - 791(196) = 180792 - 155036$$

$$|b| = 25756$$

$$b = \frac{|b|}{|A|} = \frac{25756}{1760} = 14.6341$$

$$D_{L_1} = aT_{L_1} + b \qquad (9)$$

Simplifying equation (8) with the values in table 1 for Lake 1, we obtain the linear model for Lake 1 as generated below by obtaining the value of a and b in equation (9) we have

$$D_{L_1} = 0.4136T_{L_1} + 14.6341 \qquad (10)$$

From equation (10) we obtain, the temperature model equation for Lake 1 as

$$T_{L_1} = \frac{D_{L_1} - 14.6341}{0.4136} \qquad (11)$$

Similarly, we obtain the model equation for Lake 2 as follows,

Table 2: Formulation of effect of temperature on water depth of Lake 2

DL_2	TL_2	TL_2^2	DTL_2
1	35	1225	35
2	35	1225	70
3	34	1156	102
4	32	1024	128
5	26	676	130
6	22	484	132
7	21	441	147
8	21	441	168
36	226	6672	912

$$d\sum T_{L_2}{}^2 + e\sum T_{L_2} = \sum DT_{L_2} \quad (12)$$

$$d\sum T_{L_2} + e\sum 1 = \sum D_{L_2}$$

By using the Matrix equation $ax = b$ equation (12) is transformed to become

$$\begin{pmatrix} \sum T_{L_2}{}^2 & \sum T_{L_2} \\ \sum T_{L_2} & \sum 1 \end{pmatrix}\begin{pmatrix} d \\ e \end{pmatrix} = \begin{pmatrix} \sum DT_{L_2} \\ \sum D_{L_2} \end{pmatrix} \quad (13)$$

$$\begin{pmatrix} 6672 & 226 \\ 226 & 8 \end{pmatrix}\begin{pmatrix} d \\ e \end{pmatrix} = \begin{pmatrix} 912 \\ 36 \end{pmatrix}$$

$$|k| = (6672)8 - 226(226) = 53376 - 51076 = 2300$$

$$|d| = (912)8 - 8(226) = 7796 - 8136 = -840$$

$$|e| = (6672)36 - 226(912) = 240192 - 206112 = 34080$$

$$d = \frac{-840}{2300} = 0.365217391 \simeq 0.3652$$

$$e = \frac{34080}{2300} = 14.8173913 \simeq 14.8174$$

$$D_{L_2} = DT_{L_2} + e \quad (14)$$

Simplifying equation (13) with the values in table 1 for Lake 1, we obtain the linear model for Lake 1 as generated below by obtaining the value of a and b in equation (14) we have

$$D_{L_2} = -0.3652T_{L_2} + 14.8174 \quad (15)$$

From equation (15) we obtain, the temperature model equation for Lake 2 as

$$T_{L_2} = \frac{14.8174 - D_{L_2}}{0.3652} \quad (16)$$

In addition, we obtain the model equation for Lake 3 as follows,

Table 3: Formulation of effect of temperature on water depth of Lake 3

DL_3	**TL_3**	**TL_3^2**	**DL_3TL_3**
1	34	1156	34
2	34	1156	68
3	34	1156	102
4	30	900	120
5	23	529	115
6	21	441	126
7	20	400	140

8	20	400	160
36	216	6138	865

$$f\sum T_{L_3}{}^2 + g\sum T_{L_3} = \sum D_{L_3} T_{L_3} \tag{17}$$

$$f\sum T_{L_3} + g\sum 1 = \sum D_{L_3}$$

By using the Matrix equation $ax = b$ equation (17) is transformed to become

$$\begin{pmatrix} \sum T_{L_3}{}^2 & \sum T_{L_3} \\ \sum T_{L_3} & \sum 1 \end{pmatrix} \begin{pmatrix} f \\ g \end{pmatrix} = \begin{pmatrix} \sum D_{L_3} T_{L_3} \\ \sum D_{L_3} \end{pmatrix} \tag{18}$$

$$\begin{pmatrix} 6138 & 216 \\ 216 & 8 \end{pmatrix} \begin{pmatrix} f \\ g \end{pmatrix} = \begin{pmatrix} \sum D_{L_3} T_{L_3} \\ \sum D_{L_3} \end{pmatrix}$$

$$\begin{pmatrix} 6138 & 216 \\ 216 & 8 \end{pmatrix} \begin{pmatrix} f \\ g \end{pmatrix} = \begin{pmatrix} 865 \\ 36 \end{pmatrix}$$

$$B = \begin{pmatrix} 6138 & 216 \\ 216 & 8 \end{pmatrix}$$

$$|B| = 6138(8) - 216(216) = 49104 - 46656 = 2448$$

$$f = \begin{pmatrix} 865 & 216 \\ 36 & 8 \end{pmatrix}$$

$$|f| = 865(8) - 216(36) = 6920 - 7776 = -856$$

$$f = \frac{|e|}{|B|} = \frac{-856}{2448} = -0.3497$$

$$g = \begin{pmatrix} 6138 & 865 \\ 216 & 36 \end{pmatrix}$$

$$|g| = 6138(36) - 865(216)$$

$$|g| = 220968 - 186840$$

$$|g| = 34128$$

$$g = \frac{|g|}{|B|} = \frac{34128}{2448} = 13.9412$$

$$D_{L_3} = fT_{L_3} + g \tag{19}$$

Simplifying equation (17) with the values in table 3 for Lake 3, we obtain the linear model for Lake 3 as generated below by obtaining the value of f and g in equation (19) we have

$$D_{L_3} = -0.3497T_{L_3} + 13.9412 \quad (20)$$

From equation (20) we obtain, the temperature model equation for Lake 3 as

$$T_{L_3} = -\frac{D_{L_3} + 13.9412}{0.3497} \quad (21)$$

3. RESULTS AND DISCUSSION:

The model equations obtained are given as,

$$D_{L_1} = 0.4136T_{L_1} + 14.6341 \quad (22)$$

$$D_{L_2} = -0.3652T_{L_2} + 14.8174 \quad (23)$$

$$D_{L_3} = -0.3497T_{L_3} + 13.9412 \quad (24)$$

$$T_{L_1} = \frac{14.6341 - D_{L_1}}{0.4136} \quad (25)$$

$$T_{L_2} = \frac{14.8174 - D_{L_2}}{0.3652} \quad (26)$$

$$T_{L_3} = \frac{13.9412 - D_{L_3}}{0.3497} \quad (27)$$

3.1 ANALYSIS OF RESULTS

TABLE 4: THE EFFECT OF LAKE DEPTH ON TEMPERATURE OF THE LAKE

D (m)	TL1	TL2	TL3
1	32.96446	37.83516	37.00658
2	30.54666	35.09693	34.14698
3	28.12887	32.35871	31.28739
4	25.71107	29.62048	28.4278
5	23.29328	26.88226	25.5682

6	**20.87548**	**24.14403**	**22.70861**
7	**18.45769**	**21.40581**	**19.84901**
8	**16.03989**	**18.66758**	**16.98942**

Table 4, depicts the effect of lake depth on temperature of the lake, as the depth increases the temperature decreases

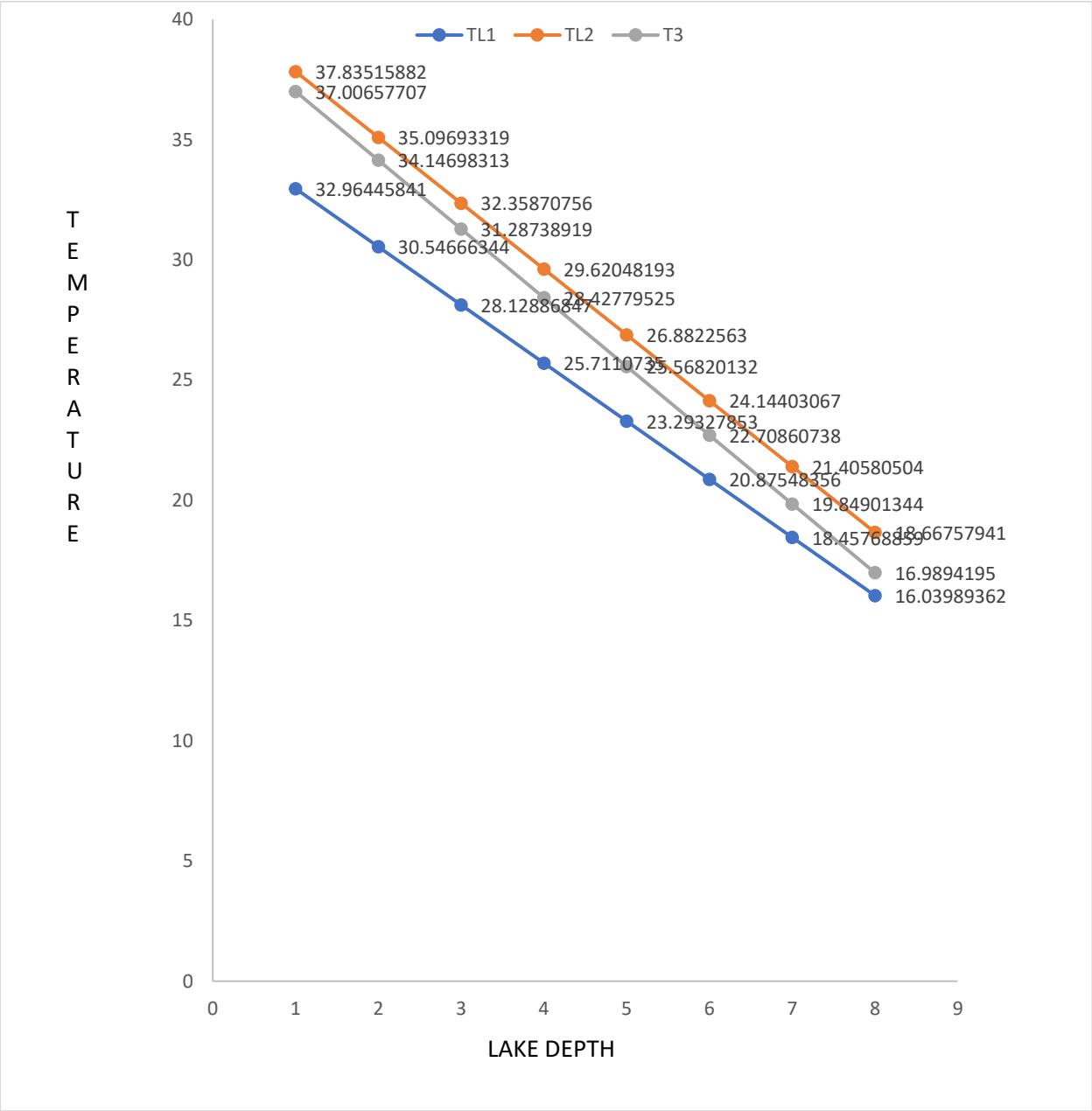

FIGURE 1: The Effect of Lake Depth on Temperature of Lake

Figure 1: shows the effect of depth of different lake on the temperature of the lake. As the depth increases the temperature reduces, this is as a result of the temperature of the surrounding as it satisfies the work of Chikwendu *et., al*. (2015).

Table 5: Thermocline Depth and Temperature of the Different Lake

LAKE TYPE	THERMOCLINE DEPTH	THERMOCLINE TEMPERATURE
LAKE 1	4.5	24.50217602
LAKE 2	4.5	28.25136911
LAKE 3	4.5	24.50217602

Table 5, shows the thermocline depth and thermocline temperature of the different lakes. The results also shows that the calculated thermocline depth and temperature for each lake agrees with reality of (4.4m, 24.50^0C), (4.4m, 28.25^0C) and (4.4m, 26.99^0C) respectively.

4. CONCLUSION

In conclusion, the model equations showing the effect of water depth on the temperature of lake 1, 2 and 3 was formulated. The thermocline depth and temperature for each lake was also determine. As the depth increases the temperature decreases, which means that the depth of lake water has a significant effect on the temperature. Linear models can be used to analyses the effect of water depths on lake's temperature and the thermocline of each lake can be determine. The linear models obtained competes favourably with other existing models.

REFERENCE

Chikwendu, C. R., Oduwole, H. K., & Okoro, S. I. (2015). An application of spline and piecewise interpolation to heat transfer (cubic case). *Mathematical Theory and Modeling*, *5*(6), 28-39.

Eville Gorham & Farrell M. Boyce **(1989):** Influence of Lake Surface Area and Depth Upon Thermal Stratification and the Depth of the Summer Thermocline. Journal of great reseach. volume 15 issues 2, 1989 page 233-245

Fondriest Environmental Learning Centre (2024): https://www.fondriest.com/environmental-measurements/parameters/water-quality/water-temperature/

https://qph.cf2.quoracdn.net/main-qimg-fafa9a305272ae54cfbe48843bfc3e84-lq

Piccolroaz, S., Zhu, S., Ladwig, R., Carrea, L., Oliver, S., Piotrowski, A. P., ... & Zhu, D. Z. (2024). Lake water temperature modeling in an Era of climate change: Data sources, models, and future prospects. *Reviews of Geophysics*, *62*(1), e2023RG000816.

Reddy, T. A., & Henze, G. P. (2023). Linear Regression Analysis Using Least Squares. In *Applied Data Analysis and Modeling for Energy Engineers and Scientists* (pp. 169-221). Cham: Springer International Publishing.

Yu, S. J., Son, J. Y., Kang, H. Y., Cho, Y. C., & Im, J. K. (2021). Effects of Long-Term Increases in Water Temperature and Stratification on Large Artificial Water-Source Lakes in South Korea. *Water*, *13*(17), 2341.

FLUID DYNAMICS AND NUMERICAL ANALYSIS

Pressure Driven Flow Through a Horizontal Annulus Filled with Bi-Disperse Porous Medium: An Exact Solution

M. K. Musa[1], L. K. Yusuf[1], M. Balarabe[1], A. M. Umar[2] and M. K. Tafida[3]

Department of Mathematics, Ahmadu Bello University, Zaria, Nigeria[1]
Division of Agricultural Colleges, Ahmadu Bello University, Zaria, Nigeria[2]
Department of Mathematics Federal College of Education, Zaria[3]

Abstract

The rapid advancements in science and technology necessitated, (depending on the industrial need), the mathematical modelling of different forms of porous materials. This work presents a theoretical analysis of fluid flow induced by an applied constant pressure gradient across a concentric cylinder filled with Bi-Disperse Porous Medium (BDPM). As distinguished from the classical single-phase porous medium, the present problem is governed by a pair of coupled second-order differential equations. The expressions for the fluid velocity profiles in either the fracture or porous phases, have been obtained in terms of the modified Bessel functions using suitable mathematical techniques. The research established that increasing in the fluid viscosity is proportional to enhancing the coefficient of momentum transfer (η) which suppresses the fluid velocities in the two phases of the porous structure. In addition, the effect of the applied pressure-gradient induces high velocities in f-phase and p-phase of the BDPM when $\delta \to 0$.

Keywords: Bi-disperse Porous Materials; Coefficient of momentum transfer; D'Alembert method; Vertical Annulus;

1.0 Introduction

Fluid flow in concentric cylinders and pipes is usually encountered in practice. In several applications, the development of mathematical models that incorporate a porous structure into the mathematical formulations is necessary. For instance, Das *et.al* (2018) examined the dynamics of blood flow through porous structure and demonstrated that the in treating some abnormal blood vessels problems, coil embolization or endovascular coiling reduces the wall shear considerably, leaving the wall pressure largely unaffected. Recently, Khanafer and Vafai (2022) presented detail and critical review of the applications of porous media in a biological system.

According to Vafai (2005), one of the classical models earlier developed (the Darcy model) simply presents a direct proportionality between the superficial average velocity (U) and the pressure difference (P) applied across the porous medium. The Darcy model was later extended to account for cases where large fluid flow (Forchheirmen's model) and boundary effects (Brinkman's model) are

[1] **Corresponding author**: mmkabirxy@yahoo.com (**ORCID: 0000-0002-0420-4014**)

required (Khaled and Vafai, 2003). Investigation of fluid flow via naturally existing porous media or scientifically developed porous structures emanates from the role porous media play in geophysical fluid flow, fluid flow in biological tissues and chemical reactors.

This article focuses on the mathematical modeling of a modified form of Brinkman's model. Interesting reports on Bidisperse porous medium have been published over the years. Nield and Kuznetsov (2013) incorporated the Forchheimer drag terms in the extended Brinkman model for Bidisperse porous medium proposed by Nield and Kuznetsov (2005) and studied the hydrodynamic stability in a channel filled with Bidisperse porous material. Narasimhan *et.al* (2012) observed that using the BDPM approach **to** thermal management, the geometry**,** and the BDPM parameters can be used to achieve pressure drop in the channel. Ajay *et.al* (2013) made a comparison between the conventional porous medium and the BDPM and their role in the surface temperature of electronic chips. They concluded that there is a reduction in average surface temperature up to about 4.21K when th**e** BDPM heat sink is used. Capone and De Luca (2021) studied the instability of a vertical fluid motion, or throughflow, in a horizontal Bidisperse porous layer heated uniformly from below and concluded that there exist a reasonable agreement between the linear instability threshold and the global nonlinear stability threshold, in the energy norm. Grosan *et.al* (2023) presented a numerical investigation on the dependence of the stream functions, isotherms and the rate of heat transfer on convectively fluid flow in a differentially heated cavity filled by a Brinkman Bidisperse porous medium. Other interesting results on the utilization of BDPM can be found in Straughan (2019), Capone *et.al* (2021) and the excellent work by Vanengmawia and Ontela (2023).

This research aims to formulate and investigate the mathematical model for the pressure driven fluid flow through a concentric annulus filled with BDPM. The effects of the drag force at the inner surface and the outer surface of the outer and the inner cylinders respectively are also examined. It is clear from the earlier research conducted that one of the challenges associated with BDPM related problems is in the decoupling the complex differential equations. Accordingly, this paper employs the use of the D'Alembert method (Ziyaddin and Huseyin, 2007) to decouple the governing differential equations. The choice of this method is to systematically decouple the governing equations without altering their initial orders.

2.0 Mathematical Analysis

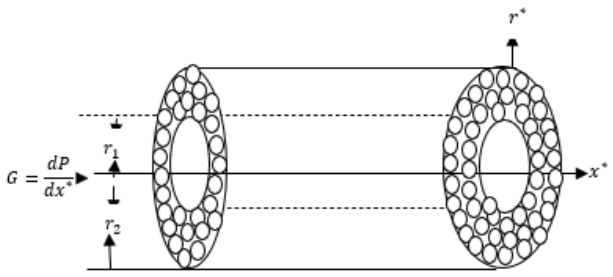

Figure 1a. The physical geometry of the problem

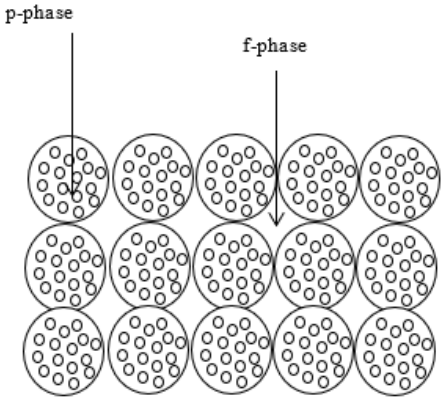

Figure 1b. Structural form of BDPM

The geometry of the problem being investigated are displayed in figures 1a and 1b. Assume a viscous, incompressible fluid contained between two horizontally oriented concentric cylinders filled with Bidisperse porous material. The $x^{'}$ −axis is taken along the axis of the concentric cylinders in the horizontal direction and the direction of the flowing fluid while $r^{'}$ is the radial coordinate.

The fluid velocities in the two phases result from the negative applied constant pressure gradient. Accordingly, following Nield and Kuznetsov (2005), the fluid velocities in both the fracture and porous phases of the Bidisperse porous medium contained in the annulus are described by a pair of coupled linear second-order differential equations:

$$G = \frac{\mu}{k_f} U_f^* + \zeta\left(U_f^* - U_P^*\right) - \bar{\mu}_f \frac{1}{r^*}\frac{d}{dr^*}\left(r^* \frac{dU_f^*}{dr^*}\right) \quad (1)$$

$$G = \frac{\mu}{k_p} U_P^* + \zeta(U_P^* - U_F^*) - \bar{\mu}_p \frac{1}{r^*}\frac{d}{dr^*}\left(r^* \frac{dU_P^*}{dr^*}\right) \quad (2)$$

Where $G = \frac{dP}{dx^*}$ represents the negative applied (constant) pressure gradient, k_f and k_p denote the permeabilities of the fracture and porous phases respectively, μ is the fluid viscosity, $\bar{\mu}_f$ and $\bar{\mu}_p$ are respectively the effective viscosities of the fluid in the fracture and porous phases. The quantity ζ is the dimensional coefficient of momentum transfer between the two phases. The selected boundary conditions consistent with the above model are given as:

$$\left.\begin{aligned} U_f^* &= U_P^* = 0 \ \ at\ r^* = r_1 \\ U_f^* &= U_P^* = 0\ at\ r^* = r_2 \end{aligned}\right\} \quad (3)$$

Where r_2 represents the radius of the outer cylinder and r_1 is the radius of the inner cylinder.

To simplify the set of equations (1) - (3), the following non-dimensional quantities are defined:

$R = \frac{r^*-r_1}{r_2-r_1}$, $\delta = \frac{r_1}{r_2}$, $Da_f = \frac{K_f}{(r_2-r_1)^2}$, $Da_p = \frac{K_p}{(r_2-r_1)^2}$, $\eta = \zeta\frac{(r_2-r_1)^2}{\mu}$, $U_f = \frac{U_f^*\mu}{(r_2-r_1)^2G}$

$U_p = \frac{U_p^*\mu}{(r_2-r_1)^2G}$, $\gamma_1 = \frac{\bar{\mu}_f}{\mu}$, $\gamma_2 = \frac{\bar{\mu}_p}{\mu}$ and by employing the transformation (Jha *et.al*, 2016),

$Z = R(1-\delta)+\delta$. So that the coupled equations (1) and (2) reduce to:

$$\frac{1}{Z}\frac{d}{dZ}\left(Z\frac{dU_f}{dZ}\right) - \frac{U_f}{Da_f(1-\delta)^2\gamma_1} - \frac{\eta(U_f-U_p)}{(1-\delta)^2\gamma_1} = -\frac{1}{(1-\delta)^2\gamma_1} \quad (4)$$

$$\frac{1}{Z}\frac{d}{dZ}\left(Z\frac{dU_p}{dZ}\right) - \frac{U_p}{Da_p(1-\delta)^2\gamma_2} - \frac{\eta(U_p-U_f)}{(1-\delta)^2\gamma_2} = -\frac{1}{(1-\delta)^2\gamma_2} \quad (5)$$

While the boundary constraints now assume the following form:

$$\left.\begin{aligned} U_f = U_p = 0 \ \ at \qquad Z = \delta \\ U_f = U_p = 0 = 0 \ at \quad Z = 1 \end{aligned}\right\} \quad (6)$$

2.1 General solutions for any arbitrary value of the coefficient of momentum transfer (η)

It is observed that the coupling together of U_f and U_p in the mathematical model (equations (4) and (5)) by the coefficient of momentum transfer (η) makes the exact solutions of the model very complex to obtain. To avoid raising the order of the governing equations if attempted to be solved by directly eliminating either of the velocities, a systematic procedure: the D'Alembert method is employed. This method enables the decoupling of the governing equations while still retaining their original (second) order.

Multiplying equation (4) by A and adding the result to equation (5) yields,

$$\frac{1}{Z}\frac{d}{dZ}\left[Z\frac{d}{dZ}\left(AU_f+U_p\right)\right] - U_f\left[\frac{A}{Da_p\gamma_1(1-\delta)^2} + \frac{\eta A}{\gamma_1(1-\delta)^2} - \frac{\eta}{\gamma_2(1-\delta)^2}\right] - U_p\left[\frac{1}{Da_p\gamma_2(1-\delta)^2} + \frac{\eta}{\gamma_2(1-\delta)^2} - \frac{\eta A}{\gamma_1(1-\delta)^2}\right] = -\frac{\gamma_1+A\gamma_2}{\gamma_1\gamma_2(1-\delta)^2} \quad (7)$$

The expressions for A and α^2 are given respectively by

$$A = \frac{Da_p\left(A\gamma_2+A\eta\gamma_2Da_f-\eta\gamma_1Da_f\right)}{Da_f\left(\gamma_1+\eta\gamma_1Da_p-\eta A\gamma_2Da_p\right)}, \quad (8a)$$

$$\alpha^2 = \frac{1}{(1-\delta)^2}\left[\frac{1}{Da_p\gamma_2} + \frac{\eta}{\gamma_2} - \frac{\eta A}{\gamma_1}\right] \quad (8b)$$

Equation (7) transformed into:

$$\frac{1}{Z}\frac{d}{dZ}\left[Z\frac{d}{dZ}\left(AU_f+U_p\right)\right] - \alpha^2\left(AU_f+U_p\right) = -\frac{\gamma_1+A\gamma_2}{\gamma_1\gamma_2(1-\delta)^2} \quad (9)$$

The general solution of equation (9) in terms of modified Bessel functions is obtained as:

$$AU_f + U_p = C_1I_0(Z\alpha) + C_2K_0(Z\alpha) + \frac{\gamma_1+A\gamma_2}{\alpha^2\gamma_1\gamma_2(1-\delta)^2} \quad (10)$$

Applying the boundary conditions, C_1 and C_2 (see Appendix) so that the particular solution of equation (10) becomes:

$$AU_f + U_p = \frac{\gamma_1+A\gamma_2}{\alpha^2\gamma_1\gamma_2(1-\delta)^2}\left[\frac{I_0(Z\alpha)(K_0(\alpha\delta)-K_0(\alpha))}{(I_0(\alpha\delta)K_0(\alpha)-K_0(\alpha\delta)I_0(\alpha))} + \frac{K_0(Z\alpha)(I_0(\alpha\delta)-I_0(\alpha))}{(K_0(\alpha\delta)I_0(\alpha)-I_0(\alpha\delta)K_0(\alpha))} + 1\right] \quad (11)$$

Solving equations (8a) and (8b) and making appropriate substitutions in equations (8b) and (11), the expressions for the fluid velocities in the fracture and porous phases are obtained as:

$$U_f = \frac{\gamma_1+A_1\gamma_2}{\alpha_1^2\gamma_1\gamma_2(1-\delta)^2(A_1-A_2)}\left[\frac{I_0(Z\alpha_1)(K_0(\alpha_1\delta)-K_0(\alpha_1))}{(I_0(\alpha_1\delta)K_0(\alpha_1)-K_0(\alpha_1\delta)I_0(\alpha_1))}+\frac{K_0(Z\alpha_1)(I_0(\alpha_1\delta)-I_0(\alpha_1))}{(K_0(\alpha_1\delta)I_0(\alpha_1)-I_0(\alpha_1\delta)K_0(\alpha_1))}+1\right]$$
$$-\frac{\gamma_1+A_2\gamma_2}{\alpha_2^2\gamma_1\gamma_2(1-\delta)^2(A_1-A_2)}\left[\frac{I_0(Z\alpha_2)(K_0(\alpha_2\delta)-K_0(\alpha_2))}{(I_0(\alpha_2\delta)K_0(\alpha_2)-K_0(\alpha_2\delta)I_0(\alpha_2))}+\frac{K_0(Z\alpha_2)(I_0(\alpha_2\delta)-I_0(\alpha_2))}{(K_0(\alpha_2\delta)I_0(\alpha_2)-I_0(\alpha_2\delta)K_0(\alpha_2))}+1\right] \quad (12)$$

and

$$U_p = \frac{A_1(\gamma_1+A_2\gamma_2)}{\alpha_2^2\gamma_1\gamma_2(1-\delta)^2(A_1-A_2)}\left[\frac{I_0(Z\alpha_2)(K_0(\alpha_2\delta)-K_0(\alpha_2))}{(I_0(\alpha_2\delta)K_0(\alpha_2)-K_0(\alpha_2\delta)I_0(\alpha_2))}+\frac{K_0(Z\alpha_2)(I_0(\alpha_2\delta)-I_0(\alpha_2))}{(K_0(\alpha_2\delta)I_0(\alpha_2)-I_0(\alpha_2\delta)K_0(\alpha_2))}+1\right]$$
$$-\frac{A_2(\gamma_1+A_1\gamma_2)}{\alpha_1^2\gamma_1\gamma_2(1-\delta)^2(A_1-A_2)}\left[\frac{I_0(Z\alpha_1)(K_0(\alpha_1\delta)-K_0(\alpha_1))}{(I_0(\alpha_1\delta)K_0(\alpha_1)-K_0(\alpha_1\delta)I_0(\alpha_1))}+\frac{K_0(Z\alpha_1)(I_0(\alpha_1\delta)-I_0(\alpha_1))}{(K_0(\alpha_1\delta)I_0(\alpha_1)-I_0(\alpha_1\delta)K_0(\alpha_1))}+1\right] \quad (13)$$

The roots A_1, A_2 and α_1, $\alpha_2$obtained from equations (8a) and (8b) respectively are defined in the Appendix.

2.2 Special cases: Extreme values of the coefficient of momentum transfer (η)

The complexity of obtaining an exact solution for the mathematical model can be traced to the parameter (η) that couples the fluid velocities in the two phases. It is interesting to note that the parameter η not only couples the velocities of the fracture and the porous phases together but also, according to Nield and Kuznetsov (2011), modifies the permeabilities k_f and k_p of the fracture and the porous phases respectively. Thus, a detailed analysis of the extreme values of η is worthwhile.

2.2.1 Weak Coupling $(\eta \to 0)$

If $\eta \to 0$ resulting to a weak coupling, equations (4) and (5) are reduced to two distinct equations of the same form.

$$\frac{1}{Z}\frac{d}{dZ}\left(Z\frac{dU_f}{dZ}\right)-a_1^2U_f=\frac{1}{(1-\delta)^2\gamma_1} \quad (14)$$

$$\frac{1}{Z}\frac{d}{dZ}\left(Z\frac{dU_p}{dZ}\right)-a_2^2U_p=\frac{1}{(1-\delta)^2\gamma_2} \quad (15)$$

Solving these equations and using equation (6), the exact solutions are obtained as:

$$U_f(Z)=\frac{Da_f(K_0(a_1\delta)-K_0(a_1))I_0(a_1Z)}{(I_0(a_1\delta)K_0(a_1)-K_0(a_1\delta)I_0(a_1))}+\frac{Da_f(I_0(a_1\delta)-I_0(a_1))K_0(a_1Z)}{(K_0(a_1\delta)I_0(a_1)-I_0(a_1\delta)K_0(a_1))}+Da_f \quad (16)$$

$$U_P(Z)=\frac{Da_P(K_0(a_2\delta)-K_0(a_2))I_0(a_2Z)}{(I_0(a_2\delta)K_0(a_2)-K_0(a_2\delta)I_0(a_2))}+\frac{Da_P(I_0(a_2\delta)-I_0(a_2))K_0(a_2Z)}{(K_0(a_2\delta)I_0(a_2)-I_0(a_2\delta)K_0(a_2))}+Da_P \quad (17)$$

Where a_1 and a_2 are defined in the Appendix

2.2.2 Strong Coupling $(\eta \to \infty)$

If $\eta \to \infty$, to the order η^{-1}, then $U_f(Z)=U_p(Z)=U(Z)$ a strong coupling is obtained. Thus equations (4) and (5) reduced to:

$$\frac{1}{\eta}\frac{1}{Z}\frac{d}{dZ}\left(Z\frac{dU}{dZ}\right)-\frac{U}{\eta\gamma_1Da_f(1-\delta)^2}=-\frac{1}{\eta\gamma_1(1-\delta)^2} \quad (18)$$

$$\frac{1}{\eta}\frac{1}{Z}\frac{d}{dZ}\left(Z\frac{dU}{dZ}\right)-\frac{U}{\eta\gamma_2 Da_p(1-\delta)^2}=-\frac{1}{\eta\gamma_2(1-\delta)^2} \quad (19)$$

Adding equations (18) and (19) and simplifying the resulting equation yields:

$$\frac{1}{Z}\frac{d}{dZ}\left(Z\frac{dU}{dZ}\right)-a_3^2U=-\frac{\gamma_1+\gamma_2}{2(\gamma_1+\gamma_2)(1-\delta)^2} \quad (20)$$

Solving equation (20) under the boundary conditions (6), the expression of the fluid velocity for the strong coupling is obtained:

$$U(Z)=\frac{Da_p\,Da_f(\gamma_1+\gamma_2)}{\gamma_1 Da_f+\gamma_2 Da_p}\left[\frac{(K_0(a_3)-K_0(a_3\delta))I_0(a_3Z)}{(K_0(a_3\delta)I_0(a_3)-I_0(a_3\delta)K_0(a_3))}+\frac{(I_0(a_3\delta)-I_0(a_3))K_0(a_3Z)}{(K_0(a_3\delta)I_0(a_3)-I_0(a_3\delta)K_0(a_3))}+1\right] \quad (21)$$

Where the expression for a_3 is given in the Appendix

2.3 Skin friction

The expressions for the dimensionless skin frictions on the outer and the inner surfaces of the two cylinders (τ_1) and (τ_δ) respectively for the two phases of the BDPM are derived and presented as follows:

$$\frac{dU_f}{dZ}\Big|_{Z=1}=\tau_1=\frac{(\gamma_1+A_1\gamma_2)}{\alpha_1\gamma_1\gamma_2(1-\delta)^2(A_1-A_2)}\left[\frac{I_1(\alpha_1)(K_0(\alpha_1\delta)-K_0(\alpha_1))}{(I_0(\alpha_1\delta)K_0(\alpha_1)-K_0(\alpha_1\delta)I_0(\alpha_1))}-\frac{K_1(\alpha_1)(I_0(\alpha_1\delta)-I_0(\alpha_1))}{(K_0(\alpha_1\delta)I_0(\alpha_1)-I_0(\alpha_1\delta)K_0(\alpha_1))}\right]-$$
$$\frac{(\gamma_1+A_2\gamma_2)}{\alpha_2\gamma_1\gamma_2(1-\delta)^2(A_1-A_2)}\left[\frac{I_1(\alpha_2)(K_0(\alpha_2\delta)-K_0(\alpha_2))}{(I_0(\alpha_2\delta)K_0(\alpha_2)-K_0(\alpha_2\delta)I_0(\alpha_2))}-\frac{K_1(\alpha_2)(I_0(\alpha_2\delta)-I_0(\alpha_2))}{(K_0(\alpha_2\delta)I_0(\alpha_2)-I_0(\alpha_2\delta)K_0(\alpha_2))}\right] \quad (22)$$

$$\frac{dU_f}{dZ}\Big|_{Z=\delta}=\tau_\delta=\frac{(\gamma_1+A_1\gamma_2)}{\alpha_1\gamma_1\gamma_2(1-\delta)^2(A_1-A_2)}\left[\frac{I_1(\delta\alpha_1)(K_0(\alpha_1\delta)-K_0(\alpha_1))}{(I_0(\alpha_1\delta)K_0(\alpha_1)-K_0(\alpha_1\delta)I_0(\alpha_1))}-\frac{K_1(\delta\alpha_1)(I_0(\alpha_1\delta)-I_0(\alpha_1))}{(K_0(\alpha_1\delta)I_0(\alpha_1)-I_0(\alpha_1\delta)K_0(\alpha_1))}\right]-$$
$$\frac{(\gamma_1+A_2\gamma_2)}{\alpha_2\gamma_1\gamma_2(1-\delta)^2(A_1-A_2)}\left[\frac{I_1(\delta\alpha_2)(K_0(\alpha_2\delta)-K_0(\alpha_2))}{(I_0(\alpha_2\delta)K_0(\alpha_2)-K_0(\alpha_2\delta)I_0(\alpha_2))}-\frac{K_1(\delta\alpha_2)(I_0(\alpha_2\delta)-I_0(\alpha_2))}{(K_0(\alpha_2\delta)I_0(\alpha_2)-I_0(\alpha_2\delta)K_0(\alpha_2))}\right] \quad (23)$$

$$\frac{dU_p}{dZ}\Big|_{Z=1}=\tau_1=\frac{A_1(\gamma_1+A_2\gamma_2)}{\alpha_2\gamma_1\gamma_2(1-\delta)^2(A_1-A_2)}\left[\frac{I_1(\alpha_2)(K_0(\alpha_2\delta)-K_0(\alpha_2))}{(I_0(\alpha_2\delta)K_0(\alpha_2)-K_0(\alpha_2\delta)I_0(\alpha_2))}-\frac{K_1(\alpha_2)(I_0(\alpha_2\delta)-I_0(\alpha_2))}{(K_0(\alpha_2\delta)I_0(\alpha_2)-I_0(\alpha_2\delta)K_0(\alpha_2))}\right]$$
$$-\frac{\alpha_1A_2(\gamma_1+A_1\gamma_2)}{\alpha_1^2\gamma_1\gamma_2(1-\delta)^2(A_1-A_2)}\left[\frac{I_1(\alpha_1)(K_0(\alpha_1\delta)-K_0(\alpha_1))}{(I_0(\alpha_1\delta)K_0(\alpha_1)-K_0(\alpha_1\delta)I_0(\alpha_1))}-\frac{K_1(\alpha_1)(I_0(\alpha_1\delta)-I_0(\alpha_1))}{(K_0(\alpha_1\delta)I_0(\alpha_1)-I_0(\alpha_1\delta)K_0(\alpha_1))}\right] \quad (24)$$

$$\frac{dU_p}{dZ}\Big|_{Z=\delta}=\tau_\delta=\frac{A_1(\gamma_1+A_2\gamma_2)}{\alpha_2\gamma_1\gamma_2(1-\delta)^2(A_1-A_2)}\left[\frac{I_1(\delta\alpha_2)(K_0(\alpha_2\delta)-K_0(\alpha_2))}{(I_0(\alpha_2\delta)K_0(\alpha_2)-K_0(\alpha_2\delta)I_0(\alpha_2))}-\frac{K_1(\delta\alpha_2)(I_0(\alpha_2\delta)-I_0(\alpha_2))}{(K_0(\alpha_2\delta)I_0(\alpha_2)-I_0(\alpha_2\delta)K_0(\alpha_2))}\right]$$
$$-\frac{A_2(\gamma_1+A_1\gamma_2)}{\alpha_1\gamma_1\gamma_2(1-\delta)^2(A_1-A_2)}\left[\frac{I_1(\delta\alpha_1)(K_0(\alpha_1\delta)-K_0(\alpha_1))}{(I_0(\alpha_1\delta)K_0(\alpha_1)-K_0(\alpha_1\delta)I_0(\alpha_1))}-\frac{K_1(\delta\alpha_1)(I_0(\alpha_1\delta)-I_0(\alpha_1))}{(K_0(\alpha_1\delta)I_0(\alpha_1)-I_0(\alpha_1\delta)K_0(\alpha_1))}\right] \quad (25)$$

3.0 Results and Discussion

In this section, a detailed analysis of the mathematical model, the role of the coefficient of momentum transfer**,** as well as the influence of the other controlling parameters on the constant pressure-driven fluid flow in a horizontal annulus filled with Bidisperse porous medium are presented. We assume that $\gamma_1=\gamma_2=1.0$ and also use the following values: $Da_f=0.1$, $Da_p=0.009$ and $\eta=2.0$ (or $\eta=0.0$ and $\eta=\rightarrow\infty$ for weak and strong coupling respectively).

Figures 2(a, b)-4(a, b) represent the velocity profiles in the two phases for any arbitrary value of the coefficient of momentum transfer (η) while figures 5(a, b)-6(a, b) and figures 7-8 represent the velocity profiles for weak and strong coupling respectively.

The effect of the applied pressure gradient which results in the high velocity of the fluid in the two phases is observed to be more pronounced when the ratio of the radii is small($\delta = 0.2$) as depicted in figures 2(a, b)-8(a, b). Also, it is found from these figures that the maximum velocity attained by the fluid is close to the region $R = 0.5$ of the concentric cylinder irrespective of the value of the coupling parameter (η). The numerical value of the maximum velocity attained however varies with the value of η with the minimum value reached when η is large (figure 2(a, b)).

Furthermore, it is also noticed from the relation $\eta = \zeta \frac{(r_2 - r_1)^2}{\mu}$ that the coefficient of momentum transfer is not dependent on the nature of the porous medium and if the region containing the fluid is kept constant, η is primarily a function of the fluid viscosity(μ), (see Nield and Kuznetsov, 2011). Thus decreasing the fluid viscosity μ, increases the coefficient of the momentum transfer η which then hinders the fluid velocities in both the f-phase and the p-phase of the BDPM (see 2(a, b)).

Figure 3(a) and 3(b) demonstrate the effect of the ratio of viscosities γ_1 and γ_2 on the fluid velocities in the porous and fracture phases of the BDPM respectively. It is observed from the figures that if the ratios $\frac{\bar{\mu}_f}{\mu}$ and $\frac{\bar{\mu}_p}{\mu}$ of the fluid in fracture and porous phases respectively are increased, the fluid resistance to motion is increased resulting in the fluid velocity in both phases of the BDPM being decreased. Physically, this is because increasing the fluid viscosity enhances the friction between the fluid layers thereby suppressing the fluid velocities in the two phases of the BDPM. It is also worth noting that this trend exhibited by the variation of the ratio of viscosities is similarly demonstrated in figures 6(a, b) and figure 8 for $\eta \to 0$ and $\eta \to \infty$ respectively.

Velocity distributions in the porous and fracture phase resulting from the variation of the measure of permeabilities (Da_f and Da_p) are displayed in figure 4(a, b) for any arbitrary value of η, figure 5(a, b) when $\eta = 0$ and figure 7 if $\eta \to \infty$. It is found that the stability of the fluid flow is attained even before the maximum velocity is reached. This trend is seen by the flatness of the velocity profiles as the measure of permeabilities of the two phases are decreased. This property exhibited by the fluid velocity emanating from the variation of the Darcy numbers, has been observed and discussed by Nield and Kuznetsov (2013) and also by Magyari (2013). From these two works and the present research, it suffices to claim that this fluid property is not influenced by the geometry of the transport medium.

Figures 9(a, b) - 11(a, b) depict the influence of the controlling parameters on the frictional (drag) force at the fluid-solid surface region for both the porous and fracture phases. A close observation of the figures revealed that for the selected values of η, γ_1, γ_2, Da_f and Da_p, the skin friction is found to be higher at the outer surface of the inner cylinder and increases with the increase in the ratio of the radii (δ) of the two cylinders. In particular, figures 9(a, b) and 10.0(a, b) show that the skin friction decreases with an increase in the coefficient of momentum transfer (η) as well as the ratio of viscosity; (γ_1 and γ_2) respectively on both surfaces of the annulus. It is also interestingly observed that at the inner surface of the outer cylinder of the fracture phase, the effect of η on the skin friction becomes less significant with an increase in η. On the other hand, figures 11a and 11b demonstrate the influence of Da_f and Da_p on the skin friction. From the figures, the skin friction is found to be increasing with an increase in the measure of the permeabilities of the two phases of the BDPM.

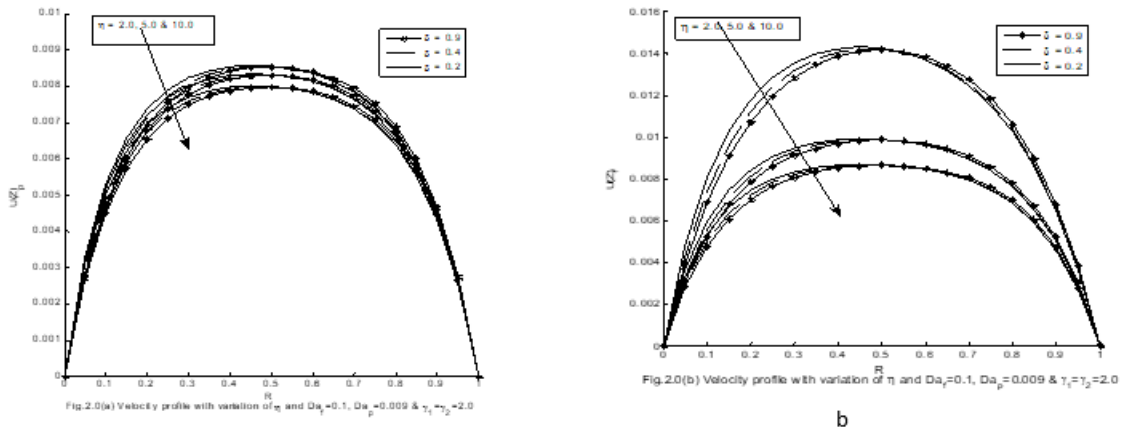

Fig.2.0(a) Velocity profile with variation of η and Da_f=0.1, Da_p=0.009 & γ_1=γ_2=2.0

a

Fig.2.0(b) Velocity profile with variation of η and Da_f=0.1, Da_p=0.009 & γ_1=γ_2=2.0

b

Figure 2. Velocity profile for the variation of η and with $Da_f = 0.1$, $Da_p = 0.009$ and $\gamma_1 = \gamma_2 = 2.0$

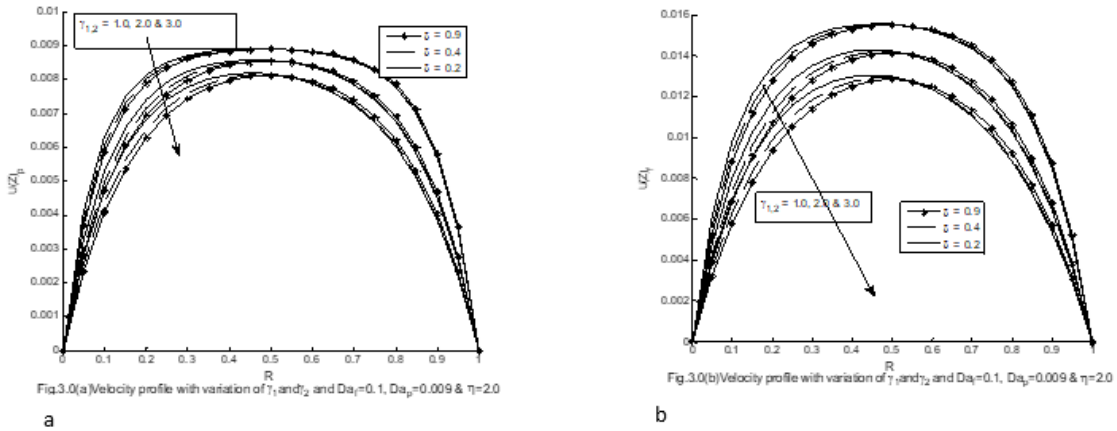

Fig.3.0(a)Velocity profile with variation of γ_1 andγ_2 and Da_f=0.1, Da_p=0.009 & η=2.0

a

Fig.3.0(b)Velocity profile with variation of $\gamma_1$andγ_2 and Da_f=0.1, Da_p=0.009 & η=2.0

b

Figure 3. Velocity profile for the variation of $\gamma_1 = \gamma_2$ and with $Da_f = 0.1$, $Da_p = 0.009$ and $\eta = 2.0$

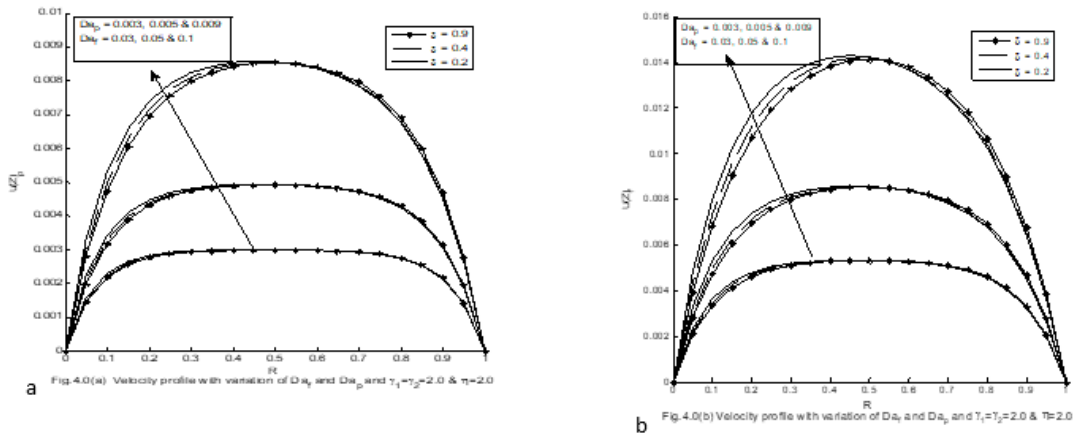

Figure 4. Velocity profile for the variations of Da_f , Da_p and with $\gamma_1 = \gamma_2 = 2.0$

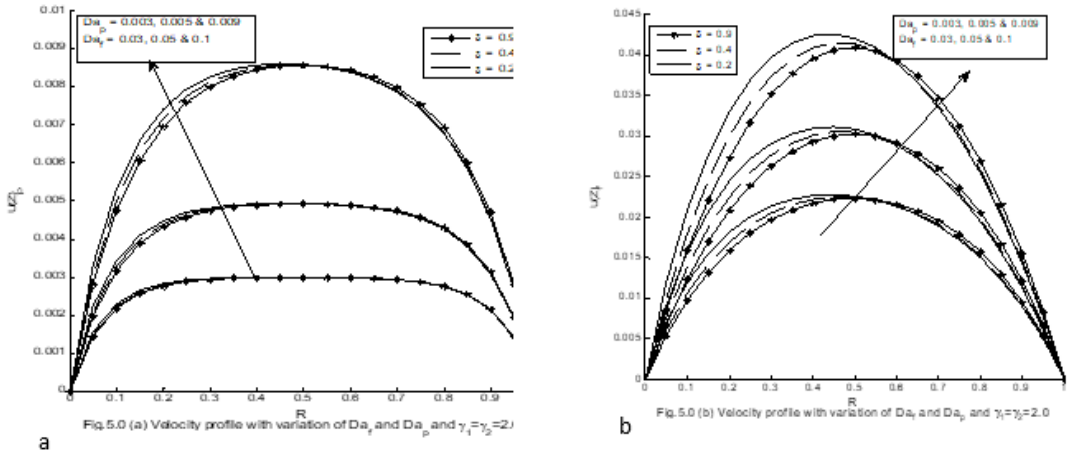

Figure 5. Velocity profile for the variations of Da_f, Da_p and with $\gamma_1 = \gamma_2 = 2.0$

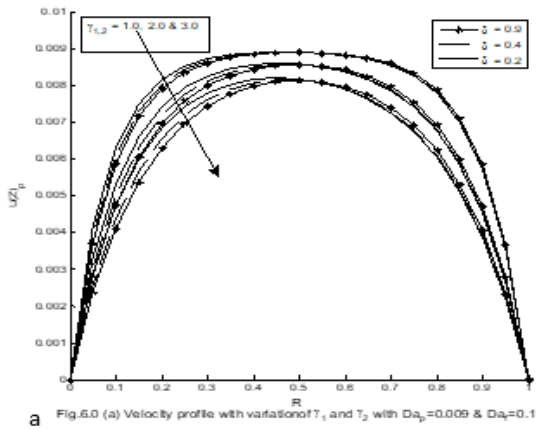

a Fig.6.0 (a) Velocity profile with variationof γ_1 and γ_2 with Da_p=0.009 & Da_f=0.1

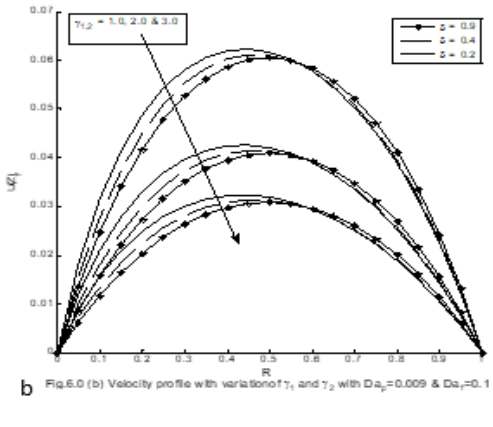

b Fig.6.0 (b) Velocity profile with variationof γ_1 and γ_2 with Da_p=0.009 & Da_f=0.1

Figure 6. Velocity profile for the variation of γ_1 and γ_2 and with $Da_f = 0.1$ and $Da_p = 0.009$

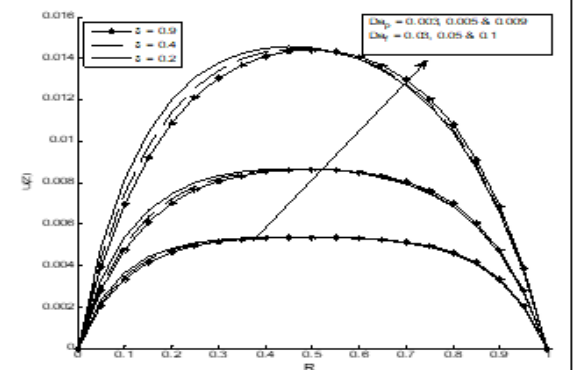

Fig. 7 Velocity profile for some values of Da_f and Da_p and γ_1=2, γ_2=2, & δ=0.4

Figure 7. Velocity profile for the variation of Da_f and Da_p and with

$\gamma_1 = \gamma_2 = 2.0$

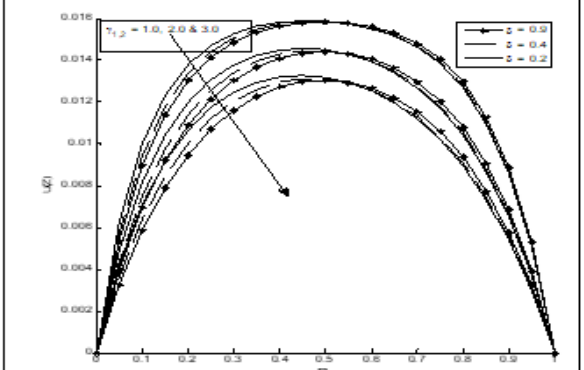

Fig.8.0 Velocity profile with variation of γ_1 andγ_2 and Da_f=0.08, Da_p=0.007 & δ=0.4

Figure 8. Velocity profile for the variation of γ_1 and γ_2

$Da_f = 0.08$ and Da_p0.007

$\gamma_1 = \gamma_2 = 2.0$ and $\delta = 0.4$

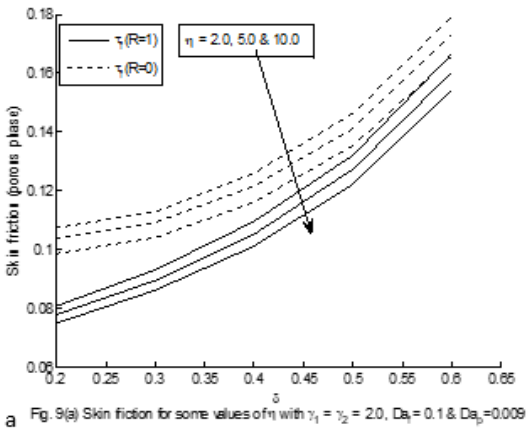

a Fig. 9(a) Skin friction for some values of η with $\gamma_1 = \gamma_2 = 2.0$, $Da_f = 0.1$ & $Da_p = 0.009$

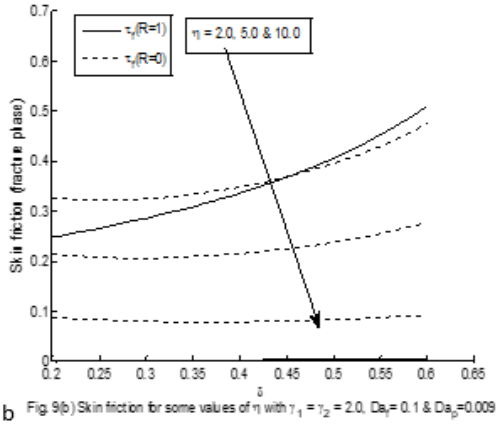

b Fig. 9(b) Skin friction for some values of η with $\gamma_1 = \gamma_2 = 2.0$, $Da_f = 0.1$ & $Da_p = 0.009$

Figure 9. Skin friction for some values of η with $\gamma_1 = \gamma_2 = 2.0$, $Da_f = 0.1$ and

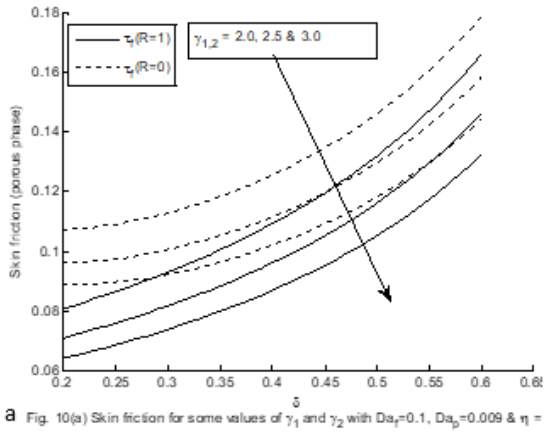

a Fig. 10(a) Skin friction for some values of γ_1 and γ_2 with $Da_f = 0.1$, $Da_p = 0.009$ & η =

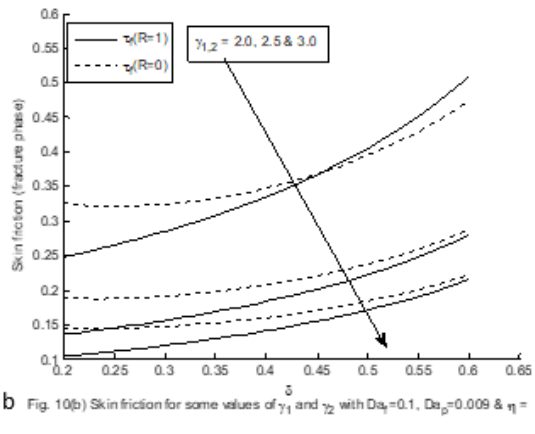

b Fig. 10(b) Skin friction for some values of γ_1 and γ_2 with $Da_f = 0.1$, $Da_p = 0.009$ & η =

Figure 10. Skin friction for some values of γ_1 and γ_2, $Da_f = 0.1$ and $Da_p = 0.009$ and $n = 2.0$

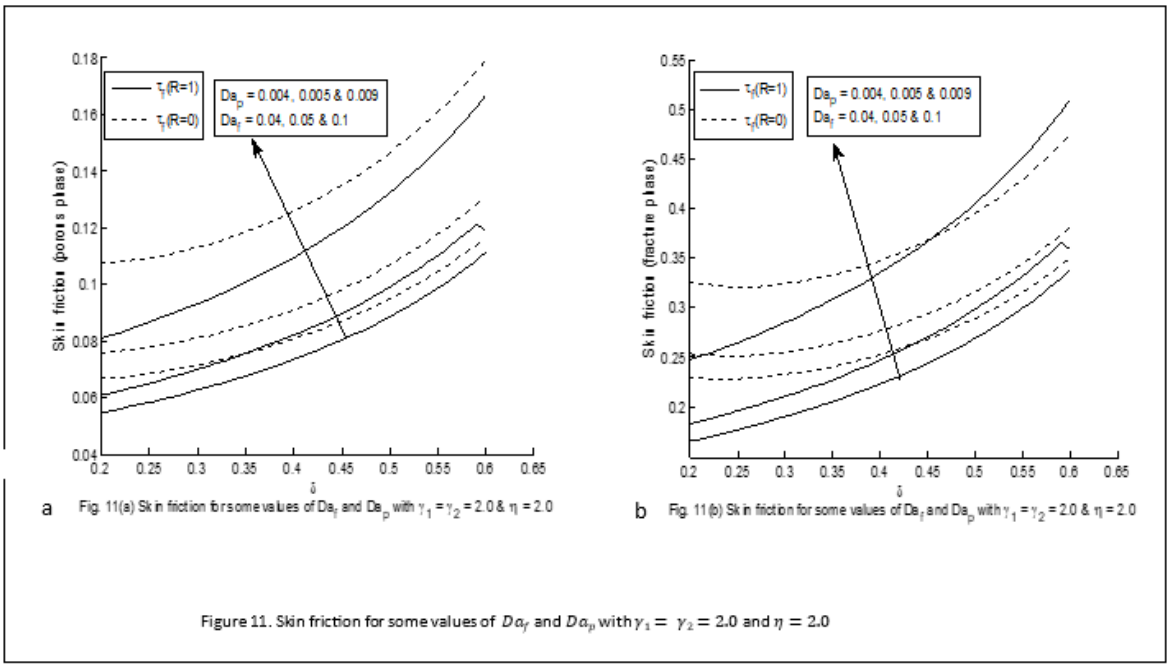

Figure 11. Skin friction for some values of Da_f and Da_p with $\gamma_1 = \gamma_2 = 2.0$ and $\eta = 2.0$

4.0 Conclusions

We have presented an analytical analysis for a pressure-driven flow in an infinitely long and horizontally oriented concentric cylinder filled with Bidisperse porous material. The fluid velocities $(U_f$ and $U_p)$in the fracture and porous phases of the BDPM are coupled to each other by the coefficient of momentum transfer (η). The D'Alembert method is used to decouple the couple governing equations without altering their initial orders. The expressions of the velocities as well as the expressions for skin friction in the two phases are obtained in terms of modified Bessel functions. It is inferred from the numerical simulation conducted that the increase of the coefficient of momentum transfer (η) as well as the ratio of viscosities (γ_1 and γ_2) exhibit a suppressive effect on the fluid velocities in the two phases of the BDPM. The research also indicates that the stability of the fluid flow resulting from the decrease in the permeabilities of the BDPM is reached even before the maximum momentum of the fluid flow is attained confirming the earlier findings by Nield and Kuznetsov (2013) and also by Magyari (2013). Furthermore, it is deduced that the skin friction increases with an increase in the coefficient of momentum transfer (η) on both surfaces of the fracture phase for the selected values of Da_f, Da_p, γ_1 and γ_2.

References

Ajay, K.P.V., Giranchandran, A.C. and Kamath, P. M. (2013). A numerical investigation to improve Heat Transfer using Bi-disperse Porous Heat Sink. *Int. J. Tech. Eng. Sci*., 1(5), 445-453.

Jha, B. K., Aina, B., Isa, S. (2016). MHD natural convection flow in a vertical micro-concentric-annuli in the presence of radial magnetic field: An exact solution. *Ain Shams Engineering Journal*, 6, 1061 – 1068.

Capone, F., and De Luca, R. (2012). Instability of vertical throughflow in Bidisperse porous media, *Physics*, *3*(4), 821-828.

Capone, F., Gentile, M., and Massa, G. (2021). The onset of thermal convection in anisotropic and rotating Bidisperse porous media. *Z. Angew Math. Phys*., 72 (169), 1-16. https://doi.org/10.1007/s00033-021-01592-w

Das, M. K., Mukherjee, P. P. and Muralidhar, K. (2018). Porous Media Applications: Biological Systems. In: Modeling Transport Phenomena in Porous Media with Applications. *Mechanical Engineering Series. Springer, Cham*. 123–15. https://doi.org/10.1007/978-3-319-69866-3_5

Grosan, T., Patrulescu F-O., and Pop, L. (2023). Natural convection in a differentially heated cavity filled with a Brinkman Bidisperse porous medium. *Int. Journal of numerical methods for heat and fluid flow*. 33 (10), 3309-3326.

Khanafer, K. Vafai, K. (2022). Applications of porous media in biological transport modeling, Modeling of Mass Transport Processes in Biological Media. *Academic Press*.1-15. https://doi.org/10.1016/B978-0-323-85740-6.00014-5

Khaled, A.R.A. and Vafia, K. (2003). The role of porous media in modeling flow and heat transfer in biological tissues. *International Journal of Heat and Mass Transfer.* 46, 4989–5003.

Magyari, E. (2013). Normal Mode Analysis of high speed channel flow in a Bidisperse porous media. *Transport Porous Media*. 97, 345-352.

Nield, D. A. and Kuznetsov, A.V. (2005). A two velocity two temperature model for a Bidisperse porous medium: forced convection in a channel. *Transport porous medium*. 59, 325-339.

Nield, D. A. and Kuznetsov, A. V. (2011). Forced convection in a channel partly occupied in a Bidisperse porous medium: symmetric case. *ASME Jr. of heat transfer*. 133, 072601.1-072601.9.

Narasimhan, A., Reddy, B.V.K. and Dutta, P. (2012). Thermal management using the Bi-disperse Porous Medium Approach. *Int. J. Heat Mass Transfer*. 55(4), 538-546.

Nield, D. A. and Kuznetsov, A.V. (2013). A note on modeling high speed flow in a Bidisperse porous medium. *Transport porous medium.* 96, 496-499.

Straughan, B. (2019). Anisotropic Bidisperse convection. *Proceedings A*. 1-18.

Vafai, K. (2005). Handbook of porous media. *Taylor & Francis Group, LLC (2nd Ed)*.

Vanengmawia, P. C., and Ontela, S. (2023). Magnetohydrodynamic forced convection in Bidisperse porous medium: Analysis of flow and temperature distributions in a parallel-plate channel. *Heat Transfer*, *53*(1), 16-43.

Ziyaddin, R., and Huseyin, K. (2007). Two-phase steady flow along a horizontal glass pipe in the presence of the magnetic and electrical fields. *Int. Journal of heat and fluid flow*. 29, 263-268.

5.0 Appendix

Nomenclature

G applied constant pressure gradient

k_f permeability of the fracture phase

k_p permeability porous phases

μ fluid viscosity

$\bar{\mu}_f$ effective viscosity of the fluid in the fracture

$\bar{\mu}_p$ effective viscosity of the fluid in the porous phase.

r' dimensional radial coordinate

R dimensionless radial coordinate

ζ dimensional coefficient of momentum transfer between fracture and the porous phases

η dimensionless coefficient of momentum transfer between fracture and the porous phases

r_1 radius of the outer cylinder

r_2 radius of the inner cylinder.

U_f dimensionless velocity in the fracture phase

U_p dimensionless velocity in the porous phase

U_f' dimensional velocity in the fracture phase

U_p' dimensional velocity in the porous phase

Da_f Darcy number of the fracture phase

Da_p Darcy number of the porous phase

γ_1 ratio of viscosities of the fracture phases

γ_2 ratio of viscosities of the porous phases

δ ratio of the radii of the outer and inner cylinders

Constant and expressions used

$$a_1 = \frac{1}{(1-\delta)\sqrt{\gamma_1 Da_f}}, a_2 = \frac{1}{(1-\delta)\sqrt{\gamma_2 Da_p}}, a_3 = \frac{1}{(1-\delta)}\sqrt{\frac{\gamma_1 Da_f + \gamma_2 Da_p}{2\gamma_1\gamma_2 Da_f Da_p}}$$

$$C_1 = \frac{(\gamma_1 + A\gamma_2)(K_0(\alpha\delta) - K_0(\alpha))}{\alpha^2\gamma_1\gamma_2(1-\delta)^2\left(I_0(\alpha\delta)K_0(\alpha) - K_0(\alpha\delta)I_0(\alpha)\right)}, C_2 = \frac{(\gamma_1 + A\gamma_2)(I_0(\alpha\delta) - I_0(\alpha))}{\alpha^2\gamma_1\gamma_2(1-\delta)^2\left(K_0(\alpha\delta)I_0(\alpha) - I_0(\alpha\delta)K_0(\alpha)\right)},$$

$$A_1 = -\frac{1}{2}\left(\frac{\gamma_2 Da_p - \gamma_1 Da_f}{\eta\gamma_2 Da_f Da_p} + \frac{\gamma_2 - \gamma_1}{\gamma_2}\right) + \frac{1}{2}\sqrt{\left(\frac{\gamma_2 Da_p - \gamma_1 Da_f}{\eta\gamma_2 Da_f Da_p} + \frac{\gamma_2 - \gamma_1}{\gamma_2}\right)^2 + \frac{4\gamma_1}{\gamma_2}}$$

$$A_2 = -\left(\frac{1}{2}\left(\frac{\gamma_2 Da_p - \gamma_1 Da_f}{\eta\gamma_2 Da_f Da_p} + \frac{\gamma_2 - \gamma_1}{\gamma_2}\right) + \frac{1}{2}\sqrt{\left(\frac{\gamma_2 Da_p - \gamma_1 Da_f}{\eta\gamma_2 Da_f Da_p} + \frac{\gamma_2 - \gamma_1}{\gamma_2}\right)^2 + \frac{4\gamma_1}{\gamma_2}}\right)$$

$$\alpha_1 = \frac{1}{1-\delta}\sqrt{\frac{1}{Da_p\gamma_2} + \frac{\eta}{\gamma_2} - \frac{\eta A_1}{\gamma_1}}, \alpha_2 = -\frac{1}{1-\delta}\sqrt{\frac{1}{Da_p\gamma_2} + \frac{\eta}{\gamma_2} - \frac{\eta A_2}{\gamma_1}}$$

Numerical Solutions of Higher Order Differential Equations via New Iterative Method

Khadeejah James Audu

Department of Mathematics, Federal University of Technology, Minna, Niger State, Nigeria.

email: k.james@futminna.edu.ng

Abstract

Higher order differential equations play a fundamental role in various scientific and engineering disciplines, but their numerical solutions often pose formidable challenges. The New Iterative Method (NIM) has emerged as a promising technique for addressing these challenges. This study is to explore and assess the efficiency and accuracy of New Iterative Method in solving higher-order differential equations. By applying NIM to a range of problems from diverse scientific disciplines, we aim to provide insights into the method's adaptability and its potential to revolutionize numerical analysis. The method is well-suited for numerically integrating both and nonlinear higher-order differential equations. To showcase the efficiency and accuracy of this approach, some numerical tests have been conducted, comparing it to existing methods. The numerical results obtained from these tests strongly suggest that the new iterative scheme outperforms the previously employed method in estimating higher-order problems, thus confirming its convergence.

Keywords: New Iterative Method, Higher Order Differential Equations, Numerical Solutions, Iterative Techniques, Computational Research.

1. Introduction

Differential equations stand out as crucial mathematical instruments employed to construct models across a diverse range of disciplines, including the sciences, engineering, economics, mathematics, physics, aeronautics, astronomy, dynamics, biology, chemistry, medicine, environmental sciences, social sciences, banking, and various other fields [1]. The general expression for nth order differential equations can be formulated as follows:

$$\frac{d^r Z(t)}{dt^r} = f\left(t, Z, \frac{dZ}{dt}, \frac{d^2Z}{dt^2}, \frac{d^3Z}{dt^3}, \frac{d^4Z}{dt^4}, ..., \frac{d^{r-1}y}{dt^{r-1}}\right) \quad r > 1$$

with initial conditions define as

$$Z(t_0) = \alpha,\ Z'(t_0) = \beta\ Z''(t_0) = \gamma, \cdots Z^{(r-1)}(t_0) = \rho$$

Higher order differential equations play a crucial role in modeling complex physical phenomena across various scientific disciplines. While analytical solutions exist for some well-defined cases, many real-world problems demand the application of numerical methods. In recent years, there has been a growing interest in the development of innovative numerical techniques to solve higher order differential equations accurately and efficiently.

Despite numerous numerical methods for higher order differential equations, many face limitations in terms of convergence and computational efficiency. This study stands out by refining an existing iterative method, addressing these limitations. Through modifications, the research enhances the method's performance, offering a more effective tool for accurately solving complex mathematical models encountered in various scientific and engineering domains. This study focuses on improving the efficiency and accuracy of solving higher order differential equations. It investigates the limitations of an existing iterative method, proposes modifications to enhance convergence and computational efficiency, and validates the refined method through comparative analysis with established numerical techniques. The aim is to provide a more effective tool for accurately solving complex mathematical models encountered in various scientific and engineering domains.

Previous research efforts have explored various methods for tackling the numerical solution of higher-order differential equations. Researchers have delved into alternative approaches, demonstrating a rich landscape of techniques aimed at enhancing accuracy, efficiency, and versatility in solving these complex mathematical problems (Falade *et al*. 2022; Tiamiyu *et al*., 2021b; Audu *et al*., 2022). While numerous researchers have delved into alternative methods for solving higher-order differential equations, it is noteworthy that the New Iterative Method (NIM) has not been extensively applied to this specific domain. This study aims to fill this gap by directing attention to the application of NIM in the numerical solution of higher-order differential equations. By exploring this uncharted territory, the research seeks to contribute fresh insights and perspectives to the ongoing discourse on efficient and accurate numerical methods for higher-order differentials. The initial section of this paper is covered in section one, with the second section focusing on describing the employed scheme, and the presentation of its convergence analysis is found in the third section. The implementation of the NIM scheme's convergence is demonstrated through numerical experiments in section four, while the conclusion of the research work is outlined in section five.

2. Description of the New Iterative Method (NIM)

Daftardar-Gejji and Jafari (2006) introduced the NIM approach that proves to be effective in addressing both linear and nonlinear functional differential equations. This method is particularly advantageous in the realm of nonlinear problems, where linearization or small perturbation may not be applicable. The NIM is characterized by its simplicity and ease of implementation, providing results that exhibit strong agreement with other methods and often requiring only a few iterations (Ali *et al*., 2022; Batiha *et al*., 2023; Audu *et al*., 2023). The formulation of the new iterative approach is articulated as follows:

Contemplate the subsequent generic functional equation

$$Z = F + L(z) + N(z) \tag{1}$$

where L, N are linear and nonlinear operators respectively, and f is a given function. The solution of equation (1) has the form

$$z = \sum_{p=0}^{\infty} z_p \tag{2}$$

Now, suppose we have the relation in (3)

$$\begin{aligned} Z_0 &= N(z_0) = f \\ Z_p &= N\left(\sum_{p=0}^{n} z_p\right) - N\left(\sum_{p=0}^{n-1} z_p\right) \end{aligned} \tag{3}$$

Then we can easily get

$$\begin{aligned} R_0 &= N(z_0) \\ R_1 &= N(z_0 + z_1) - N(z_0) \\ R_2 &= N(z_0 + z_1 + z_2) - N(z_0 + z_1) \\ R_3 &= N(z_0 + z_1 + z_2 + z_3) - N(z_0 + z_1 + z_2) + \cdots. \end{aligned} \tag{4}$$

Such that $N(z)$ can be splitted as:

$$\begin{aligned} N\left(\sum_{p=0}^{m} z_p\right) &= N(z_0 + z_1) - N(z_0) + N(z_0 + z_1 + z_2) - N(z_0 + z_1) \\ &+ N(z_0 + z_1 + z_2 + z_3) - N(z_0 + z_1 + z_2) + \cdots. \end{aligned} \tag{5}$$

To obtain a recurrence relation of the form:

$$\begin{aligned} z_0 &= f \\ z_1 &= L(z_0) + R_0 \\ z_{p+1} &= L(z_p) + R_p \qquad p = 1, 2, 3\cdots. \end{aligned} \tag{6}$$

Since L is linear, then

$$\sum_{p=0}^{n} L(z_p) = L\left(\sum_{p=0}^{n} z_p\right) \tag{7}$$

So

$$\begin{aligned} \sum_{p=0}^{n+1} z_p &= \sum_{p=0}^{n} L(z_p) + N\left(\sum_{i=0}^{n} z_p\right) \\ &= L\left(\sum_{p=0}^{n} z_p\right) + N\left(\sum_{p=0}^{n} z_p\right), \qquad p = 1, 2, \cdots. \end{aligned} \tag{8}$$

Thus,

$$\sum_{p=0}^{\infty} z_p = f + L\left(\sum_{p=0}^{\infty} z_p\right) + N\left(\sum_{p=0}^{\infty} z_p\right) \tag{9}$$

The k-term solution is given by the following form: $Z = \sum_{i=0}^{k-1} z_i$

3. Convergence Analysis

We examine the convergence of New Iterative Method for resolving any functional equation. Suppose $E = Z^* - Z$, where Z^* denotes the exact solution, Z is the approximate solution, and E is the error in the solution. Then we have

$$E(t) = f(t) + N(E(t)) \tag{10}$$

Applying the above equation to the NIM scheme, the recurrence relation becomes

$$\begin{aligned} E_0 &= f \\ E_1 &= N(E_0) \\ E_{p+1} &= N(E_0 + E_1 + \cdots + E_n) - N(E_0 + E_1 + \cdots + E_{n-}), \; p = 1, 2, \cdots. \end{aligned} \tag{11}$$

If $\| N(t) - N(s) \| \leq n \| s - t \|, 0 < n < 1,$ then we obtain

$$\begin{aligned} E_0 &= f \\ \| E_1 \| &= \| N(E_0) \| \leq n \| E_0 \|, \\ \| E_2 \| &= \| N(E_0 + E_1) - N(E_0) \| \leq n \| E_1 \| \leq n^2 \| E_0 \|, \\ &\vdots \\ \| E_{p+1} \| &= N(E_0 + \cdots + E_n) - N(E_0 + \cdots + E_{p-1}) \| \leq n \| E_p \| \leq n^{p+1} \| E_0 \|, \\ & p = 0, 1, 2, \ldots \end{aligned} \tag{13}$$

Thus $E_{p+1} \to 0$ as $p \to \infty$, which proves the convergence of the NIM for solving general functional equation.

4.Numerical Experiments, Results and Discussion

In the context of implementing the Numerical Integration Method (NIM), an exploration was conducted involving ordinary differential equations of varying orders, specifically, second, third, and fourth orders. The computational aspect of this investigation was carried out utilizing Maple 2021 software, and the resultant findings have been meticulously presented in Tables 1 to 6 for comprehensive examination and analysis.

Problem 1: We consider a real-life problem on cooling of a body temperature. The formulated problem is modelled into a 2nd order ODE as:

$$z''(t) = \frac{-z'(t)}{3}$$

with initial condition: $z(0) = 60,\ z'(0) = \frac{-80}{9}$ and exact solution: $z(t) = \frac{80}{3}e^{-\left(\frac{t}{3}\right)} + \frac{100}{3}$

(source; Kwanamu *et al*., 2021)

Table 1: Result for Problem 1

t	NIM Solution	Kwanamu *et al*. (2021)	Exact Solution
0.1	59.125762679520157388	59.12576267952015738700	59.125762679520157388
0.2	58.280186267509806339	58.28018626750980633500	58.280186267509806339
0.3	57.462331147625588618	57.46233114762558860800	57.462331147625588618
0.4	56.671288507811932107	56.67128850781193208900	56.671288507811932107
0.5	55.906179330416375308	55.90617933041637528100	55.906179330416375308
0.6	55.166153415412849564	55.16615341541284952600	55.166153415412849564
0.7	54.450388435647511050	54.45038843564751099900	54.450388435647511050
0.8	53.758089023057298472	53.75808902305729840700	53.758089023057298472
0.9	53.088485884845809762	53.08848588484580968100	53.088485884845809762
1.0	52.440834948634380011	52.44083494863437991400	52.440834948634380011

Table 2: Comparison of absolute errors for Problem 1

t	NIM	Kwanamu *et al*. (2021)
0.00	0.0000000	0.0000000
0.1	0.0000000	0.0000000
0.2	0.0000000	4.0000×10^{-18}
0.3	0.0000000	9.0000×10^{-18}
0.4	0.0000000	1.7000×10^{-17}

0.5	0.0000000	2.6000×10^{-17}
0.6	0.0000000	3.8000×10^{-17}
0.7	0.0000000	5.1000×10^{-17}
0.8	0.0000000	6.5000×10^{-17}
0.9	0.0000000	8.1000×10^{-17}
1.0	0.0000000	9.7000×10^{-17}

Problem 2: We consider the third order ordinary differential equation

$$z'''(t)'+z'(t)=0$$

with initial conditions $z(0)=0,\ \ z'(0)=1,\ \ z''(0)=2,\ \ 0\le t\le 1$ and

Exact solution: $z(t)=2(1-\cos t)+\sin t$ (Source: Folarin *et al*., 2019)

Table 3: Result for Problem 2

t	NIM Solution	Folarin *et al*. (2019)	Exact Solution
0.1	0.1098250861	0.109825086	0.1098250856
0.2	0.2385361751	0.238536175	0.2385361748
0.3	0.3848472284	0.384847227	0.3848472287
0.4	0.5472963543	0.547296351	0.5472963543
0.5	0.7242604148	0.724260408	0.7242604146
0.6	0.9139712436	0.913971232	0.9139712434
0.7	1.114533313	1.114533294	1.114533312
0.8	1.323942672	1.323942644	1.323942672
0.9	1.540106973	1.540106933	1.540106973
1.0	1.760866373	1.760866318	1.760866373

Table 4: Comparison of absolute errors for Problem 2

t	NIM	Folarin *et al*. (2021)
0.00	0.000000000	0.000000000
0.1	5.00000000×10^{-10}	$9.070000000\times10^{-11}$
0.2	3.00000000×10^{-10}	$4.125000000\times10^{-10}$
0.3	3.00000000×10^{-10}	1.243859872×10^{-9}

0.4	0.00000000000	3.402878300×10^{-9}
0.5	2.00000000×10^{-10}	6.623457000×10^{-9}
0.6	2.00000000×10^{-10}	1.147567740×10^{-8}
0.7	1.00000000×10^{-9}	1.866871200×10^{-8}
0.8	0.00000000000	2.820519300×10^{-8}
0.9	0.0000000000	4.008615600×10^{-8}
1.0	0.0000000000	5.507161900×10^{-8}

Problem 3: We consider the following fourth order homogenous linear equation

$$Z^{(iv)}(t)=2Z'''(t)-Z''(t)+Z(t);\quad z(0)=1$$

with initial conditions $z'(0)=-1,\ z''(0)=0,\ z'''(0)=1,\ 0\le t\le 1$ and

exact solution: $Z(t)=\left(\frac{1}{2}-\frac{1}{10}\sqrt{5}\right)e^{\frac{1}{2}\left(\sqrt{5}+1\right)t}+\left(\frac{1}{2}+\frac{1}{10}\sqrt{5}\right)e^{-\frac{1}{2}\left(\sqrt{5}-1\right)t}-\frac{2}{3}\sqrt{3}e^{\frac{1}{2}t}\sin\left(\frac{1}{2}\sqrt{3}\right)t$

(Source: Tiamiyu *et al*., 2021; Audu *et al*., 2022)

Table 5: Comparison Result for Problem 3

t	Exact Solution	NIM Solution
0.1	0.900179507086368372903374 4	0.900179507086368372903374 4
0.2	0.801544463014773780147434 6	0.801544463014773780147434 6
0.3	0.705598886975389102786943 4	0.705598886975389102786943 4
0.4	0.614238931291468928689510 4	0.614238931291468928689510 4
0.5	0.529808143393722026230367 6	0.529808143393722026230367 6
0.6	0.455160525903564167533023 5	0.455160525903564167533023 5
0.7	0.393732683343854693761827 0	0.393732683343854693761827 0
0.8	0.349626585274874939064009	0.349626585274874939064009
0.9	0.327704761421510586558073	0.327704761421510586558072
1.0	0.333700082480454521066471	0.333700082480454521066470

Table 6: Comparison of absolute errors for Problem 3

t	Tiamiyu *et al.* (2021)	Audu *et al*. (2022)	NIM
0.1	3.603×10^{-18}	2.985×10^{-20}	0.000×10^{-20}
0.2	3.038×10^{-17}	2.858×10^{-19}	0.000×10^{-20}
0.3	2.649×10^{-16}	6.767×10^{-19}	0.000×10^{-20}
0.4	9.765×10^{-16}	2.712×10^{-19}	0.000×10^{-20}
0.5	2.938×10^{-15}	2.507×10^{-18}	0.000×10^{-20}
0.6	4.622×10^{-15}	1.012×10^{-17}	0.000×10^{-20}
0.7	3.555×10^{-14}	2.585×10^{-17}	0.000×10^{-20}
0.8	1.839×10^{-13}	5.390×10^{-17}	0.000×10^{-20}
0.9	5.624×10^{-13}	9.947×10^{-17}	2.000×10^{-20}
1.0	1.05×10^{-12}	1.687×10^{-17}	1.000×10^{-20}

Results and Comparison:**Table 1 - Problem 1**:e NIM solutions for Problem 1 were compared with Kwanamu et al.'s method and the exact solution. The tabulated results demonstrate the close agreement between the NIM and the exact solution, confirming its accuracy. The comparison of absolute errors in Table 2 further validates the NIM's precision, with consistently low errors across all time points.

Table 3 - Problem 2:
For Problem 2, the NIM solutions were compared with Folarin *et al*.'s method and the exact solution. The NIM exhibited excellent agreement with the exact solution, as evidenced by the tabulated results. The absolute errors, outlined in Table 4, are consistently minimal, emphasizing the NIM's accuracy in estimating the solution for Problem 2.

Table 5 - Problem 3:
In the case of Problem 3, the NIM solutions were compared with Tiamiyu *et al*.'s and Audu *et al*.'s methods, along with the exact solution. The results in Table 5 show a remarkable alignment between the NIM and the exact solution. The comparison of absolute errors in Table 6 reaffirms the NIM's precision, with extremely low errors observed across all time points.

The comparison with existing methods, including Kwanamu *et al*., (2021), Folarin *et al*., (2019), Tiamiyu *et al*., (2021), and Audu *et al*., (2022), consistently favored the NIM. In multiple instances, the NIM outperformed other methods in terms of accuracy and efficiency. The obtained results strongly indicate the convergence of the NIM, providing confidence in its reliability for estimating solutions to higher-order differential equations.

5. Conclusion

In summary, this research delved into the New Iterative Method (NIM) as a promising approach for solving higher-order differential equations, prevalent in scientific and engineering disciplines. The

study demonstrated the NIM's accuracy and adaptability by applying it to various scenarios and comparing results with existing methods. Notably, the NIM consistently exhibited superior performance, showcasing its precision and convergence in estimating solutions. The findings underscore the potential of the NIM to revolutionize numerical analysis for higher-order differential equations. In terms of contribution to knowledge, this research adds valuable insights into the capabilities of the NIM, emphasizing its efficacy in both linear and nonlinear contexts. The comparative analysis with established methods highlights the NIM's superiority, providing a basis for confidence in its application. Additionally, the study contributes to the understanding of the NIM's adaptability, suggesting its potential applicability to a wide range of scientific and engineering problems. Based on the outcomes, it is recommended that future research endeavors explore the NIM in more complex scenarios and real-world applications. Continued validation across diverse problem domains will further enhance our understanding of the NIM's capabilities and limitations. Moreover, collaborative efforts within the scientific community can foster the development and refinement of the NIM, positioning it as a valuable tool for tackling intricate higher-order differential equations in various fields.

References

Ali, F., Yassen, M. F., Asiri, S. A., Nawaz, R., Zada, L., Alam, M. M. & Sene, N. (2022). New Iterative Method for Solving a Coupled System of Fractional-Order Drinfeld–Sokolov–Wilson (FDSW) and Fractional Shallow Water (FSW) Equations. *Hindawi Journal of Nanomaterials*, 1-13.

Batiha B., Ghanim, G., Batiha, K. (2023). Application of the New Iterative Method (NIM) to the Generalized Burgers–Huxley Equation, *Symmetry*, 15, 1-13.

Audu, K. J., Garba, J., Tiamiyu, A.T, & Thomas, B. A. (2022). Application of Backward Differentiation Formula on Fourth-Order Differential Equations. *Journal of Science and Technology*, *14*(2), 52-65 6.

Audu, K. J., Taiwo, A. R. & Soliu, A. A. (2023). Assessment of Numerical Performance of Some Runge-Kutta Methods and New Iteration Method on First Order Differential Problems. *Dutse Journal of Pure and Applied Sciences*, *9*(4a), 58-70.

Daftardar-Gejji, V. & Jafari, H. (2006). An iterative method for solving nonlinear functional equations, Journal of Mathematical Analysis and Applications, *316*(2), 753–763.

Falade, K. I., Tiamiyu, A. T., Edogbanya, H. O., Ibrahim, M. B. & Abubakar, A. S. (2022). On Comparison of Algorithms Techniques for Numerical Solutions of Higher Order Differential Equations. *African Journal of Mathematics and Statistics Studies*, *5*(2), 43-60.

Folaranmi, R. O., Adeniyi, R. B., Adeyefa, E. O., Yahaya, H. (2019). A Chebyshev Collocation Block Method for Solution of Third Order Initial Value Problems in Ordinary Differential Equations. *ABACUS-Science Series*, *44*(1), 1-11.

Kwanamu, J. A., Skwame, Y. & Sabo, J. (2021). Block Hybrid Method for Solving Higher Order

Ordinary Differential Equation Using Power Series on Implicit One-Step Second Derivative. *FUW Trends in Science and Technology Journal*, *6* (2), 576 – 582.

Tiamiyu, A. T., Falade, K. I., Rauf, Q. O., & Akande, S. A. (2021a). A Numerical Technique for Direct Solution of Special Fourth Order Ordinary Differential Equation Via Hybrid Linear Multistep Method. *Cankaya University Journal of Science and Engineering*. *18*(1), 47–60.

Tiamiyu, A.T., Cole, A. T. & Audu, K. J. (2021b). A Backward Differentiation Formula for Third-Order Initial or Boundary Values Problems Using Collocation Method. *Iranian Journal of Optimization*, *13*(2), 81-92.

Analysis of Magnetohydrodynamic Oscillatory Flow with Viscous Energy Dissipation

H. O. Adebayo[1,2] and R. O. Olayiwola[1]

[1]Department of Mathematics, School of Physical Sciences, Federal University of Technology Minna, Nigeria

[2]Department of Mathematics, Faculty of Physical Sciences, Ahmadu Bello University Zaria, Nigeria

[*]*Presenting author email(s):* adebayohelenolaife@gmail.com

Abstract

This paper analyses the transient laminar free convective flow of a dusty viscous fluid through a porous medium in the presence of viscous energy dissipation. The partial differential equations governing the phenomenon were non-dimensionalized using some dimensionless quantities. The dimensionless coupled non-linear partial differential equations were solved using the harmonic solution technique. The effects of model parameters on the fluid flow and temperature distribution have been analysed. The results obtained revealed that the Eckert number enhanced the temperature distribution.

Keyword: Convection, harmonic solution, heat source, magnetohydrodynamic, oscillatory flow.

1. Introduction

The study of the oscillatory flow of an electrically conducting fluid through a porous channel saturated with porous medium is important in many physiological flows and engineering applications such as magneto-hydrodynamic (MHD) generators, arterial blood flow, petroleum engineering and many more. Oscillatory flow is a periodic flow that oscillates around a zero value. Oscillatory flow is a single swing or movement in one direction of an oscillating body. They are generally used in the literature to describe the flows in which velocity, pressure or both depend on time. Oscillatory flow is always important because it has many practical applications for example in the aerodynamics of helicopter rotors or fluttering airfoils and also in a variety of bioengineering problems (Baba *et al*., 2020).

The effect of heat transfers on an oscillatory flow of an electrically conducting fluid in vertical media is encountered in a wide range of engineering areas, science and technology such as MHD power generators, plasma studies, nuclear reactors, geothermal energy extraction, electromagnetic propulsion, the boundary layer control in the field of aerodynamics. It also has numerous industrial applications in molten iron flow, recovery extraction of crude oil, electrostatic precipitation, petroleum industry and polymer technology (Mehta *et al*., 2020).

Flow of conducting fluid in external magnetic field produce a variety of new effects, which are not realized in usual hydrodynamics. Magneto-hydrodynamics (MHD) analyzes these phenomena. It also studies the arising of a flow of conducting fluid due to the current passing through the fluid (so-called electrically induced vortex-type flows). MHD is used for cleaning liquid metals of impurities as well as for the separation of multiphase systems into their components (Herman and Yeshajahu,1993).

Several authors have studied the flow and heat transfer in oscillatory fluid problems. Zubi (2018) studied MHD and mass transfer of an oscillatory flow over a vertical permeable plate in a porous medium with chemical reaction. He considered a two-dimensional, unsteady, laminar non-Darcian

mixed convection flow of an incompressible, viscous, electrically conducting fluid. He applied a magnetic field of strength vertically to the surface, neglecting the effect of induced magnetic field. Fetecau *et al*. (2021) analysed Maxwell fluid flow through a porous plate channel induced by a constant accelerating oscillating wall. They considered an incompressible fluid at rest in a porous medius and used finite Fourier sine transform to establish exact expressions for the dimensionless velocity and the shear stress fields corresponding to the two different motions of incompressible fluid.

Kodi and Mopuri (2021) studied unsteady MHD oscillatory Casson fluid flow past an inclined vertical porous plate in the presence of chemical reaction with heat absorption and soret effects. They investigated unsteady hydrodynamic flow over an inclined plate embedded in a porous medium with soret-alligned magnetic field and chemical reaction. Krsihna *et al*. (2018) discussed heat and mass transfer on unsteady MHD oscillatory flow of blood through porous arteriole. They developed a mathematical model for unsteady state situations using slip conditions. Falade *et al*. (2016) studied MHD oscillatory flow through a porous channel saturated with a porous medium. They investigated the effect of suction/injection on the unsteady oscillatory flow through a vertical channel with non-uniform wall temperature. The fluid was subjected to a transverse magnetic field and the velocity slip at the lower plate was taken into consideration. Exact solutions of the dimensionless equations governing the fluid flow were obtained.

This paper seeks to consider oscillatory fluid flow and heat transfer in a porous medium with an inclined magnetic field in the presence of viscous energy dissipation thereby extending the work of Falade *et al*. (2016).

2. Model Formulation

Consider the unsteady laminar flow of an incompressible viscous electrically conducting fluid through a channel with slip at the cold plate. An external magnetic field is placed across the normal to the channel. It is assumed that the fluid has small electrical conductivity and the electromagnetic force produced is also very small. The flow is subjected to suction at the cold wall and injection at the heated wall. We choose a Cartesian coordinate system (x', y') where x' lies along the centre of the channel, and y' is the distance measured in the normal section such that $y' = a$ is the channel's half-width.

Under the usual Bousinesq approximation the equations governing the flow are as follows:

$$\frac{\partial u'}{\partial t'} - V_0 \frac{\partial u'}{\partial y'} = \frac{1}{\rho}\frac{dP'}{dx'} + \upsilon \frac{\partial^2 u'}{\partial y'^2} - \frac{\upsilon}{k}u' - \frac{\sigma_e B_0^2}{\rho}u' + g\beta\left(T' - T_0\right) \tag{1}$$

$$\frac{\partial T'}{\partial t'} - V_0 \frac{\partial T'}{\partial y'} = \frac{k_f}{\rho C_p}\frac{\partial^2 T'}{\partial y'^2} + \frac{4\alpha^2}{\rho C_p}\left(T' - T_0\right) + \frac{\upsilon}{C_p}\left(\frac{\partial u'}{\partial y'}\right)^2 \tag{2}$$

With the initial and boundary conditions,

$$\left.\begin{aligned} &u'\left(y', 0\right) = 0, \quad u'\left(0, t\right) = \frac{\sqrt{k}}{\alpha_s}\frac{du'\left(0, t\right)}{dy'}, \quad u'\left(h, t\right) = 0 \\ &T'\left(y', 0\right) = T_0 \quad T'\left(0, t\right) = T_0, \qquad T'\left(h, t\right) = T_1 \end{aligned}\right\} \tag{3}$$

Where

$u(y,t)$ is the axial velocity, V_0 is the constant horizontal Velocity, ρ is the fluid density, P' is the fluid pressure, υ is the Kinematic viscosity, K is the porous permeability, σ_e is the electrical conductivity, B_0 Is the magnetic field intensity, g Is the gravitational acceleration, β Is the volumetric expansion, C_p is the specific heat at constant pressure, α is the term due to thermal radiation, k is the thermal conductivity, T is the fluid temperature, T_0 is the referenced fluid temperature.

2.1 Dimensional Analysis

We non-dimensionalise equation (1) - (3) using the following dimensionless variables,

$$\left.\begin{aligned} &x=\frac{x'}{h}, \quad y=\frac{y'}{h}, \quad \theta=\frac{T'-T_0}{T_1-T_0}, \quad u=\frac{u'}{U}, \quad v=\frac{v_0}{U}, \quad t=\frac{Ut'}{h}, \\ &P=\frac{P'}{\rho U^2}, \quad \frac{dP'}{dx'}=\frac{\rho U^2}{h}\frac{dP}{dx}, \quad u'=Uu, \quad t'=\frac{h}{U}t, \quad y'=hy, \end{aligned}\right\} \tag{4}$$

and we obtain,

$$\frac{\partial u}{\partial t}-v\frac{\partial u}{\partial y}=-\frac{dP}{dx}+\frac{1}{R_e}\frac{\partial^2 u}{\partial y^2}-\left(S+H_a^2\right)u+G_{r\theta}\theta \tag{5}$$

$$\frac{\partial \theta}{\partial t}-v\frac{\partial \theta}{\partial y}=\frac{1}{P_e}\frac{\partial^2 \theta}{\partial y^2}+\delta\theta+\frac{E_c}{R_e}\left(\frac{\partial u}{\partial y}\right)^2 \tag{6}$$

With corresponding dimensionless initial and boundary conditions as,

$$\left.\begin{aligned} &u(y,0)=0, \quad \left.\frac{du}{dy}\right|_{y=0}-\alpha u|_{y=0}=0, \quad u(1,t)=0 \\ &\theta(y,0)=0, \quad \theta(0,t)=0, \quad \theta(1,t)=1 \end{aligned}\right\} \tag{7}$$

2.2 Solution via Harmonic Solution Technique

Equations (5) - (7) are coupled non-linear partial differential equations and these equations can be solved by harmonic solution technique, that is the equation can be reduced to a set of ordinary differential equations which can be solved analytically. This can be done by representing the velocity, temperature of the fluid in the neighbourhood of the plate as:

$$\left.u(y,t)=u(y)e^{i\omega t}, \quad \theta(y,t)=\theta(y)e^{2i\omega t}\right\} \tag{8}$$

Substituting (8) into (5) - (7) we have,

$$\left.\begin{aligned}&\frac{d^2u}{dy^2}+b_1\frac{du}{dy}-c_1^2u=-\lambda R_e-G_{r\theta}e^{i\omega t}R_e\theta\\&\left.\frac{du}{dy}\right|_{y=0}-\alpha u|_{y=0}=0,\qquad u(1)=0\end{aligned}\right\} \tag{9}$$

$$\left.\begin{aligned}&\frac{d^2\theta}{dy^2}+b_2\frac{d\theta}{dy}-c_2^2\theta=-\frac{E_cP_e}{R_e}\left(\frac{du}{dy}\right)^2\\&\theta(0)=0,\quad \theta(1)=e^{-2i\omega t}\end{aligned}\right\} \tag{10}$$

Where $b_1=vR_e,\quad c_1=\sqrt{\left(S+H_a^2+i\omega\right)R_e},\quad b_2=vP_e,\quad c_2=\sqrt{\left(\delta-2i\omega\right)P_e}$

We let $0<G_{r\theta}<<1$ such that,

$$\left.\begin{aligned}&u(y)=u_0(y)+G_{r\theta}u_1(y)+...\\&\theta(y)=\theta_0(y)+G_{r\theta}\theta_1(y)+...\end{aligned}\right\} \tag{11}$$

and we obtain solutions to equations (9) and (10) as:

$$u(y)=\left(A_1e^{m_1y}+A_2e^{m_2y}+A_3\right)+G_{r\theta}\begin{pmatrix}A_{10}e^{m_1y}+A_{11}e^{m_2y}+A_{12}e^{m_1y}+A_{13}e^{m_2y}+\\A_{14}e^{2m_1y}+A_{15}e^{(m_1+m_2)y}+A_{16}e^{2m_2y}\end{pmatrix} \tag{12}$$

$$\theta_0(y)=\begin{pmatrix}A_4e^{m_3y}+A_5e^{m_4y}+A_6e^{2m_1y}\\+A_7e^{(m_1+m_2)y}+A_8e^{2m_2y}\end{pmatrix}+G_{r\theta}\begin{pmatrix}A_{17}e^{m_3y}+A_{18}e^{m_4y}+A_{19}e^{2m_1y}+A_{20}e^{(m_1+m_2)y}\\+A_{21}e^{3m_1y}+A_{22}e^{(2m_1+m_2)y}+A_{23}e^{(m_1+2m_2)y}+\\A_{24}e^{2m_2y}+A_{25}e^{3m_2y}\end{pmatrix} \tag{13}$$

2.3 Skin-friction of the Fluid Velocity $u(y,t)$.

The dimensionless stress tensor in terms of the skin-friction coefficient at the plate $y=0$ is given by

$$\begin{aligned}&CF_0=\left(\frac{\partial u(y,t)}{\partial y}\right)_{y=0}=\left(\frac{du}{dy}\right)_{y=0}\left(e^{i\omega t}\right)\\&CF_0=\left(A_1m_1+A_2m_2\right)+G_{r\theta}\begin{pmatrix}\left(A_{10}+A_{12}+2A_{14}\right)m_1+\\\left(A_{11}+A_{13}+2A_{16}\right)m_2+A_{15}\left(m_1+m_2\right)\end{pmatrix}e^{i\omega t}\end{aligned} \tag{14}$$

2.4 Nusselt-number of the Temperature of the Fluid $\theta(y,t)$.

The dimensionless rate of heat transfer in terms of the Nusselt number at the plate $y=0$ is given by

$$Nu_0 = -\left(\frac{\partial\theta(y,t)}{\partial y}\right)_{y=0} = \left(\frac{d\theta}{dy}\right)_{y=0}\left(e^{2i\omega t}\right)$$

$$Nu_0 = -\begin{pmatrix} A_4m_3 + A_5m_4 + 2A_6m_1 \\ +A_7\left(m_1+m_2\right) + 2A_8m_2 \end{pmatrix} + G_{r\theta}\begin{pmatrix} A_{17}m_3 + A_{18}m_4 + \left(2A_{19}+3A_{21}\right)m_1 \\ +A_{20}\left(m_1+m_2\right) + A_{22}\left(2m_1+m_2\right) \\ +A_{23}\left(m_1+2m_2\right) + \left(2A_{24}+3A_{25}\right)m_2 \end{pmatrix} e^{2i\omega t} \quad (15)$$

3. Results and discussion

The momentum and energy equations of the fluid flow are solved using the harmonic solution technique. The effects of various physical parameters on the fluid flow and temperature distribution are shown in Figure 1 and Tables 1 and 2.

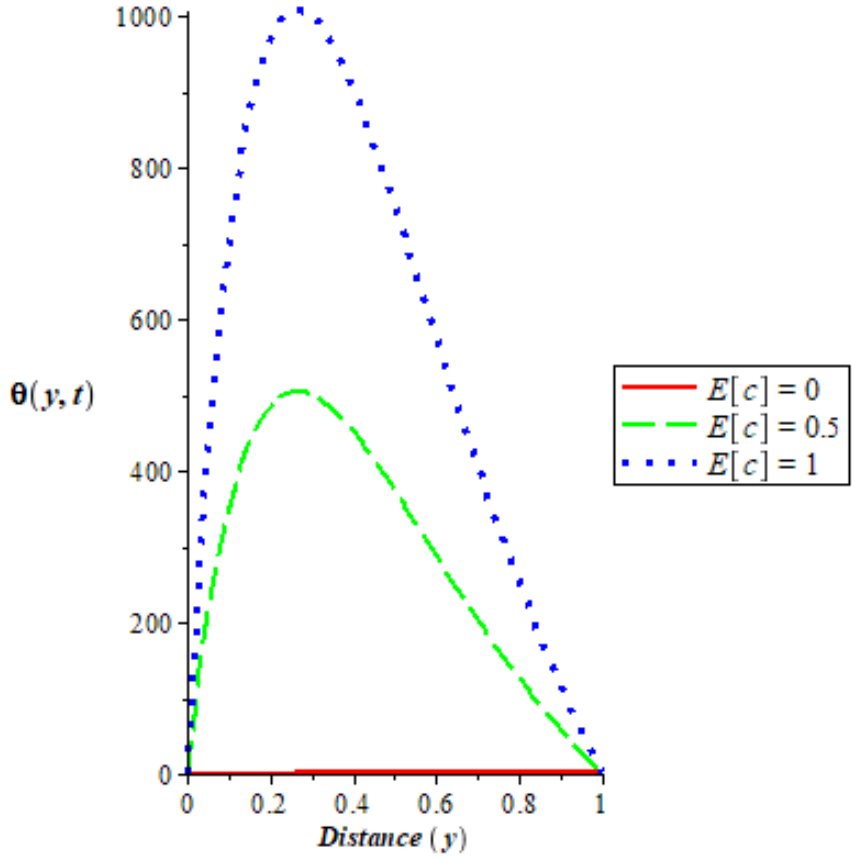

Figure 1: Effect of Eckert number (E_c) on Temperature distribution

Figure 1 displays the graph of temperature of the fluid $\theta(y,t)$ against distance for various values of Eckert number (E_c). It shows that an increase in Eckert number from 0 (no viscous heating) through 0.5 to 1 (high viscous heating) boosts temperature in the porous regime. Eckert number signifies the quantity of mechanical energy converted via internal friction to thermal energy.

Table 1: Numerical values of skin-friction coefficient at the plate $y = 0$ for various values of physical parameters

P_e	H_a	E_c	R_e	ν	$G_{r\theta}$	δ	t	CF_0
0.6	0.1	0.0000001	0.1	7	1	1	0	0.02282159761
0.7	0.1	0.0000001	0.1	7	1	1	0	0.2771784025
0.8	0.1	0.0000001	0.1	7	1	1	0	1.222821597
0.6	0.5	0.0000001	0.1	7	1	1	0	0.02270243200
0.6	0.9	0.0000001	0.1	7	1	1	0	-0.5775709957
0.6	0.1	0.0000002	0.1	7	1	1	0	-0.1771783959
0.6	0.1	0.0000003	0.1	7	1	1	0	-0.3771783893
0.6	0.1	0.0000001	0.3	7	1	1	0	0.6557569325
0.6	0.1	0.0000001	0.4	7	1	1	0	0.3670472404
0.6	0.1	0.0000001	0.1	13	1	1	0	0.5172536900
0.6	0.1	0.0000001	0.1	15	1	1	0	0.02076954027
0.6	0.1	0.0000001	0.1	7	2	1	0	0.02282160413
0.6	0.1	0.0000001	0.1	7	3	1	0	0.02282161064
0.6	0.1	0.0000001	0.1	7	1	2	0	1.022821599
0.6	0.1	0.0000001	0.1	7	1	3	0	3.022821607
0.6	0.1	0.0000001	0.1	7	1	1	0.4	0.02609456154
0.6	0.1	0.0000001	0.1	7	1	1	0.7	0.01290161830

Table 1 shows that at the plate $(y = 0)$ when the Eckert number (E_c), Reynold number (R_e), Hatmann number (H_a), kinematic viscosity and Thermal radiation parameter increase the skin friction (CF_0) decreases. The rate of skin friction increases for increasing values of Peclet number (P_e).

Table 2: Numerical values of Nusselt number at the plate $y = 0$ for various values of physical parameters.

P_e	H_a	E_c	R_e	ν	$G_{r\theta}$	δ	t	Nu_0
0.6	0.1	0.0000001	0.1	7	1	1	0	-14.56136822
0.7	0.1	0.0000001	0.1	7	1	1	0	-17.25372613
0.8	0.1	0.0000001	0.1	7	1	1	0	-19.49438297
0.6	0.5	0.0000001	0.1	7	1	1	0	-13.75969507

0.6	0.9	0.0000001	0.1	7	1	1	0	-8.417759937
0.6	0.1	0.0000002	0.1	7	1	1	0	-24.50266599
0.6	0.1	0.0000003	0.1	7	1	1	0	-34.44396367
0.6	0.1	0.0000001	0.3	7	1	1	0	-8.493814836
0.6	0.1	0.0000001	0.4	7	1	1	0	0.068118293
0.6	0.1	0.0000001	0.1	13	1	1	0	-9.856397265
0.6	0.1	0.0000001	0.1	15	1	1	0	-9.856397265
0.6	0.1	0.0000001	0.1	7	2	1	0	-24.50266594
0.6	0.1	0.0000001	0.1	7	3	1	0	-0.06553324430
0.6	0.1	0.0000001	0.1	7	1	2	0	-15.35806125
0.6	0.1	0.0000001	0.1	7	1	3	0	-16.04140800
0.6	0.1	0.0000001	0.1	7	1	1	0.4	-5.034545097
0.6	0.1	0.0000001	0.1	7	1	1	0.7	0.1168126243

Table 4.2 shows that the rate of heat transfer at the plate $(y=0)$ increases for increasing values of Reynold number (R_e), Hartmann number (H_a), and Grashof thermal $(G_{r\theta})$, but a reverse trend is observed for increasing values of Peclet number (P_e), Eckert number (E_c) and Thermal radiation parameter (δ).

4. Conclusions

The solutions for the model have been determined by the harmonic solution technique. The effects of model parameters on the fluid flow and temperature distribution have been analysed. It can be concluded that the Eckert number enhanced the temperature distribution.

References

Baba, G. A., Muhammad, S.N., Sani, U. & Adullahi, I, (2020). Unsteady Magneto Hydrodynamic Poiseuille Oscillatory Flow between Two Infinite Parallel Porous Plates. *Science World Journal*, 15(2) 2.

Falade, J. A., Joel C. U., Egere, A. C. & Samuel O. A. (2016). MHD Oscillatory Flow Through a Porous Channel Saturated with Porous Medium. *Alexandria Engineering Journal*, 56, 147–152.

Fetacau, C., Ellahi, R. & Sait, S. M. (2021). Mathematical Analysis of Maxwell Fluid Flow Through a Porous Plate Channel Induced by a Constantly Accelerating or Oscillating Wall. *Acadamic opening access publishing Mathematics*, 9(1), 90.

Herman, B. & Yeshajahu, U. (1993). Metallurgical Technologies, Energy Conversion, and Magnetohydrodynamic Flow. *Journal in Astronautic and Aeronautics*, 5(148).

Kodi, R. & Mopuri, O. (2021). Unsteady MHD Osscilatory Casson Fluid Flow Past an Inclined Vertical Porous Plate in the Presence of Chemical Reaction with Heat Absorption and Soret Effects. *Journal of Heat transfer*, 51, 733-752.

Krishna, M. V., Swarnalathamma, B. V. & Prakash, J. (2018). Heat And Mass Transfer on Unsteady MHD Oscillatory Flow of Blood Through Porous Arteriole. *Applications of fluid dynamics proceedings of ICAFD*, 207-224.

Mehta, T., Mehta, R. & Mehta, A. (2020). Oscillatory fluid flow and heat transfer through porous medium between parallel plates with inclined magnetic field, radiative heat flux and heat source. *International Journal of Applied Mechanics and Engineering,* 25(2), 88-102.

Zubi, M. A. (2018). MHD heat and mass transfer of an oscillatory flow over a vertical permeable plate in a porous medium with chemical reaction. *Modern mechanical engineering,* 8(3), 179-191.

Numerical Solution for Magnetohydrodynamics Mixed Convection Flow Near a Vertical Porous Plate Under the Influence of Magnetic Effect and Velocity Ratio

Ibrahim Yusuf[1],Umaru Mohammed[1] and Khadeejah James Audu[1]
[1]Department of Mathematics, Federal University of Technology, Minna, Niger state, Nigeria.

E-mail: ibrahimy338@gmail.com

Abstract

This paper investigates the effects of thermal radiation on MHD mixed convection flow, heat and mass transfer, Dufour and Soret effects over a porous plate having convective boundary condition under the influence of magnetic field. The governing boundary layer equations are formulated and transformed into nonlinear ordinary differential equations using similarity transformation and numerical solution is obtained by using Runge-Kutta fourth order scheme with shooting technique. The effects of various physical parameters such as velocity ratio parameter, mixed convection parameter, melting parameter, suction parameter, injection parameters, Biot number, magnetic parameter, Schmit and pranditl numbers on velocity and temperature distributions are presented through graphs and discussed.

Keywords: Dufour effect,Magnetohydrodynamics, Mixed convection, Melting, Soret effect.

1. Introduction

Magnetohydrodynamics (MHD), also called magneto-fluid dynamics or hydromagnetics is a model of electrically conducting fluids that treats all interpenetrating particle species together as a single continuous medium. It is primarily concerned with the low-frequency large-scale, magnetic behavior in plasmas and liquid metals and has applications in numerous fields including geophysics, astrophysics, engineering and medical sciences Saman *et al.* (2017). The field of MHD was initiated by Hannes Alfven 1942 for which he received noble prize in physics in 1970. The fundamental concept behind MHD is that magnetic field can induce currents in a moving conductive fluid, which in turn creates forces on the fluid and changes the magnetic field itself. The set of equations that describe MHD are combination of the Navier-Stokes equations of fluid dynamics and Maxwell's equation of electromagnetism. The effects of mass transfer on MHD second grade fluid towards stretching cylinder was explored by Alamri *et al*. (2019) analytically using homotopy analysis method and reported that the velocity decreases with increasing values of magnetic field.

Mixed convection occurs when heat transfer in a fluid or gas is influenced by both forced convection and natural convection. Forced convection is induced by external factors like fans or pumps, while natural convection occurs due to temperature gradients causing density differences. When both forced and natural convection effects are comparable, it is referred to as mixed convection Davood and Sayyid (2015). This phenomenon is important in scenarios where both mechanisms play a significant role, such as in complex ventilation systems, heat exchangers, and electronic cooling systems. Understanding the characteristics and mechanisms of mixed convection is crucial for improving heat transfer and designing efficient thermal management systems (Aaiza *et al.* 2015).

Dofour and Soret are two important mass transfer mechanism in fluid dynamics and heat transfer.The Dufour and Soret effects are two related phenomena that occur in multi-component systems, particularly in the field of fluid dynamics. These effects are named after two Swiss physicists, Jean-Baptiste Dufour and Charles Soret, who made significant contributions to understanding the behavior of mixtures and diffusion in the 19th century (Venkata *et al.*2021).

2. Literature review

Jha and Mohammed (2014) studied mixed convection effect on melting from a vertical plate embedded in porous medium with Soret and Dufour effects. Jha *et al.* (2013) studied the effects of Dofuor and Soret on melting from a vertical plate embedded in saturated porous medium. Sharma *et al.* (2018) studied the influence of heat source on MHD mixed convection stagnation point flow along a vertical stretching sheet. Reddy and Ali (2016) investigated the combined influence of suction and thermophoresis on the mixed convective mass transfer boundary layer flow of micropolar fluids through porous medium over a stretching sheet in the presence of thermo-Diffusion and Diffusion-thermo effects. Jha and Muhammad (2019) investigated the chemical reaction and diffusion thermo effect on steady fully developed free convection heat and mass transfer flow near an infinite vertical moving porous plate under nonlinear Boussinesq approximations.The impact of nonlinear thermal radiation on nonlinear mixed convection flow near a vertical porous plate with convective boundary condition has been investigated by Jha and Samaila (2020; 2021a; 2021b; 2022). Surbhi *et al.* (2023) studied the numerical investigation of micropolar fluid flow due to melting stretchy surface in a porous medium. Hemalatha and Prasad (2014) investigated the analysis of melting phenomenon with mixed convection flow and heat transfer in a fluid saturated porous medium considering the effect of applied magnetic field, viscous dissipation, and radiation by taking forchheimer extension.

Motivated by the aforementioned papers, the combined effects of magnetic effect and velocity ratio on MHD mixed convection flow has not been studied. Hence, this paper is aimed at establishing a mathematical model to analyze the effect of magnetic effect and velocity ratio on MHD mixed convection flow near a vertical porous plate with thermal radiation.

3. Methodology

Consider a hydrodynamic and boundary layer flow on a vertical porous plate influence by nonlinear thermal radiation as shown in figure 3.1. As demonstrated in the figure, the fluid is assume to move with a uniform velocity U_∞ far away from the vertical porous plate at a temperature T_∞, whereas the porous plate surface is heated through convection from a hot fluid at a temperature T_f with a heat transfer coefficient h_f. Here, the momentum equation is subjected to the Boussinesq approximation.

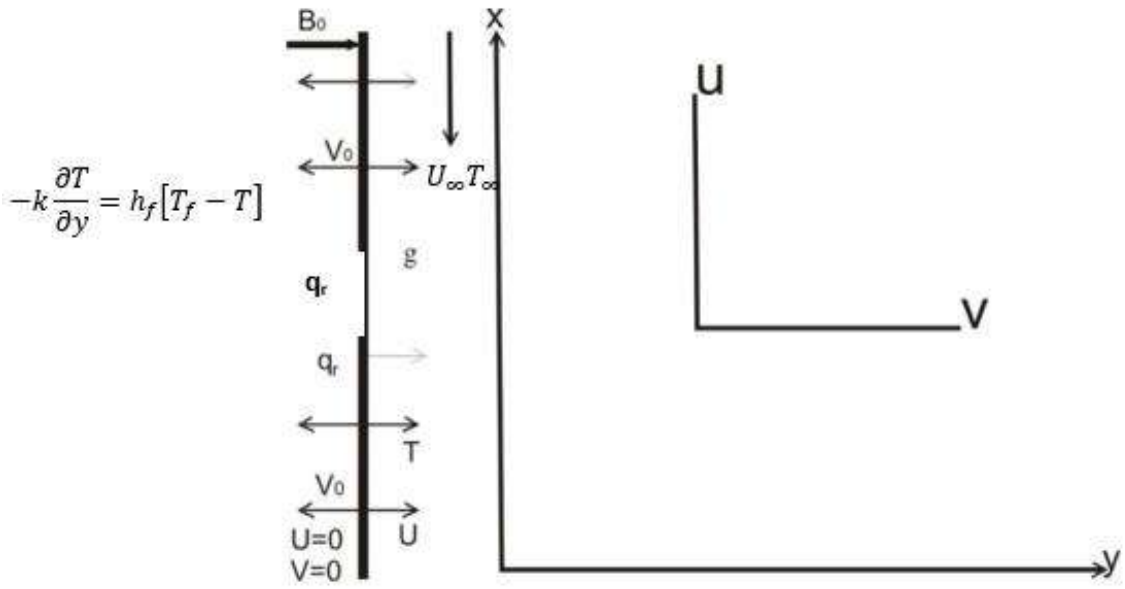

Figure 3.1: Flow configuration

Following (Jha and Samaila 2021a), the equation that governs the flow of fluid is defined as:

$$\frac{\partial u}{\partial x} + \frac{\partial v}{\partial y} = 0, \tag{1}$$

$$u\frac{\partial u}{\partial x} + v\frac{\partial u}{\partial y} = v\frac{\partial^2 u}{\partial y^2} - \frac{\sigma B_0^2}{\rho_f}(u - u_\infty) + g\beta(T - T_\infty), \tag{2}$$

$$u\frac{\partial T}{\partial x} + v\frac{\partial T}{\partial y} = \alpha\left[\frac{\partial^2 T}{\partial y^2} - \frac{1}{K}\frac{\partial q_r}{\partial y}\right] \tag{3}$$

Where T denote the dimensional temperature, Kdenote thermal conductivity, U denote velocity, v denote kinematic viscosity, and$(u,$v) are the velocity components. The quantity q_r is the radiative heat flux. However, the radiative heat flux in the x-direction is assumed to be small in comparison to that in y-direction. According to Jha *et al.* (2018), the radioactive heat flux q_r can be simplified through Rosseland diffusion approximation for an optical thick fluid as

$$q_r = -\frac{4\sigma\partial T^4}{3k^*\partial y} \tag{4}$$

Where σ and K^* represent the Stefan Boltzman constant and mean absorption respectively. Though, Rosseland approximation is only applicable for an optical thick fluid. Regardless of these limitations, it has been applied in several investigations particularly from the analysis of radiation effect on blast waves by the nuclear explosion to the transport of radiation through gasses at low density (Agha *et al.* 2014).

The boundary conditions related to the present analysis can be written as:

$$\left.\begin{aligned} &u(x,y=0)=0,\ \mathrm{v}(x,y=0)=\frac{c}{a},\ -k\frac{\partial T}{\partial y}(x,y=0)=\mathrm{h}_f\left[T_f-T(x,y=0\right] \\ &u(x,y\to\infty)=U_\infty, T(x,y\to\infty)=T_\infty, \end{aligned}\right\} \quad (5)$$

The following similarity transformations are introduced to transform equation (2) and (3).

$$\left.\begin{aligned} &\eta=y\sqrt{\frac{U_\infty}{vx}}, \\ &u=U_\infty f^{\iota}(\eta) \\ &v=\frac{1}{2}\sqrt{\frac{U_\infty v}{x}}(\eta f^{\iota}(\eta)-f), \\ &\theta=\frac{T-T_\infty}{T_f-T_\infty} \end{aligned}\right\} \quad (6)$$

Substituting equation (4) – (6) in equation (2) and (3), the momentum and energy equations and the boundary conditions are reduced to;

$$f'''(\eta)+\frac{1}{2}f(\eta)f''(\eta)+M(1-f')+Gr_x\theta(\eta)=0 \quad (7)$$

$$\theta''(\eta)\left(1+\frac{4}{3}R\left(\theta+C_T\right)^3\right)+4R\left(\left(C_T+\theta\right)^2\left(\theta'(\eta)\right)^2\right)+\frac{1}{2}Pr\theta'(\eta)f(\eta)=0 \quad (8)$$

The appropriate boundary conditions are

$$\left.\begin{aligned} &f(0)=S, \\ &f^{\iota}(0)=A, \\ &\theta^{\iota}(0)=-Bi[1-\theta(0)] \\ &f^{\iota}(\infty)=1, \\ &\theta(\infty)=0, \end{aligned}\right\} \quad (9)$$

Where prime denotes derivative with respect to η, $Gr_x=\frac{vxg\beta(T_f-T_\infty)}{{U_\infty}^2}$ is local Grashof number,$p_r=\frac{\mu C_p}{K}$ is the prandtl number, $Bi=\frac{h_f}{k}\sqrt{\frac{vx}{U_\infty}}$ is local convective heat transfer parameter,$S=\frac{-2v_0}{\sqrt{U_\infty v}}$ is suction/injection parameter, $R=\frac{4\sigma\left(T_f-T_\infty\right)^3}{k^*k}$ non linear thermal radiation parameter, $C_T=\frac{T_\infty}{T_f-T_\infty}$ temperature difference, $M=\frac{\sigma x\beta_0^2}{\rho_f}$ magnetic term parameter, $A=\frac{c}{a}$ is velocity ratio parameter.

4. Results and Discussion

The analysis of the effect of melting, Dufour and Soret effect on MHD mixed convection flow near a vertical porous plate with thermal radiation is presented. The effect of the convective boundary conditions at the porous plate surface is considered. The governing equations where transform using similarity transformation and are solved through Maple using the RKF45 algorithm. RKF45 is a default numeric scheme in Maple software because of its accuracy and lustiness. To ascertain the accuracy of the present analysis, comparisons have been made with previous literature which shows good correlation. The implication of parameters affecting fluid transport is analyzed. The default values of these flow factors are regarded as $S = 1.0$, $M = 1.5$, $Gr_x = 0.5$, $A = 0.5, B = 0.1, R = 1.0, P_r = 0.72$, $U = C_T = S_c = 0.4$,$Kr = 0.2, Me = 0.2$ and $Df(Sr) = 0.03(2.0)$.

Table 4.1: Comparison of the present results to the work of Jha and Samaila in the absence of suction/injection, magnetic effect and velocity ratio.

				Jha and Samaila (2021a)			Present Work		
Bi_x	Gr_x	Pr	R	$f''(0)$	$-\theta'(0)$	$\theta(0)$	$f''(0)$	$-\theta'(0)$	$\theta(0)$
0.1	0.1	0.72	0.1	0.36911	0.07493	0.25069	0.36911	0.07493	0.25069
1.0	0.1	0.72	0.1	0.44445	0.22287	0.77713	0.44445	0.22287	0.77713
10	0.1	0.72	0.1	0.47273	0.26702	0.97330	0.47273	0.26702	0.97330
0.1	0.5	0.72	0.1	0.49816	0.07601	0.23987	0.49816	0.07601	0.23987
0.1	1.0	0.72	0.1	0.63384	0.07693	0.23066	0.63384	0.07693	0.23066
0.1	0.1	2.0	0.1	0.35380	0.08096	0.19036	0.35380	0.08096	0.19036
0.1	0.1	7.0	0.1	0.34283	0.08663	0.13366	0.34283	0.08663	0.13366
0.1	0.1	0.72	0.5	0.37033	0.07433	0.25669	0.37033	0.07433	0.25669
0.1	0.1	0.72	0.1	0.37195	0.07354	0.26452	0.37195	0.07354	0.26452

The accuracy of the current code is illustrated in Tables 4.1, where the comparison is performed without considering suction/injection, magnetic effect, and velocity ratio parameters. The table showcases the utilization of nonlinear ODEs, employing constant values of Bi_x, Gr_x,Pr, and R while setting the suction/injection, magnetic effect, and velocity ratio values to zero. The results obtained from the present work align with the findings of Jha and Samaila (2021a).

Table 4.2: Comparison of the present approach with Jha and Samaila (2021a) on the Nusselt number $-\theta(0)$ for $Gr_x = S = R = A = M = 0$

	Jha and Samaila (2021a)			**Present work**		
$\boldsymbol{Bi_x}$	$\boldsymbol{Pr = 0.1}$	$\boldsymbol{Pr = 0.72}$	$\boldsymbol{Pr = 0.10}$	$\boldsymbol{Pr = 0.1}$	$\boldsymbol{Pr = 0.72}$	$\boldsymbol{Pr = 0.10}$
0.05	0.036844	0.042767	0.046787	0.036844	0.042767	0.046787
0.10	0.058338	0.074724	0.087925	0.058338	0.074724	0.087925
0.20	0.082363	0.119295	0.156903	0.082363	0.119295	0.156903
0.40	0.103720	0.169994	0.258174	0.103720	0.169994	0.258174
0.60	0.113533	0.198051	0.328945	0.113533	0.198051	0.328945
0.80	0.119170	0.215864	0.381191	0.119170	0.215864	0.381191
1.0	0.122830	0.228178	0.421344	0.122830	0.228178	0.421344
5.0	0.136215	0.279131	0.635583	0.136215	0.279131	0.635583
10	0.138096	0.287146	0.678721	0.138096	0.287146	0.678721
20	0.139056	0.291329	0.702563	0.139056	0.291329	0.702563

Table 4.2 examines the non-linear ODEs for model eqautions without considering the effects of nonlinear thermal radiation, suction/injection, and magnetic effect. It focuses on the scenario where Bi_x tends to infinity. The table illustrates the influence of Bi_xon the Nusselt number $-\theta'(0)$, revealing that as the values of Bi_x increase, the Nusselt number appreciates for$Pr = 0.1, Pr = 0.72,$ and $Pr = 0.10$. This finding supports the results obtained by Jha and Samaila (2021a).

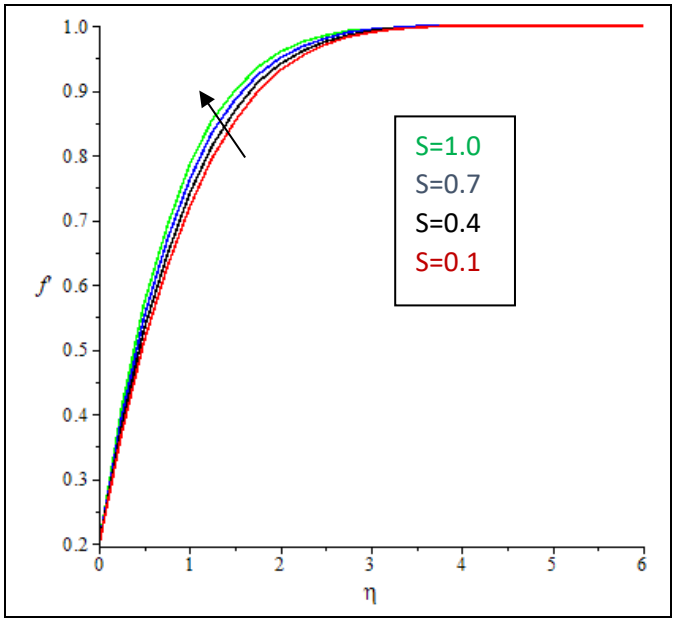

Figure 4.1: Effect of $S > 0$ Variations on $f'(\eta)$

The effect of suction on the fluid velocity distribution is depicted in figure 4.1, it is observed from the figure that the velocity f' increase as the suction $S > 0$ increases. This is because when suction increases the velocity profile is altered. The increase in suction parameter result in an increase in the velocity of the fluid near the surface where the suction is applied, this leads to narrowing of the boundary layer near the surface as the higher velocity at the surface causes greater amount of shear stress which in turn reduces the thickness of the boundary layer.

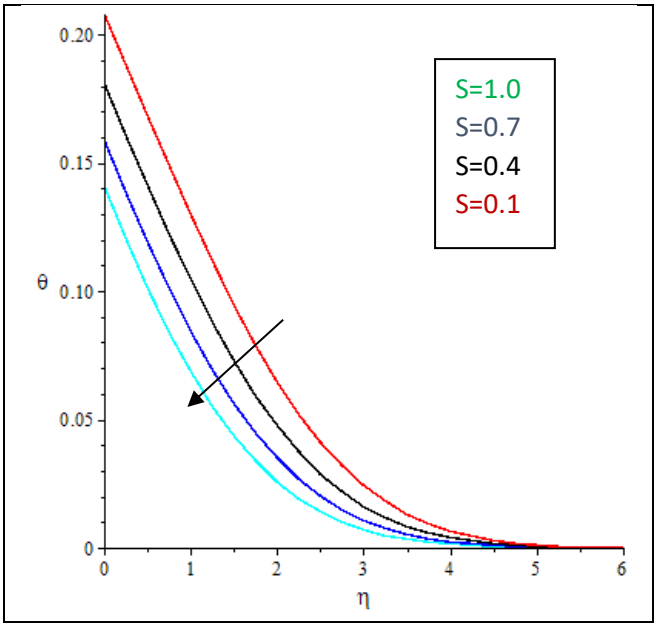

Figure 4.2: Effect of $S > 0$ Variations on $\theta(\eta)$

Figure 4.2 depict the effect of suction $S > 0$ on temperature. As shown from the figure, the temperature distribution is decrease due to the increase in suction. This is because when there is an increase in suction $S > 0$, there is more pressure being exerted on the fluid. This increase pressure can cause the fluid to flow more quickly which in turn leads to decrease in temperature of the fluid. Because, as the fluid flows more quickly it can exchange heat with its surrounding more easily. This result in a cooling effect on the fluid leading to a decrease in temperature and a thinner boundary layer.

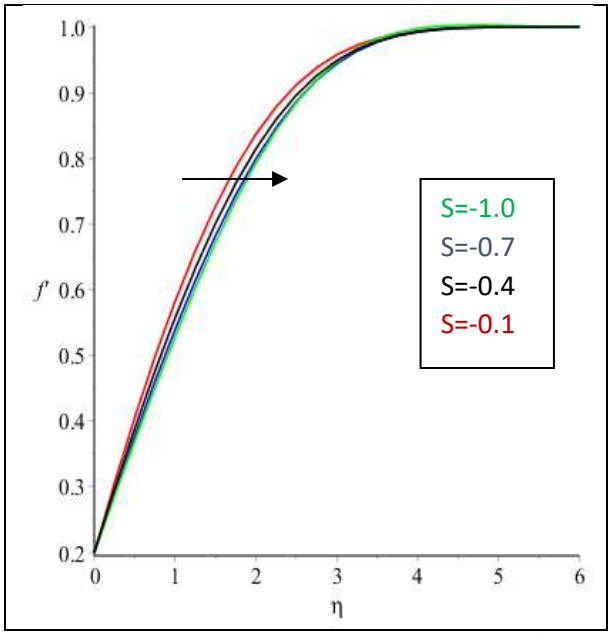

Figure 4.3: Effect of $S < 0$ Variations on $f'(\eta)$

Figure 4.3 shows the effect of injection $S < 0$ on velocity profile. As depicted from the figure the fluid velocity decreases as η increases. This indicates that with injection growth the velocity profile of the system decreases. That is, as injection parameter increases the velocity profile decreases. Because increasing the injection parameter causes more fluid to be injected into the system, increasing the overall volume and the flow rate of the fluid. This can lead to a higher pressure drop and increased turbulence within the system, resulting in a decrease in the velocity profile and a thicker boundary layer.

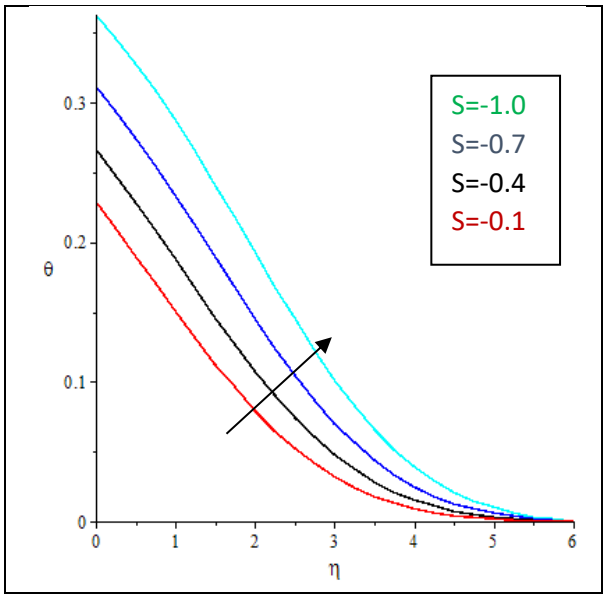

Figure 4.4: Effect of $S < 0$ Variations on $\theta(\eta)$

Figure 4.4 show the effect of injection parameter variation on temperature. As illustrated from the figure, the fluid temperature increases as η increases. This indicates that as injection parameter increases there is a corresponding increase in the temperature of the fluid. Hence, an increase in injection parameter enhances the

temperature profile of the fluid.the reason for the increase in the temperature profile is because when injection increases, there is a higher amount of energy being introduced into the fluid. This can be in in the form of flow rate, pressure, or a combination of both. As a result , the fluid is being subjected to more turbulent mixing and increase friction within the system leading to an increase in temperature.

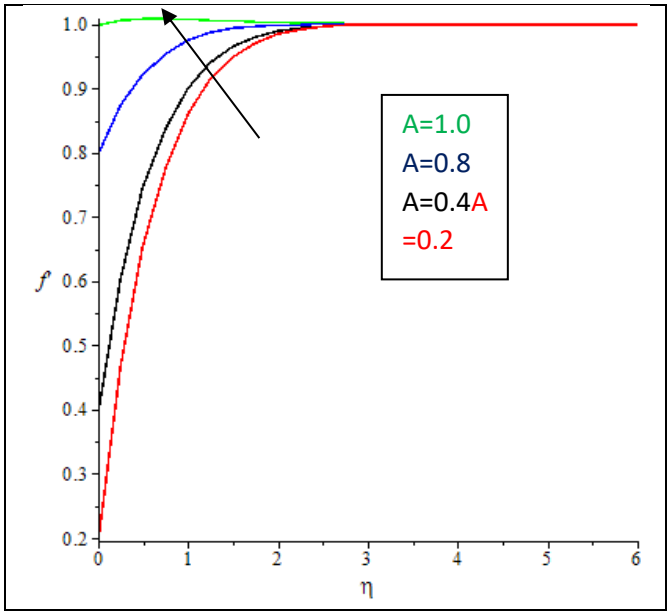

Figure 4.5: Effect of Velocity Ratio parameter A Variation on $f'(\eta)$

Figure 4.5 depict the resultant effect of velocity ratio parameter A variation on velocity profile$f'(\eta)$, which shows that as velocity ratio parameter A increases, the fluid velocity increases for both assisting and opposing flow. This is because the stretching velocity dominates the free stream velocity.

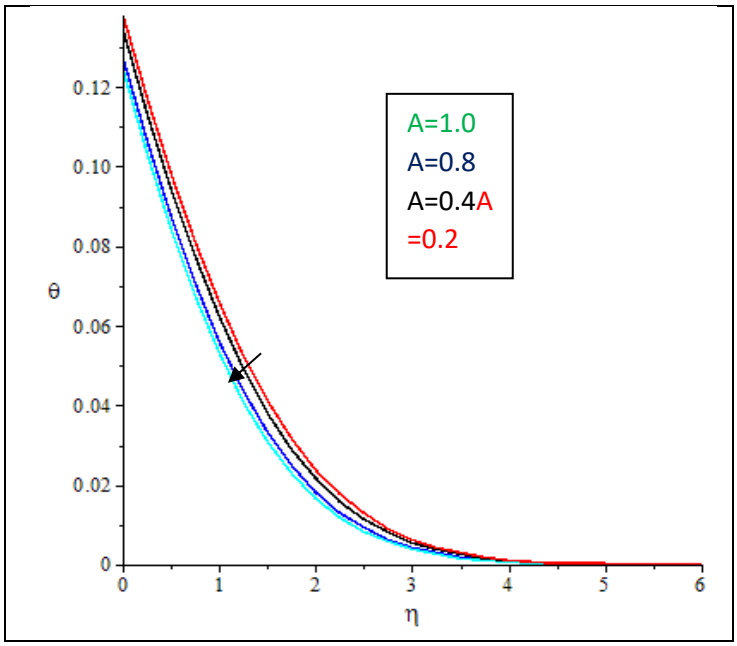

Figure 4.6: Effect of Velocity Ratio Variations on $\theta(\eta)$

Figure 4.6 depict the effect of velocity ratio parameter A variation on temperature profile. As illustrated from the figure, as velocity ratio parameter A increases the temperature profile decreases. This is because as velocity ratio parameter A increases the velocity of the system increases more rapidly, due to this the temperature profile decreases.

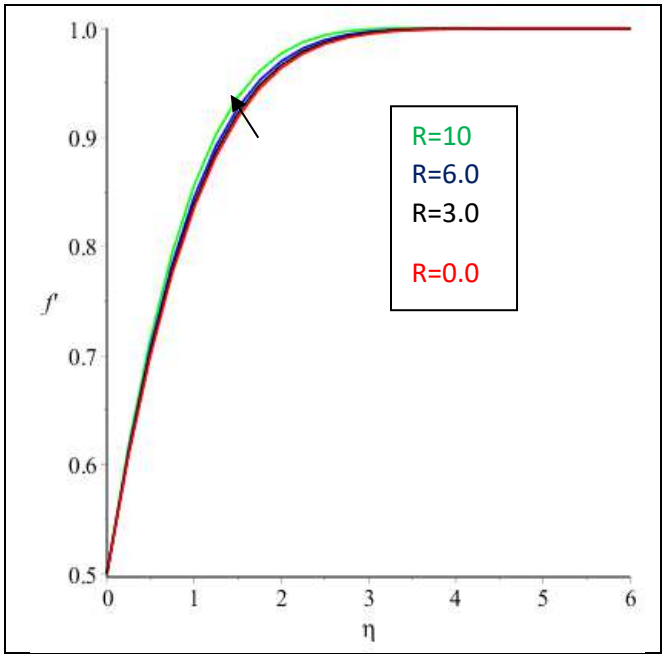

Figure 4.7: Effect of Radiation Parameter Variations on $f'(\eta)$

Figure 4.7 depict the resultant effect of Radiation Parameter R variation on velocity profile$f'(\eta)$, which shows that as Radiation Parameter R increases, the fluid velocity also increases. Hence, an increase in Radiation Parameter R enhanced the velocity profile of the fluid. This is because radiation heat transfer can contribute to the energy balance of the fluid. When radiation heat transfer is increased, more heat is transferred to the fluid, causing it to become warmer and less dense. As a result, the fluid becomes more buoyant and rises at a faster rate, leading to an increase in fluid velocity.

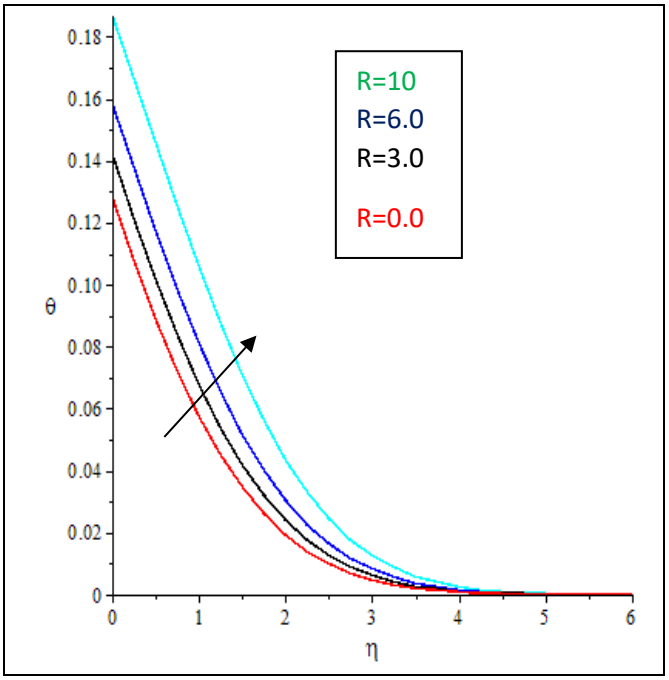

Figure 4.8: Effect of Radiation Parameter R Variations on $\theta(\eta)$

Figure 4.8 depict the resultant effect of Radiation Parameter R variation on temperature profile, which shows that as Radiation Parameter R increases, there is a corresponding increase in the temperature of the fluid. Hence, as the Radiation Parameter R increases the temperature profile of the fluid is enhanced. This is because radiation

helps in transferring heat energy from one medium to another without the need of contact. This means that as radiation parameter increases, more heat energy is being transferred to the fluid causing it to heat up and leading to an increase in its temperature profile.

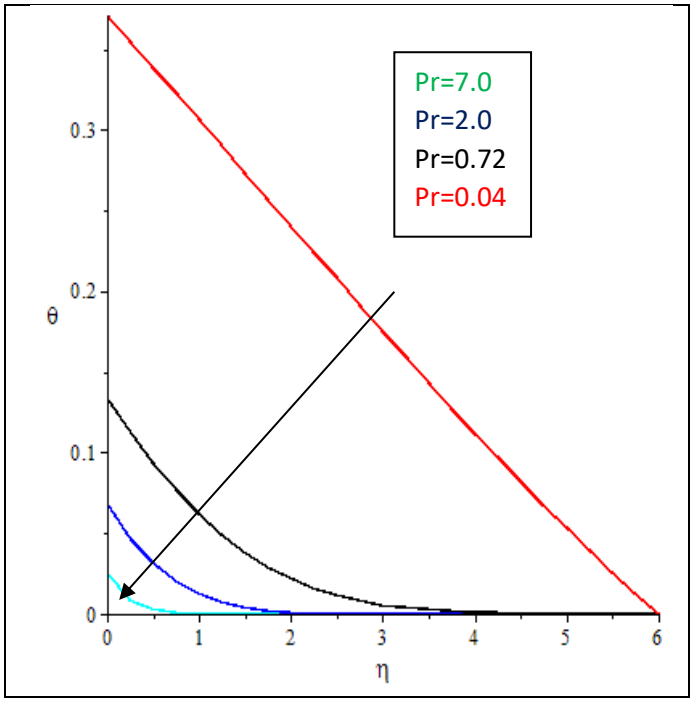

Figure 4.9: Effect of Prandtl Number Variation on $\theta(\eta)$

Figure 4.9 depict the resultant effect of Prandtl Number Variation on temperature profile $\theta(\eta)$, which shows that as Prandtl Number increases , the temperature of the fluid decreases rapidly. Henced an increase in Prandtl Number decreases the temperature profile of the fluid. This is because Prandtl number is a dimensionless number that represents the ratio of momentum diffusivity to thermal diffusivity in a fluid. When the Prandtl number is increased, it means that the thermal diffusivity of the fluid is relatively smaller compared to its momentum diffusivity. In a vertical fluid flow, an increase in the Prandtl number means that the fluid is less effective at conducting heat compared to its ability to transfer momentum. This results in a decrease in the rate of heat transfer within the fluid, leading to a flatter temperature profile.

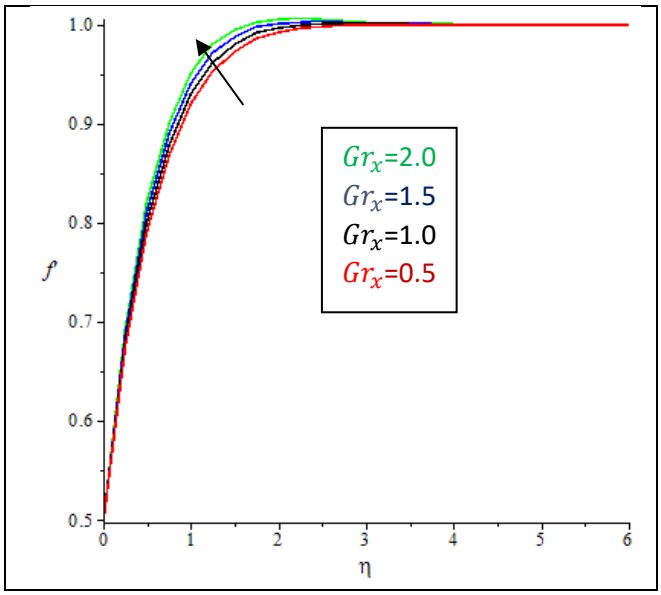

Figure 4.10: Effect of Convective Gr_x parameter on $f'(\eta)$

The consequences of Gr_x parameter on velocity profile is shown in figure 4.10. It is evident from the figure that Gr_x paramter has an increasing effect on velocity profile. This is because Gr_x strengthens the buoyancy force, and in turn enhances the fluid velocity.

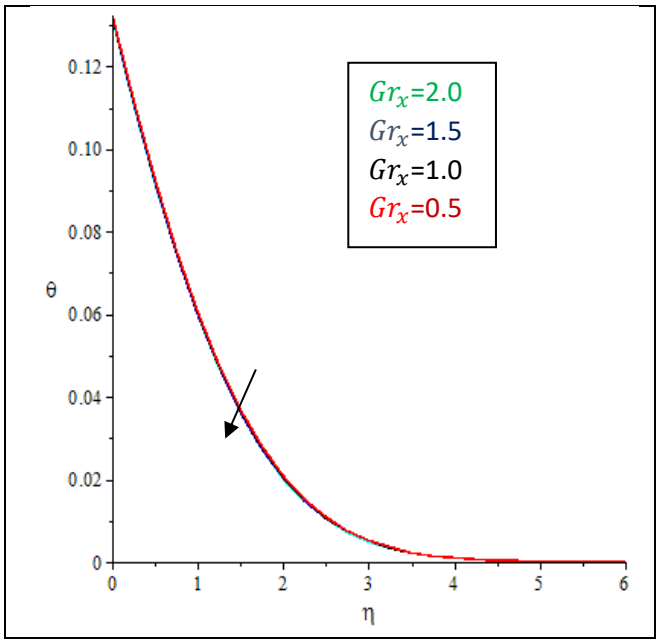

Figure 4.11: Effect of Convective Gr_x parameter on $\theta(\eta)$ for model 1

Figure 4.11 depict the resultant effect of Convective Gr_x parameter on temperature profile $\theta(\eta)$, which shows that as Convective Gr_x increases from 0.0 - 2.0, the temperature tend to decrease, although the difference in decrease from one point of Convective Gr_x parameter ranging from 0.0 - 2.0 is relatively low.

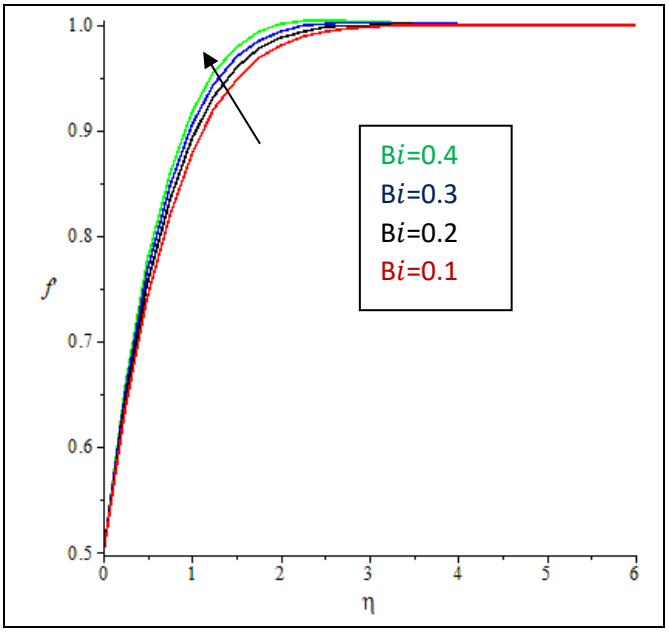

Figure 4.12: Effect of Bi number Variations on $f'(\eta)$

Figure 4.12 illustrates how varying the Bi number affects the velocity profile$f'(\eta)$. The graph demonstrates that an increase in the Bi number results in a corresponding increase in velocity profile of the system.

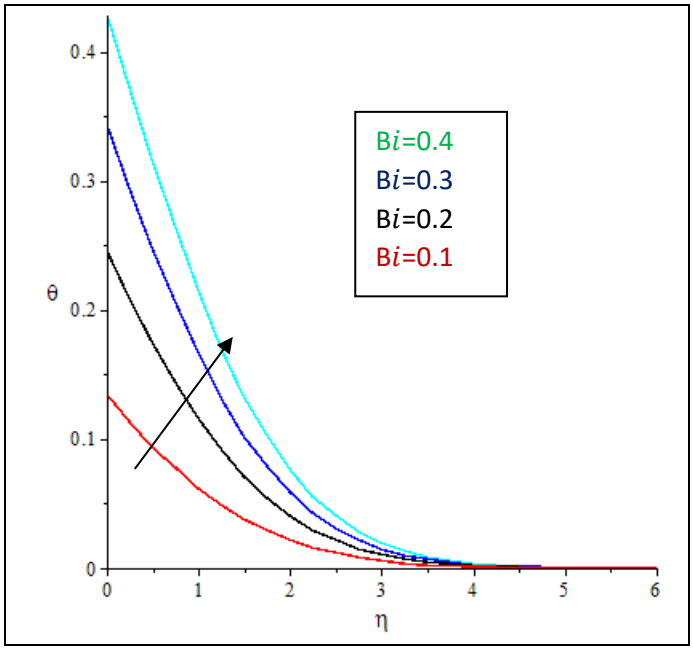

Figure 4.13: Effect of Bi variations on $\theta(\eta)$ for model 1

Figure 4.13 shows the effect of Bi number variation on temperature profile, it depicted that as the Bi number increases the temperature profile increase. This is because the Bi number is a dimensionless number used in heat transfer calculations to determine the relative importance of heat conduction within an object compared to heat convection at the object's surface. A higher Bi number indicates that convection heat transfer is more significant than conduction heat transfer. When the Bi number increases, it means that the rate of heat transfer through convection at the object's surface is higher relative to the rate of heat transfer through conduction within the object. In a fluid flow in a vertical direction, an increase in the Bi number means that there is more efficient convective heat transfer occurring at the surface of the fluid. This increased convective heat transfer leads to a more efficient exchange of heat between the fluid and its surroundings, resulting in a higher temperature profile within the fluid.

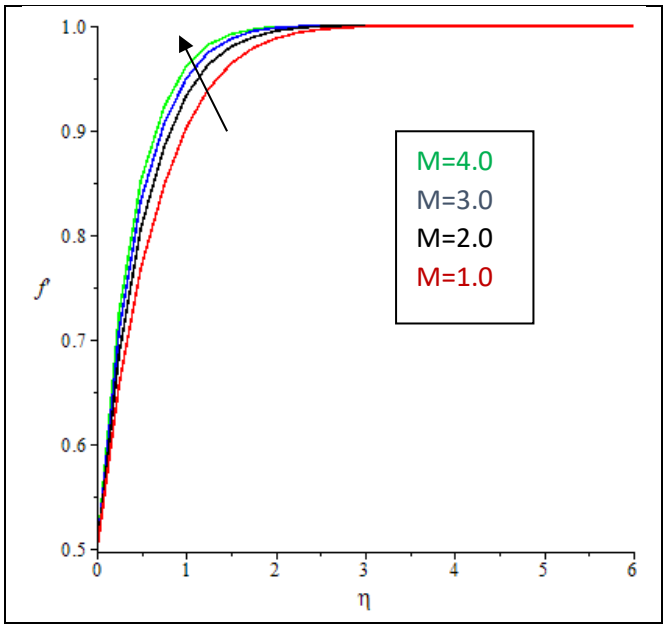

Figure 4.14: Effect of Magnetic Parameter Variations on $f'(\eta)$

Figure 4.14 show the effect of magnetic parameter variation on velocity profile, as illustrated from the figure, an increase in magnetic parameter leads to a corresponding increase in the velocity profile of the system. This is because an increase in the magnetic parameter can increase the velocity profile of the fluid due to the phenomenon known as magnetohydrodynamics (MHD). MHD is the study of the motion of electrically conducting fluids in the presence of a magnetic field. When a magnetic field is applied to a conducting fluid, it can exert a force on the fluid particles, causing them to move in a certain direction. This can lead to changes in the flow behavior of the fluid, resulting in an increase in velocity.

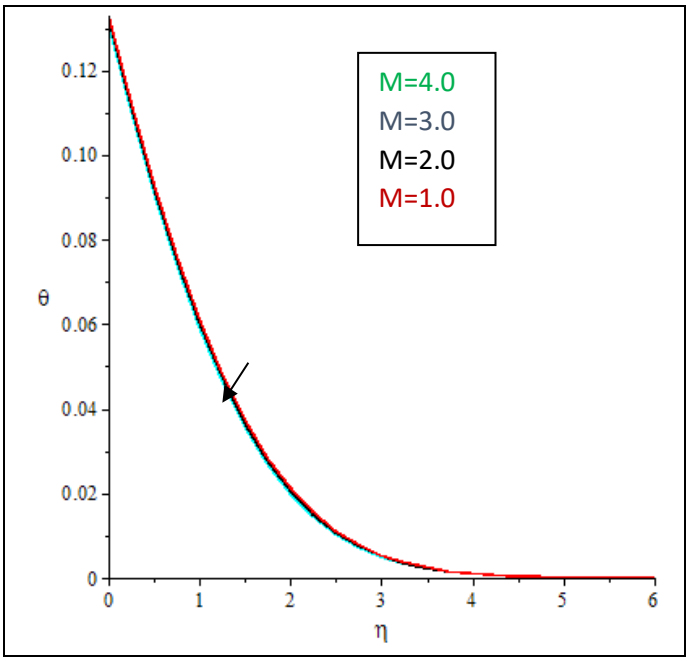

Figure 4.15: Effect of Magnetic Parameter Variations on $\theta(\eta)$

A resultant effect of magnetic parameter on temperature profile is depicted in figure 4.15. As shown from the figure, the magnetic parameter has a decreasing effect on the temperature profile. As the magnetic parameter in increase the temperature decrease relatively low. Hence the magnetic parameter has little effect on the temperature profile of the system.

5. Conclusion

The investigation of mixed convection effect on MHD flow near a vertical porous plate under the influence of magnetic effect and velocity ratio with convective boundary conditions and nonlinear thermal radiation revealed the intricacies of fluid motion and heat transfer in such systems. The findings highlighted the significance of considering these effects in the analysis of MHD flows, as they significantly influenced the velocity and temperature profiles. The major conclusions of this study are:

- The presence of mixed convection parameter enhances the velocity profile in the system, leading to a reduction in both the temperature and concentration profiles. Additionally, the boundary layer thickness increases for all profiles.
- The magnetic parameter shrinks the velocity profile and thickens the boundary layer whereas the temperature distribution rises with the boundary layer thinning thinner due to the influence of the Lorentz force.
- As the velocity ratio increases, the velocity profile is enhanced, resulting in a thicker boundary layer, whereas the temperature profile experiences a decrease.

- The Boit number results in improved velocity and temperature profiles, causing an increase in thickness for both boundary layers.

Finally the study emphasized the importance of considering these effects, as they had a substantial impact on the heat and mass transfer rates near the porous plate.

REFERENCES

Aaiza, G., Ilyas, K., & Sharidan, S.(2015). Energy Transfer in Mixed Convection MHD flow of Nanofluid Containing Different Shapes of Nanoparticles in a Channel Filled with Saturated Porous Medium. *Journal of Nano Research Letters*. 10(1), 490-504

Alamri S., Ambreen A., Mariam A., & Ellahi R. (2019). Effect of Mass Transfer on MHD Second Grade Fluids Towards Stretching Cylinder. *Journal of Physics Letters A.* 383(2-3), 276-281

Alfvén, H. (1942). Existence of Electromagnetic-Hydrodynamic Waves. *Journal of Nature*. 150(3805),405-406

Ali Agha H., Bouaziz. M.N, Hanini S.,(2014). Free Convection Boundary Layer Flow from a Vertical Flat Plate Embedded in a Darcy Porous Medium Filled with Nanofluid : Effect of Magnetic Field and Thermal Radiaton. *Arab Journal of Science Engineering*.39(11), 8331-8340.

Davood D., & Sayyid H.K. (2015). Natural,Mixed and Force Convection in Nanofluid. *JournalofApplication of Nonlinear Systems in Nanomechanics and Nanofluid*.9(6)205-269

Hemalatha K. & Prasad S.R. (2014). Melting with Viscous Dissipation on MHD Radiative flow from a Vertical Plate Embedded in Non-Darcy Porous Medium. *Journal of Applied Fluid Mechanics* 8(4), 747-752.

Jha B.K., Isah B.Y., & Uwanta I.L.,(2018). Combined Effect of Suction/Injection on MHD Free Convection Flow in a Vertical Channel with Thermal Radiation. *Ain Shams Engineering Journal*. 9(4), 1069-1088.

Jha K. B., & Mohammed U. (2014). Mixed Convection Effect on Melting From a Vertical Plate Embedded in a Saturated Porous Media. *Journal of Heat Transfer- Asian Research.* 43(7)667-676

Jha K. B., & Samaila G. (2021a). Numerical Solution for Natural Convection flow near a Vertical Porous Plate Having Convective Boundary Condition with Nonlinear Thermal Radiation. *Journal of Heat Transfer* 51(9) 45-60

Jha, B. K.,Mohammed, U. & Abiodun, O. (2013). Dufour and Soret Effects on Melting from a Vertical Plate Embedded in Saturated Porous Media. *Journal of Applied Mathematics*. 2013(1), 9-20

Jha, K., and Muhammad, S. (2019). Chemical Reaction and Dufour Effect on Nonlinear Free Convection Heat and Mass Transfer flow near a Vertical Moving Porous Plate. *Journal of Heat Transfer-Asian Research.* 49(1), 1-16.

Jha, K.and Samaila, G. (2020).Similarity Solution for Natural Convection Flow near a Vertical Plate with Thermal Radiation. *Journal of Microgravity Science and Technology*. 32(1), 1031-1038

Jha, K.B, & Samaila, G. (2021b). Impact of Nonlinear Thermal Radiation on Nonlinear Mixed Convection Flow near a Vertical Porous Plate with Convective Boundary Condition. *Journal of Process Mechanical Engineering*. 236(2)689-703

Jha, K.B. & and Samaila, G. (2022). Thermal Radiation Effect on Boundary Layer over a Flat Plate having Convective Surface Boundary Condition. *Springer Nature Journal of Applied Science*. 2(1), 381-398.

Reddy, S. & Ali, J. (2016). Soret and Dufour Effect on MHD Heat and Mass Transfer Flow of a Micropolar Fluid with Thermophoresis Particle Deposition. *Journal of Naval Architecture and Marine Engineering*.13(1) 239-270.

Saman R., Javad A., & Mahla M. (2017). Application of Magnetohydrodynamics in Biological Systems – A Review on the Numerical Studies. *Journal of Magnetism and Magntic Materials*, 439(1), 358-372.

Sharma P., Sharad S., Yadav R., & Anatoly N. (2018). MHD Mixed Convective Stagnation Point Flow along a Vertical Stretching Sheet with Heat Source/Sink. *International Journal of Heat and Mass Transfer.* 117(1) 780-786.

Surbhi S., Amit D., Amit P., Jyoti A., Qasem A., (2023). Analysis for MHD Micro Polar Fluid over a Melting Stretching Surface with Slip Effect. *Research Gate Journal* 13(1), 562-578.

Venkata, R., Anantha, K., & Sandeep, N. (2021). Impact of Soret and Dufour on MHD Casson Fluid Flow Pass a Stretching Surface with Convective-Diffusive Conditions. *Journal of Thermal Analysis and Calorimetry*. 147(1), 2653-2663.

Mathematical Analysis of Wood Pyrolysis and Combustion

Yisa, E. M.[1,2 *], Olayiwola, R. O.[1], Adamu, A. A.[1], Cole, A. T.[1]

[1]Department of Mathematics, Federal university of Technology, Minna, Nigeria

[2] Department of Mathematics and Statistics, Niger State Polytechnic, Zungeru, Nigeria

[1,2 *] emmyyisa74@gmail.com

Abstract

This paper analyses the wood pyrolysis and combustion. The partial differential equations governing the wood pyrolysis and combustion were non-dimensionalized using some dimensionless quantities. The dimensionless equations were decoupled using perturbation method and solved using Olayiwola's Generalized Polynomial Approximate Method (OGPAM). The influences of wood geometry, n on temperature distribution have been analysed. The results obtained revealed that the magnitude of temperature in the wood for the slab particle is very large compare to the cylindrical and spherical particles.

Keywords: Biomass, combustion, OGPAM, pyrolysis, wood, wood geometry

1. Introduction

Over the years, renewable energy has begun to gain attention as a possible way of supplying the world's energy demand. Biomass is one such energy source to produce renewable energy (Niranjan *et al.*, 2015). One advantage of biomass is that it is available everywhere in the world in contrast to fossil fuels such as oil and gas. Biomass actually accounts for one-third of the energy consumption in developing countries in Africa and Asia (Mate, 2016). From an environmental sustainability perspective, biomass is also a carbon-neutral energy source and combined with carbon dioxide sequestration can result in a net negative carbon footprint.

Thermochemical conversion can transform biomass into gas, liquid, or char. All the processes begin with a pyrolysis step. In pyrolysis, the biomass undergoes devolatization and is converted to char in the absence of an oxidizing agent such as oxygen. However, in combustion, biomass is oxidized in excess oxygen producing carbon dioxide and water leaving ash as the only solid residual. Gasification is a thermochemical process that converts carbonaceous materials to synthesis gas (hydrogen and carbon monoxide) by reacting them with a controlled amount of oxygen and/or steam. Employing the Fischer -Tropsch process, the synthesis gas can further be upgraded to other organic compounds such as plastics, fuel and pharmaceutical drugs (Mate, 2016).

Biomass materials, primarily in the form of wood, have been used for many different applications. Wood fuels have been used as a source of energy for cooking and heating since man developed the ability to harness fire. Wood has been widely used for building machinery and in structural applications due to the relatively high strength and availability of many species of wood (Hagge, 2005).

Furthermore, pyrolysis is a viable thermal process for efficient and economical conversion of biomass into alternative energy in forms of solid char, liquid bio oil and combustible gases (Natthaya & Chaiyot, 2013). It is generally known that, solid, liquid and gas produced from pyrolysis are of primary interest for use as a primary fuel. However, recently researchers have directed their attention towards investigating the effect of pyrolysis condition on maximizing the yield pyrolysis liquids which show promise as a substitute for petroleum based fuel.

Wood pyrolysis and combustion process can be described by a system of partial differential equation (PDE) with suitable initial and boundary conditions.

2. Literature Review

Many researchers have studied either numerically and analytically the phenomenon of wood pyrolysis and combustion. This include Long *et al.* (2015) who developed a model of pyrolysis and combustion behaviors of non-charring and intumescent-product polymers using 'firestone'. The result showed that the peak mass loss rate of the non-charring polymer material occurred near the end of burning, whereas for the intumescent-protected polymer happen shortly after the start of the experiment

Richter *et al.* (2019) investigated the effect of chemical composition on the charring of different species of wood using microscale kinetic model which include pyrolysis and char oxidation reaction. From their research they observed that the variation of cellulose, hemicellulose and lignin is small within softwood and hardwood and at microscale, the variation rate of degradation. It was also observed that at mesoscale, the difference in kinetics, including pyrolysis and char oxidation reaction proved insignificant for temperature and mass loss predictions for the charring of wood, also the tested hypothesis of kinetic of different wood species insignificantly affect the charring of wood.

Izabells *et al.* (2017) developed one dimensional numerical model and applied it to study pyrolysis and spontaneous wood ignition when subjected to transient irradiation by combining experimental and a-prior prediction. From the result, it was found that the exothermic heat of pyrolysis does not have any influence on the predictions and the reaction order of the char reaction has an impact on the mass loss rate (MLR), but it is insignificant on the temperature less than one percent. It also showed that there is strong interaction between the chemical reactions and heat and mass transfer processes involved in the thermal degradation of wood.

The effect of physical characteristics of hardwood chips on the pyrolysis was investigated by Alok *et al.* (2020) through the conservation of solid phase mass fraction of biomass. It was discovered that the equivalent length of wooden slab for G30 should vary from 73 to 74 mm which is relatively large for G50 and combination of both of them. And that the result of the proposed model provided good correlation with experimental results.

Numerous chemical and transport models have been formulated to describe the physical and chemical changes that occur during pyrolysis and combustion of wood. This research work seeks to consider the particle geometry modelled in one-dimension to be slab, cylindrical and spherical and targeted to bridge this knowledge gaps by considering the following:

(i) Two-step reaction mechanism as kinetic scheme.

(ii) Evolution of moisture in wood in the form of water vapour.

(iii) Convection and diffusion of moisture.

3. Model Formulation

Pyrolysis is mathematically described through a system of coupled equations. The basic equations are those of chemical kinetics, heat transfer and mass transfer. In this research work, wood particles of arbitrary size are considered. The particle is modelled as one dimensional, to maintain a reasonable low workload for the computation. The model can be readily extended to two or three dimensions. The following assumptions are employed in our model.

The change of the density of the wood particle is described by the following equation,

$$\frac{\partial \rho_w}{\partial t} = -A_1 \rho_w e^{-\frac{E_1}{RT}} - A_2 \rho_w e^{-\frac{E_2}{R_g T}} \tag{1}$$

The change of the density of moisture (liquid) of the wood particle is described by the following equation,

$$\frac{\partial \rho_m}{\partial t} + \frac{1}{r^n}\frac{\partial}{\partial r}\left(r^n \rho_m u_g\right) = \frac{1}{r^n}\frac{\partial}{\partial r}\left(r^n D_m \frac{\partial \rho_m}{\partial r}\right) - A_4 \rho_m e^{-\frac{E_4}{R_g T}} \tag{2}$$

The change of char densities in the wood particle is describe by the following equations,

$$\frac{\partial \rho_{c1}}{\partial t} = A_2 \rho_w e^{-\frac{E_2}{R_g T}} - A_3 \rho_{c1} \rho_{g1} e^{-\frac{E_3}{R_g T}} - \frac{M_c}{M_{ox}} S_\sigma A_5 \rho_{c1} Y_{ox} e^{-\frac{E_5}{R_g T}} \tag{3}$$

$$\frac{\partial \rho_{c2}}{\partial t} = A_3 \rho_{c1} \rho_{g1} e^{-\frac{E_3}{R_g T}} - \frac{M_c}{M_{ox}} S_\sigma A_6 \rho_{c2} Y_{ox} e^{-\frac{E_6}{R_g T}} \tag{4}$$

The change of water vapour density in the wood particle is describe by the following equation,

$$\frac{\partial \rho_v}{\partial t} + \frac{1}{r^n}\frac{\partial}{\partial r}\left(r^n \rho_v u_g\right) = A_4 \rho_m e^{-\frac{E_4}{R_g T}} \tag{5}$$

The change of densities of gases in the wood particle is describe by the following equations,

$$\frac{\partial}{\partial t}\left(\varepsilon \rho_{g1}\right) + \frac{1}{r^n}\frac{\partial}{\partial r}\left(r^n \varepsilon \rho_{g1} u_g\right) = A_1 \rho_w e^{-\frac{E_1}{R_g T}} - A_3 \rho_{g1} \rho_{c1} e^{-\frac{E_3}{R_g T}} + A_4 \rho_m e^{-\frac{E_4}{R_g T}} \tag{6}$$

$$\frac{\partial}{\partial t}\left(\varepsilon \rho_{g2}\right) + \frac{1}{r^n}\frac{\partial}{\partial r}\left(r^n \varepsilon \rho_{g2} u_g\right) = A_3 \rho_{g1} \rho_{c1} e^{-\frac{E_3}{R_g T}} \tag{7}$$

The conservation equation of gaseous species can be written as,

$$\frac{\partial}{\partial t}\left(\varepsilon\rho_g Y_{ox}\right)+\frac{1}{r^n}\frac{\partial}{\partial r}\left(r^n\varepsilon\rho_g u_g Y_{ox}\right)=\frac{1}{r^n}\frac{\partial}{\partial r}\left(r^n\varepsilon\rho_g D_{ox}\frac{\partial Y_{ox}}{\partial r}\right)-\frac{M_c}{M_{ox}}S_\sigma A_5\rho_{c1}Y_{ox}e^{-\frac{E_5}{R_gT}} - \frac{M_c}{M_{ox}}S_\sigma A_6\rho_{c2}Y_{ox}e^{-\frac{E_6}{R_gT}} \quad (8)$$

The energy conservation equation can be written as,

$$\frac{\partial}{\partial t}\left(\left(\varepsilon\sum_i^{N_g+N_v}\rho_i C_{Pi}+(1-\varepsilon)\sum_j^{N_m+N_w+N_c}\rho_j C_{Pj}\right)T\right)+\frac{1}{r^n}\frac{\partial}{\partial r}\left(r^n\varepsilon u_g\sum_i^{N_g+N_v}\rho_i C_{Pi}T\right)=$$
$$\frac{1}{r^n}\frac{\partial}{\partial r}\left(r^n K_T\frac{\partial T}{\partial r}\right)+\frac{\partial q_r}{\partial r}-\Delta h_1 A_1\rho_w e^{-\frac{E_1}{R_gT}}-\Delta h_2 A_2\rho_w e^{-\frac{E_2}{R_gT}}-\Delta h_4 A_4\rho_m e^{-\frac{E_4}{R_gT}}- \quad (9)$$
$$\Delta h_3 A_3\rho_{g1}\rho_{c1}e^{-\frac{E_3}{R_gT}}+\frac{M_c}{M_{ox}}S_\sigma A_5\Delta h_5\rho_{c1}Y_{ox}e^{-\frac{E_5}{R_gT}}+\frac{M_c}{M_{ox}}S_\sigma A_6\Delta h_6\rho_{c2}Y_{ox}e^{-\frac{E_6}{R_gT}}$$

The initial and boundary conditions are formulated as follows:

$$\left.\begin{aligned}
&\text{For } t=0,\ \forall r:\ T=T_0,\quad \rho_w=\rho_{w0},\quad \rho_m=\rho_{m0},\quad \rho_{c1}=0,\quad \rho_{c2}=\rho_{c20},\\
&\qquad\qquad \rho_v=0,\quad \rho_{g1}=0,\quad \rho_{g2}=\rho_{g20},\quad Y_{ox}=0\\
&\text{For } r=0,\ \forall t:\ \frac{\partial \mathrm{T}}{\partial r}=0,\quad \frac{\partial \rho_{\mathrm{m}}}{\partial r}=0,\quad \frac{\partial \rho_{\mathrm{v}}}{\partial r}=0,\quad \frac{\partial \rho_{\mathrm{g1}}}{\partial r}=0,\quad \frac{\partial \rho_{\mathrm{g2}}}{\partial r}=0,\quad \frac{\partial \mathrm{Y_{ox}}}{\partial r}=0\\
&\text{For } r=R,\ \forall t:\ -k^*\frac{\partial \mathrm{T}}{\partial r}=h\left(T-T_0\right),\quad -D_{ox}^*\frac{\partial \mathrm{Y_{ox}}}{\partial r}=k_{mox}\left(Y_{ox}-Y_\infty\right),\\
&\qquad\qquad -D_m^*\frac{\partial \rho_m}{\partial r}=k_{mm}\rho_m
\end{aligned}\right\}, \quad (10)$$

where

ρ_w is the density of wood, ρ_m is the density of moisture of the particle, ρ_v is the density of water vapour. ρ_{g1} & ρ_{g2} are the densities of the gases, ρ_{c1} & ρ_{c2} are the densities of the char in the particle, ρ_i, ρ_j are the species densities, C_{Pi}, C_{Pj} are the species specific heat capacities, r is the space, t is time, R is radius, R_g is the gas constant, u_g is the gas velocity, D_m is the moisture diffusion coefficient, D_{ox} is the oxygen diffusion coefficient, T is the temperature, E_1, E_2, E_3, E_4 & E_5 are the activation energies, A_1, A_2, A_3, A_4 & A_5 are the pre-exponential factor, S_σ is the specific surface of dense product of pyrolysis, Y_{ox} is the oxygen concentration, M_c is the mass of char, M_{ox} is the mass of oxygen, $\Delta h_1, \Delta h_2, \Delta h_3, \Delta h_4$ & Δh_5 are the heat of reactions, K is the permeability, q_r is the radiative heat flux, q_{ext} is the external radiative heat flux, k is the thermal conductivity of the medium, T_0 is the

interface temperature between pyrolysis and combustion, ρ_{wo} is the initial wood density, ρ_{mo} is the initial moisture density, k^* is the effective thermal conductivity of the medium, k_{mm} is the moisture convective mass transfer coefficient, k_{mox} is the Oxygen convective mass transfer coefficient, h is the convective heat transfer coefficient, ε is porosity, D_{ox}^* is the effective Oxygen diffusion coefficient, D_m^* is the effective moisture diffusion coefficient, μ is the dynamic viscosity, P is the pressure.

3.1 Dimensional Analysis

Here we make the variables in (1)—(9) dimensionless by introducing dimensionless variables

$$\left.\begin{array}{llllll} r'=\dfrac{r}{R}, & t'=\dfrac{Ut}{R}, & u=\dfrac{u_g}{U}, & \rho_1=\dfrac{\rho_w}{\rho_{w0}}, & \rho_2=\dfrac{\rho_m}{\rho_{m0}}, & \\ \rho_3=\dfrac{\rho_{c1}}{\rho_{c10}}, & \rho_4=\dfrac{\rho_{c2}}{\rho_{c20}}, & \rho_5=\dfrac{\rho_v}{\rho_{v0}}, & \rho_6=\dfrac{\rho_{g1}}{\rho_{g10}}, & \rho_7=\dfrac{\rho_{g2}}{\rho_{g20}}, & \\ \phi=\dfrac{Y_{ox}-Y_\infty}{Y_0-Y_\infty}, & \theta=\dfrac{1}{\in T_0}(T-T_0), & P'=\dfrac{P}{\rho U^2}, & a=\dfrac{E_1}{E_5}, & & \\ b=\dfrac{E_2}{E_5}, & c=\dfrac{E_3}{E_5}, & d=\dfrac{E_4}{E_5}, & e=\dfrac{E_6}{E_5}, & \in=\dfrac{R_gT_0}{E_5}, & q=\dfrac{q_{ext}}{\rho_g C_{pg}\in T_0 U} \end{array}\right\} \quad (11)$$

and we obtain,

$$\left.\begin{array}{c} \dfrac{\partial\rho_1}{\partial t}=-\alpha_1\rho_1 e^{\frac{a\theta}{1+\in\theta}}-\alpha_2\rho_1 e^{\frac{b\theta}{1+\in\theta}} \\ \rho_1(r,0)=1 \end{array}\right\} \quad (12)$$

$$\left.\begin{array}{c} \dfrac{\partial\rho_2}{\partial t}+u\dfrac{1}{r^n}\dfrac{\partial}{\partial r}(r^n\rho_2)=\dfrac{1}{P_{em1}}\dfrac{1}{r^n}\dfrac{\partial}{\partial r}\left(r^n(1+\in\theta)\dfrac{\partial\rho_2}{\partial r}\right)-\alpha_3\rho_2 e^{\frac{d\theta}{1+\in\theta}} \\ \rho_2(r,0)=1,\quad \left.\dfrac{\partial\rho_2}{\partial r}\right|_{r=0}=0,\quad \left.\dfrac{\partial\rho_2}{\partial r}\right|_{r=1}=-Sh_m\rho_2(1,t) \end{array}\right\} \quad (13)$$

$$\left.\begin{array}{c} \dfrac{\partial\rho_3}{\partial t}=\alpha_4\rho_1 e^{\frac{b\theta}{1+\in\theta}}-\alpha_5\rho_3\rho_6 e^{\frac{c\theta}{1+\in\theta}}-\alpha_6\rho_3(\phi+\gamma)e^{\frac{\theta}{1+\in\theta}} \\ \rho_3(r,0)=0 \end{array}\right\} \quad (14)$$

$$\left.\begin{array}{c} \dfrac{\partial\rho_4}{\partial t}=\alpha_7\rho_3\rho_6 e^{\frac{c\theta}{1+\theta\vartheta}}-\alpha_8\rho_4(\phi+\gamma)e^{\frac{f\theta}{1+\in\theta}} \\ \rho_4(r,0)=1 \end{array}\right\} \quad (15)$$

$$\left.\begin{aligned}&\frac{\partial \rho_5}{\partial t}+u\frac{1}{r^n}\frac{\partial}{\partial r}\left(r^n\rho_5\right)=\alpha_9\rho_2 e^{\frac{d\theta}{1+\epsilon\theta}}\\&\rho_5(r,0)=0,\qquad \left.\frac{\partial \rho_5}{\partial r}\right|_{r=0}=0\end{aligned}\right\} \tag{16}$$

$$\left.\begin{aligned}&\frac{\partial \rho_6}{\partial t}+u\frac{1}{r^n}\frac{\partial}{\partial r}\left(r^n\rho_6\right)=\alpha_{10}\rho_1 e^{\frac{a\theta}{1+\epsilon\theta}}-\alpha_{11}\rho_3\rho_6 e^{\frac{c\theta}{1+\epsilon\theta}}+\alpha_{12}\rho_2 e^{\frac{d\theta}{1+\epsilon\theta}}\\&\rho_6(r,0)=0,\qquad \left.\frac{\partial \rho_6}{\partial r}\right|_{r=0}=0\end{aligned}\right\} \tag{17}$$

$$\left.\begin{aligned}&\frac{\partial \rho_7}{\partial t}+u\frac{1}{r^n}\frac{\partial}{\partial r}\left(r^n\rho_7\right)=\alpha_{13}\rho_3\rho_6 e^{\frac{c\theta}{1+\epsilon\theta}}\\&\rho_7(r,0)=1,\qquad \left.\frac{\partial \rho_7}{\partial r}\right|_{r=0}=0\end{aligned}\right\} \tag{18}$$

$$\left.\begin{aligned}&\frac{\partial \phi}{\partial t}+u\frac{1}{r^n}\frac{\partial}{\partial r}\left(r^n\phi\right)=\frac{1}{P_{em2}}\frac{1}{r^n}\frac{\partial}{\partial r}\left(r^n(1+\epsilon\theta)\frac{\partial \phi}{\partial r}\right)-\sigma_1\rho_3(\phi+\gamma)e^{\frac{\theta}{1+\epsilon\theta}}-\\&\sigma_2\rho_4(\phi+\gamma)e^{\frac{f\theta}{1+\epsilon\theta}}\\&\phi(r,0)=0,\qquad \left.\frac{\partial \phi}{\partial r}\right|_{r=0}=0,\qquad \left.\frac{\partial \phi}{\partial r}\right|_{r=1}=-Sh_{ox}\phi(1,t)\end{aligned}\right\} \tag{19}$$

$$\left.\begin{aligned}&\frac{\partial \theta}{\partial t}+u\frac{1}{r^n}\frac{\partial}{\partial r}\left(r^n\theta\right)=\frac{1}{P_e}\frac{1}{r^n}\frac{\partial}{\partial r}\left(r^n(1+\epsilon\theta)\frac{\partial \theta}{\partial r}\right)+q\frac{\partial}{\partial r}\left(e^{-\sigma r}\right)-\delta\rho_1 e^{\frac{a\theta}{1+\epsilon\theta}}+\\&\delta_1\rho_3(\phi+\gamma)e^{\frac{\theta}{1+\epsilon\vartheta}}-\delta_2\rho_1 e^{\frac{b\theta}{1+\epsilon\theta}}-\delta_3\rho_3\rho_6 e^{\frac{c\theta}{1+\epsilon\theta}}-\delta_4\rho_2 e^{\frac{d\theta}{1+\epsilon\theta}}+\delta_5\rho_4(\phi+\gamma)e^{\frac{f\theta}{1+\epsilon\theta}}\\&\theta(r,0)=0,\qquad \left.\frac{\partial \theta}{\partial r}\right|_{r=0}=0,\qquad \left.\frac{\partial \theta}{\partial r}\right|_{r=1}=-Nu\,\theta(1,t)\end{aligned}\right\} \tag{20}$$

3.2 Solution via OGPAM

In the limit of $\epsilon\to 0$, follow the idea in Ayeni (1982) that e^{θ} can be written in quadrature form as:

$$e^{\theta}\approx 1+(e-2)\theta+\theta^2 \tag{21}$$

We obtain the solution to equations (12) – (20), using OGPAM as:

$$\rho_{10}(r,t)=e^{-\left(A_0 t+\left(c_7-c_8 r^2\right)t^2+\frac{1}{3}\left(c_9+c_{10}r^2+c_{11}r^4\right)t^3\right)} \tag{22}$$

$$\rho_{20}(r,t)=\left(B_9-B_{10}r^2\right)e^{-\left(B_6 t-\frac{1}{2}B_7 t^2-\frac{1}{3}B_8 t^3\right)} \tag{23}$$

$$\rho_{30}(r,t)=0 \tag{24}$$

$$\rho_{40}(r,t)=1 \tag{25}$$

$$\rho_{50}(r,t)=\rho_{50}\big|_{r=0}\left(1-r^2\right) \tag{26}$$

$$\rho_{60}(r,t)=\rho_{60}\big|_{r=0}\left(1-r^2\right), \tag{27}$$

$$\rho_{70}(r,t)=\left(1-r^2\right) \tag{28}$$

$$\rho_{41}(r,t)=-\left(A_{24}t+\frac{1}{2}\left(c_{160}-c_{161}r^2\right)t^2+\frac{1}{3}\left(c_{162}+c_{163}r^2+c_{164}r^4\right)t^3\right) \tag{29}$$

$$\rho_{31}(r,t)=\left(E_{43}(r)+\begin{pmatrix}E_{44}(r)+E_{45}(r)t+E_{46}(r)t^2+\\E_{47}(r)t^3+E_{48}(r)t^4+E_{49}(r)t^5\end{pmatrix}e^{A_{23}t}\right)e^{-\left(A_5t+E_{33}(r)t^2+E_{34}(r)t^3\right)}, \tag{30}$$

$$\rho_{21}(r,t)=\begin{pmatrix}c_{135}+c_{136}t+c_{137}t^2+c_{138}t^3+c_{139}t^4+c_{140}t^5+c_{141}t^6+c_{142}t^7\\+c_{143}t^8+c_{144}t^9+c_{145}t^{10}+c_{146}t^{11}+c_{147}t^{12}+c_{148}t^{13}+c_{149}t^{14}\\+c_{150}t^{15}+c_{151}t^{16}+c_{152}e^{-c_{109}t}+c_{153}t^2e^{-c_{109}t}+c_{154}t^3e^{-c_{109}t}\end{pmatrix} \tag{31}$$

$$\rho_{11}(r,t)=$$

$$\frac{1}{A_0^{10}}\left(1-\frac{1}{3}E_1(r)t^3\right)\frac{1}{A_0^{10}}\left(E_{22}(r)+\begin{pmatrix}E_{23}(r)+E_{24}(r)t+E_{25}(r)t^2+\\E_{26}(r)t^3+E_{27}(r)t^4+\\E_{28}(r)t^5+E_{29}(r)t^6+\\E_{30}(r)t^7+E_{31}(r)t^8+E_{32}(r)t^9\end{pmatrix}e^{A_0t}\right)e^{-\left(A_0t+\frac{1}{2}E_0(r)t^2\right)} \tag{32}$$

$$\phi_1(r,t)=\phi_1\big|_{r=1}.\left(\left(1+\frac{Sh_{ox}}{2}\right)-\frac{Sh_{ox}}{2}r^2\right) \tag{33}$$

$$\theta_1(r,t)=\theta_1\big|_{r=1}.\left(\left(1+\frac{Nu}{2}\right)-\frac{Nu}{2}r^2\right) \tag{34}$$

The computations were done using computer symbolic algebraic package MAPLE to generate the graphs.

4. Results and Discussion

The temperature behaviour are discussed for different dimensionless parameters involved in the governing equations.

For $n=0$, the wood particle is a slab; for $n=1$, the wood particle is cylindrical and for $n=2$, the wood particle is spherical. Graphical representations showing the variations in temperature distributions with respect to wood geometry are shown in Figures 1 – 3.

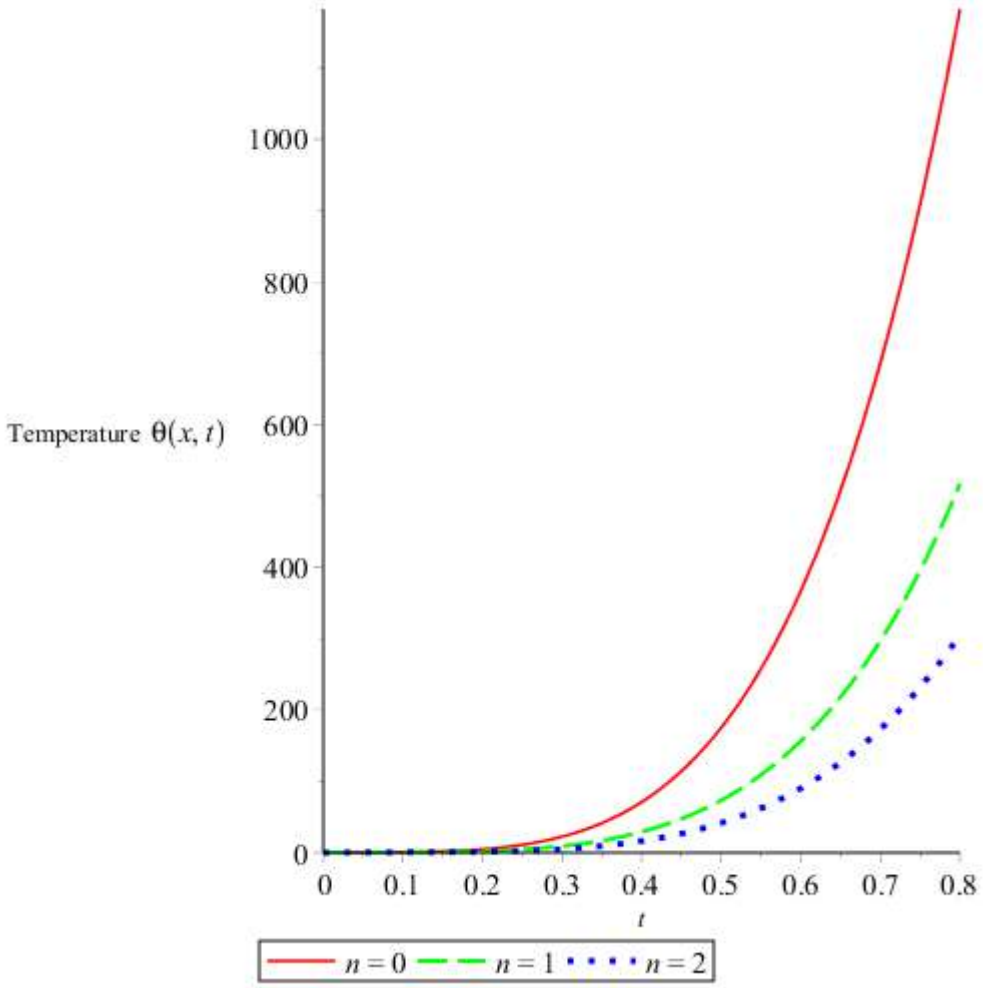

Figure 1: Effect of wood geometry, n on temperature profile.

Figure 1 shows the numerical results of the temperature history for the slab particle $(n=0)$, cylindrical particle $(n=1)$ and spherical particle $(n=2)$ against time. It is observed that the temperature increases with time for all particle and when the wood particle is a slab, the result shows much faster rise in temperature than when the wood is cylindrical or spherical. The model prediction shows that drying finishes after 12 minutes (0.2 hours), when the central temperature shows a sudden rise for all particles.

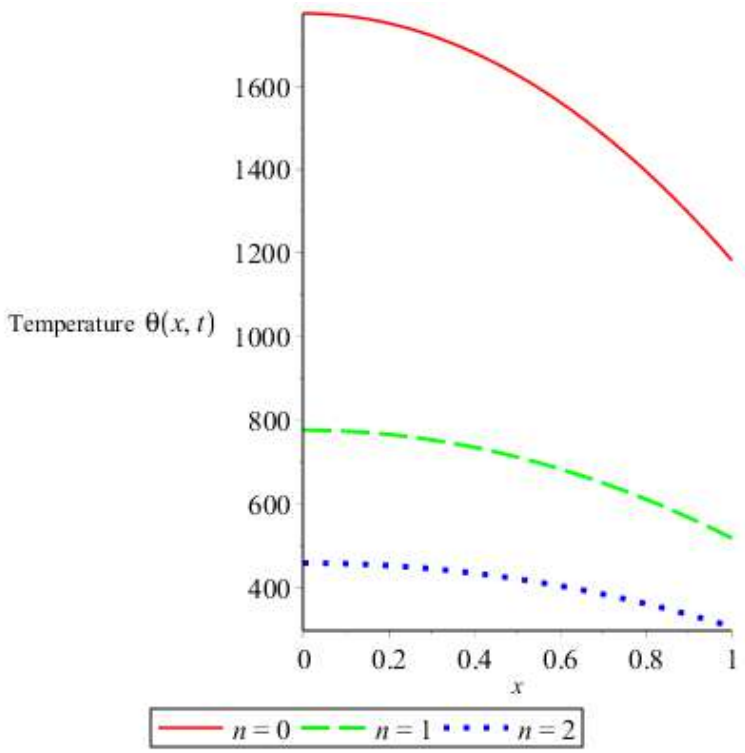

Figure 2: Effect of wood geometry, n on temperature profile.

Figure 2 shows the numerical results of the temperature history for the slab particle $(n=0)$, cylindrical particle $(n=1)$ and spherical particle $(n=2)$ against distance. It is observed that the temperature decreases a long distance for all particle and when the wood particle is a slab, the magnitude of temperature in the wood for the slab particle is very large as compare to the cylindrical and spherical particles, that is, the magnitude of temperature decreases with the increase in n. The implication is that, during pyrolysis, due to the endothermicity of the pyrolysis process, the slope of the temperature becomes smaller

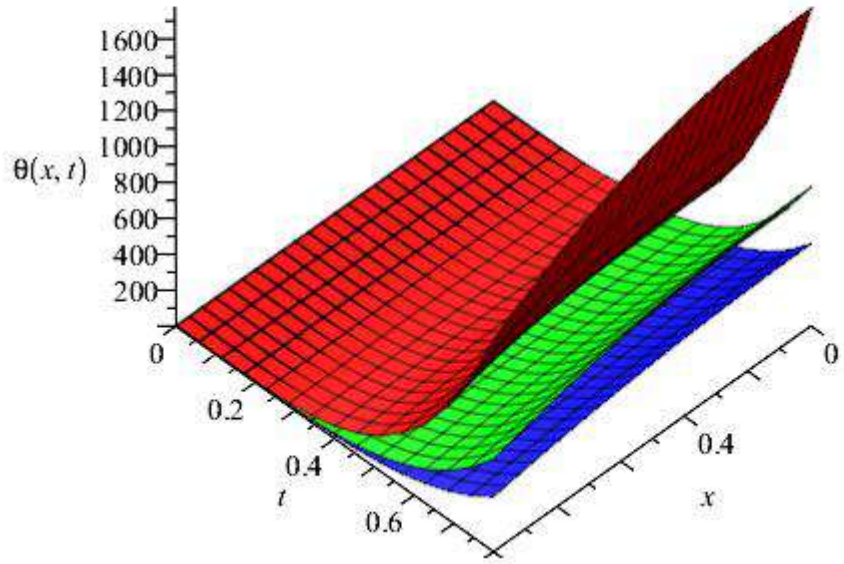

Figure 3: Effect of wood geometry, n on temperature profile.

Figure 3 shows the numerical results of the temperature history for the slab particle $(n=0)$, cylindrical particle $(n=1)$ and spherical particle $(n=2)$ against distance and time. It is replicated the combine effects observed in Figures 1 and 2.

5. Conclusion

The solution for the model have been determined by the Olayiwola's Generalized Polynomial Approximation Method (OGPAM). It can be concluded that the wood geometry has significant effect on the temperature distribution.

References

Alok, D., Suraj, B.S., and Istvan, B. (2020). Mathematical modeling of pyrolysis of hardwood (Acacia). Doi: 10.20944/preprints 202002 0094VI

Ayeni, R. O. (1978). *Thermal Runaway*. Unpublished PhD Thesis, Cornell University, USA.

Hagge, M. J. (2005). *A numerical model for biomass pyrolysis*. A PhD Thesis, Iowa State University Capstones.

Izabella, V., Matthew, J. D., Franz, R. and Elizabeth, J. W. (2017). Pyrolysis and spontaneous ignition of wood transient irradiation: experiments and a-priori predictions. *Fire safety journal*, 91 (2017): 218 – 225.

Long, S., Micheal, Y., Vasily, N. and Paul, J. (2015). Modeling the pyrolysis and combustion behaviors of non-charring and intumescent protect polymers using firestone. *Polymers*, 7: 1979-1997.

Mate M. (2016). *Numerical Modelling of Wood Pyrolysis*. Master of Science Thesis in Chemical Engineering, Royal Institute of Technology, Stockholm, Sweden.

Niranjan, F., Mohammed, A., Mahinsasa, N., Thamali, J. and Asadullahi, S. J. (2015). A mathematical model for pyrolysis of biomass. 978-1-4795-1720-2/15/&31.00

Richter, F., Arvind, A., Panagiotis, K. and Guillermo, R. (2019). The effect of chemical composition on the charring of wood across scales. *Proceedings of the combustion institute*, 000 (2019): 1 – 9.

Effect of Heat Source with Convective Surface boundary condition on MHD Heat and Mass Transfer of Chemical Reaction Flow for a Moving Vertical Plate

Danjuma Muhammad Auwal[1*] and Mustapha Mannir Gafai[2]

[1,2]Department of Mathematics and Statistics, Umaru Musa Yar'adua University, Katsina-Nigeria.

1*Auwalmuuhammad1@gmail.com

Abstract

The objective of the current work is to examine the influence of a connective border condition, internal heat generation, and chemical reaction on the thermal boundary layer MHD heat and mass transfer flow over a moving flat plate. A stream of cold fluid travels over the upper surface of the plate, creating a chemical reaction and heat source, while the lower surface of the plate is in touch with a hot fluid. By applying the appropriate transformation for a variable, the controlling nonlinear equation of flow, heat transfer, and concentration is reduced to a collection of nonlinear ordinary differential equations, which are then numerically solved using the runge-kutta fourth order approach with respect to shooting method. It is demonstrated how physical parameters affect temperature, concentration, and velocity.

Keywords: Heat Transfer, Similarity variable, Stream function, Kinematics viscosity, skin friction thermal expansion, gravitational acceleration.

Introduction

Most real-world problems in many academic fields, such as science and engineering, are first stated as mathematical models before they are addressed. These models typically yield a differential equation. A differential equation is a mathematical expression that links an unknown function to one or more of its derivatives. In many academic disciplines, including engineering and the sciences, the problems are first formulated as mathematical models and then solved. This include the investigation of mass transfer and convective flow with heat and magnetic field effects, as well as chemical reactions with heat sources. These models yield a differential equation. The chemical, petroleum, and other industries should take note of this phenomenon. A common result of these models is a differential equation. This phenomena is significant to the petroleum, chemical, and other industries. In nature, natural convection flows happen often as a result of variations in temperature, concentration, and other factors working together. Differential equations have a significant role in many branches of mathematics, including celestial mechanics and dynamics. The impact of chemical reactions and hall currents on the hydromagnetic flow of a stretching vertical surface with internal heat generation or absorption has been studied by Abdul-Aziz (2008). Given their significance for a wide range of technical applications, boundary-layer flows over a moving plate are very important, especially when it comes to the

production of fibers for the glass and polymer industries. Sakiadis's work (1961). was the first and foremost to examine boundary-layer behavior in moving surfaces in quiescent fluid. Many researchers have since worked on the issue of moving or stretching plates in many contexts. Examples of these researchers include Cortel (2007), Ishak (2009), Fang (2008), Rahimi (2017), and others. Similarity solutions are found to be helpful in the interpretation of some fluid motions at large Reynolds numbers in the boundary-layer theory. The chemical reaction, heat, and mass transfer in non-linear MHD boundary flow through a vertical porous surface in the presence of suction have all been studied by Rajeswari *eta al*.. (2009). For two dimensional, axis-symmetric, and three dimensional bodies, there are frequently similarity solutions for the stagnation point flow and flow over semi-infinite plates. In certain unique situations, in the absence of a similarity solution, one must solve a system of partial differential equations (PDEs) that are nonlinear. Auwal *eta al*.. (2023). Investigate the numerical method for the study of heat Generation in the thermal boundary layer for a plate. The impact of internal heat generation, thermal radiation, and chemical reaction on chemically responding magneto hydrodynamics was studied by Olanrewaju *eta al*.. (2016). Velocity profiles are similar for boundary layer flows with similarity. However, non-similarity flows lose this form of similarity. It is evident that boundary-layer flows with non-similarity are more significant in theory and practice, as well as having a more broad nature. Engineering uses for incompressible fluid flowing past a moving surface are numerous. This notion was then introduced by Aziz *eta al*.. (2009) with a comparable solution for a laminar thermal boundary layer over a flat plate with a convective surface of a boundary condition. Due to its many engineering applications, including post-accident heat removal in nuclear reactors, solar collectors, drying processes, heat exchangers, geothermal and oil recovery, building construction, etc., convective flow in porous media has been extensively investigated in recent years. The unstable force and free convection flow via an infinite permeable vertical plate are investigated by Daniel *eta al*.. (2013). Using a Laplace transformation approach, Basant *eta al*.. (2016) studied the combined effect of suction and injection on MHD free convection flow in a vertical channel with heat radiation. In the presence of thermal radiation, Olanrewaju (2012) investigates the similarity solution for natural convection from a moving vertical plate with internal heat generation and convective boundary condition. It's common knowledge that traditional heat-transfer fluids, such oil, Since the thermal conductivity of water and ethylene glycol mixture affects the heat transfer coefficient between the heat transfer medium and the heat transfer surface, these fluids are poor heat transfer agents. Murtala (2018). The effects of thermal radiation and thermos-diffusion on the flow of heat mass transfer with exponentially temperature dependent thermal conductivity have been studied. Over the past several years, a novel method of enhancing heat transmission through the utilization of ultratiny solid particles in the fluids has been widely applied. Makinde (2005) studied the free-convection flow over a moving vertical porous plate with thermal radiation and mass transfer. Dufour and Soret effects on mixed convection flow past a vertical porous flat plate with variable suction imbedded were studied by Alan and Rahman (2011). In this regard, Ingham *eta al*.. (2004) provided a very good description of the body of research knowledge. Olanrewaju *eta al*.. (2016) investigated the impact of internal heat generation, thermal radiation, and chemical reaction dufour Soret on magnetohydrodynamics of chemical reactions. Hussein and Hani (2018) devised a novel method for solving boundary layer theory of fluid flow via a flat plate numerically using Matlab. Given that the laminar boundary layer equation is an ordinary deferential equation of third order that is nonlinear. Using shooting techniques in

conjunction with the fourth order Runge Kutta approach, the reduction equation is numerically solved. It has been noted that variations in temperature, velocity, and concentration have an impact.

Mathematical Formulation

We examine a constant, incompressible fluid flow in two dimensions that is related to convective heat transfer across a vertical plate. a temperature-controlled stream of cold fluid (T_∞) traveling at a constant speed across the plate's right surface (U_∞) while convection from hot fluid at temperature warms the plate's left surface(T_f,) that provide the heat transfer coefficient (h_f). (Refer to Figure 1). The continuity, energy, together with momentum equation characterizing the fluid flow is been expressed as follows: the momentum equation (Boussiniceq approximation) accounts for the density change caused by the buoyancy effect.

$$\frac{\partial u}{\partial x}+\frac{\partial v}{\partial y}=0 \tag{1}$$

$$u\frac{\partial u}{\partial x}+v\frac{\partial u}{\partial y}=v\frac{\partial^2 u}{\partial y^2}+g\beta(T-T_\infty)+g\beta^*(C-C_w) \tag{2}$$

$$U\frac{\partial T}{\partial x}+V\frac{\partial T}{\partial y}=\propto\frac{\partial^2 T}{\partial y^2}+Q\theta \tag{3}$$

$$\rho C_\rho(U\frac{\partial T}{\partial x}+V\frac{\partial T}{\partial y})=K\frac{\partial^2 T}{\partial y^2}+\dot{R} \tag{4}$$

$$U\frac{\partial C}{\partial x}+V\frac{\partial C}{\partial y}=D\frac{\partial^2 C}{\partial y^2}-Kr^I C \tag{5}$$

given u and v are the x (along the plate) and the y (normal to the plate) parameter of the velocity, respectively, T is the temperature, v is the kinematics viscosity of the fluid, and α is the thermal diffusivity of the fluid and β is the thermal expansivity constant. The velocity boundary conditions can be expressed as

$$u(x,0)=v(x,0)=0 \tag{6}$$

$$u(x,\infty)=U_\infty \tag{7}$$

The boundary condition at the plate surface is far into the cold fluid which can be written as

$$-k\frac{\partial T}{\partial y}(x,0)=h_f\ [T_f\ -T(x,0)] \tag{8}$$

$$T(x,\infty)=T_\infty \tag{9}$$

given a similarity variable and a dimensionless stream function $f(\eta)$ and temperature $\theta(\eta)$ as

$$\eta=\frac{y}{\delta}=y\sqrt{\frac{U_\infty}{\vartheta_x}}=\frac{y}{x}\sqrt{Re_x}\quad,\quad \frac{u}{U_\infty}=f^I\ \ v=\frac{1}{2}\sqrt{\frac{VU_\infty}{x}}\ (\eta f^I-f)$$

$$\theta = \frac{T-T_\infty}{T_f-T_\infty} \quad \emptyset = \frac{C-C_\infty}{C_w-C_\infty} \quad Gr_x = \frac{g\beta(T_f-T_\infty)x}{U_0^2} \quad Gc_x = \frac{g\beta^*(C_w-C_\infty)x}{U_0^2} \quad \text{Bi}x = \frac{h_f}{k}\sqrt{\frac{vx}{U_0}}$$

$$Pr = \frac{v}{\alpha} \quad Sc = \frac{v}{D} \quad S_x = \frac{Q_0 x}{U_0 \rho C_\rho} \quad Kr_x = \frac{Kr^I x}{U_0}\ ,\ Nc = \frac{C_\infty}{C_w-C_\infty} \tag{10}$$

The prime symbol indicates derivative with respect to η, with the local Reynolds number is represented as $Re_x = U_\infty x/v$ Equations (1) through (9) yield

$$f^{III} + \frac{1}{2} f f^{II} + Gr_x\theta + Gc_x\emptyset = 0 \tag{11}$$

$$\theta^{II} + \frac{1}{2} Prf\theta^I + PrS_x\theta = 0 \tag{12}$$

$$\emptyset^{II} + \frac{1}{2} Scf\emptyset^I - ScKr_x\emptyset - ScKr_xNc = 0 \tag{13}$$

$$f\,(0) = f^I(0) = 0, \qquad \theta'(0) = -\,\text{Bi}_x\,[1-\theta\,(0)] \tag{14}$$

$$f^I(\infty) = 1, \qquad \theta\,(\infty) = 0 \tag{15}$$

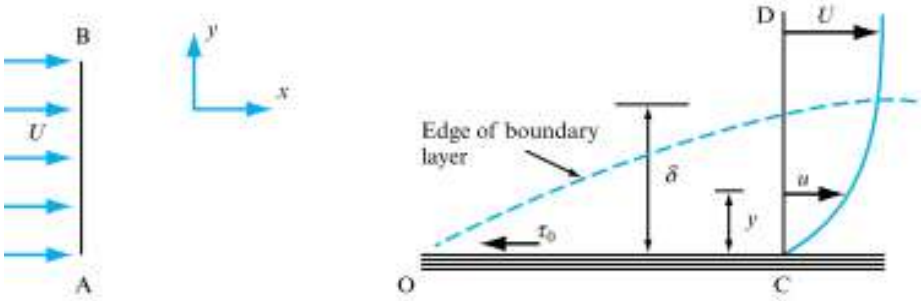

$$\text{Bi}x = \frac{h_f}{k}\sqrt{\frac{v}{U_0}}\ , \quad Pr = \frac{v}{\alpha}\ ,\ Gr_x = \frac{vxg\beta(T_f-T_\infty)}{U_0^2} \tag{16}$$

The momentum and energy equations to has a similarity solution, the parameters Gr_x and Bi_x have to be constants rather than x-dependent functions, as in Eq. 16. This requirement can be met given the heat transfer coefficient as h_f is directly proportional to $x^{-1/2}$ and the thermal expansivity term β is proportional to x^{-1}.. We consequently assume

$$h_f = cx^{-1/2}\ , \qquad \beta = mx^{-1} \tag{17}$$

where c and m are constants. Substituting Eq. (17) into Eq. (16), we have

$$Bi = \frac{c}{k}\sqrt{\frac{v}{U_0}} \quad , \qquad Gr = \frac{vmg(T_f-T_\infty)}{U_0^2} \tag{18}$$

When Bi_x and Gr_x are defined as in Eq. (16), the solutions of Equation. (11)–(15) produce the similarity solutions with Bi and Gr defined by Eq. (18). Nevertheless, the solutions generated are the local similarity solutions.

Numerical Solutions

The fourth-order Runge–Kutta approach using a shooting strategy is used to solve the coupled nonlinear Eqs. (11) and (12) with the boundary conditions in Equation. (13) and (14) on Maple (2003). The numerical solution with accuracy to the seventh decimal place is obtained using the step size 0.001 as the convergence criterion.

Result Discussion

Numerical analyses have been performed for various parameter values governing the fluid flow within the domain. The convective parameter Bi is used in the following ways: 0.05, 0.10, 0.20, 0.40, 0.6, 0.80, 1, 5, 10, and 20; the Grashof number (Grashof number Grx) is used in the following ways: Gr greater than 0. The current results exhibit great agreement with the acquired outcome when compared to past work. Our findings are presented in Tables 1 and 2 as well as Figures 1–5 below. Table 1 compares Aziz's (2009) work for the Prandtl number (Pr=0.72), and it is evident that there is a good level of consistency even in the absence of the Grashof number. Table 2 displays the skin-friction and surface heat transfer rate are positively correlated with the local Grashof number and convective surface heat transfer parameter. Moreover, a rise in the fluid Prandtl number accelerates heat transfer at the plate surface while lowering skin friction. At the plate surface, the fluid velocity is typically 0 and increases gradually toward the freestream value that satisfies the boundary conditions as one moves away from the plate. The noteworthy thing to notice is that there is a small increase in fluid velocity within the boundary layer when convective surface heat transfer intensity (Bix) increases. An increase in the local Grashof number as a result of buoyancy effects shows a similar trend. Additionally, the outcome of The fluid temperature reaches its peak near the plate's surface and then exponentially drops to zero as it gets farther from the plate, meeting the boundary requirements. It is evident from these data that the thickness of the thermal boundary layer grows as Bix increases and reduces as Grx and Pr values increase. Therefore, while an increase in the Prandtl number and the strength of buoyant force slows down the rate of thermal diffusion within the boundary layer, convective surface heat transfer increases thermal diffusion.

Table 1 Computaional presenting comparison of $f^{II}(0)$, $\theta(0)$, $\theta^{I}(0)$ and $-\emptyset^{I}(0)$ for different parameter Bi, Gr, Pr, Gc and Sc

Bi	Gr	Pr	Gc	Sc	Makinde(2013) $f^{II}(0)$	$-\theta'(0)$	$\theta(0)$	$-\emptyset^{I}(0)$	Present $f^{II}(0)$	Present $-\theta'(0)$	Present $\theta(0)$	Present $-\emptyset^{I}(0)$
0.1	0.1	0.72	0.1	0.62	-0.402271	0.078635	0.213643	0.3337	-0.4022	0.0786	0.2136	0.3337
1.0	0.1	0.72	0.1	0.62	-0.352136	0.273153	0.726846	0.3410	-0.3521	0.2731	0.7268	0.3410
0.1	0.5	0.72	0.1	0.62	-0.322212	0.079173	0.208264	0.3451	-0.3222	0.0792	0.2083	0.3451
0.1	1.0	0.72	0.1	0.62	-0.231251	0.079691	0.203088	0.3566	-0.2312	0.7970	0.2031	0.3567
0.1	0.1	0.72	0.5	0.62	0.3799184	0.080711	0.192889	0.3813	-0.0264	0.0807	0.1929	0.3814
0.1	0.1	0.72	0.1	0.62	-2.217928	0.082040	0.179592	0.4176	-0.3799	0.0820	0.1796	0.4177
0.1	0.1	1.0	0.1	0.62	-0.407908	0.066156	0.338435	0.1806	-0.4079	0.0662	0.3384	0.1807

0.1	0.1	7.10	0.1	0.62	-0.421228	0.093348	0.066513	0.4212	-0.4214	0.0819	0.0665	0.3325
0.1	0.1	0.72	0.1	0.78	-0.411704	0.078484	0.215159	0.3844	-0.4117	0.0785	0.2152	0.3845
0.1	0.1	0.72	0.1	2.63	-0.453094	0.077915	0.220841	0.7981	-0.4530	0.7792	0.2208	0.7981

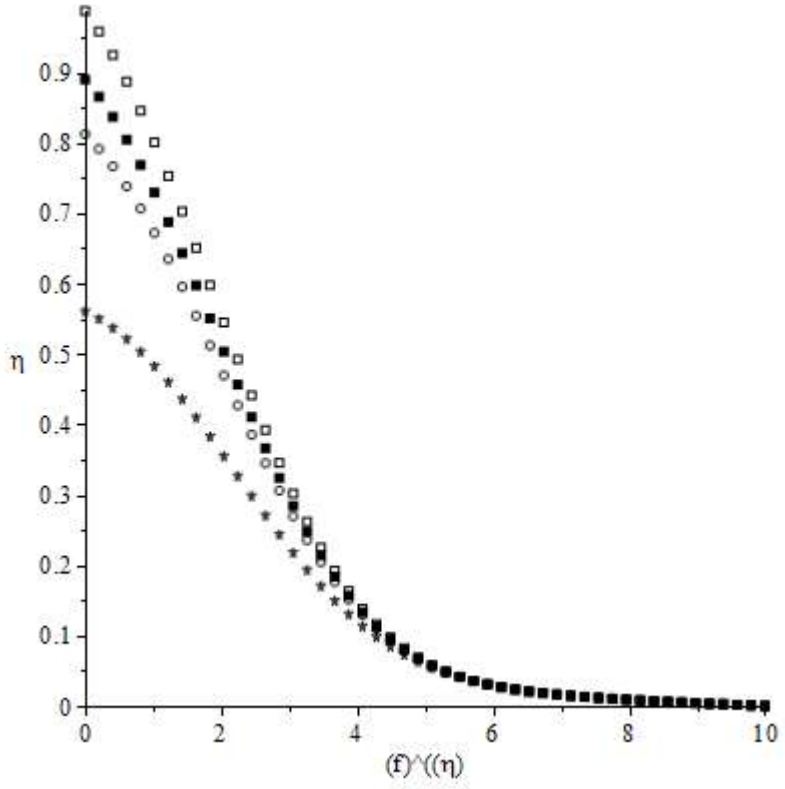

Figure 1: Velocity profile for different value of Br, Kr, Sc for Pr = 0.72, Gr = 0.1 and Gc=0.1

Table 2 computaional presenting $f^{II}(0)$ $\theta(0)$, $\theta^{I}(0)$ and $\emptyset^{I}(0)$ for different parameter

Bi	Gr	Pr	Kr	Sc	$f^{II}(0)$	$-\theta'(0)$	$\theta(0)$	$-\emptyset^{I}(0$
0.1	0.1	0.72	0.1	0.62	-0.6048	0.1548	0.5481	0.3761
1.0	0.1	0.72	0.1	0.32	-0.3585	0.1678	0.6644	0.4284
0.1	0.2	0.72	0.1	0.62	-0.3442	0.2048	0.7957	0.4300
0.1	0.2	0.72	0.1	0.62	-0.4102	0.2832	0.7167	0.4137
0.1	0.3	0.72	0.2	0.62	-0.4198	0.2652	0.7348	0.5527
0.1	0.3	0.72	0.4	0.24	-0.4287	0.2537	0.7463	0.7085
0.1	0.1	1.0	0.4	0.62	-0.4127	0.2253	0.7747	0.7096

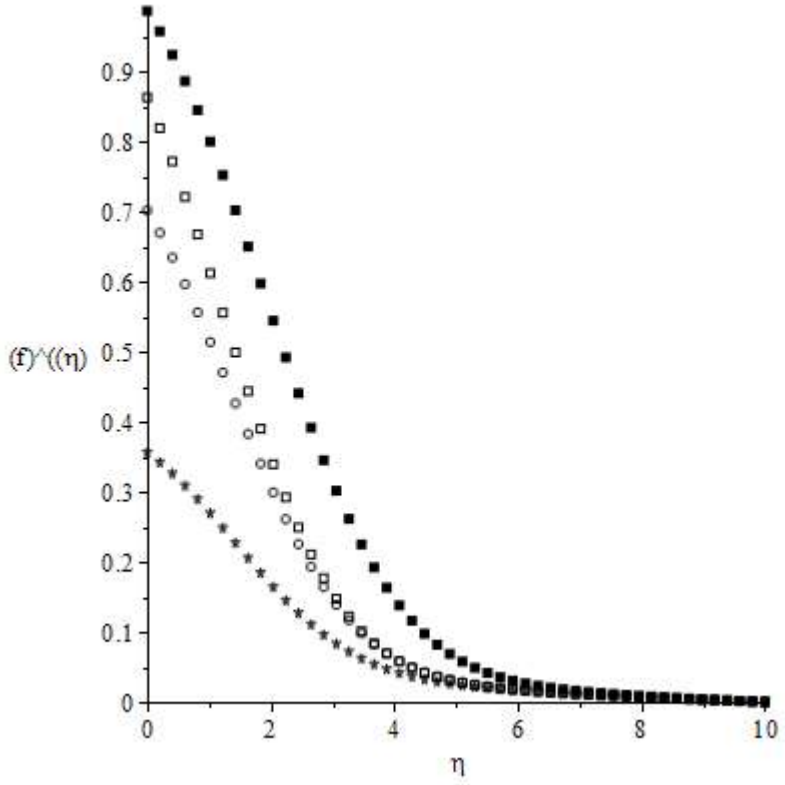

Figure 2: Temperature profile for different value of Gr, Q, Pr for Kr = 0.72, Br= 0.1 and Gc=0.1

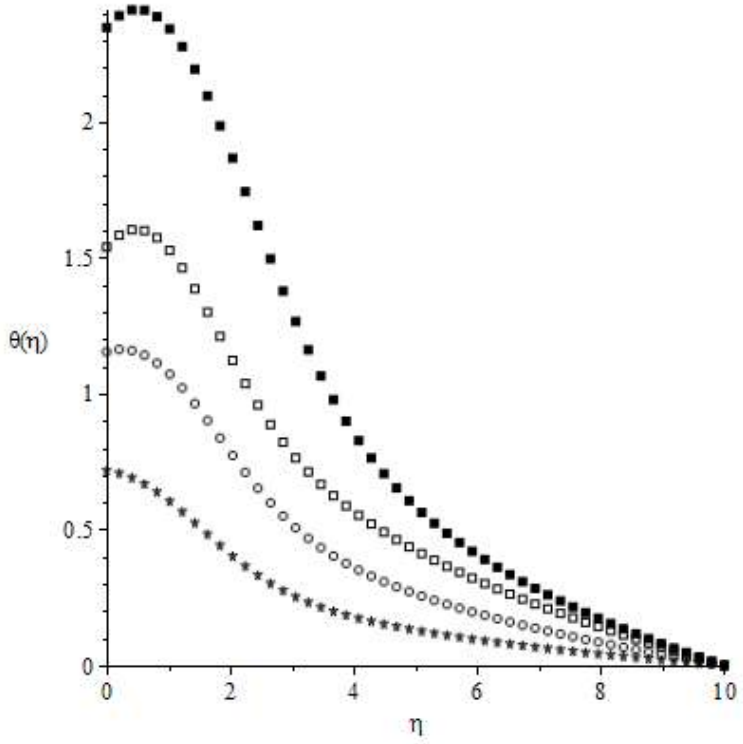

Figure 3: temperature profile for different value of Q, Gc Br for Pr = 0.72, Gr = 0.1 and Sc=0.1

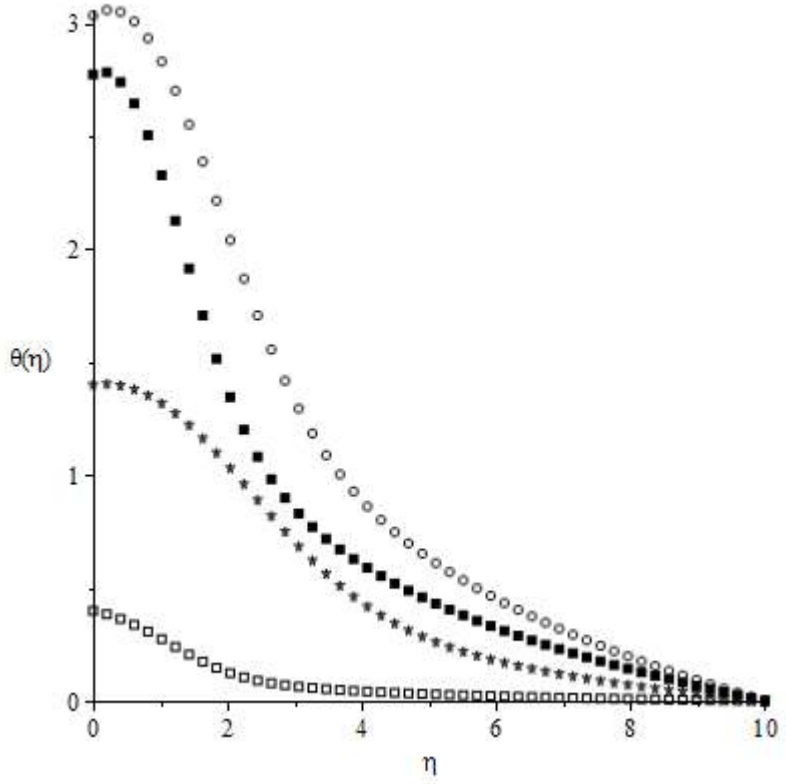

Figure 4: concentration profile for different value of Sc, Kr, Gc for Pr = 0.72, Gr = 0.1 and Gc=0.1

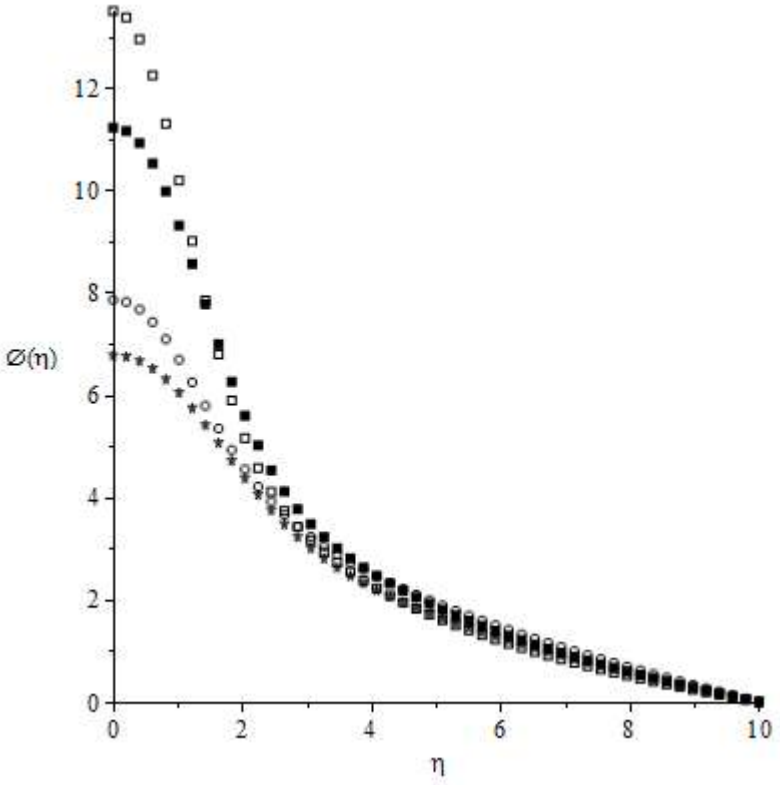

Figure 5: concentration profile for different value of Pr, Gr for Br = 0.1, Q= 0.2 and Gc=0.5

Conclusion

In the presence of a heat source, a chemical reaction, and a convective surface that provides a similarity solution for the momentum and thermal boundary layer equations, the current analysis has been conducted to investigate the heat and mass transfer of MHD flow over a vertical plate with a convective surface boundary condition. The thermal expansion coefficient β is proportional to x^{-1}, and the convective heat transfer of the fluid heating the plate on its left surface is proportional to $x^{-1/2}$. The several parameters incorporated in the problem were solved using the numerical solutions of the similarity equations. The thickness of the thermal boundary layer along the plate tends to decrease due to the growing impacts of the Grashof and Prandtl numbers. The dimensionless velocity, temperature, and mass boundary layer equations have been solved using the shooting technique with Runge-Kutta fourth-order iteration scheme. It has been demonstrated that as the source parameter increases, the plate surface temperature and Sherwood number fall while the magnitude of local skin friction and local Nusselt number increases. The local skin friction, the plate surface temperature, and the Sherwood number all increase as the strength of the chemically interacting substances increases; however, the local Nusselt number exhibits the reverse behavior. As the source and chemical reaction parameters are increased, the velocity and concentration profile becomes more pronounced and declines as the magnetic parameter increases. Boundary layer thickness increases with increasing source, mass flux boundary layer thickness, chemical reaction parameter, and plate surface convective

heat parameter; boundary layer thickness, mass boundary layer, and velocity decrease with increasing Prandtl number.

Nomenclature

(x, y) = Represent the cartesian coordinates

(u, v) = components of velocity Freestream temperature

T_f = stands for hot fluid temperature.

Gravitational acceleration equals $to\ g$

T_∞= represents the fluid temperature.

Pr = stands for Prandtl number.

U_∞ = velocity of freestream

Gr_x= is the Grashof number locally.

Bi_x = is the parameter for local convective heat transport.

K = is the heat conductivity.

References

Auwal, D. M., Gafai, M. M, Garba, A. A, and Shehu, M.(2023). "A numerical approach for the study of heat Generation in the presence of thermal boundary layer for a flat plate", 7(6), 261-266.

Aziz, A., (2009), "A Similarity Solution for Laminar Thermal Boundary Layer Over a Flat Plate With a Convective Surface Boundary Condition," *Commun. Nonlinear Sci. Numer. Simulation*,14, 1064–1068

Blasius, H., (1908), "Grenzschichten in Flussigkeiten mit kleiner reibung," *Z. Math Phys*., 56, 1–37.

Bataller, R. C., (2008), "Radiation Effects for the Blasius and Sakiadis Flows With a Convective Surface Boundary Condition," *Appl. Math. Computation*, 206, 832–840

Cortell, R., (2007), "Similarity Solutions for Flow and Heat Transfer of a Quiescent Fluid Over a Nonlinearly Stretching Surface," J. Mater. Process. Tech, l, 176–183.

Ehab Hussein and Bani-Hani. (2018). Boundary-Layer Theory of Fluid Flow past a Flat-Plate: Numerical Solution using MATLAB. *International Journal of Computer Applications,* 180(18): 0975 – 8887

He, J. H., (2003), "A Simple Perturbation Approach to Blasius Equation," *Appl. Math. Comput*., 140, 217–222.

Ingham, D. B., Bejan, A., Mamut, Eand Pop, I. (2004). Emerging Technologies and techniques in pourous Media. Kluwer, Dordecht.

Jha B.K, Isa, B. Y. and Uwanta, I. J. (2016). Combine effect of suction/injection on MHD free convection flow in a vertical channel with thermal radiation. *shams engineering journal*, http://dx.doi.org/10.1016/j.assj.2016.06.001.

Vajrevelu, K and Nayfeh, J. (1992). "Hydromagnetic convection at a cone and a wedge," *International Communications in Heat and Mass Transfer*, 19, 701–710.

Magyari, E., (2008), "The Moving Plate Thermometer," *Int. J. Therm. Sci*., 47, 1436–1441

Rahman M. M and Sattar, M. A. (2006), "Magneto-hydrodynamic convective flow of a micropolar fluid past a continuously moving vertical porous plate in the presence of heat generation/absorption," *Journal of Heat Transfer*, 128(2), 142–152.

Makinde, O. D., and Sibanda, P., (2008), "Magneto-hydrodynamic Mixed Convective Flow and Heat and Mass Transfer Past a Vertical Plate in a Porous Medium With Constant Wall Suction," *ASME J. Heat Transfer*, 130, 112-602.

Makinde, O. D., (2009), "Analysis of Non-Newtonian Reactive Flow in a Cylindrical Pipe,"

Makinde, O. D and Ogulu, A. (2005), "The effect of thermal radiation on the heat and mass transfer flow of a variable viscosity fluid past a vertical porous plate permeated by a transverse magnetic field," *Chemical Engineering Communications*,. 195(12), 1575–1584.

Murtala, S.,(2018), thermos- diffusion and thermal radiation effect on heat mass transfer flow with exponentially temperature dependent thermal conductivity, 55, 264-273.

Olanrewaju, P.O. (2012). Study the similarity solution for natural convection from a moving vertical plate with internal heat generation and convective boundary condition in the presence of thermal radiation and viscous dissipation. *Rep Opinion*, 4(8), 68-76.

Parida, S. K., Acharya, M., Dash, G. C. and Panda, S. (2011), "MHD heat and mass transfer in a rotating system with periodic suction," *Arabian Journal for Science and Engineering*, 36(6), 1139-1151.

Rajeswari, R. Jothiram, B. and Nelson, V. K. (2009). "Chemical reaction, heat and mass transfer on nonlinear MHD boundary layer flow through a vertical porous surface in the presence of suction," *Applied Mathematical Sciences*, 3, 2469–2480,

Sakiadis, B. C. (1961). Boundary-layer Behaviour on Continuous Solid Surfaces; Boundarylayer Equations for 2-dimensional and Axisymmetric Flow. *Advance International Chemical Engineering Journal*, 7, 26–28.

Weyl, H., (1942), "On the Differential Equations of the Simplest Boundary-Layer Problem," *Ann. Math*., 43,381–407

4-Step Block Hybrid Backward Differentiation Formula For Solving Second Order (BHBDF II) Ordinary Differential Equations

Hussaini Hajarat[1], Muhammad Raihanatu[2] and Yusuf Abdulhakeem[3]
[1-3]Department of Mathematics, Federal University of Technology,
Minna, Niger State, Nigeria
E-mail: hajohussy@yahoo.co.uk

Abstract

This research work presents the derivation and implementation of a 4-step linear multistep method of block hybrid backward differentiation formula for solving nonlinear second-order initial value problems of ordinary differential equations. Collocation and interpolation methods are adopted in the derivation of the proposed numerical scheme where the legendary polynomial is adopted as a basic function. The 4-step BHBDF has higher order of accuracy $p = 11$ which implies that it is consistent. The proposed numerical block method is further applied to finding direct solution to nonlinear second order ordinary differentiation equations. This implementation strategy is more accurate than some existing methods considered in the literature.

Keywords: linear multi step method, block method, hybrid, collocation and interpolation methods

1. Introduction

The differential equation is a fundamental tool utilized in the modeling of physical problems that arise across virtually all knowledge domains. In the fields of science and engineering, ordinary differential Equations (ODEs) are crucial for stimulating real-world problem. For instance, mathematical models are frequently created to facilitate comprehension of physical phenomena (Pimenov and Hendy 2015). There are various differential equations that we study in calculus to obtain closed form solutions, but not all differential equations have finite answers. Even if they have closed form solutions, obtaining them can be difficult. In such cases, depending on the need, numerical analysis researchers and scholars made significant contributions to the development and derivation of several methods for solving this type of equation (Muhammad and Yahaya, 2012; Kuboye and Omar, 2015; Abdulrahim and Omar, 2016; Muhammad, *et al*., 2020). Because exact solutions to differential equations are difficult to find, numerical methods play an important role in providing approximate solutions to them. The type and category of ordinary differential equations (ODEs) to be solved drive the creation of numerical methods such as the linear multistep approach, the single-step method, finite difference, finite element, and finite volume. The mathematical representation of physical problems leads to the approximation of ordinary differential equations (ODEs) using initial or boundary conditions (Omole *et al*., 2023). Differential equations fall into two categories: first are ordinary differential equations (ODEs) (Zwillinger, Danie and l 2021)
Zwillinger, Danie, and and Vladimir Dobrushkin. l. *Handbook of differential equations. .* 2021.

, where the unknown function is a function of just one independent variable and is expressed as follows:

$$f\left(t,u(t),\frac{du(t)}{dt},\frac{d^2u(t)}{dt^2},\frac{d^3u(t)}{dt^3},...,\frac{d^nu(t)}{dt^n}\right)=0 \qquad (1)$$

And partial differential equations (PDEs) in which the unknown function is a function of two or more independent variables and the equation involves its partial derivatives. In real life, ordinary differential equations are used to explain thermodynamics ideas, compute the movement or flow of electricity, and move an object back and forth like a pendulum.

2. Literature Review

Muhammad *et al.* (2020) reformulated an implicit block hybrid backward differentiation formula for $k = 2$ into a Runge-Kutta Type Method (RKTM of the same step number. The method so formed can be used to solve both first and second order IVPs. Mohammed *et al.* (2022) formulated block hybrid backward differentiation formula for the solution of stiff systems of ordinary differential equation through continuous collocation approach. In the research work, *k* off - grid points were incorporated at interpolation in order to retain the single function evaluation characteristic, which is peculiar to backward differentiation formula. They are frequently employed in fields like physics and engineering, where it might be challenging to get the precise answer. Akinfenwa *et al.*, (2013), Adeyeye and Omar (2016), Audu *et al.*, (2022), Cardone and D'Ambrosio (2018), Yahaya and Mohammed (2010), Mohammed and Yahaya (2010), Mohammed (2010), Muhammad *et al*. (2015a), Muhammad *et al*. (2015b). Also Akinfenwa *et al.* (2017) derived a self-starting second derivative multistep block method which uses logic behind the Simpson's 3/8 rule for quadrature using collocation and interpolation techniques to obtain approximate solutions to stiff differential equations. Their method is of order eight and A-Stable, effective and reliable for stiff systems of ordinary differential equations. Using a new class of orthogonal polynomials that Adeyefa (2017) created, a one-step hybrid block technique was developed using this new basis function. The others are Yukusak and Owolanke (2018), Abualnaja (2015), Olabode and Momoh (2016), Mohammed *et al*. (2021), and Olanegan *et al.* (2015).

3. Methodology

The derivation process starts from an orthogonal polynomial of the form:

$$U(t) = \sum_{i=0}^{r+s-1} c_j L_i(t) \qquad (2)$$

where *r* and *s* are number of interpolations and collocations points respectively, c_i's are coefficients (to be determined) of the Legendre polynomial. In this project a class of 4-step hybrid block method is proposed for solving ODEs in second order.

3.1 4-Step Block Hybrid BDF for Second Order (BHBDF II)

As specified above, the degree of the Legendre polynomial for the proposed method for approximating the exact solution of ODEs is 12 and it is given be

$$\begin{aligned} U(t) = {} & c_0 + c_1 t + \left(\frac{3}{2}t^2 - \frac{1}{2}\right)c_2 + \left(\frac{5}{2}t^3 - \frac{3}{2}t\right)c_3 + \left(\frac{35}{8}t^4 - \frac{15}{4}t^2 + \frac{3}{8}\right)c_4 + \left(\frac{63}{8}t^5 - \frac{35}{4}t^3 + \frac{15}{8}t\right)c_5 \\ & + \left(\frac{231}{16}t^6 - \frac{315}{16}t^4 + \frac{105}{16}t^2 - \frac{5}{16}\right)c_6 + \left(\frac{429}{16}t^7 - \frac{693}{16}t^5 + \frac{315}{16}t^3 - \frac{35}{16}t\right)c_7 \\ & + \left(\frac{6435}{128}t^8 - \frac{3003}{32}t^6 + \frac{3465}{64}t^4 - \frac{315}{32}t^2 + \frac{35}{128}\right)c_8 + \left(\frac{12155}{128}t^9 - \frac{6435}{32}t^7 + \frac{9009}{64}t^5 - \frac{1155}{32}t^3 + \frac{315}{128}t\right)c_9 \\ & + \left(\frac{46189}{256}t^{10} - \frac{109395}{256}t^8 + \frac{45045}{128}t^6 - \frac{15015}{256}t^4 + \frac{3465}{256}t^2 - \frac{63}{256}\right)c_{10} \\ & + \left(\frac{88179}{256}t^{11} - \frac{230935}{256}t^9 + \frac{109395}{128}t^7 - \frac{45045}{128}t^5 + \frac{15015}{256}t^3 - \frac{693}{256}t\right)c_{11} \\ & + \left(\frac{676039}{512}t^{12} - \frac{969969}{512}t^{10} + \frac{2078505}{1024}t^8 - \frac{225225}{1024}t^6 + \frac{225225}{1024}t^4 - \frac{9009}{512}t^2 + \frac{231}{1024}\right)c_{12} \end{aligned}$$

(3)

Interpolating (4) at $t=\frac{t_{i+j}}{5}, 0\le j<4, \left(t_{i+j}=t_i+jh\right)$ and collocating its second derivative at $t=t_{i+4}$, lead to the following 13×13 system of equations. *h* is a given step size.

$$\left.\begin{array}{l} U\left(t_i\right)=u_i,\ \ U\left(t_{i+\frac{1}{5}}\right)=u_{i+\frac{1}{5}},\ \ U\left(t_{i+\frac{2}{5}}\right)=u_{i+\frac{2}{5}} \\ U\left(t_{i+1}\right)=u_{i+1},\ U\left(t_{i+\frac{6}{5}}\right)=u_{i+\frac{6}{5}}\ \ U\left(t_{i+\frac{7}{5}}\right)=u_{i+\frac{7}{5}}, \\ U\left(t_{i+2}\right)=u_{i+2},\ \ U\left(t_{i+\frac{11}{5}}\right)=u_{i+\frac{11}{5}},\ U\left(t_{i+\frac{12}{5}}\right)=u_{i+\frac{12}{5}} \\ U\left(t_{i+3}\right)=u_{i+3},\ \ U\left(t_{i+\frac{16}{5}}\right)=u_{i+\frac{16}{5}},\ U\left(t_{i+\frac{17}{5}}\right)=u_{i+\frac{17}{5}} \\ U''\left(t_{i+4}\right)=v_{i+4} \end{array}\right\} \tag{4}$$

Using the matrix inversion technique via the Maple software, (5) is solved for c_j's whose values are the substituted back into (3.4) and then simplified to obtain the continuous collocation method of the form:

$$\begin{aligned} U(t)=&\alpha_0(t)u_i+\alpha_{\frac{1}{5}}(t)u_{i+\frac{1}{5}}+\alpha_{\frac{2}{5}}(t)u_{i+\frac{2}{5}}+\alpha_1(t)u_{i+1}+\alpha_{\frac{6}{5}}(t)u_{i+\frac{6}{5}}+\alpha_{\frac{7}{5}}(t)u_{i+\frac{7}{5}}+\alpha_2(t)u_{i+2} \\ &+\alpha_{\frac{11}{5}}(t)u_{i+\frac{11}{5}}+\alpha_{\frac{12}{5}}(t)u_{i+\frac{12}{5}}+\alpha_3(t)u_{i+3}+\alpha_{\frac{16}{5}}(t)u_{i+\frac{16}{5}}+\alpha_{\frac{17}{5}}(t)u_{i+\frac{17}{5}}+h^2\beta_4(t)v_{i+4} \end{aligned} \tag{5}$$

Equation (6) is the continuous scheme of the proposed method whose by the tradition of BDF has only one evaluation point which is $t=t_i+4h$. And upon implementing this, the following obtainable scheme from (6) is given below.

$$\begin{aligned} u_{i+4}=&-\frac{4899694293}{3719054980}u_i+\frac{993505500}{120322367}u_{i+\frac{1}{5}}-\frac{169955950}{10938397}u_{i+\frac{2}{5}}+\frac{94709296656}{601611835}u_{i+1}-\frac{50567692500}{120322367}u_{i+\frac{6}{5}} \\ &+\frac{4172844600}{10938397}u_{i+\frac{7}{5}}-\frac{34685775774}{54691985}u_{i+2}+\frac{10813166000}{10938397}u_{i+\frac{11}{5}}-\frac{63868346100}{120322367}u_{i+\frac{12}{5}} \\ &+\frac{9906198264}{54691985}u_{i+3}-\frac{77374571625}{481289468}u_{i+\frac{16}{5}}+\frac{96247674900}{2045480239}u_{i+\frac{17}{5}}+\frac{1120392}{54691985}h^2v_{i+4} \end{aligned} \tag{6}$$

The proposed method is aimed to be implemented to solve ODEs via block method. Hence there is need to generate additional schemes to (7) from the same continuous scheme that would meet the algebraic condition for unique solution. To do this, the second derivative of (6) is evaluated at $t_{i+j}; j=\frac{1}{5},\frac{2}{5},\frac{6}{5},\frac{7}{5},2,\frac{11}{5},\frac{12}{5},3,\frac{16}{5},\frac{17}{5},4$

$$u_{i+\frac{1}{5}} = \frac{118776743969751}{132317548848290}u_i - \frac{7430962304040}{10118400794281}u_{i+\frac{2}{5}} + \frac{2516108892252}{299360970245}u_{i+1} - \frac{13699667032800}{778338522637}u_{i+\frac{6}{5}} + \frac{762446279980}{59872194049}u_{i+\frac{7}{5}} - \frac{43811811253144}{3891692613185}u_{i+2} + \frac{11085490664136}{778338522637}u_{i+\frac{11}{5}} - \frac{369275089230}{59872194049}u_{i+\frac{12}{5}} + \frac{50435475197052}{50592003971405}u_{i+3} - \frac{999470883023}{1556677045274}u_{+\frac{16}{5}} + \frac{1674488981985}{13231754884829}u_{i+\frac{17}{5}} - \frac{727709675616}{14788431930103}h^2v_{i+\frac{1}{5}} - \frac{2064130992}{73942159650515}h^2v_{i+4} \tag{7}$$

$$u_{i+\frac{2}{5}} = -\frac{162949331766897}{6730172803077020}u_i + \frac{688549885920}{1041822415337}u_{i+\frac{1}{5}} + \frac{8642709843456}{5209112076685}u_{i+1} - \frac{49774082502690}{19794625891403}u_{i+\frac{6}{5}} + \frac{2621794350240}{1799511444673}u_{i+\frac{7}{5}} - \frac{7843200018381}{8997557223365}u_{i+2} + \frac{20104511685440}{19794625891403}u_{i+\frac{11}{5}} - \frac{427817388609}{1041822415337}u_{i+\frac{12}{5}} + \frac{513518289696}{8997557223365}u_{i+3} - \frac{2803874420295}{79178503565612}u_{i+\frac{16}{5}} + \frac{2274177560928}{336508640153851}u_{i+\frac{17}{5}} - \frac{47778918096}{1799511444673}h^2v_{i+\frac{2}{5}} - \frac{11843832}{8997557223365}h^2v_{i+4} \tag{8}$$

$$u_{i+1} = \frac{43265431323857}{303982967085952}u_i - \frac{143367625}{426884812}u_{i+\frac{1}{5}} + \frac{3314955875}{11099005112}u_{i+\frac{2}{5}} + \frac{2649296125}{1280654436}u_{i+\frac{6}{5}} - \frac{2223555125}{1494096842}u_{i+\frac{7}{5}} + \frac{1117406411}{853769624}u_{i+2} - \frac{1942982125}{1173933233}u_{i+\frac{11}{5}} + \frac{1223646125}{1707539248}u_{i+\frac{12}{5}} - \frac{964258361}{8324253834}u_{i+3} + \frac{1019235875}{13660313984}u_{i+\frac{16}{5}} - \frac{1814552875}{123369710668}u_{i+\frac{17}{5}} + \frac{164075955}{14514083608}hu_i' + \frac{693}{213442406}h^2v_{i+4} \tag{9}$$

$$u_{i+\frac{6}{5}} = -\frac{59524779287}{159151539026620}u_i + \frac{1326433964}{468092761843}u_{i+\frac{1}{5}} - \frac{83450292145}{12170411807918}u_{i+\frac{2}{5}} + \frac{1191667384144}{2340463809215}u_{i+1} + \frac{230525811560}{468092761843}u_{i+\frac{7}{5}} + \frac{132388629703}{4680927618430}u_{i+2} - \frac{3012664208}{66870394549}u_{i+\frac{11}{5}} + \frac{9969019315}{468092761843}u_{i+\frac{12}{5}} - \frac{111667102712}{30426029519795}u_{i+3} + \frac{4435631215}{1872371047372}u_{i+\frac{16}{5}} - \frac{3713585660}{7957576951331}u_{i+\frac{17}{5}} - \frac{8663210424}{468092761843}h^2v_{i+\frac{6}{5}} + \frac{236808}{2340463809215}h^2v_{i+4}$$

(10)

$$u_{i+\frac{7}{5}} = -\frac{35729475129}{31239901916740}u_i + \frac{4920894145}{643174451227}u_{i+\frac{1}{5}} - \frac{1683160836}{108587894363}u_{i+\frac{2}{5}} + \frac{539977310436}{3215872256135}u_{i+1} + \frac{42463381920}{91882064461}u_{i+\frac{6}{5}} + \frac{307950693356}{292352023285}u_{i+2} - \frac{93728957670}{91882064461}u_{i+\frac{11}{5}} + \frac{236475241011}{643174451227}u_{i+\frac{12}{5}} - \frac{163964431473}{3800576302705}u_{i+3} + \frac{9558245185}{367528257844}u_{i+\frac{16}{5}} - \frac{53101972005}{10933965670859}u_{i+\frac{17}{5}} - \frac{4725387504}{108587894363}h^2v_{i+\frac{7}{5}} + \frac{484488}{542939471815}h^2v_{i+4}$$

(11)

$$u_{i+2} = -\frac{220572654003}{153425883810892}u_i + \frac{281300270000}{29331418963847}u_{i+\frac{1}{5}} - \frac{673791569625}{34664404230001}u_{i+\frac{2}{5}} + \frac{1165672110144}{4190202709121}u_{i+1} - \frac{3771743943750}{4190202709121}u_{i+\frac{6}{5}} + \frac{220713488000}{205114817929}u_{i+\frac{7}{5}} + \frac{439481520000}{4190202709121}u_{i+\frac{11}{5}} + \frac{2032984418625}{4190202709121}u_{i+\frac{12}{5}} - \frac{2223584219904}{34664404230001}u_{i+3} + \frac{4503232956875}{117325675855388}u_{i+\frac{16}{5}} - \frac{38984754000}{5479495850389}u_{i+\frac{17}{5}} - \frac{23626937520}{380927519011}h^2u_{i+2} + \frac{484488}{380927519011}h^2v_{i+4}$$

(12)

$$u_{i+\frac{11}{5}} = -\frac{1610931429}{55387820088340}u_i + \frac{199983510}{1140337472407}u_{i+\frac{1}{5}} - \frac{4610182940}{14824387141291}u_{i+\frac{2}{5}} + \frac{9496656336}{5701687362035}u_{i+1} - \frac{155117232}{162905353201}u_{i+\frac{6}{5}} - \frac{1732516335}{325810706402}u_{i+\frac{7}{5}} + \frac{410605748388}{814526766005}u_{i+2} + \frac{577473159735}{1140337472407}u_{i+\frac{12}{5}} - \frac{1448598058281}{148243871412910}u_{i+3} + \frac{21929922459}{4561349889628}u_{i+\frac{16}{5}} - \frac{2149394970}{2769391004417}u_{i+\frac{17}{5}} - \frac{2887736808}{162905353201}h^2v_{i+\frac{11}{5}} + \frac{78936}{814526766005}h^2v_{i+4}$$

(13)

$$u_{i+\frac{12}{5}} = -\frac{737000782381}{188075458963660}u_i + \frac{13972744540}{553163114599}u_{i+\frac{1}{5}} - \frac{353004129610}{7191120489787}u_{i+\frac{2}{5}} + \frac{1571408160272}{2765815572995}u_{i+1} - \frac{893315875620}{553163114599}u_{i+\frac{6}{5}} + \frac{875764873192}{553163114599}u_{i+\frac{7}{5}} - \frac{10327761506018}{2765815572995}u_{i+2} + \frac{2546494175120}{553163114599}u_{i+\frac{11}{5}} - \frac{23121588004856}{35955602448935}u_{i+3} + \frac{35955602448935}{2212652458396}u_{i+\frac{16}{5}} - \frac{486856004716}{9403772948183}u_{i+\frac{17}{5}} + \frac{60642472968}{553163114599}h^2v_{i+\frac{12}{5}} + \frac{19215504}{2765815572995}h^2v_{i+4} \tag{14}$$

$$u_{i+3} = \frac{21843227531489}{19311753828207236}u_i - \frac{2070677464375}{283996379826577}u_{i+\frac{1}{5}} + \frac{365735910500}{25817852711507}u_{i+\frac{2}{5}} - \frac{46377146659948}{283996379826577}u_{i+1} + \frac{131376152180000}{283996379826577}u_{i+\frac{6}{5}} - \frac{11647928985875}{25817852711507}u_{i+\frac{7}{5}} + \frac{27445244184332}{25817852711507}u_{i+2} - \frac{576419714438750}{283996379826577}u_{i+\frac{11}{5}} + \frac{417083651983375}{283996379826577}u_{i+\frac{12}{5}} + \frac{751171463501875}{1135985519306308}u_{i+\frac{16}{5}} - \frac{93560142294125}{4827938457051809}u_{i+\frac{17}{5}} - \frac{716683771440}{25817852711507}h^2v_{i+3} - \frac{35531496}{25817852711507}h^2v_{i+4} \tag{15}$$

$$u_{i+\frac{16}{5}} = \frac{15521609114019}{4030212808091735}u_i - \frac{1152542307152}{47414268330491}u_{i+\frac{1}{5}} + \frac{28416106407480}{616385488296383}u_{i+\frac{2}{5}} - \frac{114114431032512}{237071341652455}u_{i+1} + \frac{61723730000688}{47414268330491}u_{i+\frac{6}{5}} - \frac{56873025990880}{47414268330491}u_{i+\frac{7}{5}} + \frac{502758613885528}{237071341652455}u_{i+2} - \frac{161062432009920}{47414268330491}u_{i+\frac{11}{5}} + \frac{88992550681380}{47414268330491}u_{i+\frac{12}{5}} + \frac{362584687682976}{3081927441481915}u_{i+3} + \frac{511877886577680}{806042561618347}u_{i+\frac{17}{5}} - \frac{1455419351232}{47414268330491}h^2v_{i+\frac{16}{5}} - \frac{4128261984}{237071341652455}h^2v_{i+4} \tag{16}$$

$$u_{i+\frac{17}{5}} = \frac{370330170269}{25192113745610}u_i - \frac{700687613545}{7557634123683}u_{i+\frac{1}{5}} + \frac{3983479568552}{22672902371049}u_{i+\frac{2}{5}} - \frac{9876629706908}{5398310088345}u_{i+1} + \frac{5337402515680}{1079662017669}u_{i+\frac{6}{5}} - \frac{34398062616676}{7557634123683}u_{i+\frac{7}{5}} + \frac{43482341208152}{5398310088345}u_{i+2} - \frac{41985676126040}{3238986053007}u_{i+\frac{11}{5}} + \frac{2611462130050}{359887339223}u_{i+\frac{12}{5}} - \frac{120657940271924}{37788170618415}u_{i+3} + \frac{48130212038465}{15115268247366}u_{i+\frac{16}{5}} + \frac{3850315744}{359887339223}h^2v_{i+\frac{17}{5}} - \frac{136668752}{1799436696115}h^2v_{i+4} \tag{17}$$

Also, the first derivative of (3.6) is evaluated at the same points as above in order to cater for the first derivative term of a general second order ODE in the implementation process of the method.

$$u_{i+\frac{1}{5}} = -\frac{8675155969326}{60196975329685}u_i + \frac{14021918174880}{9206596226893}u_{i+\frac{2}{5}} - \frac{11285871779952}{3540998548805}u_{i+1} + \frac{4482715805568}{708199709761}u_{i+\frac{6}{5}} - \frac{3135340103280}{708199709761}u_{i+\frac{7}{5}} + \frac{13130988065888}{3540998548805}u_{i+2} - \frac{3288004229664}{708199709761}u_{i+\frac{11}{5}} + \frac{1411908344280}{708199709761}u_{i+\frac{12}{5}} - \frac{14573246657904}{46032981134465}u_{i+3} + \frac{143792861982}{708199709761}u_{i+\frac{16}{5}} - \frac{480094679295}{12039395065937}u_{i+\frac{17}{5}} - \frac{121284945936}{708199709761}hu'_{i+\frac{1}{5}} + \frac{30735936}{3540998548805}h^2v_{i+4} \quad (18)$$

$$u_{i+\frac{2}{5}} = -\frac{31702636997577}{76743011328170}u_i + \frac{2216148348960}{451429478401}u_{i+\frac{1}{5}} - \frac{54994118804352}{2257147392005}u_{i+1} + \frac{20478615049620}{451429478401}u_{i+\frac{6}{5}} - \frac{1250059329792}{41039043491}u_{i+\frac{7}{5}} + \frac{4908496858083}{205195217455}u_{i+2} - \frac{13353572261120}{451429478401}u_{i+\frac{11}{5}} + \frac{5677108568586}{451429478401}u_{i+\frac{12}{5}} - \frac{401274736128}{205195217455}u_{i+3} + \frac{1126773690705}{902858956802}u_{i+\frac{16}{5}} - \frac{1873115296416}{7674301132817}u_{i+\frac{17}{5}} + \frac{71668377144}{41039043491}hu'_{i+\frac{2}{5}} + \frac{10732176}{205195217455}h^2v_{i+4} \quad (19)$$

$$u_{i+3} = -\frac{1422747654237}{209457042650042}u_i + \frac{24226868250}{560045568583}u_{i+\frac{1}{5}} - \frac{46424385000}{560045568583}u_{i+\frac{2}{5}} + \frac{5565659882328}{6160501254413}u_{i+1} - \frac{15362049976000}{6160501254413}u_{i+\frac{6}{5}} + \frac{1319675686875}{560045568583}u_{i+\frac{7}{5}} - \frac{2661475477752}{560045568583}u_{i+2} + \frac{50987263918500}{6160501254413}u_{i+\frac{11}{5}} - \frac{2924930531250}{560045568583}u_{i+\frac{12}{5}} + \frac{27262360841625}{12321002508826}u_{i+\frac{16}{5}} - \frac{1289764271250}{5512027438159}u_{i+\frac{17}{5}} - \frac{358341885720}{560045568583}hu'_{i+3} + \frac{10732176}{560045568583}h^2v_{i+4} \quad (20)$$

$$u_{i+\frac{16}{5}} = -\frac{147308208201}{48908643201535}u_i + \frac{10988954592}{575395802371}u_{i+\frac{1}{5}} - \frac{272379024720}{7480145430823}u_{i+\frac{2}{5}} + \frac{1118270418048}{2876979011855}u_{i+1} - \frac{611251923744}{575395802371}u_{i+\frac{6}{5}} + \frac{570588800320}{575395802371}u_{i+\frac{7}{5}} - \frac{5398656452112}{2876979011855}u_{i+2} + \frac{1805963499648}{575395802371}u_{i+\frac{11}{5}} - \frac{1068920095320}{575395802371}u_{i+\frac{12}{5}} + \frac{56898239340096}{37400727154115}u_{i+3} - \frac{2185664231520}{9781728640307}u_{i+\frac{17}{5}} + \frac{121284945936}{575395802371}hu'_{i+\frac{16}{5}} + \frac{30735936}{2876979011855}h^2v_{i+4} \quad (21)$$

$$u_{i+\frac{17}{5}} = \frac{215079595038}{39009452634895}u_i - \frac{271730159085}{7801890526979}u_{i+\frac{1}{5}} + \frac{20119102506272}{304273730552181}u_{i+\frac{2}{5}} - \frac{27057554793808}{39009452634895}u_{i+1} + \frac{14671221962880}{7801890526979}u_{i+\frac{6}{5}} - \frac{13562180574096}{7801890526979}u_{i+\frac{7}{5}} + \frac{122356216558752}{39009452634895}u_{i+2} - \frac{119450162548640}{23405671580937}u_{i+\frac{11}{5}} + \frac{22640428824552}{7801890526979}u_{i+\frac{12}{5}} - \frac{756052232336016}{507122884253635}u_{i+3} + \frac{16153821432210}{7801890526979}u_{i+\frac{16}{5}} + \frac{687281360304}{7801890526979}hu'_{i+\frac{17}{5}} - \frac{986965056}{39009452634895}h^2v_{i+4} \quad (22)$$

3.1 Convergence Properties of the Methods

In this section, we examine the order and error constant for consistency and also zero stability. According Lambert (1973), zero stability and consistency of a linear multistep method are necessary and sufficient conditions for its convergence.

3.3 Order and error constants

The linear differential operator L associated with (6) is defined by

$$L\left[u(t);h\right] = \sum_{j=0}^{k}\left[\alpha_j u(t+jh) - h^n\beta_j u^{(n)}(t+jh)\right] \quad (23)$$

where n is the order of the differential equation considered. Expanding (8) in Taylor series, we have

$$L\left[u(t);h\right] = c_0u(t) + c_1hu'(t) + c_2hu''(t) + \ldots + c_qh^qu^q(t) \quad (24)$$

where

$$c_0 = \alpha_0 + \alpha_1 + \alpha_2 + \alpha_3 + \ldots + \alpha_k$$
$$c_1 = \alpha_1 + 2\alpha_2 + 3\alpha_3 + \ldots + k\alpha_k$$
$$c_2 = \frac{1}{2!}\left(\alpha_1 + 2^2\alpha_2 + 3^2\alpha_3 + \ldots + k^2\alpha_k\right) - \left(\beta_0 + \beta_1 + \beta_2 + \ldots + \beta_k\right)$$
$$\vdots$$
$$c_p = \frac{1}{p!}\left(\alpha_1 + 2^p\alpha_2 + 3^p\alpha_3 + \ldots + k^p\alpha_k\right) - \frac{1}{(p-n)!}\left(\beta_1 + 2^{p-2}\beta_2 + 3^{p-2}\beta_3 + \ldots + k^{p-2}\beta_k\right)$$
$$p \geq n$$

Definition 3.1: The LMM (8) is said to be of order *p* if $c_0 = c_1 = c_2 = ... = c_p = c_{p+1} = 0$ and $c_{p+n} \neq 0$ is the error constant.

Definition 3.2: The LMM (8) is said to be consistent if it has order of accuracy *p*>1

3.2 Order and error constants of BHBDF II

Considering the discrete scheme (7), the coefficients are given as follows:

$$\alpha_0 = -\frac{4899694293}{3719054980},\ \alpha_{\frac{1}{5}} = \frac{993505500}{120322367},\ \alpha_{\frac{2}{5}} = -\frac{169955950}{10938397},\ \alpha_1 = \frac{94709296656}{601611835}$$

$$\alpha_{\frac{6}{5}} = -\frac{50567692500}{120322367},\ \alpha_{\frac{7}{5}} = \frac{4172844600}{10938397},\ \alpha_2 = -\frac{34685775774}{54691985},$$

$$\alpha_{\frac{11}{5}} = \frac{10813166000}{10938397},\ \alpha_{\frac{12}{5}} = -\frac{63868346100}{120322367},\ \alpha_3 = \frac{9906198264}{54691985},$$

$$\alpha_{\frac{16}{5}} = -\frac{77374571625}{481289468},\ \alpha_{\frac{17}{5}} = \frac{96247674900}{2045480239},\ \alpha_4 = -1,\quad \beta_4 = -\frac{1120392}{54691985}$$

and applying (9),

$$c_0 = \alpha_0 + \alpha_{\frac{1}{5}} + \alpha_{\frac{2}{5}} + \alpha_1 + \alpha_{\frac{6}{5}} + \alpha_{\frac{7}{5}} + \alpha_2 + \alpha_{\frac{11}{5}} + \alpha_{\frac{12}{5}} + \alpha_3 + \alpha_{\frac{16}{5}} + \alpha_{\frac{17}{5}} + \alpha_4 = 0$$

$$c_1 = \left(\frac{1}{5}\right)\alpha_{\frac{1}{5}} + \left(\frac{2}{5}\right)\alpha_{\frac{2}{5}} + \alpha_1 + \left(\frac{6}{5}\right)\alpha_{\frac{6}{5}} + \left(\frac{7}{5}\right)\alpha_{\frac{7}{5}} + (2)\alpha_2 + \left(\frac{11}{5}\right)\alpha_{\frac{11}{5}} + \left(\frac{12}{5}\right)\alpha_{\frac{12}{5}} + (3)\alpha_3 + \left(\frac{16}{5}\right)\alpha_{\frac{16}{5}} + \left(\frac{17}{5}\right)\alpha_{\frac{17}{5}} + (4)\alpha_4 = 0$$

$$c_2 = \frac{1}{2!}\left(\begin{array}{l}\left(\frac{1}{5}\right)^2\alpha_{\frac{1}{5}} + \left(\frac{2}{5}\right)^2\alpha_{\frac{2}{5}} + \alpha_1 + \left(\frac{6}{5}\right)^2\alpha_{\frac{6}{5}} + \left(\frac{7}{5}\right)^2\alpha_{\frac{7}{5}} + (2)^2\alpha_2 + \left(\frac{11}{5}\right)^2\alpha_{\frac{11}{5}} + \left(\frac{12}{5}\right)^2\alpha_{\frac{12}{5}} + (3)^2\alpha_3 \\ + \left(\frac{16}{5}\right)^2\alpha_{\frac{16}{5}} + \left(\frac{17}{5}\right)^2\alpha_{\frac{17}{5}} + (4)^2\alpha_4\end{array}\right) - \beta_4 = 0$$

$$c_3 = \frac{1}{3!}\left(\begin{array}{l}\left(\frac{1}{5}\right)^3\alpha_{\frac{1}{5}} + \left(\frac{2}{5}\right)^3\alpha_{\frac{2}{5}} + \alpha_1 + \left(\frac{6}{5}\right)^3\alpha_{\frac{6}{5}} + \left(\frac{7}{5}\right)^3\alpha_{\frac{7}{5}} + (2)^3\alpha_2 + \left(\frac{11}{5}\right)^3\alpha_{\frac{11}{5}} + \left(\frac{12}{5}\right)^3\alpha_{\frac{12}{5}} + (3)^3\alpha_3 \\ + \left(\frac{16}{5}\right)^3\alpha_{\frac{16}{5}} + \left(\frac{17}{5}\right)^3\alpha_{\frac{17}{5}} + (4)^3\alpha_4\end{array}\right) - (4\beta_4) = 0$$

$$c_4 = \frac{1}{4!}\left(\begin{array}{l}\left(\frac{1}{5}\right)^4\alpha_{\frac{1}{5}} + \left(\frac{2}{5}\right)^4\alpha_{\frac{2}{5}} + \alpha_1 + \left(\frac{6}{5}\right)^4\alpha_{\frac{6}{5}} + \left(\frac{7}{5}\right)^4\alpha_{\frac{7}{5}} + (2)^4\alpha_2 + \left(\frac{11}{5}\right)^4\alpha_{\frac{11}{5}} + \left(\frac{12}{5}\right)^4\alpha_{\frac{12}{5}} + (3)^4\alpha_3 \\ + \left(\frac{16}{5}\right)^4\alpha_{\frac{16}{5}} + \left(\frac{17}{5}\right)^4\alpha_{\frac{17}{5}} + (4)^4\alpha_4\end{array}\right) - \frac{1}{2!}\left(4^2\beta_4\right) = 0$$

$$c_5 = \frac{1}{5!}\left(\begin{array}{l}\left(\frac{1}{5}\right)^5\alpha_{\frac{1}{5}} + \left(\frac{2}{5}\right)^5\alpha_{\frac{2}{5}} + \alpha_1 + \left(\frac{6}{5}\right)^5\alpha_{\frac{6}{5}} + \left(\frac{7}{5}\right)^5\alpha_{\frac{7}{5}} + (2)^5\alpha_2 + \left(\frac{11}{5}\right)^5\alpha_{\frac{11}{5}} + \left(\frac{12}{5}\right)^5\alpha_{\frac{12}{5}} + (3)^5\alpha_3 \\ + \left(\frac{16}{5}\right)^5\alpha_{\frac{16}{5}} + \left(\frac{17}{5}\right)^5\alpha_{\frac{17}{5}} + (4)^5\alpha_4\end{array}\right) - \frac{1}{3!}\left(4^3\beta_4\right) = 0$$

$$c_5 = \frac{1}{5!}\left(\begin{array}{l}\left(\frac{1}{5}\right)^5\alpha_{\frac{1}{5}} + \left(\frac{2}{5}\right)^5\alpha_{\frac{2}{5}} + \alpha_1 + \left(\frac{6}{5}\right)^5\alpha_{\frac{6}{5}} + \left(\frac{7}{5}\right)^5\alpha_{\frac{7}{5}} + (2)^5\alpha_2 + \left(\frac{11}{5}\right)^5\alpha_{\frac{11}{5}} + \left(\frac{12}{5}\right)^5\alpha_{\frac{12}{5}} + (3)^5\alpha_3 \\ + \left(\frac{16}{5}\right)^5\alpha_{\frac{16}{5}} + \left(\frac{17}{5}\right)^5\alpha_{\frac{17}{5}} + (4)^5\alpha_4\end{array}\right) - \frac{1}{3!}\left(4^3\beta_4\right) = 0$$

$$c_7 = \frac{1}{7!}\left(\begin{array}{l}\left(\frac{1}{5}\right)^7\alpha_{\frac{1}{5}} + \left(\frac{2}{5}\right)^7\alpha_{\frac{2}{5}} + \alpha_1 + \left(\frac{6}{5}\right)^7\alpha_{\frac{6}{5}} + \left(\frac{7}{5}\right)^7\alpha_{\frac{7}{5}} + (2)^7\alpha_2 + \left(\frac{11}{5}\right)^7\alpha_{\frac{11}{5}} + \left(\frac{12}{5}\right)^7\alpha_{\frac{12}{5}} + (3)^7\alpha_3 \\ + \left(\frac{16}{5}\right)^7\alpha_{\frac{16}{5}} + \left(\frac{17}{5}\right)^7\alpha_{\frac{17}{5}} + (4)^7\alpha_4\end{array}\right) - \frac{1}{5!}\left(4^5\beta_4\right) = 0$$

$$c_8 = \frac{1}{8!}\left(\begin{array}{l}\left(\frac{1}{5}\right)^8\alpha_{\frac{1}{5}} + \left(\frac{2}{5}\right)^8\alpha_{\frac{2}{5}} + \alpha_1 + \left(\frac{6}{5}\right)^8\alpha_{\frac{6}{5}} + \left(\frac{7}{5}\right)^8\alpha_{\frac{7}{5}} + (2)^8\alpha_2 + \left(\frac{11}{5}\right)^8\alpha_{\frac{11}{5}} + \left(\frac{12}{5}\right)^8\alpha_{\frac{12}{5}} + (3)^8\alpha_3 \\ + \left(\frac{16}{5}\right)^8\alpha_{\frac{16}{5}} + \left(\frac{17}{5}\right)^8\alpha_{\frac{17}{5}} + (4)^8\alpha_4\end{array}\right) - \frac{1}{6!}\left(4^6\beta_4\right) = 0$$

$$c_9 = \frac{1}{9!}\left(\begin{array}{l}\left(\frac{1}{5}\right)^9\alpha_{\frac{1}{5}} + \left(\frac{2}{5}\right)^9\alpha_{\frac{2}{5}} + \alpha_1 + \left(\frac{6}{5}\right)^9\alpha_{\frac{6}{5}} + \left(\frac{7}{5}\right)^9\alpha_{\frac{7}{5}} + (2)^9\alpha_2 + \left(\frac{11}{5}\right)^9\alpha_{\frac{11}{5}} + \left(\frac{12}{5}\right)^9\alpha_{\frac{12}{5}} + (3)^9\alpha_3 \\ + \left(\frac{16}{5}\right)^9\alpha_{\frac{16}{5}} + \left(\frac{17}{5}\right)^9\alpha_{\frac{17}{5}} + (4)^9\alpha_4\end{array}\right) - \frac{1}{7!}\left(4^7\beta_4\right) = 0$$

$$\vdots$$

$$c_{13} = \frac{1}{13!}\left(\begin{array}{l}\left(\frac{1}{5}\right)^{13}\alpha_{\frac{1}{5}} + \left(\frac{2}{5}\right)^{13}\alpha_{\frac{2}{5}} + \alpha_1 + \left(\frac{6}{5}\right)^{13}\alpha_{\frac{6}{5}} + \left(\frac{7}{5}\right)^{13}\alpha_{\frac{7}{5}} + (2)^{13}\alpha_2 + \left(\frac{11}{5}\right)^{13}\alpha_{\frac{11}{5}} \\ + \left(\frac{12}{5}\right)^{13}\alpha_{\frac{12}{5}} + (3)^{13}\alpha_3 + \left(\frac{16}{5}\right)^{13}\alpha_{\frac{16}{5}} + \left(\frac{17}{5}\right)^{13}\alpha_{\frac{17}{5}} + (4)^{13}\alpha_4\end{array}\right) - \frac{1}{11!}\left(4^{11}\beta_4\right) = \frac{190648242}{1175023115234375}$$

Hence the method is of order $p = 11$ and the error constant is $c_{p+2} = \frac{190648242}{1175023115234375}$

Similar procedure is applied to the discrete schemes that constitute the block members of BHBDF II and the summary of the order and error constants is given in the tables below:

Table 3.1: Order and Error Constants of BHBDF II

Equation	Order p	Error constants c_{p+2}
3.7	11	$1.622506311 \times 10^{-9}$
3.8	11	$3.097970596 \times 10^{-9}$
3.9	11	$-9.197700413 \times 10^{-11}$
3.10	11	$3.621094306 \times 10^{-10}$
3.11	11	$9.875049942 \times 10^{-12}$
3.12	11	$6.196932974 \times 10^{-11}$
3.13	11	$8.33642171 \times 10^{-11}$
3.14	11	$3.623624551 \times 10^{-12}$
3.15	11	$3.18967290 \times 10^{-10}$
3.16	11	$-8.96155326 \times 10^{-11}$

3.17	11	-4.181635836 x 10^{-10}
3.18	11	-1.622744053 x 10^{-10}

Table 1 displays the order of accuracy of each member of the derived block method (**BHBDF II**) with its corresponding error constant. It is revealed from analysis that the block method is of uniform order p = 11 which is greater than 1. Hence the method is said to be consistent.

3.3 Zero stability

In order to characterize the method for stability, we rewrite the derived schemes as a matrix difference equation as follows:

$$P^{(1)}U_w = P^{(0)}U_{w-1} + h^n Q^{(1)}V_w \tag{25}$$

where

$$\left.\begin{aligned} U_w &= \left(u_{n+\frac{1}{5}}, u_{n+\frac{2}{5}}, u_{n+1}, u_{n+\frac{6}{5}}, u_{n+\frac{7}{5}}, u_{n+2}, u_{n+\frac{11}{5}}, u_{n+\frac{12}{5}}, u_{n+3}, u_{n+\frac{16}{5}}, u_{n+\frac{17}{5}}, u_{n+4}\right)^T \\ U_{w-1} &= \left(u_{n-\frac{1}{5}}, u_{n-\frac{2}{5}}, u_{n-1}, u_{n-\frac{6}{5}}, u_{n-\frac{7}{5}}, u_{n-2}, u_{n-\frac{11}{5}}, u_{n-\frac{12}{5}}, u_{n-3}, u_{n-\frac{16}{5}}, u_{n-\frac{17}{5}}, u_{n-4}\right)^T \\ V_{w+1} &= \left(v_{n+\frac{1}{5}}, v_{n+\frac{2}{5}}, v_{n+1}, v_{n+\frac{6}{5}}, v_{n+\frac{7}{5}}, v_{n+2}, v_{n+\frac{11}{5}}, v_{n+\frac{12}{5}}, v_{n+3}, v_{n+\frac{16}{5}}, v_{n+\frac{17}{5}}, v_{n+4}\right)^T \end{aligned}\right\}$$

and $P^{(1)}, P^{(0)}, Q^{(1)}$ are matrices whose entries are given by the coefficients of the block method, whose first characteristic polynomial is given as

$$\rho(\lambda) = \left|\lambda P^{(1)} - P^{(0)}\right| \tag{26}$$

Definition (Zero Stability) 3.3 **:** A block linear multistep method is said to be zero stable if the roots (λ_k) of the difference equation in (3.46) as $h \to 0$ is $|\lambda_k| \le 1,\ k = 1, \ldots, n$ and the multiplicity of the roots $|\lambda_k| = 1$ is not greater than the order of the ODE.

Zero Stability of BHBDF II, The first characteristics polynomial is given as:

$$\rho(\lambda) = \left|\lambda P^{(1)} - P^{(0)}\right| = 0.000013519\lambda^{12}(\lambda + 1) = 0 \tag{27}$$

$$\Rightarrow \quad \lambda = \{0,0,0,0,0,0,0,0,0,0,0,1\}$$

Hence the proposed method BHBDF II is zero stable.

4. Results and Discussion

Problem 2:

Consider the nonlinear problem in Guler *et al.* (2019): $u''+(u')^2-u^2=1-\sin t, u(0)=0, u'(0)=1$ and h = 0.01 Exact Solution: $U(t)=\sin t$

Table 4.2: Comparison of the Exact and Numerical Results for Problem 2

T	Exact solution	Numerical solution
0.1	0.099833416646828152307	0.099833416646828141012
0.2	0.19866933079506121546	0.19866933079506114447
0.3	0.29552020666133957511	0.29552020666133937661
0.4	0.38941834230865049167	0.38941834230865008339
0.5	0.47942553860420300027	0.47942553860420229076
0.6	0.56464247339503535720	0.56464247339503424468
0.7	0.64421768723769105367	0.64421768723768942938
0.8	0.71735609089952276163	0.71735609089952051408
0.9	0.78332690962748338846	0.78332690962748041151
1.0	0.84147098480789650665	0.84147098480789267764

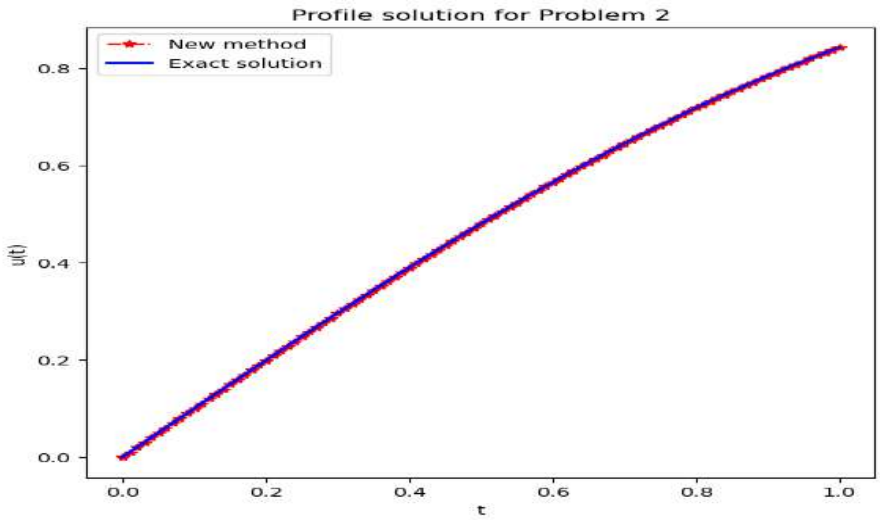

Figure 4.2: Graph of Exact and Numerical Solutions for Problem 2

Problem 3:

Consider the nonlinear problem: $u''+u^3+u=\left(\cos t+\varepsilon\sin(10t)\right)^3-99\varepsilon\sin t$, with the following initial conditions $u(0)=1, u'(0)=10\varepsilon$ and h = 0.005

Exact Solution: $U(t)=\left(\cos t+\varepsilon\sin(10t)\right)$, where $\varepsilon=10^{-10}$

Table 4.3: Comparison of the Exact and Numerical Results Problem 3

T	Exact solution	Numerical solution
0.005	0.99998750003103956190	0.99998750003104148000

0.010	0.99995000042664861944	0.99995000042666361119
0.015	0.99988750212430299300	0.99988750212435328633
0.020	0.99980000668644471149	0.99980000668656354220
0.025	0.99968751630044298218	0.99968751630067456136
0.030	0.99955003377853953694	0.99955003377893889990
0.035	0.99938756255777835656	0.99938756255841116595
0.040	0.99920010669991977454	0.99920010670086213063
0.045	0.99898767089133896263	0.99898767089267724763
0.050	0.99875026044290880042	0.99875026044473940375

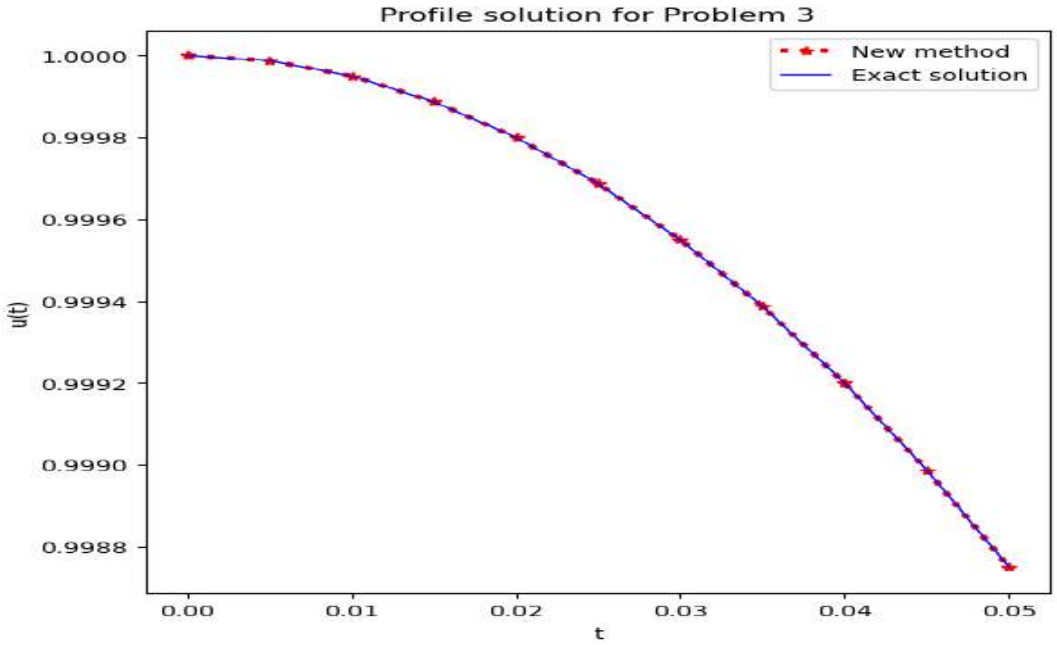

Figure 4.3: Graph of Exact and Numerical Solutions for Problem 3

Table 4.5: Comparison of Accuracy for Problem 2

T	Exact solution	Error in Guler *et al.* (2019)	Error in Ogunlaran and Kehinde (2022)	Error in BHBDF II
0.1	0.099833416646828152307	3.490×10^{-08}	9.300×10^{-10}	1.130×10^{-17}
0.2	0.19866933079506121546	1.160×10^{-07}	1.990×10^{-09}	7.099×10^{-17}
0.3	0.29552020666133957511	-	-	1.985×10^{-16}

0.4	0.38941834230865049167	1.130×10^{-07}	3.180×10^{-09}	4.083×10^{-16}
0.5	0.47942553860420300027	4.610×10^{-07}	3.230×10^{-09}	7.095×10^{-16}
0.6	0.56464247339503535720	7.800×10^{-07}	3.510×10^{-09}	1.113×10^{-15}
0.7	0.64421768723769105367	1.400×10^{-06}	3.740×10^{-09}	1.624×10^{-15}
0.8	0.71735609089952276163	4.1600×10^{-06}	3.530×10^{-09}	2.248×10^{-15}
0.9	0.78332690962748338846	1.400×10^{-05}	3.030×10^{-09}	2.977×10^{-15}
1.0	0.84147098480789650665	4.100×10^{-05}	2.750×10^{-09}	3.829×10^{-15}

Table 4.6: Comparison of Accuracy for Problem 3

T	Exact solution	Numerical solution	Error in BHBDF II
0.005	0.99998750003103956190	0.99998750003104148000	1.918×10^{-15}
0.010	0.99995000042664861944	0.99995000042666361119	1.500×10^{-14}
0.015	0.99988750212430299300	0.99988750212435328633	5.029×10^{-14}
0.020	0.99980000668644471149	0.99980000668656354220	1.188×10^{-13}
0.025	0.99968751630044298218	0.99968751630067456136	2.316×10^{-13}
0.030	0.99955003377853953694	0.99955003377893889990	3.994×10^{-13}
0.035	0.99938756255777835656	0.99938756255841116595	6.328×10^{-13}
0.040	0.99920010669991977454	0.99920010670086213063	9.424×10^{-13}
0.045	0.99898767089133896263	0.99898767089267724763	1.338×10^{-12}
0.050	0.99875026044290880042	0.99875026044473940375	1.831×10^{-12}

5. Conclusion

In this project, an effective numerical approach for solving higher-order ordinary differential equations is sought. To achieve this milestone, the research focused on developing a class of block hybrid backward differentiation formula (BDF) that simultaneously generates approximate solutions to an equation on the entire interval of integration. The techniques of interpolation and collocation are employed for the derivation of the method. In the derivation process of the method, which is four-step, that is, k = 4, a number of off-grid points were carefully selected at the interpolation points over the interval [0, 4] for the second ODE, BHBDF II. Convergence analysis of the methods reveals that BHBDF II has an order of accuracy (p + 2) of eleven. The methods are zero stable and consistent, which implies their convergence. Furthermore, numerical experiments were carried out where BHBDF II was implemented on several nonlinear second problems. The graphical illustrations displayed therein show that the method conforms to the exact solution. Further comparative analyses of BHBDF II in tables 2–4 reveal that the method has the advantage of producing smaller global errors over several existing methods in the literature, including some of the most recent ones. Error analysis in comparison with some existing methods further testifies the efficacy of the method.

References

Abdelrahim R. & Omar Z. (2016). Direct Solution of Second-Order Ordinary Differential Equations Using a Single-step Hybrid Block Method of Order Five. *Math. Comput. App.*, 21(12), doi:10.3390/mca21020012.

Abualnaja, K. M. (2015). A block Procedure with Linear Multistep Methods Using Legendre Polynomial for Solving ODEs. *App. Math. Sci. Res* 6, 717-723

Adeyefa, E. O. (2017). Orthogonal-based hybrid block method for solving general second order initial

Value Problems. *Italian Journal of Pure and Applied Mathematics,* 37, 659-672.

Adeyeye O. & Omar Z. (2016) Maximal Order Block Method for The Solution of Second Order Ordinary Differential Equations. *IAENG Int. J. App. Math*. 46(4). 46 – 63.

Akinfenwa, O.A., Jator, S.N. and Yao, N.M. (2013), Continuous Block Backwar Differentiation Formula For Solving Stiff Ordinary Differential Equations. *Computers and Mathematics with Applications,* 996 1005.

Audu K. J., Garba J., Tiamiyu A. T & Thomas B. A. (2022). Application of Backward Differentiation Formula on Fourth-Order Differential Equations. *Journal of Science and Technology* 14(2), 52-65.

Guler, C., Kaya, S. O. & Sezer, M. (2019). Numerical Solution of a Class of Nonlinear Ordinary Differential Equations in Hermite series. *Thermal Science: International* Scientific *Journal,* 23, 1205–1210.

Muhammad, R. & Yahaya, Y. A. (2012). A sixth order implicit hybrid backward differentiation formulae (HBDF) for block solution of ordinary differential equations. *American Journal* of *Mathematics and Statistics*,2(4), 89 – 94.

Muhammad, R., Yahaya, Y. A. & Abdulkareem, A. S. (2020). An implicit Runge-Kutta type method for The Solution of Initial Value Problems. *KASU Journal of Mathematical Sciences,* 1(1), 28 – 37.

Mohammed, U., Usman, A., Salihu, N. O., Ma'ali, A. I., & Akintubobo, B. (2022). Formulation of $\boldsymbol{k}$− Step Order $\boldsymbol{2k}$ Fuzzy-structured Block Hybrid Backward Differentiation Formulae Algorithms for the Approximate Solution of Fuzzy Differential Equations.

Ogunlaran, O. M., & Kehinde, M. A. (2022). A New Block Integrator for Second Order Initial Value Problems. *Neuroquantology,* 20(17), 1976 – 1980.

Olabode, B. T.& Momoh, A. L. (2016). Continuous Hybrid Multistep Methods With Legendre Basis Function for Direct Treatment of Second Order stiff ODEs. *Amer J. Compt. App. Math*., 6(2), 38-49.

Omole E. O., Obarhua F. O., Familua A. B. & Shokri A. (2023). Algorithms of algebraic order nine for Numerically solving second-order boundary and initial value problems in ordinary differential equations. *Int. J. Mathematics in Operational Research,* 25(3), 343 – 368.

Oyelami, O. A. (2018). *A Collocation Technique Based on Orthogonal Polynomial for the solution of Second order ordinary differential equatio*ns. MTech Thesis in School of Post Graduate, Federal University of Technology, Minna.

Pimenov, V. G., & Hendy, A. S. (2015). Numerical Studies for Fractional Functional differential Equations with delay based on BDF-type shifted Chebyshev approximations. In *Abstract and Applied Analysis* (Vol. 2015). Hindawi.

Yakusak, N. S. & Owolanke, A.O. (2018). A class of linear multi-step method for direct solution of Second order initial value problems in ordinary differential equations.

Zwillinger, D., & Dobrushkin, V. (2021). *Handbook of differential equations*. CRC Press.

Geophysical and Geotechnical investigation of a proposed Dam site at FUT Minna Gidan Kwano campus

A. K Nagya[1], A. A. Rafiu[2] and K. A. Salako[3]
Department of Applied Geophysics, Federal University of Technology, Minna. Niger State Nigeria.

Abstract

2D Electrical Resistivity Imaging (ERI) and A comprehensive geotechnical investigation consisting of pit digging were carried out to investigate the subsurface formation at the proposed Dam site in FUT Minna Gidan Kwano campus. The aim of this study is to thoroughly assess the integrity of a dam site structure, ensuring its long-term safety and functionality. The Wenner array method was chosen for its effectiveness in capturing subsurface resistivity variations. Electrode spacing ranged from 10 to 100 meters in 10-meters increment to allow for a particle investigation of the subsurface at varying depths. Two survey profiles (Profile A and Profile B) were established, extending 300 meters each. The profiles were strategically located to capture potential spatial variations, set at an interval of approximately 240 meters and 120 meters to the western and eastern flank respectively of the river in the study area to ensure a representative survey area. A systematic data collection approach was adopted using the ABEM SAS 4000 Terrameter, with resistance (R) measurements recorded for each electrode spacing along both profiles. The data were processed and interpreted by applying 2D inversions RES 2D software. Result from the ERI recognizes four (4) layers from the profiles as; Topsoil, gravelly sand, weathered basement and fresh basement. Result from the geotechnical tests reveals that the soils within the dam site were classified according to AASHTO soil classification system as A-5, A-6 and A-7-6 which implies high plasticity elastic silt, lean clayey soil and silt soils respectively. The result from the permeability test indicates that all the samples from the site are of low permeability. Analyzing the cohesion (N/m^2) and The angle of internal friction from the Triaxial test indicates that the samples are ideal for dam construction but might warrant careful consideration in terms of stability. Using of geophysical prospecting and geotechnical investigation is sometimes looked at as a probable rather than certain method when it comes to construct a detailed subsurface layer profiles. The correlation between dug pit information and electrical resistivity ranges was done. From the structural point of view, no faults have been detected in this location from ERI and boreholes data as well as there is no evidence of the existence of cavities or any other risky resources. There is a risk of water seepage on profile 1 of the dam site especially on the western part. As a result, profile 2 of the site is considered more suitable for construction of dam.

Introduction

A dam is a structure that is designed and constructed to obstruct and impound water in order to create a reservoir or to regulate the flow of water in a river, stream or other watercourse. Dams are typically built from various materials including concrete, earth rock, or timber, and can range in size from small, low-lying structures to massive, high-arching dams that span entire valleys. (International Community on Large Dams, 2021).

Dams have a wide range of applications, including hydroelectric power generation, irrigation, flood control, navigation, and water supply. Dams can also provide a lake used for recreational activities such as swimming, boating, and fishing. (Brown *et al.*, 2019)

Dams have been constructed for thousands of years, with some of the earliest examples dating back to ancient civilizations in Mesopotamia and Egypt. The modern era of dam building began in the late 19th century with the construction of the Aswan Low Dam in Egypt and the Hoover Dam in the United States. (World Commission on Dams, 2000).

Figure 1 A well-maintained Dam at Zungeru. (Africa Energy Portal, 2020)

Figure 2 Collapsed Dam Whaley Bridge Dam in high peak (Duncan Leatherdale, BBC News, 2019)

Area Description

The study area is located in the campus of Federal University of Technology Minna, Gidan Kwano campus. The campus is located along Minna - Bida road which is about 13km from the Minna town. The campus lies between Latitudes 9°31’15’’N and 9°32’30’’N and Longitudes 6°26’15’’E and 6°28’00’’ with an estimated land mass of 10,000 hectares. Onuigbo *et al*, 2015. The location of the dam site is roughly at about 4.8 km SW from the school Senate building. The site is accessible via an access Road, which is linked to the staff quarters road. Two alternate dam profiles were considered, Profile 1 and profile 2. Profile 1 runs approximately NW-SE across the River while profile 2 runs in an approximate E-W direction. Rice and maize were predominantly cultivated at the dam site axis. At the time of this investigation, the streams were moderately flowing forming dendritic drainage patterns. The study area lies within the basement complex of Nigeria. Crystalline igneous rocks are visible at the river bed at some portions of the downstream of the dam profiles.

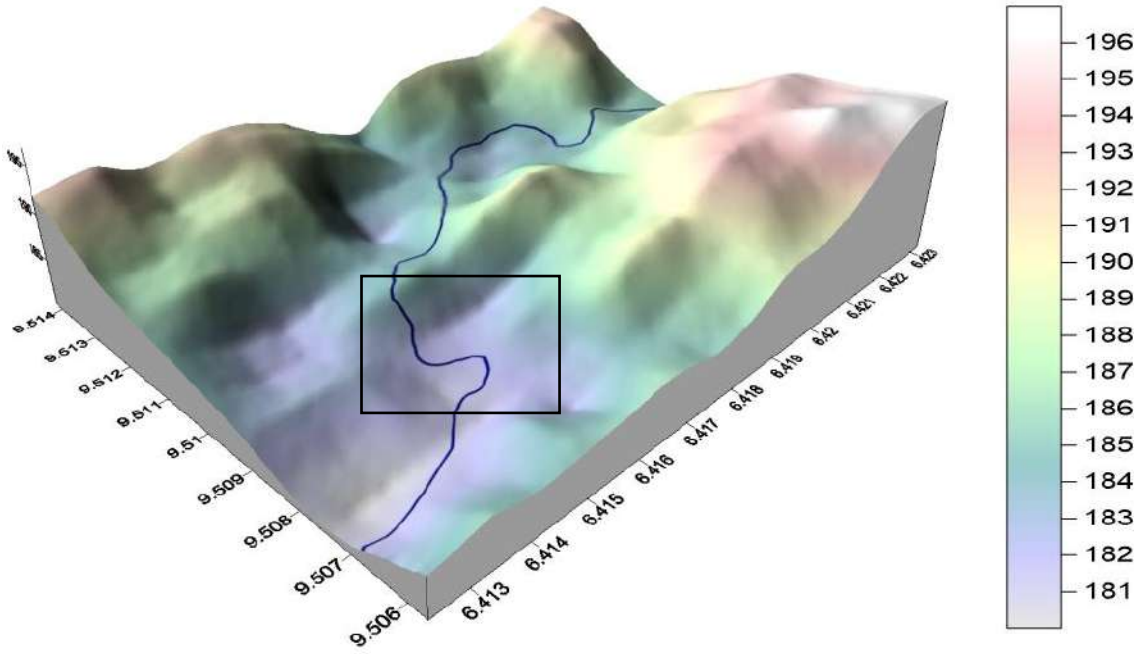

Figure 3 A 3D map showing the study area

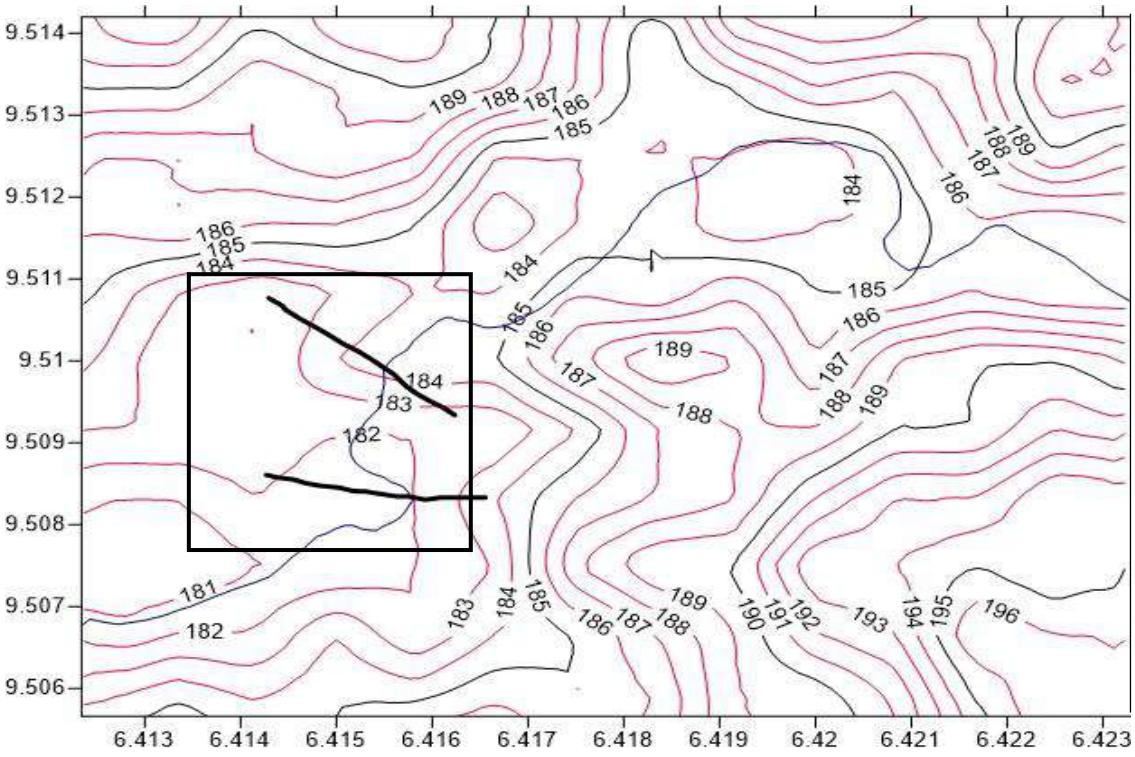

Figure 4 contour map showing the study area

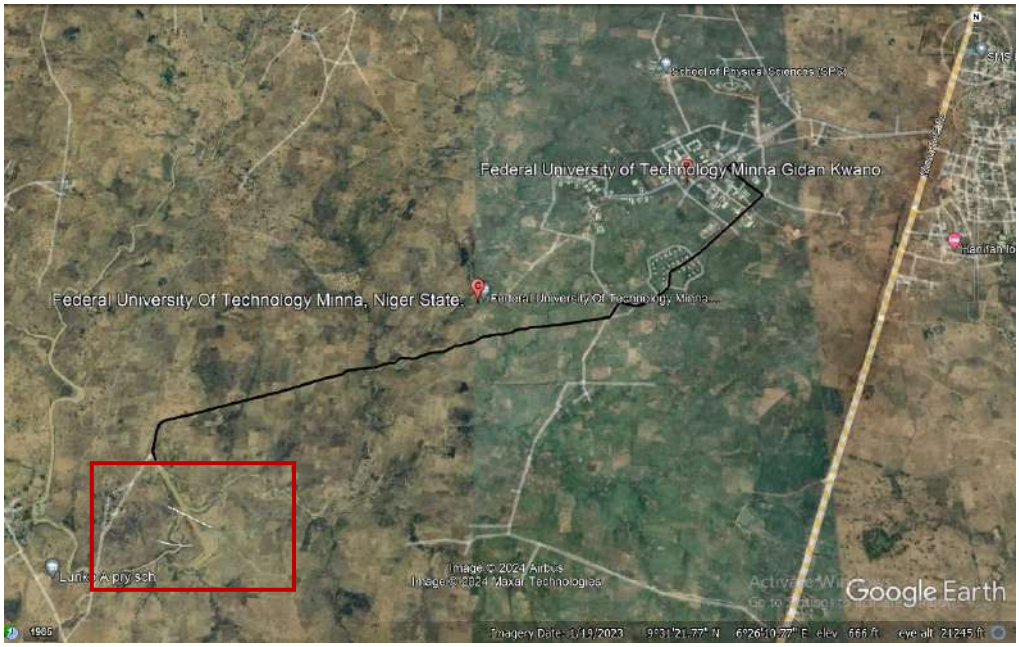

Figure 5 satelite imagery showing the study area

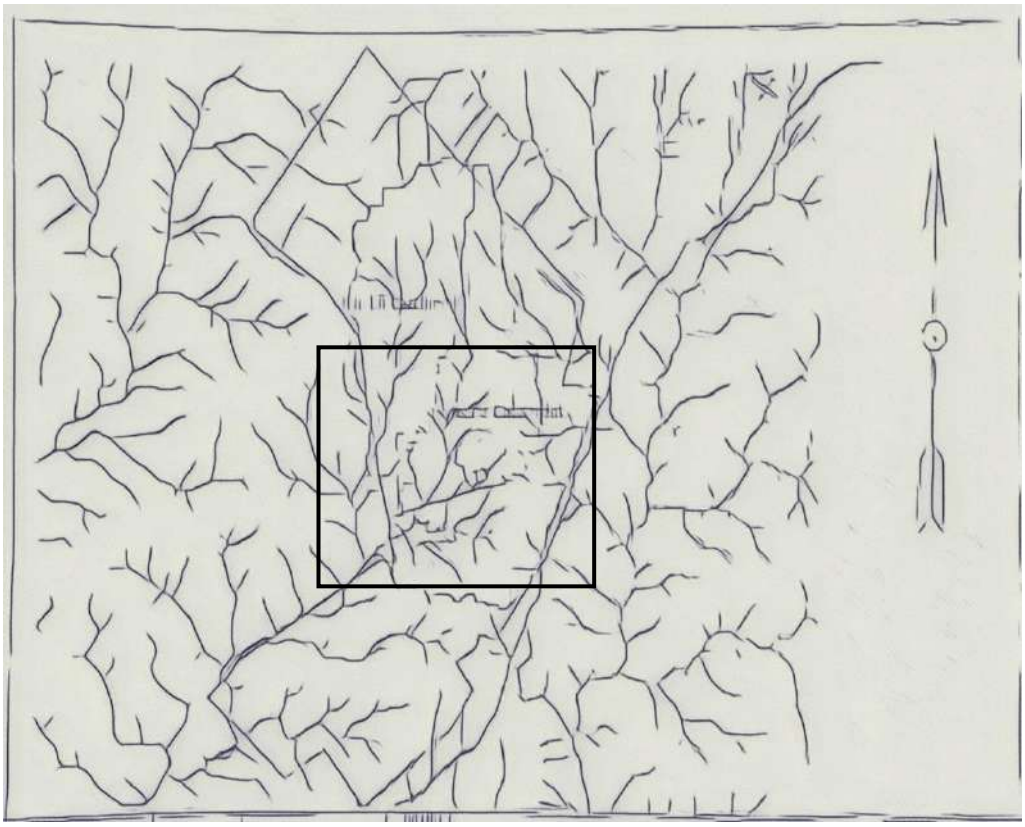

Figure 6 Drainage map showing the study area

Aim and Objective

Aim

The aim of this study is to thoroughly assess the integrity of a dam site structure, ensuring its long-term safety and functionality

Objectives

1. Evaluate the geological and geotechnical conditions of the dam site.
2. Assess the lithological conditions of the dam site.
3. Identify potential hazards and their associated consequences.

METHODOLOGY

Electrical Resistivity Imaging (ERI)

2D Electrical Resistivity Imaging (ERI) and A comprehensive geotechnical investigation consisting of pit drilling were carried out to investigate the subsurface formation at the proposed Dam site in FUT Minna Gidan Kwano campus. The Wenner array method was chosen for its effectiveness in capturing subsurface resistivity variations. Electrode spacing ranged from 10 to 100 meters in 10-meters

increment to allow for a particle investigation of the subsurface at varying depths. Two survey profiles (Profile A and Profile B) were established, extending 300 meters each. The profiles were strategically located to capture potential spatial variations, set at an interval of approximately 240 meters and 120 meters to the western and eastern flank respectively of the river in the study area to ensure a representative survey area. A systematic data collection approach was adopted using the ABEM SAS 4000 Terrameter, with resistance (R) measurements recorded for each electrode spacing along both profiles. The data were processed and interpreted by applying 2D inversions RES 2D software.

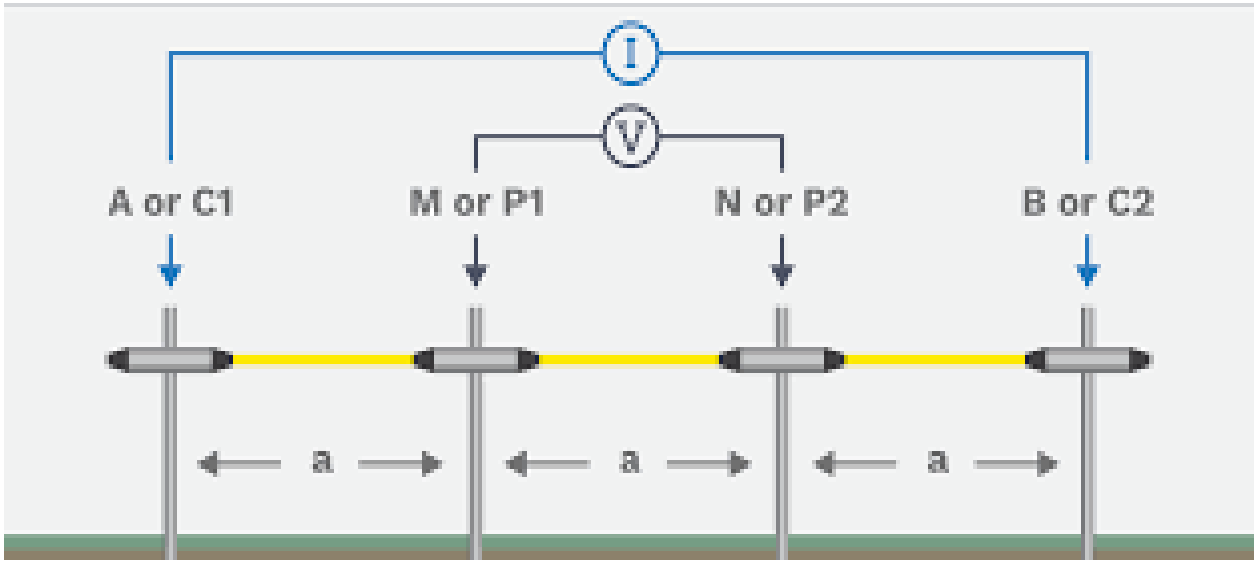

Figure 7 Wenner Array configuration

The estimated resistance (R) was inserted into Equation 1, in order to obtain the apparent resistivity.

$$\rho a = kR \qquad (1),$$

Geotechnical Analyses

Geotechnical investigation was carried out in the study area for laboratory tests of the foundation materials. Two borrowed pits (one on each flank) were dug to a depth of 1.5m and undisturbed samples A, B, C, and D were collected. The samples collected from the study area were transported to the soil test laboratory of the civil department, federal University of Technology Minna. The tests conducted include Atterberg Limit, Particle size Distribution, triaxial and Permeability test.

Atterberg Limits

Atterberg limit tests are classification tests that determine the liquid limit and plastic limit of the soil fraction finer than the No. 40 sieve (Talabi *et al*., 2021).

Particle size Distribution

Particle size Distribution primarily aims to assess the particle size distribution in soil analysis ranges and to determine its impact on soil properties. The process involves passing the material through a series of screens with distinct opening sizes.

Triaxial test

Triaxial t**es**t determines the sheer strength of a rock or soil sample. The test is performed on a cylindrical core soil or rock sample placed between two rigid caps and covered with a latex membrane and put in a Perspex cell with water. The total stress at failure is calculated using equation 1;

Total stress at failure = cell pressure + deviator stress (1)

Permeability test

Soil permeability (hydraulic conductivity) is the rate at which water flows through soil materials.

The coefficient of permeability (k) is a constant of proportionality relating to the ease with which fluid passes through a porous medium. Calculating the permeability using the following equation:

$$Coefficient\ of\ permeability\ (K) = \frac{2.303 A_p L_p}{A_{sam.} \times T \times \log\left(\frac{h_1}{h_2}\right)} \quad (2)$$

Where

k = coefficient of permeability (hydraulic conductivity) (m/s).

A_p= the inside area of the standpipe

L_p = Length of the sample.

A_{sam} = the inside area of specimen.

T = elapsed time of test (s).

h_1 = the elevation of water in the standpipe at time t=0.

h_2 = the elevation I water in the standpipe at time equal to t.

RESULTS

In the first profile, four layers were recognized (table 1). The first layer represents the topsoil which composed of variety types of clastic sediments like sand and clay with resistivity value ranges (6-160 Ohm.m). The thickness of this layer is about 0.2m. The second layer represents the gravelly sand; its resistivity value ranges (8-667 Ohm.m) with thickness about 20m. The third layer represents the

weathered basement with resistivity value ranges (254-1669 Ohm.m) and thickness of 9m. The last layer represents the fresh basement with resistivity value ranging from 2883 – 4235.

Table 1 layers identified in profile 1

layer	Rest range	thickness	Probable lithology
1	6 – 160	0 - 0.2	Topsoil
2	8 – 667	0.25 – 20.65	gravelly sand
3	254 – 1669	21 – 39.4	Weathered basement
4	2883 – 4235	45 - 53	Fresh bedrock

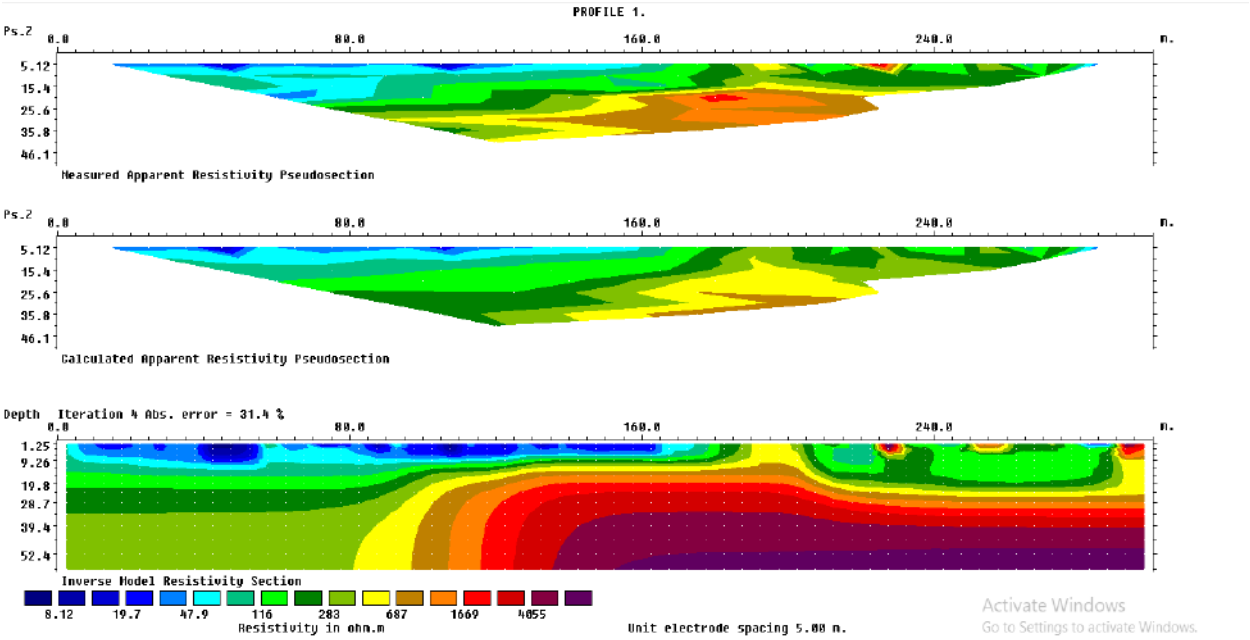

Figure 8 inversion result for profile 1

The second profile also recognized four layers (table 2). The first layer represents the topsoil which composed of variety types of clastic sediments like sand and clay with resistivity value ranges (6-500 Ohm.m). The thickness of this layer is about 0.2m. The second layer represents the gravelly sand; its resistivity value ranges (15-438 Ohm.m) with thickness about 12m). The third layer represents the weathered basement with resistivity value ranges (190-950 Ohm.m) and thickness of 6m. The last layer represents the fresh basement with resistivity value ranging from (1005 – 4235) Ohm.m.

Table 2 layers identified in profile 2

layer	Rest range	Thickness range	Probable lithology
1	6.3006 – 500	0 - 0.2	Topsoil
2	15.1 – 438	0.25 – 12	gravelly sand

3	190 – 950	12.1 – 19.8	Weathered basement
4	1005 – 4235	21 - 53	Fresh bedrock

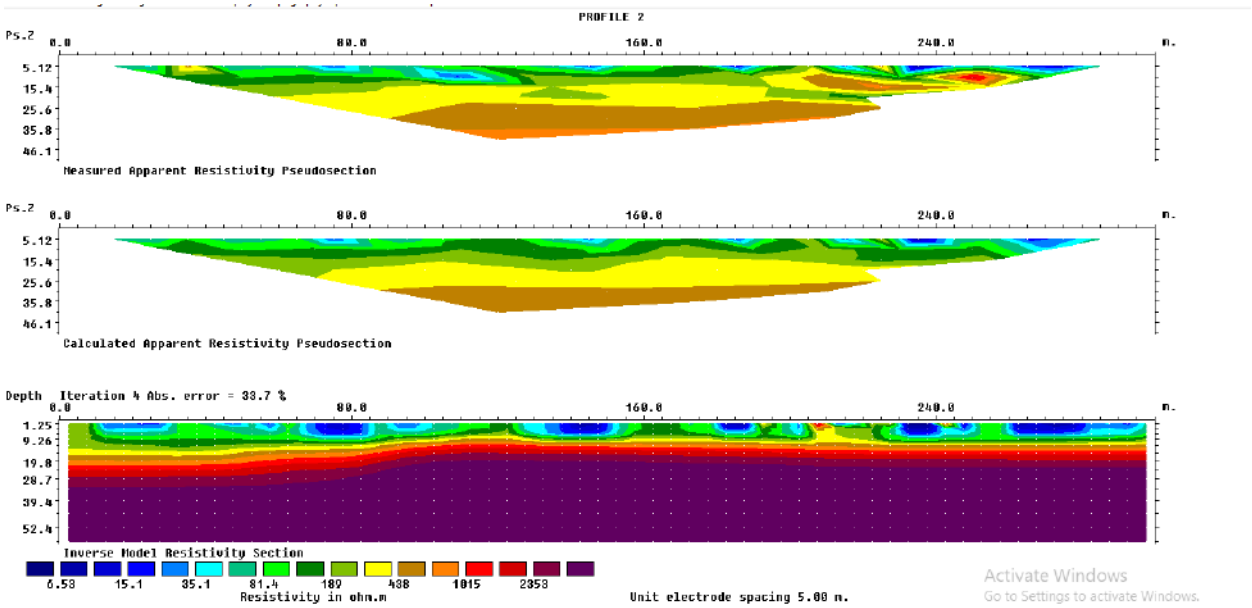

Figure 9 inversion result for profile 2

Atterberg Limits

Result from the Atterberg Limits tests reveals that the soils within the dam site were classified according to AASHTO soil classification system as A-5, A-6 and A-7-6 which implies high plasticity elastic silt, lean clayey soil and silt soils respectively.

Table 3 summary of Atterberg limit test

Property	**Sam A1**	**Sam A2**	**Sam B1**	**Sam B2**
Liquid Limit (%)	27.00	47.00	31.00	42.00
Plastic Limit (%)	19.14	21.96	19.09	25.66
Plasticity Index (%)	7.86	25.04	11.91	16.34
Passing sieve No40 (%)	79.13	71.26	77.00	72.23
Passing Sieve No200 (%)	53.69	52.66	49.59	54.99
AASHTO Classification	A-5	A-7-6	A-6	A-7-6

Sieve Analysis (ASTM D 422)

The ASTM D 422 analysis was used, which stands for "Standard Test Method for Particle-Size Analysis of Soils". This method outlines procedures for determining the particle-size distribution of soil samples.

The result of the test is represented in figure 7.

The result from the graph shows that samples A1, A2, B1, and B2 are silty sand to silt and are well graded.

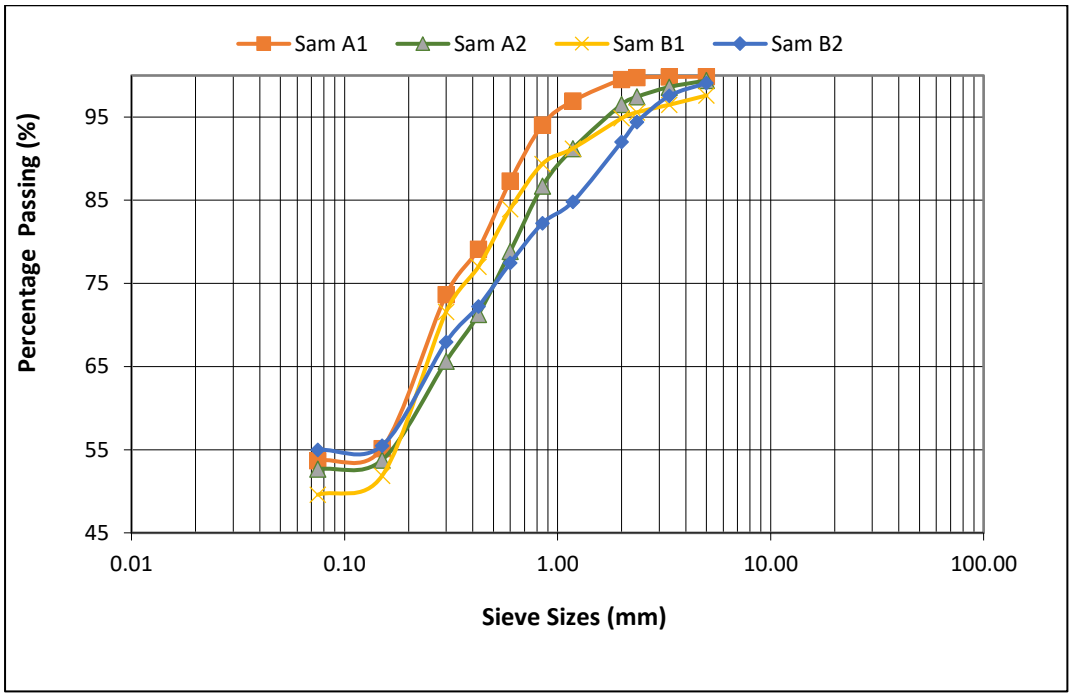

Figure 10 Graph of Sieve analysis

Permeability test

The result from the permeability test indicates that all the samples from the site are of low permeability. Results of falling head permeability obtained from samples A1, A2, B1 and B2 are shown in Table 4.

Table 4 Results of the permeability test.

Description	h1 (cm)	h2 (cm)	Test time (s)	Coefficient of permeability K (m/s)	Avg. Coefficient of

					Permeability K (m/s)
Sam A1	100	69.3	60	6.71E-03	7.96E-03
	100	46.6	120	6.98E-03	
	100	10.8	240	1.02E-02	
Sam A2	100	97.5	60	4.63E-04	6.62E-04
	100	50	1800	4.23E-04	
	100	2.7	3600	1.10E-03	
Sam B1	100	72.2	60	5.96E-03	5.97E-03
	100	57	120	5.14E-03	
	100	22.5	240	6.82E-03	
Sam B2	100	78	60	4.55E-03	4.81E-03
	100	60	120	4.67E-03	
	100	32	240	5.21E-03	

Triaxial test

Triaxial test determines the sheer strength of a rock or soil sample. The test is performed on a cylindrical core soil or rock sample. Analyzing the cohesion (N/m^2) and The angle of internal friction from the Triaxial test indicates that the samples are ideal for dam construction but might warrant careful consideration in terms of stability.

Table 5 summary of Triaxial test

Sample	A1	A2	B1	B2
Cohesion (N/m^2)	27	27	19	30
Angle of internal friction (Φ)	32.8	25.9	26	34.4

conclusion

The geophysical investigation conducted on the proposed dam site at FUT Minna Gidan Kwano campus shows that the first profile has four layers as: The topsoil which composed of variety types of

clastic sediments like sand and clay with resistivity value ranges (6-160 Ohm.m) and thickness of about 0.2m. The second layer represents the gravelly sand, its resistivity value ranges (8-667 Ohm.m) with thickness of about 20m. The third layer represents the weathered basement with resistivity value ranges (254-1669 Ohm.m) and thickness of 9m. The last layer represents the fresh basement with resistivity value ranging from 2883 – 4235. The second profile also recognize four layers as; The first layer represents the topsoil which composed of variety types of clastic sediments like sand and clay with resistivity value ranges (6-500 Ohm.m) and thickness of 0.2m. The second layer represents the gravelly sand; its resistivity value ranges (15-438 Ohm.m) with thickness about 12m). The third layer represents the weathered basement with resistivity value ranges (190-950 Ohm.m) and thickness of 6m. The last layer represents the fresh basement with resistivity value ranging from (1005 – 4235 Ohm.m. The ERI of Profile 1 shows low resistivity values with depth particularly on the western flank which might be a danger to Dam construction (seepages), low resistivity generally indicates moisture presence. The depth to bedrock is about 45m in profile 1 and about 20m in profile 2. From the result of the consistency limit tests, the soils within the dam site were classified according to AASHTO soil classification system as A-5, A-6 and A-7-6 which implies high plasticity elastic silt, lean clayey soil and silt soils respectively. The A-6 and A-7-6 (samples A2, B1 and B2), this material could be used for dam construction while the A-5 (sample A1) is not an ideal material for dam construction. The result from the permeability test indicates that all the samples from the site are of low permeability. Analyzing the cohesion (N/m^2) and The angle of internal friction from the Triaxial test indicates that the samples are ideal for dam construction but might warrant careful consideration in terms of stability. The general characteristics of the materials within the study area as reveal from geotechnical investigation indicates that they are competent as construction materials. From the structural point of view, no faults were detected in this location from ERI data as well as there is no evidence of the existence of cavities. There is a risk of water seepage on profile 1 of the dam site especially on the western part. As a result, profile 2 of the site is considered more suitable for construction of dam.

REFERENCES

A. J. Whittle, (2013) Materials testing for dams, in Geotechnical Engineering for Dams, CRC Press, pp. 377-408.

B.

A. Khan, (2019) Hydrological studies for dam safety, in Dam Safety, Risk Assessment and Management, CRC Press, pp. 41-66.

A. Khan, (2019). Hydrological studies for dam safety, in Dam Safety, Risk Assessment and Management, CRC Press, pp. 41-66.

Aina A, Olorunfemi MO, Ojo JS (1996). An integration of aeromagnetic and electrical resistivity methods in dam site investigation. Geophysics, 61(2): 349-356.

Aina, A., Olorunfemi, M. O. and Ojo, J. S., (1996). An Interpretation of Aeromagnetic and Electrical Resistivity Methods in Damsite Investigation. Geophysics. Volume 61 (2), pp. 349 – 356.

Burmister, D. M., (1949). Principles and Techniques of Soil Identification: In Proceedings of High Residential Board. Volume 29, pp. 402 – 433.

Caleb Adwangashi Tabwassah and Gabriel Ike Obiefuna, (2012). Geophysical and Geotechnical Investigation of Cham Failed Dam Project, Ne Nigeria. Research Journal of Recent Sciences Vol. 1(2), 1-18.

Cassagrande, A. M., (1948). Classification and Identification of Soils: In Transactions of the American Society of Civil Engineering. Volume 113, pp. 901 – 991.

Chen, Y., et al. (2019). Application of gravity survey in dam site integrity investigation: A case study of the Three Gorges Dam, China. Journal of Applied Geophysics, 174, 12-21.

Coduto DP (1999). Geotechnical Engineering: Principles and Practice. Prentice Hall Inc. Upper Saddle River, New Jersey 07458.

Milsch, H., & Butt, H. (2015). Geophysical Techniques for the Characterization of Foundation Soils for Dams. In Dam Foundation Grouting (pp. 79-117). Springer, Cham.

Nguyen, H., et al. (2016). Gravity survey for dam site integrity investigation: A case study of a dam in Vietnam. Journal of Applied Geophysics, 134, 225-233.

Oliveira, D., et al. (2015). Application of ground penetrating radar on dam safety: a case study. Construction and Building Materials, 93, 201-209.

Oluwakemi Olanike Adeoye-Oladapo and Michael Ilesanmi Oladapo, 2011. Geoelectric investigation of Owuruwuru Dam site, Ikere Ekiti, Southwestern Nigeria. Journal of Geology and Mining Research Vol. 3(12), pp. 325-340.

Zhang, L., Xia, J., & Tang, X. (2020). Investigation of an Earth Rock fill Dam Site Based on Electrical Resistivity Imaging. Advances in Civil Engineering, 2020, 1-13.

Zhao, Y., et al. (2013). Application of gravity survey in dam site integrity investigation: A case study of a dam in the United States. Geophysical Journal International, 194(2), 1090-1104.

On the Solution of Bar Element using Classes of Weighted Residual Approximation Techniques

[1]Oyakhire Friday Ighaghai, [2] Ekhator Monday

[1 &2] Mathematics Department, Physical sciences, Alex Ekwueme Federal University, Ndufu- Alike. Nigeria.
[2]ekhatorogie@gmail.com
*Corresponding author: [1] *Friday.oyahire@funai.edu.ng, oyakhirefriday64@gmail.com*,

Abstract

We formulate governing equation and analyzed some classical weighted residual approximation techniques for solving bar element subjected for uniformly distributed loads using Dirichlet and Neumann boundary condition that satisfies the trial solution. The classical weighted residual techniques considered are least square, collocation, sub–domain and the Galerkin's methods. The accuracy of the proposed methods is verified through numerical examples, the computed results are offered graphically and in tables for qualitative and quantitative insight in the efficiency and behavior of the proposed methods. The obtained outcomes revealed that boundary conditions satisfy the trial solution and that the Galerkin method performance is in excellent agreement with the analytic solution than other techniques with increasing value of the parameter.

Keywords: Bar element; collocation; galerkin; least-squares; sub- domain

1. Introduction

Intensive research has been performed in recent years to developed efficient and accurate numerical schemes for solving bar element because of its relevance in structural engineering**.** Analysis of partial differential equations approximate methods has been widely used (Aleksei & Alexander 2019; Amiruddin *et al.,* 2019; Chen & Yang 2006; Czeslaw 2020**;** Ding & Chen 2010). Describing system vibrations in a low dimensional system of ordinary differential equation to facilitate the use of certain technique employed for solving discrete and continuous problems. Some of these well- known techniques are the finite element method (FEM), finite difference method, and spectrum method, Least squares and point collocation that converts differential equations commonly in a weak formulation such as axially moving system to a discrete problem by applying linear constraints determinant finite sets of basis function. The application is common with great accuracy but as the complexity of the shape domain increase, accuracy becomes a challenging issue. Since some of the methods requires the presence of a predefined mesh for proper analysis and modeling of structures with complicated geometries. The FEM is associated with some shortcoming. The construction of mesh is costly and the accuracy of the stress obtained is less.

In light of the challenges caused by these numerical schemes, it is desirable to develop a class of schemes that are both high order and accurate. The emergence and growing popularity of powerful computers brought a renewed interest towards structural engineering framework. The advantage associated with weighted residual techniques is that it leads to a system of linear equation with coefficient matrix having smaller band and less computational time. (Gu & Lin, 2001). Transverse

non-linear dynamics of axially accelerating viscos-elastic beams for static and free vibration analysis of thin plate of complicated shapes using Galerkin truncation and formulation. (Han *et al* 2012) presented the Convergence and stability in collocation method of equation. (Ike, 2018; Han *et al*., 2012; Huiming & Zhanwen, 2020). Point collocation method for the analysis of Euler- Bernoulli beam on Winkler foundation, its stability and linear and non- linear third kind Volterra integral equations with non-compact operators.

Behavior of beam on elastic foundation, Shape function, modeling slippage between soil and reinforcement with large wave numbers and non-linear higher–index differential algebraic equation using element free Galerkin, least square interpolation, radial point interpolation and polynomial Least squares collocation methods (Lan, 2020; Lin *et al.,* 2011); Michael & Rowitha 2021). Approximate solution that is computationally less expensive and offered a promising results using the data of the problem without any preprocessing by restricting it to finite dimensional ansatz spaces. (Murat *et al*., 2011; Osadebe *et al.*, 2016). Application of the galerkin –Vlasov method to the flexible analysis and Vibrating system of simply supported rectangular Kirchhoff plates under uniform loads. Consistency, stability, explicit time integration and efficiency within the context of nodal integration and exact solution for non – paraxial Gaussian beams (Puse *et al.,* 2008; Sergry, 2019). (Soumyarani *et al*., 2000; Trobec *et al.,* 2009). 2D Sobolev equations with Burgers' type for non-linearity and computational complexity of meshless local Petrov Galerkin methods (MLPG) with finite difference method (FDM) and finite element method (FEM). (Wang, 2004; Wicke & Mote, 2016). Collocation method for the dynamic of the flexible continuous beam subject to impact and linear transverse vibration of axially moving state string system.

(Wu *et al.,* 2011; Y ajni *et al.,* 2015). Generalized mesh free approximation and modified least square methods for solving Helmholtz equation for flow frequencies on planet mars. (Zhang *et al.*, 2007). Complex mode Galerkin approach for solving transverse viscos-elastic string and that boundary conditions must satisfy basis function and special orthonormality relatives of the gyroscopic system. This paper is based on the views of (Zhang et *al.*, 2007: Osadebe *et al.*, 2016). Piecewise polynomial as basis function, we extended our approach by using both piecewise polynomial and trigonometry as trial displacement function and compared our results with the analytic solution using Dirichlet condition at one side and Neumann boundary conditions at the other end that satisfies the approximate solutions.

2. Formulation of the governing equation

This section deals with the formulation of the governing equation for bar element, discarding all other terms containing time derivatives of the form

$$\frac{AE\partial^2 w}{\partial x^2} + pb = 0, \qquad 0 < x < l \tag{1}$$

with boundary conditions

$$w(x=0) = w_i \qquad w(x=l) = w_{i+1}, \quad i = 1, 2, ..., n.$$

where w_i are the n unknown displacement function, A is the cross- section area of the object, E is the young's modulus ρ is the density of the material and b is body force, l is the length of the object. The governing equation requires boundary conditions which are determined according to the physics

of the problem. Suitable boundary conditions that satisfy polynomial and trigonometry approximate solution are defined as:

$$\hat{w}(x) = \sum_{i=1}^{m} \phi_i (x^i), \quad w(0) = w(1) = 0 \tag{2}$$

and

$$\hat{w}(x) = \phi_0 + \sum_{i=1}^{N} \phi_i \sin \frac{i\pi x}{l}$$
$$w(0) = w'(1) = 0 \tag{3}$$

ϕ_i 's are the coefficients in the approximate functions to be determined and the trial solution can be expressed as:

$$\hat{w} = \phi_0 + \phi_1 x + \phi_2 x^2 \tag{4}$$

Where x_1 and x_2 are nodal values at one and two point of the bar.

3. Methods

There are some questions to be answer in this study.
(1) Formulation of differential equation.
(2) Assume a trial displacement function that will satisfy the boundary conditions
(3) Applying the boundary conditions.
(4) Substitute into the governing differential equation, called the residual
(5)To avoid the danger of residual cancellation, multiply by weighting function and integrate over the domain and force the product of weight function and residual to zero.
(5) Apply the various classical weighted residual techniques.
(6) Validate the techniques using numerical example and revealed the outcomes by offering quantitative and qualitative graphs and tables.

3.1 Least square method

The integral of the weighted square of the residual is require to be minimum

$$I = \int_{\Omega} w_i R dx \tag{5}$$

Where $w = \Re^2$ and $\Re = \frac{AE\partial^2 u}{\partial x^2} + pb$ which can be expressed as:

$$\frac{\partial I}{a_i} = \int_{\Omega} R \frac{\partial R}{\partial a_i} dx = 0, \ i = 1, 2, ..., n \tag{6}$$

w_i is the weight functions. The method requires that the error function be orthogonal to each of the approximate function, which in turn yields 'n' simultaneous equation for determination of the unknown coefficients by setting the weighting average over the computational domain to zero.

3.2 Collocation

The residual R is set equal to zero at a specific point $w_i = \partial(x - x_i)$. The number of point selected equal to the number of undetermined coefficient (a_i) in the approximate function.

$$w_i R dx = 0, \ i = 1, 2, 3, ..., n. \tag{7}$$

$\partial(x - x_i) = 0$ if $x \neq x_i$ and $\partial(x - x_i) = 1$ if $x = x_i$

The existence and Uniqueness for collocation methods could be stated as:
Let $h = 1/p$ be a given step size with integer $p \geq 1$ and let the mesh on I be defined by

$$I_h : \{x_n : 0 = x_0 < x_1 < \cdots < x_N = L\} \tag{8}$$

Accordingly, the collocation points are chosen as

$$x_h : \{x_{n,i} = x_n + \phi_i h : 0 < \phi_1 < \cdots < \phi_m \leq 1 (0 \leq n \leq N - 1)\} \tag{9}$$

Where $\{\phi_i\}$ denotes a given set of collocation parameters. We approximate the solution by collocation in the piecewise polynomial spaces.

$$S_m^{(0)}(|0, L|) = \left\{ v \in C(|0, L|) : v|_{[x_n, x_{n+1}]} \in \pi_m \right\} \tag{10}$$

Where π_m denotes the set of all real polynomials of degree not exceeding m .The collocation solution is the element in this space that satisfies the governing differential equilibrium (collocation) equation (1) with Dirichlet and Neumann boundary conditions
$u(0) = u(1) = 0$ *or* $u(0) = u'(1) = 0$.

3.3 Sub-domain

The domain is sub divided into n sub-domain and the integral of the residual over the sub-domain is required to be zero. The weighted function is selected as unity $(w_i = 1)$, over the domain. The number of integration interval equal the number of the undetermined coefficients (a_i). in the approximate function defined as:

$$\frac{AE\partial^2 u}{\partial x^2} + pb = R \neq 0, \quad \int_\Omega w_i R dx = 0, \quad i = 1, 2, 3, ..., N \tag{11}$$

Where w_i is the weighted parameter.

3.4 Galerkin method

$$\int_\Omega \left(\frac{\partial w}{\partial \phi_i} \frac{AE\partial^2 u}{\partial x^2} + pb\right) dx = 0 \tag{12}$$

The number of weighting function (w_i) is equal to the number of undetermined coefficients (a_i) substituting equation (2) into equation (12) yields:

$$E_r(x_r, y) = \sum_j^n \phi_j (u_j(x)) + \rho b(x) \tag{13}$$

Where $E_r(x_r, y) = R$ is an error function or residual in equations (5), (7), (11) and (13) respectively.

Suppose a differential equation operator is of the form:

$$L\left[u = -\rho b(x)\right] \tag{14}$$

Substituting in the approximation

$$L\left|\sum \phi_i x^i\right| \tag{15}$$

$$\sum \phi_i L\left[x^i\right] = -\rho b(x)$$

With the weight function

$$u_j(x) = \frac{\partial R}{\partial \phi_i} = \frac{\partial R}{\partial \phi_j}\left\{\sum \phi_i L\left[x^i\right] - \rho b(x)\right\} \tag{16}$$

Leading to system of integral equation, so that each of the weights

$$\sum \phi_i \int L\left[x^i\right]dx + \int_{\Omega} \rho b(x)dx \tag{17}$$

The coefficient matrix of the Galerkin system of equation is symmetric provided the differential equation is linear

Integrating the above equation, we can obtain

$$w_h(x_n + \phi h) = w_h(x_n) + h\sum_{j=1}^{m} \beta_j(v) Y_{n,j}, \tag{18}$$

Where $\beta_j(v) := \int_0^v \phi_j(s)ds.$ So

$$Y_{n,i} = w_h''(x_{n,i}) - k^2 w_h(x_{n,i}) - f(x_{n,i}). \tag{19}$$

Let $n = \lambda p + 1, k \in \mathbb{Z}, l = 0,1,2,\cdots, p-1.$

4. Numerical example

Appling the trial function in equations (2), (3) or (4) for $j = 0,1,2,3$ we have a system of equations with n unknown's coefficient. Substituting the coefficients in equation (2), we obtained the numerical solution.

Problem A $\dfrac{-\partial^2 u}{\partial x^2} - \sin \pi x, \quad 0 < x < 1.$

$u(0) = 0, u(1) = 0,$ $A = 100m^2,$ $E = 210 \times 10^{-6}$

Problem B

$$\frac{-\partial^2 u}{\partial x^2} - \sin \pi x, \quad 0 < x < 1.$$

$u(0) = 0,$ $\dfrac{\partial u}{\partial x}(1) = 0,$, $A = 300m^2,$ $E = 260 \times 10^{-6}$

With the analytic solution $\dfrac{\sin \pi x}{\pi^2 AE}$

Errors are computed using $l_2 - norm = \sqrt{\sum |e|^2}$, where e is the error between the analytic and approximate solutions.

5. Results and Discussion

This section deals with results analysis for problem A using Dirichlet and Neumann boundary conditions for problem B respectively.

Table (1): Dirichlet boundary condition for problem A

Values of x	Analytic solution	Least square	Collocation	Sub-domain	Galerkin
0	0	0	0	0	0
0.10	1.4910	1.3642	2.1429	1.3642	1.6587
0.20	2.8360	2.4252	3.8095	2.4252	2.9487
0.30	3.9034	3.1831	5,0000	3.1831	3.8702
0.40	4.5887	3.6375	5.7143	3.6375	4.4031
0.50	4.8248	3.7894	5.9524	3.7894	4.6074
0.60	4.5887	3.6378	5.7143	3.6378	4.4231
0.70	3.9034	3.1831	5.0000	3.1831	3.8702
0.80	2.8360	2.4252	3.8095	2.4252	2.9487
0.90	1.4910	1.3642	2.1429	1.3642	1.6587
1.00	0	0	0	0	0

Table (2): Neumann boundary condition

Values of x	Analytic Solution	Least square	Collocation	Sub-domain	Galerkin
0	0	0	0	0	0
0.10	0.4014	0.3673	0.5769	0.3673	0.4466
0.20	0.7635	0.6529	1.0256	0..6529	0.7939
0.30	1.0509	0.8570	1.3462	0.8570	1.0420
0.40	1.2354	0.9794	1.5385	0.9794	1.1908
0.50	1.2990	1.0202	1.6026	1.0202	1.2404
0.60	1.2354	0.9794	1.5385	0.9794	1.1908
0.70	1.0509	0.8570	1.3462	0.8570	1.0420
0.80	0.7635	0.6529	1.0256	0.6529	0.7939
0.90	0.4014	0.3673	05769	0.3673	0.4466
1.00	0	0	0	0	0

In tables (1) and (2) equations (5), (7), (11) and 13) was applied to test problem A and B using Ditrichlet and Neumann boundary condition respectively with increasing value of the parameter x. The table revealed that the Galerkin method has high degree of accuracy followed by least square, sub domain and finally collocation methods.

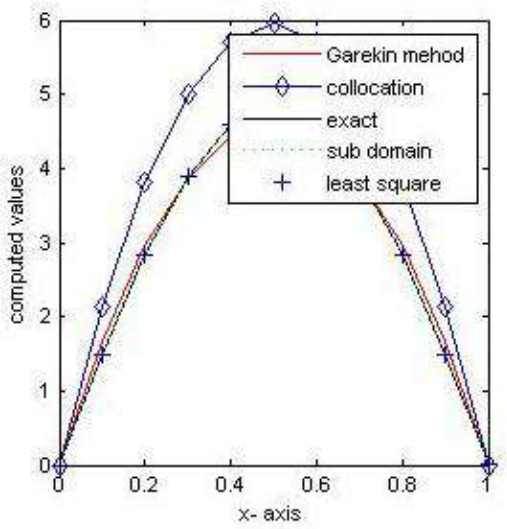

***Fig.1**. Dirichlet boundary condition*

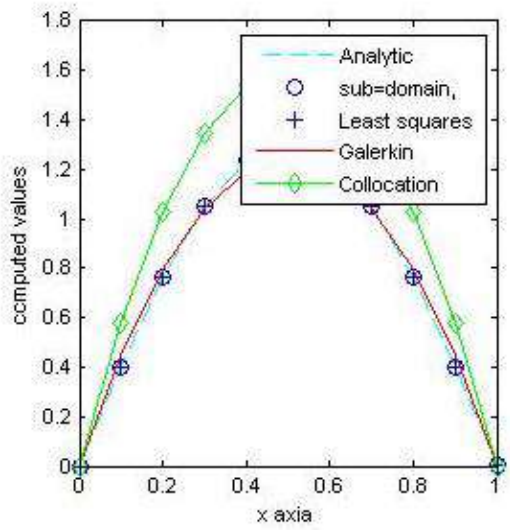

***Fig.2.** Neumann boundary condition*

Fig.1 and fig.2**,** shows the results for Dirichlet and Neumann boundary condition respectively. The graph revealed that as the lines move away from the zero point, the boundary conditions satisfy the

approximate trial solution with increasing value of the parameter and that Galerkin method performance is in excellent agreement with the analytic solution compared to other approximation techniques proposed in the study.

Table (3): Error analysis using Dirichlet boundary condition

Values of x	Analytic solution	Least square	Collocation	Sub-domain	Galerkin
0	0	0	0	0	0
0.10	1.4910	0.1268	0.6510	0.1268	0.1677
0.20	2.8360	0.4117	0.9726	0.4117	0.1118
0.30	3.9034	0.7203	1.0966	0.7203	0.0332
0.40	4.5887	0.9509	1.1256	0.9509	0.1666
0.50	4.8248	1.0354	1.1276	1.0354	0.2174
0.60	4.5887	0.9509	1.1256	0.9509	0.1666
0.70	3.9034	0.7203	1.0966	0.7203	0.0332
0.80	2.8360	0.4117	0.9726	0.4117	0.1118
0.90	1.4910	0.1268	0.6510	0.1268	0.1677
1.00	0	0	0	0	o

Table (4): Error analysis for Neumann boundary condition

Values of x	Analytic solution	Least square	Collocation	Sub-domain	Galerkin
0	0	0	0	0	0
0.10	0.4041	0.0368	-0.1728	0.0368	-0.0415
0.20	0.7635	0.1106	-0-2621	0.1106	-0.0304
0.30	1.0509	0.1939	-0.2953	0.1939	-0.0089
0.40	1.2354	0.2560	-0.3031	0.2560	-0.0446
0.50	1.2990	0.2788	-0.3036	0.2788	-0.0586
0.60	1.2354	0.2560	-0.3031	0.2560	-0.0446
0.70	1.0509	0.1939	-0.2853	0.1939	-0.0089
0.80	0.7635	0.0806	-0.2953	0.0806	-0.0304
0.90	0.4041	3.6726e+03	-0.1755	3.6726e+03	-0.0452
1.00	0	0	0	0	0

In tables (3) and (4), Dirichlet and Neumann boundary conditions using l_2- norm was applied in the computation with increasing value of parameter χ . The table revealed the desired outcome.

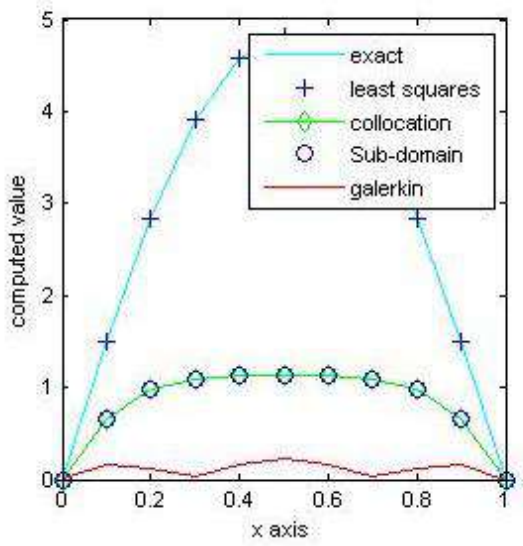

Fig.3. Dirihlet boundary condition

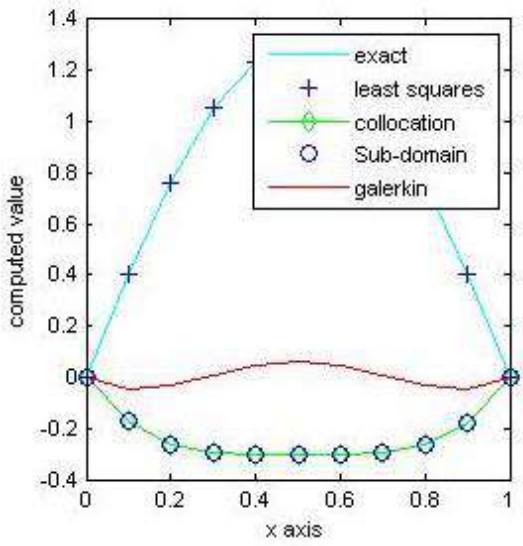

Fig.4. Neumann boundary condition

Figures (3 and (4) revealed that the trial solution satisfy boundary conditions and error is less than 0.005% with the Galerkin method with increasing value of χ compared to other proposed approximation techniques.

5. CONCLUSION

Solution of bar element was treated in this study with classes of weighted residual approximation techniques using Dirichlet boundary condition at one side and Neumann boundary condition at the other end. The results showed in tables and graphs revealed that boundary conditions satisfy the trial solution and that the Galerkin method performance is in excellent agreement with the analytic solution with error less than 0.0005% compared to other proposed approximation techniques with increasing value of the parameter.

References

Aleksei, P. K. & Alexander, B. P. (2019) Astigmatic Gaussian beams: exact solutions of the Helmholtz equation in free space. J. Phys. Comm., 3:115-127.

Amiruddin, A. B. Aziz., Muhammad, S. A. S. & Muhammad, H. N. H. (2019) Comparative study of collocation method and Galerkin method for solving nonlinear partial differential equation. Int. J. Adv. Tr. Com. Sci. and Eng., 8(5):1-5. https://doi.org/10.30534/ijatcse/2019/0181.52019.

Chen, L. Q. & Yang, X. D. (2006). Transverse non-linear dynamics of axially accelerating viscos-elastic beams based on 4th term Galerkin truncation. Chao Sol. Fra., 27(3): 748-757.

Czeslaw, M. (2020) The use of the collocation algorithm for estimating the deformation of soil-shell objects made of corrugated sheets. Res. Art. Geo Mech., 42(4): 319-399. https://doi.org/10.2478/sgen-2019-0048.

Ding, H. & Chen, L.Q. (2010) The Galerkin methods to natural technique of high speed. J. Theo. Appl. Mech., 37: 3484-3494.

Gu, Y.T. (2001) A mesh- free method for static and free vibration analysis of thin plate of complicated shape. J. Sou & Vib., 241(5): 839-855. https://doi.org/10.1006/jsvi.2000.3330.

Han,Yan Shufang . M., Yanbin, L. & Honguan, S. (2012) Convergence and stability in collocation method of equation. J. Appl. Math., 2012:125926. https://doi.org/10.1155/2012.125621.

Huiming, S. & Zhanwen, Y. (2020) Super- convergence analysis of collocation methods for linear and nonlinear third kind volterra integral equations with non- compact operators Appl. Math. & Compute., 412:126562. https//doi.org/10.1016/j.amc.2021.126562.

Ike, C.C. (2018) Point collocation method for the Analysis of Euler- Bernoulli beam on Winkler foundation. Int. J. Darshan Inst. on Eng.Res.Emerg. Tech., 7(2): Nigeria.

Lan, H.T.T. (2020) Behavior of beam on elastic foundation using element free Galerkin method. Int.J.Eng. Sci. & Tech., 12(4): 14-22.

Lin, M., Wang, J., Xiu, Y. & Shan, Z. (2011) A numerical study on the weak Galerkin method for the Helmholtz equation with large wave numbers. Comm. Comput. Phys., 15. (5):324-345

Michael, H. & Rowtha, M. (2021) Convergence analysis of Least squares collocation methods for nonlinear higher-index differential algebraic equations. J. Comput. & Appl. Math., 112514. https://doi.org/10.1016/j.cam2019.

Murat, S., Sidia, S.S. & Yesim, S. S. (2011) A procedure of the Galerkin method for a Vibrating system. J. Comput. & Math. with Appl. Elsevier 61(4): 2854-2862.

Osadebe , N.N ., Ike, C., onah .H., Nwaji, C.N. & Okafor, F.O. (2016) Application of the galerkin –Vlasov method to the flexible analysis of simply supported rectangular Kirchhoff plates under uniform loads. Nigerian J. Tech. (NJOTECH)., 35 (4): 732-738. http://dx.doi.org/10.4314/njt.v35147.

Puso M.A., Chen J.S., Zywicz, E. & Elmer, W. (2008) Mesh free and finite element nodal integration methods. Int. J. Num. Meds. Eng., 74: 416-446. https://doi..org/10.1002/nme.2181.

Sergry, V. E. (2019) Exact solution of Helmholtz equation for case of non – paraxial Gaussian beams. Institute for Time Nature Explorations., M.V. Lomonosov's Moscow state university, Leminskie gory., 1-12. Russia.

Soumyarani, M., Ambit, K. P. & Sanmya, B. (2000) Finite element Galerkin method for 2D Sobolev equations with Burgers' type nonlinearty. Appl. Math & Comput., 387. http;//doi.org/10.1016/j.amc.2020.125113.

Trobe, R., Sterk M. & Robic, B. (2009) Computational complexity and parallelization of the mesh less local Petrov–Galerkin method computers and Structures, Vol.87, pp.81-90. https://doi.org/10.106j.compstruc.2008.08.003

Wang, D. J. (2004) Using the collocation method for modelling the dynamic of the flexible continuous beam subject to impact. J. Sou & Vib., 276 :1128-1134.

Wicker, J.A. & Mote, C.D. (2016) Llinear transverse vibration of axially moving state string particular system. J. Acou. Sol. Analy., 84 (3): 63-969.

Wu C.T., Park C.K. & Chen, J.S., (2011) A generalized approximation for the mesh free analysis of solids. Int. J. Num. Meds. Eng., 85: 693 - 722. https://doi.org/10.1002.nme.2991.

Yajni, D., Why, D. & Jill, R. R. (2015) The modified Galerkin methods for solving Helmholtz equation for flow frequencies on planet mars. Asian J. Fuzzy & App. Math. (SSN2321-564x)., 03:issue 4.

Zhang, N.H., Wang, J.J. & Chen, C. J. (2007) Complex mode Galerkin approach in transverse visco-elastic string. App. Math. Mech. Eng. first edition., 28(1): 1-9.

PURE MATHEMATICS

Hybrid Fixed Point Results of Fuzzy Soft Set-Valued Maps

Mohammed Shehu Shagari[1*] and Akbar Azam[2] [1]Department of Mathematics, Faculty of Physical Sciences, Ahmadu Bello University, Zaria, Nigeria

[2]Department of Mathematics, Grand Asian University, Sialkot7KM, Pasrur Road, 51310, Sialkot, Pakistan

[1*]shagaris@ymail.com

[2]akbarazam@gaus.edu.pk

Abstract

A lot of work has been done in efforts to refine the concepts of soft set and fuzzy soft set and their applications to other domains. However, none of these investi-gations has attempted to combine the aforementioned notions in the study of functional equations involving Jaggi-type contractions. Given this background information, this work proposes the idea of Jaggi-type hybrid fuzzy soft contraction in metric space and examines novel conditions for the existence of fixed points for such mappings. The significance of the obtained principal result lies in the fact that the contractive inequali-ities can be particularized in various ways, depending on the variant of the parameters, thereby making it relatively easy to unify, deduce and improve several corresponding results.

Keywords: b-metric space; soft set; fuzzy soft set; fuzzy soft set-valued map, hybrid contraction.

2010 Mathematics Subject Classification: 46S40; 47H10; 54H25; 34A12; 46J10.

1. Introduction

The real world is filled with uncertainty, vagueness and imprecision. The problems we meet in everyday life are vague rather than precise. In recent time, researchers have taken keen interests in modelling vagueness due to the fact that many practical problems within fields such as biology, economics, engineering, environmental sciences, medical sciences involve data containing various forms of uncertainties. To handle the complexity of vagueness, one cannot successfully employ classical mathematical methods due to the presence of different kinds of incomplete knowledge. Earlier in the literature, there were four known theories for dealing with imperfect knowledge. The three most applied of these theories were: Probability theory, Fuzzy set theory and Rough set theory. All the aforementioned tools require pre-assignment of some parameters. Such pre-specifications, viewed in the backdrop of incomplete knowledge, give rise to every day problems. With this concern, Molodstov [9] initiated the concept of Soft Set Theory with the aim of handling phenomena and notions of ambiguous, undefined and imprecise environments. Soft set does not need the pre-specifications of parameters, rather, it accommodates approximate descriptions of objects. Molodstov

[9] emphasized that the models by fuzzy sets and soft sets are interrelated. Yang et al [11] observed that soft set theory needed to be expanded in different directions to stem its applications to other fields. Currently, the concept of soft sets has been refined by several researchers. By combining the ideas of soft sets and fuzzy sets, Maji et al [4] initiated the notion of fuzzy soft sets and discussed its various properties. For related developments in fuzzy soft sets, the reader can check out [5] and some citations therein. Not long ago, Mohammed and Azam [7, 8] studied the concept of soft set-valued maps and introduced the notions of e-soft fixed points and E-soft fixed points of maps whose range set is a family of soft sets. It was shown in [7] that every fuzzy mapping is a particular kind of soft set-valued map. Since every fuzzy mapping has its corresponding multifunction analogue (see [1, Theorem 2.2]), hence, the idea of e-soft invariant point theorems is a generalization of the concept of fuzzy fixed points and fixed points of crisp set-valued maps.

Following the existing literature, we notice that solutions of functional equations in the context of Jaggi-type hybrid invariant point results, using fuzzy soft sets has not been developed. Hence, this paper proposes the notion of Jaggi-type hybrid fuzzy soft contraction in metric space and examines criteria for the existence of fixed points for such contraction.

2. Literature Review

In what follows, some basic concepts are reviewed.

Definition 2.1. [2] A nonempty subset A of Ω is called proximal if, for each $\gamma \in \Omega$, we can find a $a \in A$ such that $\varrho(\gamma, a) = \varrho(\gamma, A)$.

Definition 2.2. [3, 10] A nondecreasing function $\varphi : R_+ = [0, \infty) \to R_+$ is called a (c)-comparison function if $\varphi^n(\mu) \to 0$ *as* $n \to \infty$ for every $\mu \in R_+$;

Depict by Ω, the family of functions $\varphi : R_+ \to R_+$ satisfying the following conditions:

(i) $\varphi(\mu) = 0$ if and only if $\mu = 0$.

(ii) φ is continuous.

Lemma 2.3. [10] For a (c)-comparison function $\varphi : R_+ \to R_+$, the following properties hold:

(i) each iterate φ^n, $n \in N$ is also a (c)-comparison function;

(iii) $\varphi(\mu) < \mu$ for all $\mu > 0$.

Lemma 2.4. [10] Let $\varphi : R_+ \to R_+$ be a (c)-comparison function. Then, the series $\sum_{k=0}^{\infty} \varphi^k(\mu)$ converges for every $\mu \in \mathbb{R}_+$.

Followed herewith, specific basis of soft sets and fuzzy soft sets are collated. Accordingly, let Ω be the universe of discourse, E be the parameter set $A \subseteq E$ and $P(\Omega)$ represents the power set of Ω.

Definition 2.5. [9] The pair (F, A) is called a soft set over Ω under E, where $A \subseteq E$ and F is a mapping given by $F : A \to P(\Omega)$.

We denote the set of all soft sets over Ω under E by $[P(\Omega)]^E$. Throughout this manuscript, $I = [0, 1]$ and, by I^{Ω}, we mean the family of fuzzy sets in Ω.

Definition 2.6. [4] The pair (F, A) is a fuzzy soft set over Ω, where $A \subseteq E$ and $F : A \to I^{\Omega}$ is a mapping.

For each $\gamma \in \Omega$, we represent the set of all proximal and bounded proximal subsets of Ω under E by $P^{\alpha(\gamma;e)}(\Omega)$ and $P_b^{\alpha(\gamma;e)}(\Omega)$, respectively. Let $I^{(E;\Omega)}$ denotes the family of fuzzy soft sets over Ω under E. By $A \in I^{(E;\Omega)}$, we mean the mapping $A : E \to I^{\Omega}$.

Definition 2.7. [6] The mapping $\Psi : \Omega \to I^{(E;\Omega)}$ is called fuzzy soft set-valued map.

Definition 2.8 Let $\Psi : \Omega \to I^{(E;\Omega)}$ be a fuzzy soft set-valued map $u \in \Omega, e \in Dom\Psi, \alpha \in (0,1]$. Then the α-level set of Ψ is given as

$$[\Psi(u; e)]_{\alpha} = \{\gamma \in \Omega : [\Psi(u; e)](\gamma) \geq \alpha\}$$

Definition 2.9. A point u is called fuzzy soft invariant point of $\Psi : \Omega \to I^{(E;\Omega)}$, if we can find $e \in E,\ \alpha \in (0,\ 1]$ such that $u \in [\Psi(u;\ e)]_\alpha$. The point u is said to be a common fuzzy soft invariant point of $S,\ \Psi : \Omega \to I^{(E;\Omega)}$ if $u \in [S(u;\ e)]_\alpha \cap [\Psi(u;\ e)]_\alpha$.

3. Results and Discussion

We now study hybrid invariant point results involving fuzzy soft set-valued maps. The following auxiliary results are needed in the sequel. Let $(\Omega,\ \varrho)$ be a metric space (MS). For each $\gamma \in \Omega$, consider two fuzzy soft sets $A,\ B \in I^{(E;\Omega)}$ and $\alpha(\gamma) \in I$. Assume that $[A]_{\alpha(\gamma;e)},\ [B]_{\alpha(\gamma;e)} \in P_b^{\alpha(\gamma;e)}(\Omega)$. Then, define

$$D_E{}^{\alpha(\gamma;e)}(A,\ B) = \varrho^H{}_E([A]_{\alpha(\gamma;e)},\ [B]_{\alpha(\gamma;e)});$$

where

$$\varrho_E^H([A]_{\alpha(\gamma;e)},[B]_{\alpha(\gamma;e)}) = \max\left\{\sup_{a\in[A]_{\alpha(\gamma;e)}} \varrho(a,[B]_{\alpha(\gamma;e)}),\ \sup_{b\in[B]_{\alpha(\gamma;e)}} \varrho(b,[A]_{\alpha(\gamma;e)})\right\}.$$

We now propose the following concept of Jaggi-type hybrid fuzzy soft contraction and examine conditions for the existence of fuzzy soft fixed points for such contractions.

Definition 3.1. Let $(\Omega,\ \varrho)$ be a MS and $S,\ \Psi : \Omega \multimap I$ be fuzzy soft set-valued

maps. Then, the pair $(S,\ \Psi)$ is said to form a Jaggi-type hybrid fuzzy soft contraction, if for all $\gamma,\ \varpi \in \Omega$ and $e \in E$, we can find $\alpha(\gamma;\ e),\ \alpha(\varpi;\ e) \in I$ such that

$$\varrho_E{}^E[S(\gamma;\ e)]_{\alpha(\gamma;e)},\ [\Psi(\varpi;\ e)]_{\alpha(\varpi;e)} \le \varphi J_{(S,\Psi)}^k(\gamma,\ \varpi), \qquad (3.1)$$

where

$$J^{k}_{(S,\Psi)}(\gamma,\varpi)=\begin{cases}\left[a_1\left(\dfrac{\varrho(\gamma,[S(\gamma;e)]_{\alpha(\gamma;e)})\varrho(\varpi,[\Psi(\varpi;e)]_{\alpha(\varpi;e)})}{1+\varrho(\gamma,\varpi)}\right)^{k}+a_2(\varrho(\gamma,\varpi))^{k}\right]^{\frac{1}{k}},\\ \text{for } k>0,\gamma,\varpi\in\Omega,\gamma\neq\varpi,\\ \varrho(\gamma,[S(\gamma;e)]_{\alpha(\gamma;e)})^{a_1}\varrho(\varpi,[\Psi(\varpi;e)]_{\alpha(\varpi;e)})^{a_2},\\ \text{for } k=0,\gamma,\varpi\in\Omega\setminus\mathcal{F}ix(S,\Psi),\end{cases}$$

where

$$\mathcal{F}ix(S,\Psi)=\{\gamma,\varpi\in\Omega:\gamma\in[S(\gamma;e)]_{\alpha(\gamma;e)},\varpi\in[\Psi(\varpi;e)]_{\alpha(\varpi;e)}\},$$

$\varphi\in\Omega, a_i\geq 0$ and $\sum_{i=1}^{2}a_i=1$.

Our principal result is discussed hereunder.

Theorem 3.2. Let $(\Omega,\ \varrho)$ be a complete MS and $S,\ \Psi\ :\ \Omega\ \rightarrow\ I^{(E;\Omega)}$ be fuzzy soft set-valued maps. For $e\in E$, suppose that for each $\gamma\in\Omega$, we can find $\alpha(\gamma;\ e)\in I$ such that $[S(\gamma;e)]_{\alpha(\gamma;e)}$ and $[\Psi(\gamma;e)]_{\alpha(\gamma;e)}$ are in . $P_b^{\alpha(\gamma;e)}(\Omega)$ If $(S,\ \Psi)$ forms a Jaggi-type hybrid fuzzy soft contraction, then S and Ψ have a common fuzzy soft fixed point in **Ω**.

Proof. Let $\gamma_0\in\Omega$. Then, by assumptions, we can find $\alpha(\gamma_0;\ e)\in I$ such that $[S(\gamma_0;\ e)]_{\alpha(\gamma 0;e)}\in P_b^{(\gamma 0;e)}(\Omega)$. Since e is fixed, we may write $\alpha(\gamma_0)$ instead of $\alpha(\gamma_0;\ e)$. Choose $\gamma_1\in[S(\gamma_0;\ e)]_{\alpha(\gamma 0)}$ such that $\varrho(\gamma_0,\ \gamma_1)\ =\ \varrho(\gamma_0,\ [S(\gamma_0;\ e)]_{\alpha(\gamma 0)})$. Similarly, we can find $\alpha(\gamma_1)\in I$ such that $[\Psi(\gamma_1;\ e)]_{\gamma 1}\in P_b^{\alpha(\gamma 1)}(\Omega)$. Hence, we can find $\gamma_2\in[\Psi(\gamma_1;\ e)]_{\alpha(\gamma 1)}$ such that $\varrho(\gamma_1,\ \gamma_2)\ =\ \varrho(\gamma_1,\ [\Psi(\gamma_1;\ e)]_{\alpha(\gamma 1)})$. Continuing in this manner, we can find a sequence $\{\gamma_n\}_{n\in N}$ of elements of Ω such that

$$\gamma_{2p+1}\in[S(\gamma_{2p};e)]_{\alpha(\gamma_{2p})},\gamma_{2p+2}\in[\Psi(\gamma_{2p+1};e)]_{\alpha(\gamma_{2p+1})},$$

and

$$\varrho(\gamma_{2p},\gamma_{2p+1})=\varrho(\gamma_{2p},[S(\gamma_{2p};e)]_{\alpha(\gamma_{2p})}),$$

$$\varrho(\gamma_{2p+1},\gamma_{2p+2})=\varrho(\gamma_{2p+1},[\Psi(\gamma_{2p+1};e)]_{\alpha(\gamma_{2p+1})}),p\in\mathbb{N}.$$

Since the cut sets of S and Ψ are proximal, we have

$$\varrho(\gamma_{2p},\gamma_{2p+1})\leq\varrho_E^H([S(\gamma_{2p};e)]_{\alpha(\gamma_{2p})},[\Psi(\gamma_{2p-1};e)]_{\alpha(\gamma_{2p-1})}) \tag{3.2}$$

and

$$\varrho(\gamma_{2p+1},\gamma_{2p+2})\leq\varrho_E^H([S(\gamma_{2p};e)]_{\alpha(\gamma_{2p})},[\Psi(\gamma_{2p+1};e)]_{\alpha(\gamma_{2p+1})}). \tag{3.3}$$

Suppose that $\gamma_{2p}=\gamma_{2p+1}$ for some $p\in\mathbb{N}$ and $k>0$, then,

$$J_{(S,\Psi)}^k(\gamma_{2p},\gamma_{2p+1})=\Big[a_1\left(\frac{\varrho(\gamma_{2p},[S(\gamma_{2p})]_{\alpha(\gamma_{2p})})\varrho(\gamma_{2p+1},[\Psi(\gamma_{2p+1})]_{\alpha(\gamma_{2p+1})})}{1+\varrho(\gamma_{2p},\gamma_{2p+1})}\right)$$

$$+a_2(\varrho(\gamma_{2p},\gamma_{2p+1}))^k\Big]^{\frac{1}{k}}$$

$$=\left[a_1\left(\frac{\varrho(\gamma_{2p},\gamma_{2p+1})\varrho(\gamma_{2p+1},\gamma_{2p+2})}{1+\varrho(\gamma_{2p},\gamma_{2p+1})}\right)^k+a_2(\varrho(\gamma_{2p},\gamma_{2p+1}))^{\frac{1}{k}}\right]^{\frac{1}{k}}$$

$$\leq[a_1\varrho(\gamma_{2p+1},\gamma_{2p+2})^k]^{\frac{1}{k}}=(a_1)^{\frac{1}{k}}\varrho(\gamma_{2p+1},\gamma_{2p+2})$$

$$=\varrho(\gamma_{2p+1},\gamma_{2p+2})\text{as}k\to\infty.$$

Hence, using the continuity of φ, we have

$$\varrho(\gamma_{2p+1},\gamma_{2p+2})\leq\varrho_E^H([S(\gamma_{2p};e)]_{\gamma_{2p}},[\Psi(\gamma_{2p+1};e)]_{\gamma_{2p+1}})$$

$$\leq\varphi(\varrho(\gamma_{2p+1},\gamma_{2p+2}))<\varrho(\gamma_{2p+1},\gamma_{2p+2}),$$

a contradiction. It follows that $\varrho(\gamma_{2p+1},\ \gamma_{2p+2})\ =\ 0$. Therefore,

$$\gamma_{2p}=\gamma_{2p+1}\in[S(\gamma_{2p};e)]_{\alpha(\gamma_{2p})},$$

and

$$\gamma_{2p} = \gamma_{2p+1} = \gamma_{2p+2} \in [\Psi(\gamma_{2p+1}; e)]_{\alpha(\gamma_{2p+1})} = [\Psi(\gamma_{2p}; e)]_{\alpha(\gamma_{2p})}.$$

So, γ_{2p} turns out to be the common fuzzy soft fixed point of S and Ψ. Again, for $k = 0$ and $\gamma_{2p} = \gamma_{2p+1}$, for $p \in N$, we have $J^{k}_{(S,\Psi)}\left(\gamma_{2p}, \gamma_{2p+1}\right) = 0$. Therefore, by Condition (iii) of φ, we obtain $\varrho\left(\gamma_{2p+1}, \gamma_{2p+2}\right) = 0$. Hence, on similar arguments as above, it follows that $\gamma_{2p} \in \left[S\left(\gamma_{2p}; e\right)\right]_{\alpha(\gamma 2p)} \cap \left[\Psi\left(\gamma_{2p}; e\right)\right]_{\alpha(\gamma 2p)}$. Consequently, we presume that for all $p \in N$, $\gamma_{p+1} = \gamma_{p}$ if and only if $\varrho\left(\gamma_{p+1}, \gamma_{p}\right) > 0$.

Now, in view of (3.1), putting $\gamma = \gamma_{2p}$ and $\varpi = \gamma_{2p-1}$, we have

$$J^{k}_{(S,\Psi)}(\gamma_{2p}, \gamma_{2p-1}) = \begin{cases} \left[a_1\left(\dfrac{\varrho(\gamma_{2p}, [S(\gamma_{2p}; e)]_{\alpha(\gamma_{2p})})\varrho(\gamma_{2p-1}, [\Psi(\gamma_{2p-1}; e)]_{\alpha(\gamma_{2p-1})})}{1+\varrho(\gamma_{2p}, \gamma_{2p-1})}\right)^{k} \right. \\ \left. + a_2(\varrho(\gamma_{2p}, \gamma_{2p-1}))^{k}\right]^{\frac{1}{k}}, \text{for } k > 0 \\ (\varrho(\gamma_{2p}, [S(\gamma_{2p}; e)]_{\alpha(\gamma_{2p})}))^{a_1} (\varrho(\gamma_{2p-1}, [\Psi(\gamma_{2p-1}; e)]_{\alpha(\gamma_{2p-1})}))^{a_2}, \\ \text{for } k = 0. \end{cases}$$

That is,

$$J^{k}_{(S,\Psi)}(\gamma_{2p}, \gamma_{2p-1}) = \begin{cases} \left[a_1\left(\dfrac{\varrho(\gamma_{2p}, \gamma_{2p+1})\varrho(\gamma_{2p-1}, \gamma_{2p})}{1+\varrho(\gamma_{2p}, \gamma_{2p-1})}\right)^{k} \right. \\ \left. + a_2(\varrho(\gamma_{2p}, \gamma_{2p-1}))^{k}\right]^{\frac{1}{k}}, \text{for } k > 0 \\ (\varrho(\gamma_{2p}, \gamma_{2p+1}))^{a_1} (\varrho(\gamma_{2p-1}, \gamma_{2p}))^{a_2}, \text{ for } k = 0. \end{cases}$$

The above expression implies that

$$J^{k}_{(S,\Psi)}(\gamma_{2p}, \gamma_{2p-1}) \leq \begin{cases} \left[a_1(\varrho(\gamma_{2p}, \gamma_{2p+1}) +)^{k} + a_2(\varrho(\gamma_{2p}, \gamma_{2p-1}))^{k}\right]^{\frac{1}{k}}, \text{for } k > 0 \\ (\varrho(\gamma_{2p}, \gamma_{2p+1}))^{a_1} (\varrho(\gamma_{2p-1}, \gamma_{2p}))^{a_2}, \text{ for } k = 0. \end{cases} \quad (3.4)$$

We now investigate the following two cases:

Case 1: For k> 0, suppose that $\varrho(\gamma_{2p-1}, \gamma_{2p}) \leq \varrho(\gamma_{2p}, \gamma_{2p+1})$, then, Eq. (3.4) yields

$$J^{k}_{(S,\Psi)}(\gamma_{2p},\gamma_{2p-1}) \leq [a_1(\varrho(\gamma_{2p},\gamma_{2p+1}))^k + a_2(\varrho(\gamma_{2p},\gamma_{2p-1}))^k]^{\frac{1}{k}}$$

$$= [(a_1+a_2)(\varrho(\gamma_{2p},\gamma_{2p+1}))^k]^{\frac{1}{k}}$$

Hence, from (3.1) and (3.5), we have

$$\varrho(\gamma_{2p}, \gamma_{2p+1}) \leq \varphi(\varrho(\gamma_{2p}, \gamma_{2p+1})). \tag{3.6}$$

Since φ is a (c)-comparison function, therefore, (3.6) gives $\varrho(\gamma_{2p},\gamma_{2p+1}) < \varrho(\gamma_{2p},\gamma_{2p+1})$,

a contradiction. It follows that $\varrho(\gamma_{2p}, \gamma_{2p+1}) < \varrho(\gamma_{2p}, \gamma_{2p-1})$. Consequently, (3.6) turns into

$$\varrho(\gamma_{2p},\gamma_{2p+1}) \leq \varphi(\varrho(\gamma_{2p},\gamma_{2p-1})). \tag{3.7}$$

Putting $n = 2p \in \mathbb{N}$ in (3.7), leads to

$$\begin{aligned}\varrho(\gamma_n,\gamma_{n+1}) &\leq \varphi(\varrho(\gamma_{n-1},\gamma_n)) \\ &\leq \varphi^2(\varrho(\gamma_{n-2},\gamma_{n-1})) \\ &\leq \varphi^3(\varrho(\gamma_{n-3},\gamma_{n-2})) \\ &\vdots \\ &\leq \varphi^n(\varrho(\gamma_0,\gamma_1)).\end{aligned} \tag{3.8}$$

By using the triangle inequality and (3.8), for $l \geq 1$ we obtain

$$\begin{aligned}\varrho(\gamma_n,\gamma_{n+l}) &\leq \varrho(\gamma_n,\gamma_{n+1}) + \varrho(\gamma_{n+1},\gamma_{n+l}) \\ &\leq \varrho(\gamma_n,\gamma_{n+l}) + \varrho(\gamma_{n+1},\gamma_{n+2}) + \cdots + \varrho(\gamma_{n+l-1},\gamma_{n+l}) \\ &\leq \sum_{s=n}^{n+l-1} \varphi^s(\varrho(\gamma_0,\gamma_1)).\end{aligned} \tag{3.9}$$

Applying the fact that φ is a \$c\$-comparison function in (3.9), gives $\varrho(\gamma_n, \gamma_{n+l}) \to 0$ as $n \to \infty$. Hence, $\{\gamma_n\}_{n\in\mathbb{N}}$ is a Cauchy sequence in Ω. The completeness of this space implies that we can find $u \in \Omega$ such that $\lim_{n\to\infty} \varrho(\gamma_n, \gamma_u) = 0$.

We now show that u is a common fuzzy soft fixed point of S and Ψ. By utilizing Lemma and considering the Case $k > 0$, we get

$$\begin{aligned}
\varrho(u,[S(u;e)]_{\alpha(u)}) &\le \varrho(u,\gamma_n) + \varrho(\gamma_n,[S(u;e)]_{\alpha(u)}) \\
&\le \varrho(u,\gamma_n) + \varrho_E^H([S(u;e)]_{\alpha(u)},[\Psi(\gamma_{n-1};e)]_{\alpha(\gamma_{n-1})}) \\
&\le \varrho(u,\gamma_n) + \varphi(J^k_{(S,\Psi)}(u,\gamma_{n-1})) \\
&= \varrho(u,\gamma_n) + \varphi\left[a_1\left(\frac{\varrho(u,[S(u;e)]_{\alpha(u)})\varrho(\gamma_{n-1},[\Psi(\gamma_{n-1};e)]_{\alpha(\gamma_{n-1})})}{1+\varrho(u,\gamma_{n-1})} \right)^k + a_2(\varrho(u,\gamma_{n-1}))^k \right]^{\frac{1}{k}} \\
&= \varrho(u,\gamma_n) + \varphi\left[a_1\left(\frac{\varrho(u,[S(u;e)]_{\alpha(u)})\varrho(\gamma_{n-1},\gamma_n)}{1+\varrho(u,\gamma_{n-1})} \right)^k + a_2(\varrho(u,\gamma_{n-1}))^k \right]^{\frac{1}{k}}. \quad (3.10)
\end{aligned}$$

Since φ is continuous, then, letting $n \to \infty$ in (3.10), yields

$\varrho(u,[S(u;e)]_{\alpha(u)}) \le 0$, from which we conclude that $u \in [S(u;e)]_{\alpha(u)}$ for some $\alpha(u) \in I$.

On similar steps, by considering

$$\begin{aligned}
\varrho(u,[\Psi(u;e)]_{\alpha(u)}) &\le \varrho(u,\gamma_n) + \varrho(\gamma_n,[\Psi(u;e)]_{\alpha(u)}) \\
&\le \varrho(u,\gamma_n) + \varrho_E^H([S(\gamma_{n-1};e)]_{\alpha(\gamma_{n-1})},[\Psi(u;e)]_{\alpha(u)}) \\
&\le \varrho(u,\gamma_n) + \varphi(J^k_{(S,\Psi)}(\gamma_{n-1},u)),
\end{aligned}$$

we can show that we can find $\alpha(u) \in I$ such that $u \in [\Psi(u;e)]_{\alpha(u)}$. Hence, for $k > 0$, we obtain that u is a common fixed point of S and Ψ.

Case2: For $k = 0$, using (3.11), and on account of (c)-comparison of φ, we get

$\varrho(\gamma_{2p},\gamma_{2p-1}) \le \varrho_E^H([S(\gamma_{2p-1};e)]_{\alpha(\gamma_{2p-1})},[\Psi(\gamma_{2p-2};e)]_{\alpha(\gamma_{2p-2})})$

$$\leq \varphi(J^k_{(S,\Psi)}(\gamma_{2p-1},\gamma_{2p-2}))$$

$$\leq (\varrho(\gamma_{2p-1},[S(\gamma_{2p-1};e)]_{\alpha(\gamma_{2p-1})})^{a_1}(\varrho(\gamma_{2p-2},[\Psi(\gamma_{2p-2};e)]_{\alpha(\gamma_{2p-2})})^k \qquad (3.11)$$

Assume that $\varrho(\gamma_{2p-1},\varrho(\gamma_{2p-2}) \leq \varrho(\gamma_{2p-1}),\varrho(\gamma_{2p})$, then (3.11) gives

$$\varrho(\gamma_{2p},\gamma_{2p-1}) \leq \varphi\left((\varrho(\gamma_{2p-1},\gamma_{2p}))^{a_1}(\varrho(\gamma_{2p-1},\gamma_{2p}))^{a_2}\right)$$

$$< (\varrho(\gamma_{2p-1},\gamma_{2p}))^{a_1+a_2} = \varrho(\gamma_{2p-1},\gamma_{2p}),$$

a contradiction. Thus,

$$\varrho(\gamma_{2p},\gamma_{2p-1}) < \varrho(\gamma_{2p-1},\gamma_{2p-2}). \qquad (3.12)$$

By utilizing (3.12) and (3.11), we get

$$\varrho(\gamma_{2p},\gamma_{2p-1}) \leq \varphi(\varrho(\gamma_{2p-1},\gamma_{2p-2})). \qquad (3.13)$$

We notice that (3.13) is equivalent to (3.7). It follows that $\{\gamma_n\}_{n\in\mathbb{N}}$ is a Cauchy sequence in Ω. The completeness of this space implies that $\varrho(\gamma_n,u)\to 0$ as $n\to\infty$ for some $u\in\Omega$. To see that u is a common invariant fuzzy soft fixed point of S and Ψ, we consider the inequality (3.16) for $k=0$, as follows:

$$\varrho(u,[\Psi(u;e)]_{\alpha(u)}) \leq \varrho(u,\gamma_n)+\varrho(\gamma_n,[\Psi(u;e)]_{\alpha(u)})$$

$$\leq \varrho(u,\gamma_n)+\varrho^H_E([S(\gamma_{n-1};e)]_{\alpha(\gamma_{n-1})},[\Psi(u;e)]_{\alpha(u)})$$

$$\leq \varrho(u,\gamma_n)+\varphi(J^k_{(S,\Psi)}(\gamma_{n-1},u)), \qquad (3.14)$$

where

$$J^k_{(S,\Psi)}(\gamma_{n-1},u) = (\varrho(\gamma_{n-1},[S(\gamma_{n-1};e)]_{\alpha(\gamma_{n-1})}))^{a_1}(\varrho(u,[\Psi(u;e)]_{\alpha(u)}))^{a_2}$$

$$= (\varrho(\gamma_{n-1},\gamma_n))^{a_1}(u,[\Psi(u;e)]_{\alpha(u)})^{a_2}.$$

Clearly, $\lim_{n\to\infty} J^k_{(S,\Psi)}(\gamma_{n-1},u)=0$. Under this limiting case, (3.14) reduces to

$$\varrho(u,[\Psi(u;e)]_{\alpha(u)}) \leq \varphi(0). \qquad (3.15)$$

By Property (iii) of φ, it follows from (3.15) that $\varrho(u,[\Psi(u;e)]_{\alpha(u)})=0$. Hence, $u\in[\Psi(u;e)]_{\alpha(u)}$ for some $\alpha(u)\in I$. On similar steps, we can show that we can find $\alpha(u)\in I$ such that $u\in[S(u;e)]_{\alpha(u)}$. Therefore, u is a common fuzzy soft fixed point of S and Ψ.

Corollary 3.3. Let (Ω, ϱ) be a complete MS and $\Psi : \Omega \to I^{(E;\Omega)}$ be a fuzzy soft set-valued map. For $e \in E$, suppose that for each $\gamma \in \Omega$, we can find $\alpha(\gamma; e) \in I$ such that $[\Psi(\gamma; e)]_{\alpha(\gamma;e)}$ is a proximal subset of Ω. If for all $\gamma, \varpi \in \Omega$ and $e \in E$, we can find such that

$$\varrho_E^E\left([\Psi(\gamma;e)]_{\alpha(\gamma;e)}, [\Psi(\varpi;e)]_{\alpha(\varpi;e)}\right) \leq \varphi\left(J_{(\Psi)}^k(\gamma,\varpi)\right),$$

where

$$J_{(\Psi)}^k(\gamma,\varpi) = \begin{cases} \left[a_1\left(\dfrac{\varrho(\gamma,[\Psi(\gamma;e)]_{\alpha(\gamma;e)})\varrho(\varpi,[\Psi(\varpi;e)]_{\alpha(\varpi;e)})}{1+\varrho(\gamma,\varpi)}\right)^k + a_2(\varrho(\gamma,\varpi))^k\right]^{\frac{1}{k}}, \\ \text{for } k>0, \gamma,\varpi \in \Omega, \gamma \neq \varpi, \\ \varrho(\gamma,[\Psi(\gamma;e)]_{\alpha(\gamma;e)})^{a_1}\varrho(\varpi,[\Psi(\varpi;e)]_{\alpha(\varpi;e)})^{a_2}, \text{for } k=0, \gamma,\varpi \in \Omega \setminus \mathcal{F}ix(\Psi), \end{cases}$$

where

$\mathcal{F}ix(\Psi) = \{\gamma, \varpi \in \Omega : \gamma \in [\Psi(\gamma;e)]_{\alpha(\gamma;e)}\}$, and $\varphi \in \Omega, a_i \geq 0$ with $\sum_{i=1}^{2} a_i = 1$, then Ψ has at least one fuzzy soft fixed point in Ω.

Proof. Take $S = \Psi$ in Theorem 3.2

Corollary 3.4. Let (Ω, ϱ) be a complete MS and $\Psi : \Omega \to I^{E;\Omega}$ be a fuzzy soft set-valued map. Suppose that for each $\gamma \in \Omega$, we can find $\alpha(\gamma; e) \in I$ such that $[\Psi(\gamma; e)]_{\alpha(\gamma)}$ is a proximal subset of Ω. If

$$\varrho_E^H\left([\Psi(\gamma;e)]_{\alpha(\gamma)}, [\Psi(\varpi;e)]_{\alpha(\varpi)}\right) \leq \varphi\left(\frac{1}{2}M_{(\Psi)}^k(\gamma,\varpi)\right), \text{ for all } \gamma,\varpi \in \Omega, \text{ where } \varphi \in \Omega, \text{and}$$

$M_{(\Psi)}^k(\gamma,\varpi) = \varrho(\gamma,\varpi) + \dfrac{\varrho(\gamma,[\Psi(\gamma;e)]_{\alpha})\varrho(\varpi,[\Psi(\varpi;e)]_{\alpha(\varpi)})}{1+\varrho(\gamma,\varpi)}$, then Ψ has at least one fuzzy soft fixed point in Ω.

Proof : Put $S = \Psi, a_1 = a_2 = \dfrac{1}{2}$ and $k = 1$ in Theorem 3.2

4. Conclusion

This manuscript initiated the notion of Jaggi-type hybrid fuzzy soft contraction in metric

space and examined conditions for the existence of fuzzy soft fixed points for such mappings. The preeminence of the new contractive inequalities and the associated fixed point results is that different corresponding results in the literature can easily be obtained as special cases.

Competing Interests

The authors declare that they have no competing interests.

Acknowledgement

Not applicable

References

Frigon, M. and O'Regan, D. (2002). Fuzzy contractive maps and fuzzy fixed points. Fuzzy Sets and Systems, 129(1), 39-45.

Kannan, R. and O'Regan, D. (2000). A note on the solutions of integral inclusions. Journal of Integral Equations and Applications, 12, 85-94.

Karapinar, E., and Fulga, A. (2019). New hybrid contractions on b-metric spaces. Mathematics, 7(7), 578.

Maji, P. K., Biswas, P. and A. R. Roy. (2001). Fuzzy soft sets. Journal of fuzzy mathematics, 589-602.

Mohammed, S. S. and Azam, A. (2020). An algorithm for fuzzy soft set based decision making approach. Yugoslav Journal of Operations Research 30(1), 59-70.

Mohammed, S. S. (2020). On fuzzy soft set-valued maps with application. Journal of the Nigerian Society of Physical Sciences, 2, 26-35.

Mohammed, S. S. and A. Azam, (2019). Fixed points of soft-set valued and fuzzy set-valued maps with applications. Journal of Intelligent and Fuzzy Systems, 37(3), 3865-3877.

Mohammed, S. S. and Azam, A. (2019). Integral type contractions of soft set- valued maps with application to neutral differential equation. AIMS Mathematics, 5(1), 342-358.

Molodtsov, D. (1999). Soft set theory—first results. Computers and Mathematics with Applications, 37, 19.

Rus, I. A. (2001). Generalized contractions and applications. Cluj University Press,2(6), 60-71.

Yang, X. Yu, D., Yang, J. and Wu, C. (2007). Generalization of soft set theory: from crisp to fuzzy case. Fuzzy Information and Engineering, 345-354.

On the Existence of Solutions to a Boundary Value Problem via New Weakly Contractive Operator

Rhoda Chiroma[1*] and Mohammed Shehu Shagari[2]

[1,2]Department of Mathematics, Faculty of Physical Sciences, Ahmadu Bello University, Zaria, Nigeria

[1*]E-mail: rhodaderas@fuwukari.edu.ng

[2]E-mail: shagaris@ymail.com

Abstract

In this paper, the notion of generalized quasi-weakly contractive operators in metric-like spaces is introduced, and new conditions for the existence of fixed points for such mappings are investigated. A non-trivial example which highlights the novelty of our principal idea is constructed. It is observed comparatively that the proposed concepts herein subsume some important results in the corresponding literature. Also, significant number of corollaries are pointed out and discussed.

Keywords: fixed point, metric-like spaces, weakly contractive.

1. Introduction

The Banach fixed point theorem (also known as the contraction mapping principle) is an essential tool in the theory of metric spaces. It ensures the existence and uniqueness of fixed points of specific mappings of metric spaces and pro- vides a useful search method to find these fixed points. In efforts to explore more fixed point results, several researchers have established generalizations of metric spaces. The idea of a contraction mapping principle in quasi-metric spaces was introduced by Bakhtin [4]. The latter notion was extended to b-metric spaces by Czerwik [7]. One of the earliest generalizations is the quasi-metric space de- fined by Wilson [9]. In a similar approach, Matthews [8] introduced the concept of partial metric space as a part of the investigation into denotational semantics of data flow networks. The main contribution in [8] is the establishment of the fact that self-distance in the partial metric space is not necessarily zero. As a refinement of the partial metric space, Amini-Harandi [2] proposed the notion of metric-like space metric-like space by relaxing the axiom of non-negativity and small self-distances in partial metric space.

In another direction, Alber et al. [1] introduced the idea of weak contraction mappings in the context of Hilbert space by defining additional algebraic structure on the space. Following this, Cho [5] established some fixed point results for weakly contractive mappings in metric space which extended some known results.

It is noted from the review of the existing literature that little or no work has been conducted on the quasi-weakly contractive operator as a result of metric-like space. Hence, motivated by the idea in [5], in this manuscript we introduce a new concept of a generalized quasi-weakly contractive operator in metric-like space and investigate the existence and uniqueness of fixed points of such operators. A few corollaries which compare our new concepts to other well-known ideas in the literature are presented and analyzed.

2. Literature Review

In this section, we record basic ideas needed in later sections.

Definition 2.1. [8] Let X be a nonempty set. A function $\rho : X \times X \longrightarrow R_+$ is called a partial metric on X if, for all $l, m, z \in X$, the following conditions are satisfied:

(1) $\rho(l,l) = \rho(m,m) \Leftrightarrow l = m;$

(2) $\rho(l,l) \leq \rho(l,m);$

(3) $\rho(l,m) = \rho(m,l);$

(4) $\rho(l,z) \leq \rho(l,m) + \rho(m,z) - \rho(m,m).$

The pair (X,ρ) is called a partial metric space.

Definition 2.2. [2] A mapping $\sigma : X \times X \longrightarrow R_+$ is said to be metric-like on X if for any $l, m, z \in X$, the following hold:

$(\sigma_1)\ \sigma(l,m) = 0 \Rightarrow l\ m;$

$(\sigma_2)\ \sigma(l,m) = \sigma(m,l);$

$(\sigma_3)\ \sigma(l,z) \leq \sigma(l,m) + \sigma(m,z).$

The pair (X,σ) is called metric-like space.

Definition 2.3. [2] A sequence $\{l_y\}_{y\in\mathbb{N}}$ in metric-like space (X,σ) converges to a point $l \in X$ if $(l,l) = \lim_{y\to\infty} \sigma(l_y,l)$.

Definition 2.4. [2] A sequence $\{l_y\}_{y\in\mathbb{N}}$ in metric-like space (X,σ) is called a σ-Cauchy sequence if $\lim_{y,i\to\infty} \sigma(l_y,l_i)$ exists and is finite. If there is any $l \in X$ such that for each σ −Cauchy sequence $\{l_y\}_{y\in\mathbb{N}}$

$$\lim_{y\to\infty} \sigma(l_y,l) = \lim_{y,i\to\infty} \sigma(l_y,l_i),$$

then, the metric-like space (X,σ) is said to be complete.

Definition 2.5. [6] Let (X,d) be a metric space. A self-mapping $\Upsilon : X \longrightarrow X$ is said to be a quasi-contraction if there exists $\lambda \in \left[0,\frac{1}{2}\right)$ such that for all $l, m \in X$, $d(\Upsilon l, \Upsilon m) \leq max\{d(l,m), d(l,\Upsilon l), d(m,\Upsilon m), d(l,\Upsilon m), d(m,\Upsilon l)\}$.

Definition 2.6. [1] Let (X, d) be a metric space. A mapping $Y: X \longrightarrow X$ is said to be weakly contractive, if for all $l, m \in X$,

$$d(Yl, Ym) \leq d(l, m) - \lambda(d(l, m)),$$

where $\lambda : R_+ \longrightarrow R_+$ is a continuous and non-decreasing function such that $\lambda(0) = 0$ and $\lim_{t\to\infty} \lambda(t) = \infty$

Definition 2.7. A function $f : X \longrightarrow [0, \infty)$, where X is an MS, is called lower semi-continuous if, for all $l \in X$ and $\{l_y\}_{y\in N} \subset X$ with $\lim_{y\to\infty} l_y$ we have $f(l) \leq \liminf_{y\to\infty} f(l_y)$.

Let $\Psi = \{\psi : [0, \infty) \to [0, \infty) | \psi$ be continuous and $\psi(t) = 0 \Leftrightarrow t = 0\}$. In addition, let $\Phi = \{\phi : [0, \infty) \longrightarrow [0, \infty) | \phi$ be lower semi-continuous and $\phi(t) = 0 \Leftrightarrow t = 0\}$.

Lemma 2.8. [3] Let (X, σ) be an metric-like space, and let $\{l_y\}_{y\in N}$ be a sequence in X such that if $\{l_y\}_{y\in N}$ is not a σ −Cauchy sequence in (X, σ). Then, there exist $\epsilon > 0$ and two subsequences $\{l_{y(k)}\}_{k\in N}$ and $\{l_{i(k)}\}_{k\in N}$ of $\{l_y\}_{y\in N}$, y, i are positive integers with $y(k) > i(k) > k$ such that

$$\sigma(l_{i(k)}, l_{y(k)}) \geq \epsilon \tag{2.1}$$

and

$$\sigma(l_{i(k)-1}, l_{y(k)}) < \epsilon. \tag{2.2}$$

Moreover, suppose that

$$\lim_{y\to\infty} \sigma(l_y, l_{y+1}) = 0. \tag{2.3}$$

Then, the following hold:

(1) $\lim_{k\to\infty} \sigma(l_{i(k)}, l_{y(k)}) = \epsilon$

(2) $\lim_{k\to\infty} \sigma(l_{i(k)}, l_{y(k)+1}) = \epsilon;$

(3) $\lim_{k\to\infty} \sigma(l_{i(k-1)}, l_{y(k)}) = \epsilon;$

(4) $\lim_{k\to\infty} \sigma(l_{i(k)-1}, l_{y(k+1)}) = \epsilon.$

3. Results and Discussion

In this section, we introduce the concept of a generalized quasi-weakly contractive operator in the framework of metric-like space and examine the conditions for the existence of a fixed point of such an operator.

Definition 3.1. Let (X, σ) be metric-like space. A self-mapping $\Upsilon : X \longrightarrow X$ is called a generalized quasi-weakly contractive operator, if it satisfies the following condition:

$$\psi\big(\sigma(\Upsilon l, \Upsilon l) + \sigma(\Upsilon l, \Upsilon m) + \varphi(\Upsilon l) + \varphi(\Upsilon m)\big) \leq \psi(C(l, m, \varphi)) - \phi(L(l, m, \varphi)), \quad (3.1)$$

for all $l, m \in X$, where $\psi \in \Psi, \phi, \varphi \in \Phi$ and

$$\mathcal{C}(l, m, \varphi) = \max\left\{\begin{array}{c}\sigma(l,l)+\sigma(l,m)+\varphi(l)+\varphi(m), \sigma(l,\mathrm{Y}l)+\varphi(l)+\varphi(\mathrm{Y}l), \\ +\sigma(m,m)+\sigma(m,\mathrm{Y}m)+\varphi(m)+\varphi(\mathrm{Y}m), \\ \frac{1}{2}[\sigma(l,\mathrm{Y}m)+\varphi(l)+\varphi(\mathrm{Y}m) \\ +\sigma(m,\mathrm{Y}l)+\varphi(m)+\varphi(\mathrm{Y}l)]\end{array}\right\} \quad (3.2)$$

$$\mathcal{L}(l, m, \varphi) = \max\left\{\begin{array}{c}\sigma(l,l)+\sigma(l,m)+\varphi(l)+\varphi(m), \\ \sigma(m,m)+\sigma(m,\mathrm{Y}m)+\varphi(m)+\varphi(\mathrm{Y}m)\end{array}\right\}. \quad (3.3)$$

The following is the main result of this paper.

Theorem 3.2. Let (X, σ) be a σ −complete metric-like space. If Υ is a generalized quasi-weakly contractive operator, then there exists a unique $u \in X$ such that $u = \Upsilon u$ and $\varphi(u) = 0$.

Proof. Starting from an arbitrary point $l := l0 \in X$, we will construct a recursive sequence $\{l_y\}_{y\in\mathbb{N}}$ in the following manner:

$l_0 := l$ and $l_0 := l$ and $l_y = \mathrm{Y}l_{y-1}$, for all n ∈ N.

We presume that $l_y \neq l_{y-1}$ for all $y \in N$. In fact, if for some $y \in N$, it is observed that the expression $l_y = l_{y-1} = \mathrm{Y}l_{y-1}$, then the proof is finished. By replacing $l = l_{y-1}$ and m=l_y in (3.2), we obtain

$$= \max\begin{Bmatrix} \sigma(l_{y-1}, l_{y-1}) + \sigma(l_{y-1}, l_y) + \varphi(l_{y-1}) + \varphi(l_y), \\ \sigma(l_{y-1}, l_y) + \varphi(l_{y-1}) + \varphi(l_y), \\ \sigma(l_y, l_y) + \sigma(l_y, l_{y+1}) + \varphi(l_y) + \varphi(l_{y+1}), \\ \frac{1}{2}[\sigma(l_{y-1}, l_{y+1}) + \varphi(l_{y-1}) + \varphi(l_{y+1}) \\ +\sigma(l_y, l_y) + \varphi(l_y) + \varphi(l_y)] \end{Bmatrix}. \quad (3.4)$$

We observe that

$$\frac{1}{2}[\sigma(l_{y-1}, l_{y+1}) + \varphi(l_{y-1}) + \varphi(l_{y+1}) + \sigma(l_y, l_y) + \varphi(l_y) + \varphi(l_y)]$$
$$\leq \frac{1}{2}[\sigma(l_{y-1}, l_y) + \sigma(l_y, l_{y+1}) + \varphi(l_{y-1}) + \varphi(l_{y+1}) + \sigma(l_y, l_y) + \varphi(l_y) + \varphi(l_y)]$$
$$\leq \max\{\sigma(l_{y-1}, l_y) + \varphi(l_{y-1}) + \varphi(l_y), \sigma(l_y, l_y) + \sigma(l_y, l_{y+1}) + \varphi(l_y) + \varphi(l_{y+1})\}.$$

Hence, (3.4) becomes

$$\mathcal{C}(l_{y-1}, l_y, \varphi) = \max\{\sigma(l_{y-1}, l_{y-1}) + \sigma(l_{y-1}, l_y) + \varphi(l_{y-1}) + \varphi(l_y), \sigma(l_y, l_y) + \sigma(l_y, l_{y+1}) + \varphi(l_y) + \varphi(l_{y+1})\}.$$

Similarly, we obtain

$$L(l_{y\text{-}1}, l_y, \varphi) = \max\begin{Bmatrix} \sigma(l_{y\text{-}1}, l_{y\text{-}1}) + \sigma(l_{y\text{-}1}, l_y) + \varphi(l_{y\text{-}1}) + \varphi(l_y), \\ \sigma(l_y, \mathrm{Y}l_y) + \varphi(\mathrm{Y}l_y) + \sigma(l_y, l_y) + \varphi(l_y) \end{Bmatrix}$$

$$= \max\begin{Bmatrix} \sigma(l_{y-1}, l_{y-1}) + \sigma(l_{y-1}, l_y) + \varphi(l_{y-1}) + \varphi(l_y), \\ \sigma(l_y, l_y) + \sigma(l_y, l_{y+1}) + \varphi(l_{y+1}) + \varphi(l_y) \end{Bmatrix}.$$

Consequently, (3.1) gives

$$\begin{aligned} &\psi(\sigma(l_y, l_y) + \sigma(l_y, l_{y+1}) + \varphi(l_y) + \varphi(l_{y+1})) \\ &= \psi(\sigma(\mathrm{Y}l_{y-1}, \mathrm{Y}l_{y-1}) + \sigma(\mathrm{Y}l_{y-1}, \mathrm{Y}l_y) + \varphi(\mathrm{Y}l_{y-1}) + \varphi(\mathrm{Y}l_y) \\ &\leq \psi(\mathcal{C}(l_{y-1}, l_y, \varphi)) - \phi(\mathcal{L}(l_{y-1}, l_y, \varphi)). \end{aligned} \quad (3.5)$$

If

$$\sigma(l_{y-1}, l_{y-1}) + \sigma(l_{y-1}, l_y) + \varphi(l_{y-1}) + \varphi(l_y) < \sigma(l_y, l_y) + \sigma(l_y, l_{y+1}) + \varphi(l_y) + \varphi(l_{y+1})$$

for some positive integer y, then it follows from (3.5) that

$$\psi(\sigma(l_y, l_y) + \sigma(l_y, l_{y+1}) + \varphi(l_y) + \varphi(l_{y+1}))$$
$$\leq \psi(\sigma(l_y, l_y) + \sigma(l_y, l_{y+1}) + \varphi(l_y) + \varphi(l_{y+1}))$$
$$-\phi(\sigma(l_y, l_y) + \sigma(l_y, l_{y+1}) + \varphi(l_y) + \varphi(l_{y+1}))$$

which implies that $\phi(\sigma(l_y, l_y) + \sigma(l_y, l_{y+1}) + \varphi(l_y) + \varphi(l_{y+1})) = 0.$

Hence, $\sigma(l_y,l_y)+\sigma(l_y,l_{y+1})+\varphi(l_y)+\varphi(l_{y+1})=0$, from which we notice that $l_y=l_{y+1}$, $\sigma(l_y,l_y)=0$ and $\varphi(l_y)=\varphi(l_{y+1})=0$, which is a contradiction.

Therefore, for all $y = 1,2,3,\ldots$

$$\sigma(l_y,l_y)+\sigma(l_y,l_{y+1})+\varphi(l_y)+\varphi(l_{y+1}) \leq \sigma(l_{y-1},l_{y-1})+\sigma(l_{y-1},l_y)+\varphi(l_{y-1})+\varphi(l_y). \tag{3.6}$$

Hence,

$$\mathcal{C}(l_{y-1},l_y,\varphi)=\sigma(l_{y-1},l_{y-1})+\sigma(l_{y-1},l_y)+\varphi(l_{y-1})+\varphi(l_y)$$

and

$$\mathcal{L}(l_{y-1},l_y,\varphi)=\sigma(l_{y-1},l_{y-1})+\sigma(l_{y-1},l_y)+\varphi(l_{y-1})+\varphi(l_y).$$

From (3.5), we have

$$\begin{aligned}\psi(\sigma(l_y,l_y)+\sigma(l_y,l_{y+1})+\varphi(l_y)+\varphi(l_{y+1}))&\\ \leq \psi(\sigma(l_{y-1},l_{y-1})+\sigma(l_{y-1},l_y)+\varphi(l_{y-1})+\varphi(l_y))&\\ -\phi(\sigma(l_{y-1},l_{y-1})+\sigma(l_{y-1},l_y)+\varphi(l_{y-1})+\varphi(l_y)).&\end{aligned} \tag{3.7}$$

It follows from (3.6) that the sequence $\{\sigma(l_y,l_y)+\sigma(l_y,l_{y+1})+\varphi(l_y)+\varphi(l_{y+1})\}$ is bounded below and non-increasing.

Therefore, $\sigma(l_y,l_y)+\sigma(l_y,l_{y+1})+\varphi(l_y)+\varphi(l_{y+1})\to\eta \, as \, n\to\infty$, for some $\eta \geq 0$. Suppose that $\eta > 0$. Taking limit in (3.7) as $y \to \infty$, using the continuity of ψ and the lower semi-continuity of ϕ, lead to

$$\begin{aligned}\psi(\eta) &\leq \psi(\eta)-\liminf_{y\to\infty}\phi(\sigma(l_{y-1},l_{y-1})+\sigma(l_{y-1},l_y)+\varphi(l_{y-1})+\varphi(l_y))\\ &\leq \psi(\eta)-\phi(\eta)<\psi(\eta),\end{aligned}$$

which is a contradiction. Thus, $\lim_{y\to\infty}(\sigma(l_y,l_y)+\sigma(l_y,l_{y+1})+\varphi(l_y)+\varphi(l_{y+1}))=0$, from which we have

$$\lim_{y\to\infty}\sigma(l_y,l_y)=\lim_{y\to\infty}\sigma(l_y,l_{y+1})=0 \tag{3.8}$$

and

$$\lim_{y\to\infty}\varphi(l_y)=\lim_{y\to\infty}\varphi(l_{y+1})=0. \tag{3.9}$$

Now, we prove that the sequence $\{l_y\}_{y\in\mathbb{N}}$ is Cauchy. Assume that $\{l_y\}_{y\in\mathbb{N}}$ is not Cauchy. Then, by Lemma 2.8, there exist $\epsilon > 0$ and subsequences $\{l_{y(k)}\}_{k\in\mathbb{N}}$ and $\{l_{i(k)}\}_{k\in\mathbb{N}}$ of $\{l_y\}_{y\in\mathbb{N}}$ such that (2.1) and (2.2) hold.

From (3.2), we have

$$\mathcal{C}(l_{y(k)}, l_{i(k)}, \varphi) = \max\left\{\begin{array}{c} \sigma(l_{y(k)}, l_{y(k)}) + \sigma(l_{y(k)}, l_{i(k)}) + \varphi(l_{y(k)}) + \varphi(l_{i(k)}), \\ \sigma(l_{y(k)}, \mathrm{Y}l_{y(k)}) + \varphi(l_{y(k)}) + \varphi(\mathrm{Y}l_{y(k)}), \\ \sigma(l_{y(k)}, l_{y(k)}) + \sigma(l_{i(k)}, \mathrm{Y}l_{i(k)}) + \varphi(l_{i(k)}) + \varphi(\mathrm{Y}l_{i(k)}), \\ \frac{1}{2}[\sigma(l_{y(k)}, \mathrm{Y}l_{i(k)}) + \varphi(l_{y(k)}) + \varphi(\mathrm{Y}l_{i(k)}) + \sigma(l_{i(k)}, \mathrm{Y}l_{y(k)}) \\ +\varphi(l_{i(k)}) + \varphi(\mathrm{Y}l_{y(k)})]. \end{array}\right\}$$

$$\mathcal{C}(l_{y(k)}, u, \varphi) = \max\left\{\begin{array}{c} \sigma(l_y, l_y) + \sigma(l_y, u) + \varphi(l_y) + \varphi(u), \\ \sigma(l_y, \mathrm{Y}l_y) + \varphi(l_y) + \varphi(\mathrm{Y}l_y), \\ \sigma(u, u) + \sigma(u, \mathrm{Y}u) + \varphi(u) + \varphi(\mathrm{Y}u), \\ \frac{1}{2}[\sigma(l_y, \mathrm{Y}u) + \varphi(l_y) + \varphi(\mathrm{Y}u) + \sigma(u, \mathrm{Y}l_y) \\ +\varphi(u) + \varphi(\mathrm{Y}l_y)] \end{array}\right\}. \qquad (3.10)$$

As $k \to \infty$ in (3.10), applying Lemma 2.8 and using Equations (3.8) and (3.9) yield

$$\lim_{k\to\infty} \mathcal{C}(l_{y(k)}, l_{i(k)}, \varphi) = \epsilon. \qquad (3.11)$$

On similar steps, it follows from (3.3) that

$$\mathcal{L}(l_{y(k)}, l_{i(k)}, \varphi) = \max\left\{\begin{array}{l} \sigma(l_{y(k)}, l_{y(k)}) + \sigma(l_{y(k)}, l_{i(k)}) + \varphi(l_{y(k)}) + \varphi(l_{i(k)}), \\ \sigma(l_{i(k)}, l_{i(k)}) + \sigma(l_{i(k)}, \mathrm{Y}l_{i(k)}) + \varphi(l_{i(k)}) + \varphi(\mathrm{Y}l_{i(k)}) \end{array}\right\}$$

$$= \max\left\{\begin{array}{l} \sigma(l_{y(k)}, l_{y(k)}) + \sigma(l_{y(k)}, l_{i(k)}) + \varphi(l_{y(k)}) + \varphi(l_{i(k)}), \\ \sigma(l_{i(k)}, l_{i(k)}) + \sigma(l_{i(k)}, l_{i(k)+1}) + \varphi(l_{i(k)}) + \varphi(l_{i(k)+1}) \end{array}\right\}.$$

Thus,

$$\lim_{k\to\infty} \mathcal{L}(l_{y(k)}, l_{i(k)}, \varphi) = \epsilon. \qquad (3.12)$$

From (3.1), we have

$$\psi(\sigma(l_{y(k)+1}, l_{y(k)+1}) + \sigma(l_{y(k)+1}, l_{i(k)+1}) + \varphi(l_{y(k)+1}) + \varphi(l_{i(k)+1})$$
$$\leq \psi(\mathcal{C}(l_{y(k)}, l_{i(k)}, \varphi)) - \phi(\mathcal{L}((l_{y(k)}, l_{i(k)}, \varphi)). \qquad (3.13)$$

Letting $k \to \infty$ in (3.13), and using Lemma 2.8, the continuity of ψ, the lower semi-continuity of ϕ and by using Equations (3.9), (3.11) and (3.12), we obtain $\psi(\epsilon) \leq \psi(\epsilon) - \phi(\epsilon)$, which is a contradiction because $\phi(\epsilon) > 0$. Therefore, $\{l_y\}_{y\in\mathbb{N}}$ is a Cauchy sequence. The completeness of X implies that there exists $u \in X$ such that $\lim_{y\to\infty} l_y = u$. Given that ϕ is lower semi-continuous, $\varphi(u) \leq \liminf_{y\to\infty} \varphi(l_y) \leq \lim_{y\to\infty} \varphi(l_y) = 0$, from which it follows that $\varphi(u) = 0$.

Now, from (3.2) we obtain

$$C\left(l_{y(k),u.\varphi}\right)=\max\left\{\begin{array}{c}\sigma(l_y,l_y)+\sigma(l_y,u)+\varphi(l_y)+\varphi(u),\\ \sigma(l_y,\Upsilon l_y)+\varphi(l_y)+\varphi(\Upsilon l_y),\\ \sigma(u,u)+\sigma(u,\Upsilon u)+\varphi(u)+\varphi(\Upsilon u)\\ \frac{1}{2}\left[\sigma(l_y,\Upsilon u)+\varphi(l_y)+\varphi(\Upsilon u)+\sigma(u,\Upsilon l_y)+\varphi(u)+\varphi(\Upsilon l_y)\right]\end{array}\right\}$$

$$=\max\left\{\begin{array}{c}\sigma(l_y,l_y)+\sigma(l_y,u)+\varphi(l_y)+\varphi(u),\sigma(l_y,l_{y+1})+\varphi(l_y)+\varphi(l_{y+1}),\\ \sigma(u,u)+\sigma(u,\mathrm{Y}u)+\varphi(u)+\varphi(\mathrm{Y}u),\frac{1}{2}[\sigma(l_y,\mathrm{Y}u)+\varphi(l_y)+\varphi(\mathrm{Y}u)+\sigma(u,l_{y+1})\\ +\varphi(u)+\varphi(l_{y+1})]\end{array}\right\},$$

from which we have

$$\lim_{y\to\infty}\mathcal{C}(l_y,u,\varphi)=\lim_{y\to\infty}\max\{\sigma(u,u),\sigma(u,u)+\sigma(u,\mathrm{Y}u)+\varphi(\mathrm{Y}u),\frac{1}{2}[\sigma(u,u)+\sigma(u,\mathrm{Y}u)+\varphi(\mathrm{Y}u)]$$

$$=\sigma(u,u)+\sigma(u,\mathrm{Y}u)+\varphi(\mathrm{Y}u). \qquad (3.14)$$

In like manner, we have

$$\lim_{y\to\infty}\mathcal{L}(l_y,u,\varphi)=\lim_{y\to\infty}\max\{\sigma(l_y,l_y)+\sigma(l_y,u)+\varphi(l_y)+\varphi(u),\sigma(u,u)+\sigma(u,\mathrm{Y}u)+\varphi(u)+\varphi(\mathrm{Y}u)\}$$

$$=\max\{\sigma(u,u),\sigma(u,u)+\sigma(u,\mathrm{Y}u)+\varphi(\mathrm{Y}u)\}$$

$$=\sigma(u,u)+\sigma(u,\mathrm{Y}u)+\varphi(\mathrm{Y}u). \qquad (3.15)$$

Therefore, from (3.1), we have

$$\psi(\sigma(l_{y+1},l_{y+1})+\sigma(l_{y+1},\mathrm{Y}u)+\varphi(l_{y+1})+\varphi(\mathrm{Y}u))$$

$$=\psi(\sigma(\mathrm{Y}l_y,\mathrm{Y}l_y)+\sigma(\mathrm{Y}l_y,\mathrm{Y}u)+\varphi(\mathrm{Y}l_y)+\varphi(\mathrm{Y}u))$$

$$\leq\psi(C(l_y,u,\varphi))-\phi(L(l_y,u,\varphi)). \qquad (3.16)$$

Letting $y\to\infty$ in (3.16) and employing the continuity of ψ, the lower continuity of ϕ and using Equations (3.14) and (3.13), we have

$$\psi(\sigma(u,u)+\sigma(u,\mathrm{Y}u)+\varphi(\mathrm{Y}u))$$

$$\leq\psi(\sigma(u,u)+\sigma(u,\mathrm{Y}u)+\varphi(\mathrm{Y}u))-\phi(\sigma(u,u)+\sigma(u,\mathrm{Y}u)+\varphi(\mathrm{Y}u)). \qquad (3.17)$$

The expression (3.17) implies that $\phi(\sigma(u,\mathrm{Y}u)+\varphi(\mathrm{Y}u)+\sigma(u,u))=0$ and hence

$\sigma(u,\mathrm{Y}u)+\varphi(\mathrm{Y}u)+\sigma(u,u)=0$. Therefore,

$$u=\Upsilon u,\varphi(\Upsilon u)=0 \text{ and } \sigma(u,u)=0.$$

To show that the fixed point of T is unique, suppose that p is another fixed point of T with $x=u$ and $y=p$. Then, $p=Tp$ and $\varphi(p)=0$. Now, using (3.1), we have

$$\psi(\sigma(u,u)+\sigma(u,p))+\varphi(u)+\varphi(p))=\psi(\sigma(Tu,Tu)+\sigma(Tu,Tp)+\varphi(Tu)+\varphi(Tp))$$

$$\leq\psi(\mathcal{K}(u,p,\varphi))-\phi(\mathcal{L}(u,p,\varphi))$$

$$=\psi(\sigma(u,u)+\sigma(p,u))-\phi(\sigma(u,u)+\sigma(p,u)). \qquad (3.18)$$

From, (3.18), it is clear that $\psi(\sigma(u,p)) \leq \psi(u,p)) - \phi(\sigma(u,p))$. From which $\phi(\sigma(u,p)) \leq 0$. But $0 \leq \phi(\sigma(u,p)) \leq 0$. That is, $\phi(\sigma(u,p)) = 0$. Hence, by the defining property of $\phi, \sigma(u,p) = 0$. Therefore, condition $\sigma_{(1)}$ of metric-like reveals that $u = p$.

We construct the following example to verify the hypotheses of Theorem Theorem 3.2.

Example 3.3

Let $X = 0,1,2$ together with the metric $\sigma: X \times X \in R_+$ defined by $\sigma(0,0)$

$\sigma(0,0) = \sigma(1,1) = 0$, $\sigma(0,1) = \sigma(1,0) = \frac{1}{2}$, $\sigma(0,2) = (2,0) = \frac{2}{5}$, $\sigma(2,2) = \frac{9}{20}$,

$\sigma(1,2) = \sigma(2,1) = \frac{3}{5}$. Then, (X, σ) is a σ-complete metric-like space. Notice that $\sigma(2,2) \neq 0$. Hence, σ is not a metric. In addition, $\sigma(2,2) > \sigma(2,0)$, implying that σ is not a partial metric. Define a self-mapping $Y: X \times X$ by $Y(0) = Y(1) = 0$ and $Y(2) = 1$ .To see that Y is a generalized quasi-weakly contractive operator, let $\psi(t) = \frac{4t}{5}$, $\phi(t) = \frac{2t}{5}$ and $\varphi(t) = \frac{3t}{5}$. We then consider the following cases:

$[Case1:]$ $l, m \in X, l = m;$

$[Case2:]$ $l, m \in X, l \neq m$

We demonstrate using the following Table 1 that inequality in Equation 3.1 is satisfied for each of the above cases.

Table 1

Cases	L	M	LHS of (3.1)	RHS of (3.1)
Case 1	0	0	0	0
	1	1	0	0.48
	2	2	0.96	1.32
Case 2	0	1	0	0.44
	0	2	0.88	1.14
	1	0	0	0.44
	1	2	0.88	1.14
	2	0	0.88	1.1
	2	1	0.88	1.14

In the following Figure 1, we illustrate the validity of contractive inequality (3.1) using Example 1.

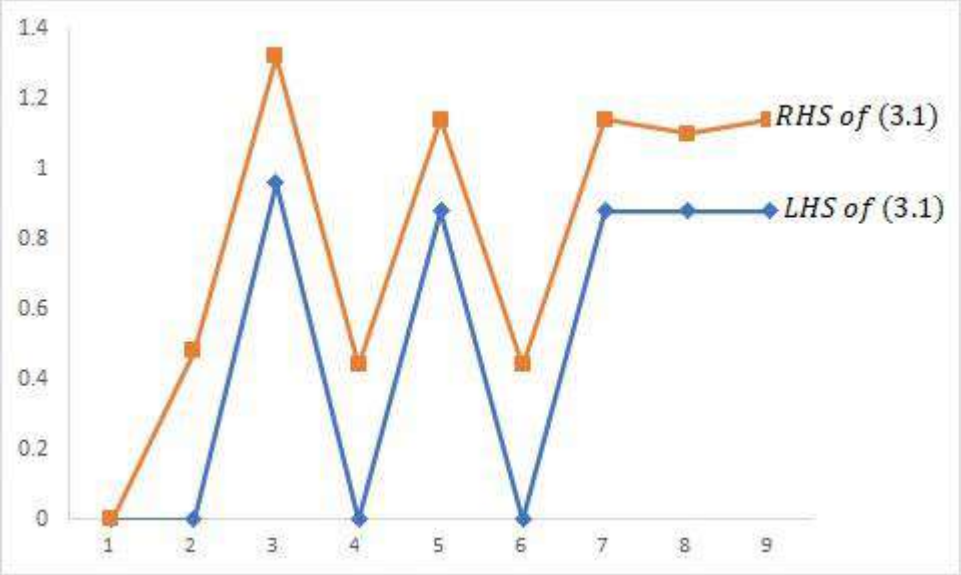

Figure 1 Illustration of contractive inequality (3.1) using Example 3.3.

Therefore, all the hypotheses of Theorem 3.2 are satisfied, and Y has a unique fixed point, $\boldsymbol{l = 0}$. Consequently, Y is a generalized quasi-weakly contractive operator.

To see that the generalized quasi-weakly contractive operator intro-duced in this manuscript is not the generalized weakly contractive operator introduced by Cho [6], let $\boldsymbol{X}$ be equipped with the Euclidean metric $\boldsymbol{d}$. Then, $(\boldsymbol{X}, \boldsymbol{d})$ is a complete metric space. However, taking any points $\boldsymbol{l, m} \in \{\mathbf{1}, \mathbf{2}\} \subset \boldsymbol{X}$, we see that

$$\psi(\sigma(\mathrm{Y}l, \mathrm{Y}m) + \varphi(\mathrm{Y}l) + \varphi(\mathrm{Y}m) = \frac{4}{5}\left(\frac{8}{5}\right) = \frac{32}{25}$$

$$> \frac{28}{25} = \frac{4}{5}\left(\frac{14}{5}\right) - \frac{2}{5}\left(\frac{14}{5}\right)$$

$$= \frac{4}{5}\left(\max\left(\frac{14}{5}, \frac{14}{5}, \frac{8}{5}, \frac{11}{5}\right)\right) - \frac{2}{5}\left(\max\left(\frac{14}{5}, \frac{8}{5}\right)\right).$$

Therefore, the generalized quasi-weakly contractive operator is not the generalized weakly contractive mapping defined by Cho [6], and so Theorem 3.2 due to Cho [6] is not applicable to this example.

In what follows, we present some consequences of Theorem 3.2.

Corollary 3.4. Let (X, σ) be a σ −complete metric-like space. Suppose that the self-mapping Υ satisfies the following condition:

$$\psi(\sigma(\mathrm{Y}l, \mathrm{Y}l) + \sigma(\mathrm{Y}l, \mathrm{Y}m) + \varphi(\mathrm{Y}l) + \varphi(\mathrm{Y}m)) \leq \psi(\mathcal{C}(l, m, \varphi)) - \phi(\mathcal{C}(l, m, \varphi)), \qquad (3.19)$$

for all $l, m \in X$, where $\psi \in \Psi$ and $\phi, \varphi \in \Phi$. Then, there exists a unique $u \in X$

such that $u = \Upsilon u$ and $\varphi(u) = 0$.

By taking $\phi(t) = 0$, for all $t \in R_+$, we have the next result.

Corollary 3.5. Let (X, σ) be a σ −complete metric-like space. Assume that the self-mapping Υ satisfies the following condition:

$$\psi(\sigma(\Upsilon l, \Upsilon l) + \sigma(\Upsilon l, \Upsilon m) + \varphi(\Upsilon l) + \varphi(\Upsilon m)) \leq \psi(\mathcal{C}(l, m, \varphi)), \quad (3.20)$$

for all $l, m \in X$, where $\psi \in \Psi$. Then, there exists a unique $u \in X$ such that $u = \Upsilon u$ and $\varphi(u) = 0$.

Corollary 3.6. Let (X, σ) be a σ −complete metric-like space. Suppose that the self-mapping Υ satisfies the following condition:

$$\psi(\sigma(\Upsilon l, \Upsilon l) + \sigma(\Upsilon l, \Upsilon m) + \varphi(\Upsilon l) + \varphi(\Upsilon m)) \leq \psi(\sigma(l, l) + \sigma(l, m) + \varphi(l) + \varphi(m)) - \phi(\sigma(l, l) + \sigma(l, m) + \varphi(l) + \varphi(m)), \quad (3.21)$$

for all $l, m \in X$, where $\psi \in \Psi$ and $\phi, \varphi \in \Phi$. Then, there exists a unique $u \in X$ such that $u = \Upsilon u$ and $\varphi(u) = 0$.

4. Conclusion

As a generalization of Banach's fixed point theorem, Amini-Harandi introduced the concept of metric-like space and derived some related fixed-point results in such space. In this manuscript, the notion of generalized quasi-weakly contractive operators in metric-like space is introduced and conditions for the existence of fixed points for such mappings are investigated. Non-trivial comparative examples have been presented to illustrate the proposed ideas and to show that they are indeed generalizations of a few concepts in the literature.

References

[1] Aber, Y., Guerre-Delabriere, S. (2011). Principles of weakly contractive maps in Hilbert spaces. New Results in Operator Theory. Ad- vances and Application, vol 98, page: 7-12.

[2] Birkhäuser, Basel(1977) Topol- ogy and its Applications 157,2778-2785 (2010).

[3] Amini-Harandi, A. (2012). Metric-like spaces, partial metric spaces and fixed points. Fixed Point Theory and Applications, 2012, Article ID: 204.

[4] Aydi, H., Karapinar, E., Erhan, I.M., Salimi, P. (2014). Best proximity points of generalized almost ψ-Geraghty contractive non-self-mappings. Fixed Point Theory and Applications, 2014(164), DOI:10.1186/1687-1812-2014-32.

[5] Bakhtin, I. (1989). The contraction mapping principle in quasi metric spaces. Functional Analysis, 30, 26-37.

[6] Cho, S. (2012). Fixed point theorems for generalized weakly contractive map- pings in metric spaces with application. Fixed Point Theory and Applications, 2018(3), DOI:10.1186/s13663-018-0628-1.

[7] Ćirić, L. B. (1974). A generalization of Banach's contraction principle. Pro- ceedings of the American Mathematical Society, 45(2), 267-273.

[8] Czerwik, S. (1993). Contraction mappings in b-metric spaces. Acta mathematica et informatica universitatis ostraviensis, 1(1), 5-11.

[9] Matthews, S.G. (1994). Partial metric topology. Annals New York Academy of Science, 728, 183-197.

[10] Wilson, W.A. On quasi-metric spaces. American Journal of Mathematics, vol 53, 675-684.

A Fixed Point Theorem of Hardy-Rogers-Type F-Contraction in C^*-Algebra Valued Metric Space

Zulaihatu Tijjani Ahmad[1] and Mohammed Shehu Shagari[2]

Department of Mathematics, Faculty of Physical Sciences, Ahmadu Bello University, Zaria, Nigeria

[1]ahmadzulaihatj@gmail.com

[2]shagaris@ymail.com

Abstract

Many researchers have studied different contractive Mappings in C^*-algebra valued metric space and their related fixed point results. However, a hybrid of Hardy-Rogers and F-contraction has not been adequately examined. Hence, this paper proposes a more general fixed point result involving the aforementioned contractive operators in C^*-algebra valued metric space. The result obtained in this work extends a few corresponding ones in the literature.

Keywords: C^*-algebra valued metric space, F-contraction, Hardy-Rogers contraction

1. Introduction

The theory of fixed point is an imminent area for various branches of mathematics and physics due to its broad applications. It is of great significance in numerical analysis and approximation theory. The earliest fixed point result known as the Banach Contraction Principle was proved by Banach in 1922. Thereafter, Many researchers studied the fixed point theory in different directions, for example, see Afra (2014), Gholamian *et al*. (2015), Wardowski (2012) and the references therein.

A C^*-algebra (see Sakai, 1971) is employed to describe physical systems in quantum theory and statistical mechanics. Subsequently, it appeared as a significant area of research. In 2014, Ma *et al*. initiated the notion of C^*-algebra valued metric space and proved fixed point theorems for contractive and expansive mappings on a complete C^*-algebra valued metric space. Since then, several authors e.g., Asim and Imdad (2020), Bai (2016), Batul and Kamran (2015), Kumar *et al*. (2021) have extended and generalized the work of Ma *et al*. (2014) in different directions with interesting theorems and applications.

In this article, motivated by the work of Shagari *et al*. (2022), Hardy and Rogers (1973), we study fixed point result of F-contraction of Hardy-Rogers type in C^*-algebra valued metric space. The result established in this work is an extension of some corresponding ones in the literature.

2. Literature Review

In this work, we assign a unital C^*-algebra by $\mathbb{A}$, X as a nonempty set, $\mathbb{A}_+$ denotes the set $\{a \in \mathbb{A} : a \geq \theta\}$ and $|a| = (a * a)^{\frac{1}{2}}$ where θ means the zero element in $\mathbb{A}$. We first give the definition of a C^*-algebra metric space due to Ma *et al*. (2014).

Definition 2.1. (Ma *et al*., 2014) Let X be a nonempty set. Suppose the mapping $d : X \times X \longrightarrow \mathbb{A}$ satisfies;

1) $\theta \preceq d(x,y)$ and $d(x,y) = \theta \Leftrightarrow x = y$ for all $x, y \in X$;
2) $d(x,y) = d(y,x)$ for all $x, y \in X$;
3) $d(x,y) \preceq d(x,z) + d(z,y)$ for all $x, y, z \in X$

Then d is called a C^*-algebra-valued metric on X and $(X, \mathbb{A}, d)$ is called a C^*-algebra-valued metric space. This concept generalizes the concept of metric space by replacing the set of real numbers by $\mathbb{A}_+$

Definition 2.2. (Ma *et al*., 2014) Let $(X, \mathbb{A}, d)$ be a C^*-algebra-valued metric space. Suppose that $(x_n)_n \subset X$ and $x \in X$, if for any $\varepsilon > 0$, there is N such that for all $n > N$, $\| d(x_n, x) \| \leq \varepsilon$, then $(x_n)_n$ is said to be convergent with respect to $\mathbb{A}$ and (x_n) converges to x. (x_n) is said to be a Cauchy sequence with respect to $\mathbb{A}$ If for any $\varepsilon > 0$, there is N such that for all $n, m > N$, $\| d(x_n, x_m) \| \leq \varepsilon$. $(X, \mathbb{A}, d)$ Is a complete C^*-algebra-valued metric space if every Cauchy sequence with respect to $\mathbb{A}$ is convergent.

Definition 2.3. (Ma *et al*., 2014) Suppose that $(X, \mathbb{A}, d)$ is C^*-algebra-valued metric space. A mapping $T : X \longrightarrow X$ is said to be a C^*-algebra -valued contractive mapping on X, if there exists an $A \in \mathbb{A}$ with $\|A\| < 1$ such that

$$d(T x, T y) \preceq A^* d(x,y) A, \qquad \forall x, y \in X.$$

Theorem 2.3. (Ma *et al*. 2014) If $(X, \mathbb{A}, d)$ is a complete C^*-algebra-valued metric space and T is a contractive mapping, then there exists a unique fixed point in X.

Theorem 2.4. (Hardy and Rogers, 1973): Let (X, d) be a metric space and T be a self-mapping satisfying the condition for $x, y \in X$

$$d(Tx,Ty) \leq ad(x,Tx) + bd(y,Ty) + cd(x,Ty) + ed(y,Tx) + f(x,y) \qquad (1)$$

Where a, b, c, e, f are nonnegative and we set $\alpha = a + b + c + e + f$. Then

a) If X is complete and $\alpha < 1$, T has a unique fixed point.
b) If (1) is modifies to the condition $x \neq y$ implies

$$d(Tx,Ty) < ad(x,Tx) + bd(y,Ty) + cd(x,Ty) + ed(y,Tx) + f(x,y) \qquad (1')$$

And in this case we assume X is compact, T is continuous and $\alpha = 1$, then T has a unique fixed point.

Definition 2.4. (Shagari *et al*., 2022) Let $F : \mathbb{A}_+ \to \mathbb{A}$ be a mapping that meets the ensuing presumptions:

A1 F is $\leq$ -increasing;

A2 for every sequence $\{A_n\}_{n \in \mathbb{N}} \in \mathbb{A}_+$, if and only if $\lim_{n \to \infty} \| F(A_n) \| = \infty$;

A3 There exists $k \in (0,1)$ such that $\lim_{A \to \theta} A^k F(A) = \theta$.

Denote the family of mappings obeying $(A1)$ - $(A3)$ by $\mathbb{A}_F$.

Definition 2.5. (Shagari *et al*., 2022) Let $(X, \mathbb{A}, d)$ be a C^*-algebra-valued metric space. A mapping $T: X \to X$ is named a C^*-algebra-valued F-contraction if there exists $A \in \mathbb{A}_+$ with $\| A \| < 1$ such that for all $x, y \in X$,

$d(Tx, Ty) \succ \theta$ implies $A + F(d(Tx, Ty)) \leq F(A^* d(x, y) A)$, where $F \in \mathbb{A}_F$.

Theorem 2.6. (Shagari *et al*., 2022) Let $(X, \mathbb{A}, d)$ be a complete C^*-algebra-valued metric space and $T: X \to X$ be a C^*-algebra-valued F-contraction. Then, T has a unique fixed point in X.

3. Results and Discussion

We now study the F-contraction of Hardy-Rogers in C^*-algebra-valued metric space.

Definition 3.1. Let $(X, \mathbb{A}, d)$ be a C^*-algebra-valued metric space. A mapping $T: X \to X$ is called a C^*-algebra-valued F-Contraction of Hardy-Rogers type if there exists $A \in \mathbb{A}_+$ with $\| A \| < 1$ and $\alpha, \beta, \gamma \in \mathbb{A}_+'$ with $\| \alpha \| + 2 \| \beta \| + 2 \| \gamma \| \leq 1$ such that for all $x \in X$, $d(Tx, Ty) \succ \theta \Rightarrow$

$$A + F(d(Tx, Ty)) \leq F\left(\alpha d(x, y) + \beta[d(x, Tx) + d(y, Ty)] + \gamma[d(x, Ty) + d(y, Tx)]\right). \quad (2)$$

Remark 3.2.

i. If $\beta = \gamma = \theta$, the definition above reduces to definition 2.5 of Shagari *et al*. (2022)

ii. If $\alpha = \gamma = \theta$, definition 3.1 reduces to definition of C^*-algebra-valued F-contraction of Kannan type.

iii. If $\alpha = \beta = \theta$, definition 3.1 reduces to definition of C^*-algebra-valued F-contraction of Chatterjea type.

iv. If $\gamma = \theta$, definition 3.1 reduces to definition of C^*-algebra-valued F-contraction of Reich type.

Our main result is presented as follows;

Theorem 3.3. Let $(X, \mathbb{A}, d)$ be a complete C^*-algebra-valued metric space. Suppose that $T: X \to X$ is continuous and T is C^*-algebra-valued F-Contraction of Hardy Rogers type. Then there exists $x \in X$ such that $Tx = x$. Moreover, if either

i. $\| \alpha \| + 2 \| \gamma \| < 1$, or

ii. $\| \beta \| + \| \gamma \| < 1$ and F is continuous,

then the fixed point is unique.

Proof

Choose $x_0 \in X$ and define a sequence $(x_n)_{n\in\mathbb{N}}$ by $x_1 = Tx_0, x_2 = Tx_1 = T^2x_0, \ldots x_{n+1} = Tx_n = T^{n+1}x_0$. If $\mathbb{A} = \theta$, then for all $n \in \mathbb{N}$ $d(x, y) = \theta$ and the result is trivial. Let $d_n = d(x_n, x_{n+1})$ $\forall n \in \mathbb{N} \cup \{0\}$.

Now, suppose $\mathbb{A} \neq \theta$ and that $\theta \prec d(x_n, Tx_n) = d(Tx_{n-1}, Tx_n)$, $n \in \mathbb{N}$. Using the contractive condition (2) with $x = x_{n-1}$ and $y = x_n$, we have

$$A + F(d(Tx_{n-1}, Tx_n)) \leq F\left(\alpha d(x_{n-1}, x_n) + \beta[d(x_{n-1}, Tx_{n-1}) + d(x_n, Tx_n)] + \gamma[d(x_n, Tx_{n-1}) + d(x_{n-1}, Tx_n]\right)$$
$$= F\left(\alpha d(x_{n-1}, x_n) + \beta[d(x_{n-1}, x_n) + d(x_n, x_{n+1})] + \gamma[d(x_{n-1}, x_{n+1}) + d(x_n, x_n)]\right)$$
$$\leq F\left(\alpha d(x_{n-1}, x_n) + \beta[d(x_{n-1}, x_n) + d(x_n, x_{n+1})] + \gamma[d(x_{n-1}, x_n) + d(x_n, x_{n+1})]\right)$$
$$= F\left((\alpha + \beta + \gamma)d(x_{n-1}, x_n) + (\beta + \gamma)d(x_{n+1}, x_n)\right).$$

By the monotonicity of F, we have

$$d(Tx_{n-1}, Tx_n) = d(x_n, x_{n+1}) \leq (\alpha + \beta + \gamma)d(x_{n-1}, x_n) + (\beta + \gamma)d(x_{n+1}, x_n)$$
$$(I - \beta - \gamma)d(x_n, x_{n+1}) \leq (\alpha + \beta + \gamma)d(x_{n-1}, x_n).$$

Since $\| \alpha \| + 2\| \beta \| + 2\| \gamma \| = 1$, then $\dfrac{\| \alpha \| + 2\| \beta \| + 2\| \gamma \|}{\| I \| - \| \beta \| - \| \gamma \|} \leq 1.$

So, $d(x_n, x_{n+1}) \leq \dfrac{\alpha + \beta + \gamma}{I - \beta - \gamma} d(x_{n-1}, x_n) = d(x_{n-1}, x_n).$

Now, $A + F(d_n) \leq F(d_{n-1})$, for all $n \in \mathbb{N}$, which implies

$$F(d_n) \leq F(d_{n-1}) - A \leq F(d_{n-2}) - 2A \leq \ldots \leq F(d_0) - nA$$
$$F(d_n) \leq F(d_0) - nA, \quad \forall n \in \mathbb{N} \qquad (3)$$

Taking the norm on both sides, we obtain $\| F(d_n) \| \to \infty$ as $n \to \infty$.

By$(A2)$,

$$\lim_{n\to\infty} d_n = \theta, \qquad (4)$$

and from $(A3)$

$$\lim_{n\to\infty} \| d_n^k F(d_n) \| = 0 \quad for \quad k \in (0,1). \qquad (5)$$

By (3), we have that for all $n \in \mathbb{N}$,

$$d_n^k F(d_n) - d_n^k F(d_0) \leq d_n^k [F(d_0) - nA] - d_n^k F(d_0)$$
$$= -nd_n^k A \leq \theta.$$

Taking the limit on both sides and using (4) and (5) in the above inequality, we obtain

$$\lim_{n\to\infty} \| d_n^k F(d_n) \| = 0.$$

Hence, there exists an $n_0 \in \mathbb{N}$ with $\theta \prec nd_n^k A \leq I$, for all $n \geq n_0$. Then,

$$\| d_n \| \leq \frac{1}{\| A \| n^{\frac{1}{k}}}, \quad \forall n \geq n_0.$$

So, for $n, p \in \mathbb{N}$ with $p > 1$, we have

$$d(x_n, x_{n+p}) \le d(x_n, x_{n+1}) + d(x_{n+1}, x_{n+2}) + \ldots + d(x_{n+p-1}, x_{n+p}) = d_n + d_{n+1} + \ldots + d_{n+p-1}$$

$$= \sum_{i=n}^{n+p-1} d_i \le \left\| \sum_{i=n}^{\infty} d_i \right\| I \le \sum_{i=n}^{\infty} \| d_i \| I = \sum_{i=n}^{\infty} \left\| \frac{A^{-1}}{i^{\frac{1}{k}}} \right\| I$$

$$\le \| A \|^{-1} \sum_{i=n}^{\infty} \left\| \frac{1}{i^{\frac{1}{k}}} \right\| I \le \sum_{i=n}^{\infty} \left\| \frac{1}{i^{\frac{1}{k}}} \right\| I$$

$$d(x_n, x_{n+p}) \le \sum_{i=n}^{\infty} \left\| \frac{1}{i^{\frac{1}{k}}} \right\| I$$

Clearly, the series above is convergent, i.e. $\| d_n \| \to 0$ as $n \to \infty$. This implies that $(x_n)_{n \in \mathbb{N}}$ is a Cauchy sequence in $(X, \mathbb{A}, d)$ and by completeness of the space, there exists $x \in X$ with $\lim_{n\to\infty} x_n = \lim_{n\to\infty} Tx_{n-1} = x$. Since T is continuous with respect to $\mathbb{A}$, then

$$d(x, Tx) = \| d(x_n, \lim_{n\to\infty} Tx_n) \| = \| \lim_{n\to\infty} d(x_n, x_{n+1}) \|$$

$$= \lim_{n\to\infty} \| d(x_n, x_{n+1}) \|$$

$$= \| d(x, x) \| = 0.$$

This implies $d(x, Tx) = \theta \iff Tx = x$.

To show uniqueness, we assume $y (\neq x)$ is another fixed point of T. Then from (2),

$$A + F(d(x, y)) = A + F(d(Tx, Ty))$$
$$\le F(\alpha d(x, y) + \beta[d(x, Tx) + d(y, Ty)] + \gamma[d(x, Ty) + d(y, Tx)])$$
$$= F(\alpha d(x, y) + \beta[d(x, x) + d(y, y)] + \gamma[d(x, y) + d(y, x)])$$
$$= F\left((\alpha + 2\gamma) d(x, y)\right).$$

Since $\| \alpha \| + 2 \| \gamma \| < 1$ and by *(A1)*,

$$\| d(x, y) \| \le \| (\alpha + 2\gamma) d(x, y) \| < \| d(x, y) \|,$$

a contraction. Hence $x = y$.

Similarly, suppose F is continuous and assume contrary that the fixed point is not unique, then

$$A + F(d(x_{n+1}, x)) = A + F(d(Tx_n, Tx))$$
$$\le F(\alpha d(x_n, x) + \beta[d(x_n, Tx_n) + d(x, Tx)] + \gamma[d(x_n, Tx) + d(x, Tx_n)])$$
$$= F(\alpha d(x_n, x) + \beta[d(x_n, x_{n+1}) + d(x, Tx)] + \gamma[d(x_n, Tx) + d(x_n, x_{n+1})]).$$

Letting $n \to \infty$ and given that $\| \alpha \| + \| \gamma \| < 1$, we obtain

$$A + F(d(x, Tx) \le F((\beta + \gamma) d(x, Tx)) \le F(d(x, Tx)),$$

a contradiction. Hence the fixed point is unique.

Corollary 3.4. Let $(X, \mathbb{A}, d)$ be a complete C^*-algebra-algebra-valued metric space. Suppose that $T: X \to X$ is continuous and T is C^*-algebra-valued F-Contraction of Kannan type. Then there exists $x \in X$ such that $Tx = x$. Moreover, if either i) or ii) of Theorem 3.3 above is satisfied then the fixed point is unique.

Proof. Put $\alpha = \gamma = \theta$ in Theorem 3.3.

Corollary 3.5. Let $(X, \mathbb{A}, d)$ be a complete C^*-algebra-algebra-valued metric space. Suppose that $T: X \to X$ is continuous and T is C^*-algebra-valued F-Contraction of Chatterjea type. Then there exists $x \in X$ such that $Tx = x$. Moreover, if either i) or ii) of Theorem 3.3 above is satisfied then the fixed point is unique.

Proof. Put $\alpha = \beta = \theta$ in Theorem 3.3.

Corollary 3.6. Let $(X, \mathbb{A}, d)$ be a complete C^*-algebra-algebra-valued metric space. Suppose that $T: X \to X$ is continuous and T is C^*-algebra-valued F-Contraction of Reich type. Then there exists $x \in X$ such that $Tx = x$. Moreover, if either i) or ii) of Theorem 3.3 above is satisfied then the fixed point is unique.

Proof. Put $\gamma = \theta$ in Theorem 3.3.

4. Conclusion

Hardy and Rogers (1973) proved a fixed point theorem of a generalization of Reich Contraction in metric space. In the present paper, we have extended Hardy-Rogers type mapping to a more general setting and established the corresponding fixed point, which can be used to solve some integral and differential equations. The result obtained in this work can be extended to a more general space like C^*-algebra- valued Partial b-metric space and some other dislocated metric space.

References

Afra, J. M. (2014), Fixed point type theorem in s-metric spaces, *Middle-East Journal of Scientific Research*, Vol. 22(6), 864–869.

Asim, M. and Imdad, M. (2020), C^*-algebra valued symmetric spaces and fixed point results with an Application, *Korean Journal of Mathematics*, Vol. 28(1), 17–30.

Bai C. (2016), Coupled fixed point theorems in C^*-algebra-valued b-metric spaces with application, *Journal of Operator theory*, Vol. 70.

Batul, S. and Kamran, T. (2015), C^*-valued contractive type mappings, *Journal of Fixed point theory and application*, Vol. 142.

Banach, S. (1922), Sur les operations dans les ensembles abstraits et leur application aux equations ´integrales. *Fundamental. Mathematica*, Vol. 3, 133–181.

Gholamian, N., Khanehgir, M. and Allahyari, R. (2017), Some fixed point theorems for C^*-algebra-valued b_2-metric spaces, *Journal of Mathematics Extention*, Vol. 11(2), 53–69.

Hardy, G. E. and Rogers, T. D. (1973), A generalization of a fixed point theorem of Reich, *Canadian Mathematics Bulleting,* Vol. 16(2).

Kumar, D., Rishi, D., Park C. and Lee J. R. (2021), On fixed point in C^*-algebra valued metric spaces using C^*-class function, *International Journal of Nonlinear Analysis and Application*, Vol. 12(2), 1157–1161.

Sakai, S. (1971), C^*-algebras and W^*-algebra. *Springer-Verlag Berlin Heidelberg*, New York,

Shagari, M. S., Alotaibi, T., Mohamed O. S., Mustafa A. O. and Bakery, A. A. (2022), On existence results of volterra-type integral equations via C^*-algebra -valued f-contractions. *AIMS Mathematics*, Vol. 8(1), 1154–1171.

Wardowski, D. (2012), Fixed points of a new type of contractive mappings in complete metric spaces. *Journal of Fixed Point Theory and Application*, Vol. 94.

A Study on Fuzzy Product Lower Approximation Operators

Mustapha Mannir Gafai[1*] and Danjuma Muhammad Auwal.[2]

[1,2]Department of Mathematics and Statistics, Faculty of Natural and Applied Sciences, Umaru Musa Yar'adua University Katsina, Nigeria

[1*]mmannirgafai@gmail.com

[2]auwalmuhammad1@umyu.edu.ng

Abstract

In this paper, we propose an approximation operators for fuzzy product rough sets (X, R), where X is a non-empty set and R is a product similarity relation on X. We also provide axiomatics to fully characterize those approximation operators. The method employed was by relaxing the R-implication of the lower semi-continuous t-norm already in the literature and adopting a Goguen implication, which is the R-implication of the product t-norm. The results obtained presents a way of computing the lower approximation operators, specifically for the product t-norm. Some related propositions and examples were also provided.

Keywords: Fuzzy-rough sets, fuzzy sets, lower approximation operator,product similarity relation, rough sets.

1. Introduction

Rough set theory proposed by Pawlak (1982) is concerned with the analysis of imprecise, uncertain or incomplete information and knowledge. The basic concept of rough set is the approximation of lower and upper spaces of a set, the approximation being the formal classification of knowledge regarding the domain of interest. Let R be a fuzzy equivalence relation, then; the lower approximation of a non empty set X with respect to R is the set of all objects which can certainly be classified in X, and the upper approximation of a non empty set X with respect to R is the set of all objects which can possibly be classified in X. If the boundary region of a non empty set X is the difference between its lower and upper approximations. If its boundary region is empty, then the set is *crisp* otherwise it is *rough*.

There are two approaches to the development of fuzzy rough set. One is the constructive approach in which the lower and upper approximation operators are constructed from fuzzy relation, the other is the axiomatic approach in which the lower and upper approximation operators satisfies a set of axioms.

The constructive approach is suitable for practical application of rough set, while the axiomatic approach is more appropriate in studying the structures of rough set algebras, takes the lower and upper approximation operators as primitive notions. In this paper, axiomatic approach will be used to establish a fuzzy product-lower approximation operator.

Throughout this paper,Π represent a product, I^X represent a fuzzy set on a set X, $I^{X\times X}$ represent a fuzzy binary relation on X, $\bigwedge$ represent an infimum and $\underline{\underline{\alpha}}$ represent a constant fuzzy set.

2. Literature Review

Fuzzy rough sets proposed by Dubois and Prade (1982) is an extension of the classical rough set theory, incorporating the concept of fuzziness to handle the problems of uncertainty and imprecision in data. Classical rough set theory, developed by Pawlak (1965) is a mathematical approach for dealing with imprecision, vagueness and uncertainty in data analysis. Fuzzy rough sets are characterized by the lower and upper approximations. The lower approximation represents the elements that certainly belong to the set, while the upper approximation represents the elements that possibly belong to the set. There are two approaches to the development of fuzzy rough set. One is the constructive approach in which the lower and upper approximation operators are constructed from fuzzy relation; the other is the axiomatic approach in which the lower and upper approximation operators satisfy a set of axioms. The constructive approach is suitable for practical application of rough set. On the other hand, the axiomatic approach which is appropriate for studying the structures of rough set algebras, takes the lower and upper approximation operators as primitive notions. Morsi and Yakout (1998) studied a set of axioms on fuzzy T-rough sets defined by a triangular norm and R-implication. However, their studies were restricted to the fuzzy rough set algebras constructed from similarity relations. In order to solidify the theory Radzikowska and Kerre (2002) through a comparative study of fuzzy rough sets presented a more general approach to the fuzzification of rough sets. Basic properties of rough sets were investigated. In particular, they define three properties of fuzzy rough sets relatively to three main classes of implication, and analyzed their properties in the contest of the basic rough equalities. Another important study about attribute reduction on fuzzy rough set concept was made by Salido and Murakami (2003), in their work, they define the more general type of fuzzy system and propose a strong infrastructure about attribute reduction application based on fuzzy rough set that can be used by constructive approaches. In their approach they used T-similarity relation which is reflexive, symmetric and have a transitive property. An axiomatic characterization of a fuzzy generalization of

rough sets by Mi and Zhang (2004) represents that in rough set theory, the lower and upper approximation operators defined by a fixed binary relation satisfies many interesting properties. The assumptions which permit a given fuzzy theoretic operator to represent an upper or lower approximation derived from a special fuzzy relation. Different classes of fuzzy rough set algebras are obtained from different types of fuzzy relations. Fuzzy-rough set-based feature selection (FS) has been shown by Cao et al (2003) to be highly useful at reducing data dimensionality but possesses several problems that renders it ineffective for large datasets.

The paper by Wu and Zhang (2004) presents a general framework for the study of fuzzy rough sets in which both constructive and axiomatic approaches are used. Tsang et al. (2005) proposed an algorithm based on discernibility matrix that can find all reduction on a fuzzy database. However, in their algorithm T-norm was used for the purpose of constructing and aggregating fuzzy similarities. Wu et al. (2003) as the dual of axiomatic systems for lower approximation, axiomatic characterization of rough set and fuzzy set without any restriction on the cardinality of the universe is also given. Beg and Rashid (2016) introduced a modified soft fuzzy rough set model, they also presented the lower and upper approximation operators and investigated their related properties. Gafai and Zulkifilu (2023) proposed an axiomatic definition for fuzzy Π-rough sets and its upper approximation operators.

3. Methodology

Axiomatic approach will be used to relaxed the T-residuated implication ϑ_T from the already existing literatures. Meanwhile, *Goguen* implication ϑ_Π shall be adopted to establish new results; the fuzzy Π-lower approximation operators.

Definition 3.1 (Morsi, 1995) A triangular norm is a binary operation on the unit interval I = [0, 1] that is associative, symmetric, monotone in each argument and has a neutral element 1

Definition 3.2 (Klement *et al*., 2004) A triangular norm T is continuous if for all convergent sequence $\{x_n\}_{n\in N}$, $\{y_n\}_{n\in N}$ we have,

$$T(\lim_{n\to\infty} x_n, \lim_{n\to\infty} y_n) = \lim_{n\to\infty} T(x_n, y_n) \quad (1)$$

Definition 3.3 (Klement *et al*., 2004) A triangular norm T is said to be left-continuous if for each y ∈[0, 1] and all non-decreasing sequence $\{x_n\}_{n\in N}$we have,

$$\lim_{n\to\infty} T(x_n, y) = T(\lim_{n\to\infty} x_n, y) \quad (2)$$

Definition 3.4 (Fodor, 2004) A triangular norm T is lower semi-continuous if and only if it is left-continuous in its first component.

Given a lower semi-continuous triangular norm T, the following binary operation on I defined ∀ α, γ ∈I by;

$$\vartheta_T(\alpha,\gamma) = \text{Sup}\{\theta \in I \mid \alpha T \theta \leq \gamma\} \quad (3)$$

is called residuation implication of T or T-residuated implication (U. Hohle, 1982).

The most popular continuous triangular norms are Minimum (denoted by m or ∧), Product (denoted by p or Π) and Lukasiewicz conjunction (denoted by T_m or W) respectively defined as, for all α, β ∈ I,

$$\alpha \wedge \beta = \min\{\alpha, \beta\} \quad (4)$$

$$\alpha \Pi \beta = \alpha\, \beta \quad (5)$$

$$\alpha \, W \, \beta = \max\{\, \alpha + \beta - 1, 0 \,\} \quad (6)$$

Their residuation implications are respectively given as follows, for all α, γ ∈ *I*by;

$$\vartheta_\wedge(\alpha,\beta) = \begin{cases} 1, & \alpha \leq \beta \\ \beta, & \alpha > \beta \end{cases} \quad (7)$$

Alternatively known as Brouwerian implication,

$$\vartheta_\Pi(\alpha,\beta) = \begin{cases} 1, & \alpha \leq \beta \\ \frac{\beta}{\alpha}, & \alpha > \beta \end{cases} \quad (8)$$

Alternatively known as the Goguen implication or the Gaines implication,

$$\vartheta_W(\alpha,\beta) = \begin{cases} 1, & \alpha \leq \beta \\ 1 - \alpha + \beta, & \alpha > \beta \end{cases} \quad (9)$$

Also known as Lukasiewicz implication (Mizumoto and Zimmermann, 1982).

Definition 3.5 (Gafai and Zulkifilu, 2023) A fuzzy binary relation R on X ($R \in I^{X\times X}$) is said to be a Π-similarity relation, if $\forall a, b, c \in X$, the following conditions are satisfied;

i. $R(a, a) = 1$ Reflexive

ii. $R(a, b) = R(b, a)$ Symmetric

iii. $R(a, c)\ \Pi\ R(a, b) \leq R(c, b)$ Π-transitive

Definition 3.6 (Gafai and Zulkifilu, 2023) A fuzzy Π-rough set (or a fuzzy Π-approximation space) is a pair (X, R) where R is a Π-similarity relation on X.

Definition 3.7 (Gafai and Zulkifilu, 2023) An operator $\overline{A}$ on I^X is said to be a fuzzy Π-upper approximation operator on Xif the following axioms are satisfied, $\forall \mu \in I^X$, $a, b \in X$ and $\underline{\underline{\alpha}} \in I$,

i. $\overline{A}\mu \geq \mu$

ii. $\overline{A}\overline{A}\mu = \overline{A}\mu$

iii. $\overline{A}\left(\bigvee_{j\in J} \mu_j\right) = \bigvee_{j\in J} \overline{A}\mu_j$

iv. $\overline{A}(1_a)(b) = \overline{A}(1_b)(a)$

v. $\overline{A}\left(\underline{\alpha}\Pi\mu\right) = \underline{\alpha}\Pi\overline{A}\mu$

Proposition 3.8 (Morsi and Yakout, 1998) The T-residuation implication ϑ of a lower semi-continuous triangular norm T, enjoys the following properties, for all α, β, γ ∈ I,

[1] $\vartheta(\gamma, 1) = 1$ and $\vartheta(1, \alpha) = \alpha$,

[2] $\vartheta(,)$is monotone in the right argument,

[3] $\vartheta(,)$ is anti-monotone in the left argument,

[4] $\vartheta(\gamma, \alpha)\mathrm{T}\vartheta(\alpha, \beta) \leq \vartheta(\gamma, \beta)$ (T-transitivity of ϑ)

[5] $\vartheta(\mathrm{V}_{\mathrm{j}\in\mathrm{J}}\,\gamma_{\mathrm{j}}, \alpha) = \Lambda_{\mathrm{j}}\,\vartheta(\gamma_{\mathrm{j}}, \alpha)$

[6] $\vartheta(\gamma, \mathrm{V}_{\mathrm{j}}\,\alpha_{\mathrm{j}}) = \mathrm{V}_{\mathrm{j}}\,\vartheta(\gamma, \alpha\mathrm{j})$

[7] $\gamma \leq \alpha$ iff $\vartheta(\gamma, \alpha) = 1$

[8] $\vartheta(\beta, \vartheta(\gamma, \alpha)) = \vartheta(\gamma, \vartheta(\beta, \alpha))$ (the exchange principle)

[9] $\vartheta(\beta\mathrm{T}\gamma, \alpha) = \vartheta(\beta, \vartheta(\gamma, \alpha)$

[10] $\vartheta(\beta\mathrm{T}\gamma, \alpha)\mathrm{T}\beta \leq \vartheta(\gamma, \alpha)$

[11] $\Lambda_{\alpha\in\mathrm{I}}\,\vartheta(\gamma\mathrm{T}\vartheta(\beta, \alpha), \alpha = \vartheta(\gamma, \beta)$

[12] $\vartheta(\vartheta(\gamma, \alpha), \alpha) \geq \gamma$

[13] $\Lambda_{\alpha\in\mathrm{I}}\,\vartheta(\vartheta(\gamma, \alpha), \alpha) = \gamma$

[14] $\vartheta(\gamma, \alpha)\mathrm{T}\beta \leq \vartheta(\gamma, \alpha\mathrm{T}\beta)$

[15] $\Lambda_{\alpha\in\mathrm{I}}\,\vartheta(\vartheta(\beta, \alpha), \vartheta(\gamma, \alpha) = \vartheta(\gamma, \beta)$

[16] $\vartheta(\gamma, \alpha) \leq \vartheta(\gamma\mathrm{T}\beta, \alpha\mathrm{T}\beta)$

[17] $\vartheta(\gamma, \mathrm{V}_{\mathrm{j}\in\mathrm{J}}\,\alpha_{\mathrm{j}}) \geq \mathrm{V}_{\mathrm{j}\in\mathrm{J}}\,\vartheta(\gamma, \alpha\mathrm{j})$

[18] $\alpha \leq \vartheta(\beta, \alpha\mathrm{T}\beta)$

4. Results and Discussion

Definition 4.1 An operator $\underline{A}$ on a fuzzy set I^X is said to be a fuzzy Π-lower approximation operator, if it satisfies the following axioms, $\forall \mu, \mu_j, \alpha \in I^X$ and for all $j \in J$ (where J is an indexed set);

$(P1)$. $\underline{A}\mu \leq \mu$.

$(P2)$. $\underline{A}\underline{A}\mu = \underline{A}\mu$.

$(P3)$. $\underline{A}\left(\Lambda_{j\in J}\,\mu_j\right) = \Lambda_{j\in J}\,\underline{A}\mu_j$.

$(P4)$. $\underline{A}\vartheta_{\Pi}\left|1_{\mathrm{x},}\underline{\alpha}\right|(y) = \underline{A}\vartheta_{\Pi}\left|1_{\mathrm{y},}\underline{\alpha}\right|(x)$.

$(P5).\ \underline{A}\vartheta_\Pi\left|\underline{\alpha}, \mu\right| = \vartheta_\Pi\left|\underline{\alpha}, \underline{A}\mu\right|.$

Proposition 4.2 Let R be a Π-similarity relation on X. Define an operator A_R on I^X as follows: for all $\mu \in I^X$ and all $x \in X$:

$$\underline{A}_R\mu(x) = \wedge_{u\in X}\,\vartheta_\Pi(\mathrm{R}(u,x),\mu(u)) \qquad (10)$$

then, $\underline{A}_R\vartheta_\Pi\left|1_x,\ \underline{\alpha}\right|(y) = \vartheta_\Pi(R(x,y),\alpha)$ for all $(x,y,\alpha) \in X \times X \times I$

$\underline{A}_R$ is a Π-lower approximation operator

i.

Proof

(i) $\underline{A}_R\vartheta_\Pi\left|1_{\mathrm{x}},\ \underline{\alpha}\right|(y) = \wedge_{u\in X}\,\vartheta_\Pi(\mathrm{R}(u,y),\vartheta_\Pi\left|1_{\mathrm{x}},\ \underline{\alpha}\right|(\mathrm{u}))$

$= \wedge_{u\in X}\,\vartheta_\Pi(\mathrm{R}(u,y),\vartheta_\Pi(1(\mathrm{x})(\mathrm{u}),\alpha))$

$= \vartheta_\Pi(\mathrm{R}(\mathrm{x},\mathrm{y}),\vartheta_\Pi(1_{\mathrm{x}}(\mathrm{x}),\alpha)\Pi\wedge_{u\neq x}\vartheta_\Pi(\mathrm{R}(u,y),\vartheta(0,\alpha))$

$= \vartheta_\Pi(\mathrm{R}(\mathrm{x},\mathrm{y}),\vartheta_\Pi(1,\alpha)\Pi\wedge_{u\neq x}\vartheta_\Pi(\mathrm{R}(u,y),1)$

$= \vartheta_\Pi(\mathrm{R}(\mathrm{x},\mathrm{y}),\frac{\alpha}{1}\Pi\wedge_{u\neq x}\vartheta_\Pi(\mathrm{R}(u,y),1)$

$= \vartheta_\Pi(\mathrm{R}(\mathrm{x},\mathrm{y}),\alpha)\Pi\wedge_{u\neq x}\vartheta_\Pi(\mathrm{R}(u,y),1)$

$= \vartheta_\Pi(\mathrm{R}(\mathrm{x},\mathrm{y}),\alpha)\ \Pi\ 1$

$= \vartheta_\Pi(\mathrm{R}(\mathrm{x},\mathrm{y}),\alpha)$

(ii) For all $\mu \in I^X$, ($\mu_j \in I^X$, for all $j \in J$), for all $x, y \in X$ and $\alpha \in I$, we get:

(P1). $\underline{A}_R\mu(x) = \wedge_{u\in X}\,\vartheta_\Pi(\mathrm{R}(u,x),\mu(u)) \le \vartheta_\Pi\big(\mathrm{R}(\mathrm{x},\mathrm{x}),\mu(\mathrm{x})\big) = \vartheta_\Pi\big(1,\mu(\mathrm{x})\big) = \mu(\mathrm{x})$

(P2). $\underline{A}_R\big(\underline{A}_R\mu\big)(x) = \wedge_{u\in X}\,\vartheta_\Pi(\mathrm{R}(u,x),\underline{A}_R\mu(u)$

$= \wedge_{u\in X}\,\vartheta_\Pi(\mathrm{R}(u,x),\wedge_{v\in X}\,\vartheta_\Pi(\mathrm{R}(v,u),\mu(v))$

$= \wedge_{u,v\in X}\,\vartheta_\Pi(\mathrm{R}(u,x),\vartheta_\Pi(\mathrm{R}(v,u),\mu(v))$

$= \wedge_{u,v\in X}\,\vartheta_\Pi(\mathrm{R}(v,u)\Pi\,\mathrm{R}(u,x),\mu(v))$

$\ge \wedge_{v\in X}\,\vartheta_\Pi(\mathrm{R}(v,u)\Pi\,\mathrm{R}(x,x),\mu(v))$

$= \wedge_{v\in X}\,\vartheta_\Pi(\mathrm{R}(v,x)\Pi\,1,\mu(v))$

$= \wedge_{v\in X}\,\vartheta_\Pi(\mathrm{R}(v,x)\,,\mu(v))$

$= \underline{A}_R\mu(x)$

Therefore, $\underline{A}_R(\underline{A}_R\mu)(x) \geq \underline{A}_R\mu(x)$ and the converse holds by (P1). Hence the equality $\underline{A}_R(\underline{A}_R\mu) = \underline{A}_R\mu$

(P3). $(\underline{A}_R(\wedge_{j\in J}\mu_j)(x) = \wedge_{u\in X}\vartheta_\Pi(\mathrm{R}(u,x), \wedge_{j\in J}\mu_j(u))$

$= \wedge_{u\in X}\wedge_{j\in J}\mu_j\,\vartheta_\Pi(\mathrm{R}(u,x), \mu_j(u))$

$= \wedge_{j\in J}\wedge_{u\in X}\mu_j\,\vartheta_\Pi(\mathrm{R}(u,x), \mu_j(u))$

$= \wedge_{j\in J}\underline{A}_R\mu_j\,(x)$

(P4). $\underline{A}\vartheta_\Pi\left|1_{x,}\underline{\alpha}\right|(y) = \vartheta_\Pi(R(x,y),\alpha)$

$= \vartheta_\Pi(R(y,x),\alpha)$

$= \underline{A}\vartheta_\Pi\left|1_{y,}\underline{\alpha}\right|(x)$

(P5). $\underline{A}_R\vartheta_\Pi\left|\underline{\alpha},\ \mu(x)\right| = \wedge_{u\in X}\vartheta_\Pi(\mathrm{R}(u,x), \vartheta\left|\underline{\alpha},\ \mu(u)\right|$

$= \wedge_{u\in X}\vartheta_\Pi(\alpha, \mathrm{R}(u,x), \mu(u)$

$= \vartheta_\Pi(\alpha, \wedge_{u\in X}\vartheta(\mathrm{R}(u,x), \mu(u))$

$= \vartheta_\Pi(\alpha, \underline{\mathrm{A}}\mu(x))$

$= \vartheta_\Pi\left|\underline{\alpha},\ \underline{A}\mu\right|(x)$

Hence, $\underline{A}_R$having satisfied (P1) – (P5) is a fuzzy Π-lower approximation operator on I^X.

The results obtained are the extension of the work of Morsi and Yakout (1998), were they studied a fuzzy rough sets based on the arbitrary T (lower semi continuous t-norm), they used a T-residuated implication ϑ_T to proposed a new definition for fuzzy T-lower approximation operator $\underline{A}$: $I^X \to I^X$of (X, R), where R is a T-similarity relation. Their definition satisfies the identities; $\overline{A}\underline{A} = \underline{A}$ and $\underline{A}\overline{A} = \overline{A}$. In this paper, we relaxed the T-residuated implication ϑ_T and adopted the Goguen implicationϑ_Π. Consequently, we established a fuzzy Π-lower approximation operator. The results obtained proffers an alternative and more precise way of computing the lower approximation operator specifically for the product case of continuous t-norms

Definition 4.3 A fuzzy set μ is said to be exact if $\overline{A}\mu = \underline{A}\mu = \mu$.

Example 4.4 Let $X = \{a, b, c\}$ and $\mu = (a_{0.2},\ b_{0.5},\ c_{0.7})$. Consider the Π-similarity relation on X;

$$R = \begin{array}{c} \\ a \\ b \\ c \end{array}\begin{array}{c} \begin{array}{ccc} a & b & c \end{array} \\ \begin{pmatrix} 1 & 0 & 0 \\ 0 & 1 & 0.3 \\ 0 & 0.3 & 1 \end{pmatrix} \end{array}$$

we find the Π-lower approximation operator on X as follows;

$$\underline{A}\mu(a) = \wedge\left(\vartheta_{\Pi}(\mathrm{R(a,a)},\mu(a)),\vartheta_{\Pi}(\mathrm{R(b,a)},\mu(b)),\vartheta_{\Pi}(\mathrm{R(c,a)},\mu(c))\right) =$$

$$\wedge(\vartheta_{\Pi}(1{,}0.2),\vartheta_{\Pi}(0{,}0.5),\vartheta_{\Pi}(0{,}0.7))$$

$$= \wedge\left(\frac{0.2}{1},\ 1,\ 1\right)$$

$$= 0.2$$

$$\underline{A}\mu(b) = \wedge\left(\vartheta_{\Pi}(\mathrm{R(a,b)},\mu(a)),\vartheta_{\Pi}(\mathrm{R(b,b)},\mu(b)),\vartheta_{\Pi}(\mathrm{R(c,b)},\mu(c))\right)$$

$$= \wedge(\vartheta_{\Pi}(0{,}0.2),\vartheta_{\Pi}(1{,}0.5),\vartheta_{\Pi}(0.3,0.7))$$

$$= \wedge(1,\frac{0.5}{1},1)$$

$$= 0.5$$

$$\underline{A}\mu(b) = \bigwedge\left(\vartheta_{\Pi}(\mathrm{R(a,c)},\mu(a)),\vartheta_{\Pi}(\mathrm{R(b,c)},\mu(b)),\vartheta_{\Pi}(\mathrm{R(c,c)},\mu(c))\right)$$

$$= \wedge(\vartheta_{\Pi}(0{,}0.2),\vartheta_{\Pi}(0.3,0.5),\vartheta_{\Pi}(1{,}0.7))$$

$$= \wedge(1,1,\frac{0.7}{1})$$

$$= 0.7$$

Therefore, $\underline{A}\mu = (a_{0.2},\ b_{0.5},\ c_{0.7}) = \mu$

Similarly, we find the Π-upper approximation operator as follows;

$$\overline{A}\mu(a) = \bigvee\left(\mathrm{R(a,a)}\ \Pi\ \mu(a),\mathrm{R(b,a)}\ \Pi\ \mu(b),\mathrm{R(c,a)}\ \Pi\ \mu(c)\right)$$

$$= \vee(1\ \Pi\ 0.2, 0\ \Pi\ 0.5, 0\ \Pi\ 0.7)$$

$$= \vee(0.2,0,0)$$

$$= 0.2$$

$$.\overline{A}(b) = \vee\left(\mathrm{R(a,b)}\ \Pi\ \mu(a),\mathrm{R(b,b)}\ \Pi\ \mu(b),\mathrm{R(c,b)}\ \Pi\ \mu(c)\right)$$

$$= \vee(0\ \Pi\ 0.2, 1\ \Pi\ 0.5, 0.3\ \Pi\ 0.7)$$

$= \mathrm{V}(0, 0.5, 0.21)$

$= 0.5$

$\overline{A}\mu(c) = \mathrm{V}\big(\mathrm{R}(\mathrm{a}, \mathrm{c}) \,\Pi\, \mu(a), \mathrm{R}(\mathrm{b}, \mathrm{c}) \,\Pi\, \mu(b), \mathrm{R}(\mathrm{c}, \mathrm{c}) \,\Pi\, \mu(c)\big)$

$= \mathrm{V}(0 \,\Pi\, 0.2, 0.3 \,\Pi\, 0.5, 1 \,\Pi\, 0.7)$

$= \mathrm{V}(0, 0.15, 0.7)$

$= 0.7$

Therefore, $\overline{A}\mu = \underline{A}\mu = \mu = (a_{0.2},\ b_{0.5},\ c_{0.7})$. Hence, μ is an exact sets

CONCLUSION

In this paper, Goguen implication was used to establish a fuzzy Π-lower approximation operator. This was achieved with the aid of some already existing definitions, theorems and propositions ont-norm, fuzzy *T*-lower approximation operator and the *T*-residuated implication. The established results proffer an easier way of finding the lower approximation operator specifically for the product case of the continuous t-norn.

REFERENCES

An, S., Hu, Q., and Wang, C. (2021). Probability granular distance-based fuzzy rough set model, *Applied Soft Computing* 102, 107064. https://doi.org/10.1016/j.asoc.2020.107064.

B. Schweizer, A. Sklar, Probabilistic Metric Spaces,, *North-Holland, Amsterdam* 1983.

Cao G., Shiu S.C.K., Wang X.Z. (2003), A fuzzy-rough approach for the maintenance of distributed case-based reasoning systems, *Soft Computing* 7 (8)491499

Dubois, D., Prade, H. (1990). Rough fuzzy sets and Fuzzy rough sets, *International Journal of General Systems* 17, 191 -208, https://doi.org/10.1080/03081079008935107.

Dubois, D., Prade, H. (1992). Putting rough sets and fuzzy sets together, *Intelligent support; Handbook of application and advances of the sets theory*, Slowiski, R.(ed.) Kluwer, 203-232, http://dx.doi.org/10.1007/978-94-015-7975-9_14.

E. Trillas and L. Valverd, , Some functionally expressable implications for fuzzy set theory, *Proc. 3rd International Seminar on Fuzzy Set Theory* , Linz, Austria (1981) 173 190

E. C. C. Tsang, D. G. Chen, D.S. Yeung, X. Z. Wang, J. W. T. Lee, Attribute reduction using fuzzy rough sets, *IEEE Trans. on Fuzzy. System* 16(2008) 11301142.

Farinas, L., Prada, H. (1986). Rough sets, twofold fuzzy sets and modal logic, fuzziness in indiscrenibility and partial information, in: A. Di. Nola, A.G.S. Ventre (Eds.) *The Mathematics of Fuzzy Systems*, TUV Rheinland, Cologne, 1986, 103-120.

Fern´andez, J. S., Murakami, S. (2003). Rough set analysis of a general type of fuzzy data using transitive aggregations of fuzzy similarity relations, *Fuzzy Sets and Systems,* 139(3), 635–660. doi:https://doi.org/10.1016/S0165-0114(03)00124-6.

Guilong, L.(2008). Axiomatic systems for rough sets and fuzzy rough sets, *International J. approximate reasoning,* 48, 857–867. https://doi.org/10.1016/j.ijar.2008.02.001

Hadrani, A., Guennoun, K., Saadane, R. & Wahbi, M. (2020). Fuzzy rough sets: Survey and proposal of an enhanced knowledge representation model based on automatic noisy sample detection, *Cognitive Systems Research* 64, 37–56. doi:https://doi.org/10.1016/j.cogsys.2020.05.001.

Hu, Q., An, S., and Yu, D. (2010). Soft fuzzy rough sets for robust feature evaluation and selection, *Information Sciences* 180 (22) (2010) 4384–4400. doi:https://doi.org/10.1016/j.ins.2010.07.010.

Janos. F. (2004), Left continuous t-norms in fuzzy logic: an overview, *Dept. of Biomaths. and inf. Fuculty of veterinary sci. Szent istvan Budapest Hungary,* U. 2, H - 1078.

Klement, E.P., Mesiar, R., Pap, E. (2004). Triangular norms. Position paper I: basic analytical and algebraic properties, *fuzzy sets and Systems*, 143, 5-26 https://doi.org/10.1016/j.fss.2003.06.007

L. Ying-Ming, L. Mao-Kang(1997). Fuzzy Topology, *World Scientific,*

L. A. Zadeh(1971), Similarity relation and Fuzzy orderings, *Inf. Sci* 3, 177 - 200.

M. M. Gafai, Z. Muazu (2023). Fuzzy Product Rough Sets as a Special Case of Fuzzy T- Rough Sets, DUJOPAS 9 (2b): 70-75, 2023 75, https://dx.doi.org/10.4314/dujopas.v9i2b.8

Mi, J.S., Zhang, W.X. (2004.) An axiomatic characterization of a fuzzy generalization of rough sets, *Information Sciences* 160 (1-4), 235–249, https://doi.org/10.1016/j.ins.2003.08.017.

Morsi, N.N., Yakout, M.M. (1998). Axiomatics for fuzzy rough sets, *Fuzzy Sets and Systems* 100, 327-342, https://doi.org/10.1016/S0165-0114(97)00104-8.

Ovchinnikov, S. (1991). Similarity relations, fuzzy partitions and fuzzy orderings, *Fuzzy Sets and Systems,* 40(1991) 107 – 126, https://doi.org/10.1016/0165-0114(91)90048-U.

Pawlak, Z. (1982). Rough sets, *Internat. J. Comput. Inform. Sci*. 11, 341 - 356j. http://dx.doi.org/10.1007/BF01001956.

Radzikowska, A. M., Kerre, E. E. (2002). A comparative study of fuzzy rough sets, *Fuzzy sets and systems* 126 (2), 137–155. https://doi.org/10.1016/S0165-0114(01)00032-X

Salido F., Murakami S. (2003), Rough set analysis of a general type of fuzzy data using transitive aggregations of fuzzy similarity relations, *Fuzzy Sets and Systems* 139(2003) 635 660.

Vluymans, S., D'eer, L., Saeys, Y. & Cornelis, C. (2015). Applications of fuzzy rough set theory in machine learning: a survey, *Fundamenta Informaticae* 142 (1-4), 53–86. http://hdl.handle.net/1854/LU-7017049.

Wang J, (2001), Reduction algorithms based on discernibility matrix: the ordered attributes method *Journal of Computer Science Technology* 16 (6) 489 504.

Yao, Y., Mi, J., Li, Z. (2014). A novel variable precision (θ, σ)-fuzzy rough set model based on fuzzy granules, *Fuzzy Sets and Systems* 236, 58–72, doi:https://doi.org/10.1016/j.fss.2013.06.012.

Zadeh, L.A. (1965). Fuzzy sets, *Information and Control* 8(3), 338-353. https://doi.org/10.1016/S0019-9958(65)90241-X.

EDUCATION, COMPUTER SCIENCE AND OTHERS

Antibacterial Activity of *Acacia Nilotica* Leaves Extract against Beta Lactamase Producing Bacteria

*[1]Kawuwa, U. A., [1]Hassan, M. M., [2]Muhammad, T. A., [2]Salawudeen A., [2]Umar A. T., [2]Jauro, H. A.
[1]*PMB 60 Gombe, Nigeria; Department of Biology, School of Secondary Education (Science), Federal College of Education (Technical)*
[2] *Gombe State University's Department of Microbiology, PMB 127, Gombe State, Nigeria*
***** Author of the correspondence:
Kawuwa, Usman Abubakar
Department of Biology, Federal College of Education (Technical), PMB 60 Gombe, Nigeria;
School of Secondary Education (Science);
Email: usmankawuwaabubakar@gmail.com

Abstract

In some regions of Northern Nigeria and West Africa, Acacia nilotica is recognized as a medicinal shrub that is used to cure ailments including dysentery and diarrhea. Because of this growing resistance to antibiotics, studies have been conducted on the phytochemical screening and antibacterial properties of Acacia nilotica leaf extracts.The plant leaves were collected from Kalshingi in Akko LGA of Gombe and authenticated at the Herbarium of Gombe State University. Phytochemical analyses using standard tests were used to detect tannins, steroids, saponins, flavonoids, glycosides, and alkaloids from the leaves. The agar-well diffusion method was employed in testing the sensitivity of the crude leaf extracts on two clinical bacterial isolates, while the tube dilution method was used to determine the minimum inhibitory concentration (MIC), and sub-culturing on nutrient agar was used to determine the minimum bactericidal concentration (MBC). Phytochemical analyses revealed tannins, steroids, flavonoids and saponins, glycosides were present in both the methanol and aqueous leaf extracts. The two extracts at concentrations varying from 6.25 mg/ml to 50 mg/ml exhibited zones of inhibition ranging from 12mm to 20mm against Escherichia coli and Klebsiella pneumoniae. The MIC test revealed that E. coli was inhibited at 1.56 mg/ml of aqueous extract and 3.12 mg/ml of methanol extract, while Klebsiella was inhibited at 3.12 mg/ml of both methanol and aqueous extracts. MBC for both bacteria was 6.25 mg/mL for each of the extracts. These results suggest that this leaf can be a potential source of an alternative to antibiotics.

Keywords: Acacia nilotica, phytochemical activity, *Escherichia coli*, *Klebsiella pneumoniae*.

INTRODUCTION

Herbal medicine (traditional) has been recognized by the WHO as an important alternative way of providing health care services and treatments for the population, especially in Ghana, which adopts this method due to its affordability (Nyarko *et al*., 2005). Man has utilized plants for a variety of reasons from the beginning of time, and as long as life exists on Earth, he will continue to do so (Abbiw, 1990). Over time, the world's population has benefited greatly from the symbiotic interaction between humans and plants.

Plants are great suppliers of several sorts of medications because they generate a wide variety of bioactive chemicals. The majority of medications, including those utilized in the conventional medical system, come from natural and synthetic compounds. Therefore, screening conventional natural compounds is a sensible method to drug development. In recent years, the usage of plant extracts has grown significantly, and several studies have been carried out globally to demonstrate the antibacterial properties of medicinal plants (Alonso-Paz *et al*., 1995). Over the years, plants have shown to be a great source of natural materials for preserving human health, particularly in the past few years with increased research into natural medicines. The World Health Organization (Santos *et al*., 1995) states that the greatest source of a wide range of medications would be medicinal plants.

Over the years, the use of plant materials to prevent and treat infectious diseases has attracted the attention of scientists worldwide due to the persistent and earnest need to find new antimicrobial mixtures with different compound structures and novel components of activity for new and reappearing irresistible illnesses. Thus turning the attention and interest of researchers towards new ways of developing better drugs against microbial infection (Falodun *et al*., 2006).

In some regions of Northern Nigeria, West Africa, North Africa, and other areas of the world, *Acacia nilotica*, also known as bagaruwa in Hausa, has been recognized and utilized as a medicinal plant for the treatment of ailments including diarrhea, dysentery, leprosy, cancer, ulcers, diabetes, etc. Opposition to antimicrobial medication resistance is not just about growth; it's also a scheduling issue for the therapeutic setting. Furthermore, a lot of information has been published on the toxicity of several therapeutic herbs. Rats' chromosomes were reportedly damaged by extracts from Bryophyllum calycinum (whole plant), Annona senegalensis root, Hymenocardia acida stem bark, Erythrophleum suaveollens leaves, and Spondiatus preussii (Sowemimo *et al*., 2007). People in rural regions employ

Acacia nilotica in traditional medicine to treat a variety of ailments. The plant's bark is often used to treat leprosy, bleeding piles, diarrhoea, colds, bronchitis, and leucoderma. Pods and delicate leaves are used in traditional medicine to treat diabetes mellitus and diarrhoea. It has been demonstrated that the plant possesses cytotoxic action, antioxidant activity, antibacterial, anti-inflammatory, vasoconstrictor, antihypertensive, and antispasmodic properties, as well as inhibitory activities against the hepatitis virus (Gilani *et al*., 1999; Del, 2009; Malviya *et al*., 2011). Secondary metabolites like alkaloids, cyanogenic glycosides, fluoroacetate, gums, terpenes (including diterpenes, essential oils, phytosterols, and triterpene genins and saponins), hydrolyzable tannins, flavonoids, and condensed tannins are known to be abundant in different parts of this plant (Seigler, 2003). Numerous uses, such as medicines, alternative medicine, natural remedies, and the preservation of raw and processed food, have been made possible by the antibacterial properties of plant extracts (Abd El-Aziz and Ali, 2013). The majority of gram-negative bacteria generate the enzymes known as beta-lactamases. They frequently cause organisms that contain them to become resistant to β-lactam antibiotics (Bush *et al*., 1995). According to Steward *et al*. (2001), ESBLs are chromosomal or plasmid-mediated enzymes that arise from spontaneous mutations in the serine active site of the old beta-lactamase enzyme. These changes add four to six additional amino acids to the enzyme's hydrolytic substrate. With the exception of carbapenems, these enzymes mediate resistance to monobactams (aztreonam) and oxymino-cephalosporins (ceftriaxone, ceftazidime, cefotaxime, and cefepime). The first extended-spectrum β-lactamase was found in Klebsiella pneumoniae in Garmany in 1983 (Knothe *et al*., 1983), and subsequently across western Europe, most likely as a result of the first clinical usage of extended-spectrum β-lactam antibiotics in those regions. The Enterobacteriaceae family is the principal host of these infections, with Klebsiella pneumoniae and Escherichia coli accounting for the majority of global reports. According to Kotra *et al*. (2002), they are to blame for 5–20% of nosocomial infection outbreaks in critical care, burn, cancer, and neonatal units. The development and controlled dissemination of these enzymes in Nigeria have been facilitated by inadequate hygiene practices, the indiscriminate use of antibiotics, and a lack of surveillance of microbial drug resistance (Arzai and Adamu, 2008). In order to ascertain the plant part's antibacterial activity against the testing isolates, screen for the presence of plant bioactive chemicals, and ultimately ascertain the plant part's minimum inhibitory concentration (MIC) and minimum biochemical concentration (MBC) against the isolates, this study was conducted.

MATERIAL AND METHODS

Collection and Preparation of Plant Materials

Using a cleaned cutlass, fresh leaves of Acacia nilotica were aseptically picked along Kalshingi and then brought to the Gombe State University microbiology lab in cleaned polythene bags and sacks. To get rid of any dirt or debris from the plant components, a soft brush was utilized (Sarker *et al*., 2006). The plant portion was identified using specimen number GSUH500 at the Botany Herbarium of the Biological Sciences Department at Gombe State University. After two weeks of air drying in the shade, the samples were ground into a powder with a mortar and pestle (Aliyu *et al*., 2008; Esimone *et al*., 2012).

Extraction of Plant Materials

Water Extraction

Fifty grams (50g) of the powdered sample of the plant was extracted by boiling in 200 ml of distilled water for 30 minutes; the extract was then filtered using What`s Man filter paper No. 2, and then the filtrate was evaporated to dryness at 40oc. (Esimone *et al*., 2012).

Methanol Extraction

An electric balance was used to weigh fifty grams (50g) of the plant's powdered sample, which was then placed into labeled conical flasks holding 200 ml of ethanol. After being shaken for two weeks on a rotary shaker, the mixture was filtered. To recover the extract, the filtrate was transferred to a new flask and boiled in a water bath (Bhojwani and Dantu, 2013).

Qualitative Phytochemical Screening of Plant Materials

Using standard techniques developed by Odebiyi and modified by Aiyelaagbe and Osamudiamen (2009), the qualitative phytochemical composition of the plant materials that demonstrated antibacterial activity was examined for the presence of alkaloid, saponin, steroids, tannin, flavonoid, and cardiac glycosides.

Screening for alkaloids (Mayer`s Reagent Test):

To acidify the sample, 2-3 drops of diluted hydrochloric acid were added to 2 mil of the extracts. Distilled water was mixed with 2 mil of Mayer's reagent, which consists of potassium iodide (KI) and mercury chloride (HgCl2). The alkaloids are present when a white to yellow precipitate forms.

Screening for saponin:

5 mil of distilled water and 2 mil of extract were combined, and the mixture was rapidly shaken for 30 seconds. Saponin is present when there is steady, continuous foaming.

Screening for tannin:

FeCL3 (1 ml) was added to 2 ml of extracts. A coloring that is either blue-green or blue-black suggests the presence of tannin.

Screening for flavonoid:

2-3 ml drops of a strong NaOH solution were added to 2 ml of extract. When diluted HCL is added, the production of strong yellow turns colorless, signifying the presence of flavonoids.

Screening for Phenol (Ferric Chloride Test):

To 2 ml of extract, 2-3 drops of ferric chloride solution were added. The presence of phenols is indicated by the production of a brilliant black hue.

Test for Glycosides (Most Classes):

10 mil of boiling distilled water were mixed with 5 mil of powdered sample, agitated, and filtered with What's Man No. 1 filter paper. The 2 mL portion of the filtrate was then supplemented with a few drops of concentrated HCL. To hydrolyze any glycosides that were present, the mixture was cooked for one minute. To make the combination alkaline, a few drops of aqueous ammonia solution were also added. Five drops of the mixture were then combined with 2 mil of Benedict's reagent and heated. The observation of a reddish-brown precipitate suggests the presence of glycosides.

Isolation of Test Organisms

The test organisms, Klebsiella pneumonia and Escherichia coli, were obtained from the Federal Teaching Hospital located in Gombe and verified by biochemical analyses. After the test organisms were aseptically subcultured on nutrient agar, the double disc synergy test (DDST) technique was used to determine whether organisms produced beta-lactamases. As Cheesbrough (2006) describes, the colonies were further subcultured to yield pure culture.

Screening for Extended Spectrum Beta-Lactamases

The approach used was the double disc synergy test (DDST), as outlined by CLSI (2010). As previously mentioned, sterile swab sticks were used to inoculate the test organisms on Mueller Hinton Agar (MHA) using standardized inocula. Every inoculated MHA had an amoxicillin/clavulanic acid disc (20/10 µg) inserted in the middle of it. The amoxicillin/clavulanic acid disc was positioned 15 mm center to center, followed by 30 µg of ceftazidime and 30 µg of cefotaxime. For twenty-four hours, the plates were incubated at 37°C. Following incubation, the formation of ESBL was indicated by an elevation of the zone of inhibition of one or both of the Ceftazidime and Cefotaxime discs towards the Amoxycillin/Clavulanic Acid discs.

Inoculum Standardization

A test tube containing normal saline was filled with enough material from an overnight culture of the test organism using an inoculation platinum wire loop, until the suspension's turbidity matched that of the 0.5 McFarland Standard (CLSI, 2012).

Preparation of Turbidity Standard

Using the procedure outlined by CLSI (2012), 1 ml of concentrated H_2SO_4 was added to 99 ml of distilled water to create a 1% v/v solution of sulfuric acid. Additionally, 0.5g of dehydrated barium chloride were dissolved in 50 ml of distilled water to create a one percent (1% w/v) solution. This was followed by mixing 0.6 ml of the barium chloride solution with 99.4 ml of sulfuric acid solution to create a 1% w/v barium sulfate suspension. After that, the turbid solution was put into the test tube to serve as the reference for analysis.

Preparation of Stock Solution of Extracts

Each of the various extracts was diluted serially by dissolving 0.2 g in 1 ml of 20% v/v dimethyl sulfoxide (DMSO) to create a 200 mg/ml concentration (Esimone *et al*., 2012).

Sensitivity Testing

The agar-well diffusion technique (Esimone *et al*., 2012) was used to perform this test, as detailed below. Each of the various extracts was diluted two times and diluted to a 200 mg/ml concentration by dissolving 0.2 g in 1 ml of 20% v/v dimethyl sulfoxide (DMSO). Two milliliters of sterile Muller-Hinton agar were used to suspend a single colony of the test isolate. As previously mentioned, the isolate solution was standardized and used to inoculate the Muller-Hinton agar surface. The extra fluid was then drained into a jar for disinfection. After allowing the infected agar surfaces to dry, the plates were properly labeled. The infected Muller-Hinton agar was hollowed out into four 6 mm diameter wells using a cork borer. Each well was filled with 50 µl of the test extracts at each concentration using a micropipette. The extracts were allowed to permeate into the agar by leaving the plates on the bench for thirty minutes. After that, the plates were incubated for twenty-four hours at 37°C. The plates were examined for inhibitory zones surrounding the wells following incubation. A meter ruler was used to measure the zone sizes to the closest full millimeter. The mean inhibition zone diameter was measured twice for each test, and it was reported to the closest full millimeter.

Minimum Inhibitory Concentration (MIC)

The tube dilution method was used to calculate the extract's minimal inhibitory concentration. The plant extracts were diluted and added to the nutritional broth in a 1:1 ratio. To ascertain the range of MIC values, preliminary approximations of the plant extract's MIC values against the test organism were determined. As a result, using the dilution formula, the following concentrations were made for each extract: 6.25, 3.12, 1.56, and 0.78. Each tube also received 0.1 ml of the test organism's reference suspension. For twenty-four hours, the tubes were incubated at 37°C. As a control, there was also a tube with extract and growth media but no inoculum. At the conclusion of the incubation period, the growth (turbid solution) or lack thereof (clear solution) was noted. The least inhibitory concentration (MIC) of an extract is defined as the lowest concentration at which no growth occurs.

Minimum Bactericidal Concentration (MBC)

By subculturing the last test dilution that had visible growth (turbidity) and all other dilutions in which there was no growth on a new extract solid medium and incubating for an additional 24 hours, the minimum bactericidal concentration (MBC) was ascertained. The minimum bactericidal concentration (MBC) was determined by using the largest dilution that did not exhibit a single bacterial colony (Baker and Silver, 2009).

RESULTS DISCUSSION, CONCLUSION

Result

The following presents the findings from the phytochemical screening and antibacterial activity of the methanolic and aqueous leaf extracts of *Acacia nilotica*

Table 1: Antibacterial activity of Methanolic (zone of inhibition) extract of *Acacia nilotica* against the tested organisms.

Concentrations	50mg/ml	25mg/ml	12.5mg/ml	6.25mg/ml
Organisms	Growth inhibition zones (mm)			
E. coli	20	12	18	13
Klebsiella pneumoniae	19	16	14	12

Table 2: Antibacterial activity of Aqueous (zone of inhibition) extract of *Acacia nilotica* against the tested organisms.

Concentrations	50mg/ml	25mg/ml	12.5mg/ml	6.25mg/ml
Organisms	Growth inhibition zones (mm)			
E. coli	17	15	12	10
Klebsiella pneumoniae	18	13	10	12

Table 3: Phytochemical Screening of Methanolic and Aqueous leaves extracts of *Acacia nilotica*.

Phytochemical components	Methanol	Aqueous
Alkaloids	-	-
Flavonoids	+	+
Saponins	-	+
Tannins	+	+
Steroids	+	+
Phenol	+	+
Glycosides	+	+

Key: -; not detected, +; present,

Table 4: Minimum Inhibitory Concentration (MIC) and Minimum Bactericidal Concentration of Methanolic and Aqueous leaves extracts of *Acacia nilotica* on tested organisms.

EXTRACTS				
Organisms	**Methanol (mg/ml)**		**Aqueous (mg/ml)**	
	MIC	**MBC**	**MIC**	**MBC**
E. coli	3.12	6.25	1.56	6.25
Klebsiella pneumoniae	3.12	6.25	3.12	6.25

Discussion

The results obtained from Table 1 showed that the Methanolic extract of the leaf plant had the highest antibacterial activity of 20mm at 50 mg/ml and 19mm at 50 mg/ml against *E. coli* and *Klebsiella pneumoniae* respectively, while the results from Table 2 showed that the aqueous extract plant exhibited the highest antibacterial activity against *E. coli* and *Klebsiella pneumoniae* with 17mm and 18mm at 50 mg/mL concentrations respectively. Methanolic leaf extract had the highest antibacterial activity against both tested isolates. Although all extracts were significant when compared with the CLSI (2014) guidelines for antimicrobial susceptibility testing, these significant activities may have resulted from reactions between components of the plant extracts that were not active themselves to improve the stability, solubility, bioavailability, or half-life of some other components, thereby making them strong and bioactive (Bone and Mills, 2013). The results obtained from this study are in line with

the findings of Oseni and Owusu (2012), who reported that a multi-blend containing different parts of the Acacia nilotica plant displayed synergistic activity on some pathogenic bacteria. However, no literature was found to support or dispute the lack of synergy between those other plant parts. Also, the result is in accordance with the findings of Philips (2010), who reported that tannins and alkaloids are natural products that have medicinal properties. The phytochemicals present could be the cause of the action seen. Numerous studies have demonstrated the antibacterial and antioxidant properties of components such as tannins, saponins, flavonoids, and terpenes (Kunle and Egharevba, 2009; Ayoola *et al*., 2008). Moreover, Tables 1 and 2 depicted the individual efficacy of the plant against the tested organisms (*E. coli* and *Klebsiella pneumoniae*), respectively, indicating its antibacterial activity against these organisms. The methanol extract of the plant exhibited the highest activity in Table 1, followed by the aqueous extract at concentrations primarily of 50 mg/mL and 25 mg/mL. These findings are consistent with Okoro *et al*. (2014), who noted strong antibacterial activity of *A. nilotica* leaf extracts against isolates. They also align with Abeer and Sanaa's (2010) observations that the methanolic extract of *A. nilotica* demonstrates superior antibacterial activity compared to the aqueous extract against certain bacterial isolates. This research corroborates Olaleyen's (2007) findings regarding the pharmacological effects of methanolic extracts of alkaloids and saponins from Hibiscus sabdariffa on bacterial isolates such as *E. coli, K. pneumoniae,* and *S. aureus*. Similarly, Abd-Ulgadir *et al*. (2015) reported higher antibacterial activity against E. coli with the methanolic extract of Acacia nilotica species. These results are also in agreement with Mahesh and Satish's (2008) studies. However, they go against the conclusions of Abubakar (2009), who found that aqueous extracts were more effective than organic extracts at preventing the development of harmful bacteria such *Proteus mirabilis, Streptococcus pyogenes, Escherichia coli, Staphylococcus aureus,* and *Pseudomonas aeruginosa*.

According to Table 3, the results of the phytochemical screening show that the extracts were found to be positive for a number of phyto-compounds, including tannins, saponins, flavonoids, phenols, steroids, and glycosides. This is in line with the results of Deshpande *et al*. (2013), who also confirmed that the leaves of Acacia nilotica contain tannins, saponins, flavonoids, phenols, and steroids. The physiological impacts and medicinal qualities of these active phytochemical elements are acknowledged, and they have an impact on the medicinal potential of plants. It has been shown that tannins, alkaloids, and saponins prevent bacterial development and provide defense against plant mycoses (Deshpande *et al*., 2013).

The results from Table 4, illustrating the MIC and MBC values obtained through individual sensitivity testing, demonstrated that the growth of beta-lactamase-producing *E. coli* and *Klebsiella pneumoniae* was halted at concentrations of 3.12 mg/mL and exhibited lethal effects at 6.25 mg/mL, respectively. This observation aligns with the findings of Okoro *et al*. (2014) and Gislene *et al*. (2000), who similarly reported MIC and MBC values for *A. nilotica* extracts and other plant samples against bacterial isolates to be 3.12 mg/mL and 6.25 mg/mL, respectively. Discrepancies in these values might arise due to variations in the methodologies employed.

Conclusion

The study findings indicated the existence of phytochemical substances like tannins, steroids, glycosides, saponins, and flavonoids in the plant components, with no detection of alkaloids. Both methanol and aqueous extracts of the plant exhibited greater antibacterial effectiveness against *E. coli* compared to *Klebsiella pneumoniae*. Hence, the plant shows promise as a potential antibacterial agent.

Reference

Abbiw, D. K. (1990). Useful Plants of Ghana: West African Uses of Wild and Cultivated Plants. Intermediate Technology Publication and the Royal Botanic Gardens, England.

Abd El-Aziz, D. M, and Ali, S. F. H. (2013). Antibacterial activity of extracts of some spices on the growth of methicillin-resistant *Staphylococcus aureus* strains, *Annals Food Science and Technology*, **14** (2): 327 – 329.

Abd-Ulgadir K. S, El-Rofaei N. A and El-Kamali H.H. (2015). Antimicrobial property of *Acacia nilotica ssp tomentosa* against some causative agents of urogenital infections. *World Journal of Pharmaceutical Research.* **4**(3): 34-35.

Abeer N. H. A and Sanaa O. Y (2010): Antimicrobial Activity of *Acacia nilotica* Extracts against Some Bacteria Isolated from Clinical Specimens; http//scialert.net/fulltext/?doi=rjmp.2007.25. 28&org=10 Pp. 1-3

Abubakar E. M (2009). The use of *Psidium guajava* L. in Treating Wound, Skin and Soft Tissue Infections. Sci. Res. Essay, **4**:605-611.

Aiyelaagbe, O. O and Osamudiamen, P. M (2009): Phytochemical Screening for Active Compounds in *Mangifera indica* Leaves from Ibadan, Oyo State, *Plant Sciences Research* **2**(1):11-13.

Aliyu B. S. (2006). Common Ethinomedicinal Plants of the Semiarid Regions of West Africa; Triumph Publishing Company Limited; Nigeria Pp 8, 26 http//:en.wikipedia.org/wiki.acacia-nilotica, 2008; *Acacia nilotica*; Pp. 1-5

Aliyu, A. B, Musa, A. M, Abdullahi, M. S., Oyewale, A. O, and Gwarzo, U.S (2008). The activity of plant extracts used in Northern Nigerian traditional medicine against Methicillin-Resistant *Staphylococcus aureus* (MRSA), *Nigerian Journal of Pharmaceutical Sciences,* **7**(1): 1-8.

Alonso-paz E, Cerdeiras M. P, Fernandez J, Ferreira F, Myona P, Soubes M (1995). Screening of Uruguayan medicinal plants for antimicrobial activity. *Journal of Ethnopharmacology*, **45**:67-70.

Arzai, A. H and Adamu, D. J. M (2008): Prevalence of beta-lactamase Producers among randomly selected bacterial pathogens in Kano, Nigeria. *Biological and Environmental Sciences Journal for the Tropics* **5** (3):218-223.

Ayoola G. A, Coker H. A. B, Adesegun S. A, Adepoju-Bello A. A, Obaweya K, Ezennia E. C, Atangbayila T. O (2008). Phytochemical Screening and Antioxidant Activities of Some Selected Medicinal Plants Used for Malaria Therapy in Southwestern Nigeria.

Bhojwani, S. S and Dantu, P. K (2013); Plant Tissue Culture: An Introductory Text, Springer India, ISBN9788132210252, pp 275 – 286.

Bush, K., Jacoby, G. A and Medeiros, A. A. (1995). A Functional Classification Scheme for β-lactamases and its correlation with molecular structure. *Antimicrob. Agents Chemother.* **39**:1211-1233.

Cheesbrough, M., (2006). District Laboratory Practice in Tropical Countries, 2nd edition, ISBN 9780521676311, pp 43 – 75.

CLSI, (2012). CLSI Document M07-A9. Methods for Dilution Antimicrobial Susceptibility Test for Bacteria that Grow Aerobically: Approved Standard. 19th Edition CLSI, Wayne.

CLSI, (2014); Guidelines for Antimicrobial Susceptibility Testing, Clinical Laboratory Science Institute.

Del WE (2009). *In vitro* evaluation of peroxyl radical scavenging capacity of water extract/fractions of *Acacia nilotica* (L.). *Afr. Journal Biotechnol*., **8**(7): 1270-1272. Deshpande S. N. (2013): Preliminary Phytochemical Analysis and In Vitro Investigation of Antibacterial Activity of *Acacia nilotica* against Clinical Isolates. Journal of Pharmacognosy and Phytochemistry; **1**(5):23-27.

Esimone, C. O., Attama, A. A., Mundi, K. S., Ibekwe, N. N., and Chah, F. K., (2012): Antimicrobial activity of *Psidium guajava* Linn. stem extracts against methicillin-resistant *Staphylococcus aureus*, *African Journal of Biotechnology* **11**(89):15556-15559.

Falodun A, Okenroba L. O, Uzoamaka N (2006). Phytochemical Screening and Anti-inflammatory Evaluation of Methanolic and Aqueous Extracts of *Euphobia hetrophylla* Linn. (Euphorbiacae). *Afri. Journal Biotechnol.* **5**(6)529-531.

Gilani A. H. (1999) Studies on Antihypertensive and Antispasmodic Activities of Methanol Extract of *Acacia nilotica* Pods. *Phytother. Res.*,**13**: 665–669.

Gislene G. F. N, Juliana L. Paulo C. F and Guiliana L. S (2000): Antibacterial Activity of Plant extract and Phytochemicals on Antibiotic-Resistant Bacteria. *Brazilian Journal of Microbiology* **31**:247-256

Jansen A. M, Cheffer J. J. C, Svendsen AB (1987). Antimicrobial activity of essential oils: a 1976-1986 literature review. Aspects of the test methods planta medica, **40**:395-398.

Knothe H, Slah P, Kramery V, Antal M, Mitsuharhi S.(1983). Transferase resistance to cefotaxime, cefoxitin, cefamandole, and cefuroxime in chemical isolates of *Klebsiella pneumonia* and *Serratiamarcescens*. Infections; **11**(6):315-7.

Kotra L. P, Samama J, Mobashery S (2002). β-lactamases and resistance to β-lactam antibiotics. In Bacterial Resistance to Antimicrobials, Lewis K, Salyers AA, Tabar HW, Wax RG (eds). Marcel Decker: New York; 123-160.

Kunle O. F and Egharevba H. O (2009). Preliminary studies on Vernonia ambigua: Phytochemistry and Antimicrobial Screening of the Whole Plant. *Ethnobotanical Leaflets* **13**: 1216-21.

Mahesh B and Satish S (2008) Antimicrobial Activity of Some Important Medicinal Plant against Plant and Human Pathogens. *World Journal of Agricultural Sciences*, **4** (S): 839-843.

Malviya S., Rawat S., Kharia A and Verma M. (2011). Medicinal attributes of *Acacia nilotica* Linn. - A comprehensive review on ethnopharmacological claims, *Intl. Journal Pharm. Life Sci.* **2**(6), 830-837.

Nyarko K. N, Aseidu-Gyekye I. J, Sittie A. A. (2005). A Manuel of Harmonized Procedures for Assessing the Safety, Efficacy, and Quality of Plant Medicines in Ghana, Ministry of Health: The Ghana National Drugs Programme

Okoro O, Smith S, Chiejina L, Lumactud R, An D, Park H. S, Voordouw J, Lomans B. P, Voordouw G (2014). Comparison of microbial communities involved in souring and corrosion in offshore oil production facilities in Nigeria. *Journal Ind. Microbiol. Biotechnol*. **41**:665-678

Olaleye M. T (2007): Cytotoxicity and Antibacterial Activity of Methanol Extract of Hibiscus Sabdariffa *Journal of Medicinal Plants Research* **1**(1): 9 – 13

Oseni L. A, and Owusu B (2012). Comparison of in vitro Growth Inhibitory Activities of Aqueous Extracts of Selected Individual Plants with the Multi-Component Concoction. *Journal of Pharmaceutical Sciences and Research*, **4**(4):1792-1796.

Philips L. (2010) Online Seminars for Municipal Arborists; Medicinal Properties of Trees; http://onlineseminars.com/index.php?=1- 3usingplants-as-sound-barrier; Pg. 1 – 5. plasmid associated with a major nosocomial outbreak. *Journal Antimicrob Chemother*. 2012. **67**(1):74-83.

Santos P. R. V, Oliveira A. C. X, Tomassini T. C. B (1995). Control microbiogicode productors. Fitoterapicos. Rev. Farm. Bioquin. **31**:35-38.

Sarker D. S, Latif Z, and Gray A. I (2006): Natural Products Isolation, 2nd edition, Humana Press Inc., ISBN 1588294471. Pp 323.

Seigler D. S (2003). Phytochemistry of *Acacia-sensu lato*. *Biochem. Syst. Ecology.*, **31**(8): 845–873.

Saxena G, McCutcheon A. R, Farmer S, Towers G. H. N, Hancock R. E. W (1994). Antimicrobial constituents of Rhus glabra. *Journal of Ethnopharmacology*, **42**:95-99.

Sofowora A (1996). Research on medicinal plants and traditional medicine in Africa. *Journal Altern.*Complement. Med. **2**(3):365-372.

Sowemimo A. A, Fakoya I. A, Awopetu I, Omobuwajo and Adesanya S. A (2007). Toxicity of some Selected Nigerian Plants; *Journal of Ethnopharmacology*, Pp. 1-6.

Steward C. W, Rasheed J. K, Hwert S. K, Biddle J. N, Rancy P. M, Anderson G. J (2001). Characterization of clinical isolates of *Klebsiella pneumoniae* from 19 laboratories using the National Committee for Clinical Laboratory Standards for detecting ESBL. *Journal ClinMicrobiol* **39**:28

Bioremediation of Polycyclic Aromatic Hydrocarbons from Kaduna Refinery Waste Contaminated Soil Using *Vernonia Amygdalina* (Bitter Leaf) Saponins

Usman Daniel[1]*, Joseph Appah[2], Jacob Bernard Kazachiang[1], Garba Aliyu[1], Joshua Akinnifesi[1]

[1]Department of Chemistry Education, Federal College of Education (Tech.) Gombe

[2] Department of Biotechnology, Nigerian Defence Academy Kaduna

*07038926453 usmandaniel26@gmail.com

Abstracts

The effect of *vernonia amygdalina* (Bitter leave) on biodegradation of Polycyclic Aromatic Hydrocarbons (PAHs) contaminated soil was studied. The Critical Micelle Concentration (CMC) of the saponins was first determined using capillary rise method. The PAHs contaminated soil was divided into four groups and treated with different saponins concentration in order to determine the effect of *V.amygdalina* saponins on biodegradation of PAHs after 7 and 18 days of incubation period at room temperature and pH value of 6.0. The targeted PAHs in this study were Naphthalene (NAP), Phenanthrene (PHE) and Benzo-A-pyrene (BAP). The Critical Micelles Concentration (CMC) of *V.amygdalina* saponins was determined to be approximately 120mg/L at a pH of nearly 6.9 (1g/500ml stock solution. There was biodegradation of PAHs when the residual mean values of the difference treatment group were compared to the values of the control group. Although not all the incubation groups have lowered the PAHs down to its reference value (0.1 $mg.kg^{-1}DW$), good number of compounds have been drastically reduced to change the soil occupation criteria. Therefore saponins from *V.amygdalina* have biodegradation effect on polycyclic aromatic hydrocarbons. Further study need to be conducted on the potentials of saponins compound from *V.amygdalina* leaves on solubilizing polycyclic aromatic hydrocarbon specifically the higher molecular weight compounds and also to establish the order of the degradation of PAHs with Saponins concentration.

Key words: Bioremediation CMC PAHs Saponins Vernonia amygdalina

1.0 INTRODUCTION

Soil, which is one of the most valuable resources that Man cannot do without is heavily polluted by both inorganic metals and organic pollutants globally (Xiao-Lan and Yong 2018). High amount of contaminants like polycyclic aromatic hydrocarbons (PAHs), petroleum and related products, pesticides, chlorophenols and heavy metals are being deposited to the soil thereby causing a serious threat to human health and natural ecosystem (Ming, *et al.*, 2015). Polycyclic Aromatic Hydrocarbons (PAHs) are chemical compounds that have two or more fused benzene rings in linear, angular or cluster shape, with only carbon and hydrogen. They are normally produced when there is low amount of Oxygen during burning under of substances (Gurjeet *et al.*, 2015). Polycyclic aromatic hydrocarbons are widely distributed owing to both natural and anthropogenic sources (Bishnoi and Mehta, 2005). Chemical and physical methods for soil cleaning of these contaminants have been unsuccessful or expensive (Ming *et al.*, 2015). Recently, use of surfactants for increasing the accessibility of PAHs from polluted soil by microbes has been promising for soil remediation (Abiram, Kongkona, Ponnusamy, Sunita, Shravani, Nikhil, Jenet, Vinoth *et al.*, 2022). Bioremediation is a process relying on microorganisms, plants or their respective enzymes to degrade pollutants (Megharaj *et al.*, 2011). The aim of this study is to determine the effect of V. *amygdalina* saponins in bioremediation of PAHs in Kaduna refinery waste contaminated soil.

2. 0 LITERATURE REVIEW

Polycyclic aromatic hydrocarbons (PAHs) are mainly categorised in two main classes: lower molecular weight PAHs, such as molecules with three or less benzene ring (naphthalene, acenaphtene, fluorene, phenanthrene, and anthracene) and higher molecular weight PAHs, such as molecules with four or more benzene rings (fluoranthene, pyrene, benzo(a)anthracene, chrysene, benzo(b)fluoranthene, benzo(k)fluoranthene, benzo(a)pyrene, and dibenzo(ah) [Megharaj *et al.,* 2001; Von Lau *et al.,* 2014).

Surfactans are widely classified as non-volatile, surface-active substances that are widespread in nature, existing mainly in the plant kingdom Hostettmann *et al.,* (2005). Surfactants produce micelles (aggregates of monomers) when the concentration is above a given value of concentration called critical micellar concentration CMC (Lakra *et al*., 2013). This characteristics of surfactant has been largely studied for decades so as to apply it in soil "cleaning technologies" (Von Lau *et al.,* 2014) or to improve mobilization of contaminants towards degrading microbes (Kobayashi *et al.,* 2012) by making the PAHs more soluble in water. *Vernonia amygdalina* is a widely known shrub or small tree that is common in tropical Africa. They are also found in Asia and are widely distributed along drainage lines and in natural forest or commercial plantation. The leaves of *V.amygdalina* can be used as condiments in making after getting rid of the bitter taste by washing. Moreover, the leaf is used to prepare a common Nigerian bitter leaf soup called Onugbo and as spice in the Cameroon dish called "Ndole. In African continent like Nigeria, the plant is processed into tonic and drank for medicinal purposes Ijeh *et al.,* (2008).

3.0 MATERIALS AND METHOD

Sample identification, collection and preparation

Fresh bitter leaf (*Vernonia amygdalina) l*eaves free from disease was collected in a sterilised polythene bag in quarter 2 area, Samaru Zaria, Kaduna state Nigeria. It was identify by Sanusi Mohammed at the herbarium of Department of Biological Science Ahmadu Bello University Zaria and identified with voucher specimen number 900179. Before the preparation, the leaves were first washed thoroughly 3 times with tap water and then once with sterile distilled water. The leave materials was dried under shade on sterile blotter and then pounded into fine powder using laboratory Pestle and Mortar.

Extraction of Saponins

The extraction of *V.amygdalina* saponins was carried out at department of Pharmacognosis, Faculty of Pharmaceutical sciences Ahmadu Bello University Zaria. Exactly five hundred grams (500g) of the powdered bitter leaves was left in 100 ml of 70%w/v Ethanol for three days to get soaked. After the three days of the extraction, the extract was filtered using Whatman No.1filter paper. The crude ethanolic extract was concentrated by evaporating the ethanol. Ethyl acetate and KOH were added for delipidization and removal of flavonoid respectively. The extract was subjected to solvent partitioning using n-butanol as water immiscible solvent to obtain the saponins extract. After complete evaporation the extract was tested for saponins using haemolytic test as described by

Sodipo *et al.,* 1990 and then measured by weighing and kept aseptically until when needed for use (Gberikon *et al.,* 2019).

Critical Micelles Concentration (CMC) of *V.amygdalina* Saponins

The CMC of the *Vernonia amygdalina* saponins was measured by the capillary rise method to determine the change in surface tension with increasing concentration of saponins as described by described by Hernan *et al*., (2001).

Soil Sample Collection

The contaminated soil sample was collected from Kaduna Refinery Petrochemical Company where both liquid and solid refinery waste are discharge in Kaduna state Nigeria which had been exposed for many decades to petroleum hydrocarbons, polycyclic aromatic hydrocarbons and trace elements. The sample was collected from different spot at same location in accordance to the distance from the source of the waste. The soil sample was taken to the department of soil science Ahmadu Bello University Zaria, air dried, sieved through a 2-mm sieve and the physicochemical properties were determined according to the methods of (Bada *et al.,* 2018).The particle size distribution of soil sample (%sand, %silt and %clay) was carried out according to Bouyoucos Hydrometer method to identify the soil texture (Umeri *et al.,* 2017).

PAHs

The Polycyclic Aromatic Hydrocarbons standards were purchased from Zayo-Sigma Chemicals Ltd.

PAHs Extraction from Soil Samples

Eight grams (8g) of sample was extracted with acetone/dichloromethane (1:1) solvent for 2 hours. After the extraction, it was allowed to evaporate on bench for 24 hours; the remaining extract was then dissolved in 10ml dichloromethane. The 1µl of the extracted solution was injected in High Performance Liquid Chromatograph (HPLC) for PAHs quantification.

Experimental System

The incubation experiment was carried out using the method described by Davin *et al., (*2018) with some modifications. In order to determine the effectiveness of PAHs degradation, the incubation experiment was done under four conditions: sample soil without saponins, sample soil with CMC of the saponins, sample soil with 2*CMC of the saponins and sample soil with 4*CMC of the saponins. Untreated soil samples were used as control and two separate incubation periods of 7 and 18 days were investigated. 15g of the experimental soil was placed at water holding capacity of 80% in a 15-ml centrifuge tubes and were pre-incubated for 3 days. After the incubation, the different concentrations of the saponins were added to the soil samples and the centrifuge tubes were closed by caps and placed in a centrifuge machine, shaken at 200 rpm at room temperature. Oxygen that is required for bioremediation was let in by opening the centrifuge tubes for 5min every day. All modalities were done in triplicate for each sample. After each of the incubation period, soils were subjected for PAHs measurement.

Statistical Analysis

The data obtain from the experiments were subjected to statistical analysis. Statistical analysis was carried out by performing calculations, analysis using one-way ANOVA and visualizing data in SPSS statistic version 23.0. The final values represented as mean (standard error) SE.

4.0 RESULTS AND DISCUSSION

Table1: Soil properties of the contaminated soil from the Kaduna refinery petrochemical company

Parameter	Value
pH in H_2O	5.6
pH in 0.01m $CaCl_2$	4.9
ECe (dSm^{-1})	0.009
Clay (%)	8
Slit (%)	10
Sand (%)	82
Texture	Loamy Sand
Organic Carbon (%)	6.94
Phosphorus (%)	0.675
Total Nitrogen (%)	0.315

*****Characterization of the contaminated soil with crude oil showed that the soil had loamy-sand texture with acidic pH both in H_2O and $CaCl_2$ (5.6 and 4.9) respectively. Rakesh (2012) presented 6.5 as the suitable pH value for the degradation of polycyclic aromatic hydrocarbons and that degradation is higher in the relatively acidic soil than alkaline soil. However there was a view that low pH (strong acidity) affected the rate of soil degradation by bacteria in oil contaminated soil Okoh (2006). The amount of phosphorus, nitrogen and organic carbon which are the soil minerals needed by the soil microorganisms for bioremediation are relatively sufficient to induce bioremediation of PAHs in the contaminated soil.

Table 2: Surface tension data for *V.amygdalina* (bitter leaf) saponins

Saponins concentration (mg/L)	0	6	10	20	40	70	100	120	130	150	200
Surface Tension(N/m)	42	41	38.5	36	35.5	28.5	26.5	25	26.5	26.5	27

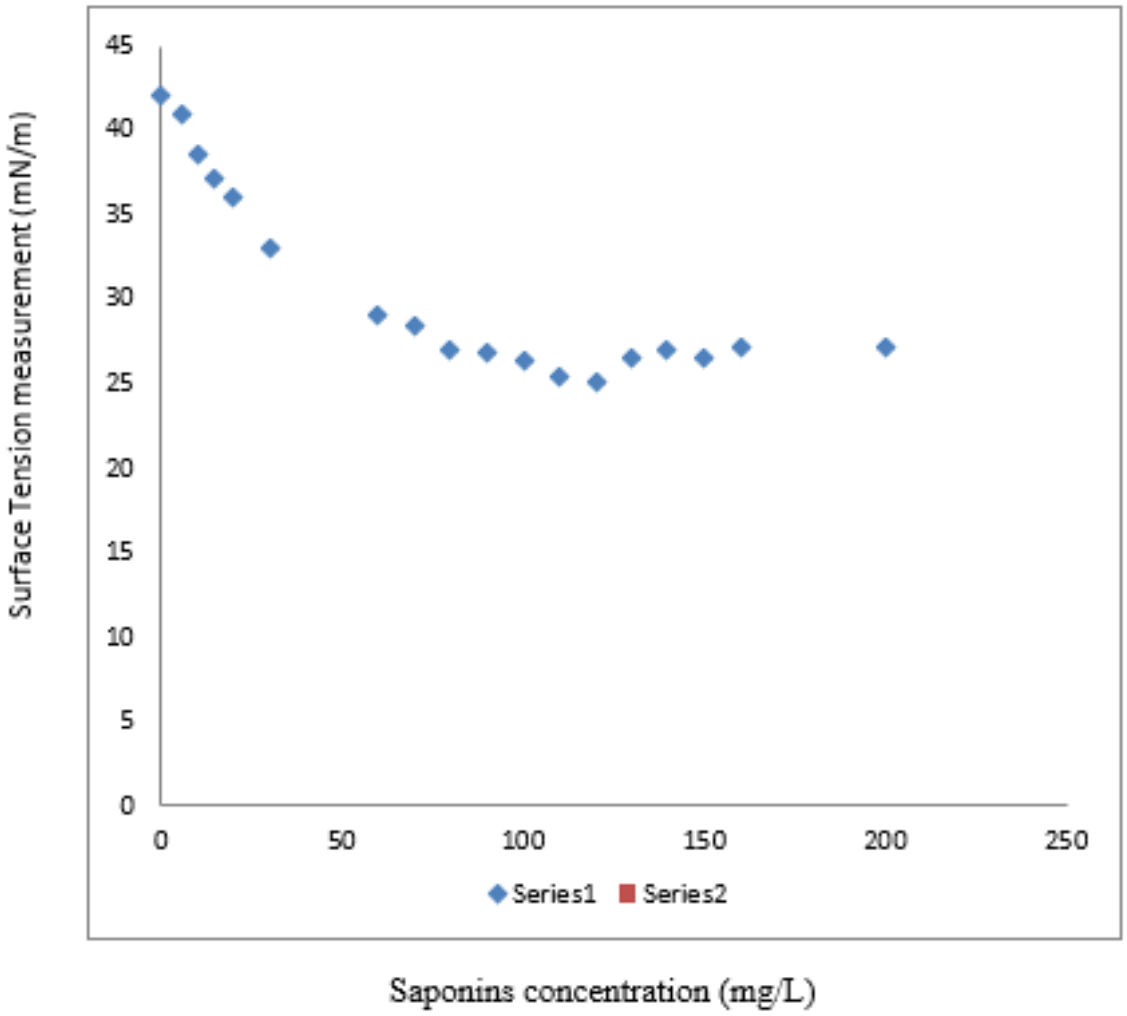

Figure 4.1Measured Surface Tension Values for Bitter leaf Saponins

There is no any available literature to the best of our knowledge that reported the critical micelles concentration (CMC) of saponins from *V.amygdalina.* Brian, (2016) presented the CMC of saponins derived from Quillaja bark to be approximately 60mg/L. Other studies conducted by Zhou *et al.,* (2011) and Stanimirova, (2011) on the same Quillaja plant presented their CMC data of 30mg/L and 247.5mg/L respectively.

Brian, (2016) also reported that the CMC of the saponins varied between manufacturers and source and importantly also from plant species to another, thus, implies that it is necessary to determine the specific CMC for the product used in this research. As such the *V.amygdalina* saponins evaluated as part of this research was determined to have CMC of approximately 120mg/L (1g/500ml stock solution). This value is within the range of CMC values determined by others as stated herein. The lower the CMC values the less quantity of the saponins is needed to induce solubilisation while the higher the CMC values the more quantity of the saponins is needed to cause solubilisation. Table 2 provides summary of the surface tension measurement taken at various saponins concentration and this result is depicted in graphical in figure 1. As proposed by Oakenfulls (1986), the relative break in

surface tension around the estimated CMC is an indication that saponins form micelles as opposed to other aggregate types.

Table 3: Residual of PAHs contents in soils treated with saponins after 7 days incubation (mg.kg^{-1}DW)

PAHs	Initial	Control	CMC	2*CMC	4*CMC	p-value
Naphthalene	48.56	26.81±0.88	1.44±0.02	1.67±0.01	1.14±0.00	0.0000
Phenanthrene	18.01	15.04±0.63	0.08±0.00	1.01±0.00	1.19±0.01	0.0000
Benzo(a) pyrene	9.00	7.31±0.28	3.49±2.79	0.68±0.01	0.66±0.04	0.0304

P-values (5% confidence level) indicate whether the amount of PAHs quantified from the soil sample treated with saponins are significantly difference from the control group. Values are means±SE, N= Sample size, CMC= Critical Micelles Concentration

Table 4: Residual of PAHs contents in soils treated with saponins after 18 days incubation (mg.kg^{-1}DW)

PAHs	Initial	Control	CMC	2*CMC	4*CMC	p-value
Naphthalene	48.56	24.87±1.05	0.76±0.03	0.88±0.16	3.65±0.98	0.0000
Phenanthrene	18.01	15.38±0.40	0.36±0.03	2.82±0.16	3.35±0.34	0.0000
Benzo (a) pyrene	9.00	8.32±0.32	4.57±0.78	0.14±0.01	4.62±0.28	0.0000

P-values (5% confidence level) indicate whether the amount of PAHs quantified from the soil sample treated with saponins are significantly difference from the control group. Values are means±SE, N= Sample size, CMC= Critical Micelles Concentration

The residual PAHs contents of both the treated and untreated soil sample after 7 and 18 days of incubation were presented in Table 3 and 4 respectively. After comparing the residual mean values of the different group treatment to the Belgian Walloon legislation norms values that are available in supplementary data it is clear that none of the incubation modalities were able to reduce the PAHs down to its reference value (0.1mg.kg^{-1}DW), even though some compounds have been relatively reduced enough to change the soil occupation criteria.

After a careful study of the each PAHs residual mean, a few deductions can be drawn after each incubation scenario: (i) in all incubation modalities Naphthalene was reduced below 25mg.kg^{-1} and 9mg.kg^{-1} (industrial and commercial intervention value) after 7 and 18 days. Phenanthrene was lowered below 16mg.kg^{-1} agricultural intervention value after the incubation period. Benzo-A-pyrene was not completely lowered in all the modalities below any of the soil occupation intervention value after 7 and 18 days. (ii) In control samples and after the two different incubation period there appeared to be no significant reduction or biodegradation of PAHs as compared to the initial concentration after 7 and 18 days.

The changes in the mean values observed in bioremediation studies are not in any linear order with the concentration of saponins addition.

Statistical analysis: (i) After comparing the residual PAHs content of the 7and 18 days incubation periods, the values in the samples treated with saponins are statistically significantly different from control samples at any of the incubation period (ii) time has no significant effect on the biodegradation of polycyclic aromatic hydrocarbons.

When the experiment was conceived, it was based on the assumption that the addition of surfactants to the contaminated soil would increase PAHs degradation as reported by the following researchers.

It was reported by Kobayashi *et al., (*2012) that the biodegradation of pyrene by *sphingomonas* sp. was increased in the presence of saponins. Likewise, the same scenarios were expected in this study, there were biodegradation of naphthalene, phenanthrene and Benzo-A-pyrene in our study also. Davin *et al.,* (2018) reported a partial degradation of polycyclic aromatic hydrocarbons by the addition of saponins. In their research only Naphthalene and Acenaphthalene were significantly degraded. Xiao-Land and Yong, (2018) also conducted a research on the application of tea saponins in the bioremediation of organic pollutant and they reported a significant effect on the increasing biodegradation efficiencies of tea saponins on organic pollutants. This research therefore is in agreement with the findings of Kobayashi *et al.,* (2012), Davin *et al.,* (2018) and Xiao-Land and Yong, (2018) all reported the biodegradation of PAHs with addition of surfactants.

5.0 Conclusion

Results of this study showed that ethanolic extract of saponins compound from *V.amygdalina* leaves have shown its potential to increase the biodegradation of polycyclic aromatic hydrocarbon by soil microorganisms specifically the lower molecular weight compounds in contaminated soil samples.

Recommendation

The changes in the mean values observed in bioremediation studies are not in any linear order with the concentration of saponins addition, therefore more studies need to be conducted to establish the order of the degradation of these organic contaminants in relation to the concentrations of the saponins added. Also there is a need to establish the specific mechanism of the degradation of these contaminants through addition of saponins from the *V.amygdalina* leaves.

References

Abiram, K.R., Kongkona, S., Ponnusamy, S.K., Sunita, V.,Shravani, K., Nikhil, B., Jenet, G. and Vinoth, K.V. (2022). Surfactants-aided mycoremediation of soil contaminated with polycyclic aromatic hydrocarbons (PAHs) progress, limitation and counter measure. *Journal of Chemical Technology and Biotechnology* (2) 391-408.

Bada, B. S., Towolawi, A. T., Anyiam, D. C. (2018). Biodegradation of polycyclic aromatic hydrocarbons in crude contaminated soil using composted market waste. *J. Appl. Sci. Environ.* Vol.22(1) 141-145.

Bishnoi,N.R., Mehta,U.(2005). Quantification of polycyclic aromatic hydrocarbons in tea and coffee samples of Mumbai city (india) by high performance liquid chromatography, *Environmon assess,cot*: 399-406.

Brian A. L. (2016). Evaluation of an alternative natural surfactant for Non Aqueous Phase Liquid Remediation .*Master's Thesis Western Michigan University.*

Davin, M.;Amandine, S.;Magali, D.;Georges, L.;Gilles, C.;Marie-Laure, F. (2008). Could saponins be used to enhance bioremediation of polycyclic aromatic hydrocarbons in age contaminated soil

Gberikon,G.M., Iyoula, F.I., Ichor,S.T (2019). Effect of bitter leaves Extract on Bacteria Isolated from soils of some mechanic and non-mechanic sites in Makurdi metropolis. *Int. J. Appl. Sci. Biotechnol. Volume7(1):81-87.*

Gurjeet, P., Kothiyal, N.C., Vaneet, K. (2015). Bioremediation of some polycyclic aromatic hydrocarbons (PAHs) from soil using sphingobium indicum, sphingobium japonicum and stenotrophonomas maltophilia Bacteria strains under Aerobic conditions. *Journal of Environmental Research and Development.* Vol. 8, No.3 pp394-405

Hernan, R., Jose, K., Alicia ,F.C. and Mariano, F.C. (2001). A simplified method for the determination of critical micelle concentration. *Journal of chemical education*, 78(3):347-

Hostettmann, K., Marston, A. (2005). Saponins: Chemistry and pharmacology of natural products. *Cambridge University Press, Cambridge, isbn*-10: 0521020174.

Ijeh II, Igwe KK and Ejike CE (2008) Effect of administration of aqueous extracts of *Vernoniaamygdalina*.Del leaves to guinea pig dams on milk production and contraction of the mammary gland and uterus. *Afri J of Trad, Compl and Altert med, Abstracts of The World Congress on Medicinal and Aromatic Plants, Cape Town*. 11:439-440.

Kobayashi T., Kaminaga H., Navarro R. & Iimura Y., 2012.Application of aqueous saponin on the remediation of polycyclic aromatic hydrocarbons-contaminated soil.J. *Environ. Sci. Health*, Part A 47 (8), 1138-1145

Lakra J., Tikariha D., Yadav T., Satnami M.L. & Ghosh K.K., 2013.Study of solubility efficiency of polycyclic aromatic hydrocarbons in single surfactant systems. *J. Surfact. Deterg.* 52016, 957-966. 521

Megharaj M., Ramakrishnan B., Venkateswarlu K., Sethunathan N. & Naidu R., (2011).Melanosi of the rectum in patients with chronic constipation. *Dis Colon Rectum 28(4):241–5.*

Ming, C., Piao, X., Guanyming, Z., Chunping, Y., Danlian, H., Jiachao, Z. (2015). Bioremediation of soils contaminated with polycyclic aromatic hydrocarbons, petroleum, pesticides, chiorophenols and heavy metals by composting: Applications, microbes and future research needs. *Biotechnology Advances* (33) 745-755.

Oakenfull, D. "Aggregation of Saponins and Bile Acids in Aqueous Solution." *Australian Journal of Chemistry* 39 (1986): 1671 – 1683.

Okoh, I.O (2006). Biodegradation alternative in the clean-up of petroleum hydrocarbon pollutants. *Biotechnology and Molecular Biology Review*, 1(2): 38 - 50.

Rakesh, M. Pawar (2012). The effect of soil pH on degradation of polycyclic aromatic hydrocarbons. *PhD thesis collection University of Hertfordshire*

Sodipo, O.A., , M.A Akanji. and Odutuga, A.A. (1990): Comparative study of the effect of saline extracts of the pulp and seeds of Garcinia kola (Heckel) on some mammalian erythrocytes. *Nig. J. Sci. 24* (182) 95 – 99.

Stanimirova, R., Mirinova, K., Tcholakova, S., Denkov, N.D., Stoyanov, S. and Pelan, E. "Surface Rheology of Saponin Adsorption Layers." *Langmuir* 27 (2011): 12486 – 12498.

Umeri, C., Onyemekowu, R.C., Moseri, H. (2017). Analysis of physical and chemical properties of some selected soils of rain forest zones of Delta Nigeria. *Agricultural Research and Technology Open Access. Vol. 4, pp 88-92.*

Von Lau E., Gan S., Ng H. & Poh P. (2014). Extraction agents for the removal of polycyclic aromatic hydrocarbons (PAH) from soil in soil washing technologies. *Environmental Pollution*, 552184, 640-649.

Xiao-Lan, Y. and Yong, H. (2018).Effective natural surfactants beneficial for soil remediation, from preparation to application.*The royal society of chemistry RSC Adv*., 8, 24312 –24321 24319.

Zhou W., Yang J., Lou L. & Zhu L., 2011.Solubilization properties of polycyclic aromatic hydrocarbon. *Colloids Surft.* A 226, 145-153.

Enhancing Breast Cancer Detection: Deep Belief Networks and Local Binary Patterns for Multi-Objective Feature Selection Using NSGA-III

Abdullahi Hameed Mohammed[1], Abdulrasheed Jimoh[2], and Ali Muhammad Usman[2]
[1]Chemistry Department, Federal College of Education (Technical), Gombe
[2]Computer Science Department, Federal College of Education (Technical), Gombe

Abstract

Breast cancer is a leading cause of cancer-related deaths among women, second only to lung cancer. Timely diagnosis and treatment are critical in reducing mortality rates. Multi- objective feature selection methods, particularly cell nucleus detection, play a vital role in breast cancer detection. However, existing deep learning approaches primarily rely on contour in- formation, often overlooking essential semantic details from shallow layers. To address this limitation, we propose a novel multi-objective feature selection method using the Non-dominated Sorting Genetic Algorithm (NSGA-III) for breast cancer detection. Our proposed methods the BreakHis dataset and incorporates data augmentation techniques to analyze internal morphological features comprehensively. Deep Belief Networks (DBNs), Local Binary Patterns (LBP), and Completed Local Binary Patterns (CLBP) are employed for feature extraction. By utilizing NSGA- III, our method selects optimal features, which are subsequently fed into a Long Short-Term Memory (LSTM) network for classification. Through the minimization of imaging features, our approach significantly enhances breast cancer detection accuracy, precision, sensitivity, and specificity. Our proposed method offers a superior approach to breast cancer detection by combining multi-objective feature selection using NSGA-III, deep learning techniques, and advanced feature extraction methods. Notably, it demonstrates faster detection of breast cancer among women while achieving remarkable accuracy and precision. Experimental results demonstrate exceptional performance measures, with accuracy, precision, F1-Score, sensitivity, and specificity rates of 97.55%, 95.98%, 92.42%, 99.22%, and 99.58%, respectively. Comparative analysis against existing methods reveals that our proposed method outperforms the majority of them in terms of both performance measures and computational time.

Keywords: Multi-objective Optimization, Nondominated Sorting Genetic Algorithms, Breast cancer, Deep Belief Net- works, Local Binary Patterns.

Introduction

Breast cancer is a major health concern worldwide, particularly among women, with high mortality rates. Early detection and accurate diagnosis are crucial for effective treatment and improved patient outcomes. In recent years, advancements in deep learning techniques have shown great potential in improving breast cancer detection. However, existing methods often overlook important semantic details from shallow layers, leading to sub-optimal performance. This paper presents a novel approach that combines deep learning with multi- objective feature selection using NSGA-III to enhance breast cancer detection accuracy.

Breast cancer is the second leading cause of cancer-related deaths in women, following lung cancer. The mortality rate associated with breast cancer is approximately 2.7%, affecting approximately 1 in 37 women Abdollahi et al. (2022). Early diagnosis and treatment are crucial for reducing mortality

rates and preventing disease progression Jafari et al. (2018). Pathological images play a vital role in the diagnosis of breast cancer, providing valuable information for doctors and researchers. Variations in morphological features of nuclei images serve as indicators for tumor detection and diagnosis Duggento et al. (2021). Therefore, accurate detection of nuclei in these images is essential for efficient breast cancer diagnosis Abdollahi et al. (2022).

Histopathological analysis is a key aspect of breast cancer diagnosis, where biopsy samples are stained and examined under a microscope by pathologists. Hematoxylin-Eosin (H- E) staining is the most widely used method, where nuclei are stained purple or blue using Hematoxylin, while the stroma and cytoplasm are stained pink using Eosin Jiang et al. (2023). The size, shape, cytoplasmic ratio, and chromatin patterns of the nuclei are important factors in assessing breast cancer- affected tissues Al-Jabbar et al. (2023). Cell nuclei detection is a core operation in computer-aided diagnosis (CAD) for cancer detection, enabling cell counting and the study of sub cellular morphology Rahimi Lifshagerd and Safari (2023). However, the detection of cell nuclei in histopathological images presents challenges due to complex structures, back- ground clutter, and artifacts Naik et al. (2023).

Existing deep learning methods for breast cancer detection primarily rely on contour information for accurate detection. However, these methods often fail to effectively extract details from shallow layers, which are crucial for precise breast cancer detection Shihabuddin and Beevi (2023). To address this limitation, this paper proposes a multi-objective feature selection method using Non-dominated Sorting Genetic Algorithm (NSGA-III) for breast cancer detection. The proposed method utilizes the BreakHis datasets and incorporates prepossessing techniques such as color variation and data augmentation. Fea- tures are then extracted using Deep Belief Networks (DBNs), Local Binary Patterns (LBP), and Completed Local Binary Patterns (CLBP) to identify salient regions in the images. The proposed multi-objective feature selection method with NSGA-III selects optimal features for subsequent classification using Long Short-Term Memory (LSTM) networks. By reducing the number of features and minimizing classification errors, the proposed method aims to enhance breast cancer detection rates.

The paper is organized as follows: Section 2 offers a comprehensive review of the relevant literature, discussing important ingredients such as Deep Belief Networks (DBN), Completed Local Binary Patterns (CLBP), and the Non- dominated Sorting Genetic Algorithm (NSGA-III). Section 3 presents the proposed methodology in detail, encompassing pre-processing techniques, a description of the datasets used, and the multi-objective feature selection approach employing NSGA-III. Section 4 showcases the results and provides a thorough discussion. The performance of the proposed method is evaluated and compared with existing approaches. Finally, Section 5 concludes the research by summarizing the key findings and emphasizing the potential impact of the proposed method in enhancing breast cancer detection rates.

Related Works

The study incorporates three major ingredients: Deep Belief Networks (DBNs), Completed Local Binary Patterns (CLBP), and the Non-dominated Sorting Genetic Algorithm III. The following sections provide a detailed description of each of these methods:

Deep Belief Networks

A Deep Belief Network (DBN) is a powerful generative model with a deep architecture. This article provides a com- prehensive understanding of DBNs, including their definition, functioning, applications, and coding implementation. DBNs are designed to address limitations in traditional neural networks with deep layers. They overcome challenges such as slow learning, convergence to local minima due to poor parameter selection, and the need for large training datasets.

A DBN consists of multiple layers of stochastic latent variables, known as binary feature detectors or hidden units. It is a hybrid generative graphical model, with the top two layers lacking direction while the higher layers have directed links to lower layers. DBNs are used for unsupervised probabilistic deep learning.

Although DBNs resemble deep neural networks, they are distinct. DBNs are feed forward neural networks with a deep architecture, comprising multiple hidden layers. They are constructed using simpler unsupervised networks like restricted Boltzmann machines (RBMs) or auto encoders, where the hidden layer of each sub-network serves as the visible layer for the subsequent layer.

The evolution of Deep Belief Neural Networks progressed from the use of Perceptrons in the First Generation of neural networks, which had limitations in handling complex technology. The Second Generation introduced Back propagation, a technique that reduces error values by comparing desired and received outputs. Belief networks, represented by directed acyclic graphs, further contributed to solving inference and learning problems. Deep Belief Networks, in particular, help generate unbiased values that can be stored in leaf nodes.

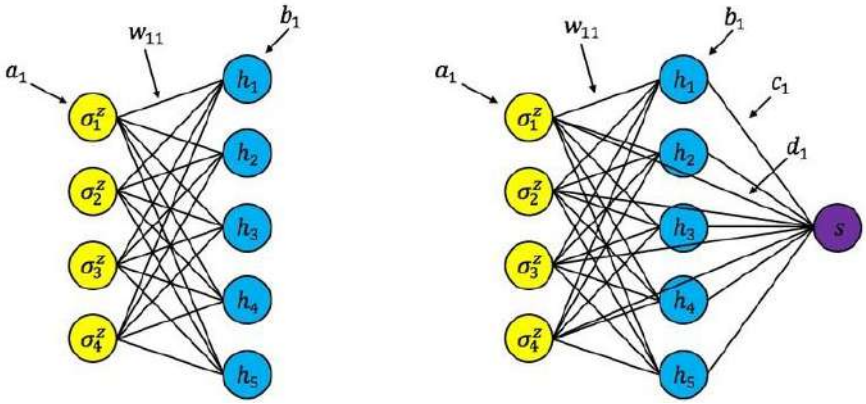

Fig. 1. Deep Belief Network

Completed Local Binary Patterns

The Local Binary Pattern (LBP) is a textural operator widely used in various computer applications such as facial recognition and target detection Muhammad et al. (2012). Singh Singh et al. (2012) introduced the LBP operator, which generates a binary code by comparing the gray value of a neighboring pixel with that of the central patch. If the neighbor pixel is smaller, it is assigned a value of 0; otherwise, it is assigned a value of 1.

The LBP operator determines the threshold value for the neighbor pixel based on the gray level of the center pixel. However, one major limitation of the LBP descriptor is that it focuses solely on the sign of the variance of the two gray values Singh et al. (2012).

To address this limitation and enhance the robustness of textural feature representation, the Complete Local Binary Pattern (CLBP) was proposed. Guo et al. introduced the concept of CLBP, which includes additional instructions not covered by the original LBP operator Singh et al. (2012). Unlike LBP, CLBP decomposes the input signal into the sign, magnitude, and different parts. This decomposition allows for

more accurate textural characterization. CLBP incorporates a local domain defined by a center pixel and the difference in magnitude between the center pixel and adjacent gray values. This information is referred to as the Local Difference Sign- Magnitude Transform, which is not included in a standard LBP texture descriptor Jegan and Jayagowri (2023).

Non-dominated Sorting Genetic Algorithm (NSGAIII)

NSGAIII was developed by Deb and Jain (2013) and has shown promising results in solving different kinds of MOPs. Thus researchers are motivated to use it and solve problems related to MOP including the work of Li et al. (2019). However, since its inception, it has never been used to solve FS imaging problems for breast cancer detection despite its proven records.

Proposed Methodology

In addition to discussing the ingredients utilized in the paper, this section provides a comprehensive description of the datasets, data processing techniques, parameter settings, and the performance measures employed.

Datasets Image Description

The proposed method utilizes the Breast Cancer Histopathological Image classification (BreakHis) datasets, comprising microscopic images of both malignant and benign breast tumors. The malignant tumor category encompasses four distinct classes: Ductal Carcinoma, Lobular Carcinoma, Mucinous Carcinoma, and Papillary Carcinoma. Conversely, the benign tumor category comprises Adenosis, Fibroadenoma, Phyllodes-tumor, and Tubular-adenoma, which are characterized by their slower growth and localized nature. The BreakHis dataset comprises a total of 9,109 breast tumor images obtained from 82 patients, employing various magnification factors such as 40x, 100x, 200x, and 400x. These images consist of 5,429 samples of malignant tumors and 2,480 samples of benign tumors, each measuring 700×460 pixels and containing three RGB channels with an 8-bit depth per channel.

Histological benign refers to lesions that lack malignant characteristics such as cellular atypia, disruptions microscopy images are randomly duplicated without adhering to fixed angles. Horizontal and vertical flipping is applied, with the latter being equivalent to rotating the image by 180 degrees prior to horizontal flipping. Additionally, shearing is utilized to distort portions of the images, creating parallelograms or altering the image shape through stretching.

Data Pre-processing and Cleaning

To ensure accurate analysis of the internal tissue morphology, the microscopic breast images from the BreakHis datasets undergo pre-processing, given that they are stained using the H-E method. However, variations in color arise due to differences in staining procedures, which can impede the model training process. To address this issue, the proposed multi-objective method employs color harmonization techniques by aligning the color characteristics of one image with another, thereby establishing color correlation. Specifically, a specific image source is selected to impose its color characteristics on the other images during pre-processing.To mitigate the risk of overfitting, data augmentation techniques are employed. These include flipping transformations, random rotations, and shearing transformations.

Parameter Settings

A jMetal library in Durillo and Nebro (2011) was used for the proposed method. The population size and the maximum iterations are 30 and 100 respectively. The mutation is set to 1/n, where n is the maximum feature size for each datasets and the cross-over probability is 0.9. Other parameters used the default settings of the library. For all the datasets, each algorithm has been run up to forty different times.

While conducting the experiments, the images of all the datasets were separated randomly into training and testing tests. While the training set takes 70% of the images whereas testing set take 30%. The proposed method was first run on the training set to select the subsets of images and later, the performance of the chosen images is computed on the test set using the support vector machine classification algorithm.

Performance Measure

The performance of the proposed were being measured based on the classification accuracy, sensitivity, specificity, precision, F1-Score, and computational time. The essence of the proposed multi-objective algorithm along with deep belief network and local binary patterns is to produce fewer features that contribute significantly to detection of breast cancer images and yet improve the detection accuracy within a shorter time. In this case, the proposed method will select the most informative features from the datasets. In addition, the selected features will be used to detect the most promising images and compared to the ones found in the literature that used similar datasets image.

The accuracy is computed using the formula in (1).

$$\text{Accuracy} = (TP + TN + FP + FN)/ (FP+FN) \quad (1)$$

The precision is computed using the formula in (2).

$$\text{Precision} = (TP) / (TP + FP) \quad (2)$$

The specificity is computed using the formula in (3).

$$\text{Specificity} = (TN) / (TN + FP) \quad (3)$$

The sensitivity is computed using the formula in (4).

$$\text{Sensitivity} = (TP) / (TP + FN) \quad (4)$$

TP , TN , FP , FN represent true positives, true negatives, false positives, and false negatives correspondingly.

Results and Discussions

The findings of the proposed method are presented in Table I and depicted in Figure 4. The evaluation metrics employed include accuracy, specificity, precision, sensitivity, and F1- score. The table clearly demonstrates that the proposed method achieves an accuracy level of 97.55%. Notably, it exhibits the highest performance in terms of sensitivity, reaching 99.22%. The precision and specificity metrics both yield a value of 95.98%. However, the F1-score reflects the lowest classification performance among the metrics.

Upon closer examination of the table, it becomes evident that sensitivity is the most prominent factor, followed by accuracy. This indicates that the utilization of deep belief networks and local binary patterns for multi-objective feature selection with the NSGA-III algorithm effectively facilitates the evolution of the optimal subset of images, leading to improved classification accuracy and sensitivity.

TABLE I Results of The Proposed Method

Performance Metrics	Proposed Method
Accuracy	97.55
Precision	95.98
F1-Score	92.42
Sensitivity	**99.22**

Specificity	95.98

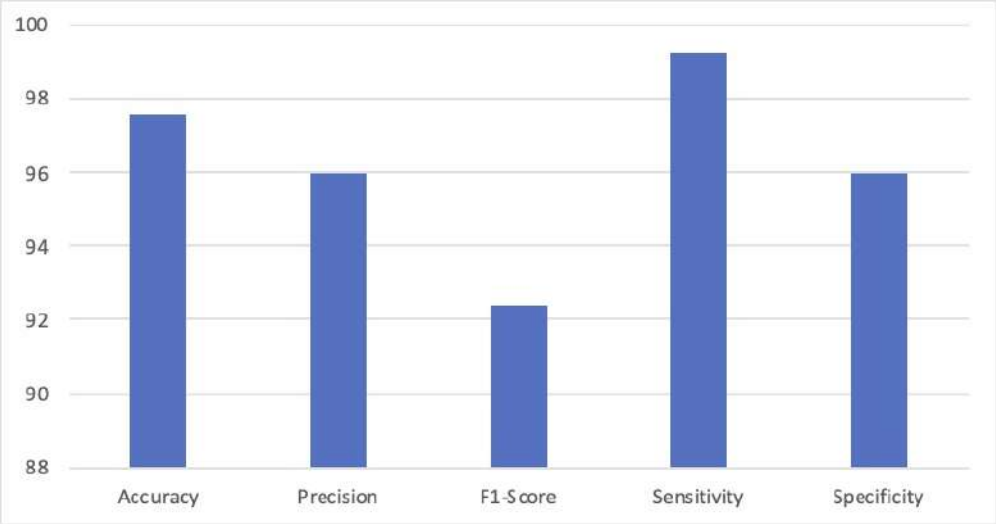

Fig. 2. Results of the Proposed Method

Comparisons Between The Proposed Method and Other Existing Methods

To ensure impartiality, the proposed method is compared to other existing approaches using the same system and similar functionalities, based on performance metrics. A comparison was initially conducted with the ACO-PSO approach hybridizing Ant Colony Optimization Algorithm with Particle Swarm Optimization Algorithm, as presented in Saturi and Premchand (2021). Although notable results were achieved by the ACO-PSO method on comparable datasets, it only attained a maximum accuracy of 95.72%, whereas the pro- posed method achieved an accuracy of 97.55%. Additionally, the proposed method outperformed ACO-PSO in terms of sensitivity, specificity, precision, and F1-score.

Furthermore, a comparison was made with the work of Wahab et al. (2019), which utilized a novel transfer learning- based deep CNN for segmentation and detection of mitoses in breast cancer histopathological images. Although the results were promising, they were not as impressive as those obtained by the proposed method in all aspects. Similarly, the work of Budak et al. (2019) employed a computer-aided diagnosis sys- tem combining FCN and BiLSTM models for efficient breast cancer detection from histopathological images. While the FCN-BiLSTM approach performed well in terms of accuracy, specificity, precision, F1-score, and sensitivity on the datasets, the proposed method surpassed it across all performance measures.

Additionally, a comparison was made with the residual recurrent CNN in Alom et al. (2019) and the multiscale RBF networks combined with DCT for breast cancer detection (MSRBF-DCT) in Beltran-Perez et al. (2020), both of which used similar datasets and obtained promising results. However, the proposed method consistently outperformed these existing works in all aspects. Consequently, the

proposed method demonstrated superior performance across all performance metrics compared to the existing approaches, while success- fully selecting optimal features for improved breast cancer detection.

Comparisons With Existing Works Based on Computational Time

The proposed method is compared to existing works in terms of computational time. Among all the methods, FCN- BiLSTM exhibits the longest detection time for breast cancer, followed by MSRBF-DCT with durations of 65 and 60 sec- onds, respectively. Conversely, ACO-PSO takes 50 seconds for breast cancer detection, while both the proposed method and CNN share the same computational time of 45 seconds. It is not surprising for CNN to be faster since it has fewer embedded algorithms compared to the other approaches. In the case of the proposed method, the application of NSGA-III algorithms treats each image feature as a pixel and employs a multi-objective approach that considers them simultaneously, leading to the observed computational time.

TABLE II Results of The Proposed Method With Existing Ones

Performance Metrics	ACO-PSO	FCN-BiLSTM	CNN	MSRBF-DCT	Proposed Method
Accuracy	95.72	93.68	92.71	93.99	97.55
Precision	94.52	92.64	90.22	91.32	95.98
F1-Score	91.57	90.62	89.66	90.11	92.42
Sensitivity	97.35	95.62	92.15	92.65	99.22
Specificity	94.54	89.44	93.27	94.35	95.98

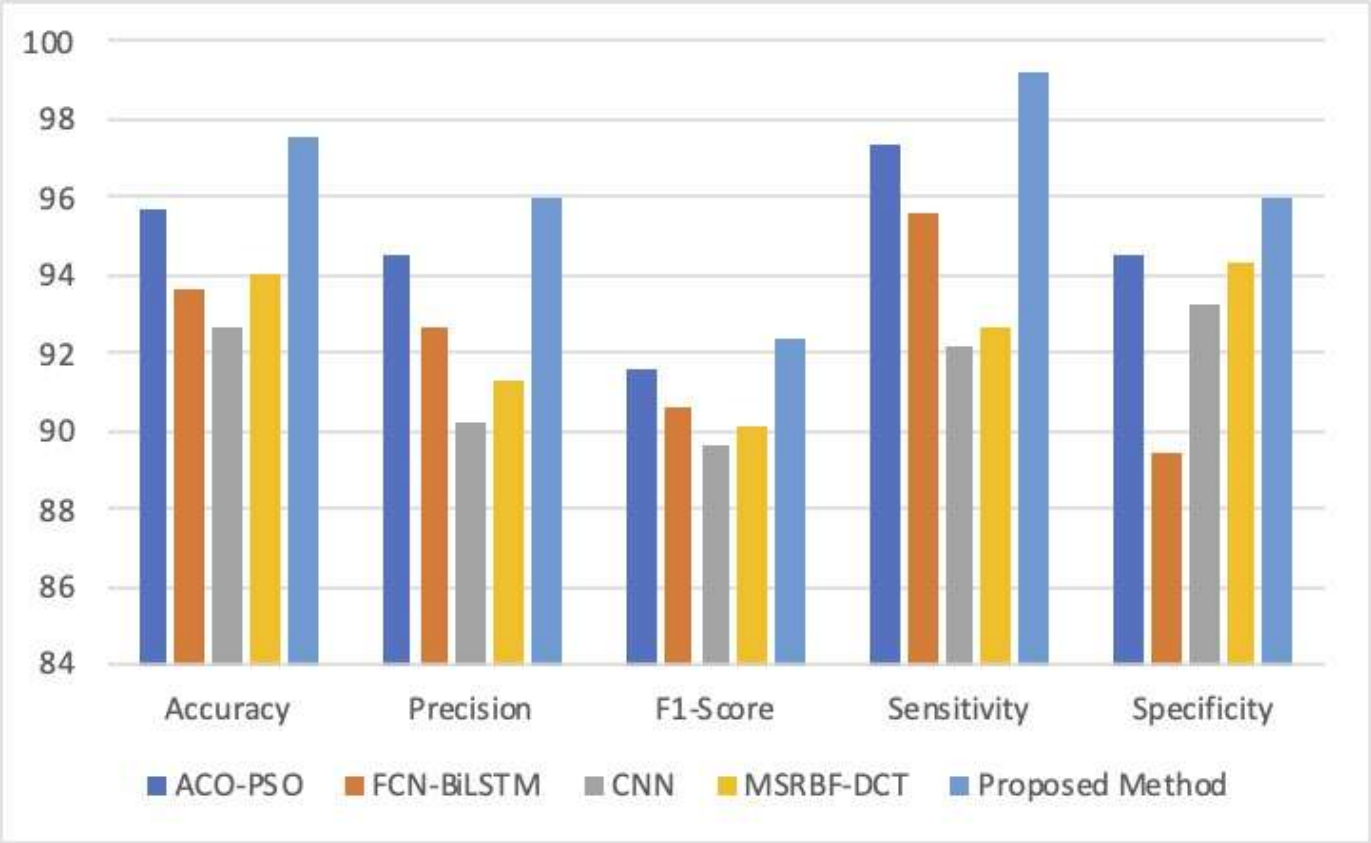

Fig. 3. Comparison of Results With The Proposed Method

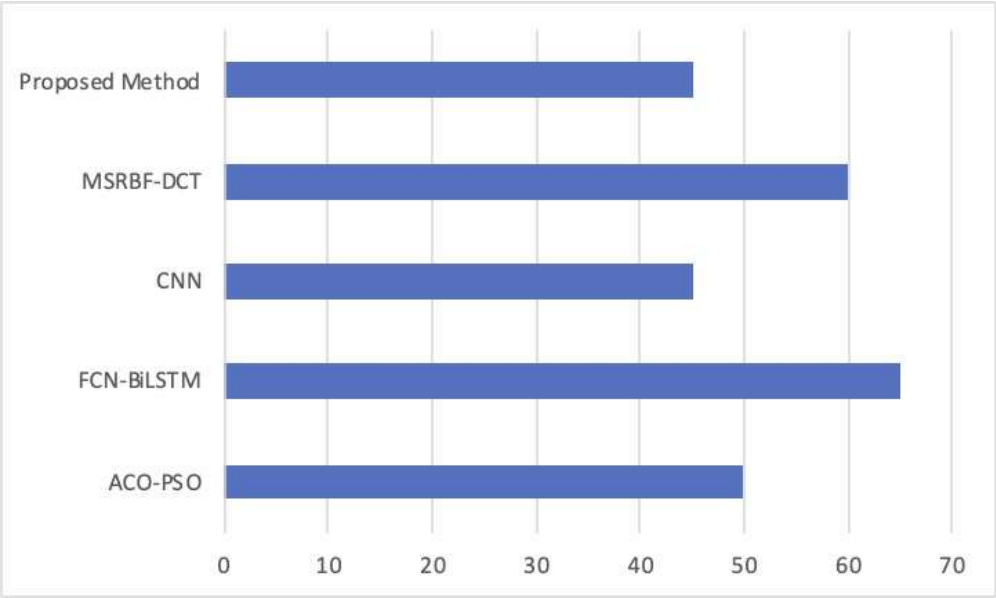

Fig. 4. Comparison of the Proposed Method With Others Based on Compu- tational Time

Conclusions and Future Directions

The findings of this study demonstrate the potential of employing Deep Belief Networks (DBNs) and Local Binary Patterns (LBP), in conjunction with NSGAIII algorithms, to improve the detection of breast cancer. The results ob- tained indicate that the proposed methods exhibited promis- ing outcomes and surpassed existing techniques across all performance measures utilized. Conventional methods often struggle to effectively extract crucial details from shallow layers, which are essential for accurate breast cancer detection. To address this issue, the proposed approach leverages the BreakHis dataset and incorporates preprocessing techniques, such as color variation and data augmentation. Images are then analyzed using DBNs, LBP, and Completed Local Binary Patterns (CLBP) to identify significant regions within the images. This process ensures that the semantic details from the shallow layers provide precise contour information, thereby enhancing the detection process.

Furthermore, the proposed method demonstrates superior computational efficiency, as evidenced by a comparison of execution times. This faster detection of breast cancer enables expedited decision-making.

In future studies, we will explore the use of various filter- based approaches to further enhance the selection of the most appropriate images for analysis. Additionally, we plan to investigate the potential of employing other multi-objective optimization algorithms for image selection. By exploring such algorithms, we anticipate the possibility of achieving even more promising results, ultimately aiding experts in making quick and accurate decisions regarding breast cancer detection.

Acknowledgement

The authors express their gratitude to Tetfund for supporting this research via its Tetfund conference grants. Additionally, heartfelt thanks are extended to the unanimous reviewers for dedicating their time to offer valuable insights and comments on the manuscripts.

References

Abdollahi, J., Davari, N., Panahi, Y., Gardaneh, M., et al. (2022). Detection of metastatic breast cancer from whole- slide pathology images using an ensemble deep-learning method: Detection of breast cancer using deep-learning. Archives of Breast Cancer, pages 364–376.

Al-Jabbar, M., Alshahrani, M., Senan, E. M., and Ahmed, I. A. (2023). Multi-method diagnosis of histopathological images for early detection of breast cancer based on hybrid and deep learning. Mathematics, 11(6):1429.

Alom, M. Z., Yakopcic, C., Nasrin, M. S., Taha, T. M., and Asari, V. K. (2019). Breast cancer classification from histopathological images with inception recurrent residual convolutional neural network. Journal of digital imaging, 32:605–617.

Beltran-Perez, C., Wei, H.-L., and Rubio-Solis, A. (2020). Generalized multiscale rbf networks and the dct for breast cancer detection. International Journal of Automation and Computing, 17:55–70.

Budak, U¨ ., Co¨mert, Z., Rashid, Z. N., S¸ engu¨r, A., and C¸ ıbuk, M. (2019). Computer-aided diagnosis system combining fcn and bi-lstm model for efficient breast cancer detection from histopathological images. Applied Soft Computing, 85:105765.

Deb, K. and Jain, H. (2013). An evolutionary many-objective optimization algorithm using reference-point-based non- dominated sorting approach, part i: solving problems with box constraints. IEEE transactions on evolutionary compu- tation, 18(4):577–601.

Duggento, A., Conti, A., Mauriello, A., Guerrisi, M., and Toschi, N. (2021). Deep computational pathology in breast cancer. In Seminars in cancer biology, volume 72, pages 226–237. Elsevier.

Durillo, J. J. and Nebro, A. J. (2011). jmetal: A java framework for multi-objective optimization. Advances in Engineering Software, 42(10):760–771.

Jafari, S. H., Saadatpour, Z., Salmaninejad, A., Momeni, F., Mokhtari, M., Nahand, J. S., Rahmati, M., Mirzaei, H., and Kianmehr, M. (2018). Breast cancer diagnosis: Imaging techniques and biochemical markers. Journal of cellular physiology, 233(7):5200–5213.

Jegan, R. and Jayagowri, R. (2023). Windowed modified discrete cosine transform based textural descriptor approach for voice disorder detection. In Implementation of Smart Healthcare Systems using AI, IoT, and Blockchain, pages 147–167. Elsevier.

Jiang, Z., Dong, Z., Fan, J., Yu, Y., Xian, Y., and Wang, Z. (2023). Breast transfg plus: Transformer-based fine- grained classification model for breast cancer grading inhematoxylin-eosin stained pathological images. *Biomedical Signal Processing and Control*, 86:105284.

Li, P., Han, Z., Jia, X., Mei, Z., Han, X., and Wang, Z. (2019). Analysis and comparison on thermodynamic and economic performances of an organic rankine cycle with constant and one-dimensional dynamic turbine efficiency. *Energy Conversion and Management*, 180:665–679.

Muhammad, G., Mesallam, T. A., Malki, K. H., Farahat, M., Mahmood, A., and Alsulaiman, M. (2012). Multidirectional regression (mdr)-based features for automatic voice disorder detection. *Journal of Voice*, 26(6):817–e19.

Naik, D. A., Mohana, R. M., Ramu, G., Lalitha, Y. S., SureshKumar, M., and Raghavender, K. (2023). Analyzing histopathological images by using machine learning tech- niques. *Applied Nanoscience*, 13(3):2507–2513.

Rahimi Lifshagerd, M. and Safari, F. (2023). Therapeutic effects of hamscs secretome on proliferation of mda-mb- 231 breast cancer cells by the cell cycle arrest in g1/s phase. *Clinical and Translational Oncology*, 25(6):1702–1709.

Saturi, R. and Premchand, P. (2021). Multi-objective feature selection method by using aco with pso algorithm for breast cancer detection. *International Journal of Intelligent Engineering & Systems*, 14(5).

Shihabuddin, A. R. and Beevi, S. (2023). Multi cnn based automatic detection of mitotic nuclei in breast histopatho- logical images. *Computers in Biology and Medicine*, 158:106815.

Singh, S., Maurya, R., and Mittal, A. (2012). Application of complete local binary pattern method for facial expression recognition. In *2012 4th international conference on intelli- gent human computer interaction (IHCI)*, pages 1–4. IEEE.

Wahab, N., Khan, A., and Lee, Y. S. (2019). Transfer learning based deep cnn for segmentation and detection of mitoses in breast cancer histopathological images. *Microscopy*, 68(3):216–233.

An Overview on the Healthcare Infection Prevention and Control During Pandemic

*Rabilu Abubakar Wakkala[1], Hassan Abubakar Dalijan [2]
[1, 2] Department of Biology, Adamu Augie College of Education Argungu, Kebbi State

[1]aburabilu2489@gmail.com , 07064294470
[2]hassandalijan87@gmail.com, 07036318081

Abstract

In the health care facilities there is need to help strengthen resistance to pathogen threats and offer proper care for patients and health workers in the way that is safe. This paper observed the healthcare infection preventive and control measures during pandemic. Identified the difficulties they are facing, the present study tries to shed light on the role of the health care layout configuration in fighting pandemics. Over the past decade, agencies have confirmed the important of global burden of health care-associated infections, many of which are caused by multidrug-resistant organisms and can cause outbursts in health care facilities and in community settings. Studies showed that, in acute care hospitals, out of every 100 patients, 7 in high-income countries and 15 in low- and middle-income countries will acquire at least one health care-associated infection during their hospital stay. Among intensive care patients, the incidence of health care-associated infections is 2 to 20 times higher in low- and middle-income countries than in high-income countries. Although no precise analysis is possible due to lack of complete data, WHO has estimated that hundreds of millions of patients are affected by health care-associated infections leading to death in 1 in 10 infected patients every year. The COVID-19 pandemic has revealed how dangerous infection prevention and control is to maintaining essential health services and ensuring patient and health worker well-being. The paper concluded that health care-associated infections and the spread of antimicrobial resistance in health care settings are a consequence of poor-quality care delivery and inadequate health infrastructure combined with inexistent or defective infection prevention and control programme. In particular, key determinants are low compliance with hand hygiene and aseptic technique practices, contaminated medical equipment and supplies, inadequate environmental cleaning, lack of trained infection prevention and control professionals and limited opportunities for staff training, exceeded bed occupancy, understaffing and limited or suboptimal infrastructure for patient isolation.

Keywords: Healthcare, pandemic, control, infection, prevention

Introduction

According to the World Health Organization (WHO), (2020), infection prevention and control (IPC) is a systematic approach and solution planned to stop harm caused by infection to patients and health workers. It is a subsection of epidemiology, and can also serve crucial function in infectious diseases.

The Active infection prevention and control is a public health concern that is necessary in patient safety and health system strengthening. The prevention of healthcare-associated infections (HAI), are deep-rooted in effective IPC measures. A guiding principle on WHO's Core Components of IPC is that "access to health care services designed and managed to minimise the risks of avoidable HAI for patients and health care workers is a basic human right".

Strengthening global infection prevention and control (IPC) is needed to fight healthcare-associated infections (HAI), antimicrobial resistance, and to respond to disease outbursts. A study published in 2021 looked at the WHO's Core Components of IPC and found that most participating countries have IPC programmes and guidelines in place; however few have set aside the necessary resources to support the programmes. There is a need to move into the implementation and monitoring stages from planning stage, particularly in countries with low economic development.

The Spread of Infectious Disease

An infection according to Wikipedia is defined as the inversion of tissues by pathogens, their multiplication, and the reaction of host tissues to the infectious agent and the toxins they produce.

In humans, infections occur when an infectious microorganism gets into the body, multiplies, and results to a reaction in the body and potential infectious disease. The spread of infectious disease requires three variables, known as the epidemiological triad

The Agent - The microorganisms that cause the infection and can be fungi, parasites, viruses or bacteria.

The Host - The target of the infection or disease.

The Environment – This is the external surroundings and conditions to the host.

Infection Spread in Healthcare

Healthcare facilities, whether hospitals or primary care clinics are an area with high risk of disease transmission due to the presence and relative ratio of susceptible individuals. One in ten patients get an infection whilst receiving care yet actual infection prevention and control reduces healthcare-associated infections by at least 30%.

In a healthcare setting, the three components required for infection spread are the following

Source - places where infectious agents survive.

Environment - patient care areas, hospital equipment, and medical devices.

People – health workers, visitors or patients.

Controlling Infectious Diseases within Communities

Infection control and prevention is a global concern and there are many procedures and guidelines that can be monitored to reduce the spread of infection within a population and globally. Detecting unprotected groups such as older people, those with chronic conditions and children can also help

guide relevant strategies to protect these vulnerable groups. The main step for infection control can start at the community level by changing their behaviour, comprising:

- Proper use of face-masks
- Applying insect repellents
- Frequent hand washing
- Taking prescribed drugs, such as antibiotics, as directed by health specialists
- Maintaining social distancing

Other steps that can be followed to control the spread within communities consist of environmental measures such as:

- Adjusting environments
- Surveillance of diseases
- Food safety
- Air quality
- Medical Interventions

There is biochemical interventions that can be applied to speed up the recovery process and in sometimes prevent viral infections absolutely. The developments of vaccinations, antivirals and antibiotics have been shown to speed up recovery, slow down the advancement and in some cases destroy infectious diseases completely.

Vaccinations

Vaccinations are used to improve immunity to a specific disease. Vaccines work by introducing small quantities of the disease-causing bacteria or virus into the host, letting them to build up natural immunity. The introduction of regular vaccines have reduced down and in some cases eliminated certain diseases such as whooping cough, measles, polio, etc. There are also vaccinations for chickenpox, nevertheless is not given regularly and is reserved for those at risk of spreading the disease to those with a weakened immune system.

Antivirals

Antibiotics give no defence for infectious diseases that are caused by viral agents such as hepatitis B, HIV, influenza and herpes. In these cases, antiviral drugs are very effective at slowing down the progression of the disease and improving the immune system. Unfortunately, as with antibiotics, viruses can mutate over time and become resistant to these antiviral drugs.

Antibiotics

Antibiotics are used to treat bacterial infections and give support to the body's natural defense system in order to eradicate the disease-causing bacterial agent. They work by killing bacteria or stopping them from spreading. Nevertheless, improper use of antibiotics has directed the increase of resistant bacteria. In some cases the combination of one or more antibiotics or stronger doses are required.

Infection Control in Healthcare Facilities

Improving practices in healthcare facilities is another important factor in controlling and preventing infection. It is the responsibility of healthcare experts worldwide to make sure they develop plans and implement policies that protect those who may be immune- compromised in order to keep susceptible patients safe from healthcare-associated infections (HAIs). Worldwide, up to 7% of patients in developed and 10% in developing countries will acquire at least one healthcare-associated infection (HAI)

Healthcare-associated infections are one of the most common harmful effects in care delivery and both the endemic burden and the occurrence of epidemics are a major public health concern. Healthcare-associated infections (HAIs) have a momentous impact on morbidity, mortality and quality of life and present an economic burden at the societal level. Conversely, a large share of healthcare-associated infections are preventable and there is a growing body of indication to help raise alertness of the global burden of harm caused by these infections, comprising strategies to decrease their spread.

Steps to Improve Infection Control

There are two tiers of recommended precautions by the Center of Disease Control and Prevention (CDC) to prevent the spread of infections in healthcare settings: (1) Standard Precautions and (2) Transmission-Based Precautions.

(1) Standard Precautions for All Patient Care:

- Perform hand hygiene
- Use personal protective equipment (PPE) to prevent exposure to infection
- Follow respiratory hygiene/cough etiquette principles
- Ensure appropriate patient placement and isolation precautions
- Properly handle, clean, and disinfect patient care equipment and medical instruments
- Handle and sterilise textiles and laundry carefully
- Follow safe injection practices and proper handling of sharps/needles
- Ensure healthcare worker safety via IPC and post-exposure prophylaxis
- Prevention of intervention-related infections (catheter-associated urinary tract infections, intravascular catheter-related infections, surgical site infections)
- The implementation of the specific isolation precaution when diagnosing some syndromes
- Improving the communication between health care workers especially when referring potentially contagious patients
- In paediatric departments or ambulatory settings, there should be efforts to decrease infection from contaminated toys. Families can be encouraged to bring their own toys

(2) Transmission-Based Precautions

Transmission-Based Precautionsused in addition to Standard Precautions for patients with infectious disease to prevent transmission:

Contact precaution: Used for patients with known or suspected infections that can be transmitted through contact. For those patients, standard precautions are needed, plus limit transport and movement of patients, use disposable patient care equipment, and thorough cleaning and disinfection strategies. Patients with acute infectious diarrhea such as Clostridium difficile, vesicular rash, respiratory tract infection with a multidrug-resistant organism, abscess or draining wound that cannot be covered need to be under contact precautions.

Droplet precautions: Used for patients with known or suspected infections that can transmit by air droplets through the mechanism of a cough, sneeze, or by talking. In such cases, it is vital to control the source by placing a mask on the patient, use standard precautions plus limitation on transport and movement. Patients with respiratory tract infection in infants and young children, petechial or ecchymotic rash with fever, and meningitis are placed under droplet precautions.

Airborne precautions: Use for patients with known or suspected infections that can be transmitted by the airborne route. Those patients require to be in an airborne infection isolation room with all the previously mentioned protections. The most important pathogens that need airborne precautions are tuberculosis, measles, chickenpox, and disseminated herpes zoster. Patients with suspected vesicular rash, cough/fever with pulmonary infiltrate, maculopapular rash with cough/coryza/fever need to be under airborne precaution.

Conclusion

There is no single solution in controlling the spread of infectious diseases, and effective infection prevention and control (IPC) surely requires government intervention and teamwork between healthcare agencies, individuals and communities. Until certain risk factors are addressed and behaviours changed, the fighting against infectious diseases will remain to be a biggest and costly health issue around the globe.

Recommendations

- Wearing face mask or avoiding crowded spaces or spaces that have little or no ventilation.
- Observing good hand hygiene.
- Keeping high touch surfaces clean.
- Monitoring sings symptoms
- Controlling the entry of healthcare workers and visitors with confirmed or suspected infections.

References

Berenholtz SM, Pronovost PJ, Lipsett PA, Hobson D, Earsing K, Farley JE, Milanovich S, Garrett-Mayer E, Winters BD, Rubin HR, Dorman T, Perl TM. Eliminating catheter-related bloodstream infections in the intensive care unit. Crit Care Med. 2004 Oct;32(10):2014-20. [PubMed]

Edmond M, Eickhoff TC. Who is steering the ship? External influences on infection control programs. Clin Infect Dis. 2008 Jun 01;46(11):1746-50. [PubMed]

Infection prevention and control [Internet]. World Health Organization. 2020 [cited 27 March 2020]. Available from: https://www.who.int/infection-prevention/about/ipc/en/

Mayhall CG. Hospital epidemiology and infection control. Lippincott Williams & Wilkins; 2012 Feb 20.from: https://www.cdc.gov/infectioncontrol/index.html

O'Boyle C, Jackson M, Henly SJ. Staffing requirements for infection control programs in US health care facilities: Delphi project. Am J Infect Control. 2002 Oct;30(6):321-33. [PubMed]

Pronovost P, Needham D, Berenholtz S, Sinopoli D, Chu H, Cosgrove S, Sexton B, Hyzy R, Welsh R, Roth G, Bander J, Kepros J, Goeschel C. An intervention to decrease catheter-related bloodstream infections in the ICU. N Engl J Med. 2006 Dec 28;355(26):2725-32. [PubMed]

Tartari E, Tomczyk S, Pires D, Zayed B, Rehse AC, Kariyo P, Stempliuk V, Zingg W, Pittet D, Allegranzi B. Implementation of the infection prevention and control core components at the national level: a global situational analysis. Journal of Hospital Infection. 2021 Feb 1;108:94-103.

Wilson J. Infection control in clinical practice. Elsevier Health Sciences; 2006 Jun 21.

World Health Organization. Guidelines on core components of infection prevention and control programmes at the national and acute health care facility level. World Health Organization; 2016.

Wright SB, Ostrowsky B, Fishman N, Deloney VM, Mermel L, Perl TM. Expanding roles of healthcare epidemiology and infection control in spite of limited resources and compensation. Infect Control Hosp Epidemiol. 2010 Feb;31(2):127-32. [PubMed]

Intelligent Tutoring System For Learning Concept Of Computer Programming Languages (ITS-CPL)

[1]Sulaiman Umar S.noma, [2]Muhammad Garba, [3]Rabiu Ibrahim, [4]Ajayi, Olugbenga Akinbola,
[1,4]Department of Computer Science, Kebbi State Polytechnic, Dakingari, Nigeria.
[2]Department of Computer Science, Kebbi State University of Sci and Tech, Aliero, Nigeria
[3]Information Communication and Technology, Federal University, Birnin Kebbi, Kebbi State

.**Email:** Sulaimanumarsnoma@gmail.com
Phone No: +2348082034443, +2347036159502

Abstract

Intelligent Tutoring System used advanced technology to create coaching programs that use artificial intelligence. ITS allows students to hone their skills by completing tasks as part of an interactive learning. In this paper, we developed an Intelligent Tutoring System to helps students study concept of programming languages called ITS-CPL. The system has four (4) modules: Domain module that provide information about the topics and subtopics to be treated in the system, Student module which keep track of student/user information, performance and current level of knowledge in the system, Tutoring module to provide necessary lesson to be learn by the student/user and User Interface Module to display interfaces that support admin/teacher and student/user in providing academic activities and conducive learning environment respectively. The ITS-CPL coach the theoretical, videos and provide resource materials for one-on-one and e-learning while exercises and multiple choices for assessing the users understanding in an independent learning process. The system was presented to lecturers and students for evaluation. The lecturers are Software Engineering professionals and National Diploma I and II students from the Kebbi State Polytechnic Dakingari in Nigeria. Both were asked to fill out a questionnaire and provide feedback using the final version of the developed system, then the average score of the questions answered was measured and the result were excellent.

Keywords: Intelligent Tutoring System, E-learning, Computer Programming Language Concept, One-on-one.

1. INTRODUCTION

The formation of knowledge for teaching is not limited to conventional instruction. It has combined with cutting-edge technology to form Intelligent Tutoring Systems (ITS), a new branch of science. These systems, which provide individualised tutorials for students with varying educational levels as professional lecturers, are founded on the idea of artificial intelligence in education.

Artificial Intelligence (AI) is part of computer science that discussed the creation of intelligent machines that behaves like humans. computers with artificial intelligence are designed for problem solving, processing languages in natural form, speech detection and learning (Pannu, 2015). Education now are day's uses computing technology to enhanced learning, educational technology uses artificial intelligence in education (AIEd). AI applications are on the rise for supporting education and have received a lot of attention in the last couple of years. Prominently adaptive learning and AI technologies featured as important developments in educational technology (Zawacki-richter *et al.*, 2019).

ITS is a computer system that gives customized instructions or feedback directly to the learner without human intervention during task execution. ITS is used in many areas such as traditional education,

distance learning, and training. This is an interdisciplinary field (Kumar, 2012). Intelligent Tutoring Systems (ITS) are promising integrated teaching tools for individualizing formal education through intelligent guidance and feedback. In recent decades, ITS has transformed teaching and learning, and related research (Guo *et al.,* 2021). This study aims to develop and evaluate an Intelligent Tutoring System for learning concept of computer programming languages.

2. REVIEW OF THE RELATED LITERATURES

Elnajjar and Abu-naser (2017) developed an intelligent tutoring system that teaches DES information security algorithms called DES-Tutor. The DES Tutor is intended for students enrolled in the Cryptography Course at the Faculty of Information Technology, Al-Azhar University, Gaza. Alawar and Naser (2017) presented a study that shows how students can learn the basics of system databases using (W3school CSS) designed as a smart tutoring system using an authoring tool named (ITSB). Oteyola et al. (2017) investigated the impact of a developed and adapted intelligent tutoring system on the academic performance of physics teachers at a university in southwestern Nigeria. The intelligent Excel teaching system, called Smart Excel Intelligent Tutoring System, aims to easily explain the usage and benefits of the system to novice students as users and teachers as material exhibitors presented in Qwaider and Abu-naser (2018). Research on Intelligent Tutoring System (ITS) to improve the future of Gaza's water environment by encouraging people to use this system to increase their awareness and knowledge of water issues discussed in (Hamed et al., 2018). Sivarasan and Rameshkumar (2017) developed an intelligent tutoring system that uses pre-quiz assessments to measure a student's knowledge level by asking them objective questions. The system automatically ranks and enrols students according to their proficiency. An intelligent tutoring system called Fuzzy Bayesian Intelligent Tutoring System "FB-ITS" developed by Eryilmaz and Adabashi (2020) using artificial intelligence methods based on fuzzy logic and Bayesian network techniques to adaptively support students in learning environments. Almurshidi and Naser (2017) presented the design and development of an intelligent tutoring system to teach students about stomach diseases and give them a clear idea of stomach ulcers. Al-nakhal and Naser (2017) designed an intelligent tutoring system to help students learn computer theory. The Intelligent Tutoring System was created using the ITSB authoring tools. King et al. (2021) presented a research that considered basic-level school students who have difficulty learning online without anyone's intervention and also their parents who are currently having difficulty teaching their children to study at home online, especially at this time of difficulty with a pandemic outbreak like COVID-19. Abueloun and Naser (2017) developed intelligent tutoring system which is called smart math tutoring system that helps many students of all ages to understand the subject as it helps students to understand the basics of mathematics and is important for addition and subtraction. Albatish et al. (2018) The Intelligent Tutoring System developed to help trainees overcome the difficulties they face when using the Arduino platform by describing the design of a desktop-based intelligent tutoring system.

3. RESEARCH GAB

According to a survey conducted by Almasri et al. (2019) and Systematic Literature Review (SLR) published by Sulaiman et al. (2022) revealed that several Intelligent Tutoring System was developed on computer programming languages (such as Java, C++, Python, C#, HTML, CSS, SQL and PHP), cloud computing, computer networking, Databases, IT security and other non-computing areas. The precise Intelligent Tutoring System that helps to understand the concept of computer programming and programming languages has not yet been developed. Therefore, it is necessary to develop an

Intelligent Tutoring System to learn the concepts of computer programming and programming languages to better understand and differentiate between the programming languages.

IV. PROPOSED INTELLIGENT TUTORING SYSTEM ARCHITECTURE

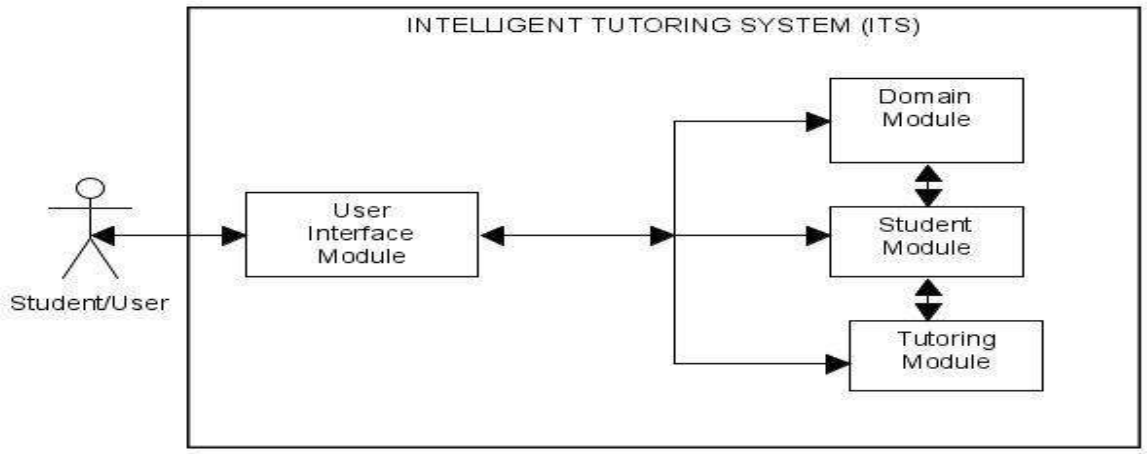

Figure 1: ITS Architecture

4. SYSTEM DEVELOPMENT

The intelligent tutoring system in this research is developed for learning concepts of computer programming and programming languages. The HTML, JAVASCRIPT and CSS scripting languages are used to develop the front-end of the system while MySQL Database is used to develop the back-end and the PHP programming language is used to communicate information between the front-end, back-end and the vice-vasa.

Intelligent tutoring systems consist of four basic components based on a general consensus amongst researchers (Sivarasan & Rameshkumar, 2017). Therefore, Figure 1 shows the architecture that constituted the components of the proposed Intelligent Tutoring System. Those components are:

i. Domain module
ii. Student module
iii. Tutoring module
iv. User Interface module

5.1 DOMAIN MODULE

This provides information about the domain/subject/lesson areas where the tutoring module will cover or be presented to the student/user (i.e it provides an explanation of what the student/user is expected to learn in the system). The step-by-step procedure in learning the system and what is expected of the student/user in the system. The lesson is organized in form of topics and subtopics and problem-solving strategies. The information about how a student/user will be evaluated by the system is also explained in this module, this is clearly stated after every topic and subtopics listed in the module. The student/user is expected to answer some questions at the end of the lesson he/she learned, the questions are informed of Multiple Choice (objectives) in order for the student/user to monitor his/her own

performance or progress about the lesson learned. This is explained at the end of particular lesson information.

The domain module for this system consists of the topics and subtopics for the concept of computer programming languages which break down as follows:

1. CONCEPT OF PROGRAMMING AND PROGRAMMING LANGUAGES
   - **i.** COMPUTER PROGRAM
     - **a.** Features of a good computer program
     - **b.** A typical programming task
   - **ii.** COMPUTER PROGRAMMING
     - **a.** Variables
     - **b.** Data Types
     - **c.** Basic syntax
     - **d.** IDEs and coding environments
   - **iii.** COMPUTER PROGRAMMING LANGUAGES
     - **a.** Machine language
     - **b.** Assembly language
     - **c.** High-level language
   - **iv.** PROGRAMMING PARADIGM
     - **a.** Unstructured programming
     - **b.** Procedural programming
     - **c.** Modular programming
     - **d.** Object-oriented programming
2. CONCEPTS OF ALGORITHMS
   - i. Flowchart
   - ii. Pseudocode
3. BASIC CODING STRUCTURES
   - **i.** SIMPLE SEQUENCE STRUCTURE
   - **ii.** SELECTION OR DECISION STRUCTURE
     - **a.** If Statement
     - **b.** If Else Statement
     - **c.** Nested If Else Statement
     - **d.** Switch Statement
   - **iii.** REPETITION OR ITERATION STRUCTURE
     - **a.** While Loop
     - **b.** Do While Loop
     - **c.** For Loop

4.2 STUDENT MODULE

The student module keeps track of student/user information and the current level of knowledge of a student/user about the lesson learned in the system. The module provides a student/user performance table that always displays the performance of a user in the system, user can also download his/her performance on Pdf, CSV and Excel or view the performance on a histogram chart at the same time student/user can copy or print his/her performance. The module also keeps track of days and times the student/user accessed the system which served as attendance to the student/user. The module automatically evaluates the student/user knowledge based on the end of the lesson test and exam the

user has taken in the tutoring module. Finally, the module provides all the necessary information, knowledge base and performance of a student/user.

4.3 TUTORING MODULE

The tutoring module uses the information from the domain and student module to provide necessary lessons to be learned by the student/user. For new student/user, the system will automatically start the tutoring lesson from the beginning as it was in the domain module while for existing student/user the system keeps track of where the student/user left in the last login/use and provide the lesson at that particular point where he/she stop in the last use of the system. The module keeps track of the learner's knowledge progress to present the tutoring lesson step-by-step to the student/user. At the end of every lesson multiple choice (objectives) questions and options are provided by the system in order to evaluate the performance of a learner in that lesson learned. If the student/user has taken the objectives test for a particular lesson the system will automatically assign him/her to the next lesson following the domain knowledge base while the previous lesson performance will be saved in the performance table under the student module. After all the lesson has been taken by the student/user a final exam in form of multiple choice (objectives) is presented and the result is sent to the performance table under the student module. During learning, the student/users can watch the uploaded videos as well as read the materials online or download the videos and materials for further explanation and study.

4.4 USER INTERFACE MODULE

The intelligent tutoring system in this research has been developed for learning the concept of computer programming and programming languages. The system has an interface that supports students/users and another interface that supports admin/teacher. The admin or teacher can add lessons, examples, and material resources such as pdf documents, word documents and videos tutorials, he/she can also set multiple choice questions to the student/user, view the individual performance as well as general performance of the enrolled student/user in the system. The student/user can view the lessons to be learned in form of a curriculum as explained in the domain module, learn the lesson step-by-step as in the tutoring module, takes test and exam, download videos to watch offline or watch videos online and download materials. A screenshot of some interfaces are shown in Figure 2 – Figure 12.

Figure 2: System home page

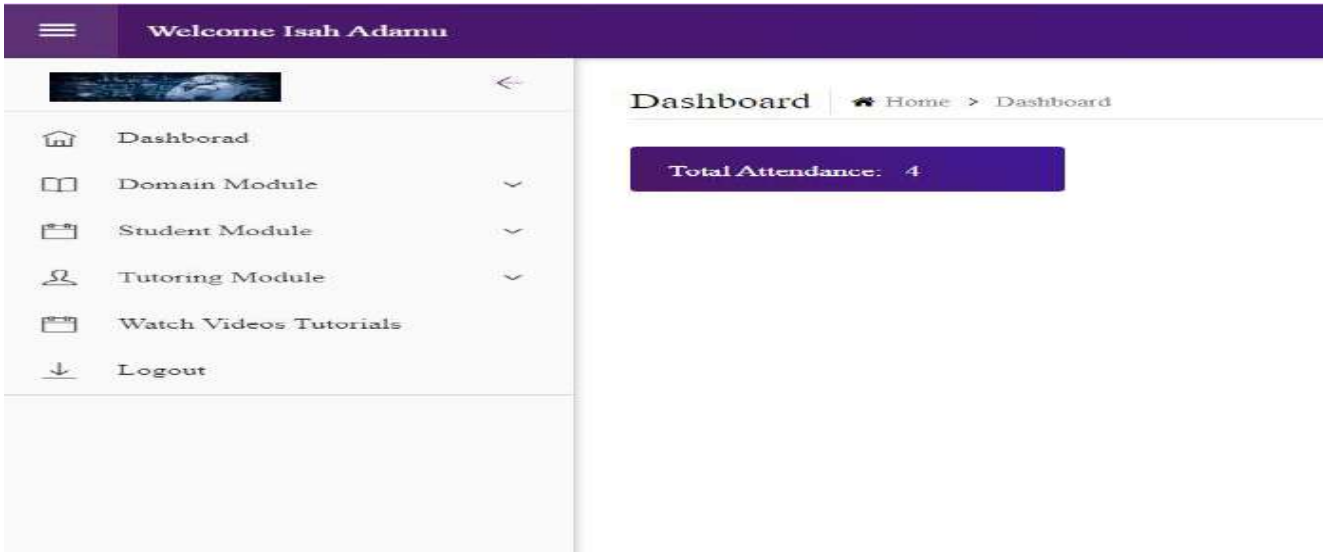

Figure 3: System dashboard

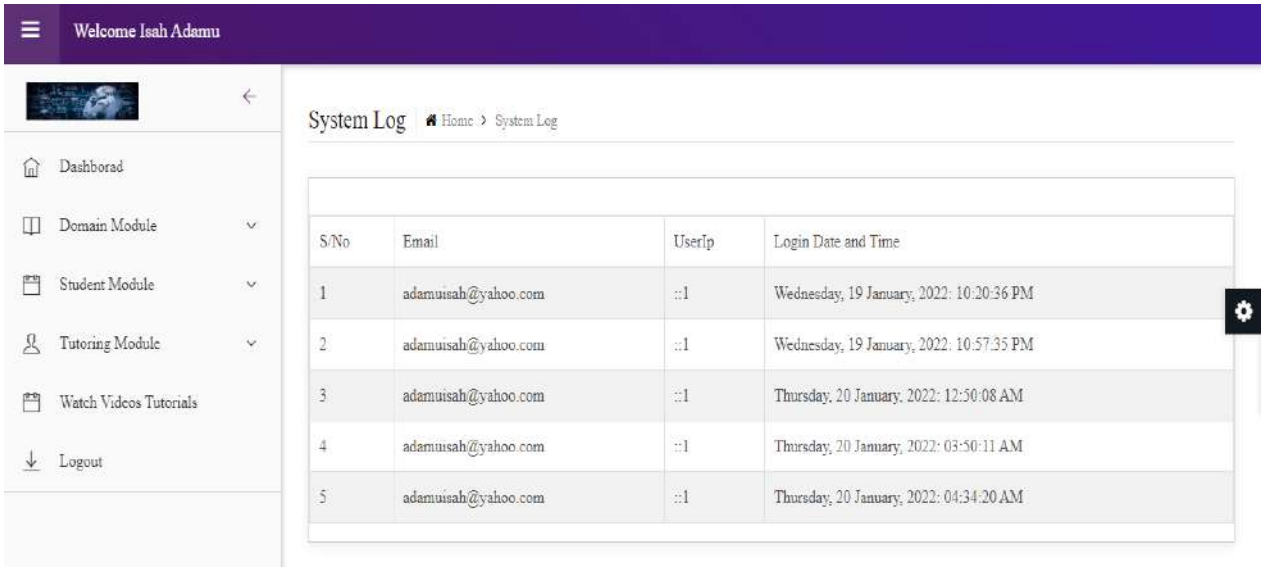

Figure 4: Attendance or System logs

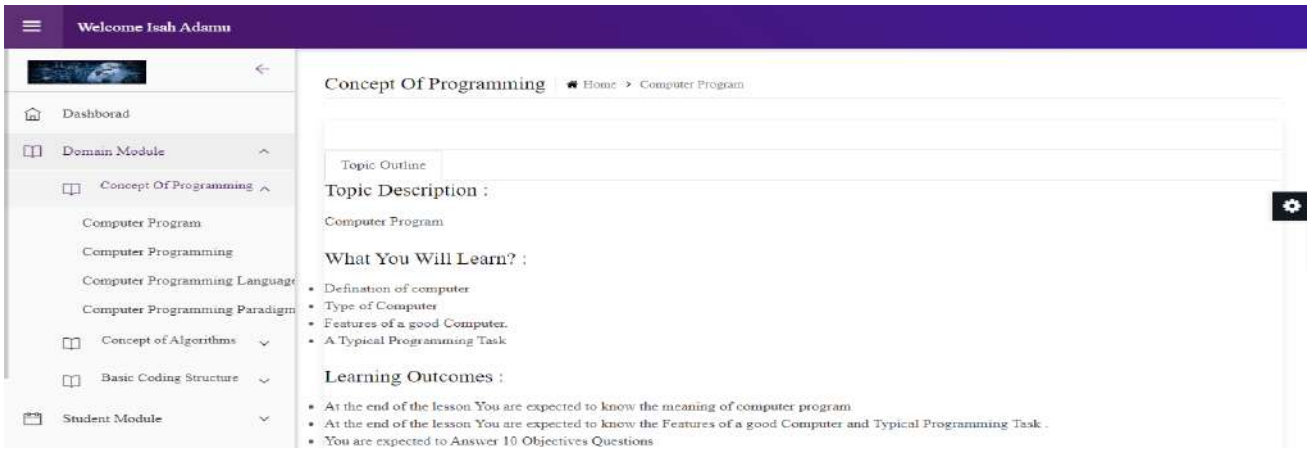

Figure 5: Domain module displaying what student is expected to learn on the programming

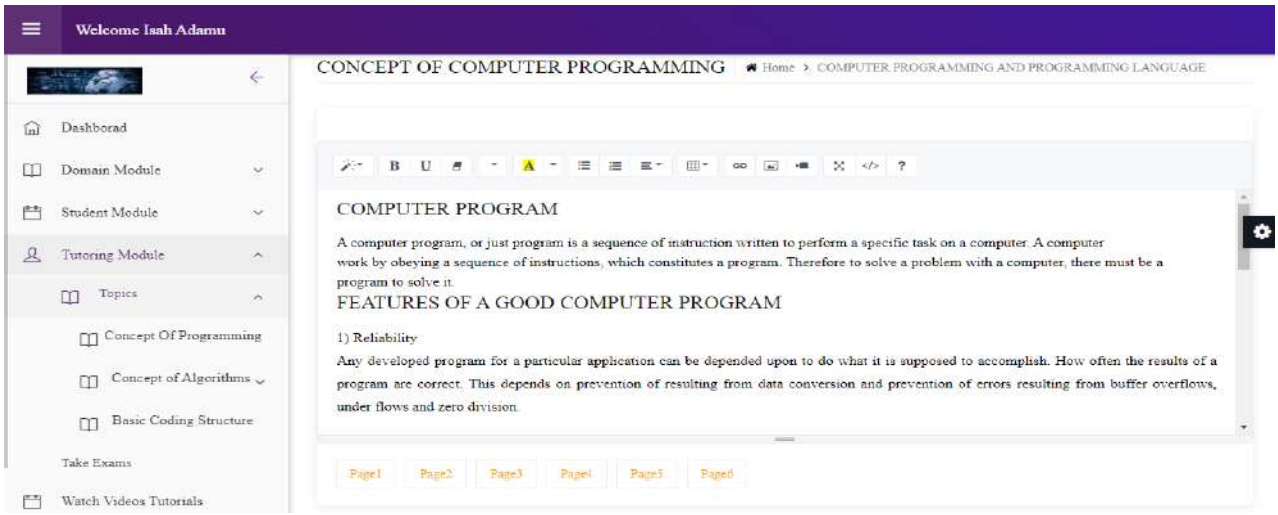

Figure 6: Displaying the lesson on the concept of computer programming

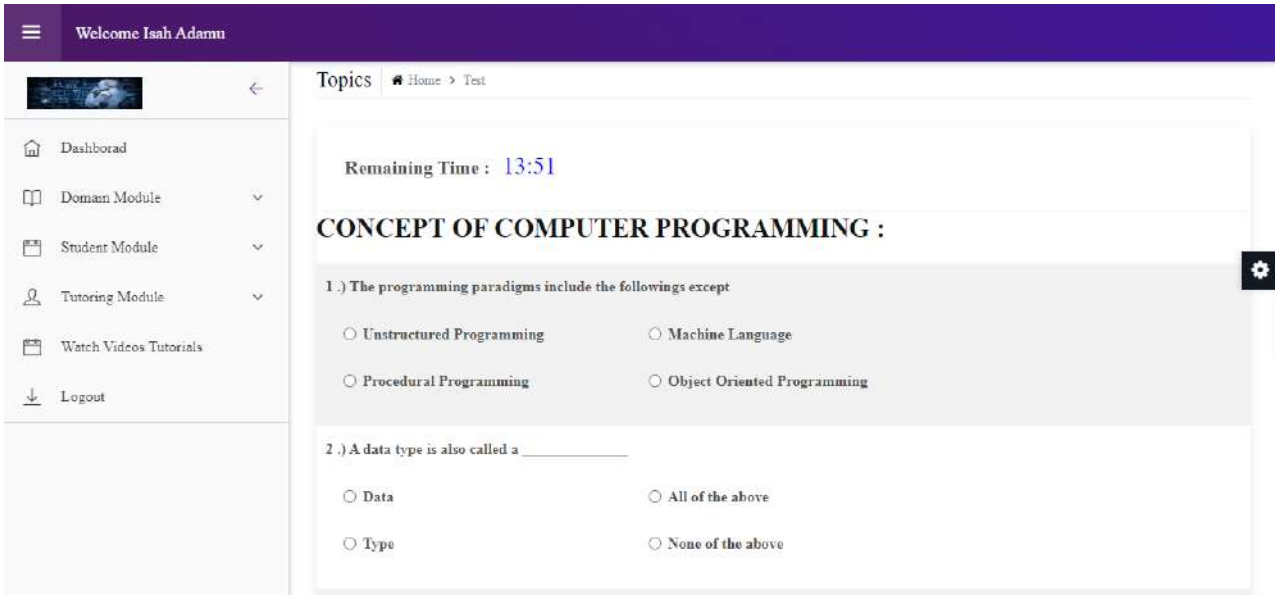

Figure 7: Displaying the test question on the concept of computer programming

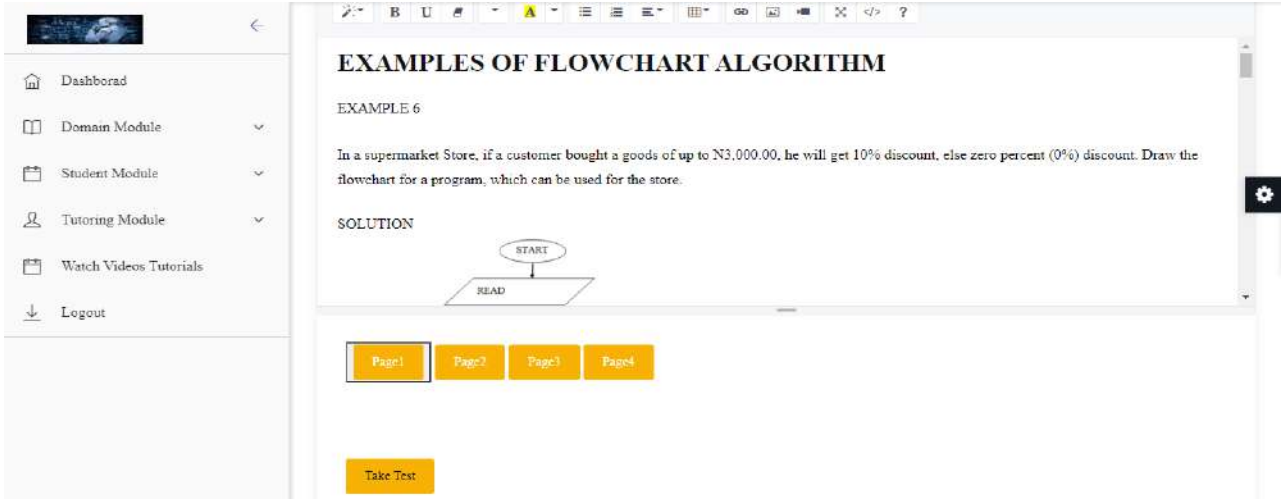

Figure 8: Displaying the examples of flowchart

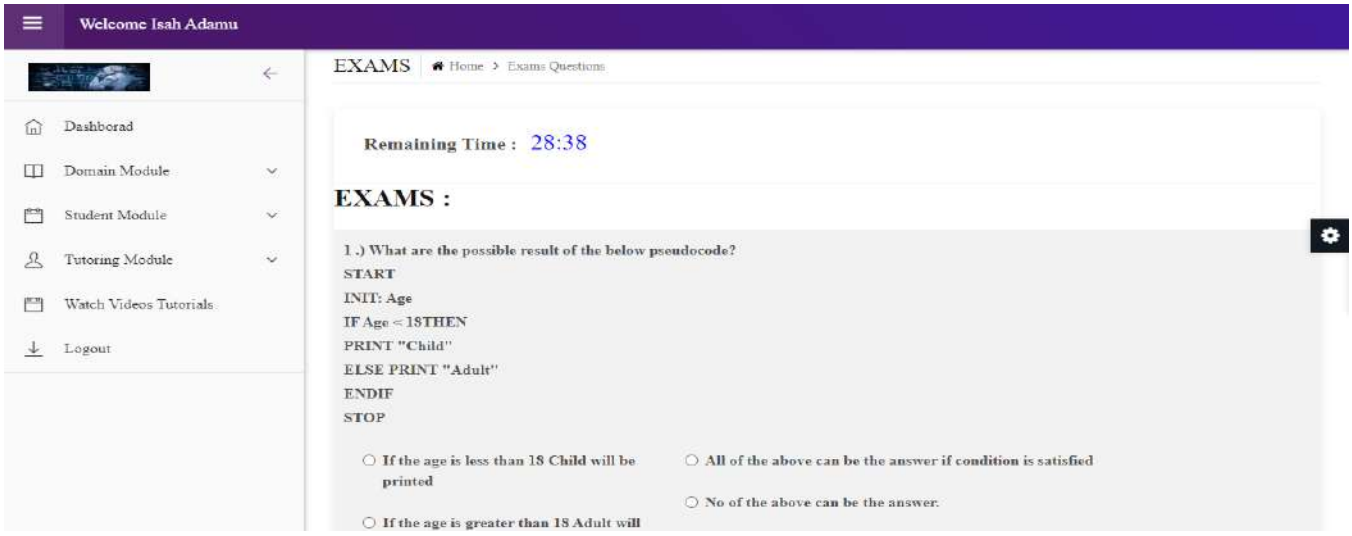

Figure 9: Displaying exam questions

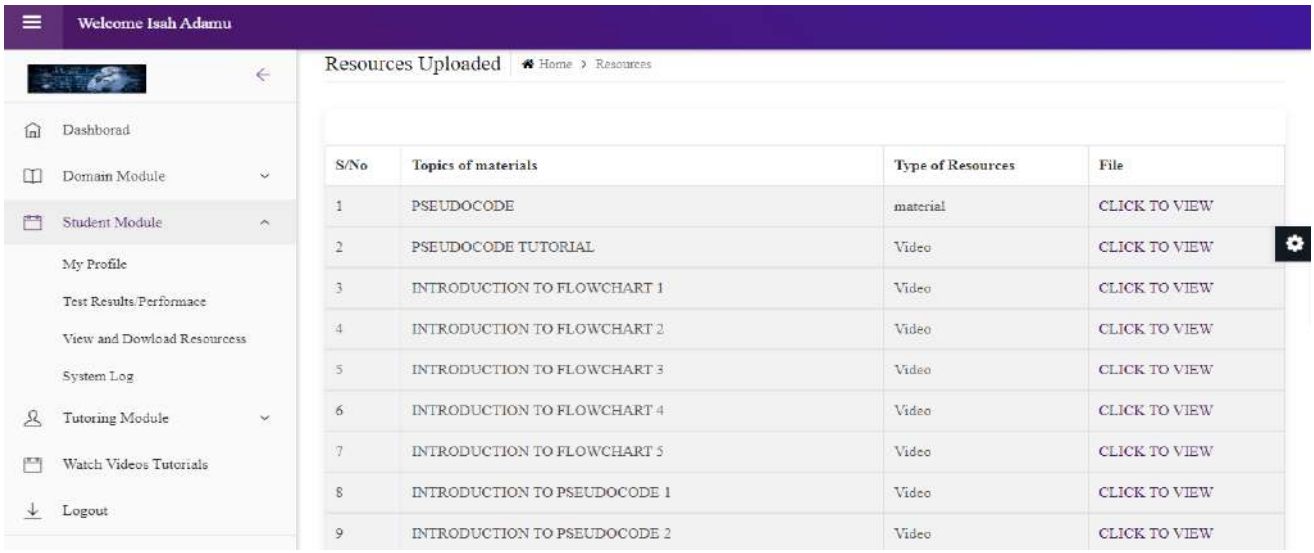

Figure 10: Displaying uploaded resources videos and pdf materials

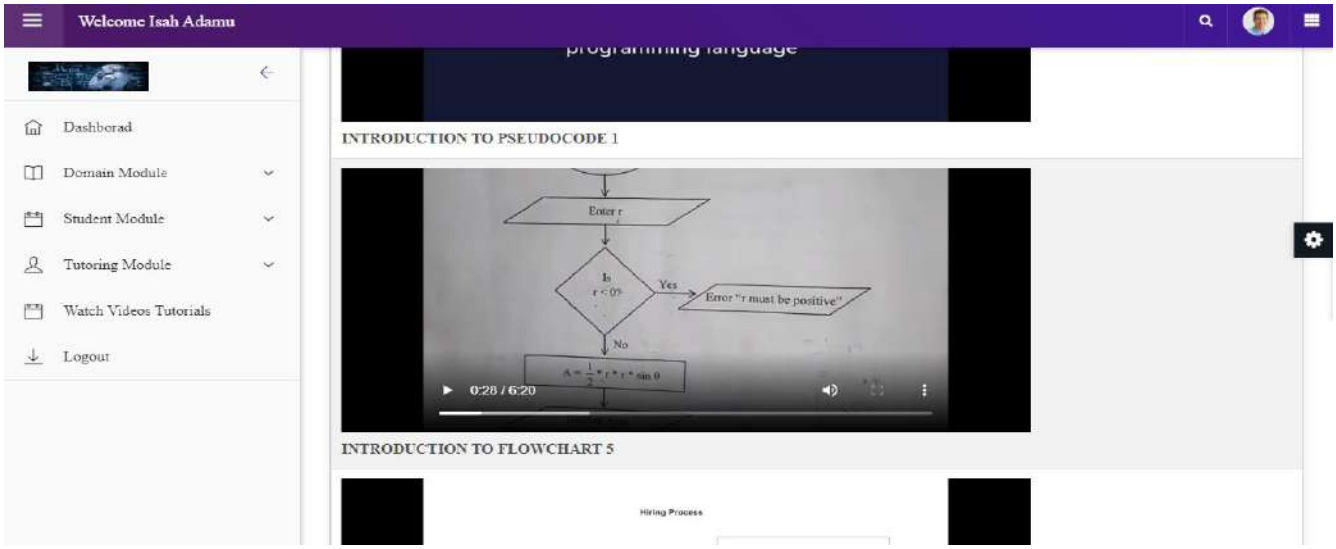

Figure 11: Watching online videos (All the uploaded videos will display at once here)

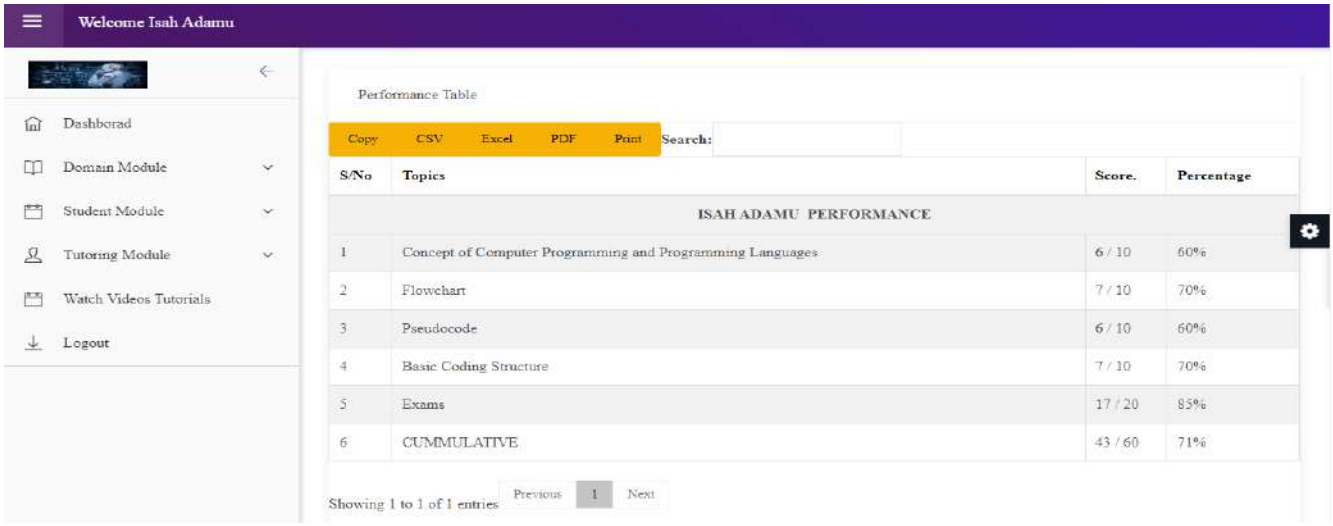

Figure 12: Performance result of a student/user.

6. SYSTEM USABILITY EVALUATION PROCEDURES

The developed ITS system has been presented to the ten (10) lecturers and thirty (30) experimental students. The lecturers were drawn from some Universities and the Polytechnics in the North-western region Nigeria. The students consists of the experimental group who's participated in learning the concept of Computer programming and programming languages using the Intelligent Tutoring System at Kebbi State Polytechnic Dakingari. Both of them were asked to evaluate the developed ITS system and to fill the questionnaire. The questionnaire was prepared by the researchers and approved by an expert.

7. RESULT AND DISCUSSION

7.1 RESULT OF THE QUESTIONNAIRE RESPOSES BY THE LECTURERS ON THE SYSTEM USABILITY EVALUATION

Table 1 outlines each question and its average percentage. Figure 13 shows a bar chart of each question and its percentage.

Table 1: Result of questions asked to lecturers

Question No.	QUESTIONS	AVERAGE (%)
Q1	How easy to use the ITS system?	VE = 9 (90%)
Q2	What are the qualities of the system design?	VS = 9 (90%)
Q3	How easy to learn concept of programming languages using the system?	VE = 8 (80%)
Q4	How easy are the step-by-step examples provided in the system?	VE = 9 (90%)
Q5	Do you benefit from using ITS system?	Y = 10 (100%)
Q6	Would you like to see similar ITS in other courses?	Y = 10 (100%)
Q7	What are the qualities of materials provided in the system?	VS =10 (100%)
Q8	Do you recommend this ITS to the students?	Y = 10 (100%)
Q9	System development opinion	It is very good especially when it

		comes to learning in the modern days now.

VE = Very Easy; VS = Very Satisfied; Y = Yes.

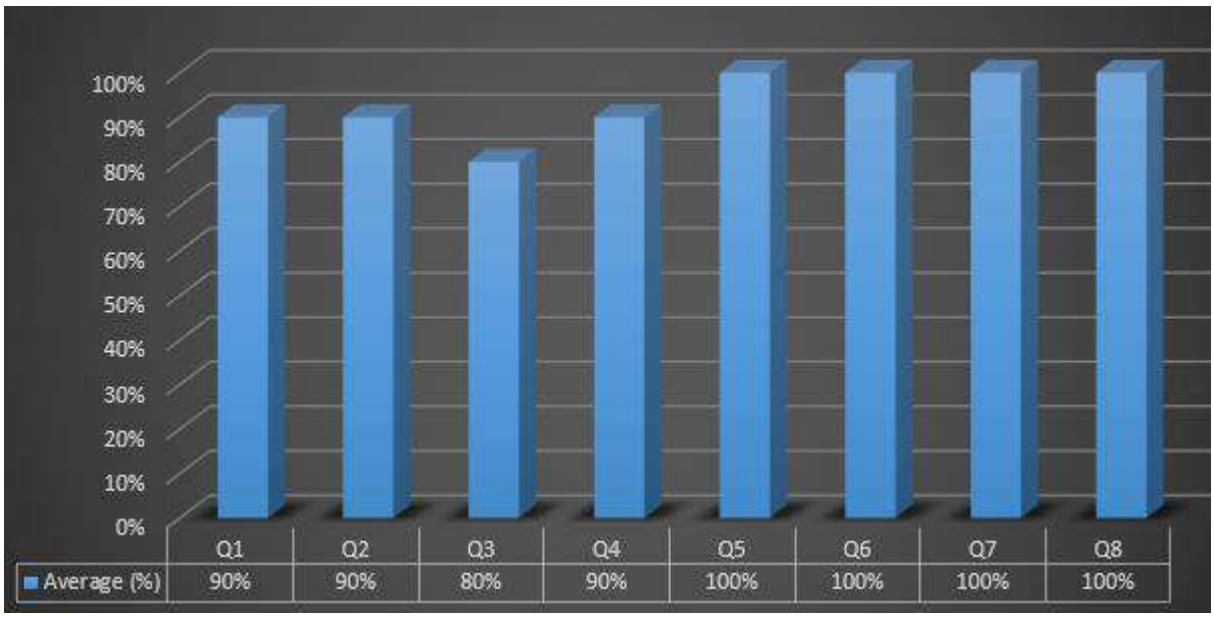

Figure 13: Result of questions asked to lecturers

7.2 RESULT OF THE QUESTIONNAIRE RESPOSES BY THE EXPERIMENTAL STUDENTS ON THE SYSTEM USABILITY EVALUATION

Table 2 shows each question and its average percentage. Figure 14 shows a bar chart of each question and its average percentage.

Table 2: Result of questions asked to experimental students

Question No.	QUESTIONS	AVERAGE (%)
Q1	How easy to use the ITS system?	VE =28 (93%)
Q2	What are the qualities of the system design?	VS =29 (97%)
Q3	How easy to learn concept of programming languages using the system?	VE =25 (83%)
Q4	How easy are the step-by-step examples provided in the system?	VE =29 (97%)
Q5	Do you benefit from using ITS system?	Y = 30 (100%)
Q6	Would you like to see similar ITS in other courses?	Y = 30 (100%)
Q7	Do you enjoy the materials provided in the system?	Y = 30 (100%)
Q8	Do you recommend this ITS to other students?	Y = 30 (100%)

VE = Very Easy; VS = Very Satisfied; Y = Yes.

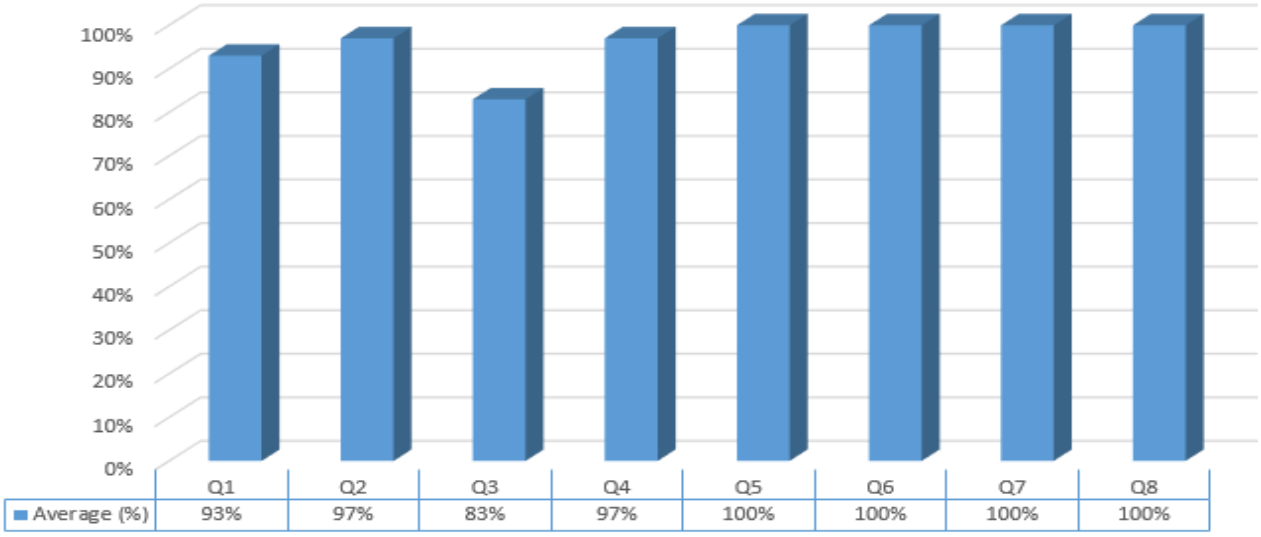

Figure 14: Result of questions asked to experimental students

In evaluating the developed ITS system, evaluators were required to use the system. After that, they were asked to provide their feedback about the ITS system through filling the questionnaire which consisted of the nine (9) questions for the lecturers and eighth (8) questions for the students.
The usability results of the developed ITS system were measured as shown in the Table 1 and Figure 13 for the lecturers and Table 2 and Figure 14 for the students. The average score of the questions answered was measured and the result were excellent.

8. CONCLUSION

No doubt that ITS plays a vital role in teaching and learning. One could argue that a number of researches were carried out in the field in other ascertain issues with ITS and how to improve them. Our result presented in this research may be useful to novice ITS developers and in the area of educational artificial intelligence or educational technology.

9. RECOMMENDATION

Based on the findings of this research, the following recommendations are provided:

1. Intelligent Tutoring System for other computer programming languages should be developed in order to ease the stress on both lecturer and students because it makes individuals learn at their comfort times.
2. Awareness and how to use ITS should be timely organised by the governments and institutions, especially in the areas where banditries and Boko haram become a threat.
3. Parents/guardians/teachers should educate their children on the use of an Intelligent Tutoring System in order to reduce the cost of the extra lessons.

REFERENCES

Abueloun, N. N., & Naser, S. S. A. (2017). Mathematics intelligent tutoring system. *International Journal of Advanced Scientific Research*, *2*(1), 11–16. www.allscientificjournal.com

Al-nakhal, M. A. M., & Naser, S. S. A. (2017). Adaptive Intelligent Tutoring System for Learning Computer Theory. *European Academic Research*, *IV*(10), 8770–8782. https://doi.org/10.1007/978-3-319-67450-6_3

Alawar, M. W., & Naser, S. S. A. (2017). CSS-Tutor : An intelligent tutoring system for CSS and

HTML. *International Journal of Academic Research and Development*, *2*(1), 94–98.

Albatish, I., Mosa, M. J., & Abu-Naser, S. S. (2018). ARDUINO Tutor : An Intelligent Tutoring System for Training on ARDUINO. *International Journal of Engineering and Information System (IJEAIS)*, *2*(1), 236–245.

Almasri, A., Ahmed, A., Al-masri, N., Sultan, Y. A., Mahmoud, A. Y., Zaqout, I., Akkila, A. N., & Abu-naser, S. S. (2019). Intelligent Tutoring Systems Survey for the Period 2000- 2018. *International Journal of Academic Engineering Research (IJAER)*, *3*(5), 21–37.

Almurshidi, S. H., & Naser, S. S. A. (2017). Stomach disease intelligent tutoring system. *International Journal of Advanced Research and Development*, *2*(1), 26–30.

Elnajjar, A. E., & Abu-naser, S. S. (2017). DSE-Tutor : An intelligent tutoring system for teaching DES information security Algorithm DSE-Tutor : An intelligent tutoring system for teaching DES information security Algorithm. *International Journal of Advanced Research and Development*, *2*(1), 69–73.

Eryılmaz, M., & Adabashi, A. (2020). Development of an intelligent tutoring system using bayesian networks and fuzzy logic for a higher student academic performance. *Applied Sciences*, 1–18. https://doi.org/doi:10.3390/app10196638

Gavrilović, N., & Jovanovic, S. (2015). IMPLEMENTING ITS (INTELLIGENT TUTORING SYSTEMS) FOR JAVA PROGRAMMING E-LEARNING. *The Sixth International Conference on E-Learning (ELearning-2015)*, 24–25.

Guo, L., Wang, D., Gu, F., Li, Y., Wang, Y., & Zhou, R. (2021). Evolution and trends in intelligent tutoring systems research : a multidisciplinary and scientometric view. *Asia Pacific Education Review*, *22*(3), 441–461. https://doi.org/10.1007/s12564-021-09697-7

Hamed, M. A., Abu-naser, S. S., & Abualhin, K. S. (2018). Intelligent tutoring system effectiveness for water knowledge and awareness. *International Journal of Academic Information Systems Research (IJAISR)*, *2*(4), 18–34.

King, C. L., Vincent, Kelvin, Warnars, H. L. H. S., Nordin, N., & Utomo, W. H. (2021). Intelligent Tutoring System: Learning Math for 6th-Grade Primary School Students. *Education Research International*, *2021*, 1–10. https://doi.org/10.1155/2021/5590470

Kumar, P. (2012). Development of an intelligent tutoring system framework for game based learning. In *M. Tech thesis, IIT Bombay*. Indian Institute of Technology, Bombay.

Oteyola, T. A., Idowu, L., & Adeyanju, L. J. (2017). European Journal of Education Studies PRE-SERVICE PHYSICS TEACHERS ' ACADEMIC PERFORMANCE IN COLLEGES OF EDUCATION ON SOUTHWESTERN NIGERIA. *European Journal of Education Studies*, *3*(6), 560–578. https://doi.org/10.5281/zenodo.573353

Pannu, A. (2015). Artificial Intelligence and its Application in Different Areas. *International Journal of Engineering and Innovative Technology (IJEIT)*, *4*(10), 79–84.

Qwaider, S. R., & Abu-naser, S. S. (2018). Excel Intelligent Tutoring System. *International Journal of Academic Information Systems Research (IJAISR)*, *2*(2), 8–18.

Sivarasan, R., & Rameshkumar, D. G. . (2017). Intelligent Tutoring System for Teaching Java. *International Journal of Advanced Research in Computer and Communication Engineering*, *6*(1), 46–51. https://doi.org/10.17148/IJARCCE

Zawacki-richter, O., Marín, V. I., Bond, M., & Gouverneur, F. (2019). Systematic review of research on artificial intelligence applications in higher education – where are the educators ? *International Journal of Educational Technology in Higher Education*, 1–27.

Abueloun, N. N., & Naser, S. S. A. (2017). Mathematics intelligent tutoring system. *International Journal of Advanced Scientific Research*, *2*(1), 11–16. www.allscientificjournal.com

Al-nakhal, M. A. M., & Naser, S. S. A. (2017). Adaptive Intelligent Tutoring System for Learning Computer Theory. *European Academic Research*, *IV*(10), 8770–8782. https://doi.org/10.1007/978-3-319-67450-6_3

Alawar, M. W., & Naser, S. S. A. (2017). CSS-Tutor : An intelligent tutoring system for CSS and HTML. *International Journal of Academic Research and Development*, *2*(1), 94–98.

Albatish, I., Mosa, M. J., & Abu-Naser, S. S. (2018). ARDUINO Tutor : An Intelligent Tutoring System for Training on ARDUINO. *International Journal of Engineering and Information System (IJEAIS)*, *2*(1), 236–245.

Almasri, A., Ahmed, A., Al-masri, N., Sultan, Y. A., Mahmoud, A. Y., Zaqout, I., Akkila, A. N., & Abu-naser, S. S. (2019). Intelligent Tutoring Systems Survey for the Period 2000- 2018. *International Journal of Academic Engineering Research (IJAER)*, *3*(5), 21–37.

Almurshidi, S. H., & Naser, S. S. A. (2017). Stomach disease intelligent tutoring system. *International Journal of Advanced Research and Development*, *2*(1), 26–30.

Elnajjar, A. E., & Abu-naser, S. S. (2017). DSE-Tutor : An intelligent tutoring system for teaching DES information security Algorithm DSE-Tutor : An intelligent tutoring system for teaching DES information security Algorithm. *International Journal of Advanced Research and Development*, *2*(1), 69–73.

Eryılmaz, M., & Adabashi, A. (2020). Development of an intelligent tutoring system using bayesian networks and fuzzy logic for a higher student academic performance. *Applied Sciences*, 1–18. https://doi.org/doi:10.3390/app10196638

Gavrilović, N., & Jovanovic, S. (2015). IMPLEMENTING ITS (INTELLIGENT TUTORING SYSTEMS) FOR JAVA PROGRAMMING E-LEARNING. *The Sixth International Conference on E-Learning (ELearning-2015)*, 24–25.

Guo, L., Wang, D., Gu, F., Li, Y., Wang, Y., & Zhou, R. (2021). Evolution and trends in intelligent tutoring systems research : a multidisciplinary and scientometric view. *Asia Pacific Education Review*, *22*(3), 441–461. https://doi.org/10.1007/s12564-021-09697-7

Hamed, M. A., Abu-naser, S. S., & Abualhin, K. S. (2018). Intelligent tutoring system effectiveness for water knowledge and awareness. *International Journal of Academic Information Systems Research (IJAISR)*, *2*(4), 18–34.

King, C. L., Vincent, Kelvin, Warnars, H. L. H. S., Nordin, N., & Utomo, W. H. (2021). Intelligent Tutoring System: Learning Math for 6th-Grade Primary School Students. *Education Research International*, *2021*, 1–10. https://doi.org/10.1155/2021/5590470

Kumar, P. (2012). Development of an intelligent tutoring system framework for game based learning. In *M. Tech thesis, IIT Bombay*. Indian Institute of Technology, Bombay.

Oteyola, T. A., Idowu, L., & Adeyanju, L. J. (2017). European Journal of Education Studies PRE-SERVICE PHYSICS TEACHERS ' ACADEMIC PERFORMANCE IN COLLEGES OF EDUCATION ON SOUTHWESTERN NIGERIA. *European Journal of Education Studies*,

3(6), 560–578. https://doi.org/10.5281/zenodo.573353

Pannu, A. (2015). Artificial Intelligence and its Application in Different Areas. *International Journal of Engineering and Innovative Technology (IJEIT)*, *4*(10), 79–84.

Qwaider, S. R., & Abu-naser, S. S. (2018). Excel Intelligent Tutoring System. *International Journal of Academic Information Systems Research (IJAISR)*, *2*(2), 8–18.

Sivarasan, R., & Rameshkumar, D. G. . (2017). Intelligent Tutoring System for Teaching Java. *International Journal of Advanced Research in Computer and Communication Engineering*, *6*(1), 46–51. https://doi.org/10.17148/IJARCCE

Zawacki-richter, O., Marín, V. I., Bond, M., & Gouverneur, F. (2019). Systematic review of research on artificial intelligence applications in higher education – where are the educators ? *International Journal of Educational Technology in Higher Education*, 1–27.

The Potentials of UAVs, IOT, And ML in the Detection and Analysis of Common Rice Diseases in Kebbi State, Nigeria

Anas Shehu[1], Zauwali Sabitu Paki[2]

[1]Department of Computer Science, Kebbi State Polytechnic Dakindari-Nigeria
[2]Department of Computer Science, Yusuf Maitama Sule University, Kano-Nigeria
Email and Phone No: Anasshehu8@gmail.com/08031399779

Abstract

Food security is a global issue. Rice is a staple crop in the world and it is a major cash crop in Nigeria. It has contributed to Nigeria's GDP in recent years. This contribution is considerably limited by the widespread of different rice diseases. Crop diseases hamper the chance of attaining food security due to the losses they cause to farmers. The productivity of our farmers is substantially affected by these diseases. Effective crop disease monitoring and analysis are key to achieving food self-reliance. Recent technologies like blockchain, Internet of Things (IoT), Machine Learning (ML), and Unmanned Arial Vehicles (UAV) present promising opportunities for real-time monitoring of crops. They are the major constituents of smart agriculture. IoT provides the technology for acquiring on-site data about plant nutrient deficiencies, plant stress conditions, pests, and diseases. These data are highly invaluable for the effective monitoring of plant health on farms. Blockchain technology facilitates the secure transmission of these data to a server for analysis and necessary action. Machine learning techniques support the processing and analysis of the huge volume of data collected from the farms. In this work, we review the recent developments in these technologies and assess the level of adoption of them in Kebbi state Nigeria. We also, present the opportunities and benefits of the adoption of these technologies to both farmers and Nigeria's achievement of food security in a short time.

Keywords: Blockchain, Food security, IoT, machine learning, smart agriculture, UAV.

Introduction

Food security is a critical and multifaceted issue that remains at the forefront of global concerns, particularly in developing nations such as Nigeria. Nigeria the Africa's most populous country with over 200 million people and is the largest producer of rice, but the country's production levels are still relatively low compared to its consumption demand (Adenowuro, 2023). The report on rice production in Africa 2021 by (Sasu, 2023) shows, Nigeria is the top producer of rice in West Africa, with a production of 8.1 million tonnes, more than any other country in the region, including Mali (3.0 million tonnes), Ghana (0.6 million tonnes), Burkina Faso (0.4million tonnes), Chad (0.3 million tonnes), and Niger (0.1 million tonnes). Despite this production, Nigeria faces the complex challenge of ensuring a reliable and sustainable food supply for its increasing population due to climate change, agricultural inputs that either reduce or increase and socio-economic disparities that continue to pose threats to the nation's ability to achieve and maintain food security(Rebecca, 2020). Water scarcity is a major global environmental problem in agriculture, rainfall pattern, soil type and climatic regime on crop water use efficiency are among the factors that causes crop diseases (Mbava et al., 2020) this crop diseases

contribute negatively on Nigeria food security which require urgent need for effective monitoring and analysis strategies.

Recent advancements in technology, such as blockchain, Internet of Things (IoT), Machine Learning (ML), and Unmanned Aerial Vehicles (UAV), present promising avenues for real-time monitoring of crops—constituting the pillars of what is commonly referred to as smart agriculture. The aim of this research is to integrate these technologies and evaluate their adoption in Kebbi state, Nigeria for effective monitoring and plan health on farm, with the view of presenting the opportunities and benefits of the adoption of these technologies to both farmers and Nigeria. Fig. 1 gives the various application areas of ML and DL in agriculture.

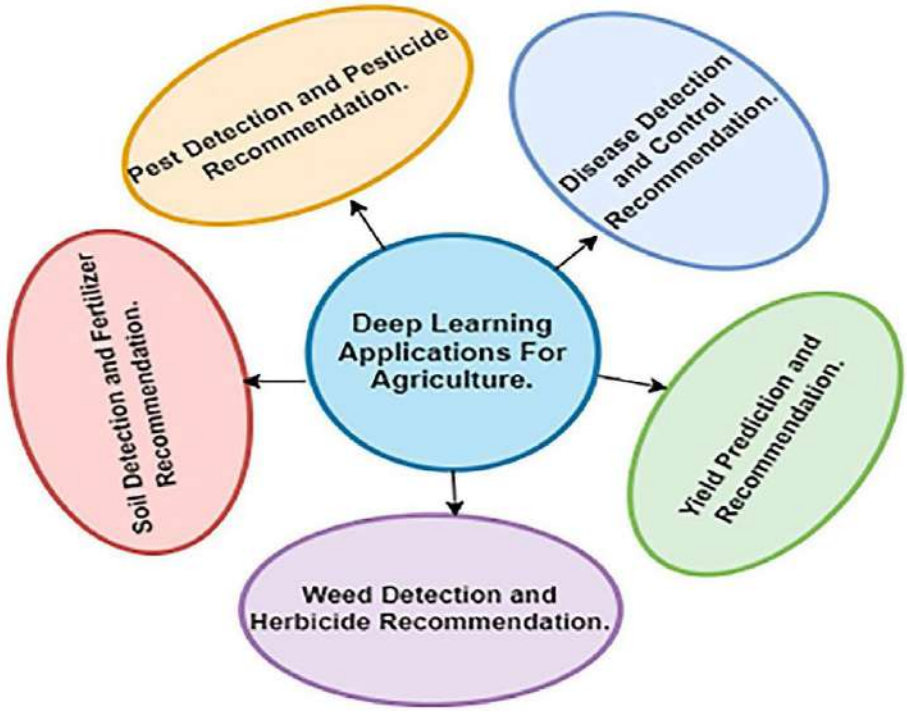

Fig. 1. DL applications in agriculture curled from (Saranya et al., 2023)

As can be seen from Fig. 1, deep learning has been applied in different aspects of agriculture such as pest detection and pesticides recommendation. This is done with the help of different technologies such as satellite, ground-based, and airborne sensors (Darra et al., 2023). The data collected by these sensors are parsed and analyzed using deep learning algorithms to detect the kind of pests that infiltrate a given farm and recommend the best pesticides to control them. This can be done in real-time so that the effects of the pests can be minimized to the lowest minimum. The use of machine learning in agriculture cannot be over emphasized especially with regards to the pests and disease control in very large farmlands were physical monitoring and surveillance is very difficult, expensive, ineffective, and time consuming.

2 Recent Technological Advancements in Agriculture

There has been tremendous improvement in agriculture due the advancement of technology especially the artificial intelligence. These technological advancements are motivating data scientists and agronomists to develop analytical methods and tools to streamline field management and address contemporary issues. Based on data and task automation, these innovative solutions need professional assistance to satisfy farmers' needs and enable them to maximize their agricultural output. Smart agriculture makes extensive use of artificial intelligence (AI), which combines a number of digital technologies such as big data, deep learning, and the Internet of Things (IoT) (Darra et al., 2023). Deep learning has recently revolutionized the agricultural sector. Darra *et al.* (2023) has succinctly presented the major areas where deep learning has changed the agricultural practices. The major areas are:

Crop monitoring: By analyzing photos of crops, deep learning systems can provide precise data on the health and growth of the plants. In order to increase agricultural productivity, this can assist farmers in identifying problems early on, such as nutrient shortages or disease outbreaks, and in taking appropriate action.

Yield prediction: Deep-learning models can accurately forecast agricultural yields by evaluating data from sensors, satellites, and other sources. This can assist farmers in managing their crops and helping them plan their harvests.

Plant disease detection: By analyzing plant photos, deep learning algorithms are able to identify pests, illnesses, and other problems. This can assist farmers in spotting issues early on and taking appropriate steps to stop the disease from spreading (Dogra et al., 2023).

Irrigation optimization: Deep learning models can make recommendations about when and how much to irrigate crops based on their analysis of weather data and soil moisture levels. Farmers can increase crop productivity and conserve water by doing this.

Pest and weed identification. To identify weeds and pests in crop photos, deep learning systems can evaluate the photographs. This can lessen the demand for chemical pesticides and herbicides by assisting farmers in weed and pest detection and management. Through extensive image dataset training, deep learning models are able to recognize various weed and pest species with accuracy in real time, empowering farmers to manage their crops accordingly.

Identification of plant stress: Deep learning algorithms are capable of examining plant photos in order to identify indicators of stress, such as illness, nutrient shortages, and water stress. This can assist farmers in spotting issues early on and implementing the necessary fixes to enhance plant health and productivity. Deep learning models may identify minute indicators of stress that might not be obvious to the human eye by using enormous image datasets for training. This allows farmers to monitor crop health more precisely and effectively.

In general, deep learning has the ability to greatly increase agricultural productivity and efficiency while assisting farmers in making knowledgeable crop management decisions (Asadi and Shamsoddini, 2024; Coulibaly et al., 2022; Dogra et al., 2023).

2.1 IoT and UAVs in crop disease detection

Agriculture is one of the fields that generates huge amount of data that needs to be processed and analyzed for improved agricultural production. Several sensors are now used to collect real-time data about crops on the farmland and transmit for processing. This is a component of smart agriculture (Han, 2023). Components of smart farming are summarized in Fig. 2.

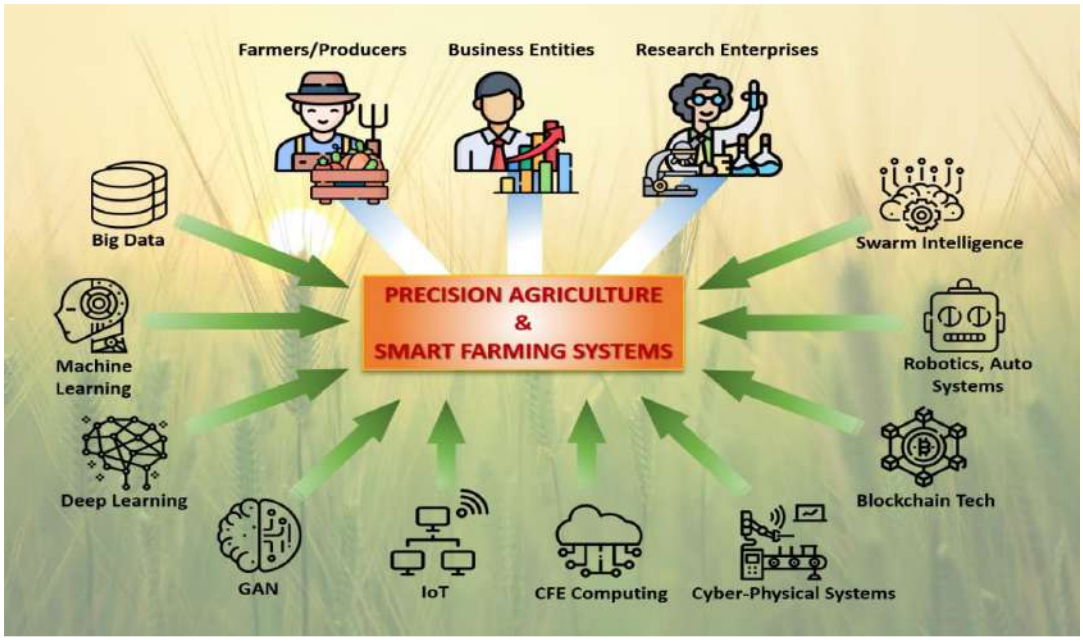

Fig. 2. Component of smart agriculture (Han, 2023)

The internet-of-things (IoT) links various objects so that data about them can be exchanged online with people all over the world. Agriculture is progressing to a new level with the application of IoT and DL in wireless sensor networks (WSN). The amount of research in this field has not stopped, and the Internet of Things has made agricultural development more adaptable to shifting weather patterns. To help farmers make the most of their land and crops and ensure that they are as productive and healthy as possible, it has made use of information and communication technology (ICT) (Han, 2023). Through the implementation of site-specific agricultural methods, the Internet of Things guarantees sustainability, profitability, and environmental protection. To compute the water requirements of urban areas, for example, the smart irrigation system makes use of the Internet of Things. Based on temperature and soil moisture content, it advises when to irrigate crops. This system gathers information regarding the test bed's temperature, humidity, and direction of wind (Han, 2023).

The advancement of unmanned aerial vehicle (UAV) remote sensing has led to its application in field-scale trait evaluation, including oilseed rape, spinach, and rice yield estimate, biomass dynamic monitoring, and time series canopy phenotyping of genetic variations in soybeans. Researchers who investigated the viability of using unmanned aerial vehicle (UAV) remote sensing to assess the severity of narrow brown leaf spots in rice discovered that the vegetation index—which is generated from RGB (red, green, and blue) images—achieved the best detecting performance (Shaodan et al., 2023).

2.2 Machine learning (ML) and Deep Learning (DL) in agriculture

Machine learning (ML) and deep learning (DL) present several opportunities for making useful analysis and predictions from large volume of agricultural data. Agricultural data is mostly muti-dimensional and complex. ML is a sub-field of artificial intelligence (AI) that gives computers the skills or talents to learn on their own without being programmed explicitly (Liakos et al., 2018). DL, on the other hand, if a powerful technique that has found a central role in data analysis and image processing applications (Attri et al., 2023). DL frameworks have the ability handle the complexity and multidimensionality of agricultural data. DL is a concept that mimics the cognitive work of human brain and hence used in improving the accuracy of predictions (Sanaeifar et al., 2023).

Machine learning and deep learning have been found to be very instrumental for the successes achieved in healthcare sector. For example, ML has found its role in recognising anomalies in medical images for effective diagnosis. For drug discovery, DL can process a large volume of clinical datasets and quickly predict drug candidates for an ailment. In finance, ML and DL are used for fraud detection and algorithmic trading in which any suspicious transaction can be effectively detected and predictive model for price fluctuations can be developed in real-time. Also, they used in a retail situation to build efficient recommender and inventory management systems.

Machine learning and deep learning have been employed in different aspects of agriculture. Islam *et al.* (2023) built a deep transfer learning model for the prediction of cotton leaf diseases. The authors used pretrained models with the help of hyperparameter tuning; VGG-16, VGG-19, Xception, and Inception-V3 on publicly available cotton disease dataset. The authors reported that their model achieved 98.70% accuracy. Agricultural produce can be substantially affected by weak/poor weed management. Farmers deploy different strategies for weed control on their farmers ranging from manual identification and removal to the use of herbicides. Being able to effectively separate weeds from the actual crops can be a challenging task. Deep learning models can effectively detect disease, pests, and weeds (Attri et al., 2023). For example, Nagothu *et al*. (2023) built a convolutional neural network (CNN) that detects weeds from images captured using unmanned arial vehicle (UAV) with good performance. In a similar effort, Xia *et al.* (2023) used multimodal data fusion captured using UAV, and deep learning to build a comprehensive weed resistance score (CRS) which enabled real-time assessment of weeds resistance to herbicides over very large farmlands.

In the area of plant stress, different deep learning models have been employed. Stress is a situation or chemical that affects the effective plant's metabolism and growth (Attri et al., 2023). Plant biotic stress are caused by deleterious organisms such as bacteria, fungi, viruses, pests, and insects; whereas the abiotic are as a result of unfavourable environmental such as the salinity, drought, chemical damage, and deficiency of nutrients (Cándido-Mireles et al., 2023) For instance, Cándido-Mireles et al. (2023) built CNN models for the identification of grapevine plants with stress symptoms from RGB images with help of EfficeintNetB3 architecture. The best model achieved 97.2%.

Moreover, prediction of crop yield has a central role in accurate and reliable crop monitoring systems for agricultural planning and the attainment of national food security (Ju et al., 2021). Crop yield prediction is the process of estimating the average yield of a specific crop in a given area prior to

harvest (Ning et al., 2023). Crop prediction provides information on food production potentials to several decision-makers (farmers, government agencies, individuals), and hence, is very well linked to national and global food security. From time to time, agricultural managers determine the sorts of crops to grow and the size of the cultivation farm. This forms the basis upon which they estimate crop yields. Accurate, reliable, and timely crop yield prediction help in setting up policies such as domestic crop pricing , crop import-export policy (Yalcin, 2019), and food self-sufficiency (Ju et al., 2021). There is a huge volume of both on-farm and off-farm data that we can gain useful insight into if they are well processed and properly organized. These data come in different forms, emanating from various sources and at varying speeds. Having the right analytic tools to process and organize them will be of great help to both farmers and policymakers Crop yield prediction is known to be complex because of the complex interaction between different factors such as crop genotype, environmental, and management factors (Khaki and Wang, 2019; Saravi et al., 2020). In recent times, impressive performances have been achieved with the use of deep learning frameworks (Khaki et al., 2020).

Crop yield prediction relies on the availability of the relevant data. With advancement of remote sensing technology, researches are now using the remote sensing data for yield prediction due to its ease of acquisition and scalability (Barbedo, 2023; Coulibaly et al., 2022; Gadiraju and Vatsavai, 2020; Liakos et al., 2018). Remote sensing is a way of obtaining optical data about an object using a sensor in the field or landscape in a non-intrusive way without coming into contact with the sampling units(Barbedo, 2023). Process-based biophysical (PB) (Fathi et al., 2023; Jeong et al., 2021) and machine-learning (ML) models are the two primary model categories that can be used to predict agricultural production data. PB models, such as the Decision Support System for Agro-Technology Transfer (DSSAT) and the Agricultural Production System Simulator (APSIM), use accurately calibrated crop growth models to dynamically simulate crop yield. In this architecture, state variables in a model are frequently updated, recalibrated, or reinitialized at a greater spatial resolution than the driving data using RS data. However, process-based model calibration at bigger scales continues to be difficult and necessitates a variety of field observations.

3 Prospects of technology in crop disease detection and mitigation for Kebbi state

As can be seen from the previous sections, there are several opportunities the advancement in recent computer technologies has brought to streamline agriculture. It is long overdue for our farmers to adopt these technologies in their agricultural practices because of their cost effectiveness, efficiency, time saving, and scalability. Kebbi state being one of the key producers of rice in Northern Nigeria is expected to adopt these technologies, in the areas of pests and diseases detection and mitigation, drought prediction and mitigation, crop yield prediction, and the farm management.

3.1 Harnessing technology for improved yield

Harnessing technology in agriculture is crucial for achieving sustainable and competitive food production (Bajac et al., 2023). Technological innovations play a significant role in increasing food security (Dimitrova, 2022). Over the years, agriculture has witnessed the adoption of various technologies, from mass production techniques to genetic testing and digitization (Sandhu et al., 2021). These advancements have been applied in different sectors of agriculture, such as dairy farming,

poultry farming, and organic farming (Sharma et al., 2021). The use of information and communication technologies, including the Internet of Things, sensors, and blockchain, can optimize agricultural management practices, improve yield, and provide real-time information to farmers and extension workers. By harnessing technology, the agriculture sector can enhance productivity, optimize resource utilization, and promote sustainable practices, ultimately contributing to the overall development of the industry.

3.2 level of adoption of technology in agriculture in Kebbi State

The Kebbi State being one of the key producers of rice in Northern Nigeria with 21 local governments, it produces paddy rice from almost all the local governments with a high prospect for increase in production over the years over other states(Ayuba et al., 2023) , Despite this production our investigation found that farmers in the state are not adopting technology in Agriculture, they only rely on manual method of monitoring crop yield, farm management with normal method of Insecticide and fertilizer when need arise. This method can only be effective with small farmers but is time consuming, and cannot address the issues of diseases detection and mitigation, drought prediction and mitigation, crop yield prediction, and the farm management in time. But the use of computer in agriculture technology has solve all through several sensors that are now used to collect real-time data about crops on the farmland and transmit for processing.

It is the high time for our farmers to adopt these technologies in their agricultural practices because of their cost effectiveness, efficiency, time saving, and scalability.

4 Conclusion

In this work, we have reviewed the recent development in agricultural production in relation to the adoption of modern technologies in Kebbi State. Our investigation found that farmers in the state are not adopting technology in Agriculture, they only rely on manual method of monitoring crop yield, farm management with normal method of Insecticide and fertilizer when need arise.

The study present the opportunities and benefits of the adoption of these technologies to both farmers and Nigeria's achievement of food security in a short time in terms of enhance productivity, optimize resource utilization, and promote sustainable practices, ultimately contributing to the overall development of the industry By harnessing technology.

References

Adenowuro, O. J. (2023). *The role of financial support and rice farming education in rice farming sustainability: Acase of rice farmers association of Nigeria (RIFAN), Ebonyi state.* (Master), Estonian university of life sciences, Institute of Agricultural and Environmental Sciences.

Asadi, B., & Shamsoddini, A. (2024). Crop mapping through a hybrid machine learning and deep learning method. *Remote Sensing Applications: Society and Environment, 33*, 101090.

Attri, I., Awasthi, L. K., Sharma, T. P., & Rathee, P. (2023). A review of deep learning techniques used in agriculture. *Ecological Informatics*, 102217.

Ayuba, G., Aliyu, D., Josiah, S., Asmau, A., & Dorh, L. E. (2023). Economic Analysis of Paddy Rice Marketing in Kebbi State, Nigeria. *International Journal of Applied and Scientific Research (IJASR)*

1(2), 147-156.

Bajac, B. M., Bajac, M., & Stošić, L. (2023). APPLIED INFORMATION TECHNOLOGIES IN AGRICULTURE. *Social Informatics Journal, 2*(1), 15-20.

Barbedo, J. G. A. (2023). A review on the combination of deep learning techniques with proximal hyperspectral images in agriculture. *Computers and Electronics in Agriculture, 210*, 107920.

Cándido-Mireles, M., Hernández-Gama, R., & Salas, J. (2023). Detecting vineyard plants stress in situ using deep learning. *Computers and Electronics in Agriculture, 210*, 107837.

Coulibaly, S., Kamsu-Foguem, B., Kamissoko, D., & Traore, D. (2022). Deep learning for precision agriculture: A bibliometric analysis. *Intelligent Systems with Applications, 16*, 200102.

Darra, N., Anastasiou, E., Kriezi, O., Lazarou, E., Kalivas, D., & Fountas, S. (2023). Can Yield Prediction Be Fully Digitilized? A Systematic Review. *Agronomy, 13*(9), 2441.

Dimitrova, A. (2022). Technological Innovations in Agriculture as a Way to Increase Food Security. *Economic Thought journal*(6), 692-704.

Dogra, R., Rani, S., Singh, A., Albahar, M. A., Barrera, A. E., & Alkhayyat, A. (2023). Deep learning model for detection of brown spot rice leaf disease with smart agriculture. *Computers and Electrical Engineering, 109*, 108659.

Fathi, M., Shah-Hosseini, R., & Moghimi, A. (2023). 3D-ResNet-BiLSTM Model: A Deep Learning Model for County-Level Soybean Yield Prediction with Time-Series Sentinel-1, Sentinel-2 Imagery, and Daymet Data. *Remote Sensing, 15*(23), 5551.

Gadiraju, K. K., & Vatsavai, R. R. (2020). *Comparative analysis of deep transfer learning performance on crop classification.* Paper presented at the Proceedings of the 9th ACM SIGSPATIAL International Workshop on Analytics for Big Geospatial Data.

Han, D. (2023). Big Data Analytics, Data Science, ML&AI for Connected, Data-driven Precision Agriculture and Smart Farming Systems: Challenges and Future Directions *Proceedings of Cyber-Physical Systems and Internet of Things Week 2023* (pp. 378-384).

Islam, M. M., Talukder, M. A., Sarker, M. R. A., Uddin, M. A., Akhter, A., Sharmin, S., . . . Debnath, S. K. (2023). A deep learning model for cotton disease prediction using fine-tuning with smart web application in agriculture. *Intelligent Systems with Applications, 20*, 200278.

Jeong, S., Ko, J., & Yeom, J.-M. (2021). Predicting rice yield at pixel scale through synthetic use of crop and deep learning models with satellite data in South and North Korea. *Science of the Total Environment*. doi: https://doi.org/10.1016/j.scitotenv.2021.149726

Ju, S., Lim, H., Ma, J. W., Kim, S., Lee, K., Zhao, S., & Heo, J. (2021). Optimal county-level crop yield prediction using MODIS-based variables and weather data: A comparative study on machine learning models. *Agricultural and Forest Meteorology, 307*.

Khaki, S., & Wang, L. (2019). Crop yield prediction using deep neural networks. *Frontiers in plant science, 10*, 621.

Khaki, S., Wang, L., & Archontoulis, S. V. (2020). A cnn-rnn framework for crop yield prediction. *Frontiers in Plant Science, 10*, 1750.

Liakos, K. G., Busato, P., Moshou, D., Pearson, S., & Bochtis, D. (2018). Machine learning in agriculture: A review. *Sensors, 18*(8).

Mbava, N., Mutema, M., Zengeni, R., Shimelis, H., & Chaplo, V. (2020). Factors affecting crop water use efficiency: A worldwide meta-analysis. *ELSEVIEW, Agricultural Water Management 228 (2020) 105878, 228*, 105878.

Nagothu, S. K., Anitha, G., Siranthini, B., Anandi, V., & Prasad, P. S. (2023). Weed detection in agriculture crop using unmanned aerial vehicle and machine learning. *Materials Today: Proceedings*.

Ning, W., Zhong, M., Pengcheng, H., Xi, L., Zhao, H., & Kedi, L. (2023). 3D Convolutional Neural Network with Dimension Reduction and Metric Learning for Crop Yield Prediction Based on Remote Sensing Data. *Applied Sciences, 13*(24), 13305.

Rebecca, N. (2020). International Plant Pathology: Past and Future Contributions to Global Food Security. *The American Phytopathological Societ • 2020 • 110:245-253 • https://doi.org/10.1094/PHYTO-08-19-0300-IA, 110*(2), 245-253.

Sanaeifar, A., Guindo, M. L., Bakhshipour, A., Fazayeli, H., Li, X., & Yang, C. (2023). Advancing precision agriculture: The potential of deep learning for cereal plant head detection. *Computers and Electronics in Agriculture, 209*, 107875.

Sandhu, S. K., Morozov, A. Y., Holt, R. D., & Barfield, M. (2021). Revisiting the role of hyperparasitism in the evolution of virulence. *The American Naturalist, 197*(2), 216-235.

Saranya, T., Deisy, C., Sridevi, S., & Anbananthen, K. S. M. (2023). A comparative study of deep learning and Internet of Things for precision agriculture. *Engineering Applications of Artificial Intelligence, 122*, 106034.

Saravi, B., Nejadhashemi, A. P., & Tang, B. (2020). Quantitative model of irrigation effect on maize yield by deep neural network. *Neural Computing and Applications, 32*(14), 10679-10692.

Sasu, D. D. (2023). Rice production in Africa 2021, by country. Retrieved 21 January, 2024, from https://www.statista.com/statistics/1322372/rice-production-in-africa-by-country/

Shaodan, L., Yue, Y., Jiayi, L., Xiaobin, L., Jie, M., Haiyong, W., . . . Dapeng, Y. (2023). Application of UAV-Based Imaging and Deep Learning in Assessment of Rice Blast Resistance. *Rice Science*.

Sharma, A., Devadas, V., Sharma, H., Kartha, D., Pandey, H., Soni, G., . . . Kumari, N. (2021). Advancement of agricultural technology in farming of India. *Bhartiya Krishi Anusandhan Patrika, 36*(4), 313-319.

Xia, F., Lou, Z., Sun, D., Li, H., & Quan, L. (2023). Weed resistance assessment through airborne multimodal data fusion and deep learning: A novel approach towards sustainable agriculture. *International Journal of Applied Earth Observation and Geoinformation, 120*, 103352.

Yalcin, H. (2019). *An approximation for a relative crop yield estimate from field images using deep learning.* Paper presented at the 2019 8th International Conference on Agro-Geoinformatics (Agro-Geoinformatics).

STATISTICS AND OPTIMIZATION

On Unobserved Traits and its Measurements: A Note on Modern Item Response Modelling Approach

O. M. Adetutu

Department of Statistics, Federal University of Technology Minna, Nigeria
*adetutuolayiwola@gmail.com

Abstract

Often, scientists are interested in studying traits and other unobservable attributes of individuals which can only be measured with instruments such as questionnaire, test let, construct, and so on. These instruments are useful in extracting information on these hidden traits. Traditionally, Karl Pearson's classical approach were in used in modelling these traits with its attendant shortcoming ranges from variant estimates to its challenges of validity and reliability. This study present a better and modern item response modelling that remedy shortcomings of classical approach yielding reliable, consistent, and valid estimate through item response functions.

Keywords: unobservable, attributes, traits, reliability, validity

1 Introduction

Unobserved traits are mental and emotional activities that cannot be directly observed or measured, examples are: $(i.)$ psychological constructs such as intelligence, self-esteem, depression, academic proficiency, aptitude achievement, attitude or belief, $(ii.)$ psychological traits and behaviour such as thinking, memory, perception, problem-solving, and decision-making are all hidden traits which can only be estimated through questionnaire, test lets, constructs, schedules, and so on (Embretson *et al.*, 2000).

Two approaches toward measurement of unobserved traits are: classical test theory (CTT), and item response theory (IRT). The former is a body of related psychometric theory that predicts outcomes of psychological testing based on the fact that person's observed or obtained score on a test, construct, and questionnaire is sum of a true score and error score (NCME, 2017). This approach is a sample (test, questionnaire, or schedule) based rather than item base. The model for this approach is positioned in equation (1)

$$X = T_x + E_x: \tag{1}$$

Such that: $E(E_x) = 0$

$Cov(T_x, E_x) = 0$

$$Cor((T_x, E_x) = 0$$

Where: X is the obtained score

T_x is a true score

E_x is an error score

The focus of CTT is to understand and improve the reliability and validity of unobserved traits using the entire sample. Furtherance to this, Hambleton *et al.*, (1991) identified various shortcomings of CTT which are: inseparability of respondent's and construct's characteristics, assumptions of equal standard errors for all respondents, construct oriented rather than item oriented, and impossibility of making predictions on how well on individual respondents or even group of respondents may do on a given construct item.

The latter is a modern technique of modelling unobserved traits called latent trait theory, strong true score theory or modern mental test theory. Adetutu and Lawal, (2020) described item response theory modelling as a paradigm for the design, analysis, and scoring of tests, constructs, questionnaire, schedule and other instruments used in measuring hidden traits. This approach makes use of item response functions which make it item base rather than sample base.

Assumptions

Potency of IRT and its assumptions that places IRT over CTT as enumerated by Adetutu and Lawal (2023) are: *(i.)* the number of traits that underlies respondents' behaviours or performances. This could be unidimensional or multi-dimensional; for unidimensional, only one trait is being measured, otherwise, multidimensional. The differences in observing response between respondents would be due to their traits when this assumption hold. *(ii.)* Local independence assumption implies that items in the construct are uncorrelated and hence, response to separate item is mutually independent (Lim, 2020). *(iii.)* A non-linear regression curve relates the probability of response on the item to trait being measured, this is a distinction between different latent models, sometime called trace lines or item response functions, and *(v.)* invariant properties of IRT which guarantee unchanging parameters' estimates even when the characteristics of the respondents change. These assumptions have made it possible to estimate individual, and item properties rather than sample based of CTT.

Properties

Discrimination parameter of modern latent traits theory determines the rate at which the probability of correct response option to an item or construct changes as a function of ability or trait continuums. This is often called slope of item response curves whereby negative values are discarded, hence, it is a monotonic increasing because as ability or trait increases, probability of endorsing correct response category to a construct or test also increases and vice-versa (Baker and Kim, 2004). In addition, *difficulty* parameter describes how easy or hard an item of a construct is being perceived by the respondent in binary IRT, while this is tagged 'propensity of endorsing a response option' in a polytomous IRT (Linden, 2018). However, the third property is *pseudo-guessing* parameter which only apply to educational setting, and this is the impact of chance on observed response. This means a lower trait respondent may have non-zero probability of endorsing an item in a test correctly; even an item that seems to be difficult to endorse.

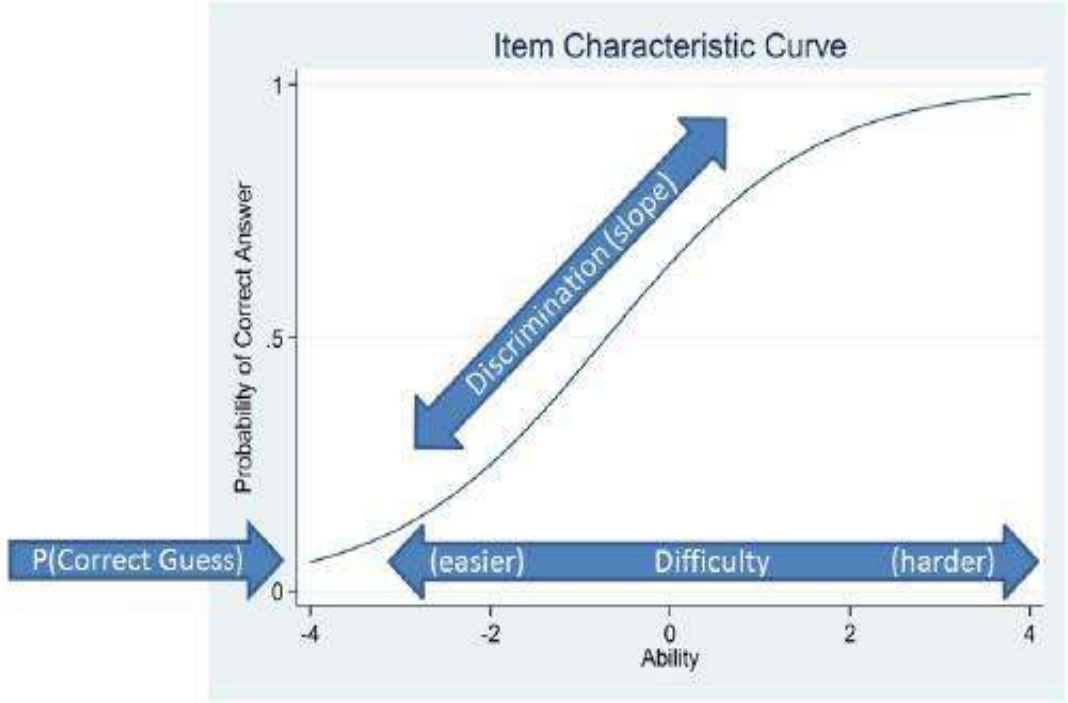

Figure 1: Properties of Unobserved Ability or Traits Model

Vertical axis of the Figure 1 displays probability of correct responses to an item while horizontal axis represent trait or ability continuum; this means, any point on the response curve is a function of respondents' traits with a specific probability of response. The implication of

this is that items and individual respondent characteristics can be estimated at any point on the item characteristic curve which is a plus for IRT modelling.

The Aim and Objectives

The study was motivated by the need to efficiently measures and models latent, hidden, not yet manifested, personality characteristic, or trait of respondent devoid of drawbacks associated with traditional approach of CTT. The specific objectives are to describe how to estimate the:

i. Value of an assumed latent trait (discrimination, and difficulty/location parameter)

ii. Attributes of the individual (trait/ability)

iii. Describe variation of the latent parameters among individuals

2. Methodology

2.1 Study Designs and Measures

A well structure construct, questionnaire, multiple choice question, likert-scales or instruments that are scored dichotomous and polytomous would be suitable in extracting information from respondents using suitable sampling techniques on area of interest is applicable here.

2.2 Methods

Responses from the respondents are coded polytomously to form $n \times p$ matrix depending on number of respondents and items on the construct, after which graded response model (GRM) proposed by Samejima (1969) which allowed categorical or ordered item responses function is used.

2.3 Graded Response Model

The likelihood of a respondent with trait θ responds in response category k of item i is:

$$\Pr\left(Y_{ij} \geq k \middle| a_i, b_i, \theta_j\right) = \frac{\exp\{a_i(\theta_j - b_{ik})\}}{1+\exp\{a_i(\theta_j - b_{ik})\}} \; : \qquad \theta_j \sim N(0,1) \tag{2}$$

Where:

a_i is the discrimination parameter index for item i, and

b_i is the difficulty (location) parameter of category (threshold) for item i

$i(i = 1,2, \ldots, I)$

The principle of GRM is based on operating characteristic functions which indicates the likelihood of responding to a particular category given trait or ability level θ are computed by subtracting adjacent $P^*_{ik}(\theta)$ as defined in equation (3).

$$P_{ik} = P^*_{ik} - P^*_{ik+1} \tag{3}$$

Where:

$$P^*_{ik} = \frac{e^{\{a_i(\theta_j - b_{ik})\}}}{1+e^{\{a_i(\theta_j - b_{ik})\}}} \tag{4}$$

$$P^*_{ik+1} = \frac{e^{\{a_i(\theta_j - b_{ik+1})\}}}{1+e^{\{a_i(\theta_j - b_{ik+1})\}}} \tag{5}$$

2.4 Parameters Estimation in Graded Response Model

The parameterization of equation (2) in term of slope-intercept is presented as

$$\Pr(Y_{ij} \geq k | \gamma_i, \omega_i, \theta_j) = \frac{\exp\{\gamma_i(\theta_j - \omega_{ik})\}}{1+\exp\{\gamma_i(\theta_j - \omega_{ik})\}} \tag{6}$$

$$\left.\begin{aligned} a_i &= \gamma_i \\ b_{ik} &= \frac{\omega_i}{\gamma_i} \end{aligned}\right\} \tag{7}$$

When y_{ij} is the observed response for Y_{ij} and

$$p_{ij} = \Pr(Y_{ij} = y_{ij} | \gamma_i \omega_i) \tag{8}$$

Conditional density for respondent j is

$$f(y_j | \boldsymbol{G}, \theta_j) = \prod_{i=1}^{I} p_{ij} \tag{9}$$

Where:

$y_j = (y_{1j}, y_{2j}, \dots, y_{Ij})$

$\boldsymbol{G} = (\gamma_1, \gamma_2, \dots, \gamma_I, \omega_1, \omega_2, \dots, \omega_I)$ and I is the number of items.

The likelihood of the respondent j is

$$L_j(\boldsymbol{G}) = \int_{-\infty}^{\infty} f(y_j|\boldsymbol{G}, \theta_j)\emptyset(\theta_j)d(\theta_j) \quad (10)$$

Where: $\emptyset(\theta_j)$ is the density function for standard normal distribution.

For N respondents

$$1ogL(\boldsymbol{B}) = \sum_{j=1}^{N} 1ogL_j(\boldsymbol{G}) \quad (11)$$

Equation (11) is intractable, numerical method such adaptive quadrature would be implemented in Stata or R software.

4.0 Item Category Characteristic Curve and Discussions

A typical item category characteristic curve is a non-linear regression curves that displays likelihood of respondent responding in each of the mutually exclusive response categories.

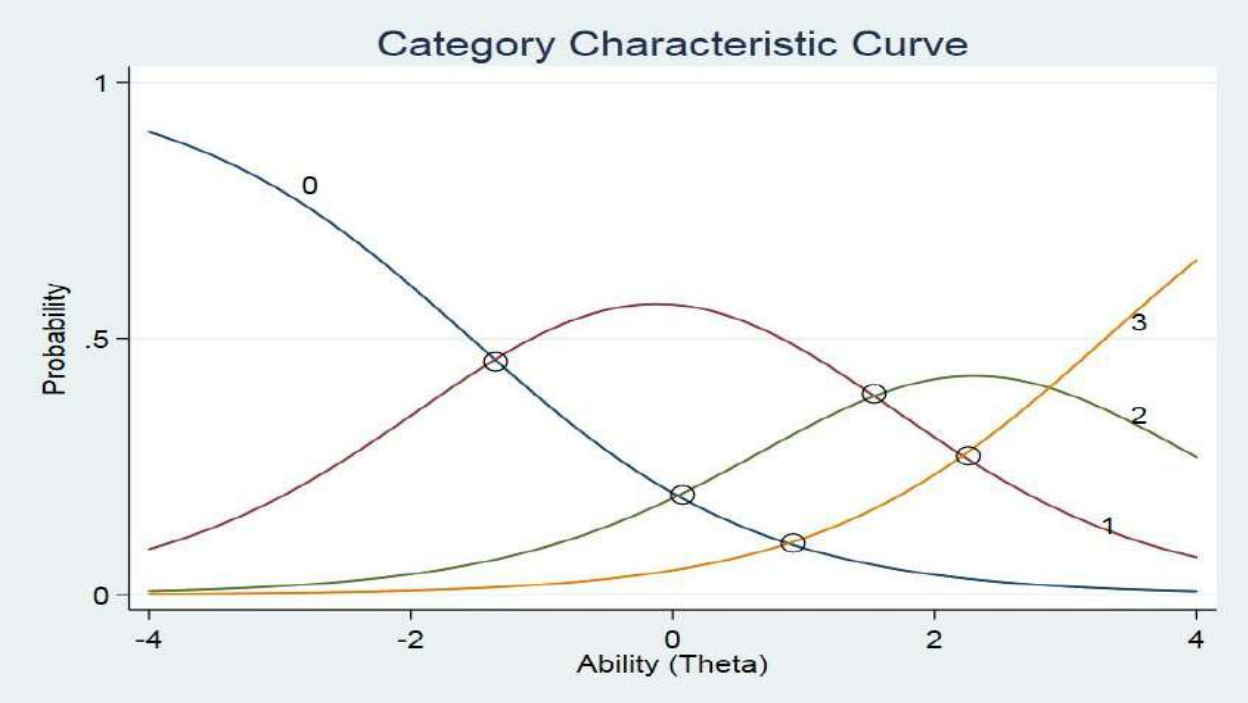

Figure 2: A Typical Category Characteristic Curve of an Item

In Figure 2, there are four responses to this item, curve 1, is taken as a base. The lower trait respondents are most likely to respond to this particular item by endorsing curve 1 instead of a base curve 0 with the corresponding likelihood or probability of endorsing the response option, this is because the first curve to cross base curve from the left is curve 1. This have negative index on ability axis. Moreover, an average individual most likely to endorse curve 2 instead of the base response, this is because where it crosses base curve on the ability axis is close to 0 while those respondents endorse curve 3 have higher trait, this is because curve 3 is the last to cross the base curve towards right.

In addition, response option tagged curve 3 would mostly discriminate respondents. This is because of all the response options, it has the largest slope and curve 2 would have the least, hence least in classifying respondents in term of their abilities.

5. Conclusions

The results from item response theory modelling is item base rather than sample, therefore attributes of individual item such as discriminating and location indices, and respondents' traits are estimable at any point of item response curve, this places IRT over CTT. In addition, parameters estimates remain unchanged under IRT even when attributes of respondents and environment surrounding estimation changes; this is a plus for IRT over CTT. The major focus and challenge of CTT is improving validity and reliability of estimates which are already be taken care of by IRT when its assumptions hold.

6. References

Adetutu, O. M. and Lawal, H. B. (2023). Applications of Item Response Theory Models to Assess Item Properties and Students' Abilities in Dichotomous Responses Items. Open Journal of Educational Development (ISSN: 2734-2050), 3(1), 01-19. Available from https://doi.org/10.52417/ojed.v3i/.304

Adetutu, O. M., and Lawal, H. B., (2020). On comparisons of Frequentist to Bayesian Estimation for item response theory models in the presence of dichotomous response of Science, Technology, Mathematics, and Education, 16(4), 128-137. https//:www.jostmed.futminna.edu.ng

Baker, F. B., and Kim, S. H. (2004). Item Response Theory: Parameter Estimation Techniques (2nd ed.). New York: Taylor and Francis.

Embretson, Susan E.; Reise, Steven P. (2000). Item Response Theory for Psychologists. Psychology Press. ISBN 9780805828191.

Hambleton, R., Swaminathan, H., Rogers, H. (1991). Fundamentals of Item Response Theory. Newbury Park, California: Sage Publications, Inc.

Lim, S. (2022). Review: A Course in Item Response Theory and Modelling with Stata, and Using R for Item Response Theory Model Applications. Structural Equation Modelling: A Multidisciplinary Journal, 27(4), 657-659, doi: 10.1080/10705511.2020.1740886, Available from https://doi.org/10.1080/10705511.2020.1740886

Linden, A. (2018). Review of Tenko Raykov and George Marcoulides's A Course in Item Response Theory and Modeling with Stata. The Stata Journal: Promoting Communications on Statistics and Stata, 18(2), 485–488. https://doi.org/10.1177/1536867X1801800213

National Council on Measurement in Education (2017) http://www.ncme.org/ncme/NCME/Resource_Center/Glossary/NCME/Resource_Center/Glossary1.aspx?hkey=4bb87415-44dc-4088-9ed9-e8515326a061#anchorC Archived 2017-07-22 at the Wayback Machine

Samejima, F. (1969). Estimation of Latent Ability Using a Response Pattern of Graded Scores. Psychometrika Monograph Supplement, No. 7

Predicting the Number of Fire Accidents Occurrence in Federal Capital Territory (FCT) Using Grey-Artificial Neural Network Model

[1]Fadipe, Faith O., [2]Lawal Adamu, [3]Somma Samuel A.

[1,2,3] Department of Mathematics, Federal University of Technology Minna, Niger State.

Email the corresponding author: faithmatthew113@gmail.com

Abstract

This paper presents a hybrid model for predicting fire accidents in FCT, integrating the Artificial Neural network and the Grey Model. The model made use of historical accident data to enhance prediction accuracy. The findings demonstrated superior performance as compared to the standalone Grey GM (1,1) model. Results from this model could help in assessing the risk levels of fire accident occurrence in FCT and planning and executing firefighting strategies.

Keywords: Artificial Neural Network, Grey System Model, Grey-Artificial Neural Network, Fire Accident

1. Introduction

When a material burns in an exothermic process, it quickly oxidizes, producing heat, light, and other reaction products. This process is known as fire. (Charles, 2000).
When a flammable or combustible substance is exposed to heat or air above the fuel's flash point and can maintain a rate of rapid oxidation that triggers a series of reactions, in addition to an adequate amount of an oxidizer, such as oxygen gases or another oxygen-rich compound, a fire can start. (Yusuf, 2012). Accidents involving fires can cause terrible damage and severe human injuries. Nigeria experiences fire accidents that result in property worth billions of Naira each year. Serious injuries, such as burns to the entire body, can occur to victims of fire accidents.

In addition to burns, smoke inhalation, and poisonous gas exposure can result in mortality in fire incidents. Residential fires in general present the highest risk to human life and the environment due to their increased potential for catastrophic outcomes (Ceyhan *et al*., 2013). Fires are often started by a single fuel source. The temperature of the smoke layer rises as more objects catch fire, giving off more heat and reflecting it to more objects. The unburned items may ignite almost instantaneously in compact compartments. We refer to this circumstance as a flashover.

In large compartments, it is more likely that objects will ignite sequentially. The sequence of the ignition depends on the fuel arrangement and composition and ventilation available to support the combustion of available fuels (Idayat, 2021). The main concern for residents of the Federal Capital Territory (FCT) is the annual loss of billions of naira in property and human life caused by fire accidents. Business owners in FCT have suffered enormous losses because of multiple fire incidents. Since many of these companies are still in their infancy, there are worries that the incidents may harm investments in the area (Odeniyi, 2022). Recently, on

November 6th, 2023, A fire mishap destroyed the Samsung office in Wuse 2 District's well-known Banex neighborhood. (The Punch, 2023). On the 6th of November 2023, a part of the Canadian High Commission in FCT was destroyed by fire, leaving two individuals dead and the same number injured. (Channels, 2023). Located in the Jahi neighborhood of the Federal Capital Territory (FCT), Abuja, Next Cash and Carry is one of the best department stores in the city. On December 26, 2021, a fire destroyed the store, destroying items valued at billions of naira. (Vanguard Newspaper, 2021).

2. Literature Review

Modeling and predicting fire incidents are crucial elements of fire management strategy. Many academics from all around the world have put out several strategies to offer data that can help reduce the frequency of fire incidents. A few of these studies are described here.

Idayat (2021) developed a stochastic model aimed at predicting the number of fire incidents in Niger State using the Viterbi Algorithm. This model was based on a three-state stochastic framework, according to Markov's principles, with each state presenting four potential outcomes. The model's parameters were derived from fire accident data sourced from the Niger State Fire Service archives. Following parameter estimation, the model underwent training with the Baum-Welch Algorithm to optimize for maximum likelihood. Testing for the model's validity revealed it to be 75% accurate in making short-term predictions, but only 50% accurate for predictions over a longer term. The researcher deduced that while the model is reliable for short-term forecasts, its long-term predictive capability is limited. Consequently, it was suggested that the insights gained from the model could help governmental agencies in crafting policies aimed at reducing fire incidents within the state.

Jiyu *et al* . (2020) The study evaluated the precision of fire accident forecasts in China using two different stochastic approaches: Grey theory and Grey-Markov theory. Despite a noticeable rise in fire incidents in China in 2013, there has been a subsequent decrease in fatalities, injuries, and property damage from fires since 2014. The comparison revealed that the Grey-Markov theory outperforms the Grey theory in forecasting accuracy, with the Grey theory achieving a maximum relative error of 5.8% compared to Grey-Markov's more accurate 5% maximum relative error.

Saeed *et al.* (2021) The study implemented the Grey-System Model GM (1,1) to forecast vehicular accident occurrences on the Lokoja-Abuja-Kaduna Expressway in Nigeria, analyzing data gathered over a decade (2010-2019) from the Federal Road Safety Corps of Nigeria archives. The model achieved a prediction accuracy of 85.97%. Based on this high level of accuracy, the researchers determined that the model is reliable for predicting vehicular incidents and suggested that its predictions could be valuable in guiding policymaking and decision processes for enhancing road safety on highways.

Reported (Chunxia *et al.,* 2016). The article focused on developing an enhanced version of the Grey neural network model, aimed at predicting transportation delays. The objective was to

refine the Grey neural network approach, and the model's effectiveness was then evaluated through empirical research. This was done to help businesses forecast market demand more accurately in the event of transportation disruptions.

Enhancing the selection criteria for the number of neurons in the input layer of Backward Propagation (BP) neural networks, increasing the model's predictive accuracy and fit, and elevating the stability and dependability of its forecasts are among the ways the advanced grey neural network model surpasses the traditional Grey model GM (1,1). The model particularly excels when handling raw data exhibiting exponential growth, provided that the fluctuations in the data remain within a moderate range. Moreover, this refined model proves effective in predicting sequential data during instances of sudden changes or disruptions in transportation, thereby aiding in the anticipation of transportation disturbances.

3. Methodology

3.1 Grey System GM (1,1) Model.

By adding these data from the first in the Accumulating Generation Operator (AGO), the grey GM(1,1) model uses the discrete data series to create an equation of grey continuous differential equations, which can then be solved to conduct forecasting. (Li Q *et al.*, 2007).
Let the study's raw data series now be represented by:
$x_{(k)}^{(0)}$; k=1,2, 3…n, $x^{(0)}{}_{(k)} \geq 0$ (non-negative). It can also be represented by

$$X^{(0)}{}_{=} \qquad (x_{(1)}^{(0)}, x_{(2)}^{(0)}, x_{(3)}^{(0)}, \dots, x_{(n)}^{(0)}) \qquad (3.1)$$

Let $X^{(1)}{}_{=} \qquad (x_{(1)}^{(1)}, x_{(2)}^{(1)}, x_{(3)}^{(1)}, \dots, x_{(n)}^{(1)})$ (3.2)

Equation (3.2) is the accumulated generated sequence (AGO) of the grey GM (1, 1) model.
Where, $X^{(1)}{}_{=}\sum_{i=1}^{k} x_{(i)}^{(0)}$, k=1, 2…n
$X^{(1)}$is called the Accumulated Generating Operation of $X^{(0)}$ denoted by 1-AGO.
By differentiating $X^{(1)}$ a whitened differential equation is obtained

$$\frac{dx^{(1)}}{dt} + ax^{(1)} = b \qquad (3.3)$$

Equation (3.3) can be represented by

$$x_{(k)}^{(0)} + az_{(k)}^{(1)} = b \qquad (3.4)$$

and is called the differential equation of GM (1,1) model.
Where $Z_{(k)}^{(1)} = \frac{1}{2}(x_k^{(1)} + x_{(k-1)}^{(1)})$
(3.5)
and $\hat{x}_{(k)}^{(0)}$is a grey derivative where a and b are called a grey input and developing coefficient, respectively, and it maximizes the information density for a given series to be simulated.

$$\hat{x}_{(k+1)}^{(1)} = (x_{(0)}^{(1)} - \frac{b}{a})e^{-ak} + \frac{b}{a} \quad (3.6)$$

Parameter *a* and *b* in equation (3.6) are estimated using the least square method as follow.

$$\begin{bmatrix} a \\ b \end{bmatrix} = \left[B^T \quad B \right]^{-1} B^T Y \quad (3.7)$$

Where,

$$Y = \left[x_{(2)}^{(0)}, x_{(3)}^{(0)}, x_{(4)}^{(0)}, \dots, x_{(n)}^{(0)} \right]^T \quad (3.8)$$

$$B = \begin{bmatrix} -Z_{(1)}^{(1)} & 1 \\ -Z_{(2)}^{(1)} & 1 \\ -Z_{(3)}^{(1)} & 1 \\ . & \\ . & \\ . & \\ -Z_{(n)}^{(1)} & 1 \end{bmatrix} \quad (3.9)$$

MAPE

$$MAPE = \frac{1}{n} \sum_{i=1}^{n} \left| \frac{y_i - \hat{y}_i}{y_i} \right| \times 100\% \quad (3.10)$$

Where;

$\hat{y}_i$ is the Grey Model predicted value.

y_i is the Grey-Model actual value.

n is the number of predictions samples.

Lewis (1982) divided the prediction accuracy of models into four grades and the division of prediction accuracy grades as presented in the Table 3.1

Table 3. 1

MAPE	Prediction Accuracy
$<10\%$	High
$10\%-20\%$	Good
$20\%-50\%$	Feasible
$>50\%$	Low

3.2 Grey-Artificial Neural Network Model.

The Grey-Artificial Neural Network represents a hybrid model that merges the Grey system model for a single variable (GM (1,1)) with an Artificial Neural Network (ANN) model. Within this integrated model, the ANN is employed to enhance the functioning of the Grey-system GM(1,1) model, leveraging the strengths of both approaches for improved performance. (Sifeng *et al*., 2016).

$$\hat{X}^{(0)}(i,l) = \hat{X}^{(0)}(i) + \hat{e}^{(0)}(l) \quad (3.11)$$

4 Result And Discussion

4.1 Application of Grey GM (1,1) model in predicting the annual number of fire accident in FCT Abuja from 2009 to 2022.

The data utilized in this paper was collected from the achieves of FCT fire service, Asokoro Headquarters for a period of fourteen years (2009-2022) to ensure comprehensive coverage of relevant information. This forms the original data sequence of the annual number of fire accident in FCT in the table below:

Table4.2: FCT Fire accident Statistics from 2009 to 2022

S/N	Year	Number of Fire accident
1	2009	324
2	2010	335
3	2011	542
4	2012	491
5	2013	427
6	2014	623
7	2015	486
8	2016	418
9	2017	443
10	2018	442
11	2019	338
12	2020	507
13	2021	570
14	2022	547

We begin the application by substituting the raw data in table 2 into equation (3.1), to obtain equation (3.11) below:

$$X^{(0)} = (324,335,542,491,427,623,486,418,443,442,338,507,570,547) \quad (3.12)$$

Using equation (3.2), we obtain the accumulated generating sequence from equation (3.13) as given below:

$$X^{(1)} = (324,659,1201,1692,2119,2742,3228,3646,4089,4531,4869,5376,5946,6493) \quad (3.13)$$

Using equation (3.5), we obtain equation (3.14) below:

$$Z^{(1)} = (491.5,930,1446.5,1905.5,2430.5,2985,3437,3867.5,4310,4700,5122.5,5661,6219.5) \quad (3.14)$$

Using equation (3.8), we obtained equation (3.15)

$$Y = \begin{bmatrix} 335 \\ 542 \\ 491 \\ 427 \\ 623 \\ 486 \\ 418 \\ 443 \\ 442 \\ 338 \\ 507 \\ 570 \\ 547 \end{bmatrix} \quad (3.15)$$

Using equation (3.9), we obtained equation (3.16)

$$B = \begin{bmatrix} -491.5 & 1 \\ -930 & 1 \\ -1446.5 & 1 \\ -1905.5 & 1 \\ -2430.5 & 1 \\ -2985 & 1 \\ -3437 & 1 \\ -3867.5 & 1 \\ -4310 & 1 \\ -4700 & 1 \\ -5122.5 & 1 \\ -5661 & 1 \\ -6219.5 & 1 \end{bmatrix} \quad (3.16)$$

Using equation (3.7) by the help of Maple 23 software, we obtained

$$\hat{a} = \begin{bmatrix} -0.00943 \\ 442.974 \end{bmatrix} = \begin{bmatrix} a \\ b \end{bmatrix} \quad (3.17)$$

Where a= -0.00943 and b= 442.974

Substitute for a and b in equation (3.6), we obtained equation below:

$$\hat{x}^{(1)}(k+1) = 47298.97349e^{0.00943k} - 46974.97349 \quad (3.18)$$

Evaluating equation (3.18) for k=0, 1, 2, …, 13 we obtained equation (3.19) below:

$$\hat{x}^{(1)} = (324,772,1225,1681,2142,2608,3077,3552,4030,4514,5001,5494,5992,6493) \quad (3.19)$$

We compute the stimulated value of the equation (3.20)

$$\hat{x}^{(0)} = \hat{x}^{(1)}(k) - \hat{x}^{(1)}(k-1) \quad (3.20)$$

The stimulated values are presented in equation (3.21) below.

$$\hat{X}^{(0)} = (324,448,453,456,461,466,469,475,478,484,487,493,498,502) \quad (3.21)$$

Equation (3.21) is the stimulated values from 2009 -2022 and is presented in table 4.3 below.

Table 4.3: Grey Stimulated values

S/N	Year	Fire incident	Grey Stimulated value of Fire accidents	Residual Error	Relative Error (%)
1	2009	324	324	0	0
2	2010	335	448	-113	-33.73
3	2011	542	453	89	16.42
4	2012	491	456	35	7.13
5	2013	427	461	-34	-7.96
6	2014	623	466	157	25.20
7	2015	486	469	17	3.50
8	2016	418	475	-57	-13.64
9	2017	443	478	-35	-7.90
10	2018	442	484	-42	-9.50
11	2019	338	487	-149	-44.08
12	2020	507	493	14	2.76
13	2021	570	497	73	12.80
14	2022	547	502	45	8.22

From Table 4.3 using equation (3.10) we observed that:

MAPE=13.76% which is the error of the stimulated values, which is described as good accuracy when compared with table 3.1.

Hence, the accuracy is calculated as:

ACCURACY=100%-13.76%=86.24%, this shows that the stimulated accuracy is good.

Hence, can be used for prediction.

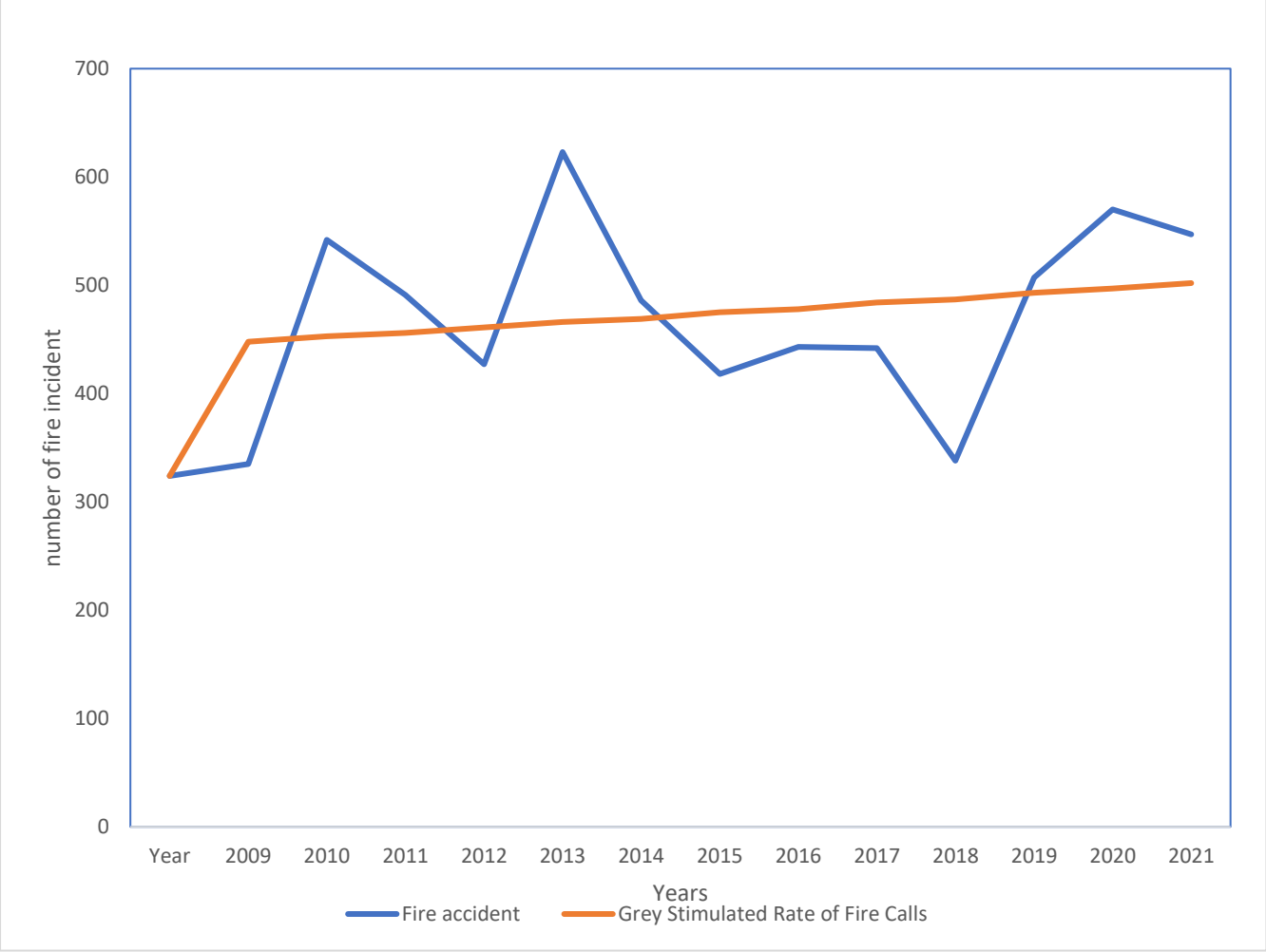

Fig 4.1: The Line graph of Actual and Grey Model stimulated values of the number of fire accident in FCT

4.2 Application of Grey-Artificial Neural Network model for Prediction of the number of Fire Accident in Abuja.

In this study, we utilize an Artificial Neural Network (ANN) as a novel forecasting model, concentrating on predicting the frequency of fire incidents in the FCT. Our method entails the creation and training of an ANN designed to mimic the error patterns generated by the Grey

system model. To optimize the model, we employed a trial-and-error process to construct multiple backpropagation neural networks. The performance of each model was meticulously assessed using metrics like root mean square error (RMSE), the coefficient of determination, and the coefficient of correlation. The model showcasing the strongest correlation coefficient and minimal RMSE emerged as the optimal choice for precisely forecasting the number of Fire Accidents in the FCT.

Table 4.4: Actual value, Grey stimulated value and predicted residual to generate the GRANNM in FCT from 2009-2022

S/N	Year	Actual values	Grey stimulated values	Predicted Residual	GRANNM values
1	2009	324	324	0	324
2	2010	335	448	-115	333
3	2011	542	453	55	508
4	2012	491	456	32	488
5	2013	427	461	-51	410
6	2014	623	466	82	548
7	2015	486	469	25	494
8	2016	418	475	-62	413
9	2017	443	478	-30	448
10	2018	442	484	-31	453
11	2019	338	487	-114	373
12	2020	507	493	42	535
13	2021	570	497	63	560
14	2022	547	502	56	558

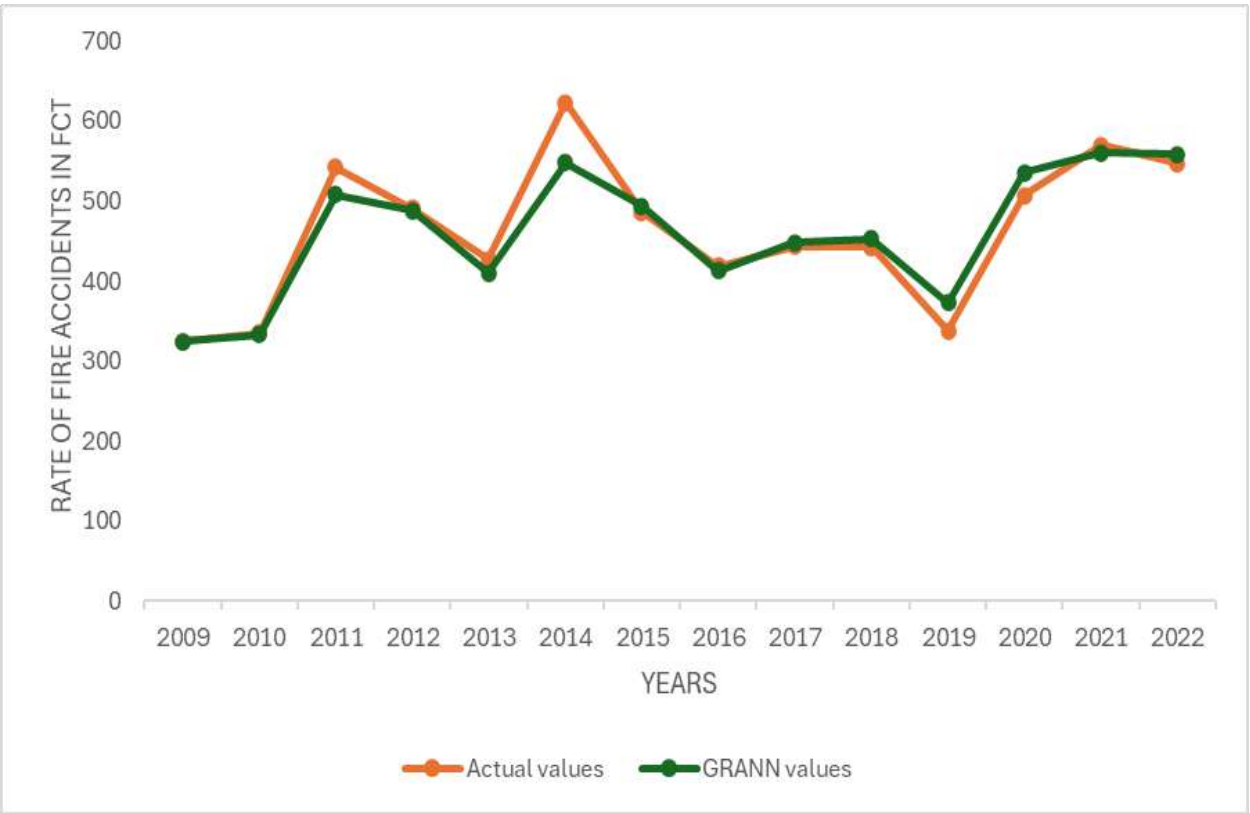

Fig 4.2: The Line graph of Actual and GRANN Model stimulated values of the number of fire accident in FCT

5. Conclusion.

In this paper the Artificial neural network values were gotten using Python 3.11. The combination of two highly efficient prediction models has yielded a combined accuracy superior to the performance of Grey GM (1,1) Model only.

Reference

Ceyhan, E., Ertuğay, K. & Düzgün, Ş. (2013). Exploratory and inferential methods for spatio-temporal analysis of residential fire clustering in urban areas. *Fire Safety Journal, 58, pp. 226-239.*

Channels Television (2023) "Two Dead, Others Hospitalized As Fire Guts Canadian High Commission In Abuja".https://www.channelstv.com/2023/11/06/casualties-recorded-as-fire-guts-canadian-high-commission-in-abuja/ retrieved on 6/11/2023

Charles J. (2000), "Fire Technology", *Malaysia International Conference*, Vol. 35, No1

Chunxia L., Tong S., Shou C., Shouyang W., Kin K. L. , Lu Gan F(2016). An improved grey neural network model for predicting transportation disruptions. Expert Systems With Applications Vol 45: 331-340

Idayat (2021).A Stochastic Model For Predicting Number Of Fire Incident Occurrence In Niger State Using Viterbi Algorithm. An Unpublished master's thesis submitted to federal University of Technology Minna.

Jiyu Z., Lingbo Z., Jiankun G., & WenkunW. (2020) Feature Analysis and Comparison of Prediction Methods for Fire Accidents International Journal of Safety and Security Engineering. Vol. 10, No. 5, pp. 707-712

Lewis, C.D. (1982). Industrial and Business Forecasting Methods: A Practical guide to exponential smoothing and curve fitting, Butterworth-Heinemann, London

Li Q., Hu Q., Zangh P., (2007). Application of Grey-Markov Model in Predicting Traffic Volume. Proceeding of 2007 IEEE International Conference on Grey System and Intelligent Services, November 18-2-, 2007, Nianjin, China.

Saeed. O. B., Abubakar U. Y., Lawal A., & Usman A. (2021). Prediction Of Vehicular Incidents Along Lokoja-Abuja-Kaduna Express Way Nigeria Using Grey-System Model GM(1,1). Journal of Science, Technology, Mathematics and Education (JOSTMED), 17(3),pp87-94

Punch Newspaper (2023) "Fire guts Abuja showroom" https://punchng.com/breaking-fire-guts- abuja-showroom/ retrieved on 4/11/2023

Sifeng L., Yingjie Y., Jeffery F. (2017). Grey Data Analysis: Methods, Models and Applications.

Solomon O., (2022). "Incessant fire outbreaks in Abuja raise fear, investors lament as unemployment worsens" https://punchng.com/incessant-fire-outbreaks-in-abuja-raise-fear-investors-lament-as-unemployment-worsens/retrieved on 10/4/2022

Vanguard Newspaper (2021) "Fire razes Abuja's Next Cash and Carry store as FCT launches probe" https://www.vanguardngr.com/2021/12/fire-razes-abujas-next-cash-and-carry-store-as-fct-launches-probe retrieved on 10/4/2022

Yusuf O. (2012), "A literature review of fire incidence with an emphasis on urban residential fires", Vol.8 116-130

Linear Programming for Profit Maximization of Agricultural Stock

Jacob Rebecca[1], Nyor Ngutor[2] and Khadeejah James Audu[3]

[1-3]Department of Mathematics Federal University of Technology Minna, Niger State

E-mail: rebeccajacob428@gmail.com

Abstract

This paper discusses a few common issues that are specific to agricultural investing, such as the challenge of choosing which stocks to buy in order to maximize returns. The linear programming model was applied to ten (10) agricultural stocks, and the simplex approach was used as the numerical technique to calculate the best possible outcome. The TORA programmer was used to verify the best option, and the findings indicated that not every item should be invested in order to maximize profit.

Keywords: agricultural stock, linear programming (LP), mathematical programming, profit maximization, sensitivity analysis, simplex method.

1. INTRODUCTION

One of the problems that humanity faces is producing enough revenue to maintain a sustainable quality of life. Due to its ability to generate money, its employment potential, and the barriers it places on the expansion of other industries, farming is vital to the Nigerian economy (Nwibo and Mbam, 2013). It is not overstatement to say that the growth and development of any country is largely dependent on the growth of agriculture, since even industrial enterprises depend on agricultural endeavours to produce the raw materials that are then converted into capital goods through the application of human resources. Agriculture is, therefore, defined as intentional work that uses natural resources to meet human needs. Among its many advantages are national cash earnings, food, clothes, fibres, housing, a variety of raw materials for industrialization, investment and job possibilities, and capital development. For farmers' communities and countries, agriculture is an essential business. However, Nigerian agriculture is subsistence-level, with many farmers working on dispersed, small, and fragmented land plots with hand tools and traditional farming techniques like planting on mounds, land rotation, superficial hand tillage, mixed cropping with several carefully planned crop associations, mixed farming, etc (Odoemenem, et al. 2013). Maintaining a household's income raises the likelihood of making investments in the future. Income raises collateral in a loan market, credit rating, and repayment capacity indirectly (Osondu et al. 2015).

A subset of mathematical programming, linear programming (LP) is a quantitative analytical method for choosing how to accomplish a goal. It is used to find the problem's most ideal solution within a set of limitations. It consists of linear inequalities as the goal function and certain restrictions expressed as either linear equations or inequalities. Depending on certain restrictions expressed in the linear relationship, this approach is used to maximize or minimize the objective function of the supplied mathematical model, which consists of the collection of linear inequalities. According to Danzig and Thapa (1997), LP deals with the maximization or minimization of a linear objective function in a number of variables while adhering to restrictions on linear equality and inequality. LP assists in

effectively allocating resources to maximize profits, minimize losses, or make the best use of production capacity (Srinath, 2018).
The goal of Nyor et al. (2019) was to maximize the demands of the Federal University of Technology Minna, Nigeria, which has two campuses, in terms of both student and agency transportation. Software for solving linear programmes was used to tackle the problem using the simplex approach. 10%, 6%, 17%, and 3% student percentage increases were shown in the linear programming formulation result for the corresponding example under consideration. The goal of Ruby et al. (2022) was to surreptitiously ascertain how the merchant saw that particular consumer group in order to adjust the product mix. The emphasis is on small businesses in little communities that lack the resources to successfully coordinate choices about the product mix. Ten representatives and five supervisors participated in in-person interviews to gather the data, which was done in accordance with the manufacturing department's existing papers and datasheet, which was slightly modified to create the final product. The information covered a single season, from April to March. Profits from pre- and post-linear programming were examined using data analysis. Using a linear programming process, they determine the advantage of each period and the present asset consumption level of one of the garment manufacturing companies. Real resource consumption was computed in order to assess profit after using linear programming to determine costs and waste. After LP, resource utilization increased by 54% as compared to product-wise utilization. Similar to this, while using linear programming, the profit more than doubled due to low costing and waste and high revenue. The paper concentrated on utilising Excel (Solver) LINGO to discover the product mix using the straightforward fundamentals of linear programming.

2.**Methodology**

For the purpose of this research, personal (direct interview) with the middle men in Paiko market, Paiko Minna was made in June 2023 as the source of data. The data used in these work has not been in used but were obtained for the purpose of this study. The analysis of data was earned out using optimization software for the models used such as LP with TORA.

2.1 Mathematical Formulation of Linear Programming Problems

the steps in formulating linear programming problem are as follows;

Step 1: Identify the decision variables.
Step 2: Express the objective function in terms of decision variables.
Step-3: Write down the constraints with the help of which the objective function is to be optimized.
Step-4: Write down the non- negative constraints.

2.2 Formulation of Linear Programming Problem

The general form of linear programming problem (LPP) with decision variables and constraints can be stated as follows:

Decision variables $(x_1, x_2, x_3, \dots, x_n)$.

Objective function: it is the function to optimize and it is written in terms of the decision variable.

Linear program is given by $(Max\ or\ min)\ z = c_1x_1 + c_2x_2 + \dots + c_nx_n$

Subject to Linear Constraints of the form

$$\begin{aligned} a_{11}x_1 + a_{x1,x212}x_2 + \cdots + a_{1n}x_n \ (\leq, =, \geq)\ b_1 \\ a_{12}x_1 + a_{22}x_2 + \cdots + a_{2n}x_n \ (\leq, =, \geq) b_2 \\ \vdots \qquad\qquad \vdots \\ a_{m1}x_1 + a_{m2}x_2 + \cdots + a_{mn}x_n \ (\leq, =, \geq) b_m \\ x_1, x_2, x_3, \ldots, x_n \geq 0 \end{aligned} \tag{1}$$

Constraints: they are the conditions under which the objective function is optimized

And, $x_j > 0;\ \ j = 1,2, \ldots, n$ (non negative condition)

And, $x_j > 0;\ \ j = 1,2, \ldots, n$ (non negative condition)

2.3 Problem Description

An investor has a fixed sum of ₦50,000,000 to invest in any of the ten (10) agricultural stocks namely; Maize, Guinea corn, Millet, White Beans, Brown Beans, Soya Beans, Melon, Unpeeled Rice, Groundnut, and Dry Pepper; and at most the sum of ₦5,000,000 for the storage of the stock. This investment is to be made before August and December of the current year and sold between March and July of the following year. Let $x_1, x_2, x_3, \ldots x_n$ designate the amount of bag to be allocated to Maize, Guinea corn, Millet, White Beans, Brown Beans, Soya Beans, Melon, Unpeeled Rice, Groundnut, and Dry Pepper respectively. Table 3.1 shows the cost, future expected price and the cost of storing the agricultural stock (August - December 2022: march-July 2023).

2.4 Model Formulation

Let $x_i$be the share of stock i purchase then the linear programming problem is formulated as

$$Max\ F(x) = 30x_1 + 40x_2 + 45x_3 + 48x_4 + 51x_5 + 31x_6 + 50x_7 + 35x_8 + 80x_9 + 35x_{10}$$

$$(expected\ price)$$

Subject to

$$21x_1 + 25x_2 + 27x_3 + 40x_4 + 42x_5 + 25x_6 + 35x_7 + 25x_8 + 50x_9 + 25x_{10} \leq 50000$$

$$(purchase\ cost)$$

$$3.6x_1 + 3.6x_2 + 3.25x_3 + 3.8x_4 + 3.8x_5 + 3.25x_6 + 3.2x_7 + 3.2x_8 + 3.7x_9 + 3.2x_{10} \leq 5000 \qquad \text{(cost of storage)}$$

$$x_1, x_2, x_3, x_4, x_5, x_6, x_7, x_8, x_9, x_{10} \geq 0 \tag{2}$$

Table 2.1: Data Collection

s/no	Stock	Purchase cost Per Bag (in thousands naira)	Future expected price (in thousands naira)	Cost of storage (in thousand naira)
1	Maize	21	30	3.6
2	Guinea corn	25	40	3.6
3	Millet	27	45	3.25
4	White beans	40	48	3.8
5	Red beans	42	51	3.8
6	Soya beans	25	31	3.25
7	Melon	35	50	3.2
8	Unpeel rice	25	35	3.2
9	Groundnut	50	80	3.7
10	Dry pepper	25	35	3.2

Source: Personal interview (June 2023).

NB: storage = Chemical + Cost of store + Cost of transportation

3. Results and Discussion

Applying simplex method to equation 3.1, then by standardizing we have

$$Max\ F(x) = 30x_1 + 40x_2 + 45x_3 + 48x_4 + 51x_5 + 31x_6 + 50x_7 + 35x_8 + 80x_9 + 35x_{10} + 0s_1 + 0s_2$$

Subject to

$$21x_1 + 25x_2 + 27x_3 + 40x_4 + 42x_5 + 25x_6 + 35x_7 + 25x_8 + 50x_9 + 25x_{10} + s_1 = 50000$$

$$3.6x_1 + 3.6x_2 + 3.25x_3 + 3.8x_4 + 3.8x_5 + 3.25x_6 + 3.2x_7 + 3.2x_8 + 3.7x_9 + 3.2x_{10} + s_2 = 5000$$

$$x_1, x_2, x_3, x_4, x_5, x_6, x_7, x_8, x_9, x_{10}, s_1, s_2 \geq 0$$

Where s_1, s_2 are slack variables associated with the respective constraints

Table 3.1 initial table

Basis	x_1	x_2	x_3	x_4	x_5	x_6	x_7	x_8	x_9	x_{10}	s_1	s_2	solution	Ratio
z	-30	-40	-45	-48	-51	-31	-50	-35	-80	-35	0	0	0	
s_1	21	25	27	40	42	25	35	25	50	25	1	0	50000	
s_2	3.6	3.6	3.25	3.8	3.8	3.25	3.2	3.2	3.7	3.2	0	1	5000	

Simplex iterations start at the origin $x_1, x_2, x_3, x_4, x_5, x_6, x_7, x_8, x_9, x_{10} = (0,0,0,\ldots,0)$ whose associated set of nonbasic variables $(x_1, x_2, x_3, x_4, x_5, x_6, x_7, x_8, x_9, x_{10})$ and basic variables (s_1, s_2).The starting solution is not optimal because some of the z-row coefficient associated with nonbasic variables are negative. Locate the Entering variable: This is the most negative coefficient in the objective. Locate the Leaving variable: This is the minimum value of the non negative ratio of the right hand side of the equation to the corresponding constraint coefficients under the entering variables. Identify Pivot element: These correspond to the intersection of pivot row and pivot column.

The swapping process in the simplex method is based on the Gauss-Jordan row operation which has two types of computations

i. Pivot row
   a. Replace the leaving variable in the basic column with the entering variable
   b. New pivot row = current row ÷ pivot element
ii. All other rows including z
   New row = current row – (its pivot column coefficient × new pivot row)

These computations are applied to the preceding tables in the same manner until the optimal solution is obtained.

Table 3.2 iteration 1

Basis	x_1	x_2	x_3	x_4	x_5	x_6	x_7	x_8	x_9	x_{10}	s_1	s_2	solution	Ratio
z	-30	-40	-45	-48	-51	-31	-50	-35	-80	-35	0	0	0	
s_1	21	25	27	40	42	25	35	25	50	25	1	0	50000	1000
s_2	3.6	3.6	3.25	3.8	3.8	3.25	3.2	3.2	3.7	3.2	0	1	5000	1351.1

The entering variable is x_9 and the leaving variable is s_1, therefore the pivot element is 50, then we reduce the pivot element to unity and other element in column 10 to zero using row operation. New Row $R_3 = R_3 \div 50$, New Row $R_4 = R_4 - (3.7 \times newR_3)$,

New Row $R_2 = R_2 - (-80 \times newR_3)$

Table 3.3 iteration 2

Basis	x_1	x_2	x_3	x_4	x_5	x_6	x_7	x_8	x_9	x_{10}	s_1	s_2	solution	Ratio
z	3.60	0	-1.8	16	16.2	9	6	5	0	5	1.60	0	8000	
x_9	0.42	0.5	0.54	0.80	0.84	0.50	0.70	0.50	1	0.50	0.02	0	1000	1851.85
s_2	2.05	1.75	1.25	0.84	0.69	1.40	0.61	1.35	0	1.35	-0.07	1	1300	1040

The entering variable is x_3 and the leaving variable is s_2 , therefore the pivot element is 1.25, then we reduce the pivot element to unity and other element in column 4 to zero using row operation. New Row $R_3 = R_3 - (0.54 \times newR_4)$, New Row $R_4 = R_4 \div 1.25$,

New Row $R_2 = R_2 - (-1.8 \times newR_4)$

Table 3.4 iteration 3

Basis	x_1	x_2	x_3	x_4	x_5	x_6	x_7	x_8	x_9	x_{10}	s_1	s_2	solution
z	6.54	2.52	0	17.21	17.1	11.01	6.88	6.4	0	6.4	1.49	1.44	81869.01
x_9	-0.46	-0.25	0	0.44	0.54	-0.10	0.44	-0.08	1	-0.08	0.05	-0.43	43.30
x_3	1.63	1.40	1	0.67	0.55	1.12	0.4	1.08	0	1.08	-0.06	0.80	1038.34

Based on the optimal condition the z-row coefficient associated with the non basic variable are nonnegative, hence we have obtained the optimal solution. In this case the optimal solution is

$x_1 = 0,\ x_2 = 0,\ x_3 = 1038.34,\ x_4 = 0,\ x_5 = 0,\ x_6 = 0,\ x_7 = 0,\ x_8 = 0,$

$x_9 = 439.30, x_{10} = 0$. Where the variables are the numbers of bag the investor should purchase, and then the maximum profit is ₦81869.01

LINEAR PROGRAMMING OUTPUT SUMMARY

Title: profit maximazation
Final Iteration No.: 3
Objective Value = 81869.01

Variable	Value	Obj Coeff	Obj Val Contrib
x1: maize	0.00	30.00	0.00
x2: guniea corn	0.00	40.00	0.00
x3: millet	1038.34	45.00	46725.24
x4: white beans	0.00	48.00	0.00
x5: brown brown	0.00	51.00	0.00
x6: soyabeans	0.00	31.00	0.00
x7: melon	0.00	50.00	0.00
x8: unpeelrice	0.00	35.00	0.00
x9: groundnut	439.30	80.00	35143.77
x10: dry pepper	0.00	35.00	0.00

Constraint	RHS	Slack-/Surplus+
1 (<)	50000.00	0.00
2 (<)	5000.00	0.00

Sensitivity Analysis

Variable	Current Obj Coeff	Min Obj Coeff	Max Obj Coeff	Reduced Cost
x1: maize	30.00	-infinity	36.54	6.54
x2: guniea corn	40.00	-infinity	42.52	2.52
x3: millet	45.00	43.20	70.27	0.00
x4: white beans	48.00	-infinity	65.21	17.21
x5: brown brown	51.00	-infinity	68.19	17.19
x6: soyabeans	31.00	-infinity	42.01	11.01
x7: melon	50.00	-infinity	56.88	6.88
x8: unpeelrice	35.00	-infinity	41.94	6.94
x9: groundnut	80.00	64.26	83.33	0.00
x10: dry pepper	35.00	-infinity	41.94	6.94

Constraint	Current RHS	Min RHS	Max RHS	Dual Price
1 (<)	50000.00	41538.46	67567.57	1.49
2 (<)	5000.00	3700.00	6018.52	1.44

Figure 3.1.1 summary of model 1

The model was solved by analyzing the data using TORA software.

$$F(x) = 30(0) + 40(0) + 45(1038.34) + 48(0) + 51(0) + 31(0) + 50(0) + 35(0) + 80(439.30) + 35(0) = 81869.01$$

Optimal Decision: The results require that the investor should invest on only Millet of 1038.34 bags and Groundnuts of 439.30 bags in order to maximized profit and also it is noticed that if the investor embarks on this plan the following results would follow:

a. The money invested shall be fully exhausted /utilized.

b. The cost of storing the stock shall be fully used.

4.1 Sensitivity Analysis for model

The goal of sensitivity analysis is to determine how much the input data may be modified while still maintaining a relatively constant output from the linear programming model. The investor need to look closely at the sensitivity analysis of the stock from fig 3.1.1

In order to attain the same result the cost of a bag of Maize, Guinea Corn, White Bean, Brown Beans, Soya Beans, Melon, Unpeeled Rice, and Dry Pepper is at the minimum of any amount and the maximum should be at ₦36540, ₦42520, ₦65210, ₦68100, ₦42010, ₦56880, ₦41400 and ₦41400 respectively. While minimum cost of Millet is at ₦43200 and maximum at ₦70270 also that minimum cost of Groundnut is at ₦64260 and maximum at ₦83330.
The investor can invest the minimum of ₦41,538,460 and maximum of ₦67,567,570 instead of ₦50,000,000 and the minimum cost of storing are ₦3,700,000 and maximum of ₦6,018,520 instead of ₦5,000,000 and the profit made will remain unchanged.

5. **Conclusion**

In this paper, the concept of linear programming to model 10 agricultural stocks which the data were collected through direct interview in paiko market was used. Based on the analysis carry out on the model, the results require that the investor should invest on only Millet of 1038.34 bags and Groundnuts of 439.30 bags in order to maximized profit. Sensitivity Analysis is useful for investors who must work in a dynamic environment with imprecise estimates of the coefficients because it shows how changes in values of decision variable affect the optimal solution within certain ranges in the objective function coefficients and the right hand value.

References

Dantzig G B, Thapa MN. (1997). *Linear programming 1:Introduction*. Springer-Verlag New York, Inc.

Nwibo, S.U., and Mbam, B.N. (2013). Determinants of savings and investment capacities of farming households in Udi Local Government Area of Enugu State, Nigeria. *Research Journal of Finance and Accounting:* 4(15): 59 -68.

Nyor, N., Evans, O., Audu, S., Henry, S. (2019). Linear programming formulations for optimum student transportation need in a university with two campuses. *Nigeria journal of mathematics and applications.*B(29);78-90

Odoemenem, I. U., Ezihe, J. A. C and Akerele, S. O. (2013). Saving and investment pattern of small-scale farmers of Benue State, Nigeria. *Global Journal of Human Social Science, Sociology and Culture,* 13(1): 7 – 12

Osondu, C. K., Obike, K. C. and Ogbonna, S. I. (2015). Savings, income and investment patterns and its determinants among smallholder Arable crop farmers in Umuahia, Abia State, Nigeria. *European Journal of Business and Innovation Research,* 3 (1): 51 – 70.

Ruby, chanda., vanishree, pabalkar., sudeepa, Gupta. (2022). A study on application of linear programming on product mix for profit maximization and cost optimization. *Indian journal of science and technology*. 15(22):1067-1074

Srinath, L.N. (2018) *Linear Programming*: *Principles and applications. Second Edition*. Basingstoke, England: Palgrave Macmillan.

Statistical Analysis of Computer Management Information System in First Bank Minna Niger State

[1]Batagi, S., A., [1]Yahaya, A., [2]A., Abdulazeed, S., [2]Iliyasu, M., A., [3]Hassan, S [3]Umar, A., M., [4]Gidado, I., I.

EMAILS: maimunaanwar5@gmail.com, abuahmad4u@gmail.com, aburumaisawu@gmail.com, awwaliliyasu@gmail.com, hsuleiman457@gmail.com **aliyu.umar@fedpoffaonline.edu.ng,Ismailibrahim054@gmail.com,**

[1]Department of Statistics, Niger State polytechnic Zungeru.
[1]Department of Mathematic, Federal polytechnic Bida.
[2] Department of Library and Information Management, Niger State polytechnic Zungeru.
[2] Department of computer Science Education, Niger State College of education Minna.
[3] Department of Urban and Regional planning, Niger State polytechnic Zungeru.
[3] Department of Mathematics, Federal polytechnic Offa, Kwara State
[4]Department of Mathematics, Federal polytechnic Kabo, Kano State.

Abstract

Business managers in Nigeria see the installation of information systems as a way to battle competition by increasing productivity, profitability, and, most importantly, organizational performance. The extent to which Nigerian banks use information systems has not yet been determined. This study investigated the link between information systems and bank organizational performance, utilizing the First Bank PLC Minna branch as a case study. This study looked into the role of information systems (IS) in bank organizational performance by administering a structured questionnaire to 20 randomly chosen staff members from the First Bank Minna branch in Niger State, Nigeria, and analyzing the results using descriptive (percentage and frequency) statistical analysis. The research found that First Bank workers understand the significance of information systems to businesses and ensure that the available information systems within their branches are well used by their staff and customers, however there is still a gap when compared to developed countries. The researchers recommended that First Bank spend more money on information technology procurement, which would boost the organization's chances of survival in the face of challenging situations.

Key words: Computer instruction, Logical Solution, Design Requirement, Binary Codes, Control Function and Information System

Introduction

Computers have become highly powerful instruments in the corporate sector due to their ability to store, process, and disseminate huge amounts of information in a consistent, efficient, and effective manner, allowing for quick decision-making.

A computer is an electronic device that accepts data, interprets it, conducts certain operations on it, and reports the results. As a result, it acts as a tool manager, assisting in the complex and time-consuming process of generating information.

It took centuries for the computer to reach the fourth generation, which marked the start of serious attempts to simplify mathematical procedures. A huge number of people were involved in the computer's creation, and while several of the scientists who made those valuable contributions did not plan to build a computer, their ideas proved to be a critical step toward computer development (Patterson and Hennessy 2016).

A computer may be built with a few simple instructions, and any problem having a logical answer can be reduced to a solution based on a limited set of those instructions. Several years later, John Michael (2015) broke down the design criteria for a modern computer as follows:

1. Data processing instructions, including program change.
2. Binary codes are used to represent data and instructions in a way that does not distinguish between the two while yet allowing for storage space in the computer.

The contemporary computer owes its existence to the work and innovations of these scientists and others. IT underwent a succession of improvements, resulting in the fourth computer generation, which preceded what we now know as contemporary computers. However, the introduction of this general-purpose processor and programming languages greatly expanded computer utility, notably in management information systems (MIS), which are concerned with how information is acquired, processed, and used. Computers are increasingly indispensable machines in corporate activities as electronic data processing expands and consumers seek speed, precision, and efficiency when dealing with security issues. Other applications of information technology include marketing, accounting, inventory management, and manufacturing. According to Lutter Quick (2014), the notion of management information systems (MIS) was created during a speech at the Rochester Institute of Technology in October 1960. It became evident and imperative that information play a critical part in the price-meal approach to solving business and management problems, with a concentration almost totally on the automating of all office duties. Essentially, management information systems aim to provide managers at all levels with the information they need to run their firms. It provides a corporation with adaptable integrated tools for planning and controlling activities, as well as the ability to produce information requirements at all management levels.

According to Michael (2015). Management information system (MIS) is the process of properly and efficiently sharing information both within and outside of a company.

The management information system (MIS) is primarily designed to distribute, plan, and regulate information to all levels of management, allowing for sound decision-making. As a result, it accomplishes this by gathering data, inputting and processing it into information, and then providing that information to their terminal. As a result, we can categorize management

information systems as functional information systems, such as marketing information systems, financial information systems, and personnel information systems, depending on the information system that an organization requires at the time. The management information system offers management with varied information dependent on level, resulting in increased organizational efficiency and better management decisions. (Andrew and Tanenbaum 2015).

However, as businesses have evolved, so has the flow of information, to the point where face-to-face interactions and even the creation of memos are no longer required for successful communication or data processing. These organizations' management information systems have recently failed to keep up with the increased demand for information, leaving manual methods of operation overburdened with data to handle. As a result, data collection and processing is slow and inaccurate. Delays may lead to incorrect conclusions. There is also the issue of essential document abuse and file theft.

Statement of Problem

Several years ago, the whole company's data was processed manually. This technique was not always satisfactory due to its slowness. Most firms in this country have had business information challenges as a result of the manual approach taken. These difficulties affect their productivity and service quality.

Furthermore, there are issues with the organization's international structure and functions, such as personnel turnover, record loss, expensive communication, equipment, record, and storage system issues, such as information collection, processing, storage, retrieval, and distribution, all of which have an impact on decision-making processes.

Early bank personnel were denied access to modern technologies that could assist them give more efficient and effective service while performing their professional obligations.

Given this understanding, the researcher chose the topic: A study of computers in management information systems to address the issue of an ineffective information system that has plagued businesses for many years.

The Aim of Study

This study aims to investigate ineffective information damaging First Bank's accomplishment in terms of service delivery and shortcomings in Minna, Niger State.

Objectives of the Study

The objectives of this study are to:

1. Examine the information management system at First Bank Minna, Niger State.
2. How does First Bank's management information system contribute to achieving its goals?
3. Identify gaps in the management information system of First Bank plc in Minnesota.

4. Provide graphical simulations of the service delivery management information system (MIS).

Significance of the Study

The study will benefit not only First Bank Plc Minna, but also other companies that serve customers in Nigeria and other nations. It will also benefit individuals, the public sector, including state and federal government organizations that use computer-based management information systems.

It will also function as a database for future research and additions to the library's existing resources. The findings will also be useful for universities that offer management information systems courses, as well as businesses wishing to form a management information system union.

It will also address the force discovered on current users of the system, which contains some irregularities.

Scope of the Study

This study focuses on the utilization of management information systems at First Bank Plc Minna, Niger State, and other firms that provide similar services.

Research Question

The following questions will be used in writing the project:

1. What are the type of computer Information Systems in First Bank, Minna, Niger State
2. What are the contributions of management information system towards the achievement of First Bank's goal?
3. What are the lapses in the management and utilization information system of First Bank plc Minna.

Methodology

This present research will be adopted in carrying out the various research design, sample population, sampling techniques, validation of research instrument, reliability of the instrument, Method of data collection, and data analysis.

Research Design

This study used a descriptive survey approach. The results were reported in percentages and numbers. The population included all employees of First Bank plc branches in Niger State, Nigeria. The research design used in this study enables a researcher to investigate a wide range of factors within the research disciplines. Descriptive survey methods are considered appropriate because they focus on factual results from respondents.

Area of the Study

The study area is first bank branch, Minna, Niger State, Nigeria. It is the capital of Niger State in North Central Nigeria. It has two major ethnic groups: Gbagyi and Nupe. It has an estimated population of 202,151 as at 2006, according Nigerian Census Figures (National Bureau of Statistics, 2011). It lies between Latitudes 9^0 33' and 9^0 45' North of the equator and Longitudes 6^0 29' and 6^0 35' East of the Greenwich Meridian (Idowu *et al.*, 2020). It is connected to Abuja, Nigeria's capital by road with a distance of 150 km. The city experiences a distinct wet and dry seasons with annual rainfall varying from 1100mm to 1600mm. The rainy season starts from the month of April to October with peak in June to September. The main agricultural products of the city include cotton, guinea corn, yam, and ginger.

Figure 3.1: Map of Niger state, showing First Bank, Minna

Source: Geographical Map from Google Area view (2023).

Population of the Study

The population of the study consists of all the employees of the first bank, Minna, Niger state. The target population for the study will be 35-bank staffs of first bank, Minna, Niger State.

Sample and Sampling Procedure

A simple random selection strategy was used to select 15 bank workers, whilst purposive sampling and comprehensive enumeration were used to encompass all personnel with a first

degree or higher education. This resulted in a total of twenty bankers. The sample represents 40% of the target population of academic personnel from the university's selected schools. This is consistent with the recommendations of Nwana (1981) and Levy Lemeshow (2013), who proposed a 40% sample size for all studies. A simple random sample procedure will be used to select 20 respondents from the study's captive population.

Instrument for Data collection

The data was gathered via a questionnaire titled "Computer Management Information System in First Bank". The questionnaire was divided into four pieces. Section A: Demographic Profile; Section B: The Impact of Information System utilization on Bank Organizational Performance; Section C: How can management information systems help First Bank achieve its goals?; and Section D: Factors that limit information system utilization. Respondents are asked to provide comments on some of the elements they believe influence the efficient use of information systems at First Bank plc.

Reliability of the Instrument

The instrument was verified by information management professionals, and Cronbach's alpha was used to assess the reliability of each of the four components separately. The results were as follows: Section A: 0.84, Section B: 0.58, Section C: 0.76, and Section D: 0.80. The total result was 0.75. The researchers disseminated the questionnaire and gathered replies.

Method of Data Collected

The researchers gathered data from the first bank, Minna Branch, in order to facilitate the instrumental design. It was administered to responders and collected at the agreed-upon time by study assistants. The data was collected over four weeks , processed and analyzed using the statistical software SPSS.

Method of Data Analysis

The data was analyzed using the Statistical Package for Social Sciences (SPSS V.16). Descriptive statistics were employed to determine the frequency distribution of all variables on the questionnaire.

Demographic Profile of Respondents

Table 1: Gender of respondents

Characteristics	Categories	Frequency	Percentage
Gender	Male	7	35%
	Female	13	65%
Total		20	100%

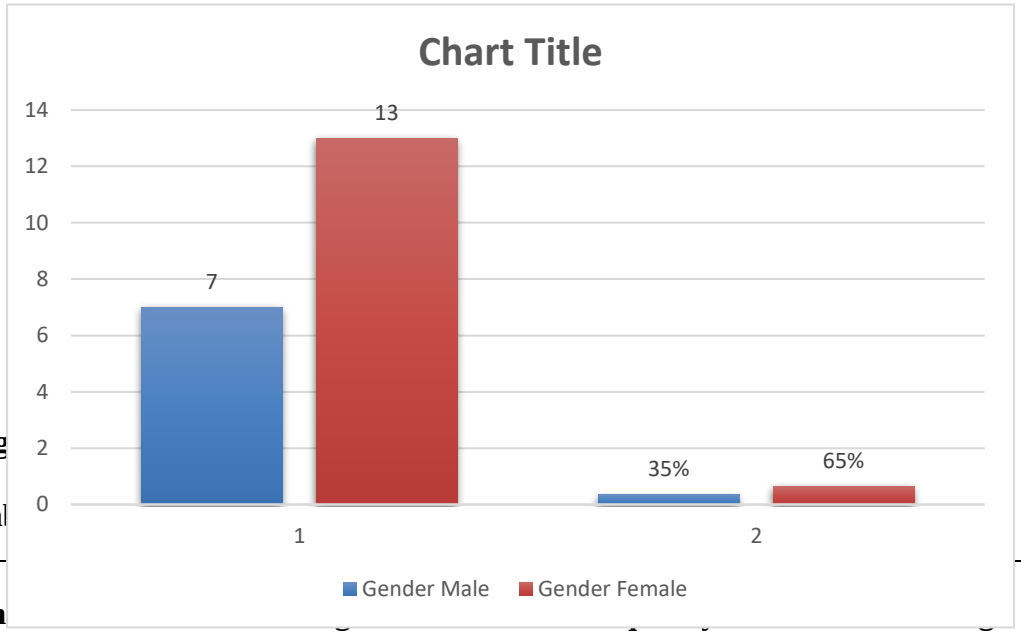

Fig

Tab

Ch			
Age (in years)	21-30	10	50%
	31-40	5	25%
	Above > 40	5	25%

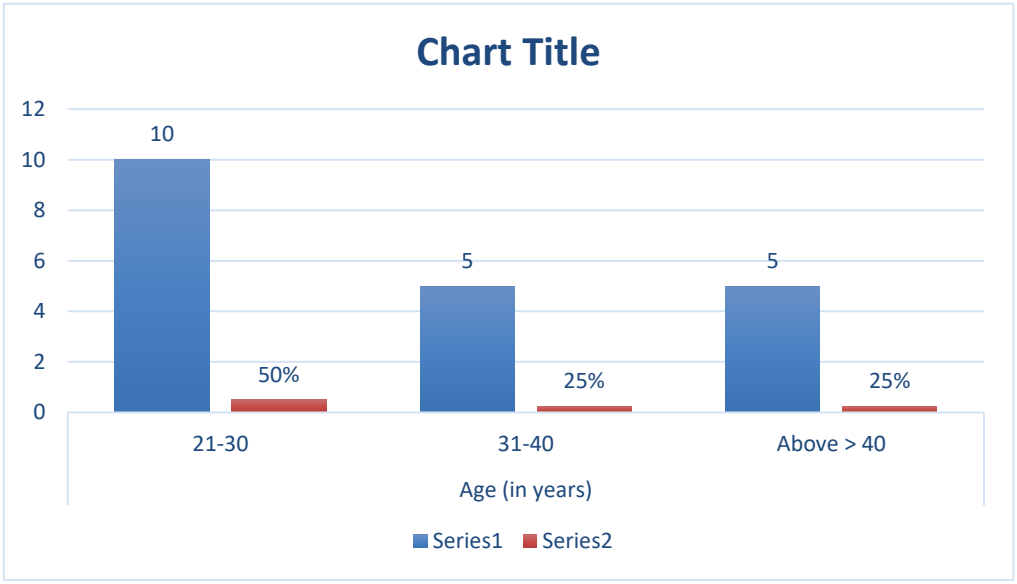

Figure 2: Age in years of respondents

Table 3: Marital status of respondents

Characteristics	Categories	Frequency	Percentage
Marital Status	Single	11	60%
	Married	9	40%

Table 4: Educational Level of Respondents

Characteristics	Categories	Frequency	Percentage
Educational Level	Diploma	6	30%
	BA/B.SC/HND	9	45%
	Master	5	25%

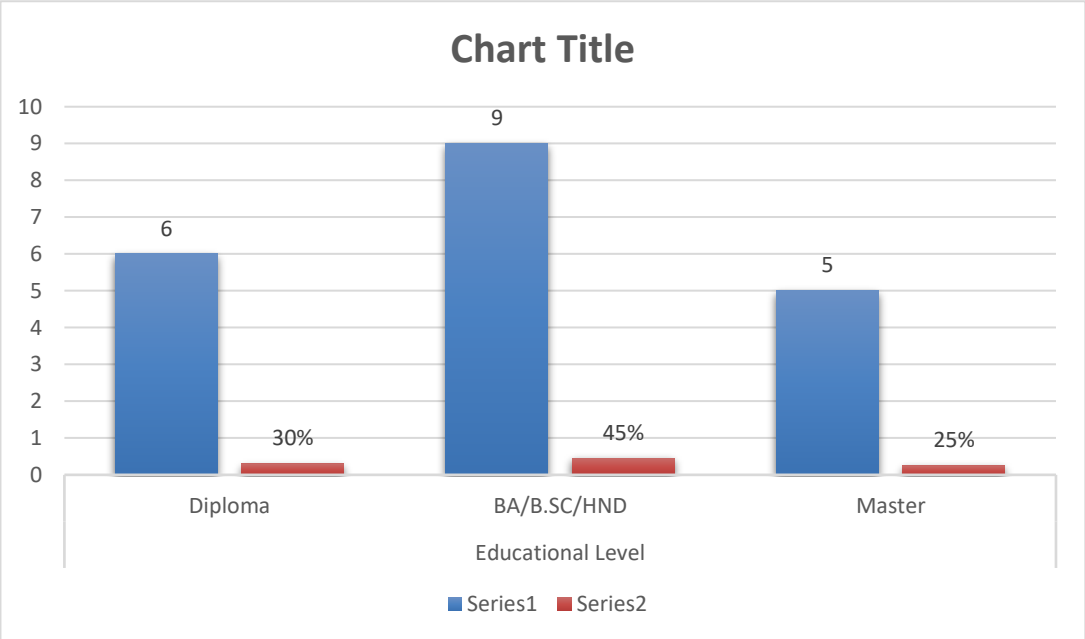

Figure 4: Educational Level of Respondents

Table 5: Working Years' Experience of Respondents

Characteristics	Categories	Frequency	Percentage
How long have you Been working in the department	1 – 5 Year	6	30%
	6 – 10 Year	9	45%
	More than 10 Years	4	25%

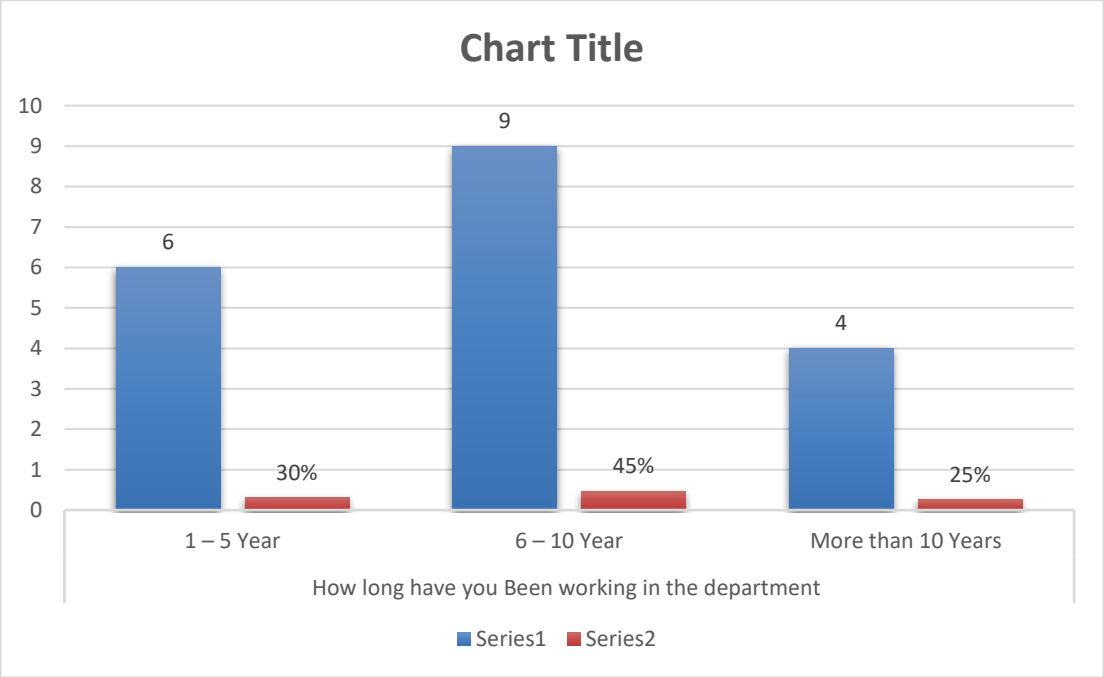

Figure 5: Working Years' Experience of Respondents

According to the findings reported in Figures 1-5 above, 35% of all respondents are males and 65% are female. This implied that the majority of First Bank respondents are females. In terms of marital status, single respondents led the study (60%). The majority of responses are BA/BSc/HND holders.

Finally, the majority of respondents have been with First Bank for 6-10 years, with 25% having worked for more than ten years, indicating that they have sufficient experience to provide appropriate responses.

Research Questions:

Research Question one: What are the types of computer information systems at First Bank, Minna, Niger State

Table 6: Types of Information Systems used in First Bank?

S/N	Types of Information System available	Responses
1.	Transaction Processing Systems (ATMs)	20 (100%)
2.	Management Information Systems	20(100%)
3.	Executive Support System	20(100%)
4.	Office Automation Systems	20(100%)
5.	Electronic Communication Systems	20(100%)
6.	Decision- Support Systems	10(50%)
7.	Knowledge-Based Information Systems	4(20%)

Table 1 shows the captured transaction processing systems (ATMS) of First Bank, with just 50% claiming a decision support system in their branch and 20% claiming a knowledge-based information system. First Bank has practically all types of information systems, suggesting that they are technologically sophisticated and understand the role information systems play in influencing organizational performance.

Research Question two: How does the How does the management information system help First Bank achieve its goals?

When asked if First Bank's information systems influence organizational performance, 90% replied yes, with 10% saying no.

Table 7: Relevance of information system on First Bank's organizational performance

S/N	Relevance of Information System within First Bank	SA	A	D	SD
1.	Is imposing security and control	11 (55%)	7(35%)	2(10%)	0%
2.	Is threat to my bank	0%	0%	7(35%)	13(65%)
3.	Computer virus and many other fraudulent manipulations are threat to exposure of confidential information confronting my bank.	6(30%)	5(25%)	0%	9(45%)
4.	Is has made service continuity a more appropriate term than business continuity.	12(60%)	6(30%)	0%	2(10%)
5.	Is has made decisions leading to the achievement of my bank objectives attainable.	0%	0%	4(20%)	16(80%)
6.	Is a major issue that affects my bank survival?	0%	0%	6(30%)	14(70%)
7.	Accurate and well-presented information is available to improve our productivity.	19(95%)	1(5%)	0%	0%
8.	Is enables planning, coordinating, organizing and controlling functions of management,	16(80%)	0%	3(15%)	1(5%)
9.	Is the Life Blood of my bank?	19(95%)	1(5%)	0%	0%
10.	From My Own Perspective, IS is that least important	0%	0%	1(5%)	19(95%)
11.	Is has a profound contribution on our Operation	16(80%)	2(10%)	1(5%)	1(5%)
12.	Strategic ability to deal with Crisis and Interruptions effectively is again of IS	17(85%)	2(10%)	1(5%)	0%
13.	Is has made decisions leading to the achievement of my bank objectives attainable.	16(80%)	2(10%)	1(5%)	1(5%)
14.	With is accurate, timely well-presented information is available to improve our productivity.	14(70%)	**3(15%)**	2(10%)	1(5%)
15.	With is accurate and well-presented information is available to improve our productivity.	17(85%)	2(10%)	1(5%)	0%

16.	Is enables planning, coordinating, organizing and controlling functions of management.	12(60%)	0%	5(25%)	3(15%)

Table 2 demonstrates that 70% of respondents strongly disagreed that the information system is a critical issue threatening First Bank's survival, while 65% strongly disagreed that the information system poses a security and control risk to First Bank. Also, 30% believe that computer viruses and other fraudulent activities represent a threat to First Bank. 60% strongly agreed that information systems had made service continuity more suitable than business continuity. Table 2 indicated that information systems are crucial in businesses such as banks.

Research Question two: What are the problems in the management and use of First Bank plc Minna's information system?

This section contains questions that prompted responses that contributed in identifying the barriers to the usage of information systems within the first bank.

Table 8: Factors That Hinder the Utilization of Information Systems in First Bank:

Budgetary allocation	35%
Privacy issues	25%
Integration of new systems	25%
Lack of Job security	15%

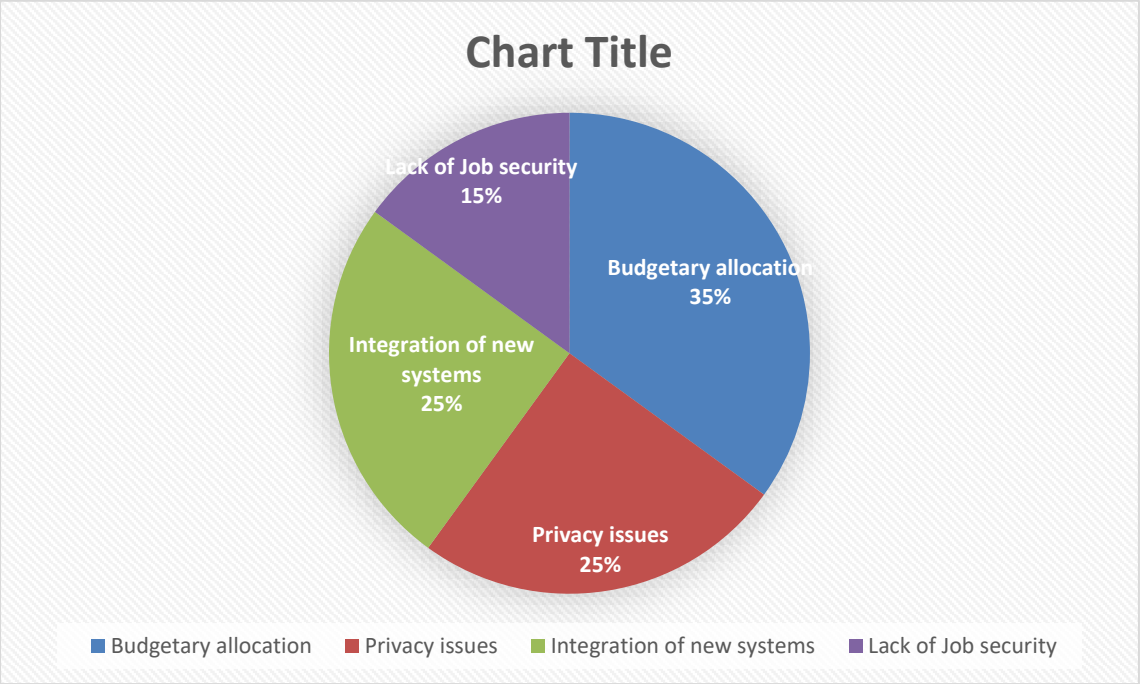

Figure 6: Factors that hinder the utilization of information systems in First Bank

Figure 6 depicts the respondents' responses when asked about the factors that impede the use of information systems at First Bank, with 35% citing budgetary allocation and 25% citing privacy concerns as the major barriers to information system utilization, 25% claiming that integration of new systems is also a factor, and 15% citing a lack of job security. As processes become more automated, unemployment did not

Discussion

The study's findings revealed that 90% of respondents thought information systems were crucial to First Bank's organizational effectiveness. The survey also revealed that the majority of respondents believed information systems were vital to their daily banking operations. Furthermore, the study's tested hypothesis indicates a considerable link between information systems and organizational performance. This observation is consistent with Kling's (1996) contention that incorporating information technologies into a bank's operations frequently results in a significant change in workflow.

This study also found that the bank conducted the majority of its operations using an information system, and when asked if information systems have an impact on performance, respondents agreed. This is consistent with Kasasbeh's (2007) findings, which explored the effect of information systems in increasing the efficiency of the Free Zones Corporation. Jordan's performance from 1996 until 2005. Armstrong's (2009) remark adds legitimacy to the conclusions that the overall goal of information systems is to develop and improve the performance of individuals, teams, and hence organizations.

The examination indicated that the bank rarely carried out actions without the use of an information system. Eaton and Bawdon (1991) emphasized the relevance of information systems for all institutions because information is now one of the most significant assets to service providers, such as banks, as it allows for speedy decision making.

The majority of respondents stated that financial allocation, privacy concerns, and the integration of new systems are the key barriers to the bank's smooth operations. Many reliable hard drives and software are costly, and others demand the purchase of user licenses.

Conclusion

The adoption of computers in Nigerian banking had a significant and positive impact on the business. Transactions now take much less time to complete, customer expectations are met, and the volume of commercial transactions has expanded significantly, benefiting both banks and their clients. All banks understand its significance to the long-term profitability of their operations. As a result, information systems should be given special attention because they are crucial to banks' competitive existence and profitability.

Recommendations

Based on the study's findings, the researchers suggest that First Bank reconsider its current investments, close the information technology gap discovered when compared to developed countries, and allocate more funds to the purchase of information systems, increasing the organization's chances of survival in the face of formidable challenges.

First Bank's top management must devise a strategy to overcome the challenges to efficiently deploying this significant investment in information systems, distribute it throughout the organization, build a shared vision, and address all critical areas of information systems.

REFERENCES

Aboelmaged, M.G., &Gebba T.R. (2013). Mobile banking adoption: an examination of TAM and Theory of Behaviour. International Journal of Business Research and Development, 2(1), 35-50.

ACM, (2019). Association for Computing Machinery: https://www.acm.org/

AlfredT.Y.,(2019). Computer Systems Management Thesis:

Shttps://www.researchgate.net/publication/337224753.

Al-Jabri, I.M., &Sohail, M.S., (2012). Mobile Banking Adoption: Application of the Diffusion Innovation Theory. Electronic Commerce Research, 13(4), 379-391.

Al-Shiha, F. M. (2018). IT Service Management: A Guide for ITIL Foundation Exam Candidates. Springer.

Alter, S. (2013). Information Systems: Foundation of E-Business. Pearson.

Andrew S. &Tanenbaum., 2015). "Structured Computer Organization"

APM and MoM, (2012). Symbiotic Solution Sets". APM Digest.

Bates, M. J. (2005). Information and Knowledge: An Evolutionary Framework for Information Science. Information Research, Vol. 10(4).

Bawden, D., & Robinson, L. (2012). Introduction to information science. Facet Publishing.

Brookshear J. G., and David T. S., (2015) Computer Science: An Overview". Vol. 12, pp. 3-443

Chaffey, D., & White, G. (2017). Business Information Management: Improving Performance Using Information Systems. Pearson.

Chaitin, G. J. (2007). Algorithmic information theory. Cambridge University Press.

Chuvakin, A., &Halpert, R. (2016). Security Information and Event Management (SIEM) Implementation. McGraw-Hill Education.

Davenport, T. H. (2013). Process Innovation: Reengineering Work through Information Technology. Harvard Business Press.

David A. P. and John L. Hennessy L., (2016). "Computer Organization and Design: The Hardware/Software Interface"

David A. Patterson and John L. Hennessy (2016). "Computer Organization and Design: The Hardware/Software Interface"

Davis, F. D. (2012). User acceptance of information technology: toward a unified view. MIS Quarterly, 27(3), 425-478. [22] Yu, C.S. (2012)

Edubirdie, (2022). Advantages and Disadvantages of Technology in Banking Sectorhttps://edubirdie.com/examples/advantages-and-disadvantages-of-technology-in-banking-sector/

Floridi, L. (2010). Information: A Very Short Introduction. Oxford University Press.

Floridi, L. (2019). The Logic of Information: A Theory of Philosophy as Conceptual Design. Oxford University Press.

Galliers, R. D., &Leidner, D. E. (Eds.). (2014). Strategic Information Management: Challenges and Strategies in Managing Information Systems (4th ed.). Routledge.

Gleick, J. (2011). The Information: A History, a Theory, a Flood. Vintage.

Glenn B. J. and Dennis B. (2019). Computer Science: An Overview"

Haag, S., Cummings, M., McCubbrey, D., &Pinsonneault, A. (2018). Management Information Systems for the Information Age. McGraw-Hill Education.

Huang, Y. (2017). Computer System Management: Design, Implementation, and Management. CRC Press.

Kim, H. M. (2016). Strategic Information Management: Challenges and Opportunities in the Digital Age. IGI Global.

Kim, S., & Solomon, M. G. (2015). Fundamentals of Information Systems Security. Jones & Bartlett Learning.

Laudon, K. C., & Laudon, J. P. (2016). Management Information Systems: Managing the Digital Firm. Pearson Education.

Laudon, K. C., & Laudon, J. P. (2020). Management Information Systems: Managing the Digital Firm. Pearson.

Luciano, F. (2019). Information: A Historical Companion. Oxford University Press.

McLeod, R. Jr., & Schell, G. P. (2018). Management Information Systems. Pearson.

McLeod, R., & Schell, G. P. (2019). Management Information Systems. Pearson.

Michael S., (2015). "Introduction to the Theory of Computation"

Morris, S. (2015). Computer Systems: Theory, Technology, and Management. Springer.

NB, (2020). Nigerian Banker: www.nigerianbanker.com/first-bank-of-nigeria-limited/

O'Brien, J. A., &Marakas, G. M. (2018). Management Information Systems. McGraw-Hill Education.

O'Brien, J. A., &Marakas, G. M. (2019). Introduction to Information Systems. McGraw-Hill Education.

Oz, E. (2018). Management Information Systems. Cengage Learning.

Russell, J. C., &Gangemi, G. T. (2013). Information Security: Principles and Practices. Prentice Hall.

Shaikh, A.A., &Karjaluoto, H. (2015). Making the most of information technology and systems usage: a literature review, framework and future research agenda. Computers in Human Behaviour, 40, 541-566.

Snedaker, S. (2014). Business Continuity and Disaster Recovery Planning for IT Professionals. Syngress.

Stair, R. M., & Reynolds, G. W. (2018). Principles of Information Systems (13th ed.). Cengage Learning.

Stair, R. M., Reynolds, G. W., & Chesney, T. (2019). Fundamentals of Information Systems. Cengage Learning.

Stallings, W. (2018). Operating Systems: Internals and Design Principles. Pearson.

Tanenbaum, A. S., &Bos, H. (2014). Modern Operating Systems. Pearson.

Turban, E., &Volonino, L. (2019). Information Technology for Management: On-Demand Strategies for Performance, Growth, and Sustainability. John Wiley & Sons.

Turban, E., &Volonino, L. (2019). Information Technology for Management: Digital Strategies for Insight, Action, and Sustainable Performance. Wiley.

van Bon, J., & de Jong, J. (2011). Foundations of IT Service Management with ITIL 2011. Van Haren Publishing.

Ward, J., &Peppard, J. (2016). The Strategic Management of Information Systems: Building a Digital Strategy (4th ed.). John Wiley & Sons.

A Retrospective Overview of Responses Towards Transmission Dynamics and Control of COVID-19 Pandemic in Nigeria

N. I. Akinwande[1], O. M. Adetutu[2]*, S. A. Somma[1], N. O. Abdurrahman[1], T. T. Ashezua[3], F. A. Oguntolu[1], R. I. Gweryina[3], R. O. Olayiwola[1], T. P. Adajime[4], F. A. Kuta[5], S. Abdulrahman[6], A. I. Enagi[1], G. A. Bolarin[1], M. D. Shehu[1], A. Usman[2]

[1]Department of Mathematics, Federal University of Technology Minna, Nigeria
[2]Department of Statistics, Federal University of Technology Minna, Nigeria
[3]Department of Mathematics, Federal University of Agriculture, Makurdi, Nigeria
[4]Department of Epidemiology and Community Health, Benue State University, Makurdi, Nigeria.
[5]Department of Microbiology, Federal University of Technology Minna, Nigeria.
[6]Department of Mathematics, Federal University, Birnin-Kebbi, Nigeria.
*adetutuolayiwola@gmail.com

Abstract

A retrospective review of responses from several programmes initiated by government of Nigeria towards educating general public on awareness, symptoms, pharmaceutical interventions, and non-pharmaceutical protocols to halt the spread of COVID-19 pandemic were x-rayed using item response approach to ascertain degree of public awareness, keeping to non-pharmaceutical practices, and assert pharmaceutical mediations across different segments of society. Responses from 2500 respondents spread across Federal Capital Territory Abuja and 4 selected states were assessed, coded, and modelled using non-linear item response functions to known respondents' dispositions to COVID-19 pandemic of various social strata. While all levels of society acknowledge COVID-19, and its symptoms, radio/television were very effective in enlightening low income individuals, only high income individuals attested to testing, vaccination centres as well as received COVID-19 doses. Government in her efforts need to do more to enable low income earners to access and accept pharmaceutical interventions. This research findings can be a road map for future efforts towards pandemic awareness, preventions and control.

Keywords: awareness, interventions, pharmaceutical, responses, retrospective

1 Introduction

World Health Organization (WHO) declared coronavirus disease 2019 (COVID-19) a pandemic in March 2020 (WHO, 2020a), it is a novel coronavirus typically a new strain of infectious disease that has not been previously identified in human beings (WHO, 2020b). These are large family viruses that are responsible for illness ranging from common cold to more severe respiratory syndrome coronavirus 2, pneumonia and death (WHO, 2020c). The disease as a global pandemic had affected over 200 countries and territories around the globe which had been responsible for past and current social economic disorders affecting lives and livelihoods (Akande-Sholabi and Adebisi, 2020). In Nigeria, the first case of the novel

coronavirus was reported and confirmed on 27th February, 2020 by Nigeria Centre for Disease Control (NCDC). As of June 8, 2022, the total number of confirmed cases has risen to 252,187 as reported by NCDC. Of the confirmed cases, 249,063 individuals have recovered while 3,124 deaths were recorded (NCDC, 2020). Symptoms of this novel coronavirus disease includes dry cough, tiredness (fever and fatigue) as most common, while others are running nose, diarrhoea, skin rashes, sore throat, pains, difficulty in breathing, headache, toes or fingers discolouration (WHO, 2020d).

The extracted data from NCDC website spanned from March 31 to May 29, 2020 was used by Ogundokun *et al.,* (2020) to measure the impact of travelling history and contact on COVID-19 confirmed cases thereby used in predicting the prevalence of COVID-19 in Nigeria using a linear regression model. They conducted the model before and after travel restriction was enforced by Federal Government of Nigeria, and their findings revealed that government made right decision in enforcing restriction because they observed that travelling history and contacts have increased chances of people being infected with COVID-19 by 85% and 88% respectively.

What the daily new cases of COVID-19 would have been ten days after lockdown was eased in Nigeria was modelled by Adesina *et al.,* (2020) using Autoregressive Fractionally Integrated Moving Average (ARFIMA) and compared to the actual new cases for the period when the lockdown was eased. The proposed model ARFIMA was compared with autoregressive integrated moving average (ARIMA), ARIMA (1, 0, 0), and ARIMA (1, 0, 1) thereby discovered that ARFIMA performs better than classical ARIMA. Their findings show that the rate of COVID-19 spread would have been significantly lesser if the restrict had continued, and ARFIMA model was further used to model what new cases of COVID-19 would be ten days ahead starting from 31st of August 2020.

The accuracy of diverse time-series models was explored by Folorunso *et al*., (2021) in COVID-19 epidemic detection in all the 36 states and the Federal Capital Territory (FCT) in Nigeria with the maximum count of daily cumulative of confirmed, recovered, and death cases as of November 4, 2020. In their work, 14-step forecast system for active coronavirus cases for six different deep learning-stimulated and statistical time-series models were built, analysed and compared using two openly accessible datasets. The findings revealed that ARIMA model obtained the best values for four of the states (0.002537, 0.001969.12E-058, 5.36E-05 values for Lagos, FCT, Edo and Delta states, respectively) based on Random Mean Standard Error (RMSE) metric.

A suitable Autoregressive Integrated Moving Average (ARIMA) model was developed by Didi *et al.,* (2021) and used to forecast daily confirmed and death cases of COVID-19 in Nigeria, suitability check was carried out after developing the model and eight months forecast was made before recommendations were sent to the Nigerian health sector. A forecast of 239 days starting from 6th May to 31st December 2020 was conducted using the fitted models, they observed that the COVID-19 data had an upward trend and was best forecasted within a short period.

The intrinsic patterns in the COVID-19 spread in Nigeria was studied and analysed by Ortese et al., (2021) using the Box-Jenkins procedure whereby data of daily confirmed cases

of COVID-19 in Nigeria from NCDC official website from 27th February to 31st October 2020 was used to identify the series components and estimate parameters. An appropriate stochastic predictive model was developed and used to forecast future trend of the novel virus. The results shown that Autoregressive Integrated Moving Average (ARIMA) of order (0,1,1) was identified as the most suitable model based on the analysis of the autocorrelation, partial autocorrelation functions and Akaike Information Correction (AIC) value. R software version 4.0.3 was used to analyse the trend which smoothen the series by using 8point moving average in extracting the irregular component as well as differencing the series one step further to obtain a stationary series. Augmented Dickey-Fuller Unit root test, parameter estimation and Ljung-Box test were performed to check the proposed model's conformity to the stationary univariate process.

Predictive distributions and models such as Bernoulli, Poisson, Gaussian, and most importantly, the simplest epidemiological susceptible-infectious (SI) model were clearly explained and illustrated by Qiwei, (2022) using Bayesian inference of the discrete time Markov chain with applications in biology. The concepts of the discrete-time Markov chain, a stochastic model which describe a sequence of possible events in which probability of each event depends only on the state attained in previous event was used.

Count regression models like: Poisson Regression (PR), Negative Binomial Regression (NBR), and Generalized Poisson Regression (GPR) models were adopted by Adams *et al.,* (2020) to model the daily cases of COVID-19 deaths in Nigeria. They examined appropriate count regression model to the confirmed, active, and critical cases of COVID-19 in Nigeria after 130 days using daily COVID-19 cases update released by the NCDC online data base from February 28 to July 6 2020. The extracted data was used in simulation of Poisson, Negative Binomial, and Generalized Poisson Regression models with the aids of Stata 14 Standard Edition, fitted the data at 5% significance level, and the best model was selected on the basis of -2logL, AIC, and BIC selection criteria. The results from their analysis revealed that Poisson Regression incapable of capturing over-dispersion, therefore other count regression such as Negative Binomial and Generalized Poisson Regression models were used in the estimation and discovered that when over-dispersion is present, Generalized Poisson Regression was the best.

The COVID-19 data on confirmed cases, deaths, and recovered obtained from the website of the Nigerian Centre for Disease Control (NCDC) from April 2 to August 24, 2020 was used by Chigbu et al., (2021) to study some epidemiological characteristics of the Nigerian COVID-19 data in order to help the government and university administrators toward making informed decisions on the safety of personnel and students. In their work, infection rate, prevalence, ratio, cause-specific death rate, and case recovery rate were used to assess the epidemiological faces of the pandemic in Nigeria, exponential smoothing was adopted in modelling the time series data and forecasting the pandemic in Nigeria up to January 31, 2021. Their findings revealed that the pandemic had infection rate of at most 3 infections per 1 million per day from April to

August 2020. The death rate was 5 persons per 1 million during the period of study while recovery rate was 747 persons per 1000 infections. Analysis of forecast data showed steady but gradual decrease in the daily infection rate and death rate and substantial increase in the recovery rate, 975 recoveries per 1000 infections. During the pandemic, it is very important to do retrospective study appraisal of effective sources of information on COVID-19 in Nigeria.

Item response theory (IRT) modelling comprises of related statistical methods and models that explain non-linear relationship between observed responses on the construct to respondent's trait: social status levels (Adetutu and Lawal, 2022). It mainly focused on each item of the constructs, compares respondents' responses to the construct and likelihood of their positive responses thereby adopting an explicit model for each possible response to the questionnaires (Lim, 2022). This probability is derived as a function of the latent trait and some questionnaires' parameters. It is widely used today in analysing health responses, items bank development, computer adaptive testing, and so on (Linden, 2018).

The three basic components of IRT are: *Item Response Functions* (IRFs) which are non-linear regression models that relate latent trait (social status) to the probability of endorsing an item in the questionnaire (Adetutu and Lawal, 2020), *Item Information Function* (IIF) is an indication of item (questionnaire) quality, and item's ability to segregate among the respondents, and *invariance* that shows the position on the latent (social status) continuum that can be estimated by any item with known IRFs and item characteristics which are population independent within a linear transformation (Lim, 2020).

However, five assumptions of item response modelling discussed in Adetutu and Lawal (2022) includes: *unidimensional* which implies that the questionnaires is measuring a single concept, and all items are contributing in the same way to the underlying latent trait, *local independence* of IRT infers that questionnaires items are uncorrelated for the respondents of same trait , *monotonicity* assumption focuses on item response functions which shows non-linear relationship between respondents' traits, propensity and probability of endorsement. The probability of a respondent endorsing an item increases as the respondent's social status (latent trait) level increases, on *item invariance,* parameters estimates by IRT would not change even when characteristics of respondents changes, and *qualitatively homogeneous populations* of IRT implied that the same item response functions applied to all respondents.

On awareness of COVID-19, there had been abundant evident on vital role played by health campaign in pandemic. No doubt that information technology and social media have transformed the way information reach people during pandemic. Sources of information about wellness and hygiene especially hand washing, use of sanitizers, social distancing and so on are examples of roles played by heath organization in the response to COVID-19 pandemic. On control of COVID-19 pandemic, protective behaviours of non-pharmaceutical protocols such as use face mask, hand washing, social distancing and so on are the keys to managing pandemic, and pharmaceutical interventions such as first, second and booster doses of vaccines could be a key protective behaviour for COVID-19 (Reiter *et al.*, 2020).

The study is motivated by the outgoing spread of the third wave of the coronavirus including most African country- Nigeria with sole aim of appraising our public health strategy towards curbing this pandemic. To brilliantly achieve this aim, item response approach is used

to cross examine observed responses of the respondents towards COVID-19 awareness, symptoms, and vaccine acceptability. The approach would enable us detect public health strategy that need improvement through the behaviour of various item response functions.

2 Methods

2.1 Study design

A stratified incorporated simple random sampling technique was used in administering a well prepared questionnaires to elicit useful information on COVID-19 awareness, symptoms and vaccinations through the responses made to the construct by 2500 respondents equally spread over four selected states: Benue, Lagos, Niger, Rivers and Federal Capital Territory (FCT) in Nigeria. The responses were later entered into an excel spread sheet followed by quality check and data cleansing to ensure accuracy.

2.2 Measures

COVID-19 Awareness: A well structure questionnaire was used to gather responses on awareness, and sources of information on COVID-19 which were followed by items on acknowledging, and listing of COVID-19 testing and vaccination centres.

Symptoms of COVID-19: Some items in the questionnaires were meant to assess respondents ability in identifying symptoms of this pandemic listed in the questionnaires.

Use of Non-pharmaceutical protocols: Items were devoted to know how often the respondents wear face mask, and practice of any non-pharmaceutical protocols listed in the questionnaires.

Practice of COVID-19 Vaccine: Items were geared towards knowing level of practice for pharmaceutical interventions (first, second, and booster doses) among respondents.

2.3 Data Analysis

In this retrospective study, data in excel were coded dichotomously to form 2500 by 38 matrix based on the principle of one parameter logistic modelling of Rasch, (1966) applied in Adetutu and Lawal (2022) which employed unity of discrimination with varied social status parameters in assessing various responses reference to social status of the respondents. Thereafter, coefficients of social status are used in adjudging strata of society who responded most positively to COVID-19 awareness, symptoms, and vaccination in Nigeria. Stata 17 Standard Edition on window platform are used for the analysis.

2.4 Rasch Modelling

As a special one-parameter binary logistic model, responses yes and no were coded as 1 and 0 respectively then modelled by equation (1). A specialised Conditional Maximum Likelihood (CML) estimation procedure was used due to the availability of sufficient statistic for the resulting matrix (Baker and Kim, 2004). Needed information was extracted from set of item response functions (item characteristic curves) which described non-linear regressions of observed responses from respondents with varied social status (θ) and their likelihood of endorsing their preferred responses in according to equation (1).

$$\Pr\left(R_{ij}=1 \mid b_i, \theta_j\right)=\frac{e^{\left(\theta_j-b_i\right)}}{1+e^{\left(\theta_j-b_i\right)}} \quad (1)$$
$$i=1,2,...,38$$
$$j=1,2,...,2500$$

Where b_i is respondent $j^{'}s$ capability of responding yes to item i in the questionnaires θ_j is respondent's j trait indicating his or her social status level
R_{ij} is the response from respondent j to item i in the questionnaires.

Primary to Item Characteristic Curves (ICC) is a table displaying respondents' capability indices on the basis of their social status levels. An average respondent with moderate social status is designated *0*; as the parameter increases, it means social status improves, and vice versa. In practical, status ranges between *-4*, *4* except in extreme cases (Raykov and Macrolides, 2018).

2.5 Parameter Estimation

If r_{ij} be the observed response for R_{ij} outcome for item i from respondent j, and referring r_{ij} = 1 as yes, and r_{ij} = 0 as no, the probability of j^{th} respondent with traits level θ_j responds yes to item i is as position in equation (1), b_i and θ_j were as defined accordingly then the slope-intercept form is presented in equation (2)

$$P\left(R_{ij}=1 \mid \beta_i, \theta_j\right)=\frac{e^{\left(\theta_j+\beta_i\right)}}{1+e^{\left(\theta_j+\beta_i\right)}} \quad (2)$$

and the transformation between the parameterization is

$$b=-\beta_i \quad (3)$$

Let

$$p_{ij}=P\left(R_{ij}=1 \mid \beta_i, \theta_j\right) \quad (4)$$
$$q_{ij}=1-p_{ij}$$

Conditional on θ_j for respondent j since item responses are assumed to be independent, is given by the equation (5)

$$f\left(r_j \mid \Omega, \theta_j\right)=\prod_{i=1}^{38} {p_{ij}}^{r_{ij}}\ {q_{ij}}^{1-r_{ij}} \quad (5)$$
$$r_j=\left(r_{1j},...,r_{38j}\right)$$
$$\Omega=\left(\beta_1,...,\beta_{38}\right),$$

and 38 is the number of items in the questionnaires.

The likelihood for respondent j is computed by integrating out the latent variable from the joint density

$$\mathrm{L_j}(\boldsymbol{\Omega}) = \int_{-\infty}^{\infty} f\left(r_j \mid \boldsymbol{\Omega}, \theta_j\right) \phi(\theta_j) d\theta_j \tag{6}$$

$\phi(.)$ is a density function for standard normal distribution. For 2500 respondents, the sum of log likelihood is given in equation (7)

$$logL\left(\Omega\right) = \sum_{j=i}^{2500} logL_j\left(\Omega\right) \tag{7}$$

Since the integral for $L_j(\boldsymbol{\Omega})$ is generally not tractable, we used 21 points adaptive Gauss-Hermite quadrature with Newton-Raphson maximization technique in (Stroud and Secrest, 1966) implemented on Stata 17 SE.

4 Results

The results of the analysis display respondents on different level of social status responding positively to the items in the questionnaires are presented in Table 1 where negative, zero, and positive indicators indicate respondents' low, average, and high social status which are illustrated by Figures 1 to 4.

Table 1: Social Status Indicators for Respondents (Positive Response)

Item	Benue	FCT	Lagos	Niger	Rivers	Combine
Awareness	-6.095683	-6.800279	-6.953285	-4.529761	-5.95334	-5.717256
Rad/TV	-2.099262	-3.637553	-2.295092	-1.774495	-4.32166	-2.564053
Internet	-0.463852	-1.57596	-1.034459	-1.822069	-3.88709	-1.492284
Friends	-0.361675	-1.534956	-0.986957	-1.580841	-3.54777	-1.384523
Newspaper	-0.040206	-1.0295	-0.472879	-0.601047	-3.26667	-0.875
P/Campaign	0.899362	-0.160296	-0.757171	-0.179579	-2.49937	-0.407602
T/Centres	0.7462	0.3231773	0.1229541	1.149185	0.428348	0.5503601
1st centre	0.811198	0.3027144	0.2371468	1.114479	0.22844	0.5357007
2nd centre	1.262401	1.476079	1.201324	2.491204	6.874038	1.899761
V/centres	1.337789	0.3848623	-0.998779	0.8497551	0.312453	0.3741304
1st centre	1.262401	0.3848623	-0.84768	0.8817545	0.322966	0.3967428
2nd centre	1.692674	1.722664	0.6393139	2.314381	6.874038	1.874127
C/symptoms	-5.159317	-4.675566	-3.099036	-3.342459	-3.54777	-3.687732
Fever	-1.862486	-2.756052	-1.71107	-1.854475	-3.0579	-2.167245
Cough	-1.960416	-3.273561	-2.105333	-2.630519	-2.84217	-2.485064
Tiredness	0.159491	-1.377426	-0.745974	-1.190768	-2.62375	-1.029326

Loss of taste	1.312435	-0.503887	-0.537372	-0.343518	-2.67595	-0.413829
Sore throat	0.411784	-1.57596	-1.218302	-0.905169	-2.42853	-1.022278
Headache	0.330487	-0.928448	-0.813538	-0.745031	-2.10883	-0.774552
Aches/Pains	1.262401	-0.220421	-0.313806	-0.093572	-2.93143	-0.285978
Diarrhoea	1.993285	0.6158735	0.8716261	0.6934666	-3.0579	0.3679718
Skin rashes	2.17253	0.7350926	0.894314	1.080178	-2.80419	0.5085536
Red/irritated eyes	1.909719	-0.050219	0.4361713	0.5322985	-2.23052	0.1764229
S/breath	0.229673	-1.984426	-1.413147	-1.214902	-2.90118	-1.27834
Loss of speech	1.536152	0.6373372	0.6937563	0.7345887	-1.26793	0.4711215
Chest pain	0.866086	-0.270628	-0.430183	-0.520646	-1.29547	-0.306489
W/face mask	-3.156249	-3.442347	-2.275234	-2.099473	-3.19424	-2.734813
Always	1.893428	0.0800661	0.894314	0.7345887	1.277746	0.9318009
Occasionally	-1.443472	0.1102229	-0.624316	-0.724172	-0.47686	-0.618143
Not at all	3.749688	3.595569	3.789708	2.314381	1.110411	2.530566
Hand washing	-2.779203	-3.585769	-2.913708	-2.386733	-1.97552	-2.647116
Sanitizer	-2.154152	-2.756052	-1.756684	-1.938106	-3.33421	-2.295631
S/distancing	-0.525785	-1.302062	-0.355965	-0.560696	1.902087	-0.212422
S/isolation	1.312435	0.5944971	1.092216	1.012702	2.893602	1.282043
R/etiquette	1.402231	1.007283	0.3940047	1.219894	2.713967	1.262129
1st dose	2.249591	1.722664	0.5531294	1.959375	0.771708	1.370797
2nd dose	2.599577	2.322311	1.417993	2.514845	1.052305	1.874127
b/dose	3.587013	3.411772	3.015023	3.759464	1.427782	2.74177

5 Discussions

5.1 On awareness of COVID-19

Outcome of the analysis in Table 1 suggested convincingly that all various segment of respondents overwhelmingly aware of COVID-19 pandemic, evidences were abound that lower social status upward were aware of the pandemic: Benue *(-6.10)*, FCT *(6.80)*, Lagos *(-6.95)*, Niger *(-4.53)*, Rivers *(-5.93)*, Combined *(-5.72)*.

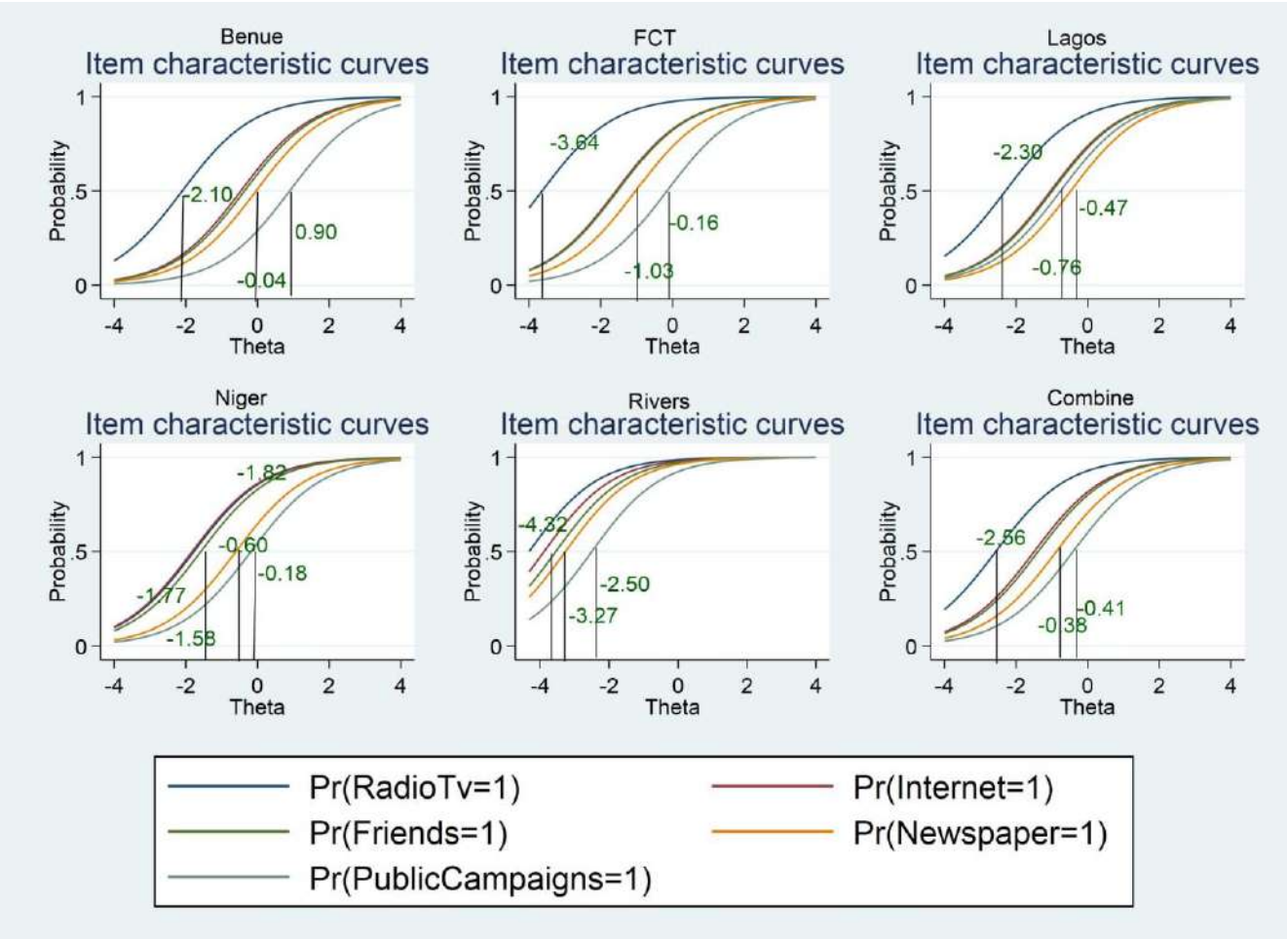

Figure 1: Sources of COVID-19 Information in Nigeria

On sources of information, Figure 1 graphically presented varied categories of respondents' traits (social status) who got COVID-19 information on horizontal *(x)* denoted as *Theta* (θ), and the probability of making their responses on vertical *(y)* axis in consonant with Table 1. Result from Benue attested to the fact that lower social status respondents most likely got information on COVID-19 pandemic from Radio/Television *(-2.10)*, internet *(-0.46)* and friends *(-0.36)* in that order. The parameter estimates in Table 1 for radio/television, internet and friends also agreed with graphical findings. Apart from these, at least only moderately social status respondents had assessed to COVID-19 pandemic information from Newspapers *(-0.04)*, and public campaigns *(0.90)* as the graph and Table 1 suggested. It is better to emphasize here that of all this sources, Radio/Television had done well. In addition, findings from FCT revealed that though at least, lower social status respondents received information on COVID-19 pandemic from radio/television *(-3.64)* most likely, internet *(-1.58)*, friends *(1.54)*, newspaper *(-1.03)*, and public campaigns *(-0.16)* in accordance to their social status as suggested by Figure 1 and supported by Table 1.

Likewise from Lagos, finding revealed that lower status respondents were informed of COVID-19 pandemic through radio/television *(-2.30)* first, followed by internet *(-1.03)*, friends *(-0.99)*, newspaper *(-0.47)*, and public campaign *(-0.76)*. In Niger, both radio/television *(-1.77)* and

internet *(-1.82)* were discovered to have same profound impact in disseminating COVID-19 pandemic information on lower social status respondents than friends, newspaper, and public campaigns has shown in both Figure 1 and Table 1. On the other hand, results from Rivers suggested that mostly likely all these sources of information were geared towards sensitizing and impacting lower social status while radio/television *(-4.32)* performed exceptionally well. Internet *(-3.89)*, friends *(-3.55)*, newspaper *(-3.27)*, and public campaign *(-2.50)* were all taking cares of lower social status in our survey.

Our findings in Nigeria (combined) as a whole suggested that radio/television *(-2.56)* had more impact on at least lower social status respondents than other mediums, followed by internet *(-1.38)*, friends *(-1.38)*, newspaper *(-0.88)*, and public campaign (-0.41). Comparatively, radio/television was discovered to be more effective in disseminating information to lower social status individuals/citizenry in Rivers and FCT than any other areas. Public campaigns in Benue was not felt by lower social status respondents like other areas, however, government agencies in charge of public campaigns need to arise to their duties.

On COVID-19 testing centres, the findings presented in Table 1 revealed that none of the lower social status respondents acknowledge any testing centre. Few respondent who acknowledge testing centre were at least moderate social status respondents: Benue (0.74), FCT (0.32), Lagos (0.12), Niger (1.15), Rivers (0.43), and combined (0.55). This was the reason why it was impossible for lower social status respondents to list at least a COVID-19 testing centre in their domains. This has been set back for government efforts, only high social status respondents were able to list two COVID-19 testing centres. On vaccination centres, only in Lagos (-1.00) we have lower social status respondents who were able to admit the existence of COVID-19 vaccination centres while it took only moderate or more social status from Benue (1.33), FCT (0.38), Niger (0.85), Rivers (0.31) to acknowledge vaccination centre.

The resultant of this is that only in Lagos we had a lower social status respondents who were able to list a COVID-19 vaccination centres (Lagos =-0.85) whereas most respondents finding it difficult to name a COVID-19 vaccination centres not to talk of two in other locations. It must be emphasized here that only those on high social status were able to acknowledge and list at most one: Benue (1.26, 1.69), FCT (0.38, 1.72), Lagos (-0.85, 0.64), Niger (0.88, 2.31), Rivers (0.32, 6.87), and combined (0.40, 1.87). This means, it was mostly possible for respondents in Lagos and FCT to list two centres than respondent in Benue to list just a centre, and most likely impossible for anyone to list two centres from Rivers!

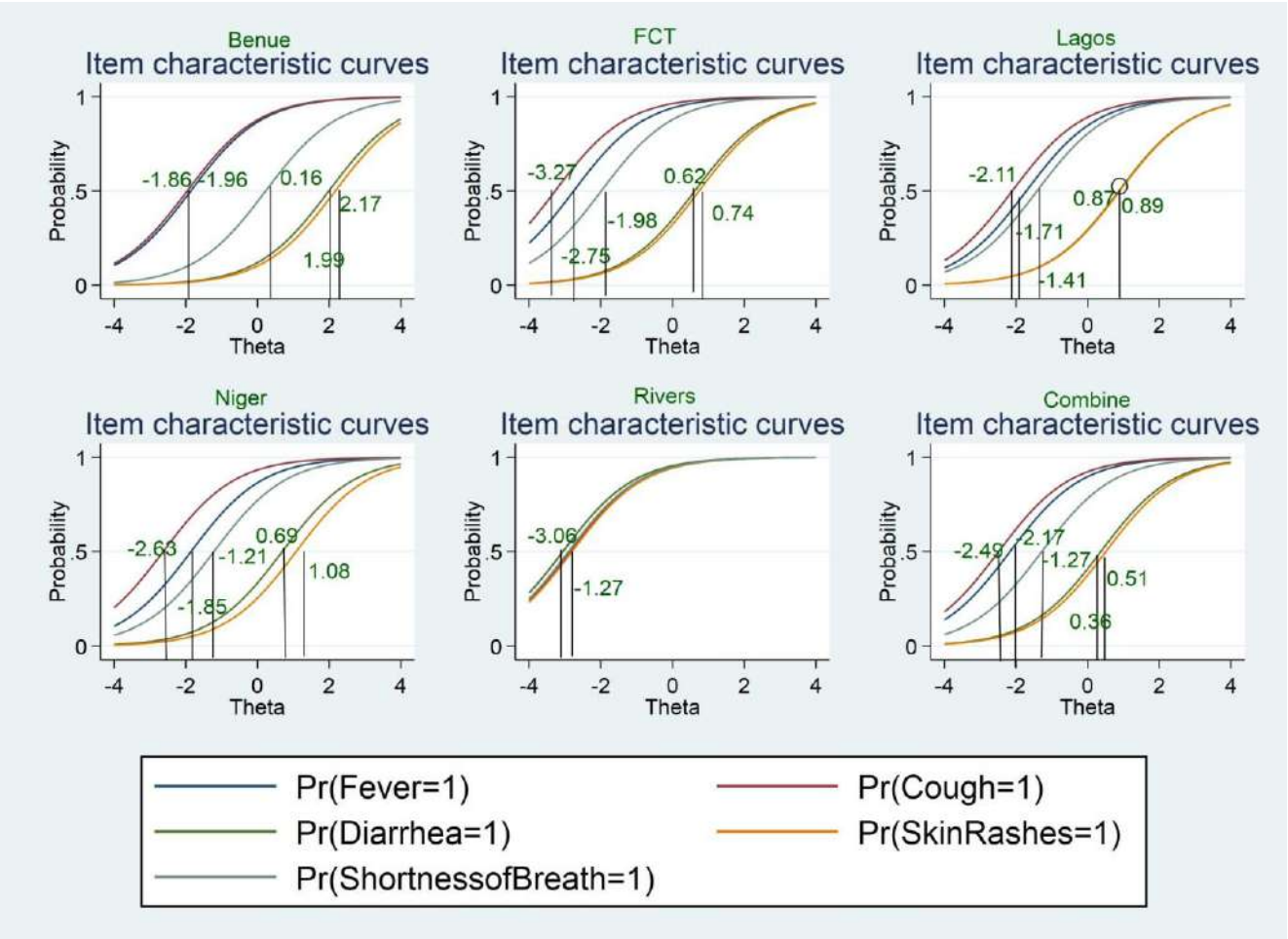

Figure 2: Some Symptoms of COVID-19 Acknowledged in Nigeria

5.2 On symptoms of COVID-19

The results in both Table 1 and Figure 2 show that at least lower social status respondents acknowledged different symptoms of COVID-19: Benue(-5.16), FCT(-4.68), Lagos(-3.10), Niger(-3.34), Rivers(3.55), combined (-3.69). A further breakdown of these symptoms revealed that at least lower social status respondents attested to Cough followed by Fever in Benue (-1.96,-1.86), FCT (-3.27, -2.76) , Lagos (-2.11, -1.71), Niger (-2.63, -1.85) Nigeria as a whole (-2.49, -2.16) Rivers (-3.06, -2.84). On the other-hand, only high social status respondents were able to acknowledge, diarrhoea, skin rashes/discolouration of the fingers and shortness of breath in Benue (2.17), FCT (0.74), Lagos (0.89) , Niger (1.08), except Rivers (-2.80). This call for more efforts to enable lower social status individuals to be aware of these symptoms.

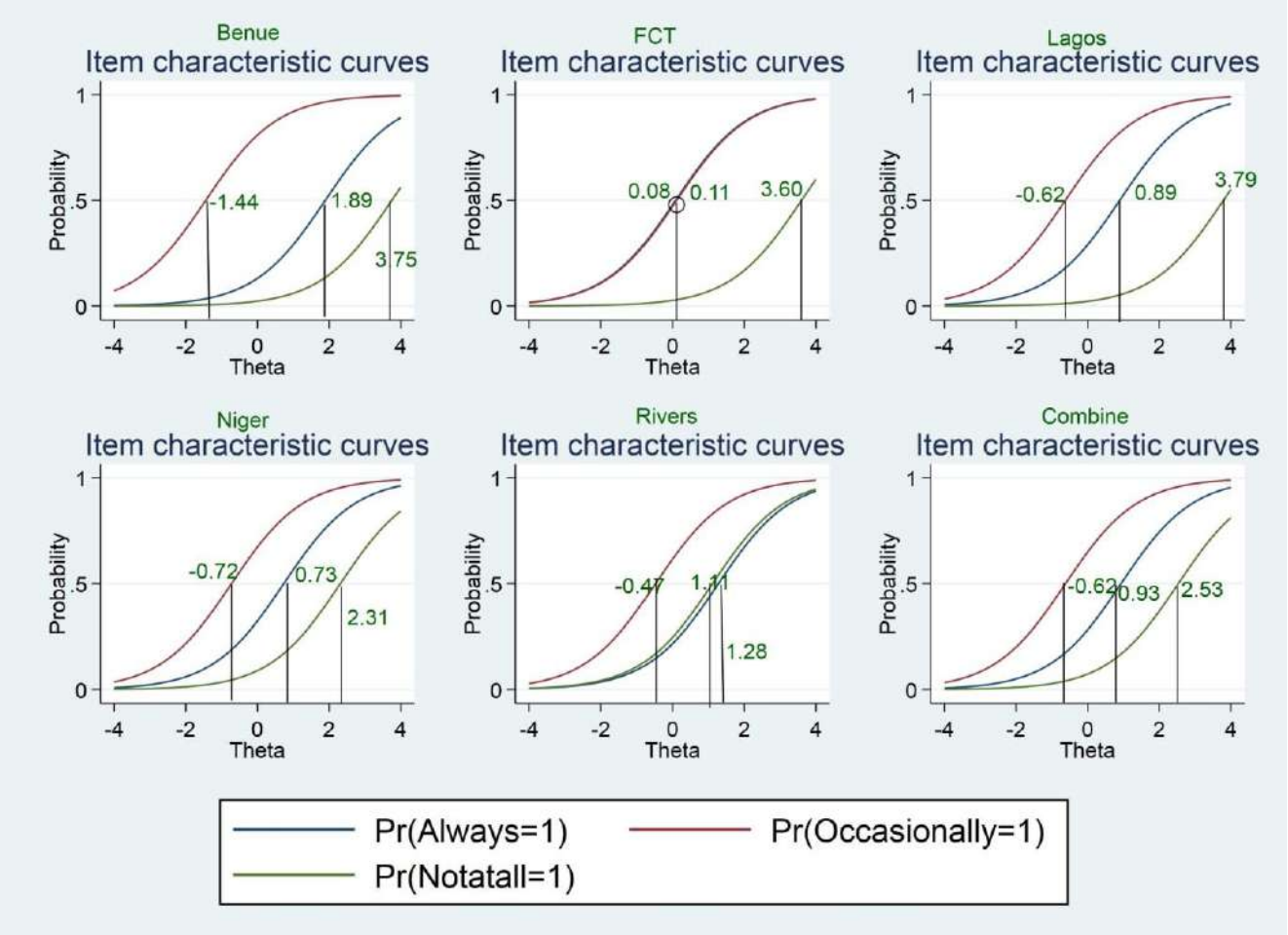

Figure 3: Usage of Face Mask in Nigeria

5.3 On the use of face mask

Our findings here show that most likely lower social status respondents aligned with the use of this non-pharmaceutical protocols (wearing of face mask): Benue (-3.15), FCT (-3.44), Lagos (-2.28), Niger (-2.10), Rivers (-3.19), and combined (-2.74) as fully displayed in Table 1. Unbundle wearing of face mask, we discovered that lower social status respondents occasionally wear face mask in public place as suggested in Figure 3, moderate social status respondents were always wearing face mask, and high social status respondents wear face mask not at all as non-pharmaceutical protocols in curbing transmission of COVID-19 pandemic.

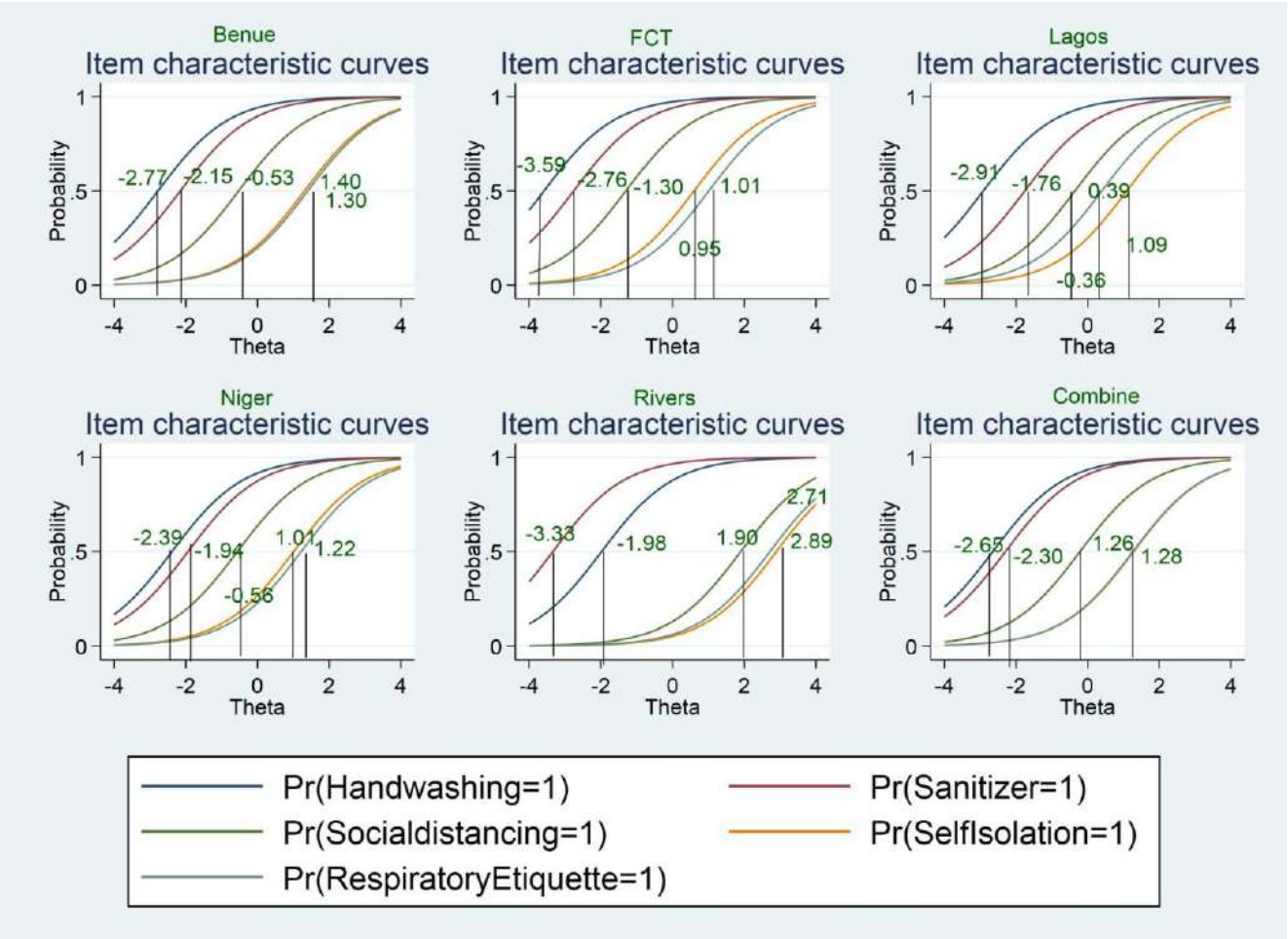

Figure 4: Practice of Non-Pharmaceutical Protocols in Nigeria

5.4 On the Practice of Non-pharmaceutical Protocols of COVID-19

The study discovered that lower social status segment of the respondents aligned with hand washing, sanitizer, and social distancing in that order. The scientific evidence abound as Benue (-2.78, -2.15 , -0.53), FCT (-3.59, -2.76, -1.30), Lagos (-2.91, -1.76, -0.36), Niger (-2.39,-1.94, -0.56), Rivers (-1.98 , -3.33, -1.90), Combine (-2.65, -2.30, -0.21); however, high social status respondents practised self-isolation, and respiratory etiquette as presented and displayed in Table 1 and Figure 4 respectively. On the other hand, scientific evidences also show that moderate, high, and higher social status respondents took first, second, and booster doses of the COVID-19 vaccines. Inferentially, lower social status respondents were less likely to take COVID-19 vaccine.

6 Conclusion

If awareness of COVID-19 testing, and vaccination centres together with vaccine acceptability were properly done among the lower social status individuals, it would be a key public strategy to reduce overall diseases burden due to COVID-19. Our study provides a retrospective insight

into the COVID19 awareness, symptoms, and vaccination; with results indicating that most likely lower social status may be willing to receive first, second, and booster doses of the vaccine if and only if there were much awareness of testing, and vaccination centres. The findings further revealed that vaccine acceptability differs on the basis of social status. There was vaccine acceptability among the high social status individuals; rather, greater work would be needed among lower status individuals to accept first, second, and booster doses of COVID-19 vaccine. These findings can help guide the planning, and development of future efforts to increase awareness of pharmaceutical intervention of COVID-19 vaccine.

Acknowledgement

We acknowledged the great efforts of our field workers, data collators in data acquisition, and the Tertiary Education Trust Fund, (TETfund) Nigeria with the award of the National Research Fund 2020 grant, reference number TETF/ES/DR&D-CE/NRF2020/SETI/82/VOL.1 to the research group which enabled us to team up and carry out this research work.

References

Adams, S. O., Bamanga, M. A., Olanrewaju, S. O., Yahaya, H. U. and Akano, R. O. (2020). Modeling COVID-19 Cases in Nigeria Using Some Selected Count Data Regression Models. *International Journal of Healthcare and Medical Sciences*, 6(4): 64 -73, doi: https://doi.org/10.32861/ijhms.64.64.73.

Adesina, O. S., Onanaye, S. A. Okewole, D. and Egere, A. C. (2020). Forecasting of New Cases of COVID-19 in Nigeria Using Autoregressive Fractionally Integrated Moving Average Models. *Asian Research Journal of Mathematics*, **16**(9):135- 146. DOI: 10.9734/ARJOM/2020/v16i930226.

Adetutu, O. M. and Lawal, H. B. (2020) On Comparisons of Frequents to Bayesian Estimation for Item Response Theory Models in the Presence of Dichotomous Response. *Journal of Science, Technology, Mathematics, and Education*, 16, 128-137. Available at: *https//:www.jostmed.futminna.edu.ng*

Adetutu, O. M. and Lawal, H. B. (2022). Applications of Item Response Theory Models to Assess Item Properties and Students' Abilities in Dichotomous Responses Items. *Open Journal of Educational Development* (ISSN: 2734-2050), **3**(1), 01-19. Available from *https://doi.org/10.52417/ojed.v3i/.304*

Akande-Sholabi, W. Adebisi, Y. A. The Impact of COVID-19 Pandemic on Medicine Security in Africa: Nigeria as a Case Study, *Pan African Medical Journal*, 2020, **35** (2) 73.

Baker, F. B. and Kim, S. H. (2004). Item Response Theory: Parameter Estimation Techniques (Second Edition). New York: *Taylor and Francis*.

Didi, E. I., Kingdom, N. and Harrison, E. E. (2021). ARIMA Modelling and Forecasting of COVID-19 Daily Confirmed and Death Cases: A Case Study of Nigeria. *Asian Journal of Probability and Statistics*, **12**(3): 59-80. DOI: 10.9734 /AJPAS/ 2021/v12i330289.

WHO, WHO Director-General's Opening Remarks at the Media Briefing on COVID-19 16 March 2020 [Internet], 2020 Mar [cited 2022 May 5]. Available from: https://web.archive.org/web/20200317011700/https://www.who.int/dg/speeches/detail/who-director-general-s-opening-remarks-at-the-media-briefing-on-covid-19—16-

World Health Organisation (WHO). Coronavirus Disease (COVID-19) Pandemic, 2020. Available at *https://www.who.int/emergencies/diseases/novel-coronavirus-2019*

World Health Organisation (WHO). Questions and Answers on Coronaviruses (COVID19), 2020.*https://www.who.int/emergencies/diseases/novel-coronavirus-*19/questions-an answers-hub/qa-*detail/q-a-coronaviruses* (Accessed on July 16 2020)

WHO, Operational Considerations for Case Management of COVID-19 in Health Facility and Community [Internet], 2020. Available from: https://web.archive.org/web/20200411165155/https://www.who.int/publications-detail/operational-considerations-for-case-management-of-covid-19-in-health-

Nigeria Centre for Diseases Control (NCDC), 2020, COVID-19 Nigeria. Available at: *https//covid19.ncdc.gov.ng/report/* (Accessed on June 8, 2022.)

Ogundokun, R. O., Lukman A. F., Kibria, G. B. M., Awotunde, J. B. and Aladeitan, B. B. (2020). Predictive modelling of COVID-19 confirmed cases in Nigeria. *Infectious Disease Modelling* 5 (2020) 543e548. https://doi.org/10.1016/j.idm.2020.08.003.

Folorunso, S. O., Awotunde, J. B., Banjo, O. O. Ogundepo, E. A., and Adeboye, N. O. (2021) Comparison of Active COVID-19 Cases per Population Using Time-Series Models. *International Journal of E-Health and Medical Communications*, **13**(2): 1–21, doi: 10.4018 /IJEHMC.20220701.oa 6

Ortese, C. E., Ieren, T. G. and Tamber, A. J. (2021). A Time Series Model to Forecast COVID-19 Infection rate in Nigeria Using Box-Jenkins Method. *Nigeria Annals of Pure and Applied Sciences*, **4**(1):75– 85. https//doi.org/10.46912/napas.232

Qiwei, L. (2022). Bayesian Analysis of Infectious Diseases: COVID-19 and Beyond. *The American Statistician*, **76**(2): 199-199, doi:10.1080/00031305.2022.2054625

Schneble, M., de Nicola, G., Kauermann, G. and Berger, U. (2021). A statistical model for the dynamics of COVID-19 infections and their case detection ratio in 2020. *Biometrical Journal, 63:1623*–1632. https://doi.org/10.1002/bimj.202100125.

Chigbu, B. C., Edikpa, E. C., Onu, E. A., Nwabueze, A. I., Aneke, M. C., Vita-Agundu, U. C. and Adepoju, E. B.(2021). Analysis and forecasting of confirmed, death, and recovered

cases of COVID-19 infections in Nigeria: Implications for University Administrators. *Medicine*, 100:31(e26776).

Lim, S. (2022). Review: A Course in Item Response Theory and Modelling with Stata, and Using R for Item Response Theory Model Applications. Structural Equation Modelling: *A Multidisciplinary Journal*, **27**(4), 657-659, doi: 10.1080/10705511.2020.1740886, Available from *https://doi.org/10.1080/10705511.2020.1740886*

Linden, A. (2018). Review of Tenko Raykov and George Marcoulides's A Course in Item Response Theory and Modelling with Stata. *The Stata Journal: Promoting Communications on Statistics and Stata*, **18**(2), 485–488, https://doi.org/10.1177/1536867X1801800213

Reiter, P. L., Pennell, M. L. and Katz, M. L. (2020) Acceptability of a COVID-19 Vaccine Among Adults in the United States: How Many People Would Get Vaccinated? *Vaccine*, 38, 6500-6507. Available at *https://doi.org/10.1016/j.vaccine2020.08.4*

Rasch, G. (1966). An Item Analysis Which takes Individual Differences into Account. *British Journal of Mathematics and Statistical Psychology*, 19, 49-57.

Raykov, T. and Marcoulides, G. A. (2018). A Course in Item Response Theory and Modelling with Stata. College Station, TX: Stata Press College Station.

Stroud, A. H. and Secrest, D. (1966) Gaussian quadrature formulas. Englewood Cliffs.

ADDENDUM

An Assessment of Nigeria's State of Preparedness in the Management and Control of Diseases, Epidemics and Pandemics in the Wake of the Corona Virus Pandemic

[1]Auwal Umar and [2]Okoh I. Simon Peter

[1]Department of Physical and Health Education, School of Science Federal College of Education (Technical), Gombe
[2]Department of Social Sciences and Humanities Education, School of General Studies Education Federal College of Education (Technical), Gombe

Abstract

A recurrent reality in the modern-day world has to do with the rise in the scale, magnitude and effects of diseases, epidemics and pandemics and their effects on the global economy. The globalization process has made this a source of worry as well for developing countries like Nigeria where, sadly, lapses abound in health management and preparedness for such huge impacts as the Corona Virus Pandemic threw to the fore with regards to the Nigerian experience. This paper investigates the state of readiness and preparedness of the Nigerian Polity for any future occurrences looking at health policies in that regard and budgetary allocations for such as well as the state of manpower resource in the health sector. Hinging upon the systems theory of analysis in the social sciences, the paper tries to show the need for greater and more purposeful devotion of attention to the management of diseases, epidemics and pandemics in Nigeria. Using data and statistics, the paper shows that lapses abound despite records of success and argues for more concerted government intervention towards preparing ahead for any exigencies in this area.

Key Words: Preparedness, Management and Control, Disease, Epidemic and Pandemic

Introduction

More than ever before in human history, the reality of living in a fast globalizing and consequently volatile world appears to have become more apt to keen observers. The world, as we know it today, has become, probably, more prone to exigencies and encumbrances (natural and manmade) that are capable of altering the socioeconomic lot of mankind, bringing about disequilibrium and inducing protracted anxiety on the populations. This has constituted a recurrent reality and challenge for the entire world, particularly, for developing spheres of the planet. Outbreaks of diseases such as HIV Aids (between 1970 and 1980s), Ebola (between 1979 and 1994 and between 2014 and up to January 2023), Marburg (in 1999 and 2000) in the republic of Congo, Angola between 2004 and 2005), Zika (1960s to the 80s, and 2016 to 2017), and the Corona Virus Pandemic, which brought the world to a standstill literally, are but some notable experiences that have tested the strength of health institutions and governments globally besides triggering anxiety. Not only did these incapacitate governments but induced stressful conditions and experiences on people globally; most especially in the developing spheres.

The Nigerian state has had its fair share of the hit too particularly as lives were lost, the state of readiness of the country's health care delivery system was tested and stretched, businesses were shut

down and many never recovered nor resurfaced in its aftermath. Sources of livelihoods were disrupted and income and wealth creation and generation took a dive down south statistically too. These generated worry and mental health conditions for a lot of Nigerians particularly in the non-formal sector which according to (BOI, (2022) constitutes economic activities and sources of income that are not fully regulated by the government and other public authorities. This sector accounts for 92.3% of the country's labor force, in contrast to about 8% in the formal sector (Falaiye, 2023). Obviously, the former would, naturally, be more affected and thrown off balance by the situation and its consequences. The Nigerian government responded and indeed rose to the occasion of making attempts to contain and salvage the situation. through lock down measures to curb the spread and transmission of the virus by people, awareness creation measures, testing and tracing of suspected cases for isolation, creation of isolation centers for quarantining and treatment of infected persons among other efforts.

The COVID 19 Pandemic and its Effects on the Nigerian Polity

The coronavirus disease gained spotlight in 2019. Its cause has been traced to "…Severe Acute Respiratory Syndrome Virus 2; S.A.R.S.-CoV-2" (W.H.O., 2020) and it was first reported in December of the year 2019 by Health Authorities in China following an outbreak of pneumonia of unknown origin in Wuhan, Hubei Province (Li, 2019). The disease appears to be of zoonotic origin and is similar to S.A.R.S. as well as the Middle East Respiratory Syndrome (M.E.R.S.). It is transmitted between humans through respiratory droplets and fomites (Patel, 2020). The World Health Organization (W.H.O.) declared it a Public Health Emergency of International Concern on January 30, 2020 (Jee, 2020) as it spread to more countries and became a cause of escalating, devastating human mortality rates. It was declared a pandemic by the WHO on March 11, 2020 with calls for urgent and aggressive action to contain and reduce its spread (Cucinotta and Vanelli, 2020), (W.H.O., 2020); a call the Nigerian government wasted no time in heeding.

Nigeria's status as the most populous country in Africa and the sixth most populous nation in the world makes the country a significant focal point given the prediction at the onset of the pandemic that it would affect the African continent drastically (World Economic Forum, 2021) and given the fact that the country's was facing this challenge in the context of a polity with an ailing health delivery system in dire need of resuscitation and repositioning for greater efficiency coupled with a fragile economy just emerging from a period of economic recession as well as socio-economic, political and security concerns. Fortunately, for the Nigerian government, the country had, in 2014, been given a wakeup call by the Ebola epidemic experience which created room for the sensitization of its health system, creating some level of awareness for the government and communities with regard to the realities of highly infectious diseases in a fast globalizing world and the need to prepare ahead proactively for future occurrences (Shuaib 2014).

Four years later, the World Health Organization undertook a joint external evaluation of International Health Regulations core capacities in 2017 to assess the capacities of countries to prevent, detect and

respond to public health risks. In the areas of prevention and response. Nigeria scored poorly in the areas of response and prevention (Dixit 2020). This source notes that Nigeria's average score of 1.9 across fifteen Joint External Evaluation (JEE) indicators in the 'prevent' category is suggestive of limited capacity to prevent biological, chemical or radiation health risk. Again, in the 'detect' category, across 13 indicators, Nigeria's average score was 2.6 suggesting development of some capabilities to detect new health risks through real time surveillance as well as laboratory capacities to test the diseases. However, as this source concurs, the sustainability of these capacities is still in doubt. The country, as this source shows, performed badly as well, in the 'respond' category with an average score of 1.5 across 20 indicators indicating limited capacity to respond to sudden health risk. It is important, given the recurrent nature of outbreak of diseases in recent times and proneness of the developing world to be caught off guard by such exigencies, for governments to put in place measures, systems and requisite infrastructures that would serve as deflectors that could reduce initial impacts and give the governments some form of leverage and strategic advantage in terms of power to act effectively. If the World Health Organizations results from its evaluation of Nigeria's state of preparedness to deal with and manage outbreaks is anything to go by, it leaves room for concern and worry as the data below alludes.

Figure 1. Nigeria's Average Score on Preparedness to Tackle Public Health Risk

These realities, probably, gained expression in the face of the COVID 19 pandemic in Nigeria. It is worthy of mention as well that experiences of persistence outbreaks that could be regarded as epidemics such as Lasa fever outbreaks as well as diphtheria outbreaks (Chukwuma (2023). Prevention, Detection and Response in the case of COVID-19 were areas fraught with challenges that overwhelmed the Nigerian healthcare delivery system. It was almost impossible to prevent spread of the virus as movement and transmission defied the lockdown measures and could only be barely reduced. Though the government continued to provide information daily on new cases and increment in infection and deaths and to create awareness, it is doubtful if prompt and concise detection of cases was the case given the preexisting situation of adequate data, access to and availability of health related facilities and infrastructure among others. The response system was probably the most appalling as many Nigerians were not even open to accepting the scourge as a reality let alone subjecting themselves to being identified by calling the lines provided by the government which, could be argued, were not to be fully patronized. Besides, there were general complains of poor response from the N.C.D.C. response mechanism.

The Nigerian government appears to be contented with the status quo. The Nigerian government, through its NCDC director and chief executive officer has assured that the country is ready and prepared to prevent, contain next pandemic (Chukwuma, 2023) asserting that progress has been made setting the nation ahead of its pre-pandemic reality. Some notable areas of progress according to this source include 1) Stepping up the number of laboratories with diagnostic capacity for COVID -19 in the country from the previous 3 to 200 laboratories (public and private) within our network that can be activated in the event of an emergency. 2) Developing regional laboratories to decentralize the

reference laboratory system. 3) Establishment of a digitalized surveillance network through Surveillance Outbreak Response Management and Analysis System (SORMAS), 'SitAware' and other tools in all local governments that help accelerate reporting. 4) Training of disease notification officers (DNOs) in all the states of Nigeria through the Regional Disease Surveillance Systems Enhancement (REDISSE) project, and building a strong frontline of public health workers at subnational level for surveillance through Integrated Training of Surveillance Officers in Nigeria (ITSON). The presence of more public health emergency operations centers (PHEOCs) enabling coordination of response to public health threats (from the twenty-nine nationwide pre-pandemics statue to 35 across the states and the FCT. This government assures that Nigeria also has an adequately trained workforce to respond in case of public health events and more treatment and isolation centers facilitating improved case management during outbreaks. Perhaps, the emergence of a Centre for Disease Control (CDC) given requisite might and wherewithal by the government for enhanced diagnostic and surveillance capacity in the country added more tenacity to the countries preparation for future exigencies given the role the CDC played during the Pandemic.

In 2022, the Nigerian Health minister alluded to the fact that Nigerian doctors were migrating from the country but asserted that Nigeria had enough doctors suggesting that the percentage of doctors leaving was not a threat. Prior to this, in 2019, the government, via its minister for labor and employment asserted that there were enough doctors in Nigeria suggesting that the percentage leaving were out of the surplus the country has.

The Systems theory of Analysis

The 'Systems Theory' is a multidisciplinary approach that sees complex entities as systems of interconnected parts. This can refer to organizations and societies. The key principle is that no part can be understood in isolation from the whole. Change in one part will inevitably lead to change in other parts of the system.

The Nigerian Healthcare Delivery System operates within a system and is a component of an entire system. This is probably why matters of healthcare and health related challenges fall within its purview and constitute its area of jurisdiction. It is the sector of the Nigerian system charged with the responsibility of seeing to it that health care and health security related challenges are addressed effectively. Failure of this sub system will affect and clog the wheel of progress for the entire system as this will affect the very indices that constitute its labor force and have an effect of slowing down and reducing productivity. This subsystem cannot function meaningfully without requisite input to galvanize it by the system it functions for and thus the interrelatedness that needs to be understood. A correlation therefore exists between the Government and the health care delivery sector.

The country's healthcare system based on a three-tier system care comprising of 1.) the Primary Health Care (PHC) which operates at the community level and is the first point of contact for patients, 2.) the

Secondary Health Care which is an intermediate healthcare level and 3.) the Tertiary Health Care which is at the federal healthcare level, and the Federal Ministry of Health which is responsible for policy making, technical support, national health management, health services delivery (Pharmchoices, 2024). The government remains a cardinal factor for the stimulation of the sector for preparedness and effectiveness in Nigeria

The Nigerian healthcare system appears to be weak and in dire need of concerted fortification for even more effective health care delivery let alone readiness for another pandemic. It was ranked 187thout of 195 countries on a global health care index in terms of healthcare delivery in 2018 (Odubola, 2018). Five years later, the country ranked **157th** Best Health System in the World Published (Owoyele, 2023). The pandemic stretched the health system grimly culminating in severe decline in services and their related qualities rendered in the hospitals. Some of the facility units / departments were temporarily closed due to COVID-19 pandemic.

In Nigeria, most patients fund their medical care out of their earnings unlike the advanced countries where insurance schemes and taxes take care of such needs. The National Health Insurance Scheme (NHIS) which is also a positive health care delivery development in Nigeria, does not cover the totality of health care needs nor does it cover the health insurance of most of the population. (Pharmachoices, 2024). The healthcare system in Nigeria suffers from lack of proper health funding and investment it observes that the government commits about 5% of the budget to health. Nigeria's ranking by the World Health Organization based on the quality of the medical system and health care delivery is low; 156th out of 191 countries.

Problems such as access to quality health care (affordability and quality of service), Health care delivery infrastructure (availability of quality infrastructure in hospitals) and hospital standards, quality of emergency response services in health care delivery, the issue of skills, education and knowledge (training and opportunities for career development while in service), insurance of health workers and practitioners in the healthcare delivery sector, financial incentives and rewards for doctors and practitioners in the healthcare delivery sector as well as funding and adequate access to funds remain major areas where challenges continue to hamper readiness and preparedness for greater effectiveness of health care delivery in Nigeria. (CcHUB 2014).

In recent times, particularly in the aftermath of the pandemic, there has been mass exodus of medical practitioners from the Nigerian polity to other climes and economies deemed to be more rewarding than Nigeria. A research survey sustains that eighty-eight percent of Nigerian doctors are considering work opportunities abroad (Ihua, 2017). This source reveals destinations and the percentages of medical practitioners from Nigeria to each such as the United Kingdom (93%), the United States of America (86%) Canada (60%), Saudi Arabia (59%), Australia (52%) UAE (Dubai) (29%), The Caribbean Islands (17%), Ireland (15%)and South Africa (4%). This source cites issues such as poor salary emoluments, lack of proper infrastructure, low work satisfaction, huge knowledge gap, high taxes and deductions from salaries, poor quality of practice, inadequate opportunities for career

progression, poor working environment and poor treatment by government. (Ihua, 2017). In November 2021, the Nigeria Medical Association (NMA) President noted that current doctor to population ratio in the country was about one doctor to between 4,000 and 5,000. Data from the World Health Organization shows that Nigeria has more doctor-population ratio than many African countries (I.C.I.R., 2022) asserting that in every ten thousand Nigerians, there are three hundred and seventy medical doctors (Motolani,2024). However, a ratio of four doctors to attend to 10,000 people is the observed ratio according to ICIR, (2022) reports for Nigeria noting that the trend has remained so in the past two decades. This source, citing W.H.O. records, reports that in 2003, a ratio of (2.6) doctors attending to 10,000 people was the case and observes that this figure peaked at 4.49 in 2016 and 3.81 in 2018. Ironically, W.H.O. data on global doctors' population among countries reveal that some African nations have more doctors to attend to their population than Nigeria. (ICIR, 2022). The United Nations and the WHO recommended one physician to 600 persons. WHO reports suggest that any country with fewer than 10 doctors per 10,000 people could be described as having an "insufficient" number of healthcare professionals. This would mean Nigeria, for its 226.9 million citizens, would need 198,000 doctors to move out of the "insufficient" bracket. These findings contradict the assertion that Nigeria has enough doctors as the former Health and Labor / Employment ministers would have Nigerians believe.

Recommendations

No people centered government and ideal democracy sleeps over security related issues bothering the polity and health security remains one of such security challenges the Nigerian government cannot afford to play politics with. The Nigerian government has taken notable steps on the ladder of preparation and being prepared but must not be contented or deceived to believe it is ready yet. The nature of pandemics has been that of being caught unaware, the need to understand causal factors which always takes time, the need to trace contain and quarantine infected persons to avoid further contagion and spread and these are areas where even the developed countries still have to contend and struggle. The Nigerian government must work even harder to;

1. Consolidate on lessons learnt thus far from the COVID 19 pandemic and related experiences to prepare for future occurrences via increased surveillance and monitoring even at peace time. The rankings and findings in the postulations and reports of international bodies should be a source of worry and concern for the Nigerian government. The need for synergy with other advanced nations in terms of discerning more effective best practices cannot be overemphasized.

2. There is need for greater health care delivery infrastructural development; the provision of larger and more accessible health care facilities equipped with diagnostic capacities at all the three levels with experts on ground manning these stations as much as possible. Most of our healthcare delivery points are grossly ill equipped for the business of healthcare delivery and are bereft of basic facilities for the achievement of their goals and objectives.

3. Effective policy implementation and requisite funding remain areas that must be wrenched from politicization and mismanagement. Government cannot afford to leave this totally to the private sector given the fact that our economy is not an ideally capitalist one yet nor can it be said to be ready for capitalist practices of that sort.

4. The issue of non-availability of medical practitioners and technicians due to migration must be addressed and stemmed. Even among the remnant of medical practitioners left in the country, a great percentage will not hesitate to opt to leave for more rewarding climes if given the opportunity. This is not only a problem affecting the health sector. Even the teachers and educational institutions training and preparing these doctors are losing their bests to these other climes too begging the question of quality of the crop of future generations of medical practitioners in the country. The remuneration and reward system must be reviewed and addressed to have some degree of semblance with what other nations benefit and this is not impossible for Nigeria given the billions been stolen and looted by political elites and yet the country still thrives.

Summary and Conclusion

Government has embarked on drastic measures in times past to intervene and stem the challenge of disease outbreaks and epidemics and rose to the challenge of mitigating the COVID-19 Pandemic. However, evidence shows that cannot be said to have gotten to the point of declaring itself prepared as findings allude and speak to the contrary seriously. It is still too early to suggest that the country has done enough to declare the Nigerian polity ready to manage, prevent or contain any other possible outbreak in the manner touted by the governments representatives and in the manner they have asserted. The issues raised and highlighted above abound and continue to remain prevalent realities the nation must deal willingly, purposefully and decisively with in the spirit of people centeredness as a quality of good governance and good will towards the population.

References

Bank of Industry (2022). Economic Development Through Nigeria's Informal Sector; A BOI perspective. https://www.boi.ng/

Cucinotta D, Vanelli M. (2020). WHO Declares COVID-19 a Pandemic. Acta Biomed. doi: 10.23750/abm.v91i1.9397. PMID: 32191675; PMCID: PMC7569573.

Chukwuma M. (2023) Nigeria prepared to prevent, contain next pandemic, NCDC boss says. https://guardian.ng/features/health

Dixit S., Ogundji Y.K., Onujekwe O. (2020) How well has Nigeria Responded to COVID-19? https://www.brookings.edu/articles

Centre for Democracy and Development (CDD) (2022) Fact Check: Are There Enough Doctors I in Nigeria as Health Minister Ehanire Claimed? https://dailytrust.com

Falaiye H. (2023). Experts decry High Informal Employment Rate. in the Punch Newspaper online. 13 /09/2023. https://punchng.com/

Ihua B. (2017) Emigration of Nigerian Medical Doctors. DOI:10.13140/RG.2.2.31532.77440 www.researchgate.net/publication/319546816

International Centre for Investigative Reporting (ICIR) (2022) Four Doctors to 10,000 Population, Nigeria's highest in two decades – Data. https://www.icir.nigeria.org

Jee Y. (2020). WHO International Health Regulations Emergency Committee for the COVID-19 Outbreak. Epidemiol Health. doi: 10.4178/epih.e2020013. Epub 2020 Mar 19. PMID: 32192278; PMCID: PMC7285442.

Journal of Global Health. (2020). Nigeria's public health response to the COVID-19 Pandemic: January to May 2020. Published online 2020 Oct 26. doi: 10.7189/jogh.10.020399

Motolani A. (2024). WHO says there are 370 medical doctors in every 10,000 Nigerians. https://www.pulse.ng

Odubola I. (2018). Nigeria's health care system ranks 187th globally https://businessday.ng/health/article

Owoyele T. (2023). Nigeria Ranked Country with 157th Best Health System in the World. Foundation for Investigative Journalism https://www.fij.ng/article

Patel A, Jernigan DB, Abdirizak F, Abedi G, Aggarwal S, Albina D. (2020) Initial Public Health Response and Interim Clinical Guidance for the 2019 Novel Coronavirus Outbreak - United States, **MMWR Morb Mortal Wkly Rep**. 2020;69:140- 6. 10.15585/mmwr.mm6905e1

Shuaib F, Gunnala R, Musa E, Mahoney F, Oguntimehin O, Nguku PM. (2020). Epidemiological Profile of the Ebola Virus Outbreak in Nigeria July September 2014

The Pan African Medical Journal, 31 (2015) https://doi.org/10.11604/pamj.2015.21.331.5834 PMID: 26587177 PMCID: PMC4633745

World Health Organization. (2020). Naming the coronavirus disease (COVID-19) and the virus that causes it. https://www.who.int

World Health Organization. (2020) Report of the W.H.O. China Joint Mission on Coronavirus Disease 2019 (COVID-19). Geneva, W.H.O.

World Health Organization. (2020) WHO Director-General's opening remarks at the media briefing on COVID-19, Geneva, W.H.O. https://www.who.int/dg/speeches/

The Effect of a Source Term Inflow and Shockwaves Evaluation of Traffic Flow Model for a Single-Lane Highway

A. Hamisu[1] and D.M. Auwal[2]

[1,2]Department of Mathematics and Statistics, Umaru Musa Yar'adua University Katsina, Katsina State-Nigeria.

Email Address: hamisuaminu2015@gmail.com

Abstract

This paper, studies macroscopic traffic flow based on the Lighthill-Whitham-Richard Model. The study investigates the Effect of a Source Term Inflow and Shockwaves Evaluation on Traffic Flow Model for a Single-lane Highway. The paper also studies Explicit Upwind difference schemes for solving first order Partial Differential Equations based on macroscopic traffic flow model appended with initial and boundary conditions. The Traffic Flow Model with a single Source Term had been modified to include a Shockwave Speed term which produces some noise with regards to the existing model and assisted in the evaluation of the shockwaves. The method of characteristics was used to solve the non-linear partial differential equation. The Lighthill-Whitham-Richard Model combined with the velocity-density relationship were used to obtain the analytical and numerical solutions. The model is treated as an Initial Boundary Value Problem and the numerical solutions are change to an Explicit Upwind difference scheme. We visualize the effect of the dissipation term employed in the model and evaluate the shockwave speed by different maximum velocity considerations. The stability and physical constraint conditions of the scheme were also established. MATLAB Software is used to carry out numerical simulations for various traffic parameters for the implementation of the explicit upwind difference scheme. The model revealed a good rate of convergence in L1 norm which is quite acceptable.

Keywords: Difference scheme, Explicit Upwind, Macroscopic traffic flow model, Shockwaves, Source term.

INTRODUCTION

Most problems of physical sciences are modelled as differential equations before they can be solved. Most interesting and physically relevant real world problems are difficult to solve analytically. An alternative method is by using computers to find approximate solutions.

Traffic flow is a physical phenomenon that is extremely complicated to model mathematically. Nevertheless, traffic flow problem is one that we cannot avoid, but rather we find a solution to, by developing a mathematical model.

Due to rapid growth in the world's population, the rise in traffic congestion among towns and cities in the urban areas across the globe has become a mighty challenge to traffic engineers.

Since the beginning of the twentieth century, many researchers started to think of a mathematical model that can describe the behavior of traffic flow in urban areas. There have been two approaches in the formulation of the mathematical model of traffic flow. The first one is the microscopic view, which

studies the single movement of vehicles and the interactions between vehicle pairs. The other approach studies the macroscopic features of traffic flow such as flow rate q, traffic density k and travel speed v. The basic relationship between the three variables is $q = vk$.

The pioneers of this concept were (Lighthill and Whitham, 1955) and separately (Richard, 1956). They were the first ones to describe traffic flow with equations coming from fluid dynamics, Usinga nonlinear hyperbolic partial differential equation (PDE) popularly known as the continuity equation and is written as;

$$\frac{\partial k(x,t)}{\partial t} + \frac{\partial q(x,t)}{\partial x} = 0 \qquad 1.0$$

where x denotes the spatial co-ordinate in the direction of the traffic flow, t is the time, k is the density and q denotes the flow rate. Also adding a dissipation and shockwave velocity terms as proposed by Saxena and Jain (2017) equation 1.0.1 becomes;

$$\frac{\partial k(x,t)}{\partial t} + \frac{\partial q(x,t)}{\partial x} = v_s + \beta(t,x,k) \qquad 1.1$$

2.0 METHODOLOGY

The LWR model (Lighthill and Whitham, 1955, Richard 1956) describe the traffic flow model using the concept of dynamic difference equation such that the law of the conservation of the vehicles in traffic can be written as;

$$n(x)\frac{\partial k(x,t)}{\partial t} + \frac{\partial q(x,t)}{\partial x} = 0 \qquad (2.1)$$

where

q=$kv(k)$: Traffic density in vehicles per lane per kilometer at location x and at time t.

$n(x)$: The number of lanes at position x.

$q(x,t)$: The traffic flow (traffic intensity) in vehicles per hour at location x and at time t.

The variables $k(x,t)$ and $q(x,t)$ are continuous functions of space and time. The equation expresses the physical principles of the traffic flow.

$$\frac{\partial k}{\partial t} + \frac{\partial (kv(k))}{\partial x} = v_s + \beta(t,x,k) \qquad (2.2)$$

where

$\beta(t,x,k)$is the source term denoting inflow or outflow in a particular location of a single-lane highway and v_s is the shockwave speed propagating along the road sections. To avoid complexity of this model, we consider $\beta(t,x,k)$as a constant and equation (2.2) become;

$$\frac{\partial k}{\partial t} + \frac{\partial (kv(k))}{\partial x} = v_s + \beta \qquad (2.3)$$

We adopt the velocity-density relationship as formulated by Greenshields (1935) given by:

$$v(k) = v_{max}\left(1 - \frac{k}{k_{max}}\right) \qquad (2.4)$$

where v_{max} is the maximum velocity and k_{max} is the maximum density of the road. Incorporating the linear velocity – density relationship (2.4) in (2.3), we obtain the specific first order non-linear partial differential equation of the form:

$$\frac{\partial k}{\partial t} + \frac{\partial}{\partial x}\left[kv_{max}\left(1 - \frac{k}{k_{max}}\right)\right] = v_s + \beta \qquad (2.5)$$

Multiplying k through the bracket in (2.5) above we obtain

$$\frac{\partial k}{\partial t} + \frac{\partial}{\partial x}\left[v_{max}\left(k - \frac{k^2}{k_{max}}\right)\right] = v_s + \beta \qquad (2.6)$$

In this paper, we investigate the traffic equation (2.6)

3.0 Analytical solution of the model

The non-linear PDE (2.6) can be solved if we know the traffic density at a given initial time, that is, if we know the traffic density at a given time t_o ,we can predict the traffic density for all future time $t \geq t_o$. We then need to solve an initial value problem of the form:

$$\frac{\partial k}{\partial t} + \frac{\partial}{\partial x}\left[v_{max}\left(k - \frac{k^2}{k_{max}}\right)\right] = v_s + \beta \quad (3.1)$$

$k\,(x,t_o)=k_o\,(x)$

We now use method of characteristics to solve the IVP (3.1) as follows

The PDE in (3.1) can be written as;

$$\frac{\partial k}{\partial t} + \frac{\partial q(k)}{\partial x} = v_s + \beta,$$

Where $q(k) = v_{max}\,(k - \frac{k^2}{k_{max}})$ *and* $v_s = \frac{(qb - qa)}{(kb - ka)}$

a and b are the upper and lower boundaries of the road section, $a \leq x \leq b$.

$$\frac{\partial k}{\partial t} + \frac{\mathrm{d}q}{\mathrm{d}k}.\frac{\partial k}{\partial x} = v_s + \beta$$

$$q'(k) = v_{max}\left(1 - \frac{2k}{k_{max}}\right)$$

$$\frac{\partial k}{\partial t} + v_{max}\left(1 - \frac{2k}{\rho_{max}}\right)\frac{\partial k}{\partial x} = v_s + \beta$$

Again $\frac{\mathrm{d}k}{\mathrm{d}t} = \frac{\partial k}{\partial t} + \frac{\mathrm{d}x}{\mathrm{d}t}.\frac{\partial k}{\partial x} = v_s + \beta$

$$\frac{\mathrm{d}x}{\mathrm{d}t} = v_{max}\left(1 - \frac{2k}{k_{max}}\right) \quad (3.2)$$

$$\frac{\mathrm{d}k}{\mathrm{d}t} = v_s + \beta \quad (3.3)$$

By integrating equation (3.3) we obtain

$$\int \mathrm{d}k = \int (v_s + \beta)\,\mathrm{d}t$$

$$= \int \boldsymbol{v_s} dt + \int \beta\,\mathrm{d}t$$

$$k(x,t) = v_s t + \beta t + c_1 \quad (3.4)$$

Where $c_1$is the constant of integration, then putting $t = 0$ and $x = x_0$ in equation (3.4) we have;

$$k_o(x_o) = k\,(x_o, 0) = v_s(o) + \beta(o) + c_1$$

$$\therefore c_1 = k_o\,(x_o)$$

Now, substituting $c_1$in equation (3.4), we have;

$$k(x,t) = v_s t + \beta t + k_o\,(x_o) \quad (3.5)$$

Also by integrating equation (3.2) we have;

$$\frac{\mathrm{d}x}{\mathrm{d}t} = v_{max}\,(1 - \frac{2k}{k_{max}})$$

$$\int \mathrm{d}x = \int v_{max}\,(1 - \frac{2k}{k_{max}})\,\mathrm{d}t$$

$$x(t) = v_{max}\left(1 - \frac{2k}{k_{max}}\right)\int dt$$

$$\therefore x(t) = v_{max}\left(1 - \frac{2k}{k_{max}}\right)t + c_2 \quad (3.6)$$

Where $c_2$is the constant of integration. Also putting t=0, equation (3.6) becomes:

$$x(t) = v_{max}\left(1 - \frac{2k}{k_{max}}\right)t + x_o \quad (3.7)$$

Therefore equation (3.7) is referred to as the characteristics curve of the initial value problem (IVP) in equation (3.1) above.

Now from equation (3.7)

$$x_o = x(t) - v_{max}\left(1 - \frac{2k}{k_{max}}\right)t \quad (3.8)$$

Then substituting equation (3.8) in (3.5) we have,

$$k(x,t) = v_s t + \beta t + k_o\left(x - v_{max}\left(1 - \frac{2k}{k_{max}}\right)t\right) \quad (3.9)$$

4.0 Numerical Solution using Explicit Upwind Difference Scheme

In this section, we consider a finite difference scheme for the non-linear LWR traffic flow model. In order to develop the Explicit Upwind Difference Scheme (EUDS), we consider our specific non -linear traffic flow model problem as an initial boundary value problem (IBVP):

$$\frac{\partial k}{\partial t} + \frac{\partial q(k)}{\partial x} = v_s + \beta\ ,\ t_o \le t \le T,\ a \le x \le b \quad (4.1)$$

with initial condition$k(to, x) = k_o(x_o),\ a \le x \le b$

and boundary condition$k(t, a) = k_a(t),\ t_o \le t \le T$

Since, we only consider a single-lane for our specified length of the road, therefore, a one sided boundary condition is used so that the density of the vehicles will move with respect to the time 't' along the section 'a' of the highway.

where

$$q(k) = v_{max}\left(k - \frac{k^2}{\rho_{max}}\right) \quad (4.2)$$

Finite difference methods provide efficient approach to numerical solutions of partial differential equations (PDE). The finite difference method proceeds by replacing the derivatives in the partial differential equation by the finite approximation.

To develop the scheme, we discretize the space and time. We discretize the time derivative $\frac{\partial k}{\partial t}$ and space derivatives $\frac{\partial q}{\partial x}$ in the (IBVP) (4.1) at any discrete point(t^n,x_i) for i= 1,2,3,…M and n= 0,1,2,…….N-1.We assume the uniform grid spacing $t^{n+1} = t^n + g$ and $x_{i+1} = x_i + h$. The discretization of $\frac{\partial k}{\partial t}$ is obtained by first order forward difference in time and the discretization of $\frac{\partial q}{\partial x}$ is obtained by first order backward difference in space.

5.0 Forward Difference (FD) in Time:

From the Taylor's series expansion, we can write;

$$k(x, t+g) = k(x,t) + g\frac{\partial k}{\partial t} + \frac{g^2}{2!}\frac{\partial^2 k}{\partial t^2} + \ldots \quad (5.1)$$

$$g\frac{\partial k}{\partial t} = k(x, t+g) - k(x,t)$$

Dividing both sides by g wehave,

$\frac{\partial k}{\partial t} = \frac{k(x,t+g) - k(x,t)}{g} + 0(g)$

$\frac{\partial k}{\partial t} \approx \frac{k(x,t+g) - k(x,t)}{g}$

$\therefore \frac{\partial k(t^n, x_i)}{\partial t} \approx \frac{k_i^{n+1} - k_i^n}{\Delta t}$ (5.2)

where $g = \Delta t$

6.0 Backward Difference (BD) in Space:

From Taylor's series expansion we can write;

$q(x-h,t) = q(x,t) - h\frac{\partial q}{\partial x} + \frac{h^2}{2!}\frac{\partial^2 q}{\partial x^2} - \ldots\ldots$ (6.1)

$h\frac{\partial q}{\partial x} = q(x,t) - q(x-h,t)$

dividing both sides by h, we have

$\frac{\partial q}{\partial x} = \frac{q(x,t) - q(x-h,t)}{h} + 0(h)$

$\frac{\partial q}{\partial x} = \frac{q(x,t) - q(x-h,t)}{h}$

$\therefore \frac{\partial q(t^n, x_i)}{\partial x} \approx \frac{q_i^n - q^n{}_{i-1}}{\Delta x}$ (6.2)

Inserting (5.2) , (6.2) in (4.1) and substituting k_i^n for $k(t^n, x_i)$, the discrete version of the non-linear PDE formulates the first order explicit upwind difference scheme of the form:

$\frac{k_i^{n+1} - k_i^n}{\Delta t} + \frac{q(k_i^n) - q(k^n{}_{i-1})}{\Delta x} = v_s + \beta$

$\frac{k_i^{n+1}}{\Delta t} - \frac{k_i^n}{\Delta t} + \frac{q(k_i^n) - q(k^n{}_{i-1})}{\Delta x} = v_s + \beta$

$\frac{k_i^{n+1}}{\Delta t} = \frac{k_i^n}{\Delta t} + (v_s + \beta) - \frac{1}{\Delta x}[q(k_i^n) - q(k^n{}_{i-1})]$

Multiplying both sides by Δt, we have

$k_i^{n+1} = k_i^n + (v_s + \beta)\Delta t - \frac{\Delta t}{\Delta x}[q(k_i^n) - q(k^n{}_{i-1})]$ (6.3)

Where $q(k_i^n) = v_{max}\left(k_i^n - \frac{(k_i^n)^2}{\rho_{max}}\right)$ (6.4)

7.0 Stability and Physical Constraint Condition

The implementation of the EUDS scheme is not straight forward. Since vehicles are moving in only one direction, so the characteristics speed $\frac{\partial q}{\partial x}$ must be positive. Therefore, one needs to ensure the well-posedness (physical constraint) condition:

$q'(k_i^n) = v_{max}\left(1 - \frac{2k_i^n}{k_{max}}\right) \geq 0$ (7.1)

Since the maximum velocity $v_{max} > 0$

$1 - \frac{2k_i^n}{k_{max}} \geq 0$ and $\frac{2k_i^n}{k_{max}} \leq 1$

Hence, $k_{max} \geq 2k_i^n$ (7.2)

Which is the condition for well-posedness

$q'(k_i^n) \leq v_{max}$ (7.3)

Re-writing the non-linear PDE in (4.1) as

$$\frac{\partial k}{\partial t} + q'(k)\frac{\partial (k)}{\partial x} = v_s + \beta$$

The explicit finite difference scheme (6.3) takes the form:

$$k_i^{n+1} = k_i^n - q'(k)\frac{\Delta t}{\Delta x}[k_i^n - k^n{}_{i-1}] + (v_s + \beta)\Delta t$$

$$k_i^{n+1} = (1-\lambda)\, k_i^n + \lambda k^n{}_{i-1} + (v_s + \beta)\Delta t \quad (7.4)$$

Where, $\lambda = q'(k)\frac{\Delta t}{\Delta x}$ (7.5)

Since, we are considering the source term "β" to be constant, equation (7.4) implies that

If $\lambda \leq 1$, then the solution at the new time space is weighted average of the solution at the old time space. Implying that;

$$\lambda = q'(k)\frac{\Delta t}{\Delta x} \leq 1 \quad (7.6)$$

Then condition (7.6) can be guaranteed via (7.3) by

$$\gamma = \frac{v_{max}\Delta t}{\Delta x} \leq 1 \quad (7.7)$$

Which is the stability condition involving the parameter v_{max}.

Thus, whenever one employs the stability condition (7.7), the physical constraints condition (7.2) can be guaranteed immediately by choosing

$$k_{max} = \alpha max_i k_0 (x_i),\ \alpha \geq 2 \quad (7.8)$$

8.0 Incorporation of Initial and Boundary Data

In order to perform numerical simulation, we consider the exact solution:

$$k(x,t) = v_s t + \beta t + k_o\,(x - v_{max}\,(1 - \frac{2k}{k_{max}})t)$$

We consider the initial condition $k_o\,(x) = \frac{1}{2}x$, then we have;

$$k(x,t) = v_s t + \beta t + \frac{1}{2}\,(x - v_{max}\,(1 - \frac{2k}{k_{max}})t) \quad (8.1)$$

$$k(x,t) = v_s t + \beta t + \frac{1}{2}\,(x - v_{max}t) + \frac{1}{2}(\frac{2v_{max}k}{k_{max}})t)$$

$$k(x,t) = v_s t + \beta t + \frac{1}{2}\,(x - v_{max}t) + \frac{v_{max}kt}{k_{max}}$$

$$k(x,t) = \frac{v_s t + \beta t + (x - v_{max}t)/2}{1 - v_{max}t/k_{max}} \quad (8.2)$$

We prescribe the corresponding boundary value by the equation

$$k_a\,(t) = k_a\,(t, x_a) = \frac{v_s t + \beta t + (x_a - v_{max}t)/2}{1 - v_{max}t/k_{max}} \quad (8.3)$$

Where x_a denotes the position of the left boundary. To present the numerical solution, we avoid the term βt from the right hand side of equation (8.3). Hence the boundary condition takes the following form:

$$k_a\,(t) = k_a\,(t, x_a) = \frac{\frac{x_a - v_{max}t}{2}}{1 - v_{max}t/k_{max}} \quad (8.4)$$

To implement the numerical result we need to use the EUDS in (6.3) above.

9.0 Model Assumptions

To illustrate the analysis presented, we consider the following assumptions:

i. A highway in the range of 20km.

ii. A source term inflow at β=10km.

iii. A space grid size Δx =0.25km in model simulation.

iv. A time grid size Δt=3 secs in model simulation.

v. A maximum time t_{max}=12 minutes.

Vi. $k(0,x) = 25 * \sin\left(\frac{x}{4}\right) + 30$ as the initial condition.

vii. A maximum density of$k$=100cars/km.

viii. Maximum velocities v_{max}=15km/h, v_{max}=20km/h, v_{max}=25km/h and v_{max}=30km/h were used to visualize the effect of source term and shockwave evaluation in our traffic equation.

10.0 Numerical Scheme Algorithm

The algorithm was developed to describe the step-by-step process of the traffic simulation for a non-linear partial differential equation (pde). The outputs of the algorithm are measured in terms of traffic length, travel time and total number of vehicles passing through the section of the highway. The flow-chart also describes the process by which the flow of the traffic is implemented along with defined parameters coupled with first order EUDS.

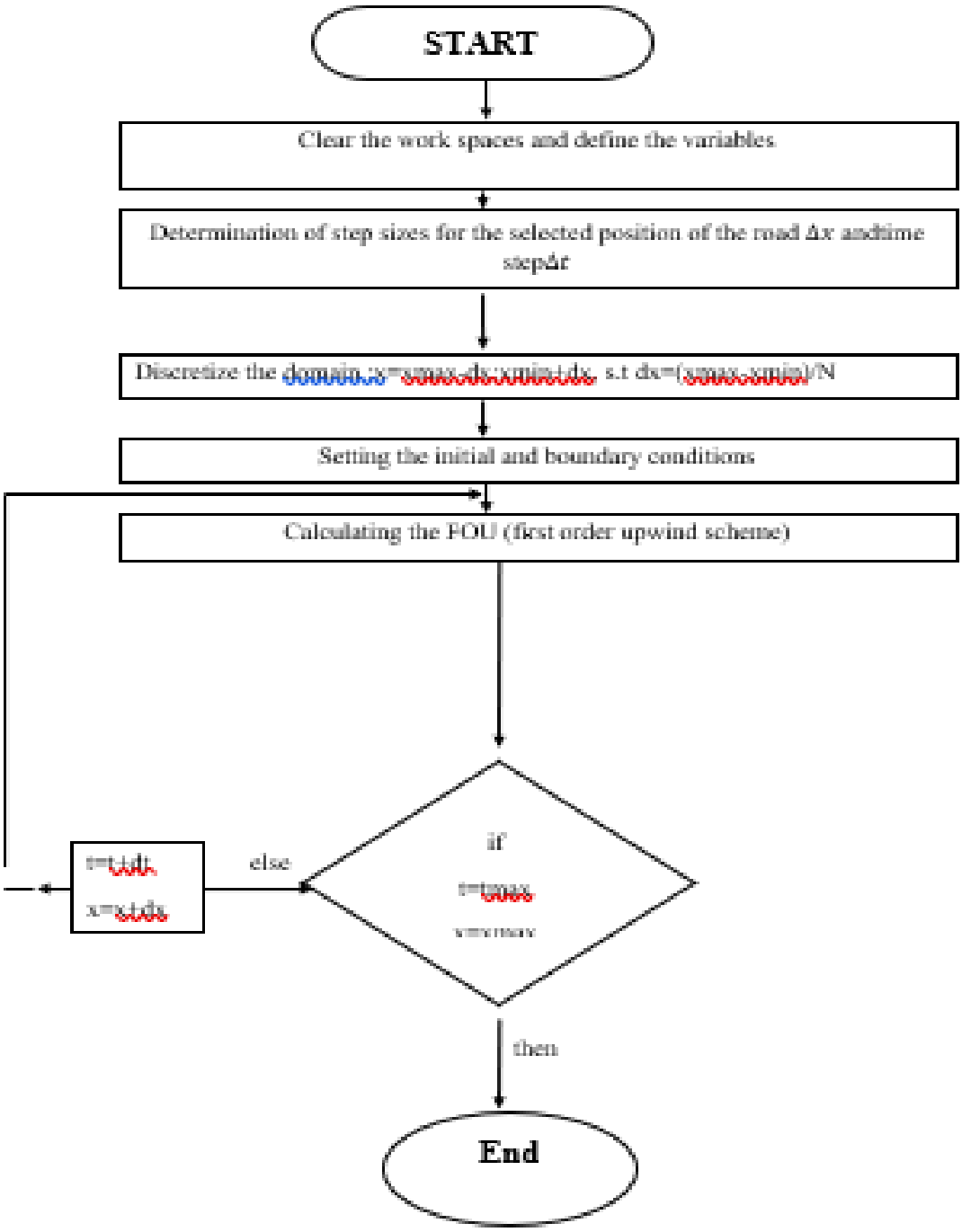

Figure 10.1 Flow Chart for the (EUDS) numerical scheme algorithm

RESULTS AND DISCUSSION

11.0 Introduction

In this section we present some numerical experiments conducted with the scheme introduced in the previous chapter, which is the first order Explicit Upwind Difference Scheme (EUDS) obtained in equation (6.3). In order to implement the Numerical scheme, we developed a computer program in MATLAB (version 7.5.0(R2007b), 2007) and performed numerical simulations as presented below.

11.1 Comparison of Analytical and Numerical Results in case of EUDS

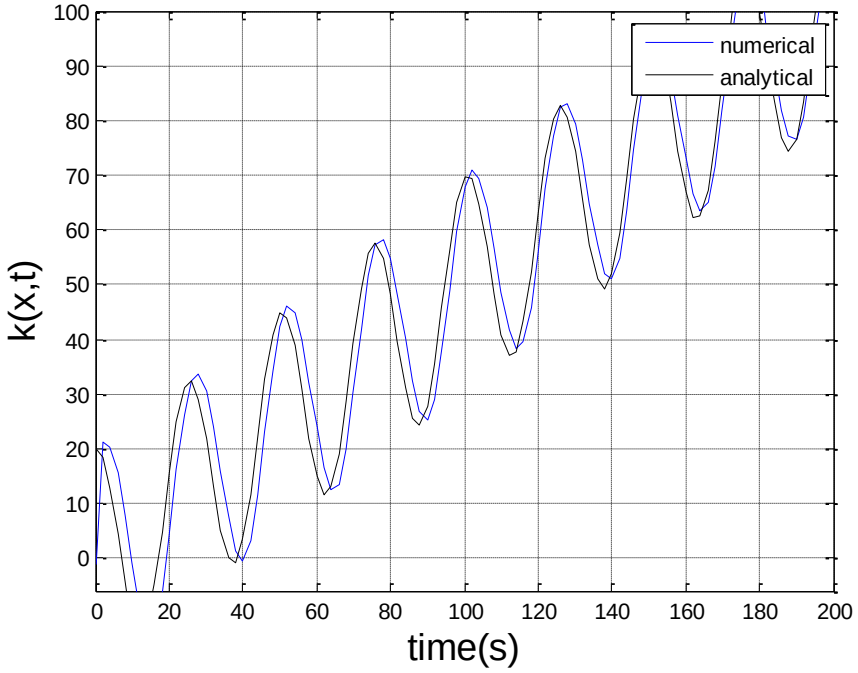

Partial Validation of the finite difference scheme formulation of equation (6.3) and (6.4) has been performed by solving the finite difference formulation, and comparing those numerical results to the analytical solution expressed by equation (3.9). We discretized the spatial domain into some specific points and assumed that vehicles entering the inflow will caution the drivers' behavior of driving on the highway, thereby reducing the speed at which they are moving towards the inflow source**.**

Figure 11.1.1: Analytical and Numerical Results Comparison profile in case of EUDS

11.2 Velocity Profile Using EUDS

The following figures show the velocity profile for car position in 12 minutes with different maximum velocity level consideration. The velocity is computed by the specific linear-density relationship according to Greenshields (1935).

This specific relation is of the following form:

$$v(k) = v_{max}\left(1 - \frac{k}{k_{max}}\right)$$

The first order Explicit Upwind Difference Scheme (5.2) coupled with the above velocity-density relation were used to visualize the effect of the source term in the traffic flow model.

The program was run initially with *t=0* for the values of time step size $\Delta t = 3$secs and space step size Δx=0.25m.

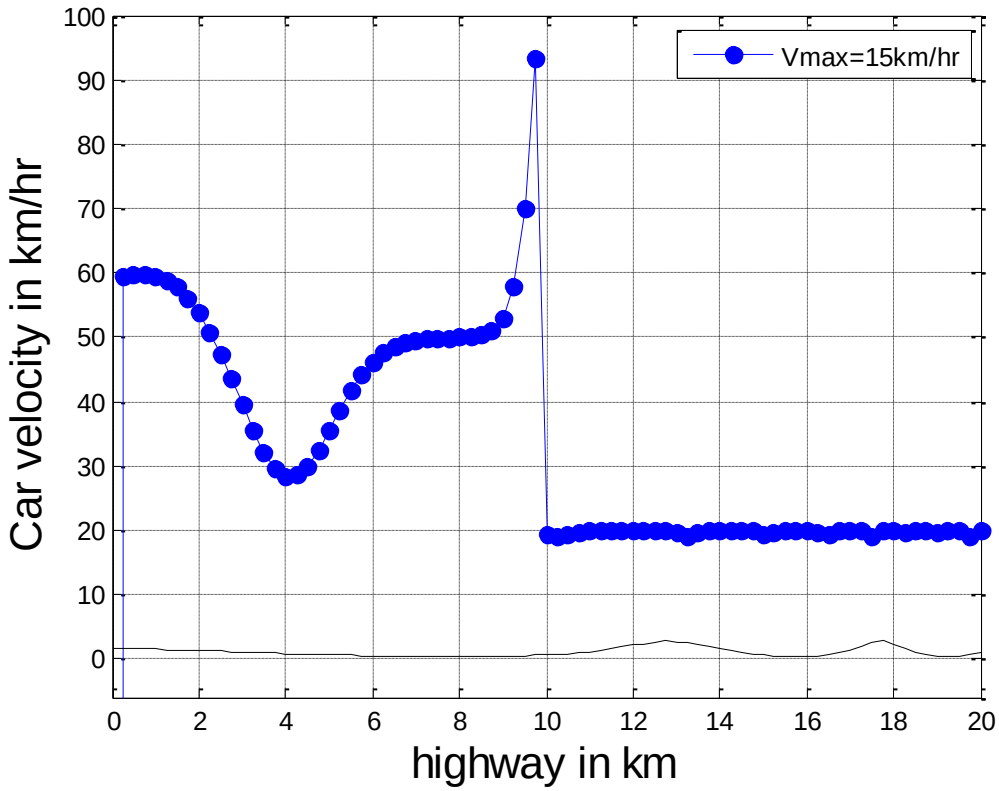

Figure 11.2.1.Velocity profile for car position in case of EUDS when v_{max}=15km/h

According to the behavior of car velocity marked by "dot-dash line" in the above velocity profile diagram, we see that the inflow is acting on the 10^{th} km position, so that for high density at that position, the velocity of cars suddenly decrease, allowing the vehicles to slow down and adjust to the position of the chosen parameter.

The above figure 11.2.1, also illustrate the behavior of vehicular shockwave as the traffic moves at a loss density, as such a state of free flow where vehicles moves freely on the highway is experienced. However, density increases to accommodate most of the flow at the long run whereby the speed drops as following vehicles also have to decelerate.

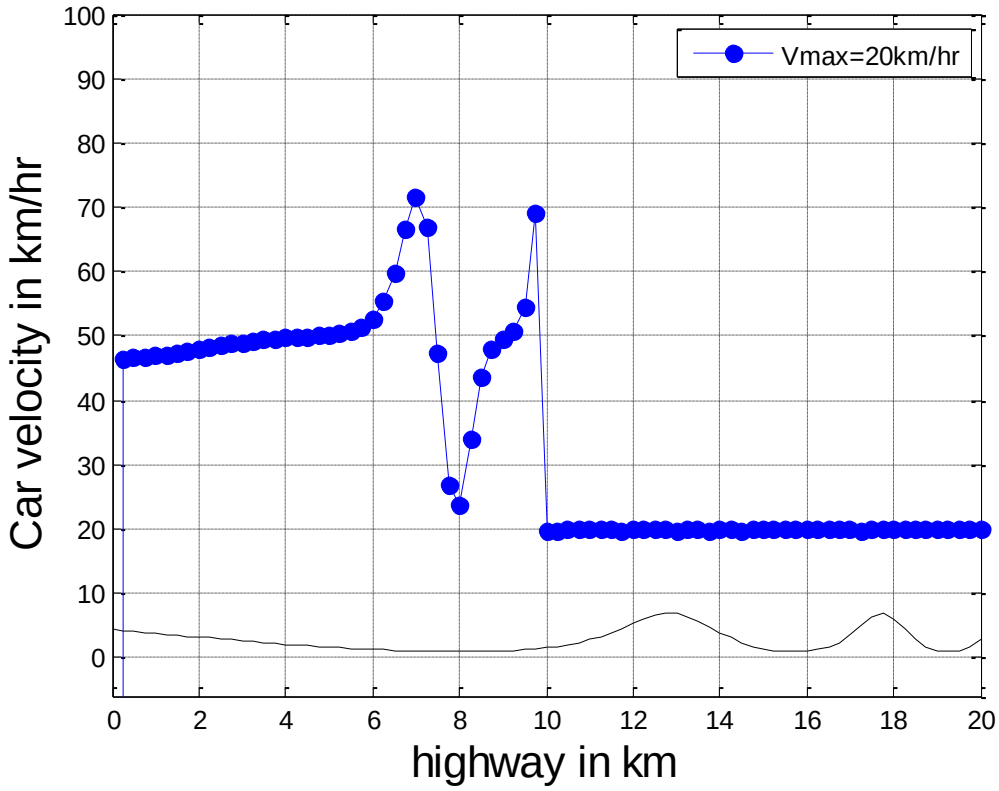

Figure 11.2.2.Velocity profile for car position in case of EUDS when v_{max}=20km/h

The result displayed in figure 11.2.2. is the velocity profile diagram indicating car velocity marked by "dot-dash line", it is observed that a constant rate inflow acted on the 10th km position as well, so that for high density at that position, the speed of cars suddenly decrease allowing the vehicles to slow down and adjust to the position of the chosen parameter.

In figure 11.2.2 above, the formation of a shockwave speed on a single-lane road is presented. Initially, we can see that at the sections of the road fewer vehicles moving with higher speed at a free flow state suddenly decelerate due to increase in density of vehicles on the road where the velocity of a following vehicle cannot be greater than that of the car right ahead. Otherwise, collision will occur. A transient state is observed for a while as a result of the shockwave formed which propagate along the road.

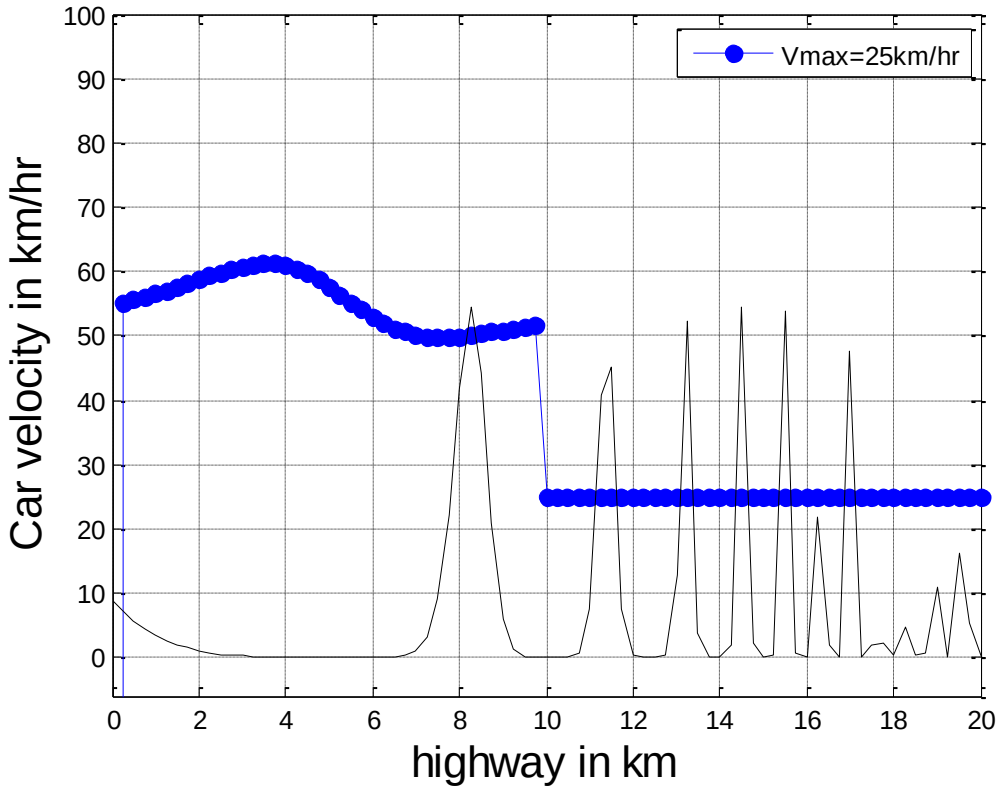

Figure 11.2.3.Velocity profile for car position in case of EUDS when v_{max}=25km/h

In the above velocity profile diagram showing car velocity marked by "dot-dash line", it is clearly seen that a constant rate inflow acted on the 10^{th} km position as well, so that for high density at that position, the speed of cars suddenly decrease allowing the vehicles to slow downand adjust to the position of the chosen parameter.

For the shockwave speed depicted in the above figure 11.2.3, it can be observed that the wave of an increased density propagate upward to the left section of the road slowing down to a free flow state by the right section of the single-lane highway. The vehicular shockwave at the transient state as can be seen clearly above is due to the continuous slow down of all vehicles following the leading vehicle as a result of high density. Therefore, the leading vehicle on the right section has to slow down in order to avoid collision, until free flow is restored over the total affected road section.

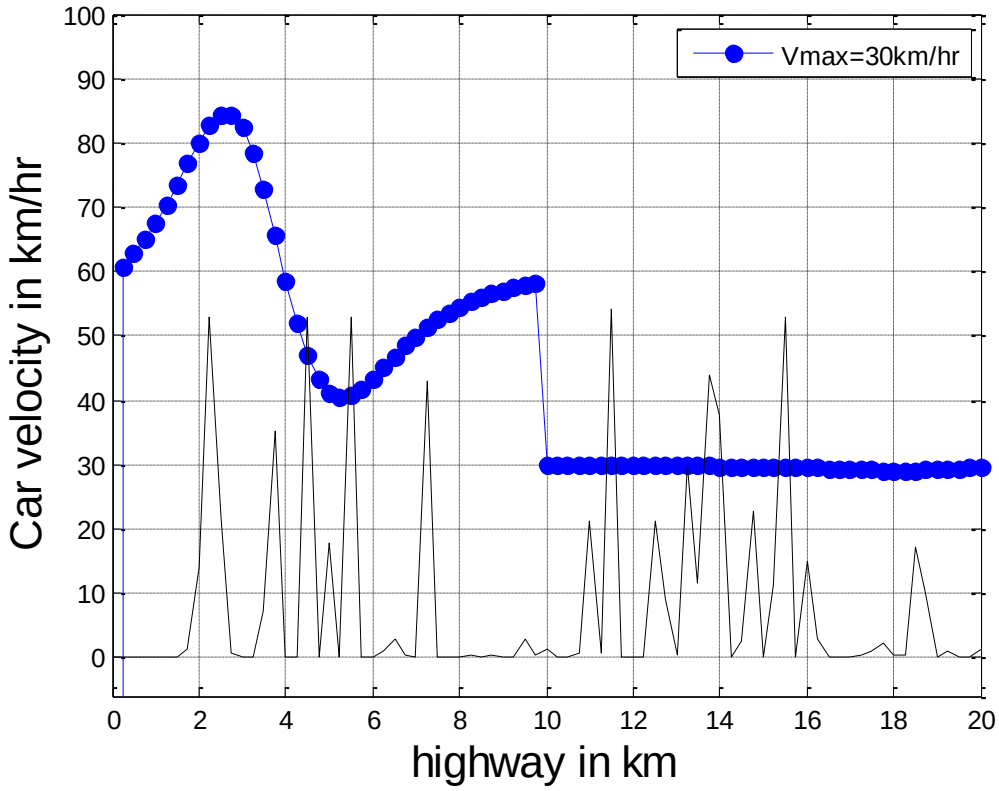

Figure 11.2.4 Velocity profile for car position in case of EUDS when v_{max}=30km/h

The velocity profile diagram in figure 11.2.4 above depicts the car velocity marked by "dot-dash line", it revealed that an inflow is acting on the 10^{th} km position of the single-lane highway considered as 20km, so that for high density at that position, the speed of cars suddenly decreases allowing the vehicles to slow down and adjust to the position of the chosen parameter.

For the shockwave speed it can be clearly seen that as more and more vehicles occupy the road space the flow decreases, thereby resulting to drop in speed by the vehicles that causes fluctuation in the shockwave speed with which vehicles enters the transient state. As the density increases the equilibrium flow enters the congested phase.

SUMMARY, CONCLUSION AND RECOMMENDATIONS

12.0 Introduction

In this paper, a general overview of the work is presented. Recommendations on the method adopted in the paper and fields of further research are suggested.

12.1 Summary

In this paper, effect of a source term in a traffic flow model for a single-lane highway is investigated and a shockwave evaluation is presented. An analytical solution of the non-linear partial differential equation for the traffic flow equation is obtained by characteristics method; result obtained is verified using Explicit Upwind Difference Scheme by developing a computer program in MATLAB (version

7.5.0(R2007b), 2007). Similarly some numerical experiments conducted with different traffic parameters were presented and discussed.

12.2 Conclusion

In this paper, the traffic flow model presented gave the expected results. The LWR model has been verified for a particular position of the road using dissipation and a shockwave speed terms and the results were found to be consistent with the values of the parameters chosen. The method of characteristics was used to solve the PDE which yield a characteristics curve of the form $k(x,t) = v_s t + \beta t + k_o\ (x - v_{max}\ (1 - \frac{2k}{k_{max}})t\ )$.

Consequently, our numerical scheme was derived using Taylor's series expansion. The finite difference scheme has been used to solve the traffic flow model. Matlab software was used in carrying out the simulation in order to implement the EUDS. We evaluated the model performance by a shockwave speed and a dissipation term. The outcome of different traffic parameters such as dissipation term, shockwave speed term and varying maximum velocities, has also been presented. Stability and physical constraint conditions were also established.

12.3 Recommendations

Numerically, it was clearly seen that the dissipation term effect and the shockwaves on our roads can be viewed directly with some varying maximum velocities.

To prevent congestion and to improve efficiency, traffic should move at a density corresponding to maximum traffic flow. Therefore it is recommended that we should use other methods to solve the LWR model instead of the method of characteristics. The effect of shockwaves on multilane models with bottleneck should be investigated. This is left for future research.

REFERENCES

Ahasan, H.M. and Johnnie, B.E. (2014). Effect of Rainfall on Traffic Flow Shockwave Propagation. Proceeding of Malaysian Universities Transportation Research Forum and Conference. ISSN 978-967-57700-8-1

Ali, A., Andallah**,** L.S. and Hossain, Z.(2015). Numerical Solution of a Fluid Dynamics Traffic Model Associated with a Constant Rate Inflow. American Journal of Computational and Applied Mathematics, 5(1): pp. 18-26.

Ali, A., Andallah, L.S. (2016). Inflow Outflow Effect and Shock Wave Analysis in a Traffic FlowSimulation. American Journal of Computational Mathematics, 06, pp. 55-65.

Anuar, K. and Cetin, M. (2017). Estimating Freeway Traffic Volume Using Shockwaves and ProbeVehicle Trajectory data. Transportation Procedia. Vol.22, pp. 183-192.

Coclite, G. M., Garavello, M. and Piccoli, B. (2005).Traffic Flow on a Road Network. SIAM J.Mathematical Analysis. 36(6), pp. 1862-1886.

Daganzo, C. F. (1995). A Finite Difference Approximation of the Kinematic Wave Model of Traffic Flow, Transportation Research Part B: Methodological Volume 29,Issue 4, pp.261- 276.

Dass, H.K. (2013).*Advanced Engineering Mathematics*, 21st Revised edition, S. Chand & Company Ltd., Ram Nagar, New Delhi, India.

Doboszczak, S. and Forstall, V.(2013). Traffic flow Mathematical modeling by differential equations.http://www.norbertwiener.umd.edu/Education/m3cdocs/Presentation2.pdf. Accessed: 25thNovember, 2021-5:07pm.

Elfar, A., Xavier, C., Talebpour, A. and Mahmassan, H. (2018). Traffic Shockwave Detection in a connected Environment Using the Speed Distribution of IndividualVehicles. Transportation Research Record Journal, Volume 2672, Issue 20, pp. 203-214.

Gupta, A.K. and Katiyar, V.K. (2005). Analyses of Shockwaves and Jam in Traffic Flow. Journal of Physics, A, Mathematical General, 38, pp. 4069-4083.

Gani, M.O., Hossain, M.M. and Andallah, L.S. (2011). A finite Difference Scheme for a Fluid Dynamic Traffic Flow Model Appended with two-point Boundary Condition. Jahangirnagar, Bangladesh Mathematical Society (ISSN 1606-3694) 31, pp. 43-52.

Greenshield, B.D. (1935). A Study of Traffic Capacity. Highway Research Board, 14, pp. 448-477.

Kabir, M.H, Gani, M.O and Andallah, L.S. (2010). Numerical Simulation of a Mathematical TrafficFlow Model based on a non-linear velocity-density function, Journal of Bangladesh Academy of Sciences,Vol. 34, No. 1, pp. 15-22.

Kabir, M.H., Afroz, A. and Andallah, L.S. (2012). Finite Difference Scheme for a Macroscopic traffic Flow Model based on non-linear density-velocity relationship. Bangladesh Journal of Scientificand Industrial Research 47(3), pp. 339-346.

Li, T. (2001). L_1 Stability of Conservation Laws for a Traffic Flow Model, Electronic Journal of Differential Equations, Vol. 14, pp. 1-18. ISSN: 1072-6691.

Li, T. (2002). Well-posedness Theory of an inhomogeneous Traffic Flow Model. Discrete and Continuous Dynamical Systems-Series B Vol. 23, pp. 401-414.

Lighthill, M. J. and Whitham, G. B. (1955), On Kinematic Waves. II. A Theory of Traffic Flow on Long Crowded Roads, Proceedings of Royal Society of London. Series. A.,229(1178), pp. 317-345.

MATLAB (2007). Language of Technical Computing, version 7.5.0 (R2007b). License Number: 161052 USA.

Richard, P.I. (1956). Shockwaves on the highways, Operations Research, 4, pp. 42-51.

Rodrigue, J.P. (2009). Definition of Congestion. International Journal of Business and Social Sciences,Vol. 4, Centre for Promoting Ideas, USA

Saxena, N. and Jain, N. (2017). Evaluation of Road Traffic Congestion by Shockwave Theory and Reduction Strategies. International Journal on Recent and Innovation Trends in Computing and Communication. ISSN: 2321-8169, pp. 125-129.

Sahin, I., Kusakci, S.S. and Aydin, G. (2016). Shockwaves in Highway Traffic: Macroscopic and Microscopic Investigation with Wavelet Transform. https://samsun.imo.org.tr/resimler/ekutuphane/pdf/17807-11-33.pdf. Accessed: 11th July, 2021-12:02pm.

Vikram, D., Chackroborty, P. and Mittal, S. (2013). Exploring the Behaviour of LWR Continuum Models of Traffic Flow in the Presence of Shockwaves. 2nd Conferences of Transportation Research Groups of India. pp. 412-421.

Wu, X. and Liu, X.H. (2011). A Shockwave Profile Model for Traffic Flow on Congested Urban Arterials. Transportation Research Part B: Methodological, Vol. 45, issue 10, pp. 1768-1786.

Wikipedia (2021) https://en.wikipedia.org/wiki/wiki/Traffic_flow. Accessed: 9th April, 2021- 9:08am.

Wikipedia (2021) https://en.wikipedia.org/wiki/wiki/Shock_wave. Accessed: 20th November, 2021-11:23pm.

Wikipedia (2021) https://en.wikipedia.org/wiki/wiki/Method_of_characteristics. Accessed: 4th June,2021- 2:34pm.

Wikipedia (2021) https://en.wikipedia.org/wiki/wiki/Finite_difference_method. Accessed: 21stAugust, 2021-03:06pm.

Wikipedia (2021) https://en.wikipedia.org/wiki/wiki/Taylor_series. Accessed: 7th May, 2021-08:17am.

Wikipedia (2021) https://en.wikipedia.org/wiki/wiki/Initial_value_problem. Accessed: 16th February, 2021-10:13am.

Wikipedia (2021) https://en.wikipedia.org/wiki/wiki/Initial_boundary_value_problem. Accessed: 16thFebruary, 2021-10:15am.

Wikipedia (2022) https://en.wikipedia.org/wiki/wiki/Continuity_equation. Accessed: 2th January, 2022- 04:18pm.

APPENDIX

Matlab Program

```
Clear                    %clear workspaces
clc
%define variables
xmin=0;  %minimum value of x
xmax=20;  %maximum value of x
N=100;  %no.of nodes-1
dt=0.3;  %timestep
kmax=100;  %maximum density
s=10;  %source term
t=0;  %time
h=5;            % vmax increment
Vmax=15+h;  %Maximum velocity
dx=0.25;
k0=0.5;
k1=15+h;
k2=30+h;
q1=20+h;
q2=25+h;
x=xmin-dx:dx:xmax+dx;      %discretise the domain
%set initial conditions
ko=25*sin(x/4)+30;
k=ko;
kn=Vmax*(1-k/kmax);
vs=(q2-q1)/(k2-k1)
qpn=pn;
knk1=qkn;
%loop through time
nsteps=tmax/dt;
for n=1:nsteps          %calculate boundary conditions
        kn(1)=k(3);
    kn(N+3)=k(N+1);
%calculate the FOU scheme
for i=2:N+1
    qkn(i)=Vmax*(kn(i)-((kn(i).^2)/kmax));
    knk1(i)=kn(i)+(s*dt)-(dt/dx)*(qkn(i)-qkn(i-1));
end
%update t and k
  t=t+dt;
  k=knk1;
```

```
%plot solution
   plot(x,k,'bo-','Markerfacecolor','b');
hold on
   plot(x,vs,'m','Markerfacecolor','g');
   grid on
axis([xmin xmax -6 100])
xlabel('highway in km','fontsize',16);
ylabel('Car velocity in km/hr','fontsize',16)
   legend('velocity');
   title(sprintf('time=%1.3f',t),'fontsize',16)
   shg
   pause (dt);
end
```

Mathematical Model and Analysis of Dynamics of Lassa Fever in Nigeria with Influence of Treatment

[1]Yahaya A. Abdullahi, [2]Abdullahi M. Auwal and [1]Umar Muhammad

[1]Gombe state Polytechnic Bajoga

[2]Mathematics and Statistics Department, Federal Polytechnics Bauchi

∗Correspondence: Email:yahyaalimaibuhu@gmail.com

Abstract

In this study, we used standard incidence rate to examine the treatment impact on infected patients and developed, grew, and analyzed an SEIR deterministic mathematical model of Lassa fever in Nigeria. Empirical and mathematical models demonstrate the model's viability.

The basic reproduction number R_0 that depends on ten parameters which is the important threshold has been obtained, together with the basic control parameters say transmission coefficient β_h and treatment coefficient γ that can help us to control the spread of the Lassa fever disease. Both the endemic and disease-free equilibrium points, which are demonstrated to be present in the model, are asymptotically stable both locally and globally, provided specific threshold parameters are fulfilled. Additionally, we demonstrated that treating affected populations early lowers the number of infected people, which in turn lowers the dynamics of Lassa fever disease spread within a community.

Keywords: Lassa fever, mathematical model, basic reproduction number, stability analysis, control Parameters.

Introduction

A zoonotic viral infection, Lassa fever is also known as Lassa hemorrhagic fever. It is caused by the Lassa virus, a single-stranded RNA virus belonging to the Arenaviridae family [(Peterson et al.,2014, Ibrahim and Denes (2021)]. The primary host of this virus, which is prevalent in Sub-Saharan Africa and one of the most frequent rodent species, is the mastomys natalensis, also known as the multimammate rat [(Zhao et al., 2020), (Gibb et al., 2017)& Richmond and Baglole (2013)]. The virus that causes Lassa fever was initially discovered in 1969 in the northern Nigerian state of Borno.

However, the estimated annual prevalence in West African regions, both eastern and western, varies from 100,000 to 500,000 cases, with approximately 5,000 fatalities [(Grenenky et al., 2017), (Mariem et al., 2019) & (Olugasa et al., 2015)]. This momentum made it necessary for the World Health Organization (WHO) and the Centers for Disease Control and Prevention (CDC) to declare Lassa fever an endemic disease in Western Africa. Therefore. Liberia, Guinea, Sierra Leone, and Nigeria are among the nations most at risk of contracting Lassa fever (belt) [(Greenky et al., 2017), (Musa et al., 2020), (Davies et al., 2019) & (Peter et al.,2020)]. There have been numerous breakouts from the aforementioned countries over the years, with Nigeria reportedly experiencing the worst pandemic.

Although there are a number of factors, including inadequate healthcare facilities, a dirty environment, and inadequate personal hygiene, that contribute to the annual rise in Lassa virus infections, rainfall and the transportation of produced food into our communities are also important considerations. Lassa fever prevalence is dependent on human efforts to lower the disease's transmission proportion. These activities are linked to an improvement or increase in the host reservoir (mastomys rodents) to migrate from their natural habitation to the human environment [(Zhao et al., 2020), (Onah and Collins (2020)]. Given that Lassa fever has an incubation period ranging from six to twenty-one days, infected individuals are anticipated to exhibit clinical symptoms after this exposure period. Despite the fact that only a small percentage of infected persons experience symptoms like fever, headaches, sore throats, coughing, muscle discomfort, and weakness. However, in more severe situations, an infected person may experience additional side effects such low blood pressure, face swelling, nasal bleeding, and respiratory distress [(Ibrahim and Denes (2021), (Peter et al., 2020) & (Bakare et al., 2020)]. In a more dire circumstance, neurological issues caused by this disease may result in death fourteen days after the onset of symptoms [(Ibrahim and Denes (2021), (Bakare et al., 2020)]. The main way that humans contract the Lassa virus is through human. Since there is currently no vaccine to prevent Lassa fever, infection prevention is crucial to limiting the disease's spread throughout the general public. Since it is currently impractical to eradicate the mastomys rodent population, measures to prevent the infection's spread include encouraging good personal hygiene to prevent coming into contact with the secretions or excretions of infected rodents and putting in place standard medical facilities for efficient patient testing, diagnosis, and treatment (Davies et al., 2019).

Although there is currently no known vaccine or cure for Lassa fever, ribavirin, an antiviral medication, has been shown to be an effective treatment for patients with Lassa fever when given early in the infection cycle (Mariem et al., 2019; Musa et al., 2020). Therefore, our understanding of the virus's transmission dynamics is still incomplete and far from complete. As a result, it's critical to carry out a variety of studies and investigate fresh approaches and strategies right once in order to improve our comprehension of the virus's spread and contain its spread. In the past ten years, mathematical models have developed into essential resources for researching the dynamics of diseases within a certain community. The usage has recently developed. Onah et al. (2020) employed optimal control theory to ascertain the most economical means of mitigating disease transmission. This was achieved by incorporating various control intervention strategies, including treatment, isolation, external protection, and rodent control, into an extended SIR-SI-type compartmental model. A forward bifurcation between the endemic and disease-free equilibriums with a stability switch was demonstrated by Musa et al. (2020). Their approach explains hospitalization, seclusion, and quarantine as well as human-rodent interactions. Zhao et al. (2020) examined the epidemiological characteristics of Lassa outbreaks throughout different parts of Nigeria and found a relationship between rainfall and the number of reproductions. Reproduction numbers estimated from four different growth models, models fitted to Lassa surveillance data, and other factors were used to determine Lassa's infectivity.

The Model System Description and Formulation

This research will focus on how treatments affects the dynamics of Lassa fever virus diseases and how far along the infection spreads in the human population. Thus, in the following ways, our suggested models build upon the work of James et al. (2015)

i. Incorporating exposed, treatment and recovered compartments with treatment as control measure, is not considered in James *et al.* (2015).
ii. Sub dividing the reservoir population (rodents) In to susceptible and infected compartments. is not considered in James *et al.* (2015).
iii. We Extend our model to SEIR type while SIR model type was used in James *et al.* (2015).
iv. The Probability or proportion of susceptible to be becomes infectious in both humans and reservoir (rodents) population, is not considered in (James *et al.*, 2015).
v. Standard incidence rate used while bilinear incidence rate was used in (James *et al.*, 2015).

Thus, the proposed extended model is formulated based on the following considerations.

(a) Homogeneous mixing of members of the population under consideration with equal chances of transmitting the virus.
(b) the Probability of susceptible individuals to be becomes infectious in the population under consideration by the proportion of $(1-\theta)$, with the transmission rate β and $0 \leq \theta \leq 1$.
(c) Successful treatment of individuals to becomes recovered, does not guarantee permanent immunity. But they do confer some immunity from their primary infection, and since there is no absolute cure for Lassa fever, they may also have a relapse of the disease back into the infectious class.

Hence, the total human and population at time t, is divided into five (5) compartments such that $N_h(t) = S_h(t) + E_h(t) + I_h(t) + T_h(t) + R_h(t)$ and the total rodents population at time t is divided in to two (2) compartments such that $N_r(t) = S_r(t) + I_r(t)$.

In the model (1), $S_h(t); E_h(t); I_h(t); T_h(t); R_h(t); S_r(t)\ and\ I_r(t)$ are the state variables used to represent the Susceptible human, Exposed human, Infected human, Recovery human, Treated human, Susceptible mastomys rats' and Infected mastomys rats compartment respectively, with the assumptions that all parameters in the model (1) are constants.

Thus, the susceptible population with risk of Lassa virus infection $S_h(t)$ is generated by recruitment of humans at a constant rate Λ_h (all humans recruited into the population are assumed to be at risk of Lassa-infection), All infected individuals move into the susceptible population due to treatment failure at rate φ, the population is decreased by natural death at a rate μ, following the effective contact with β_h the human-to-human contact rate and β_r a mastomys rat-to-human contact rate.

The exposed population $E_h(t)$ is produced following the effective contact with β_h the human-to-human contact rate and β_r a mastomys rat-to-human contact rate, and further reduce by the proportion of susceptible individuals that becomes infectious at $(1-\theta)$ and natural death at a rate μ.

The infected population $I_h(t)$ is increased by ξ the proportion of exposed individuals that becomes infectious at $(1-\theta)$, which decreased by ϕ a recovery rate of infectious human, and rates at which infected humans move to treatment class γ together with natural death of human population μ and the induced death of infectious individual at α_1.
The population of treated individuals $T_h(t)$ is generated as a result of treatment of infected individuals at rate γ, and diminished by the ψ rate of recovery, all infected individuals move into the susceptible

population due to treatment failure at rate φ,natural death at a rate μ, together with α_2 the induced death of individual under treatment.

The population of recovered individuals $R_h(t)$ is composed as a result of recovery of treated individuals at rate ψ together with recovery rate of infected individuals and decreased by natural death at a rate μ.

Similarly, the population of susceptible mastomys rat (rodents) $S_r(t)$ is generated by recruitment of rodents at a constant rate Λ_r, which decreased by the population of natural death at a rate ϑ, following the effective contact with β_r the transmission rate of mastomys rat-to-mastomys rat.

The population of infected mastomys rats (rodents) $I_r(t)$ is produced following the effective contact with β_r the transmission rate of mastomys rat-to-mastomys rat. and only diminished by natural death of mastomys rat's (rodents) at a rate ϑ.

Thus, the transfer diagram of the model system shown in Fig. 1. Together with above descriptions, yield the following model equations:

$$\frac{dS_h}{dt} = \Lambda_h + \varphi T_h - (\lambda_h + \mu)S_h$$

$$\frac{dE_h}{dt} = \lambda_h S - [\xi(1-\theta) + \mu]E_h$$

$$\frac{dI_h}{dt} = \xi(1-\theta)E_h - (\phi + \gamma + \mu + \alpha_1)I_h$$

$$\frac{dT_h}{dt} = \gamma I_h - (\psi + \varphi + \mu + \alpha_2)T_h \qquad (1)$$

$$\frac{dR_h}{dt} = \phi I_h + \psi T_h - \mu R_h$$

$$\frac{dS_r}{dt} = \Lambda_r - (\lambda_r + \vartheta)S_r$$

$$\frac{dI_r}{dt} = \lambda_h S_r - \vartheta I_r$$

With $\lambda_h = \frac{\beta_h I_h + \beta_r I_r}{N_h}$ and $\lambda_r = \frac{\beta_r I_r}{N_r}$ (2)

where β_h is the effective contact rate for human-to-human transmission, β_r is a mastomys rat-to-human effective contact rate.

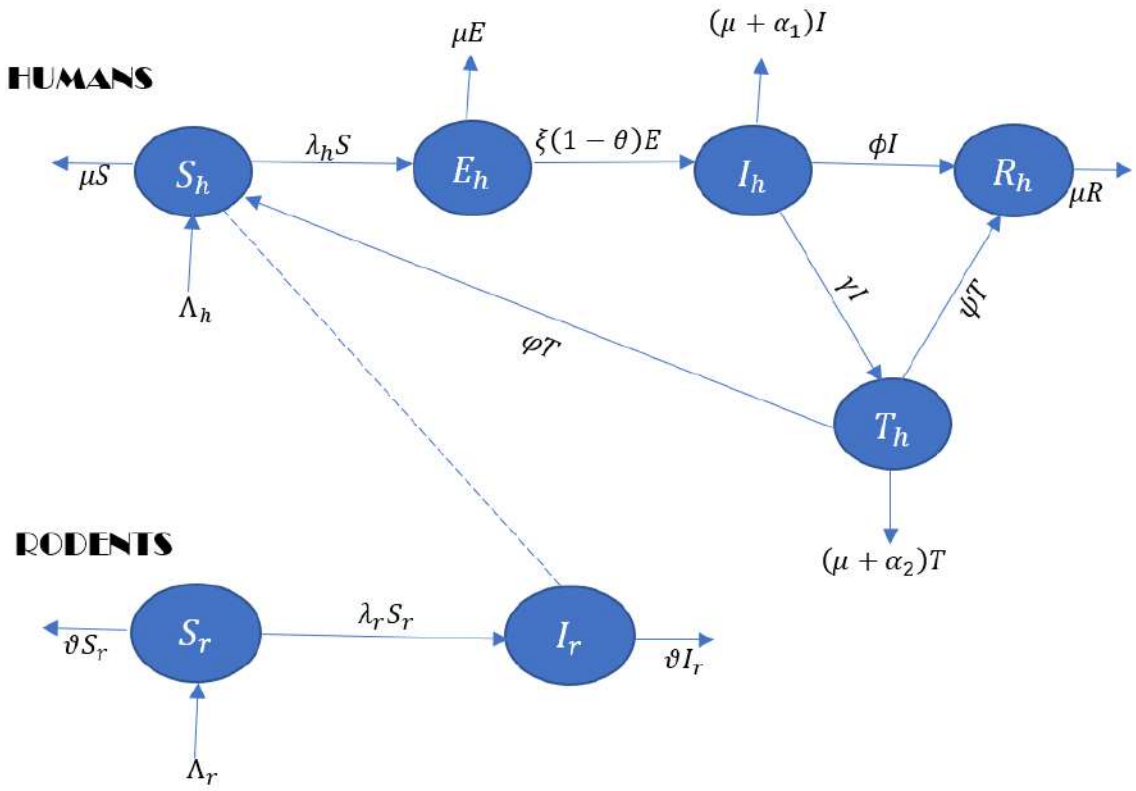

Figure 1. The Lassa fever flow diagram for human and rodent population

Description of the state variables and the parameters of the flow chart model

Table 1. The State Variables of the Flow Chart Model System

Symbol of the Variable	Description
$S_h(t)$	Susceptible human compartment
$E_h(t)$	Exposed human compartment
$I_h(t)$	Infected human compartment
$T_h(t)$	Treatment compartment
$R_h(t)$	Recovery human compartment
$S_r(t)$	Susceptible mastomys rats' compartment
$I_r(t)$	Infected mastomys rats' compartment

Table 2. The Parameters of the Flow Chart Model System

Symbol of the Parameters	Descriptions
$\Lambda_h and \Lambda_r$	Rate of recruitment of susceptible human and mastomys rat's population
μ	Rate of natural death in human
ϑ	Rate of natural death in mastomys rat's
Ψ	Recovery rate of treated individuals
ϕ	Recovery rate of infected individuals
φ	Rate of treatment failure
γ	Rate of treatment (Rates at which infected humans move to treatment class)
$(1-\theta)$	Proportion of new exposed individual that become symptomatically infected
ξ	Rate at which an exposed individual becomes infectious
α_1 and α_2	Rate of induced death of infectious individual and individual under treatment. Respectively
β_h	The Transmission rate of human population
β_r	The Transmission rate of mastomys rat's population

Positivity and Boundedness

To verify that the differential equation system in (1) is both mathematically and biologically meaningful, let us now demonstrate the positivity and boundedness of our model's solutions.
Theorem1.*Let the initial coditions* $S_h(0)>0, E_h(0)>0, I_h(0)>0, T_h(0)>0, R_h(0)>0, S_r(0)>0,$ *and* $I_r(0)>0,$ *then the solution of* $S_h(t), E_h(t), I_h(t), T_h(t), R_h(t),$ $S_r(t)$ *and* $I_r(t)$ *of the model system* (1) are positive for all $t \geq 0$.

Proof. Suppose $S(t)$ is not positive, then there exists a first time, say $t^* > 0$, such that $S_h(t) > 0$ For all $t \in [0, t^*)$ and $S_h(t^*) = 0$. By inspection of the equation of $E_h(t)$, we have that

$$\frac{dE_h}{dt} \geq -[\xi(1-\theta)+\mu]E_h(t), for\ \ t \in [0, t^*),$$

Hence, it follows that,

$$E_h > 0\ for\ t \in [0, t^*).$$

Thus, it is clear from the first equation of model system (1) that

$$\frac{dS_h}{dt} \geq -(\lambda_h + \mu)S_h(t), for\ t \in [0, t^*).$$

It follows that $S_h(t^*) > 0$ which contradicts $S_h(t^*) = 0$. therefore, $S_h(t)$ is positive. Using similar approach as that for $S_h(t)$,it is easy to show that$E_h(0) > 0, I_h(0) > 0, T_h(0) > 0, R_h(0) > 0, S_r(0) > 0,\ and\ I_r(0) > 0$. Hence the proof.

Invariant Region

In order to retain the biological feasible region of the model system (1) we consider the biologically feasible region consisting of

$$\Delta = \Delta_h \times \Delta_r \in \mathbb{R}_+^5 \times \mathbb{R}_+^2$$

with

$$\Delta_h = \{S_h, E_h, I_h, T_h, R_h \in \mathbb{R}_+^5 : N_h \leq \frac{\Lambda_h}{\mu}\}$$

And

$$\Delta_r = \{S_r, I_r, \in \mathbb{R}_+^2 : N_r \leq \frac{\Lambda_r}{\vartheta}\}$$

It can be shown that the set Δ is a positively invariant set and global attractor of this system. This implies any phase trajectory initiated anywhere in the nonnegative region $\mathbb{R}_+^7$ enters the feasible region Δ and remains in thereafter.

Lemma 1. The biological feasible region $\Delta = \Delta_h \cup \Delta_r \subset \mathbb{R}_+^5 \times \mathbb{R}_+^2$ of the Lassa fever model (1) is positively invariant with nonnegative initial conditions in $\mathbb{R}_+^7$.

Proof

The following steps are followed to establish the positive invariance of Δ (i.e., solutions in Δ remain in Δ for all $t > 0$). The rate of change of the total human and rodent populations $N_h$and N_r respectively, are obtained by adding the respective components of model (1) which result to

$$\frac{dN_h(t)}{dt} = \Lambda_h - \mu N_h(t) - \{(\alpha_1)I_h(t) + (\alpha_2)T_h(t)\}\ and$$

$$\frac{dN_r(t)}{dt} = \Lambda_r - \vartheta N_r(t)$$

so that,

$$\frac{dN_h(t)}{dt} \leq \Lambda_h - \mu N_h(t)\ and\ \frac{dN_r(t)}{dt} \leq \Lambda_r - \vartheta N_r(t) \qquad (2)$$

Hence, $N_h(t) \leq \mu N_h(0)e^{\mu t} + \frac{\Lambda_h}{\mu}(1 - e^{-\mu t})\ and\ N_r(t) \leq \vartheta N_r(0)e^{\vartheta t} + \frac{\Lambda_r}{\vartheta}\left(1 - e^{-\vartheta t}\right)$.

In particular, $N_h(t) \leq \frac{\Lambda_h}{\mu}\ and\ N_r(t) \leq +\frac{\Lambda_r}{\vartheta}$ if the total human population and rodent population at the initial instant of time, $N_h(0) \leq \frac{\Lambda_h}{\mu}\ and\ N_r(0) \leq +\frac{\Lambda_r}{\vartheta}$, respectively. So, the region Δ is positively invariant. Thus, it is consequently adequate to consider the dynamics of Lassa fever governed by model

(1) in the biological feasible region Δ , where the model is considered to be epidemiologically and mathematically well posed see (Lakshmikanthan, *et al* 1989; Ojo, *et al*, 2017).

Existence and Stability of Lassa Fever Free Equilibrium (LFFE)

Setting the right-hand side of equation (1) to zero will result in the steady-state solution where the Lassa fever free equilibrium of model (1) is reached in the absence of Lassa fever infection. such that $S_h^* = E_h^* = I_h^* = T_h^* = R_h^* = S_r^* = I_r^* = 0$ and solve it simultaneously we get the disease-free equilibrium state denoted by $\mathcal{E}_0$ and is given by

$$\mathcal{E}_0 = (S_h^*, E_h^*, I_h^*, T_h^*, R_h^*, S_r^*, I_r^*) = \left(\frac{\Lambda_h}{\mu}, 0,0,0,0, \frac{\Lambda_r}{\vartheta}, 0\right) \quad (3)$$

Basic Reproduction Number

The next-generation matrix method is used on system (1) for determining the reproduction number $\mathcal{R}_0$. The epidemiological quantity $\mathcal{R}_0$, called the reproduction number, measures the typical number of Lassa fever cases that a Lassa fever-infected individual can generate in a human population that is completely susceptible (Lakshmikantham, *et al,* 1989; Oke, *et al,* 2020).

The matrices F and V for the new infection terms and the remaining transfer or transition terms are shown below, it follows that the basic reproduction number of model system (1) is calculated as follows

$$\begin{vmatrix} Gain\ to\ E \\ Gain\ to\ I \\ Gain\ to\ T \\ Gain\ to\ \ I_r \\ losses\ from\ E \\ losses\ from\ I \\ osses\ from\ T \\ losses\ from\ \ I_r \end{vmatrix} \begin{vmatrix} (\frac{\beta_h I_h + \beta_r I_r}{N_h})S_h \\ 0 \\ 0 \\ (\frac{\beta_r I_r}{N_r})S_r \\ [\xi(1-\theta)+\mu]E_h \\ -\xi(1-\theta)E_h + (\phi+\gamma+\mu+\alpha_1)I_h \\ -\gamma I_h + (\psi+\varphi+\mu+\alpha_2)T_h \\ \vartheta I_r \end{vmatrix}$$

That is by considering the most relevant equations in the model system (1) say, $E_h(t), I_h(t), T_h(t)\ and\ I_r(t)$, thus, the gain (the new infection terms) and losses (the transfer or transition terms) expressions associated with the model (1) using next generation method gives

$$\text{Gain} \Rightarrow F = \begin{pmatrix} 0 & \beta_h & 0 & \beta_r \\ 0 & 0 & 0 & 0 \\ 0 & 0 & 0 & 0 \\ 0 & 0 & 0 & \beta_r \end{pmatrix}$$

$$\text{Losses} \Rightarrow V = \begin{pmatrix} K_1 & 0 & 0 & 0 \\ -K_2 & K_3 & 0 & 0 \\ 0 & -\gamma & K_4 & 0 \\ 0 & 0 & 0 & \vartheta \end{pmatrix}$$

$$V^{-1} = \begin{pmatrix} \frac{1}{K_1} & 0 & 0 & 0 \\ \frac{K_2}{K_1K_3} & \frac{1}{K_3} & 0 & 0 \\ \frac{\gamma K_2}{K_1K_3K_4} & \frac{\gamma}{K_3K_4} & \frac{1}{K_4} & 0 \\ 0 & 0 & 0 & \frac{1}{\vartheta} \end{pmatrix}$$

Where $K_1 = [\xi(1-\theta)+\mu], K_2 = \xi(1-\theta), K_3 = (\phi+\gamma+\mu+\alpha_1)\ and\ K_4 = (\psi+\varphi+\mu+\alpha_2)$ (4)

Thus, the spectral radius of the next-generation FV^{-1},is the basic reproduction $\mathcal{R}_0$ of the model (1) it follows then that the associated reproduction number denoted by $\mathcal{R}_0$, is obtained as follows:

$$\mathcal{R}_0 = \frac{\vartheta\beta_h K_2 + \beta_r K_1 K_3}{K_1 K_3 \vartheta} \quad (5)$$

With $\mathcal{R}_{0h} = \frac{\beta_h K_2}{K_1 K_3}\ and\ \mathcal{R}_{0r} = \frac{\beta_r}{\vartheta}$ (6)

Where $\mathcal{R}_{0h}$ defined the basic reproduction number of human population and $\mathcal{R}_{0r}$ defined the basic reproduction number of rodents respectively.

Stability Analysis

Lemma 2: The disease – free equilibrium (DFE) of the (LASV) model system (1), given $\mathcal{E}_0$, is locally asymptotically stable if $\mathcal{R}_0 < 1$ and ε_0 is unstable if $\mathcal{R}_0 > 1$.

Proof.

We prove the Lemma 2 using linearization method. The Jacobian matrix associated with the LASV model at the DFE, $\mathcal{E}_0 = (S_h^*, E_h^*, I_h^*, T_h^*, R_h^*, S_r^*, I_r^*) = \left(\frac{\Lambda_h}{\mu}, 0,0,0,0, \frac{\Lambda_r}{\vartheta}, 0\right)$ is given by

$$J(\varepsilon_0) = \begin{pmatrix} -\mu & 0 & -\beta_h & \varphi & 0 & 0 & \beta_r \\ 0 & -K_1 & 0 & 0 & 0 & 0 & 0 \\ 0 & K_2 & -K_3 & 0 & 0 & 0 & 0 \\ 0 & 0 & \gamma & -K_4 & 0 & 0 & 0 \\ 0 & 0 & \phi & \psi & -\mu & 0 & 0 \\ 0 & 0 & 0 & 0 & 0 & -\vartheta-\beta_r & \\ 0 & 0 & 0 & 0 & 0 & 0 & -\vartheta \end{pmatrix} \quad (7)$$

With $K_1, K_2, K_3,\ and\ K_4$ same as in (4)

The eigenvalues can be determined by solving the characteristic equation $|J - \lambda I| = 0$. Now Evaluating the eigenvalues of the Jacobian matrix J we found that the following eigenvalues $-K_4, -K_3, -K_1, -\vartheta, -\mu, -\vartheta\ and\ -\mu$ are all real and negative. Hence,ε_0 is locally asymptotically stable whenever $\mathcal{R}_0 < 1$, and the above lemma has been proved accordingly.

Global Stability of Lassa Fever-Free Equilibrium

The global stability of the Lassa fever-free equilibrium $\mathcal{E}_0$ of the model system (1), can be examine since $\mathcal{E}_0$ is locally asymptotically stable from above lemma.

Theorem 2 The Lassa fever disease-free equilibrium $\mathcal{E}_0$ is globally asymptotically stable (GAS) of model system (1) if $\mathcal{R}_0 < 1, in\ the\ interior\ of\ \Delta$.

Proof. Comparisons theorem allow us to prove the above theorem in the following sense. Now let consider the next generation matrix together with the infected compartments as

$$F = \begin{pmatrix} 0 & \beta_h & 0 & \beta_r \\ 0 & 0 & 0 & 0 \\ 0 & 0 & 0 & 0 \\ 0 & 0 & 0 & \beta_r \end{pmatrix},\ V = \begin{pmatrix} K_1 & 0 & 0 & 0 \\ -K_2 & K_3 & 0 & 0 \\ 0 & -\gamma & K_4 & 0 \\ 0 & 0 & 0 & \vartheta \end{pmatrix} \text{ and } Z = \begin{pmatrix} E_h \\ I_h \\ T_h \\ I_r \end{pmatrix}$$

Then the rate of change of the infected compartments of model (1) can be written in the form

$$\frac{dZ}{dt} = (\mathrm{F} - \mathrm{V})\mathrm{Z} - \mathrm{JZ} \qquad (8)$$

So that

$$\mathrm{JZ} = \begin{pmatrix} -K_1 & \beta_h & 0 & \beta_r \\ K_2 & -K_3 & 0 & 0 \\ 0 & \gamma & -K_4 & 0 \\ 0 & 0 & 0 & \beta_r - \vartheta \end{pmatrix} \begin{pmatrix} E_h \\ I_h \\ T_h \\ I_r \end{pmatrix} - \begin{pmatrix} \frac{\beta_h I_h + \beta_r I_r}{N_h})S_h - [\xi(1-\theta) + \mu]E_h \\ \xi(1-\theta)E_h + (\phi + \gamma + \mu + \alpha_1)I_h \\ \gamma I_h + (\psi + \varphi + \mu + \alpha_2)T_h \\ (\frac{\beta_r I_r}{N_r})S_r - \vartheta I_r \end{pmatrix}$$

$$\mathrm{JZ} = \begin{pmatrix} 0 & \beta_h\left(1 - \frac{S_h}{N_h}\right) & 0 & \beta_r\left(1 - \frac{S_r}{N_r}\right) \\ 0 & & 0 & 0 \\ 0 & 0 & 0 & \\ 0 & 0 & 0 & \beta_r\left(1 - \frac{S_r}{N_r}\right) \\ & 0 & & \end{pmatrix} \begin{pmatrix} E_h \\ I_h \\ T_h \\ I_r \end{pmatrix}$$

With $J = \begin{pmatrix} 0 & \beta_h\left(1 - \frac{S_h}{N_h}\right) & 0 & \beta_r\left(1 - \frac{S_r}{N_r}\right) \\ 0 & 0 & 0 & 0 \\ 0 & 0 & 0 & 0 \\ 0 & 0 & 0 & \beta_r\left(1 - \frac{S_r}{N_r}\right) \end{pmatrix}$

It can be observed that J is a non-negative matrix since $S_h(t) \leq N_h(t) \leq \frac{\Lambda_h}{\mu}$ and $S_r(t) \leq N_r(t) \leq \frac{\Lambda_r}{\vartheta}$ In the invariant set. Hence it follows that

$$\frac{dZ}{dt} \leq (F - V)Z \qquad (9)$$

Considering the fact that eigenvalues of the matrix $F - V$ all have negative real parts, which coincide with our local stability result, where $\rho(FV^{-1}) < 1$ if $R_0 < 1$, (Van den Driessche and Watmough 2002)). It follows that the linearized differential inequality of (9) is stable whenever $R_0 < 1$.

Consequently, $(E_h, I_h, T_h, I_r) \to (0,0,0,0)\ as\ t \to \infty$. Thus, by comparison theorem, $(E_h, I_h, T_h, I_r) \to (0,0,0,0)\ as\ t \to \infty$. Substituting $E_h = I_h = T_h = I_r = 0$ in (8) gives $S_h(t) \to S_h^*$ as $t \to \infty$ and $S_r(t) \to S_r^*$ as $t \to \infty$. Thus, $(S_h(t), E_h, I_h(t), T_h, R_h, S_r(t), I_r(t)) \to (S_h^*, 0,00,0,, S_r^*, 0)\ as\ t \to \infty$ for $R_0 < 1$. Thus, ε_0 is GAS if $R_0 < 1$.

Existence and stability of Endemic Equilibria

Lassa fever endemic equilibrium points of model (1) is obtained at the steady-state solution in the presence of Lassa fever infection in the population. there in by setting the right-hand side of equation (1) equal to zero and solve it simultaneously in terms of the associated form of infection we get the Lassa fever endemic equilibrium points state denoted by $\mathcal{E}_1$ and is given by $\mathcal{E}_1 = ({S_h}^{**}, {E_h}^{**}, {I_h}^{**}, {T_h}^{**}, {R_h}^{**}, S_r^{**}, I_r^{**})$, Therefore, the endemic equilibrium point of the model system (1) is obtained as

$$ {S_h}^{**} = \frac{K_1 K_3 K_4 \Lambda_h}{(K_1 K_3 K_4 - \gamma\varphi K_2)\lambda_h^{**} + \mu K_1 K_3 K_4} $$

$$ {E_h}^{**} = \frac{K_3 K_4 \Lambda_h \lambda_h^{**}}{(K_1 K_3 K_4 - \gamma\varphi K_2)\lambda_h^{**} + \mu K_1 K_3 K_4} $$

$$ {I_h}^{**} = \frac{K_2 K_4 \Lambda_h \lambda_h^{**}}{(K_1 K_3 K_4 - \gamma\varphi K_2)\lambda_h^{**} + \mu K_1 K_3 K_4} $$

$$ {T_h}^{**} = \frac{K_2 \gamma \Lambda_h \lambda_h^{**}}{(K_1 K_3 K_4 - \gamma\varphi K_2)\lambda_h^{**} + \mu K_1 K_3 K_4} \quad (10) $$

$$ {R_h}^{**} = \frac{(\gamma\psi + \phi K_4)\, K_2\, \gamma\, \Lambda_h \lambda_h^{**}}{((K_1 K_3 K_4 - \gamma\varphi K_2)\lambda_h^{**} + \mu K_1 K_3 K_4)\mu} $$

$$ S_r^{**} = \frac{\Lambda_r}{\lambda_r^{**} + \vartheta}\ , \qquad I_r^{**} = \frac{\lambda_r^{**} \Lambda_r}{\vartheta(\lambda_r^{**} + \vartheta)}. $$

With the force of infections

$$ \lambda_h^{**} = \frac{\beta_h I_h^{**} + \beta_r I_r^{**}}{N_h^{**}} \ and \ \ \lambda_r^{**} = \frac{\beta_r I_r^{**}}{N_r^{**}} \qquad (11) $$

Where $N_h^{**} = ({S_h}^{**} + {E_h}^{**} + {I_h}^{**} + {T_h}^{**} + {R_h}^{**})\ and\ \ N_r^{**} = (S_r^{**} + I_r^{**})$

From equation (9) $\lambda_r^{**} = \frac{\beta_r I_r^{**}}{N_r^{**}}$

implies that

$$ \lambda_r^{**} N_r^{***} - \beta_r I_r^{**} = 0 $$

$$\Rightarrow (\lambda_r^{**} - \beta_r) I_r^{**} + \lambda_r^{**} S_r^{**} = 0.$$
$$\Rightarrow (\lambda_r^{**} - \beta_3) \frac{\lambda_r^{**}\Lambda}{\vartheta(\lambda_r^{**} + \vartheta)} + \lambda_r^{**} \frac{\Lambda}{(\lambda_r^{**} + \vartheta)} = 0$$
$$\Rightarrow \frac{\lambda_r^{**}\Lambda(\lambda_r^{**} - \beta_r + \vartheta)}{\vartheta(\lambda_r^{**} + \vartheta)} = 0$$

Thus, $\lambda_r^{**} - \beta_r + \vartheta = 0$ since $\lambda_r^{**} \neq 0$,
and so $\lambda_r^{**} = \beta_r - \vartheta$ (13)

Also, From (9) $\lambda_h^{**} = \lambda_h^{**} = \frac{\beta_h I_h^{**} + \beta_r I_r^{**}}{N_h^{**}}$
implies that

$\lambda_h^{**} N_h^{**} - (\beta_r I_r^{**} + I_h^{**} \beta_h) = 0$
$\Rightarrow \lambda_h^{**}(S_h{}^{**} + E_h{}^{**} + I_h{}^{**} + T_h{}^{**} + R_h{}^{**}) - (\beta_r I_r^{**} + I_h^{**} \beta_h) = 0$ (14)

Substituting (8) and (10) into (11) we have the following quadratic equation in team of λ_h^{**}

$$a\lambda_h^{**2} + b\lambda_h^{**} + c = 0 \quad (15)$$

With

$a = \Lambda_h \vartheta \left(\gamma \mu K_2 + \gamma \psi K_2 + \mu K_2 K_4 + \mu K_3 K_4 + \phi K_2 K_4\right)$
$b = K_1 K_3 K_4 \Lambda_h \vartheta \mu (1 - \mathcal{R}_{0h}) + K_1 K_3 K_4 \Lambda_r \vartheta \mu (1 - \mathcal{R}_{0r}) + K_2 \gamma \varphi \mu \Lambda_r (\beta_r - \vartheta)$
$c = \mu^2 K_1 K_2 K_4 \Lambda_r \vartheta (1 - \mathcal{R}_{0r})$

It can be observed that the coefficient a is always positive while the sign of b and c depends on the values of the reproduction numbers $\mathcal{R}_{0h}$and $\mathcal{R}_{0r}$ $with\ \beta_r - \vartheta \neq 0. since\ \mathcal{R}_0 < 1$, it follows by Descartes rule of signs that,

i. If $R_{0h} > 1$ and $R_{0r} > 1$, then $b < 0$ and $c < 0$ then there is only one sign change in the sequence of coefficients a, b, c. Thus, there is one positive real root of (15).
ii. If both b and c are positive when $R_{0h} < 1$ and $R_{0r} < 1$. Then there is no change in the sequence of coefficients, therefore, equation (15) has no positive real root.
iii. If $R_{0h} > 1$ and $R_{0r} < 1$ then there either two sign changes or no sign change in the sequence of coefficients of (15). Then there two or no positive real root of (15).
iv. If $R_{0h} < 1$ and $R_{0r} > 1$, there is one sign change in the sequence of coefficients a, b, c . Then there exists at most one positive real root of (15)

Consequently, apart from the root $\lambda_h^{**} = 0$, by Descartes rule of signs, there exists at least one positive real root for (15) whenever $\mathcal{R}_0 > 1$. Hence, the model (1) has at least one endemic equilibrium point whenever $\mathcal{R}_0 > 1$.

Conclusions

In this paper, a deterministic mathematical model of Lassa fever epidemic with influence of treatment was formulated and analyzed. We obtain the basic reproduction number $\mathcal{R}_0$ via next generation matrix method, we have shown that if $\mathcal{R}_0$ is greater than one, means the disease is spreading and also the number of infected individual increases as well. the disease-free equilibrium points and the endemic

equilibrium point has been established. We have proven that the disease – free equilibrium (DFE) of the (LASV) model system is locally asymptotically stable if $\mathscr{R}_0 < 1$ and $_0$ is unstable if $\mathscr{R}_0 > 1$. This show that the early treatment of Lassa fever is necessary and meaningful.

Recommendations

To decrease the transmission of disease;

i. Keeping the remaining parameters constant, the transmission rate (β_h) and the coefficient (ξ) should be less than 0 respectively.
ii. Keeping the remaining parameters constant, the treatment failure rate (φ) should be less than 0.
iii. Keeping the remaining parameters constant, the Lassa fever induced death rate for infectious individual rate (α_1) should be greater than 0.
iv. Keeping the remaining parameters constant, the treatment rate (γ) should be greater than 1.
v. Government needs to increase or adopt the principle of screening or testing, and managing population of infected family with effective and sufficient medication to protect non-infected population.

Acknowledgement

Authors are grateful to the Gombe State Polytechnic and TETfund IBR Grants for their financial support throughout this research.

References

Alsaedi, A., Nieto, J. J. & Venktesh, V. (2015): Fractional electrical circuits. Adv. Mech. Eng. 7(12), 1687814015618127.

Bakare, E., Are, E., Abolarin, O., Osanyinlusi, S., Ngwu, B. and Ubaka, O. N. (2020): Mathematical modelling and analysis of transmission dynamics of Lassa fever. J. Appl. Math.

Davies, J., Lokuge, K. and Glass, K. (2019): Routine and pulse vaccination for Lassa virus could reduce high levels of endemic disease: a mathematical modelling study. Vaccine 37(26), 3451–3456

Diethelm, K. (2010).: The Analysis of Fractional Differential Equations: An Application-Oriented Exposition Using Differential Operators of Caputo Type. Springer.

Gibb, R., Moses, L. M., Redding, D. W. & Jones, K. E. (2017).: Understanding the cryptic nature of Lassa fever in West Africa. Pathogens Global Health 111(6), 276–288

Greenky, D., Knust, B. and Dziuban, E. J. (2018): What pediatricians should know about Lassa virus. JAMA Pediatr. 172(5), 407–408

Hamblion, E., Raftery, P., Wendland, A., Dweh, E., Williams, G., George, R., Soro, L.,

Katawera, V., Clement, P., Gasasira, A., et al. (2018): The challenges of detecting and responding to a Lassa fever outbreak in an Ebola-afected setting. Int. J. Infect. Dis. 66, 65–73

Ibrahim, M. A. and Dénes, A. (2021): A mathematical model for Lassa fever transmission Dynamics in a seasonal environment with a view to the 2017–20 epidemics in Nigeria. Nonlinear Anal. Real World Appl. 60, 103310.

James, T. O., Abdulrahman, S., Akinyemi S. and Akinwade, N. I. (2015): Dynamics transmission of Lassa fever disease, International Journal of Innovation and Research in Educational Sciences, 2(1), ISSN (Online), 2349-5219.

Ma, M., Baleanu, D., Gasimov, Y. S. and Yang, X .-J. (2016): New results for multidimensional diffusion equations in fractal dimensional space. Rom. J. Phys. 61, 784–794.

Mariën, J., Borremans, B., Kourouma, F., Baforday, J., Rieger, T., Günther, S., Magassouba, N., Leirs, H. & Fichet-Calvet, E. (2019): Evaluation of rodent control to Fght Lassa fever based on feld data and mathematical modelling. Emerg. Microbes Infect. 8(1), 640–649

Maxmen, A. (2018): Deadly Lassa-fever outbreak tests Nigeria's revamped health agency. Nature 555, 7697

Musa, S. S., Zhao, S., Gao, D., Lin, Q., Chowell, G. & He, D. (2020): Mechanistic Modelling of the large-scale Lassa fever epidemics in Nigeria from 2016 to 2019, J. Theoret. Biol. 110209.

Musa, S. S., Zhao, S., Gao, D., Lin, Q., Chowell, G., He, D. (2020): Mechanistic Modelling of the large-scale Lassa fever epidemics in Nigeria from 2016 to 2019. J. Theor. Biol. 493, 110209

Nigeria Centre for Disease Control: Weekly epidemiological report. Available from https://ncdc.gov.ng/reports/ weekly.

Nobel Lectures, Physiology or Medicine 1901-1921. Elsevier Publishing Company, Amsterdam, 1967.

Olugasa, B. O., Odigie, E. A., Lawani, M., Ojo, J. F., et al. (2015): Development of a time-trend model for analyzing and predicting case-pattern of Lassa fever epidemics in Liberia, 2013–2017. Ann. Afr. Med. 14(2), 89

Onah, I. S. & Collins, O. C. (2020).: Dynamical system analysis of a Lassa fever model with varying socioeconomic classes. J. Appl. Math.

Onah, I. S., Collins, O. C., Madueme, P.-G.U. & Mbah, G.C.E. (2020): Dynamical system Analysis and optimal control measures of Lassa fever disease model, Int. J. Math. Math. Sci. 2020 7923125.

Peter, O. J., Abioye, A. I., Oguntolu, F. A., Owolabi, T. A., Ajisope, M. O., Zakari, A.G. and Shaba, T. G. (2020): Modelling and optimal control analysis of Lassa fever disease. Inform. Med. Unlocked 20, 100419

Peterson, A. T., Moses, L. M. and Bausch, D. G.(2014): Mapping transmission risk of Lassa fever in West Africa: the importance of quality control, sampling bias, and error weighting. PLoS ONE 9(8), 100711.

Richmond, J. K. and Baglole, D. J. (2003).: Lassa fever: epidemiology, clinical features, and social consequences. BMJ 327(7426), 1271–1275

World Health Organization (2007): Options for the use of human H5N1 influenza vaccines and the WHO H5N1 vaccine stockpile. http://www.who.int/csr/resources/publications/

Zhao, S., Musa, S. S., Fu, H., He, D. & Qin, J. (2020): Large-scale Lassa fever outbreaks in Nigeria: quantifying the association between disease reproduction number and local rainfall. Epidemiol. Infect. 148, 10

Zhao, S., Musa, S. S., Fu, H., He, D. & Qin, J. (2020): Large-scale Lassa fever outbreaks in Nigeria: Quantifying the association between disease reproduction number and local rainfall, Epidemiol. Infect. 148

Deforestation Rate and its Effects on Biodiversity in Dukku/Kwami Forest Cover

Ali Zakari, Idris Aliyu, Mohammed Dodo Kwairanga, Kubra Yahaya Umar and Abdullahi Aminu Yarima
Biology Department, Federal College of Education (Technical), Gombe
PMB 60, Ashaka Road, Gombe State.
alizakari5@gmail.com, aliyummalwa@gmail.com, alizakari5@gmail.com, sulaimanshuaibufky@gamil.com, kubrayahaya8@gmail.com, aminu_yarima55@yahoo.com
*alizakari5@gmail.com, 08066027655

Abstract

In the past years there was a thick vegetation cover in Dukku/Kwami axis and its Biodiversity. The loss in the biodiversity is due to a number of reasons which tree cutting is a major. The current study aimed at accessing the rate of deforestation and its effects on biodiversity. Questionnaire and interview schedule methods were the tools used in data collection. Five different plots were used to analyze the loss of valuable flora of the study area, while remote sensing method was used to obtain data from the plots. The data were analyzed using simple statistical techniques. NDVI Resulting Image indicates that there was a decrease in the vegetation cover in the source areas after the first three years by 0.223742 from 2013-2015. Therefore, there was a decrease of vegetation cover after the second three years with -0.093396 from 2016-2019. Out of 986 trees; 884, 904, 706, 1,023 and 620 were completely lost in plot 1, 2, 3, 4 and 5 respectively. 42.7% of the respondents pointed to fuel wood collection as the key factor affecting Biodiversity loss on vegetation in the source area. It was concluded that deforestation rates are currently higher in the study area; this means that the forest cover was drastically reduced in size between 2013 to 2019. Hence, recommended that legislation should be re-enforced to curtail unnecessary bush burning and tree cutting and farmers should be advised to practice a selective method of cutting trees.

Keywords: Biodiversity, Deforestation, Forest

Introduction

Environment is the sum total of the condition within which living organisms live and interact with nonliving ones. Environment in which an organization operates includes air, water, land and natural resources. It also affects the life, nature, behavior and growth, development and maturation of living organism (Barrow, 1993).

Forests are largely known as source of various essential goods and services (DWAF, 2005). In addition to the physical contribution to the environment, forests also provide ecological, economic, social, religious and cultural benefits (Mainagwa, 2010). According to Nzeh and Eboh (2007), forests contribute directly and indirectly to rural household livelihoods through the generation of income and employment from the sale and exchange of gathered and unprocessed non-timber forest products.

It is obvious that Nigerian vegetation cover has consistently reduced since the 1990s, at an average of 410,000 hectares (ha) per annum. FAO (2009) reveals that about 60 percent of the world's total deforestation (3,900 million cubic meters) from forests and trees outside forests are used for fuel. Generally in world, the total net reduction in forest area in the period 2000–2010 is valued at 5.2

million ha per year, which is correspondent to a loss of more than 140 square kilometers of forest per day (FAO, 2010). This is due to deforestation which is considered to be as the cutting down of trees from forest cover from the forest- or the long-term destruction of the tree canopy cover at a level lower than the minimum 10 percent threshold (FAO, 2010).

In the years there was a thick vegetation cover in Dukku/Kwami axis and its Biodiversity; also games were available as they enjoyed the protection of thick vegetation cover in the area.

Objectives of the Study

i. To determine the deforestation rate in the study area from 2013 - 2019.
ii. To determine the source of fuel wood consumed in the study area.

Methodology

Research Design

The plot base biodiversity analysis by quadrat method was used in mapping out the plot (100 m^2). Five different plots were used to analyze the loss of valuable flora of the study area.

Method of Data Collection

Questionnaire and interview schedule methods were the tools used in data collection. The data were analyzed using simple statistical techniques, such as mean and standard deviation and NDVI model of remote sensing.

Method of Data Analysis

Descriptive statistical techniques such as mean and standard deviation were employed to analyze the data collected.

$$Mean\ (X) = x/n$$

$$SD = \sqrt{\frac{(x - X^2}{n}}$$

S.D = standard deviation

x = Total quantity of trees removed

n = Total number of Quadrat

Results

Biodiversity loss on vegetation in the source area from 2013 – 2019.

This section reveals the findings of the analysis undertaken using Remote Sensing (RS) that explores the pattern of vegetation change from 2013 - 2019 in Dukku/Kwami axis.

Change detection analysis (supervised and use/land vegetation cover classification) was employed to show the rate of vegetation cover loss, health and density (NDVI) using the resulted values generated from satellite imagery.

Vegetation Change Patterns

The NDVI is a dimensionless index, so it values varies from -1 to +1 with higher value showing denser and healthier vegetation such in tropical forests, average values present shrubs and grassland, while least values of 0.1 and below are common to water and non-vegetated areas. Furthermore, high values shows high photosynthetic activity and low values represent o low photosynthetic activities.

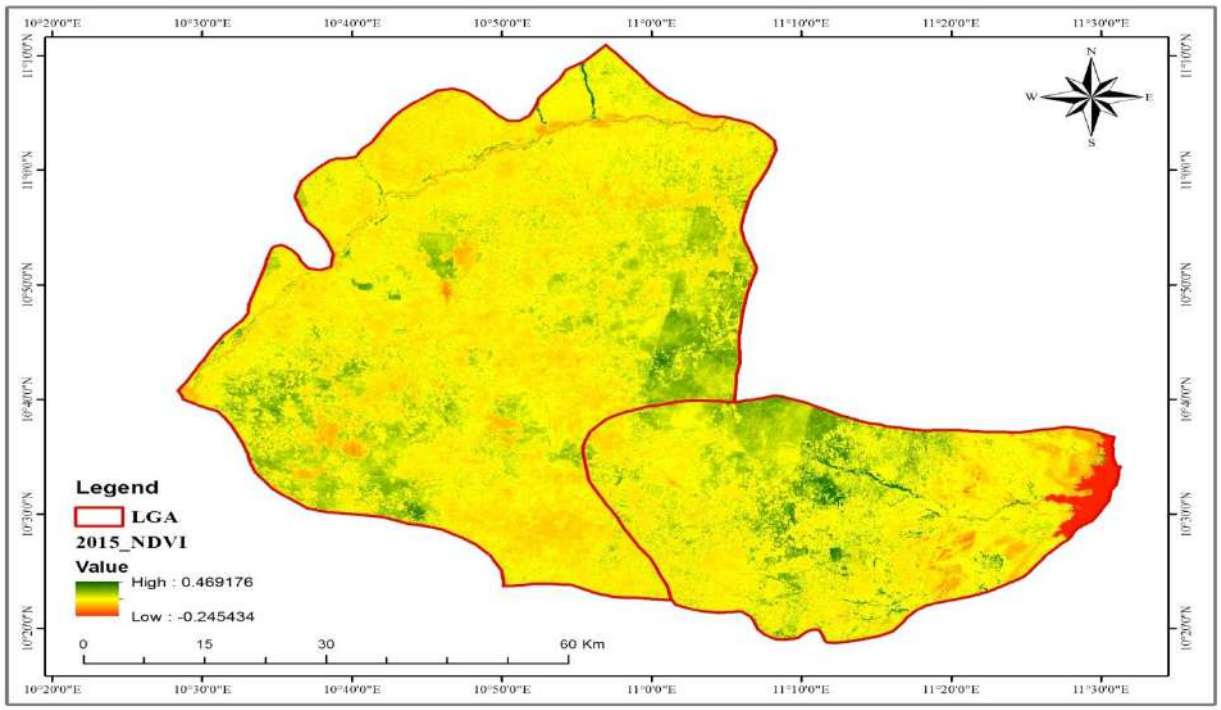

Figure 1: Vegetation Change Patterns (2013 – 2015)

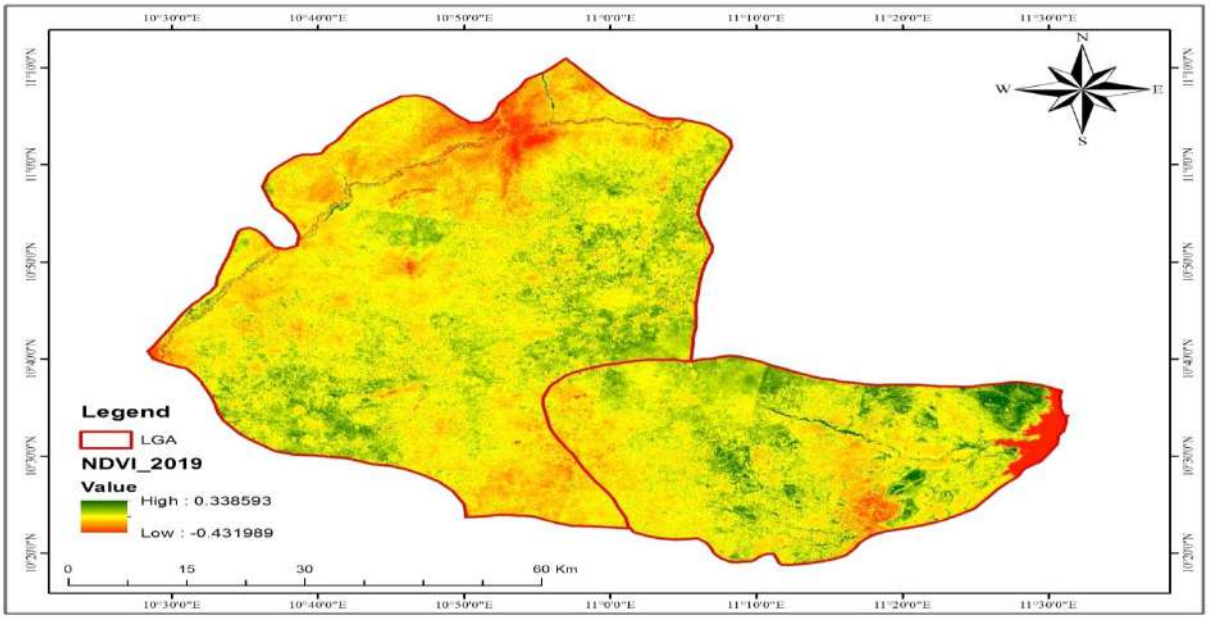

Figure 2: Vegetation Change Patterns (2016 – 2019)

The values in figure 1 and 2 describe the dimension index of the study areas vegetation cover within the study period in terms of high, moderate and low vegetation accordingly from the findings NDVI images.

From the NDVI Resulting Image, it shows that there was a decrease in the vegetation cover source areas after the first three years by 0.223742 (i.e. moderate vegetation) from 2013-2015 (Figure 1). At

the same time, there was a decrease of vegetation cover after the second three years by -0.093396 (i.e. very low vegetation) from 2016-2019 (Figure 2). This indicate that the vegetation was drastically reduced in size between 2013 and 2019.

Overall, the NDVI images further revealed that the resulting values was drastically reduced by 0.254714 (from 0.3855106 to 0.1307966) for the periods of six years (2013 to 2019), hence moderate vegetation.

The result in a visit to Dajin Dille Dukku Local Government Area, shows that the rate of cutting down trees are factors responsible for deforestation and the loss of valuable biodiversity of the source area especially floral diversity.

Table 1: Result of plot base Biodiversity analysis using quadrat methods

Plot	Cut Trees	Regenerated Trees	Standing Trees	Lost Trees
1	962	78	24	884
2	966	62	31	904
3	725	19	21	706
4	1,048	25	18	1,023
5	638	18	23	620
Total Mean	**867.8**	**40.4**	**23.4**	**827.4**

Table 1 described the loss of the trees in the five plots between 2013 to 2019. Out of 986 trees in plot 1 884 were completely lost, 904 were also lost in plot 2 while 706, 1,023 and 620 were also lost in plot 3, 4 and 5 respectively. This gave a significant value of total mean tree loss of 827.4.

Table 2: Causes of Biodiversity loss on vegetation

S/N	Parameters	Frequency	Percentage (%)
1	Demand for fuel wood	12	42.72
2	Over population	3	10.7
3	Demand for Agriculture	2	7.12
4	Demand for constructional materials	1	3.6
5	Poverty	2	7.12
6	Lack of employment	1	3.6
7	Lack of alternative energy	2	7.12
8	Demand for Herbs	2	7.12
9	Global warming	1	3.6
10	Demand for games (through hunting)	1	3.6
11	Demand for Grazing	1	3.6

Table 2 presented 28 respondents with various evidence for the potential cause(s) of Biodiversity loos on forest cover. 12 respondents (42.7%) pointed to fuel wood collection as the key factor affecting

Biodiversity loss on vegetation in the source area, followed by population increase with frequency of 3 (10.7%) as the source of deforestation, who emphasized that the population has significantly increased in recent times compared to the past. They reported that the need for fuel wood and housing as result of larger population can only be provided by the present vegetation resources,That is why there is vegetation reduction. Demand for Agriculture, Poverty, Lack of alternative energy and Demand for Herbs have frequency of 2 (7.12%) while others with unit frequency (3.6%) of the respondents identified various reasons for the loss of biodiversity in the source area.

Discussion

A moderate reduction in the vegetation cover in the source areas was observed after the first three years by 0.223742 from 2013-2015. Fawzi, Husna and Helms (2018) reported a decline in 2011 of deforestation rate to around 68 ha/year, and was around 112 ha/year in 2017. Furthe more, there was high decrease in vegetation cover after the second three years by -0.093396 from 2016-2019. This indicates that the forest cover has drastically reduced in size between 2013 and 2019.

The result in a visit to Dajin Dille Dukku Local Government Area, shows that the rate of cutting down trees are factors responsible for deforestation and the loss of valuable biodiversity of the source area especially floral diversity. Tropical deforestation is a major threat to global biodiversity (Asunción *et al.,* 2019).

The use of fuel wood has been on the increase due to increase in cost and scarcity of alternative sources (Paul, 2008). The recent study tagged fuel wood collection as the key factor affecting Biodiversity loss on vegetation with the highest frequency of 12(42.72) out of the 28 respondents, which is in line with the finding of Sambo (2008), need for energy is higher because more than 80% of households use fuel wood for their cooking. Acheampong *et al.* (2019) identified firewood production, forest fires and agriculture expansion (Boafo, 2013) as the major causes of deforestation. Population increase with frequency of 3(10.7%) was also identified in the present study as the cause of deforestation.

Conclusion

Deforestation rates are currently higher in the study area than what was obtained in the past. Fuel wood collection pattern of commercial vendors in the study area, has changed from that of previous household collection to an organized trade and from the clearing of dead woods to the cutting down of live trees.

Recommendations

Base on the findings of this study the following recommendations are made:

i. Emphasis should be made on tree planting campaign and more trees should be planted after cutting the existing ones.
ii. Farmers and the fuel wood vendors should also be encouraged to practice a selective method of cutting the trees.
iii. Legislation also should be re-enforced to curtail unnecessary bush burning and tree cutting.
iv. Alternative sources of energy should be provided, in order to reduce the over dependence on firewood.

References

Acheampong, O. E., Macgregor, C. J., Sloan, S. & Sayer, Y. (2019). Deforestation is driven by agricultural expansion in Ghana's forest reserves. *Scientific African, 5*; e00146

Asunción, S., Julieta, D., Matthias, B., Juan, M. B., Micaela, C., Bibiana, G., Tobias, K. (2019). Biodiversity loss in deforestation frontiers: Linking occupancy modelling and physiological stress indicators to understand local extinctions. *Biological conservation ELSEVIRE, 236*; 281-288.

Barrow, C. J. (1993). *Developing the Environment: Problems and Management*. UK Longman Scientific and Technology. pp230-241.

Boafo, J. (2013). The impact of deforestation of forest livelihoods in Ghana. Africa Portal Backgr., 49 (1), 1-7

Department of Water Affairs and Forestry, DWAF. (2005). Pilot State of the Forest Report. A pilot report to test the national criteria and indicators. Institute of Natural Resource.Scottsville. Investigational Report Number: 253.

Fawzi, N. I., Husna, V. N. & Helms, J. A. (2018). Measuring deforestation using remote sensing and its implication for conservation in Gunung Palung National Park, West Kalimantan, Indonesia. *IOP Conf. Series: Earth and Environmental Science 149*; 012038 doi :10.1088/1755-1315/149/1/012038

Food and Agriculture Organization of the United Nations (FAO) (2010). Global Forest Resources Assessment 2010 Country Report Nigeria. FRA2010/Pp.151. Rome, FAO.

Mainagwa, M. G. (2010). Fuelwood Markets in Sub-Saharan Africa: *Factors whichImpede, and Incentives which will accelerate their Development*. 6(1): 36 – 48.

Nzeh, C. E. P. and Eboh, E. C. (2007). Analysis of Income Effects of Forest Products Activities Among Rural Households in Enugu State, Nigeria. *J. Agric. Soc. Res. 7*(1):23-33.

Paul, J. (2008). Comparative Analysis of household Energy use in Yola Metropolitan Area. An unpublished M.Sc Thesis Department of Agricultural Economics and Extension, Federal University of Technology, Yola Adamawa state Nigeria.

Sambo, A. S. (2008 a). *Renewable Energy Options for the Environment and Sustainable Development in Nigeria.* Paper Presented at The National Workshop On Energy *Investment* and Private Sector and Participation at The Petroleum Training Institute, Warri.

Multivariate Analysis of Variance on the Academic Performance of Secondary School Students in National Examinations in Niger State, Nigeria

Adamu R., Usman A. & R. A. Adeyemi
Department of Statistics, Federal University of Technology, Minna, Nigeria
Email: adamuramatu@futminna.edu.ng

Abstract

The objective of this research is to evaluate the scholastic performance of secondary school students in Niger State, Nigeria, with a specific focus on their performance in National Examinations. This would be accomplished through the utilisation of multivariate analysis of variance. A random selection process was employed to choose two educational institutions from each geopolitical zone within the state. The research employed data obtained from the Senior Secondary School Certificate Examinations (SSSCE) administered by the West African Examinations Council (WAEC) and the National Examinations Council (NECO) spanning a decade, specifically from 2011 to 2020. According to the official gazettes of WAEC and NECO, the data was acquired. Multiple test techniques are utilised in the Multivariate Analysis of Variance (MANOVA), including as Wilks' Lambda, Pillai Bartlet, Hotelling T2, and Roy's Characteristics Root. In order to ascertain the characteristic roots of the sum of squares and sum squares cross products for the respective source of variation, it is necessary to solve an equation for each of these operations. The findings revealed significant variances in the academic performance of students within the three geopolitical zones of the state, as well as variations in the organisations responsible for conducting the examinations (WACE and NECO). The study has assessed the influence of national examinations on students' scholastic achievements, revealing that the academic performance of students in NECO surpasses that of WAEC.

Keywords: WAEC, NECO, MANOVA, Academic Performance, Examination, English, Mathematics And Biology

1.0 INTRODUCTION

Education is a complex process that helps people develop their talents, improve their cognitive capacities, and gain knowledge. Serving as a crucial conduit between basic and higher education levels, secondary schools in Nigeria are an essential part of the country's educational system. Asikhai (2010) asserts that secondary school education is essential for setting the groundwork for obtaining advanced knowledge in postsecondary educational settings. This entity serves as a double component that accelerates a nation's social, political, technological, scientific, and cultural advancements while also acting as an investment. Regretfully, the performance of contemporary secondary schools on external evaluations falls short of expectations. Public criticism of secondary school students' continuous low academic performance in public exams has been strong. Nwokocha and Amadike (2005) assert that a nation's ability to educate its citizens is mostly determined by the academic success of its pupils. Therefore, it is imperative to uphold an exceptional level of performance in internal and, for the most part, external assessments. Academic performance, as defined by Wikipedia (2013), is the degree to which a learner, teacher, or organisation has successfully completed their course of study. A student's success can be defined as their evaluation of their performance on tests that are directly related to their courses and on several other types of exams. Japo published in 2014.

Rofikul and Zebun (2017) propose that education is a crucial tool for promoting societal change by dismantling beliefs and superstitions and fostering rationality and knowledge in individuals. Everyone agrees that education plays a vital role in developing the skills and personal growth of citizens in a state or country. It takes on a pivotal role in driving a nation's progress by fostering the personal development and advancement of its citizens. For a country to progress in the domains of science and technology, which are essential for a nation's economic well-being, it needs an informed populace.

1.1 Objectives of the study

This paper has the following objectives: - To

i. check whether there is any significant difference between the zones
ii. know whether there is any significant difference between the examinations bodies

2.0 Literature Review

Mildin and Rubio (2021) conducted a multivariate analysis to look into senior high school students' academic achievement in the areas of attitudes, self-efficacy, and statistics. The researchers employed a five-point Likert scale to collect the data. The interval measurement scale is used to analyse Likert-scale data. To generate a composite score, the mean or sum of four or more Likert-type questions must be determined. As a result, the composite score is examined within the interval measurement scale. The mean, which indicates central tendency, and standard deviations, which assess variability, are the suggested statistical metrics for interval scale items. The degree of self-efficacy beliefs, attitudes towards statistics, and performance in statistics among senior high school students were assessed using the mean and standard deviation. Box's M and Levene's test were used to assess the data's homogeneity and normalcy before the significant difference test was finished. In this study, the impact of various levels of independent factors, either alone or in combination, on the dependent variables was ascertained using the application of Multivariate Analysis of Variance (MANOVA). The study's conclusions show that, of the different demographic variables examined, only the type of school had a statistically significant impact on senior high school statistics students' self-efficacy beliefs, attitudes towards statistics, and academic achievement.

In the context of university students' academic achievement, Okeke et al. (2018) looked into the relationship between descriptive statistics and multivariate analysis of variance (MANOVA). An initial assessment was carried out to examine the normality and equality of variance of the data in order to establish whether the data were suitable for the analysis of variance test. The Doormik-Hansen test yielded a p-value of greater than 0.05, suggesting a robust adherence to normalcy in the data. Strong evidence for the equality of covariance matrices among the groups was found by the Box M test, which produced a p-value greater than 0.05. A p-value of 0.306 was obtained from the Wilks Lambda test, exceeding the predetermined level of significance ($\alpha = 0.05$). The results show that there is no significant correlation between Federal University Wukari 300 level students' academic achievement and their affiliation with a particular faculty.

Endris (2016) conducted a multivariate analysis to look at the variables that affect the academic performance of grade 10 students in Hawassa City, Ethiopia. The Education Department supplied the secondary data on students' results in the five chosen subjects (Mathematics, Biology, Physics, Chemistry, and English) on the Ethiopian General Secondary Education of Certificate Examination (EGSECE). The data were analysed using multivariate multiple linear regression, factor analysis, and descriptive analysis. The findings of the study indicate that students from both government and non-government schools performed poorly in physics but excelled in English. Students attending non-governmental schools outperformed students attending governmental schools in terms of academic performance on average.

In the setting of Kwara State, Udokang and Odeyemi's (2021) study looked at the impact of extra teaching hours on secondary school students' academic performance in the areas of English language and mathematics. Multivariate Analysis of Variance was utilised to examine the impacts. The results of the MANOVA analysis show that students' academic performance in mathematics and English language is significantly impacted by the choice and duration of supplemental courses. However, the statistical analysis showed that there were no noteworthy results from the association between these parameters. Analysis of Variance (ANOVA) was used to further examine the relationship between the length and type of supplemental instruction sessions and students' academic performance in mathematics and English language.

3.0 Materials and Method

A thorough synopsis of the study population, research topic, sample and sampling methodology, data collection tool, data collection process, and data analysis method is given.

3.1 Design of the study

The study used multivariate analysis to assess senior secondary school students' academic performance across many schools and zones. Its goal was also to evaluate the level of correlation that existed between the dependent variable (students' academic performance) and the independent variables (schools and zones) in the areas of English language, general mathematics, and biology among senior secondary school students taking the WAEC and NECO exams.

3.2 Data collection and data source

The dataset used for analysis includes the academic performance of pupils who took part in the English language, general mathematics, and biology National Examinations (WaEC and NECO). Grades are given and then converted into percentages to evaluate performance.
The research makes use of secondary data that was obtained for the internal examinations conducted in May/June and June/July from the gazettes of the West African Examinations Council (WAEC) and the National Examinations Council (NECO). The Test and Measurement Unit, which is run by the Niger State Ministry of Education, provided the data used in this investigation. The data set includes the years 2011 through 2020. Two public schools were selected from each geopolitical zone, for a total of six schools that were part of the data collection procedure. Additionally, two local government districts from each zone were chosen for the study. There are a total of 25 Local Government Areas (LGAs) in Niger State, which are divided into three zones: A, B, and C. There are eight Local Government Areas (LGAs) in Zone A, nine in Zone B, and eight in Zone C. Three topics were selected for examination: English Language, Mathematics, and Biology for each of the approved public secondary schools.

Sample and sampling technique

A randomly selected subset of the population is known as a simple random sample. Every member of the population has an equal chance of getting chosen thanks to this sampling technique.

3.3 Method of Analysis

Multivariate analysis of variance

A statistical method called multivariate analysis of variance (MANOVA) expands on the ideas of univariate analysis of variance (ANOVA). ANOVA is used to examine differences between group means for a single response variable. The response variable count is increased to two or more in the MANOVA model. The comparison of group mean vectors lies at the heart of the theory. In terms of comparing two groups, the outcomes align with Hotelling's T2 methodology. The F-test's multivariate extension is not

entirely simple to use. Furthermore, there exist multiple test statistics that can be employed, including Wilks' Lambda and Lawley's trace. Because it is inherently difficult to precisely calculate the true distributions of the given data, approximations based on the F-distribution are used. Because MANOVA has advantages over univariate Analysis of Variance (ANOVA) when working with a single response variable, it is used in this study. An independent analysis of variance (ANOVA) study can include biology, mathematics, and English language proficiency as independent response variables. The matrix technique is utilised for the MANOVA computations due to the existence of many response variables, specifically the academic accomplishment of pupils in the subjects of biology, mathematics, and English language. In this study, the independent variables are the year, schools, zones, and examination bodies (WaEC and NECO). The univariate two-way model proposed by Xijk is used to describe the kth observation at level i of zones and level j of tests. The equation provided splits the total sum of squares of and cross product matrix (SSCPT) into two components: a within the sum-of-squares and cross-products matrix (SSCPW) and a between the sum-of-squares and cross-products matrix (SSCPB).

$$X_{ijk} = \mu + \alpha_i + \beta_j + (\propto \beta)_{ij} + e_{ijk} \qquad (3.1)$$

Where

i = 1, 2, . . ., r, j = 1, 2, . . ., c and k = 1, 2, . . ., n

α_i The variable "r" represents the number of zones in Niger state.

β_j The variable "c" represents the number of examination bodies that have been selected for the investigation.

where

$\sum_{i=1}^{r} \alpha_i = \sum_{j=1}^{c} \beta_j = \sum_{i=1}^{r} \sum_{j=1}^{c} (\propto \beta)_{ij} = 0$ and e_{ijk} are independent N(0, σ^2) random variables. Here, μ represents an overall level, α_i represents the fixed effects of factor 1 (α), β_j represents the fixed effect of factor 2 (β), and $(\alpha\beta)_{ij}$ is the interaction between zones and examination bodies the expected response at the i^{th} level of zones and the j^{th} level of examination bodies is thus

$$E(X_{ijk}) = \mu + \alpha_i + \beta_j + (\propto \beta)_{ij} \qquad (3.2)$$

i = 1, 2, . . ., *r and j = 1, 2, . . c*

The presence of interaction λ_{ij}, implies the factor effects are not additive

$$X_{ijk} = \bar{X}_{...} + (\bar{X}_{i..} - \bar{X}_{...}) + (\bar{X}_{.j.} - \bar{X}_{...}) + (\bar{X}_{ij.} - \bar{X}_{i..} - \bar{X}_{.j.} + \bar{X}_{...}) + (\bar{X}_{ijk} - \bar{X}_{ij.}) \qquad (3.3)$$

Let X_ijk represent the total number of observations about the academic achievement of the students throughout the zones and examination bodies. The average academic performance of pupils across all zones and examination bodies is represented by the symbol X_. The average academic achievement of pupils at the ith level within the zones is denoted by X_(i..). The average academic performance of students in the examination bodies for the jth level is represented by X_(.j.), whereas the average academic performance of students in the zones and examination bodies for the ith and jth levels is represented by X_(ij.).

The matrix technique is used in computer computations to obtain the p-value and the F-ratio, which are then used to evaluate the viability of the subsequent hypotheses.

Hypothesis

In this study, the researchers will examine the following hypothesis.

Hypothesis 1

H_{01}: There is no significant difference between academic performance of students and zones
Vs
H_{11}: There is significant difference between academic performance of students zones

Hypothesis 2

H_{02}: There is no significant difference between academic performance of students and examination bodies
Vs
H_{12}: There is significant difference between academic performance of students and examination bodies

Hypothesis

H_0: $\alpha_1 = \alpha_2 = \alpha_3$

H_1: $\alpha_1 \neq \alpha_2 \neq \alpha_3$

H_0: $\beta_1 = \beta_2$

H_1: $\beta_1 \neq \beta_2$

Sum of squares cross product

$$SS_{zones} = cn\sum_{i=1}^{r}(X_{i..} - \bar{X}_{...})^2 = cn\sum_{i}^{r}(X_{i..} - \bar{X}_{...})(X_{i..} - \bar{X}_{...})' \quad (3.4)$$

$$SS_{Exams\ bodies} = rn\sum_{j=1}^{c}(X_{.j.} - \bar{X}_{...})^2 = rn\sum_{j}^{c}(X_{.j.} - \bar{X}_{...})(X_{.j.} - \bar{X}_{...})' \quad (3.5)$$

$$SS_{int} = n\sum_{i=1}^{r}\sum_{j=1}^{c}(X_{ij.} - X_{i..} - \bar{X}_{.j.} - \bar{X}_{...})^2 = n\sum_{i=1}^{r}\sum_{j=1}^{c}(X_{ij.} - X_{i..} - \bar{X}_{.j.} - \bar{X}_{...})(X_{ij.} - X_{i..} - \bar{X}_{.j.} - \bar{X}_{...})' \quad (3.6)$$

$$SS_{res} = \sum_{i=1}^{r}\sum_{j=1}^{c}\sum_{k=1}^{n}(X_{ijk} - \bar{X}_{ij.})^2$$

$$= \sum_{i=1}^{r}\sum_{j=1}^{c}\sum_{k=1}^{n}(X_{ijk} - \bar{X}_{ij.})(X_{ijk} - \bar{X}_{ij.})' \quad (3.7)$$

$$SS_{Total} = \sum_{i=1}^{r}\sum_{j=1}^{c}\sum_{k=1}^{n}(X_{ijk} - \bar{X}_{...})^2$$

$$= \sum_{i=1}^{r}\sum_{j=1}^{c}\sum_{k=1}^{n}(X_{ijk} - \bar{X}_{...})(X_{ijk} - \bar{X}_{...})'$$

(3.8)

Table3.1: MANOVA Table for comparing effects of two factors and their interaction

Source of variation (SV)	**Sum of squares (SS)**	**Degrees of freedom (df)**
Zones	$SS_{zones} = cn\sum_{i=1}^{r}(X_{i..} - \bar{X}_{...})(X_{i..} - \bar{X}_{...})'$	r – 1
Exams Bodies	$SS_{Exams} = rn\sum_{j=1}^{c}(X_{.j.} - \bar{X}_{...})(X_{.j.} - \bar{X}_{...})'$	c – 1
Interaction	$SS_{int} = n\sum_{i=1}^{r}\sum_{j=1}^{c}(X_{ij.} - X_{i..} - \bar{X}_{.j.} - \bar{X}_{...})(X_{ij.} - X_{i..} - \bar{X}_{.j.} - \bar{X}_{...})'$	(r – 1)(c – 1)
Residual (error)	$SS_{res} = \sum_{i=1}^{r}\sum_{j=1}^{c}\sum_{k=1}^{n}(X_{ijk} - \bar{X}_{ij.})(X_{ijk} - \bar{X}_{ij.})'$	rc(n – 1)
Total (corrected)	$SS_{cor} = \sum_{i=1}^{r}\sum_{j=1}^{c}\sum_{k=1}^{n}(X_{ijk} - \bar{X}_{...})(X_{ijk} - \bar{X}_{...})'$	rnc – 1

Source: Johnson and Wichern, (1944)

The F-ratio of the mean squares, $SS_{zones}/(r-1)$, $SS_{Exams}/(c-1)$ and $SS_{int}/(r-1)(c-1)$ to the mean square, $SS_{res}/[rc(n-1)]$ can be used to test for the effects of zones, exams and zones – exams interaction respectively.

3.4 Test statistic for Multivariate Analysis of Variance (MANOVA) and hypotheses

Four test statistics are typically used in multivariate analysis of variance. The subsequent section offers a comprehensive elucidation of the aforementioned statistics.

1. **Wilks's lambda (∧)**: - The product of the unexplained variance on each of the variates.

$$\wedge = \prod_{i=1}^{n} \frac{1}{1+\lambda_i} \quad (3.9)$$

i =1, 2, …, n

Though it's crucial to remember that the symbol denotes multiplication rather than addition, it shares characteristics with the summation symbol (ʒ). The aforementioned test is frequently employed in situations where the independent variables give rise to more than two distinct groups. The centroids, or vectors, of the means on the independent variables are used to quantify the differences between the groups. The differences grow as lambda () diminishes. The importance of lambda is ascertained by using Bartlett's transformation of lambda(). Lambda. For each variable, the SS_E/SS_T ratio is calculated, which shows the ratio of error variance to total variance.

Or

Wilks Lambda

$$\wedge^* = \frac{|E|}{|H+E|} \quad (3.10)$$

E represents the sum of squared errors, H represents the hypothesis, and H + E is the total sum of squared errors.

In this case, the determinant of the total sum of squares and cross-product matrix T = H + E is divided by the determinant of the error sums of squares and the cross-products matrix E. The total of H and E will be more than E if H is greater than E. Hence, when the Wilks lambda value is very small, close to 0, the null hypothesis is considered invalid.

Hotelling-Lawley Trace: By using the formula = ∑_(i=1)n⁒_i, the Hotelling-Lawley trace is computed by adding the Eigen values corresponding to each variable. This is the currently accepted standard test for two different groups. The "SSCP_H/SSCP_T" statistic is a straightforward comparison to the F ratio in an ANOVA since it measures the ratio of explained variance to unexplained variance for every variable.

Or

Hotelling-Lawley Trace

$$T_0^2 = trace(HE^{-1}) \quad (3.11)$$

2. The process involves multiplying matrix H by matrix E's inverse, then figuring out the trace of the resulting matrix. The Hotelling-Lawley trace will show a significant magnitude if H is a significant amount bigger than E. The null hypothesis will be rejected if it is found that the test statistic is large.
3. **Pallai – Bartlett trace**: - The formula V = ∑_(i=1)n⁒κ_i/(1+ κ_i) represents the Pillai trace mathematically, where n is the number of eigenvalues for each discriminant variate. The total explained variance on the distinguishing variants—variables derived using the canonical coefficients for a particular set of roots—is referred to as Pillai's trace. Thus, by convention, a high value denotes a significant difference and is similar to the explained variance to total variance ratio.

Or

Pallai Trace

$$\boldsymbol{V = trace(H(H+E)^{-1})} \quad (3.12)$$

4. In this case, H is multiplying by the cross product matrix T=H+E, which is the inverse of the total sum of squares. The Pillai trace will take a significant value if H is large in relation to E. Thus, in the event that the test statistics are high, we will reject the null hypothesis.
5. **Roy's greatest characteristic roots**: - The largest root of Roy's equation is represented by the eigenvalue of the first variable. According to Michael's (2010) research, the Hotelling-Lawley trace is comparable to the trace described above, with the exception of the first variable. The ratio of unaccounted variance to unaccounted variance (SSCP_H/SSCP_E) is represented by the previously indicated statistic with respect to the first distributive function. While this approach is comparable to the Pillai Bartlett trace, it places more focus on the early—and hence, more significant—root. Sometimes the largest Eigen value is thought to be equal to the greatest root of Roy. The result described above is equivalent to the F-ratio in univariate analysis of variance (ANOVA) and denotes the greatest possible difference between groups based on the information gathered. The test statistic shows less robustness in comparison to the other tests when the multivariate normality assumption is violated.
6. or

Roy's Maximum Root: Largest eigenvalue of HE^{-1}

In this case, the largest eigenvalue of the resultant matrix is calculated by multiplying the matrix H by the inverse of the matrix E. Roy's root will also have a bigger value if H has a greater value than E. Consequently, the null hypothesis is disproved if the test statistic is high. The table that follows, Table 3.1, gives detailed information about the F approximations for the four test statistics that are commonly used in multivariate analysis of variance.

Table 3.2: Test Statistics used to compare sample mean vectors with Approximate F-test

Test	**Statistic**	**F**	***df₁***	***df₂***	**Comment**
Pillai's Trace	V	$(n-m-p+s)V\big(d(s-V)\big)^{-1}$	*Sd*	S(n-m-p+s)	$d = \max(p, m-1)$ $s = \min(p, m-1)$ = number of positive eigen values
Wilks's Lambda	∧	$\left\{\left(1-\wedge^{\frac{1}{t}}\right)\wedge^{\frac{1}{t}}(df_2 \times df_1^{-1})\right\}$	P(m -1)	wt – (df_1x0.5) + 1	$w = n-1(p+m)0.5$ $t = [(df_1^2-4) \times (p^2 + (m-1)^2 - 5)^{-1}]^{0.5}$ If $df_1 = 2$, set t = 1
Hotelling's Trace	U	$df_2 U \times (sdf_1)^{-1}$	S(2A+s+1)	2(sB + 1)	*s is as for pillai's trace* $A = (\lvert m-p-1\rvert - 1) \times 0.5$ $B = (n-m-p-1) \times 0.5$ The significance level obtained is a lower bound
Roy's Largest Root	λ_1	$(df_2 \times df_1^{-1})\lambda_1$	D	n – m – d – 1	$d = \max(p, m-1)$ $s = \min(p, m-1)$ = number of positive eigen values

Source: Manly (2005)

4.0 Data Analysis

Multivariate analysis of variance is the statistical technique used for the investigation. Because the data were complex, statistical software called SPSS version 21 was used for the analysis.

The output of the SPSS statistical programme was used to calculate the matrices that reflect the sum of squares and cross-products, as indicated in Appendix I. The following are these matrices:

$$SSCP_{ZONES} = \begin{pmatrix} 25664.227 & 35605.209 & 24189.398 \\ 35605.209 & 118362.984 & 47232.619 \\ 24189.398 & 47232.619 & 25510.287 \end{pmatrix}$$

The sum of squares and cross product for the zones ($SSCP_{ZONES}$) in Niger State

$$SSCP_{EXAMS} = \begin{pmatrix} 17285.444 & -9231.023 & 10301.014 \\ -9231.023 & 4929.685 & -5501.097 \\ 10301.014 & -5501.097 & 6138.743 \end{pmatrix}$$

The sum of squares and cross product for the Examination bodies ($SSCP_{EXAMS}$)

$$SSCP_{Error} = \begin{pmatrix} 2122819 & 885393.114 & 844003.525 \\ 885393.114 & 2780950.653 & 921317.664 \\ 844003.525 & 921317.664 & 1965926.210 \end{pmatrix}$$

The sum of squares error and cross product for the zones and examinations ($SSCP_{ERROR}$)

Calculation of the MANOVA test statistics

1. **Zones:** the test statistics for the zones (academic performance base on zones) are as computed below.

   (a) Wilks's lambda

$$\wedge = \frac{|E|}{|H+E|}$$

$$|E| = \begin{vmatrix} 2122819.665 & 885393.114 & 844003.525 \\ 885393.114 & 2780950.653 & 921317.664 \\ 844003.525 & 921317.664 & 1965926.210 \end{vmatrix}$$

$$2122819.665 \times \begin{vmatrix} 2780950.653 & 921317.664 \\ 921317.664 & 1965926.210 \end{vmatrix}$$
$$- 885393.11\,4 \times \begin{vmatrix} 885393.114 & 921317.664 \\ 844003.525 & 1965926.210 \end{vmatrix}$$
$$+ 844003.525 \times \begin{vmatrix} 885393.114 & 2780950.653 \\ 844003.525 & 921317.664 \end{vmatrix}$$

$$2122819.665 \times (5.4671 \times 10^{12} - 8.4883 \times 10^{11}) - 885393.114 \times (1.7406 \times 10^{12} - 7.7760 \times 10^{11}) + 844003.525 \times (8.1573 \times 10^{11} - 2.3471 \times 10^{12})$$

$$9.8038 \times 10^{18} - 8.5263 \times 10^{17} - 1.2925 \times 10^{18}$$

$$|E| = 7.6587 \times 10^{18}$$

$$|H+E| = \begin{vmatrix} 2148483.892 & 920998.323 & 868192.923 \\ 920998.323 & 2899313.637 & 968550.283 \\ 868192.923 & 968550.283 & 1991436.497 \end{vmatrix}$$

$$2148483.892 \times \begin{vmatrix} 2899313.637 & 968550.283 \\ 968550.283 & 1991436.497 \end{vmatrix} - 920998.323 \times \begin{vmatrix} 920998.323 & 968550.283 \\ 868192.923 & 1991436.497 \end{vmatrix} + 868192.923 \times \begin{vmatrix} 920998.323 & 2899313.637 \\ 868192.923 & 968550.283 \end{vmatrix}$$

$$2148483.892 \times (5.7738 \times 10^{12} - 9.3809 \times 10^{11}) - 920998.323 \times (1.8341 \times 10^{12} - 8.4089 \times 10^{11}) + 868192.923 \times (8.9203 \times 10^{11} - 2.5172 \times 10^{12})$$

$$1.0389 \times 10^{19} - 9.1474 \times 10^{17} - 1.4110 \times 10^{18}$$

$$|H+E| = 8.0638 \times 10^{18}$$

$$\wedge = \frac{|E|}{|H+E|} = \frac{7.6587 \times 10^{18}}{8.0638 \times 10^{18}}$$

$$= 0.950$$

b) **Pallai Trace**

$$\boldsymbol{V = trace(H(H+E)^{-1})}$$

$$trace\left(\begin{pmatrix} 25664.227 & 35605.209 & 24189.398 \\ 35605.209 & 118362.984 & 47232.619 \\ 24189.398 & 47232.619 & 25510.287 \end{pmatrix}\begin{pmatrix} 2148483.892 & 920998.323 & 868192.923 \\ 920998.323 & 2899313.637 & 968550.283 \\ 868192.923 & 968550.283 & 1991436.497 \end{pmatrix}^{-1}\right)$$

$$trace\begin{pmatrix} 0.0061 & 0.0086 & 0.0053 \\ 0.0104 & 0.0400 & 0.0225 \\ 0.0035 & 0.0136 & 0.0046 \end{pmatrix}$$

$$V = 0.0061 + 0.0400 + 0.0046$$

=0.051

(c) **Hotelling Lawlay Trace**

$$\cup = HE^{-1}$$

$$\begin{pmatrix} 25664.227 & 35605.209 & 24189.398 \\ 35605.209 & 118362.984 & 47232.619 \\ 24189.398 & 47232.619 & 25510.287 \end{pmatrix} \times \begin{pmatrix} 2122819.665 & 885393.114 & 844003.525 \\ 885393.114 & 2780950.653 & 921317.664 \\ 844003.525 & 921317.664 & 1965926.210 \end{pmatrix}^{-1}$$

$$= trace\begin{pmatrix} 0.0062 & 0.0090 & 0.0054 \\ 0.0105 & 0.0416 & 0.0226 \\ 0.0035 & 0.0143 & 0.0048 \end{pmatrix}$$

$$\cup = 0.0062 + 0.0416 + 0.0048$$

$$= 0.052$$

(d) **Roy's Characteristic Root**
Largest eigenvalue of HE^{-1}
$\lambda_{max} = 0.052$

The computed values are the same with the values obtained from the SPSS out in Appendix II (see Zones (A B and C))

2. **Examination Bodies**: - The test statistics for the examination bodies (WAEC and NECO) are as computed below.

(a) Wilks's lambda

$$\wedge = \frac{|E|}{|H+E|}$$

$$|E| = \begin{vmatrix} 2122819.665 & 885393.114 & 844003.525 \\ 885393.114 & 2780950.653 & 921317.664 \\ 844003.525 & 921317.664 & 1965926.210 \end{vmatrix}$$

$$2122819.665 \times \begin{vmatrix} 2780950.653 & 921317.664 \\ 921317.664 & 1965926.210 \end{vmatrix} - 885393.114 \times \begin{vmatrix} 885393.114 & 921317.664 \\ 844003.525 & 1965926.210 \end{vmatrix} + 844003.525 \times \begin{vmatrix} 885393.114 & 2780950.653 \\ 844003.525 & 921317.664 \end{vmatrix}$$

$$2122819.665 \times (5.4671 \times 10^{12} - 8.4883 \times 10^{11}) - 885393.114 \times (1.7406 \times 10^{12} - 7.7760 \times 10^{11}) + 844003.525 \times (8.1573 \times 10^{11} - 2.3471 \times 10^{12})$$

$$9.8038 \times 10^{18} - 8.5263 \times 10^{17} - 1.2925 \times 10^{18}$$

$$|E| = 7.6587 \times 10^{18}$$

$$|H + E| = \begin{vmatrix} 17285.444 & -9231.023 & 10301.014 \\ -9231.023 & 4929.685 & -5501.097 \\ 10301.014 & -5501.097 & 6138.743 \end{vmatrix} + \begin{vmatrix} 2122819.665 & 885393.114 & 844003.525 \\ 885393.114 & 2780950.653 & 921317.664 \\ 844003.525 & 921317.664 & 1965926.210 \end{vmatrix}$$

$$= \begin{vmatrix} 2140105.109 & 876162.091 & 854304.539 \\ 876162.091 & 2785880.338 & 915816.567 \\ 854304.539 & 915816.567 & 1972064.953 \end{vmatrix}$$

$$2140105.109 \times \begin{vmatrix} 2785880.338 & 915816.567 \\ 915816.567 & 1972064.953 \end{vmatrix} - 876162.091 \times \begin{vmatrix} 876162.091 & 915816.567 \\ 854304.539 & 1972064.953 \end{vmatrix} + 854304.539 \times \begin{vmatrix} 876162.091 & 2785880.338 \\ 854304.539 & 915816.567 \end{vmatrix}$$

$$2140105.109 \times (5.4939 \times 10^{12} - 8.3872 \times 10^{11}) - 876162.091 \times (1.7278 \times 10^{12} - 7.8239 \times 10^{12}) + 854304.539 \times (8.0240 \times 10^{11} - 2.380 \times 10^{12})$$

$$|H + E| = 7.7865 \times 10^{18}$$

$$\wedge = \frac{|E|}{|H + E|} = \frac{7.6587 \times 10^{18}}{7.7865 \times 10^{18}}$$

$$= 0.984$$

(b) **Pallai Trace**

$$\boldsymbol{V = trace(H(H + E)^{-1})}$$

$$trace\left(\begin{pmatrix} 17285.444 & -9231.023 & 10301.014 \\ -9231.023 & 4929.685 & -5501.097 \\ 10301.014 & -5501.097 & 6138.743 \end{pmatrix} \begin{pmatrix} 2140105.109 & 876162.091 & 854304.539 \\ 876162.091 & 2785880.338 & 915816567 \\ 854304.539 & 915816.567 & 1972064.953 \end{pmatrix}^{-1} \right)$$

$$trace \begin{pmatrix} 0.0094 & -0.0078 & 0.0048 \\ -0.0050 & 0.0042 & -0.0026 \\ 0.0056 & -0.00\,47 & 0.0029 \end{pmatrix}$$

$V = 0.0094 + 0.0042 + 0.0029$
=0.016

(c) **Hotelling Lawlay Trace**

$$\cup = HE^{-1}$$

$$\begin{pmatrix} 17285.444 & -9231.023 & 10301.014 \\ -9231.023 & 4929.685 & -5501.097 \\ 10301.014 & -5501.097 & 6138.743 \end{pmatrix} \times \begin{pmatrix} 2122819.665 & 885393.114 & 844003.525 \\ 885393.114 & 2780950.653 & 921317.664 \\ 844003.525 & 921317.664 & 1965926.210 \end{pmatrix}^{-1}$$

$$= trace\begin{pmatrix} 0.0095 & -0.0080 & 0.0049 \\ -0.0051 & 0.0043 & -0.0026 \\ 0.0057 & -0.0047 & 0.0029 \end{pmatrix}$$

$\cup = 0.017$

(d) **Roy's Characteristic Root**
Largest eigenvalue of HE^{-1}

$\lambda_{max} = 0.017$

a) The calculated figures are consistent with the values obtained from the SPSS software, as shown in Appendix II, which also contains the test organisations (WAEC and NECO). the test calculation's F-statistics computation. Data interpretation
The statistical data obtained above are used to the four multivariate procedures to compute the F-values.
Zone-based academic performance (A, B, C)

b) Wilks's Lambda ($\wedge$)
Where n = 10286; m = 3, p = 3, d = 3, s = 2 and $\wedge = 0.950$

$$F = \left(\frac{1-\wedge}{\wedge}\right)^{\frac{1}{t}}\left(\frac{df_2}{df_1}\right) = \left(\frac{1-0.950}{0.950}\right)^{\frac{1}{2}} \times \left(\frac{20562}{6}\right) = 89.102$$

c) Pillia's trace (V)

$$F = \frac{(n-m-p+s)V}{d(s-V)} = \frac{(10286-3-3+2)0.051}{3(2-0.051)} = 89.684$$

d) Hotelling Lawley Trace

$$F = \frac{df_2 \cup}{Sdf_1} = \frac{20560 \times 0.052}{2 \times 6} = 89.093$$

e) Roy's Characteristics root

$$F = \left(\frac{df_2}{df_1}\right)\lambda_{max} = \frac{10279}{3} \times 0.043 = 147.332$$

a) The null hypothesis H01 is to be rejected if the estimated F value is higher than the critical F value of 0.05, yielding a value of 2.61 at a significance level of 5%. The calculated values of 89.102, 89.684, 89.093, and 147.332 are over the critical value, per the test findings. Consequently, there is a statistically significant difference in academic achievement between zones A, B, and C, demonstrating the rejection of the null hypothesis. academic achievement as determined by the WAEC and NECO Examination Bodies

Wilks's Lambda ($\wedge$)

Where n = 10286; m = 3, p = 2, d = 3, s = 2 and $\wedge = 0.984$

$$F = \left(\frac{1-\wedge}{\wedge}\right)^{\frac{1}{t}}\left(\frac{df_2}{df_1}\right)$$

$$= \left(\frac{1-0.984}{0.984}\right)^{\frac{1}{2}} \times \left(\frac{20564}{4}\right) = 41.627$$

b) Pillia's trace (V)

$$F = \frac{(n - m - p + s)V}{d(s - V)}$$

$$= \frac{(10286 - 3 - 2 + 2)0.016}{3(2 - 0.016)} = 27.632$$

c) Hotelling Lawley Trace

$$F = \frac{df_2 \cup}{Sdf_1}$$

$$= \frac{20562 \times 0.017}{2 \times 4} = 43.694$$

d) Roy's Characteristics root

$$F = \left(\frac{df_2}{df_1}\right)\lambda_{max}$$

$$= \frac{10280}{2} \times 0.017 = 87.380$$

If the estimated F value is higher than the critical F value of 0.05, the null hypothesis H02 is rejected, resulting in a value of 3.00 at a significance level of 5%. The computed values of 41.627, 27.632, 43.694, and 87.380 are shown to exceed the critical value by the acquired test results. It can be concluded that there is a difference in academic performance between the examination boards, namely WAEC and NECO, as a result of the null hypothesis being rejected.
In summary
Academic achievement was shown to be statistically significantly correlated with the zones and examination bodies that were the subject of the study. The findings imply that there is no statistically significant impact of zones on the academic achievement of state residents' children. It's also critical to recognize that exam bodies have no bearing whatsoever on students' academic performance.

Reference

Adeleke B. L., Yahaya W. B. & Usman A. (2015). A comparison of Some Test Statistics for Multivariate Analysis of Variance Model with Non – Normal Responses. *Journal of Natural Science Research, 5(15),* 1 – 9 www.iiste.org p-ISSN 2224-3186 e-ISSN 2225-0921

Anthony E. U & Ekemini G. (2020) Multivariate Analysis of Academic Performance of Undergraduate Students Admitted Through Unified Tertiary Matriculation Examination and Direct Entry. *Journal of Mathematics 7(2),* 1 – 10 www.researchjournali.com

Bashir M. I. & Luka K. M. (2022) Comparative Analysis of Students' Performance in WAEC and NECO English Language and General Mathematics Examinations of Senior Secondary Schools in Kano State, Nigeria *AJSTME, 8(1),* 480-487, https://www.ajstme.com.ng ISSN: 2251-0141

Bryan F. J. Manly (2005). *Multivariate Statistical Methods. A Primer Third Edition*. Florida 33431: Chapman and Hall/CRC

C. Chatfield A. J. Collins (1984). *Introduction to Multivariate Analysis. First Edition.* London: Chapman & Hall

Endris, E. A. (2016). Multoivariate Analysis of Factors Influencing Achievement of Students in Selected Subjects at School Level: A Case Study of Grade 10 Students at Hawassa City, Ethiopia. *Global Journal of Human Social Science, XVI*(II), 25 - 37.

Jonhson R. A & Wichern D. W. (1944). *Applied Multivariate Statistical Analysis. Sixth Edition.* London 9780131877153: Pearson Prentice Hall.

Okeke E. N., Okeke J. U. & Adashu, D. (2018). Multivariate Analysis of Variance of University Students' Academic Performance. *International Journal of Applied Mathematics and Statistical Sciences (IJAMSS), 7*(1), 13 - 19

Paul M., Peter M., Emmanuel G. & Baah-Korang K. (2015) Multivariate Analysis of Academic Performance of Ghanaian Secondary School Students *International Invention Journal of Education and General Studies, 1(1),* 9-17. http://internationalinventjournals.org/IIJEGS

Udokang A. E. & Odeyemi J. B. (2021) Multivariate Analysis of Variance of Effect of Extra Lesson on Secondary School Students' Academic Performance in English Language and Mathematics in Kwara State *International Journal of Engineering and Applied Sciences (IJEAS), 8(2),* 7-12 www.ijeas.org

Usman A. (2014). Analysis of ChlorophyII "A" and "B" in Randomly selected Varieties of Surgarcane Leaves Using Multivariate Analysis of Variance. *Journal of Mathematics, 10(2),* 26 – 32 www.iosrjournals.org e-ISSN: 2278-3008, p- ISSN:2319-7676.


6.15%
7^2